Modelling, prevalence and immobilisation of per- and poly-fluoroalkyl substances

by

Julie Anne Sleep

Bachelor of Science (Applied Physics)

Bachelor of Information Technology (Computing and Mathematics)(Honours)

Master of Science (Mathematics)

A thesis submitted for the degree of

Doctor of Philosophy

UniSA STEM

Future Industries Institute



University of South Australia

December 2025

Contents

List of figures . . . x
List of tables . . . xiii
Glossary and abbreviations . . . xv
Summary . . . xviii
Declaration . . . xix
Acknowledgments . . . xix
Author contributions . . . xx

1 Introduction **1**
1.1 Background . . . 1
1.1.1 Molecular structure . . . 1
1.1.2 Toxicity . . . 2
1.1.3 Prevalence . . . 3
1.1.4 Sorption . . . 4
1.2 Research aims . . . 5
1.3 Structure . . . 7
1.4 List of publications . . . 10

2 A review of immobilisation-based remediation of per and poly-fluoroalkyl substances (PFAS) in soils **11**
2.1 Introduction . . . 13
2.2 Immobilisation . . . 15
2.2.1 Activated carbon-based amendments . . . 15
2.2.2 Biochar-based amendments . . . 17
2.2.3 Clay-based amendments . . . 17
2.2.4 Composite and other amendments . . . 18
2.2.5 Amendment additions and binding agents . . . 18
2.3 Remediation effectiveness . . . 19
2.4 Mechanisms of immobilisation . . . 22
2.5 Conclusions and future research needs . . . 24

I Modelling **29**

3 Modelling of PFAS-surface interactions: Effect of surface charge and solution ions **33**
3.1 Introduction . . . 36
3.2 Materials and methods . . . 36
3.2.1 Monte Carlo simulations . . . 36

3.2.2 Intermolecular potential calculations . . . 37
3.2.3 Short-range electrostatic interactions . . . 37
3.2.4 van der Waals interaction . . . 37
3.2.5 Long-range electrostatic interactions . . . 37
3.2.6 Implementation and computation . . . 38
3.3 Results and discussion . . . 38
3.3.1 Neutral surface and molecules . . . 38
3.3.2 Positively charged surfaces . . . 39
3.3.3 Negatively charged surfaces . . . 39
3.3.4 Surfaces with mixed charge . . . 40
3.3.5 Relative contributions of van der Waals and Coulomb potentials . 40
3.4 Conclusions and outlook . . . 40

4 R-MCMolecSim: Original R-based software and extended numerical methods for Monte Carlo molecular simulations incorporating long-range interactions 45
4.1 Introduction . . . 45
4.2 Setup and initialisation . . . 47
4.2.1 Simulation box set up and periodic boundary conditions . . . 47
4.2.2 Input parameters and other simulation features . . . 47
4.2.3 Simulation initialisation . . . 50
4.3 Calculations . . . 51
4.3.1 Atom-atom potentials . . . 52
4.3.2 Electrostatic interaction . . . 52
4.3.3 Lennard-Jones potential . . . 52
4.3.4 Long-range electrostatic interactions . . . 53
4.4 Monte Carlo simulation . . . 56
4.4.1 Rotations and translations . . . 56
4.4.2 Long-range force implementation . . . 57
4.4.3 Change in potential calculation . . . 57
4.5 Analysis . . . 58
4.5.1 Single simulation run statistics . . . 58
4.5.2 Density calculations and plots . . . 59
4.5.3 Long-range force plots . . . 61
4.6 Conclusions and future work . . . 61

II Environmental investigations 65

5 Perfluoroalkyl, fluorotelomer sulfonate, and perfluorooctane sulfonamide contamination in biosolids: Composition, co-contamination and re-use implications 69
5.1 Introduction . . . 71
5.2 Material and methods . . . 72
5.2.1 Biosolid samples and characterisation . . . 72
5.2.2 PFAS extraction and analysis . . . 72
5.2.3 Total oxidisable precursor assay . . . 72
5.2.4 QA/QC . . . 72

5.2.5 Statistical analysis . . . 73
5.3 Results and discussion . . . 73
5.3.1 Total PFAS concentrations . . . 73
5.3.2 PFAS composition . . . 74
5.3.3 Historical biosolid stockpiles . . . 74
5.3.4 Relationships between PFAS and biosolid characteristics . . . 75
5.3.5 Precursors and transformation . . . 76
5.3.6 Biosolid contamination guidelines . . . 76
5.4 Conclusions . . . 76

6 Composition and transformation of PFAS contamination profiles in AFFF impacted soils and leachates 81
6.1 Introduction . . . 81
6.2 Materials and methods . . . 83
6.2.1 Soil sampling and preparation . . . 83
6.2.2 Chemical analysis . . . 83
6.2.3 Leaching procedure . . . 84
6.2.4 Statistical analysis . . . 85
6.3 Results . . . 85
6.3.1 PFAS concentrations in field collected soil samples . . . 85
6.3.2 PFAS concentrations and temporal changes in Angus Fire impacted soil . . . 88
6.3.3 Correlations . . . 90
6.3.4 PFAS concentration in soil post-TOP assay . . . 92
6.3.5 Relationships between samples . . . 94
6.3.6 PFAS concentrations in leachate . . . 98
6.3.7 Soil-leachate comparison . . . 101
6.3.8 PFAS concentration in leachate post-TOP assay . . . 103
6.4 Conclusions and future work . . . 105

7 Measurement and prediction of PFAS immobilisation in AFFF-contaminated soils with RemBind® formulations 107
7.1 Introduction . . . 107
7.2 Materials and Methods . . . 109
7.2.1 Soil sampling, preparation and immobilisation . . . 109
7.2.2 PFAS leachability, analysis and QA/QC . . . 110
7.2.3 Statistical analysis and model fitting . . . 111
7.3 Results and Discussion . . . 111
7.3.1 PFAS concentration in soil pre-amendment . . . 111
7.3.2 PFAS leaching in soil pre-amendment . . . 114
7.3.3 Soil-leachate comparison prior to amendment . . . 116
7.3.4 Leachates after amendment: amendment efficacy . . . 119
7.3.5 Modelling PFAS immobilisation . . . 122
7.4 Conclusions and future work . . . 128

8 Conclusions and future work **131**
8.1 Conclusions . . . 131
8.1.1 Limitations . . . 134
8.2 Future Work . . . 134
8.2.1 Short-term . . . 135
8.2.2 Medium-term . . . 135
8.2.3 Long-term . . . 136

Bibliography **137**

Appendices **147**

A Supplementary information: Modelling of PFAS-surface interactions: Effect of surface charge and solution ions **149**

B Supplementary information: Perfluoroalkyl, fluorotelomer sulfonate, and perfluorooctane sulfonamide contamination in biosolids: Composition, co-contamination and re-use implications **169**
B.1 Chemicals and reagents . . . 170

C Supplementary information for Chapter 6 **177**

D Supplementary information for Chapter 7 **193**

E Monte Carlo simulation source code **217**
E.1 Monte Carlo simulation . . . 218
E.2 Long-range force calculation . . . 233
E.3 Monte Carlo simulation with long-range forces . . . 238
E.4 Analysis of initial output . . . 254
E.5 Analysis of output with long-range forces . . . 261
E.6 Long-range force visualisation . . . 266
E.7 Density plotting of multiple simulations . . . 268

F Documentation **273**
F.1 Authorship statements . . . 273
F.2 Publication reprinting permissions . . . 278
F.2.1 Elsevier permissions . . . 278
F.2.2 Springer Nature permissions . . . 278

List of Figures

1.1 Example structural formulas of selected PFAS obtained from Molview utilising data from Pubchem [1]: PFOS, PFOA and 8:2 Fluorotelomer sulfonic acid (8:2 FTS) where 8 designates the number of fluorinated and 2 the unfluorinated carbon atoms in the backbone. 2
1.2 Methods of possible interactions of PFAS and soil particles: Electrostatic and divalent cation bridging (with charged mineral surfaces), and hydrophobic (with organic matter) 4
1.3 Possible PFAS structural formations: Bilayers and micelles 5
1.4 Conceptual diagram of thesis 8

2.1 Composition of PFAS contamination from three locations 14
2.2 Comparison of PFCA immobilisation efficacy 19
2.3 Comparison of PFSA, FTS and FOSA immobilisation efficacy 20
2.4 Change in PFOA and PFOS leachability following treatment of soil with amendments 21
2.5 Assessment framework for the design, optimisation and validation of PFAS immobilisation efficacy and longevity 23

3.1 Structure of PFBS, PFOS 37
3.2 Inhomogeneous density distributions of PFAS molecules 39
3.3 Inhomogeneous density distributions of PFAS anions 40
3.4 PFOS anion simulation positions at 20,000 iterations 41
3.5 Inhomogeneous density distributions of PFAS anions 41
3.6 PFOS anion simulation positions at 20,000 iterations 42
3.7 Heat maps showing ion count during simulation 43

4.1 Structure of the R-MCMolecSim simulation code 46
4.2 Simulation box of dimensions $2b \times 2b \times 2b$ showing fixed surface atoms (grey), mobile PFOA anions (clusters of spheres), and mobile Ca^{2+} ions (single green spheres). Molecule colours are standard CPK colours. . . . 48
4.3 Structure of the combined R list object containing all the PFAS and ions, with each list item containing values for the 9 listed parameters 51
4.4 The structure of the eight half-quadrants around the simulation box (top view). The integration for the external field contribution, Eq 4.4, is performed over all space external to the shaded region. 54
4.5 Conceptual diagram of the replacement of the square based prism of half-width b by a circular cylinder of radius a of equal volume (top view) . . . 54

4.6 Plot of external potential contribution, v_{ext}, as a function of radial distance r. Shown are external potential for three values of z for a PFDA + Ca^{2+} system. 55
4.7 Example potential energy plot as a function of iteration number for a PFOA ion only system with a positive surface charge. 59
4.8 Snapshot of the simulation system in its final configuration for the case of PFOA with Ca^{2+} ions and a negative surface charge. 60
4.9 Plots of number density profiles as a function of distance from the surface. The results compared the distributions obtained from independent simulation of PFOA and PFDA both involving Ca^{2+} ions and a negative surface charge. 60
4.10 2D density plots for (a) PFDA and (b) H^+ on surface of mixed charge . . 62
4.11 Plots of ensemble-averaged charge density distributions as a function of distance z from the surface for a system comprising PFDA anions, Ca^{2+} ions and a negative surface charge. Shown are individual charge distributions and the net charge distribution. 63
4.12 Plots of external potential as a function of z experienced by a positive and negative unit charge respectively for the case of a system of PFDA anions, with Ca^{2+} counterions and a negative surface charge. 63

5.1 Concentration and composition of PFAS in biosolids from 12 Australian waster water treatment plants 73
5.2 Individual PFAS concentration in WWTP biosolid samples from aged WWTP3 biosolid stockpiles. 74
5.3 Correlation between PFAS and biosolid physico-chemical properties, ordered by hierarchical clustering 75
5.4 Mean change in post-oxidation PFAS concentration (mg kg-1) for WWTP2, 3 and 10. 77

6.1 PFAS soil concentrations ($\mu g\ kg^{-1}$) for (a) Σ_{28}PFAS, (b) PFSAs, (c) PFCAs, and (d) FTSs and FOSA. 86
6.2 Composition of PFAS in soils (a) pre- (original samples) and (b) post-TOP assay 87
6.3 Change in individual PFAS concentration ($\mu g\ kg^{-1}$) in P20 over time for (a) all PFAS, (b) excluding 6:2 and 8:2 FTS 89
6.4 Correlation plot of PFAS and elements present across soils with hierarchical clustering. The colour and size of each circle corresponds to the Pearson correlation co-efficient (shown in the right-hand side legend) and indicates if there is a positive or negative association between each pair of variables, and the strength of this. 91
6.5 PFAS concentration ($\mu g\ kg^{-1}$) in soils pre vs post- TOP assay (a) Σ_{28}PFAS (b) PFSAs (c) PFCAs (d) PFOA. A 1:1 relationship is detailed by a dotted line, while P20 soils are labelled in (a) and circled in (c) and (d). 93
6.6 PFAS plotted against the first two principal components. Variables are coloured by the magnitude of their contribution to the components. . . 95
6.7 Individual samples plotted against the first two principal components. Points are coloured by their representation quality. 96

6.8 Values of the coordinates for the contributions of each PFAS to each of the dimensions. 97
6.9 Scree plot showing percentage of variance in the data that is explained by each principal component 98
6.10 Composition of PFAS in (a) pre and (b) post TOP assay leachate. 100
6.11 PFAS concentration (μg L^{-1}) in leachate pre vs post- TOP assay (a) Σ_{28}PFAS (b) PFSAs (c) PFCAs (d) PFOA. A 1:1 relationship is detailed by a dotted line, while P20 soils are labelled in (a) and within a box in (c) and (d). 103

7.1 PFAS composition across soils Z2-Z4 and Z7-Z9 in the <2 mm soil particle size fraction. 113
7.2 PFAS composition across soils Z2-Z4, and Z7-Z9 following leaching using ASLP (AS4439) (1997). 116
7.3 PFAS immobilisation efficacy at application rates of 1%, 2.5%, 5% and 10% w/w as a function of soil and PFAS for (a) RB100 and (b) RB300. Applications shown in different shades, while soils are depicted as different shapes. 120
7.4 PFOA experimental leachate concentrations (points) and fitted models (coloured lines) for soils Z2, Z3 and Z9 and amendments RB100 and RB300. Horizontal lines show leachate guideline values of 0.56 (unlined; solid), 5.6 (single composite lined; dashed) and 56 μg L^{-1} (double composite lined; dotted). 123
7.5 PFOS + PFHxS experimental leachate concentration (points) and fitted model (coloured lines) for soils Z2, Z3 and Z9 following amendment with (a) RB100 and (b) RB300. Horizontal lines show leachate guideline values of 0.07 (unlined; solid), 0.7 (single composite lined; dashed) and 7 μg L^{-1} (double composite lined; dotted). 124

A.1 PFOS simulation run with ±10% OPLSAA parameter values 152
A.2 PFOS simulation runs with different random starting configurations . . . 152
A.3 Potential energy at teach step of simulation 153
A.4 Net charge as a function of z, external potential as a function of z, external potential over charge as a function of r (multiple figures) 154
A.5 PFBS and PFOS simulation positions at 20,000 iterations (multiple figures) 162

B.1 Correlation between PFAS and biosolid physico-chemical properties . . . 172

C.1 PFAS leachability vs fluorinated carbon chain length. Points shown at zero had detectable PFAS concentrations in the soil but not in the leachate. 186
C.2 PFAS leachability vs initial concentration (a) all soils (b) soils with lower initial concentrations. Points shown at zero had detectable PFAS concentrations in the soil but not in the leachate. Higher (> 150%) leachability values are observed at lower concentrations, which may be reflective of variability in concentrations closer to the limits of quantification along with impacts of adjustments for dilution factors. 187

D.1 Heat map of PFAS concentrations across soils Z2-Z4 and Z7-Z9 in the <2 mm soil fraction, normalised per PFAS. Colour scale indicates row-normalised concentration Z-score. 195
D.2 Heat map of PFAS concentrations across soils Z2-Z4, and Z7-Z9 in leachable fraction, normalised per PFAS. Colour scale indicates row-normalised concentration Z-score. 196
D.3 Leachable PFAS reduction (µg L^{-1}) in (a) Z2 (b) Z3 (c) Z4 (d) Z7 and (e) Z9 soil amended with RB100. Points indicate experimental data, connecting lines for visualisation purposes only. 201
D.4 Leachable PFAS reduction (µg L^{-1}) in (a) Z2 (b) Z3 (c) Z4 (d) Z7 and (e) Z9 soil amended with RB300. Points indicate experimental data, connecting lines for visualisation purposes only. 202
D.5 PFAS concentration in leachable fraction following immobilisation with RB 100: (a) Z2, (b) Z3, (c) Z4, (d) Z7, (e) Z9. Points indicate experimental data and coloured lines the fitted model. 203
D.6 PFAS concentration in leachable fraction following immobilisation with RemBind 300: (a) Z2, (b) Z3, (c) Z4, (d) Z7, (e) Z9. Points indicate experimental data and coloured lines the fitted model. 204
D.7 Fitted exponentials by PFAS family: Short chain PFCAs. Points indicate experimental data. 205
D.8 Fitted exponentials by PFAS family: Medium chain PFCAs. Points indicate experimental data. 206
D.9 Fitted exponentials by PFAS family: Long chain PFCAs. Points indicate experimental data. 207
D.10 Fitted exponentials by PFAS family: Short chain PFSAs. Points indicate experimental data. 208
D.11 Fitted exponentials by PFAS: PFHxS. Points indicate experimental data. 209
D.12 Fitted exponentials by PFAS: PFHpS. Points indicate experimental data. 210
D.13 Fitted exponentials by PFAS: PFOS. Points indicate experimental data. . 211
D.14 Fitted exponentials by PFAS family: Long chain PFSAs. Points indicate experimental data. 212
D.15 Fitted exponentials by PFAS family: FOSAMs. Points indicate experimental data. 212
D.16 Fitted exponentials by PFAS family: FTSAs. Points indicate experimental data. 213
D.17 Fitted exponentials: PFOS+PFHxS. Points indicate experimental data. . 214

List of Tables

2.1 Laboratory and field-based immobilisation studies detailing the impact of soil amendment on PFAS leachability 16

3.1 Details of the system setup for the 12 different simulation scenarios . . . 38

4.1 Variable input parameters 49
4.2 Example structure of primary molecule input file format, for PFOA . . . 49
4.3 Simulation output variables 58

6.1 Dilution factor adjusted leachate concentrations as a percentage of soil concentrations (%, 3.s.f.). * denotes detection in leachate but not soil, 0 detection in soil but not leachate, and blank - detection in neither sample. 102

7.1 Mean soil PFAS concentrations in AFFF-impacted soil prior to immobilisation (μg kg^{-1}, 3 s.f.). MeFOSA, MeFOSE, EtFOSA, EtFOSE, 4:2 FTS and PFTeDA were <LOR for all soils. Replicate measure varied for concentrations greater than the LOR by an average of ±12%. 112
7.2 Local guideline values for garden soil, ecological and public land, residential soil and industrial land [2] and soils failing these at initial concentration measurements. 114
7.3 Mean leachate PFAS concentrations prior to immobilisation (μg L^{-1}, 3 s.f.). MeFOSA, MeFOSE, EtFOSA, EtFOSE, 4:2 FTS, 10:2 FTS, PFTrDA and PFTeDA were <LOR for all leachates. Replicate measure varied for concentrations greater than the LOR by an average of ±15%. . 115
7.4 Suitability of unamended soils for landfill disposal based on landfill acceptance criteria [2] including leachable concentration (Guideline 1) and soil concentration (Guideline 2). 117
7.5 Dilution adjusted leachate concentrations as a percentage of soil concentrations (%, max 3 s.f.). Cells marked with * denote the PFAS was detected in leachate but not in soil, 0 denotes detected in soil but not in leachate, and blank indicates detection in neither sample. 118
7.6 Σ_{28}PFAS immobilisation efficacy (%) of RB100, RB300 and relative efficacy of RB100 vs RB300 as a function of application rate (w/w %) and soil. 10% application rate was not applied to Z7 soil due to low initial PFAS concentrations. 121
7.7 Fitted exponential model parameters a and r (3 s.f.) for PFAS immobilisation using RB100 and RB300. 125

7.8 Table of percentage required to get below leachable concentration guideline values for disposal in double composite lined (Double CL), clay/single composite lined (Clay SL) and unlined landfills. Cells marked with * were not fitted using the exponential model, as the minimum required data points were unavailable due to concentrations <LOR. 127

A.1 3D structure, Lennard jones parameters, partial charges for PFBS anion 151
A.2 3D structure, Lennard jones parameters, partial charges for PFOS anion 151

B.1 PFAS analysed in this study, abbreviations used and limits of reporting . 171
B.2 WWTP details 172
B.3 Individual and total PFAS concentrations 173
B.4 Correlation coefficients between PFAS concentrations and physico-chemical properties 174
B.5 Correlation coefficients between PFAS concentrations 175
B.6 Correlation coefficients between physico-chemical properties 176

C.1 PFAS compounds fell into the broad groups of perfluoroalkyl sulfonic acids (PFSAs), perfluoroalkyl carboxylic acids (PFCAs), perfluorooctane sulfonamide-based substances (FOSAMs) and fluorotelomer sulfonic acids (FTSAs). 178
C.2 Surrogate recovery and oxidation efficiency values for pre- and post-TOP assay analyses of P1-P13 and P20 soils. 179
C.3 PFAS concentrations in P1-P13 soils (μg kg^{-1}, max 3 significant figures, s.f.) and % of Σ_{28}PFAS (max 2 s.f.). 180
C.4 PFAS concentrations in P20 soil (μg kg^{-1}, max 3 s.f.) and % of Σ_{28}PFAS (max 2 s.f.). 181
C.5 Differences in PFAS concentrations in P1-P13 soils pre vs post- TOP assay (μg kg^{-1}, 3 s.f.), and percentage change (%, 3 s.f.), which is blank when the PFAS was not detected in the original sample. 182
C.6 Differences in PFAS concentrations in P20 soil pre vs post- TOP assay (μg kg^{-1}, 3 s.f.), and percentage change (%, 3 s.f.), which is blank when the PFAS was not detected in the original sample. 183
C.7 PFAS concentrations in P1-P13 leachates (μg L^{-1}, max 3 s.f.) and % of Σ_{28}PFAS (max 2 s.f.). 184
C.8 PFAS concentrations in P20 leachates (μg L^{-1}, max 3 s.f.) and % of Σ_{28}PFAS (max 2 s.f.). 185
C.9 Suitability of soils for landfill disposal based on landfill acceptance criteria [2] including leachable concentration (Guideline 1) and soil concentration (Guideline 2). 186
C.10 PFAS concentrations in P1-13 post-TOPA leachates (μg L^{-1}, max 3 s.f.) and % of Σ_{28}PFAS (max 2 s.f.). 188
C.11 PFAS concentrations in P20 post-TOPA leachates (μg L^{-1}, max 3 s.f.) and % of Σ_{28}PFAS (max 2 s.f.). 189
C.12 Changes in PFAS concentrations in leachate with application of the TOP assay. First row is raw difference in concentration (μg L^{-1}, max 3 s.f.), alternate rows are percentage change (%, max 3 s.f.). * denotes the PFAS was not present in the initial sample, blank that the PFAS was not present in either sample. 190

C.13 Changes in PFAS concentrations in leachate with application of the TOP assay for P20 samples. 191

D.1 PFAS level of reporting (LOR) for liquid and solid matrices, grouped into perfluoroalkyl sulfonic acids (PFSAs), perfluoroalkyl carboxylic acids (PFCAs), perfluorooctane sulfonamide-based substances (FOSAMs) and fluorotelomer sulfonic acids (FTSAs). 194
D.2 RB100 PFAS immobilisation efficacy at an application of 1% w/w. Where leachate values were <LOR, an immobilisation range was calculated using leachate values of 0 and LOR. 197
D.3 RB300 PFAS immobilisation efficacy at an application of 1% w/w. . . . 197
D.4 RB100 PFAS immobilisation efficacy at an application of 2.5% w/w. . . . 198
D.5 RB300 PFAS immobilisation efficacy at an application of 2.5% w/w. . . . 198
D.6 RB100 PFAS immobilisation efficacy at an application of 5% w/w. 199
D.7 RB300 PFAS immobilisation efficacy at an application of 5% w/w. 199
D.8 RB100 PFAS immobilisation efficacy at an application of 10% w/w. . . . 200
D.9 RB300 PFAS immobilisation efficacy at an application of 10% w/w. . . . 200
D.10 Residual sum of squares (RSS), total sum of squares (TSS) and R^2 values for RB100 fitted models. 215
D.11 Residual sum of squares (RSS), total sum of squares (TSS) and R^2 values for RB300 fitted models. 216

Glossary and abbreviations

4:2 FTS	4:2 Fluorotelomer sulfonate
6:2 FTS	6:2 Fluorotelomer sulfonate
6:2 FTAB	6:2 Fluorotelomer sulfonamidoalkyl betaine
8:2 FTOH	8:2 Fluorotelomer alcohol
8:2 FTS	8:2 Fluorotelomer sulfonate
10:2 FTS	10:2 Fluorotelomer sulfonate
Å	Angstrom
AC	Activated carbon
ADONA	Ammonium 4,8-dioxa-3H-perfluorononanoate
AFFF	Aqueous film forming foam
APFO	Ammonium perfluorooctanoate
ASLP	Australian standard leaching procedure
BAF	Bioaccumulation factor
C	Coulombs
CB	Cement binder
Cl-PFESA	Chlorinated polyfluorinated ether sulfonate
CNT	Carbon nanotubes
CSIRO	Commonwealth Scientific and Industrial Research Organisation
DEP	Department of environmental protection
DI	Deionised
DMOA	Perfluorinated dimethyloctanoic acid
ECF	Electrochemical fluorination
EtFOSA	N-ethyl perfluorooctane sulfonamide
EtFOSAA	N-ethyl perfluorooctane sulfonamido acetic acid
EtFOSE	N-ethyl perfluorooctane sulfonamido ethanol
eV	Electron volts
FOSAMs	Perfluorooctane sulfonamides
FOSAA	Perfluorooctane sulfonamido acetic acid
FHxSA	Perfluorohexane sulfonamide
FOSA, PFOSA	Perfluorooctane sulfonamide
FT	Fluorotelomer
FTOH	Fluorotelomer alcohol
FTCA	Fluorotelomer carboxylic acid
FTS	Fluorotelomer sulfonate
FTSA	Fluorotelomer sulfonic acid
FtTAoS	Fluorotelomer thioether amido sulfonate
GAC	Granular activated carbon
GAF	Grass accumulation factor

GenX	Ammonium 2,3,3,3-tetrafluoro-2-(heptafluoropropoxy) propanoate
HPFHpA	7H-Perfluoroheptanoic acid
IMS-MS	Ion Mobility Spectrometry-Mass Spectrometry
K_d	Partitioning coefficient
K_{oc}	Organic carbon partitioning coefficient
K_{ow}	Octanol-Water partitioning coefficient
LC-IMS-MS	Liquid Chromatography-Ion Mobility Spectrometry-Mass Spectrometry
LC-MS-MS	Liquid Chromatography-Mass Spectrometry-Mass Spectrometry
LEAF	Leaching environmental assessment framework
LJ	Lennard-Jones
LOAEL	Lowest observable adverse effect level
LOD	Limit of detection
LOQ	Limit of quantification
LOR	Limit of reporting
MC	Monte Carlo
MeFOSA	N-methyl perfluorooctane sulfonamide
MeFOSAA	N-methyl perfluorooctane sulfonamido acetic acid
MeFOSE	N-methyl perfluorooctane sulfonamido ethanol
MOA	Mode of action
MWCNT	Multi-walled carbon nanotubes
NAPL	Non-aqueous phase liquids
NATA	National association of testing authorities
NEMP	National environmental management plan
OC	Organic carbon
PAC	Powdered activated carbon
PCA	Principal component analysis
PELMO	Pesticide leaching model
PFAS	Per- and poly-fluoroalkyl substances
PFBA	Perlfuorobutanoic acid
PFBS	Perfluorobutane sulfonic acid
PFCAs	Perfluoroalkyl carboxylic acids
PFDA	Perfluorodecanoic acid
PFDoA, PFDoDA	Perfluorododecanoic acid
PFDoS	Perfluorododecane sulfonic acid
PFDS	Perfluorodecane sulfonic acid
PFHpA	Perfluoroheptanoic acid
PFHpS	Perfluoroheptane sulfonic acid
PFHxA	Perfluorohexanoic acid
PFHxS	Perfluorohexane sulfonic acid
PFHxSAm	Perfluorohexane sulfonamide amine
PFNA	Perfluorononanoic acid
PFNS	Perfluorononane sulfonic acid
PFOA	Perfluorooctanoic acid
PFOS	Perfluorooctane sulfonic acid
PFOSA, FOSA	Perfluorooctane sulfonamide
PFOSF	Perfluorooctane sulfonyl fluoride
PFPrA	Perfluoropropanoic acid

PFPrS	Perfluoropropane sulfonic acid
PFSAs	Perfluoroalkyl sulfonic acids
PFTeDA	Perfluorotetradecanoic acid
PFTrDA	Perfluorotridecanoic acid
PFUnDA	Perfluoroundecanoic acid
PolyDADMAC	Polydiallyldimethylammonium chloride
QA	Quality assurance
QC	Quality control
QTOF-MS	Quadrupole time of flight mass spectrometry
RB	RemBind®
RB+	RemBind Plus®
RB100	RemBind® 100
RB100X	RemBind® 100X
RB300	RemBind® 300
SPLP	Synthetic precipitation leaching procedure
TCLP	Toxicity characteristic leaching procedure
TFA(A)	Trifluoroacetic acid
TFSA	Trifluoromethanesulfonic acid
TOC	Total organic carbon
TOP	Total oxidisable precursor
TOPA	Total oxidisable precursor assay
UPLC	Ultraperformance liquid chromatography
USEPA	United States Environmental Protection Agency
WWTP	Waste-water treatment plant

Summary

Per- and polyfluoroalkyl substances (PFAS) are a class of persistent, toxic and bioaccumulative contaminants of growing global concern. Historically, research has predominantly focused on experimental work pertaining to a small number of well-known PFAS, however thousands of different PFAS exist and their behaviour varies widely. Sorption of PFAS to surfaces plays an important role in both PFAS prevalence in the environment and efficacy of methods for harm reduction such as immobilisation in soils. It was proposed that investigating the role of factors such as carbon chain length, surface charge and solution ions across both theoretical and experimental data may contribute to the understanding, generalisation and ultimately prediction of sorption behaviour across different PFAS and environmental conditions. This thesis approached this in a multi-pronged way, with a literature review, theoretical modelling and analysis of experimental data. An important focus was on the role that modelling and theory can play in the understanding and interpretation of observed PFAS concentrations, sorption and transformation behaviour, and these themes are carried across each part of this work.

Findings from the quantitative global review into the efficacy of soil amendments for PFAS immobilisation in soils, found activated carbon amendments to be best performing for a wide range of PFAS. Following from this, modelling work resulted in both a novel application of Monte Carlo molecular simulation to PFAS-surface interactions and creation of the R-MCMolecSim original software for performing such simulations in the R environment. The applied simulation studies examined the effect of PFAS size and charge, solution ions and surface charge on PFAS sorption and interactions with carbon surfaces. Findings highlighted the importance of surface charge and additional effects including divalent cation bridging and electrolytic screening.

Experimental data analysis investigated 28 PFAS with respect to their prevalence in contaminated soils and biosolids, and the effects of immobilisation amendments. Investigations across multiple soils and biosolids unearthed relationships between both PFAS, pH and other contaminants, between contamination source type and proximity, and contamination composition profiles. PFAS transformation was studied in samples by both ageing and application of the total oxidisable precursor assay, which additionally aided in estimation of PFAS precursor populations. Subsequent analysis and modelling of effectiveness of different formulations of a composite activated carbon based amendment, RemBind®, were then conducted across multiple contaminated soils. Both RemBind® 100 and 300 were shown to effectively immobilise PFAS across a range of soils.

The insights resulting from both theoretical and experimental data, linked by examination of observed and theoretical sorption behaviour, contributed to the growing body of knowledge necessary for effectively understanding and addressing environmental PFAS contamination.

Declarations

This thesis is submitted as a Thesis Containing Published Research in accordance with University of South Australia Policy AB-58 Research Degrees, Appendix AB-58 AD2: Content and Form of the Research Degree Thesis.

I declare that:
this thesis presents work carried out by myself and does not incorporate without acknowledgment any material previously submitted for a degree or diploma in any university; to the best of my knowledge it does not contain any materials previously published or written by another person except where due reference is made in the text; and all substantive contributions by others to the work presented, including jointly authored publications, is clearly acknowledged.

Signed:  date: 13/06/2025

Acknowledgments

I would like to thank the team of supervisors and co-authors that I have interacted with during my candidature: Professor Albert Juhasz, Professor Stanley Miklavcic, Dr Jackie Wright, Professor Christopher Chow and Associate Professor Craig Styan for their contributions to and feedback on both my thesis and included publications, my work has been improved by all of your comments and advice. I am indebted to technical staff at ALS Global Ltd, Envirolab Services Pty Ltd and the University of South Australia for sample preparation and chemical analyses across Chapters 5-7. I am appreciative of the University of South Australia for providing me with office accommodation and access to the High Performance Computing facility Tango 2.0 for Chapter 3 calculations. Finally, I acknowledge the financial support provided by an Australian Government Research Training Program Scholarship, which made this undertaking possible.

Author contributions

The authors for the published works were Julie Sleep (JAS), Albert Juhasz (ALJ) and Stanley Miklavcic (SJM). The author contributions to the published work contained within this these were as follows:

A review of immobilisation-based remediation of PFAS in soils, Current Pollution Reports

Task	JAS	ALJ
Conceptualisation	50	50
Formal Analysis	80	20
Visualisation	80	20
Writing - Original Draft	80	20
Writing - Review and Editing	60	40
Total %	70	30

Modelling of PFAS-Surface Interactions: Effect of Surface Charge and Solution Ions, Chemosphere

Task	JAS	SJM	ALJ
Conceptualisation	90	5	5
Methodology	80	15	5
Software	100	0	0
Formal Analysis	100	0	0
Visualisation	100	0	0
Writing - Original Draft	100	0	0
Writing - Review and Editing	50	45	5
Total %	89	9	2

Perfluoroalkyl, fluorotelomer sulfonate, and perfluorooctane sulfonamide contamination in biosolids: Composition, co-contamination and re-use implications, Environmental Pollution

Task	JAS	ALJ
Conceptualisation	0	100
Methodology	70	30
Formal Analysis	100	0
Visualisation	100	0
Writing - Original Draft	80	20
Writing - Review and Editing	60	40
Total %	68	32

Chapter 1

Introduction

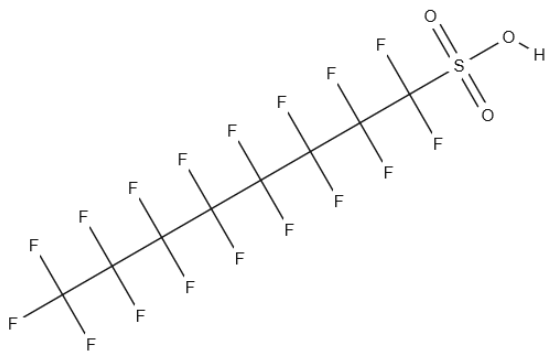
1.1 Background

Per- and poly-fluoroalkyl substances, more commonly referred to as PFAS, are man-made compounds utilised in a variety of industrial and consumer products such as aqueous film forming foams (AFFF), fabric treatments, and food packaging materials. Their usefulness stems from their unique physicochemical properties which include high surface activity, chemical and thermal stability and oil and water repellency. Although they have been considered useful chemicals, their persistence, toxicity and bioaccumulative nature have raised concerns regarding the presence of these compounds in the environment resulting in the listing of some PFAS[1] in the Stockholm convention [3, 4], prohibiting or restricting their use.

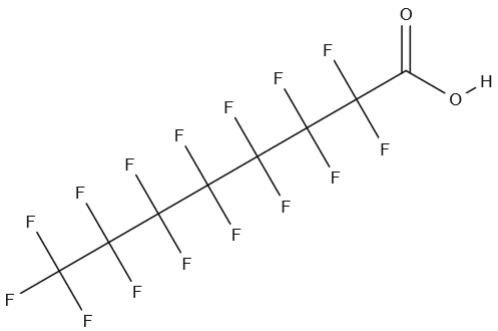
1.1.1 Molecular structure

Structurally, PFAS are based on a fully or partially fluorinated carbon backbone, along with a varying functional group. PFAS families are defined by their functional group, the most common being the perfluoroalkyl carboxylic acids (PFCAs), the perfluoroalkyl sulfonic acids (PFSAs) and the fluorotelomer sulfonic acids (FTSAs). Examples of these are shown in Figure 1.1. PFAS may also be categorised based on the length of their carbon chain backbone, resulting in the classifications of long-chain ($C \geq 8$), short chain ($4 \leq C \leq 7$) and ultra-short chain ($2 \leq C \leq 3$) PFAS [5]. Both the carbon chain lengths and the functional groups influence PFAS fate and toxicity in the environment [6]. It is the strength of the carbon-fluorine bonds within the molecules that makes these substances persistent (i.e. long-lived) in the environment. While there are over 8,000 substances containing at least one CF3 or CF2, it was shown by Buck et al. [7] that 256 of these

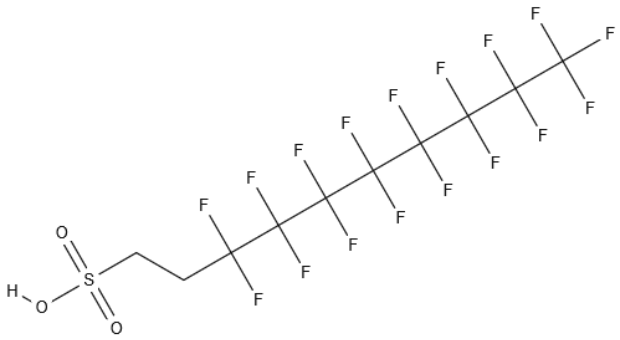
[1] Perfluorooctane sulfonic acid (PFOS), associated salts and perfluorooctane sulfonyl fluoride (PFOSF) were listed in Annex B, perfluorohexane sulfonic acid (PFHxS), perfluorooctanoic acid (PFOA), both their associated salts and related compounds were listed in Annex A.



PFOS



PFOA



8:2 Fluorotelomer sulfonic acid

Figure 1.1: Example structural formulas of selected PFAS obtained from Molview utilising data from Pubchem [1]: PFOS, PFOA and 8:2 Fluorotelomer sulfonic acid (8:2 FTS) where 8 designates the number of fluorinated and 2 the unfluorinated carbon atoms in the backbone.

are considered to be commercially relevant substances.

1.1.2 Toxicity

PFAS toxicological effects encompass a broad spectrum of potential impacts including hepatotoxicity, neurotoxicity, immunotoxicity and developmental toxicity and include the induction of tumours and disruption of the endocrine system [8]. Their toxicity varies according to factors such as physicochemical properties (carbon chain length and functional group), exposure variables (duration, dose and bioavailability), species and gender. It has been recently shown that adverse effects from PFAS exposure may be irreversible even without bioaccumulation [9]. More studies of the underlying molecular mechanisms behind PFAS toxicity are required for these effects to be fully understood [10, 11].

Between organisms, PFAS toxicity varies widely, with bees being one of the more sensitive species [12]. While a reasonable amount of toxicological data for the most common PFAS (e.g. PFOS and PFOA) is available for aquatic organisms, terrestrial wildlife data is still somewhat lacking [13]. Robust human toxicity data is also lacking, and further complicating this is the gap in understanding of modes of action (MOA) of both individual PFAS and PFAS mixtures [14]. Further complicating the issue of assessing PFAS toxicity, is that common replacements for PFOA and PFOS, such as Genx chemicals and PFBS, have been found in drinking and surface water and have been shown to have detrimental health effects in animal studies [15, 16]. These replacements, while not illegal, raise problems in that they add to the pool of chemicals that need to be assessed. Many replacement chemicals have subsequently been found to be either as toxic or more so than the chemicals they replace [17].

1.1.3 Prevalence

PFAS have emerged as ubiquitous environmental pollutants in both soil and water, being detected in remote locations worldwide from the Arctic [18] to the Antarctic [19]. Background environmental PFAS concentrations in areas distant from contamination zones were recently reviewed for North America [20] with average soil values ranging from 0.059-1.838 $\mu g\ kg^{-1}$ for PFOA and 0.018-1.956 $\mu g\ kg^{-1}$ for PFOS. Mean freshwater background concentrations ranged from 0.65-43.4 ng L^{-1} for PFOA and 0.6-46 ng L^{-1} for PFOS.

Elevated concentrations of PFAS may enter the environment as a consequence of chemical releases from sources such as fluorochemical plants [21], use of AFFF at fire-fighting training grounds and airports, reuse of biosolids from waste water treatment plants (WWTP) [22, 23], recycled water use [24] and via landfill leachates [25]. Soil and water PFAS concentrations arising from these sources vary widely (μg to g kg^{-1}) and are dependent on a variety of factors including source concentrations, PFAS mobility, distance from source zones, and frequency of use. For example, one study of soil-PFAS concentration near a fluorochemical manufacturing plant identified diminishing PFOS (56-7800 $\mu g\ kg^{-1}$) and PFOA concentrations (2-114 $\mu g\ kg^{-1}$) with increasing distance from the plant [21]. PFAS soil concentrations have also been found to vary in the vertical direction, between the top soil and deeper soil layers, with directionality depending on PFAS C chain length [26]. Similar gradients have also been detected in soil-water bodies [27]. The assessment of environmental PFAS concentrations in soils and biosolids is important for the determination of contamination exposure pathways for humans and wildlife. This may occur through direct contact or through transfer and accumulation from soil and water bodies, into plants and animals, at all trophic levels [28, 29].

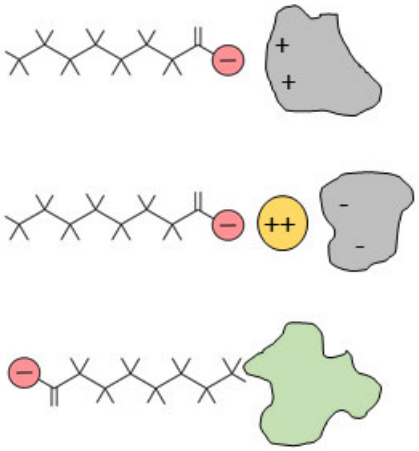


Figure 1.2: Methods of possible interactions of PFAS and soil particles: Electrostatic and divalent cation bridging (with charged mineral surfaces), and hydrophobic (with organic matter)

1.1.4 Sorption

At a fundamental level, PFAS distribution in the environment is determined by sorptive processes, a phenomenon which may be exploited in the design and implementation of strategies to immobilise PFAS in soil, as well as for the removal of compounds from water [30]. PFAS consist of a hydrophobic tail with multiple fluorine atoms, and a hydrophilic group. At environmental pH, the majority of commonly used PFAS such as those in the PFCA and PFSA families usually form anions. These anions interact with surfaces via electrostatic interactions either directly with positively charged surfaces or indirectly through forming bridges with divalent cations to interact with negatively charged surfaces [31], as depicted in Figure 1.2. Hydrophobic interactions, promoting micelle and bilayer formation, as depicted in Figure 1.3, may also be important [30, 32], while van der Waals interactions and H-bonding have been reported as allegedly insignificant [30, 31].

Both the functional group and the length of the carbon chain influence the extent of PFAS sorption. The former can be seen in the difference between the PFSA and PFCA families, with PFSAs more readily participating in sorption than PFCAs, noting that PFSAs are also more hydrophobic [30]. Increasing the C-F chain length of a PFAS molecule increases its hydrophobicity, which facilitates greater sorption when hydrophobic interactions are driving the sorption process [30]. Along with PFAS molecular properties, many soil properties affect PFAS sorption. Li et al. [31] observed that pH, organic carbon and clay content all played an important role. pH also plays a role in sorption capacity, with sorption generally decreasing with increasing pH [30]. However,

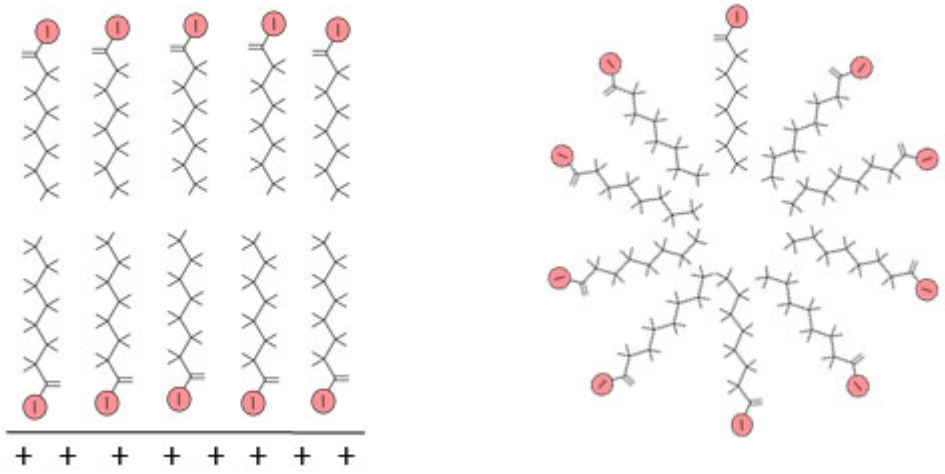


Figure 1.3: Possible PFAS structural formations: Bilayers and micelles

increasing pH can also create more basic sites for divalent cation bridging, thus sometimes contributing to an increase in sorption. Sorption kinetics can also be strongly influenced by the size of any pores and the diameter of the adsorbent particles [30]. As mentioned earlier, the presence of divalent cations in solution can result divalent cation bridging with anionic PFAS, which will, in turn, favour sorption. The understanding of PFAS sorption processes at the molecular level is in its early days. Unfortunately the high number of PFAS has impeded the experimental investigation of sorption of all molecules in every PFAS family, under a wide range of experimental conditions. This difficulty raises an important question of whether theoretical modelling may be able to assist.

1.2 Research aims

This thesis investigates the prevalence and behaviour of PFAS, spanning three main areas of research. These areas are modelling of PFAS-surface interactions, prevalence of PFAS in environmental soil and biosolid samples, and immobilisation of PFAS in soils. The research gaps and questions to be addressed are detailed below. The overarching question connecting these studies is how can the underlying mechanisms driving PFAS sorption help us to understand PFAS prevalence and behaviour in soils and biosolids, and aid with their subsequent immobilisation.

Soil amendments, with and without the use of binders, have emerged as an increasingly investigated method to immobilise PFAS in soils - a strategy to reduce exposure. The aim of the immobilisation review contained in this thesis, was to identify the best amendments among those in the wide range already studied to achieve this. The re-

search questions addressed included both what is the best performing amendment type, and the issues surrounding the quantitative comparison of effectiveness of different soil amendments under differing experimental conditions. Additionally it was of interest to investigate how immobilisation efficacy varies with PFAS carbon chain length and functional group in the combined study data. The question of how might a future, more comprehensive framework for assessing immobilisation efficacy appear was also of interest.

The outcomes of PFAS-soil interactions, such as sorption and leaching, play important roles in PFAS transport and toxicity. Previous studies have found these to be dependent upon soil properties including pH, organic material and particle size, as well as PFAS properties such as functional group and carbon chain length. Many laboratory and field-based measurements have been performed and continue to be conducted regularly, but associated modelling work has been performed less frequently, and generally limited to regression analyses against soil parameters or the fitting of kinetic equations for a single soil. The modelling presented within this thesis aimed to investigate, at a fundamental, molecular level, the theoretical interactions between PFAS and various surfaces . This required unique bespoke software development, involving highly complex calculations and the development of some components of the underlying theory. The modelling work sought to investigate the relative contributions of intermolecular van der Waals and electrostatic interactions to the overall system free energy. Of particular interest was examination of different scenarios encompassing positive, neutral, negative and mixed surface charges. The influence of H^+, OH^- and Ca^{2+} ions in solution was a second area of focus, as was the influence of carbon chain length. The latter consideration was investigated by including both C_4 (PFBS) and C_8 (PFOS) molecules in solution.

The majority of analytical studies undertaking measurement of PFAS concentrations focus on only one or two PFAS molecules, such as PFOS or PFOA. The analytical study conducted here aimed instead to investigate AFFF contaminated soil samples for a greater number of PFAS, beyond those few already regulated. Motivated by the role they play in laying as a pathway for the transport of PFAS, the study will also measure the extent of PFAS contamination (for the subset of 28 PFAS examined[2]) found in WWTP biosolids. The contamination composition was examined, along with temporal trends, and the relationships between PFAS concentrations, pH and other contaminants. For both soil and biosolid samples, an assessment against current local and global concentration guideline values was undertaken. Finally, the utility of the total oxidisable precursor (TOP) assay as a mechanism for determining potential future PFAS transformation and degradation was investigated.

[2]More extensive measurement of total PFAS contamination would be aided by non-target analyses and measurement of total organic fluorine.

As a final contribution to this thesis, a case study involving a composite activated carbon based amendment, Rembind® was undertaken with the aim of investigating the effectiveness of immobilisation across a large range of factors, such as different soil properties, application rates and Rembind® formulations. The research questions included how all these varied across different PFAS molecules, and how amendment efficacy could be modelled in order to calculate the application rate required to enable PFAS leachability to be below relevant guideline values.

1.3 Structure

The structure of the thesis consists of both published papers and unpublished chapters addressing a range of research topics related to PFAS immobilisation, PFAS prevalence in soils and biosolids, and modelling of PFAS surface sorption at the molecular level. These are interrelated by the underlying mechanisms of interactions between PFAS molecules and surfaces. The research in the thesis is structred into eight chapters, which are arranged as per Figure 1.4, and described below.

Chapter 1 consists of background information on the problem of PFAS contamination and information on several subtopics in support of the research contained in the rest of the thesis. This begins with an explanation of the structural properties of PFAS and their toxicity. Their prevalence in the environment is then discussed, along with the mechanisms of sorption that underpin each of the following chapters. Further, specific background information on modelling, biosolids and immobilisation are included at the beginnings of the respective chapters.

Chapter 2 contains a literature review entitled "A review of immobilisation-based remediation of PFAS in soils" as published in the journal *Current Pollution Reports*, 7, 524–539 (2021). This review of immobilisation amendments in soils contains an in-depth quantitative study of amendment effectiveness across a range of soils and PFAS molecules. Amendments examined include different forms of activated carbon, biochar, chitosan, minerals, clays, cement binders and their combinations. Immobilisation efficacy was calculated and compared across 18 different PFAS molecules, and the underlying mechanisms of immobilisation behind their differing effectiveness are discussed.

The main body of research following these two chapters is arranged into two parts: "Modelling" and "Environmental investigations". The first of these, **Part I** containing the modelling components of the thesis, comprises Chapters 3 and 4.

Chapter 3 applied Monte Carlo molecular modelling methodology to assess a suite of simulation scenarios involving interactions of PFBS and PFOS molecules with a carbon (graphite) surface. Simulations comprised varying combinations of solution ions (Ca^{2+}, OH^- and H^+) and surface charges. Density of molecules and solution ions in

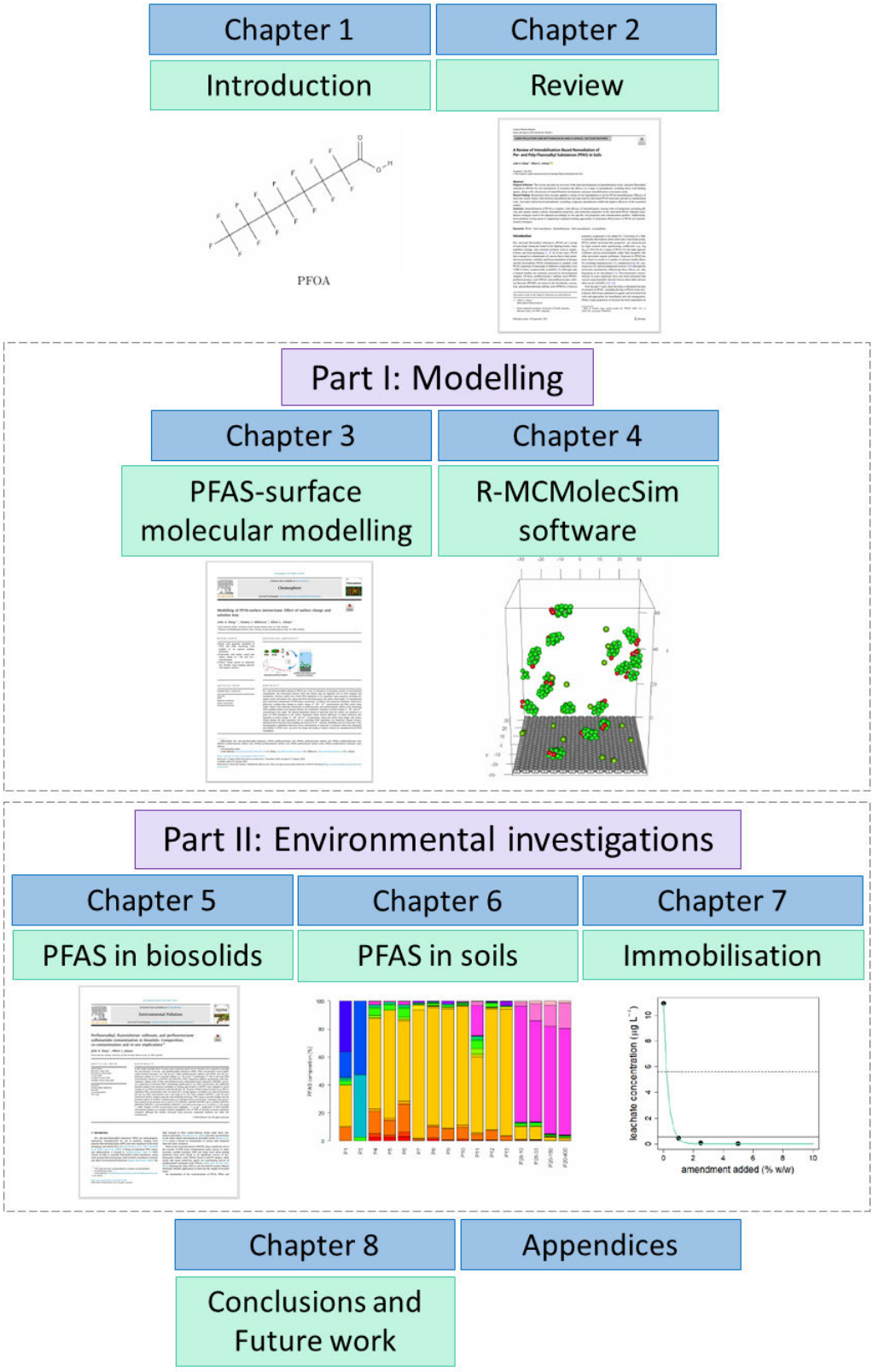


Figure 1.4: Conceptual diagram of thesis

relation to the surface during the simulation was measured and compared across scenarios. Relative contributions of van der Waals and Coulomb potentials were measured and possible sorption mechanisms across the different scenarios discussed. This chapter was published in the journal *Chemosphere*, as "Modelling of PFAS-surface interactions: Effect of Surface charge and solution ions", 319, 137910 (2023).

Chapter 4 sets forth the modelling methodology and R-MCMolecSim software written for the assessment of PFAS sorption to a model carbon surface. This was a series of programming scripts, written in the language R for performing molecular simulations based on the Monte Carlo method. R-MCMolecSim calculates the theoretical interactions between molecules and surfaces inside a simulation box containing a surface, an aqueous electrolyte solution and PFAS molecules. In this chapter we also describe the necessary van der Waals and electrostatic interactions, including long-range interaction potentials, and additional theory required to numerically evaluate the latter. Also described here are other simulation details such as the periodic boundary conditions applied to avoid edge effects, simulation box size, molecular structure, partial charge distributions, Lennard-Jones parameters, surface charges, and the concentrations and charges of solution ions.

Part II comprises environmental investigations on biosolids, soil and immobilisation, contained in Chapters 5, 6 and 7 respectively.

Chapter 5 presents the results of an investigation into biosolid samples from twelve Australian WWTPs, including historical biosolid stockpiles dating back to the pre-1970s. It includes investigations into the composition of PFAS contamination, discusses the relationship between PFAS concentrations, pH and other contaminants of concern, and compares concentrations to a range of guideline values. The TOP assay was applied to these samples in order to evaluate precursor populations and potential transformation. This chapter was published in the journal Environmental Pollution as "Perfluoroalkyl, fluorotelomer sulfonate, and perfluorooctane sulfonamide contamination in biosolids: Composition, co-contamination and re-use implications", Environmental Pollution, 266 (1), 115120 (2020).

Chapter 6 gives an account of an investigation into PFAS contamination of multiple soils historically impacted by PFAS-containing AFFF. A spiked AFFF soil, aged for varying periods of time was also included in the study. The composition of the contamination across 28 PFAS was examined in both soil and leachate samples. The TOP assay was also applied to compare pre- and post-TOP assay data to examine potential PFAS precursor concentrations and transformation. Correlations between PFAS and elemental concentrations were calculated and discussed.

Chapter 7 takes an in depth look at one class of immobilisation amendment identified in Chapter 2, exploring the concept of enhancing sorption as a risk management strategy for PFAS-contaminated soil. Several different formulations of the composite

activated-carbon based soil amendment, RemBind®, were applied across five AFFF contaminated soils, at a number of different application rates. PFAS leachate concentrations were examined and contrasted with soil concentrations. Post-immobilisation leachate concentrations were examined and compared to guideline values. The rate of application required to bring soils below guideline values for leachable PFAS was modelled, and this was performed for multiple soils of differing properties and initial contamination concentrations.

Chapter 8 comprises a discussion of conclusions spanning research addressed in each preceding chapter, and outlines areas of future research needs arising from the research undertaken.

These chapters are followed by the combined bibliography for the unpublished chapters and their respective appendices. Appendices A, B, C and D contain supplementary information for Chapters 3, 5, 6 and 7 respectively. Appendix E contains the key pieces of code used in Chapters 3 and 4, while Appendix F contains supporting administrative documents as per University requirements.

1.4 List of publications

A. Julie A. Sleep and Albert L. Juhasz, A review of immobilisation-based remediation of PFAS in soils, *Current Pollution Reports*, 7, p524-539 (2021). Accepted 1 July 2021; Available online on 28 September 2021.

B. Julie A. Sleep, Stanley J. Miklavcic, Albert L. Juhasz, Modelling of PFAS-surface interactions: Effect of Surface charge and solution ions, *Chemosphere*, 319, 137910, (2023). Received 17 August 2022; Received in revised form 1 December 2022; Accepted 17 January 2023; Available online 24 January 2023.

C. Julie A. Sleep and Albert L. Juhasz, Perfluoroalkyl, fluorotelomer sulfonate, and perfluorooctane sulfonamide contamination in biosolids: Composition, co-contamination and re-use implications, *Environmental Pollution* 266 (1), 115120 (2020). Accepted 26 June 2020; Received in revised form 17 June 2020; Available online 8 July 2020.

Chapter 2

A review of immobilisation-based remediation of per and poly-fluoroalkyl substances (PFAS) in soils

This chapter reviews immobilisation-based remediation strategies for reducing the leachability of per and poly-fluoroalkyl substances (PFAS) in soils. It provides a quantitative assessment of immobilisation methods and study results found across the published literature up to June 2021. The immobilisation amendments examined included activated carbon, biochar, clay and cement binder-based immobilisation agents, and combinations thereof. Methods were assessed according to reduction in leachability and immobilisation efficacy across eighteen different PFAS. Activated carbon (AC) based amendments, including composite AC-based amendments such as RemBind®, were observed to have the highest efficacies of those studied. This chapter was published in the journal, Current Pollution Reports[1] as "A review of immobilisation-based remediation of per and poly-fluoroalkyl substances (PFAS) in soils".

Since the publication of that review a number of additional immobilisation studies have been published. Biek et al. [33] applied RemBind at 0.5-5% application rates to a PFAS contaminated soil and measured both leachability and uptake into a grass species. Consistent with the results in our review on RemBind efficacy, they found both a significant reduction in leachability (88.7-99.8%) and a 5-12 fold reduction in plant uptake. Navarro et al. [34] performed a longer term study, finding that AC was an effective immobilisation agent over both the long and short term, while biochar based immobilisation was only effective in the short term. Wang et al. [35] also verified the effectiveness of activated carbon for reduction of PFAS leaching, but the higher effective-

[1]Reprinted courtesy of Springer, Current Pollution Reports (See Appendix F for license).

ness of organoclays in reduced toxicity to a soil nematode and an aquatic plant, results leading to the suggestion of a composite AC based clay amendment. A montmorillonite clay based amendment incorporating the nutrients choline and carnitine was studied by Hearon et al. [36], and it was reported that bioavailability was reduced by up to 74%, and PFAS residues were significant reduced in cucumbers. Esmaeilian et al. [37] found that compost had no impact on PFOS sorption, but that 0.1% w/w addition of activated carbon increased sorption by over 80%. They additionally modelled how effective this might be in the long term by simulation of leaching to groundwater caused by rainfall. These recent findings are consistent with the conclusions of the review that activated carbon based amendments are effective PFAS immobilisation agents.

Current Pollution Reports
https://doi.org/10.1007/s40726-021-00199-z

LAND POLLUTION (GM HETTIARACHCHI AND A JUHASZ, SECTION EDITORS)

A Review of Immobilisation-Based Remediation of Per- and Poly-Fluoroalkyl Substances (PFAS) in Soils

Julie A. Sleep[1] · Albert L. Juhasz[1]

Accepted: 1 July 2021
© The Author(s), under exclusive licence to Springer Nature Switzerland AG 2021

Abstract

Purpose of Review This review provides an overview of the latest developments in immobilisation of per- and poly-fluoroalkyl substances (PFAS) for soil remediation. It examines the efficacy of a range of amendments, including those with binding agents, along with a discussion of immobilisation mechanisms and post-immobilisation assessment needs.

Recent Findings Researchers have recently applied a variety of soil amendments to soil for PFAS immobilisation. Efficacy of these has varied widely, both between amendment and soil types and for individual PFAS molecules present in contaminated soils. Activated carbon based amendments, including composite amendments exhibit the highest efficacies of the examined studies.

Summary Immobilisation of PFAS is complex, with efficacy of immobilisation varying with soil properties including pH, clay and organic matter content, amendment properties, and molecular properties of the individual PFAS. Optimal remediation strategies need to be adjusted accordingly to site specific soil properties and contamination profiles. Additionally, bioavailability testing needs to supplement standard leaching approaches to determine effectiveness of PFAS soil immobilisation strategies.

Keywords PFAS · Soil remediation · Immobilisation · Soil amendments · Leachability

Introduction

Per- and poly-fluoroalkyl substances (PFAS) are a group of man-made chemicals found in fire-fighting foams, water repellent coatings, and consumer products such as carpets, textiles and food packaging [1, 2]. In recent years, PFAS have emerged as contaminants of concern due to their potential for persistence, mobility and bioaccumulation in humans and the environment. PFAS contamination is complex, with PFAS consisting of thousands of different compounds (over 3,000 of these commercially available) [3] although only a limited number are routinely assessed in environmental samples. Of these, perfluorooctan`e sulfonic acid (PFOS), perfluorooctanoic acid (PFOA) and perfluorooctane sulfonyl fluoride (PFOSF) are listed in the Stockholm convention, and perfluorohexane sulfonic acid (PFHxS) is listed as potential compounds to be added [4]. Consisting of a fully or partially fluorinated carbon chain and a functional group, PFAS exhibit surfactant-like properties, are characterised by high octanol-water partitioning coefficients (e.g. log K_{OW}=3.94-6.56 for a range of PFAS [5]) but high aqueous solubility and are proteinophilic rather than lipophilic like other persistent organic pollutants. Exposure to PFAS has been shown to result in a number of adverse health effects [6] including hepatotoxicity [7], immunotoxicity [8], neurotoxicity [9], and developmental toxicity [10] although the molecular mechanisms influencing these effects are only beginning to be elucidated [11]. Environmental concentrations in some organisms have also been measured that exceed experimentally derived lowest observable adverse effect levels (LOAEL) [12, 13].

Over the past 5 years, there has been a substantial increase in research on PFAS[1], including the fate of PFAS in the environment, their bioaccumulation in aquatic and terrestrial food webs and approaches for remediation and risk management. While a large proportion of research has been undertaken on

This article is part of the Topical Collection on *Land Pollution*

✉ Albert L. Juhasz
albert.juhasz@unisa.edu.au

[1] Future Industries Institute, University of South Australia, Mawson Lakes, SA 5095, Australia

[1] Web of Science topic search results for "PFAS" 2016: 141, vs 2020: 561, accessed 15/06/2021.

Published online: 28 September 2021

PFAS impacted water, and associated technologies for its removal, less information is available on strategies for the treatment of contaminated soil. PFAS contamination of soil is prevalent at fluorochemical manufacturing sites [14], fire-fighting training grounds [15], landfill sites [16], airports and air-force bases [17] along with sites where PFAS contaminated biosolids [18], wastewater [19] or recycled water [20] have been utilised. Given the number of possible per and poly-fluoroalkyl congeners in commercial products, PFAS contamination from different sources may vary widely in terms of concentration and composition. For example, Brusseau et al. [21] determined that the median background concentration of

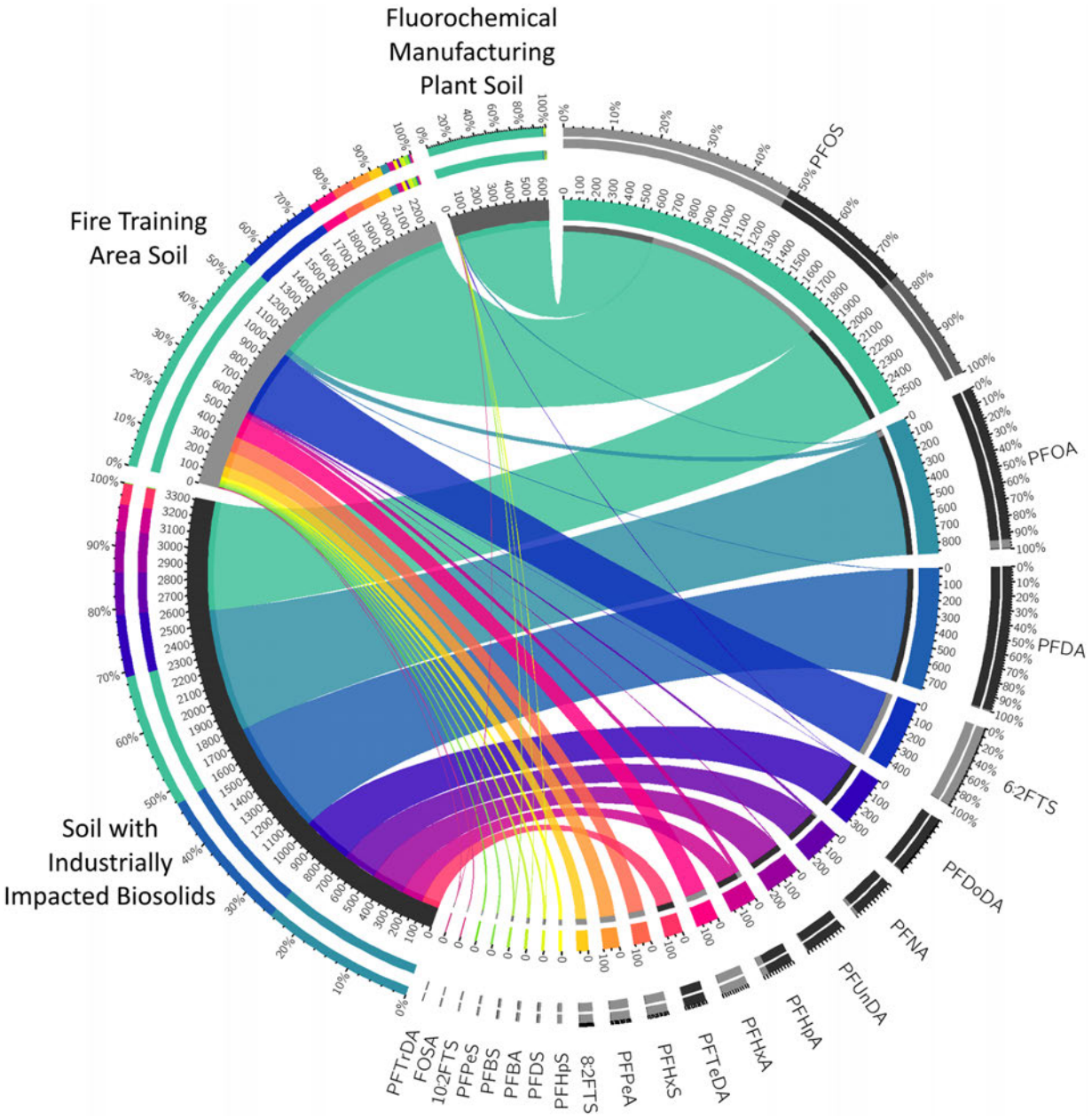


Fig. 1 Composition of PFAS contamination from three locations; soil from an AFFF fire-fighting training ground, a soil with industrially impacted biosolids [22], and a soil from a fluorochemical manufacturing plant [14]. On the right hand side of the circle, moving clockwise, individual PFAS are shown ordered by decreasing concentration (μg kg^{-1}). This is followed by location type, ordered by decreasing total PFAS concentration. The size of the link connecting an individual PFAS with a location type represents the concentration, sized according to the inner numbered scale (μg kg^{-1})

PFOS and PFOA in soil from a large range of international sites where neither primary nor secondary PFAS contamination occurred, was 2.7 μg kg^{-1} compared to up to 460 g kg^{-1} (PFOS) and 11 g kg^{-1} (PFOA) at contaminated sites. PFAS congeners in contaminated soil may vary considerably, as depicted in Fig. 1 where three example PFAS contamination profiles representing impacts from fluorochemical manufacturing, the use of aqueous film-forming foam (AFFF) at fire-fighting training grounds and biosolid amended soil are shown. PFAS profiles may range from being dominated by a single compound (e.g., perfluorooctane sulfonic acid, PFOS) in impacted soil from a manufacturing plant [14] to having a wide range of congeners present. A soil from a fire-fighting training area contained significant proportions of both PFOS and 6:2 fluorotelomer sulfonic acid (6:2 FTS), along with smaller amounts of perfluorohexanoic acid (PFHxA) and PFHxS among others. Due to wastewater treatment plants (WWTPs) having PFAS inputs from multiple sources, biosolids and biosolid-amended soil [22] may contain a range of PFAS often dominated by long-chain PFAS ($\geq C_7$) due to their preferential retention (in biosolids) during wastewater processing [23].

Irrespective of the activity leading to soil contamination, potential adverse environmental health effects associated with PFAS exposure has necessitated the development and application of remediation technologies. However, due to the unique physicochemical properties of PFAS, some traditional remediation strategies are ineffective for PFAS remediation. In particular, the strength of the C-F bond limits the application of chemical oxidation and bioremediation strategies and in some cases, oxidation of poly-fluoroalkyl and/or precursor compounds may increase the concentration of recalcitrant perfluorinated carboxylic acids (PFCAs) [24]. Soil washing results in secondary liquid waste that requires additional treatment, while phytoremediation is slow, treatment zones are dependent on plant root depth, and uptake may be limited by mass transfer effects. While thermal treatment technologies, such as incineration with excess oxygen, gasification and pyrolysis have the potential to destroy PFAS by breaking C-F bonds, temperatures in excess of 1000 °C are required to minimise the production of greenhouse gases [25, 26].

Immobilisation techniques, whilst not removing PFAS from the soil matrix, offer a risk management strategy through a reduction in leachability and/or bioavailability. The effectiveness of immobilisation strategies is influenced by a wide variety of parameters, including soil and amendment properties in addition to PFAS profiles in contaminated soil. While recent PFAS remediation reviews have provided a synopsis of the application of established technologies for PFAS contaminated soil and sediment [27–31] or focused on emerging treatment strategies [32], this paper provides a comprehensive overview of soil-based PFAS immobilisation approaches including amendment properties, treatment efficacy, immobilisation mechanisms, existing data gaps and future research priorities.

Immobilisation

Immobilisation is a strategy which reduces the mobility and bioavailability of contaminants through the addition of 'sorptive' soil amendments, thereby reducing exposure for human and ecological receptors. Amendments may be applied either in situ or ex situ and used with or without additional binding agents (e.g. Portland cement). Soil amendments offer the advantage of ease of application, cost-effectiveness and commercial viability, however, selecting suitable amendments that exhibit high sorptive capacity is critical for delivering sustainable immobilisation approaches. While immobilisation strategies are well developed for many legacy contaminants (e.g. metal(loid)s, PAHs), amendments and immobilisation approaches for PFAS have only recently gained research, development and commercial attention. Table 1 provides details of amendments that have been applied for PFAS immobilisation including activated carbon, biochar, clay, polymer and composite sorptive phases. A comparison of physicochemical properties which influence PFAS sorptive capacity and immobilisation efficacy, which in many cases, may be manipulated during amendment development; along with advantages and disadvantages of each amendment type are discussed in detail in the following sections.

Activated Carbon-Based Amendments

Activated carbon is a commonly used sorbent for the removal of contaminants from (waste)water due to its high surface area, high pore volume and surface functional groups. This sorbent has also been applied to contaminated soil for the immobilisation of a variety of organic and inorganic compounds including PFAS [43, 45, 46]. Activated carbon's effectiveness for PFAS sorption is due its high surface area, size and number of pores. However, physicochemical properties and sorptive potential of activated carbon varies depending on the carbon source and temperature used for its production [47]. These parameters influence porosity, surface area and surface functional groups whereby increased production temperature decreases surface functional groups, and in doing so, increases surface charge [47]. Activated carbon has the ability to form both electrostatic and hydrophobic interactions with PFAS, and possibly hemi-micelle and micelle formation in pores [48]. Charge-assisted hydrogen bonding was also suggested from experimental spectroscopy of PFAS interacting with functional groups on the surface of activated carbon [49].

Table 1 Laboratory and field-based immobilisation studies detailing the impact of soil amendment on PFAS leachability

Amendment category	Amendment type(s)	Technique	Application rate (w/w)	Ageing period	Soil properties	Initial soil conc. ($\mu g\ kg^{-1}$)	PFAS tested	Leaching method/details	Author, year and reference
Activated carbon	CB + GAC	Stabilisation and solidification	15% CB, 0.2% GAC	12 months	AFFF contaminated (sand 30%, clay 42%, silt 28% pH 8.6, OC 6%)	Not stated	C_{5-8} PFCAs, $C_{4,6,8}$ PFSAs, 6:2 FTS, PFOSA, 3:2 FTOH, HpF-PipB	EN 12457/in situ, 0.1-2.0 mm particles	Sörengård et al. (2021) [33]
Activated carbon	Colloidal activated carbon (PlumeStop®)	Sorbent amendment (injection)	1%	10 months	Spiked 0.6 mg kg^{-1} 10 soils with varying OC, clay	Σ_{18}=10,800	$C_{3-11,13,15,17}$ PFCAs, $C_{4,6,8}$ PFSAs, 6:2,8:2 FTS, PFOSA	1:7 liq:soil, 0.45 μm filter	Sörengård et al. (2019b) [34]
Biochar	Activated and unactivated waste timber biochar	Sorbent amendment (ex situ)	0-5%	Not stated	AFFF contaminated, 1 low, 1 high TOC	Σ_{21}=1200-3800	$C_{4,6,7,8,10}$ PFSAs, $C_{4-10,12-14,16}$ PFCAs, 4:2, 6:2, 8:2 FTS, HPFHpA, DMOA	Modified CEN EN 12457 <1mm, 1.2 μm filter	Sørmo et al. (2021) [35]
Biochar	Biochar (pine, 750 °C)	Sorbent amendment	0-5%	Not stated	Spiked sandy clay, loamy sand	Not stated*	$C_{6,8}$ PFCAs, $C_{6,8}$ PFSAs	0-96 hours, 0.22 μm	Askeland et al. (2020) [36]
Biochar	Activated and unactivated biochar	Sorbent amendment	0-20%	2 weeks	Industrially contaminated	Σ_4=1,125-3,671	$C_{6,8}$ PFCAs, $C_{6,8}$ PFSAs	EN 12457-2	Silvani et al. (2019) [37]
Composite	RemBind®, RemBind Plus®	Sorbent amendment	5-30%	2 months	AFFF contaminated	Σ_{12}=2,400-14,000	$C_{4,6,8}$ PFSAs, C_{4-10} PFCASs	24 h, 0.45 μm filter	Bräunig et al. (2021) [38]
Composite	Modified clay (MatCARE^{TM})	Sorbent amendment	10%	1 week-1 year	AFFF impacted sandy, clay and sandy clay loams	Σ_i=9,262-74,379	PFOS	0.45 μm filter, 24 h	Das et al. (2013) [39]
Multiple	RemBind® PAC (FiltraSorb^{TM} 400)	Sorbent amendment	5%	2 weeks	AFFF contaminated. loamy sand (1), sandy (1)	Σ_{21}=700-37,200	$C_{4-8,10}$ PFSAs, C_{4-13} PFCAs, PFOSA, 4:2, 6:2, 8:2, 10:2 FTS,	ASLP	Kabiri et al. (2021a,b) [40, 41]
Mulitple	CB + bentonite, CaCl, chitosan, hydrotalcite, PAC, pulverized zeolite, RemBind®	Stabilisation and solidification	10% CB 0.2% amend	4 months	Loamy sand (spiked)	Σ_{14}=6240-7310	C_{3-10} PFCAs, $C_{4,6,8}$ PFSA, 6:2, 8:2 FTS, PFOSA	0.1-2.0 mm particles, modified EN-12457-1	Sörengård et al. (2019a) [42]

Table 1 (continued)

Amendment category	Amendment type(s)	Technique	Application rate (w/w)	Ageing period	Soil properties	Initial soil conc. (μg kg^{-1})	PFAS tested	Leaching method/details	Author, year and reference
Mulitple	Activated carbon, compost soil, montmorillonite	Sorbent amendment	3%	Not stated	Sandy AFFF contaminated	Σ_{12}=6.4-2,510	C_{4-10} PFCAs, $C_{4,6,8}$ PFSAs, 6:2, 8:2 FTS	Modified EN 12457-2. 1:1 soil water, 8 days, 0.7 μm filter	Hale et al. (2017) [43]
Multiple	AC (coal-based), Biochar (mixed wood, paper-mill waste)	Sorbent amendment	4%	2 weeks (sorption)	Natively AFFF contaminated	Σ_{15}=780-3,600	PFOS, PFOA, PFHxS	47 μm filter	Kupryianchyk et al. (2016) [44]

AC activated carbon, *ASLP* Australian Standard Leaching Procedure, *CB* concrete binder, *DMOA* perfluoro-3,7-dimethyl octanoic acid, *FTOH* fluorotelomer alcohol, *FTS* fluorotelomer sulfonate, *GAC* granular activated carbon, *HPFHpA* 7H-dodecafluoro heptanoic acid, *HpFPipB* heptafluoropiperidin butane, *OC* organic carbon, *PAC* powdered activated carbon, *PFCAs* perfluoroalkyl carboxylic acids, *PFSAs* perfluoroalkyl sulfonic acids, *PFOSA* perfluorooctanesulfonamide, *TOC* total organic carbon

**Spiked with 5 μg L^{-1} per PFAS

A number of activated carbon products are available for PFAS sorption including powdered activated carbon (PAC), granular activated carbon (GAC) and colloidal/liquid activated carbon, such as PlumeStop®. Smaller particle size activated carbon has the advantage of higher surface area but is problematic to apply due to dust issues, however, colloidal/liquid activated carbon formulations have overcome these issues. Activated carbon amendments have been found to have the highest sorption capacity across a range of PFAS compared to other immobilisation amendments. In a PFAS sorption study using 44 adsorbents in water, Sörengård et al. [50] identified that activated carbon amendments (GAC, PAC, RemBind®) had the highest sorption capacity across most PFAS, with mean log K_d values of 3.5 for PFCAs and 4.2 for PFSAs, PFOSA and fluorotelomer sulfonates (FTSAs). Similarly, GAC was found to be superior at removal of PFAS compared to zeolite and sludge in another comparative study [51].

Biochar-Based Amendments

Biochar is used as an amendment due to its high cation exchange capacity (CEC), surface area and pore volume [52]. It is a carbonaceous material alternative to activated carbon, being produced from sustainably sourced materials [53] for carbon sequestration. As with activated carbon, biochar physico-chemical properties are influenced by carbon source material and pyrolysis temperature. Higher pyrolysis temperatures result in more organised carbon layers, with less functional groups, especially those containing O-H groups (a result of deoxygenation and dehydration) [52]. Higher temperatures also result in higher porosity, specific surface area, pH and ash content with a concomitant decrease in CEC and volatile matter [52]. Animal and solid-waste biochars tend to have lower surface area and volatile matter, but higher CEC than wood and crop-based biochars. The impact of these properties on PFAS sorption are complex, but generally result in biochars being less effective in sorption compared to their more homogenous activated carbon counterparts.

In an attempt to increase sorption capacity, research has been undertaken whereby surface functional groups are modified through biochar treatment. For example, biochar treated with $MgCl_2$ was found to have the highest mean log K_d for PFCAs (0.93) and PFSAs (0.87) of the non-activated carbon sorbents, while the untreated, MnO and $FeCl_3$ treated biochars were less effective at sorbing PFAS [50].

Clay-based Amendments

Of the non-carbon-based amendments, clays, such as zeolite, bentonite, hydrotalcite, montmorillonite and kaolinite have been utilised as a sorbent phase for PFAS immobilisation due to their large surface area and recognised potential

to sorb organic contaminants (e.g. PAHs). Clay minerals are hydrophilic, chemically stable and have high cation exchange capacities [54]. The abovementioned clays differ in their constituent molecules, structures and interlayer spacing which drives sorptive capacity. For example, Zhang et al. [55] determined that kaolinite had a higher PFOS sorption capacity (77.6 μg g^{-1}) than montmorillonite (54.5 μg g^{-1}), however, PFOS was observed to sorb in the montmorillonite interlayer. A study of PFAS sorption on kaolinite in water [56] found that adsorption of $\leq C_4$ molecules was not thermodynamically favourable. Clay minerals may also be modified to increase their PFAS sorptive capacity [54]; some of these modified clays are discussed in the following section on composite amendments.

Composite and Other Amendments

To improve the efficacy of soil amendments for PFAS immobilisation, composite products have been developed that comprise a variety of sorptive phases in combination. The philosophy behind composite amendments is to utilise different components exhibiting different physicochemical properties to enable multiple sorptive mechanisms for PFAS retention. Composite amendments used for PFAS immobilisation include RemBind®, RemBind Plus® and MatCARE.

RemBind® is a composite amendment, consisting of aluminium hydroxide, kaolin, and activated carbon. It is proposed that the aluminium hydroxide component of RemBind® interacts via electrostatic forces with anionic PFAS, binding the functional group. The activated carbon and organic matter components of RemBind® bind to the PFAS 'tail' through hydrophobic and Van der Waals forces. This provides a twopronged reaction mechanism for binding PFAS anions. In addition, the kaolinite and organic matter component of RemBind® provides the ability to bind cationic compounds through electrostatic interactions, regardless of the length of the CF backbone. The activated carbon component also binds PFAS cations through hydrophobic interactions. Most long-chain PFAS ($\geq C_8$) bind to activated carbon, however, smaller compounds ($\leq C_4$) may not bind efficiently as there are limited contact points with the carbon surface and Van der Waals forces are weak. In RemBind®, short-chain compounds are bound through electrostatic interactions as detailed above. RemBind Plus® [38] contains a higher quality and amount of both activated carbon and aluminium oxyhydroxides.

MatCARE^{TM}, is another composite amendment that consists of clay (palygorskite-based, an Mg-Al phyllosillicate), which has been modified with an unsaturated fatty amine (oleylamine), and also contains quartz, kaolinite, dolomite, amorphous materials and traces of NaCl [39]. It was reported to have a PFOS adsorption capacity of 0.09 mmol g^{-1}, which was higher than the activated carbon product, Hydraffin (0.07 mmol g^{-1}) from the same study [39]; however, the sorptive performance for other PFAS and environmental implication related to the use of the oleylamine modification has not been reported.

Other amendments investigated for their PFAS sorptive capacities include polymers, carbon nanotubes and nanoparticles with ligands. In an aquifer solids sorption study, the cationic polymers polydiallyldimethyl ammonium chloride (polyDADMAC) and polyamine [57] were found to increase sorption of PFSAs and PFCAs by a factor ranging from 2.0 to 6.1. For example, K_D values for PFOS increased from 1.44 L kg^{-1} for the untreated soil, to 2.94L kg^{-1} and 8.75 L kg^{-1} for polyDADMAC and polyamine respectively. It was proposed that the increase in PFAS sorption was due to the increase in carbon content, but also due to enhanced exchange interactions between the cationic polymers and anionic PFAS [57]. Similarly, a study of two polyquaternium polymers, poly-(dimethylamine-co-epichlorohydrin) and poly-(diallyldimethylamonium) in water/soil suspensions, found that PFOS was bound, predominantly in soil-polymer-PFOS complexes, with respective affinities of 9.3×10^4 and 7.3×10^4 M^{-1} [58].

PFOS sorption onto Gold nanoparticles with different combinations of dual ligands has been demonstrated by Liu et al. [59], while the adsorption of PFOA onto multi-walled carbon nanotubes (MWCNT) and MWCNT with embedded Fe, Co, Al, Mg, Mn, Fe_2O_3, Cu and Zn has been demonstrated in several studies [60–62]. Carbon nanotubes are useful sorbents due to their large surface areas; however, the cost of MWCNT is generally prohibitive relative to GAC and PAC for large scale applications.

Amendment Additions and Binding Agents

The amount of amendment added to a contaminated soil will influence treatment costs, and may also influence whether the soil is able to be reused post-treatment. Application rates for immobilisation studies included in Table 1 range from 0.1% to 30%. Soil amendments may also be added to contaminated soil in conjunction with binding agents such as cement and lime. Binders are added to reduce the hydraulic conductivity and to increase or maintain unconfined compressive strength so that it is compatible with the intended site end use. The co-addition of amendments and binders provides a two-pronged approach for minimising PFAS leaching through adsorptive and encapsulation processes, as described in "Mechanisms of Immobilisation". Binding agents listed in Table 1 have typically been added at 10% w/w, and cured for a number of months.

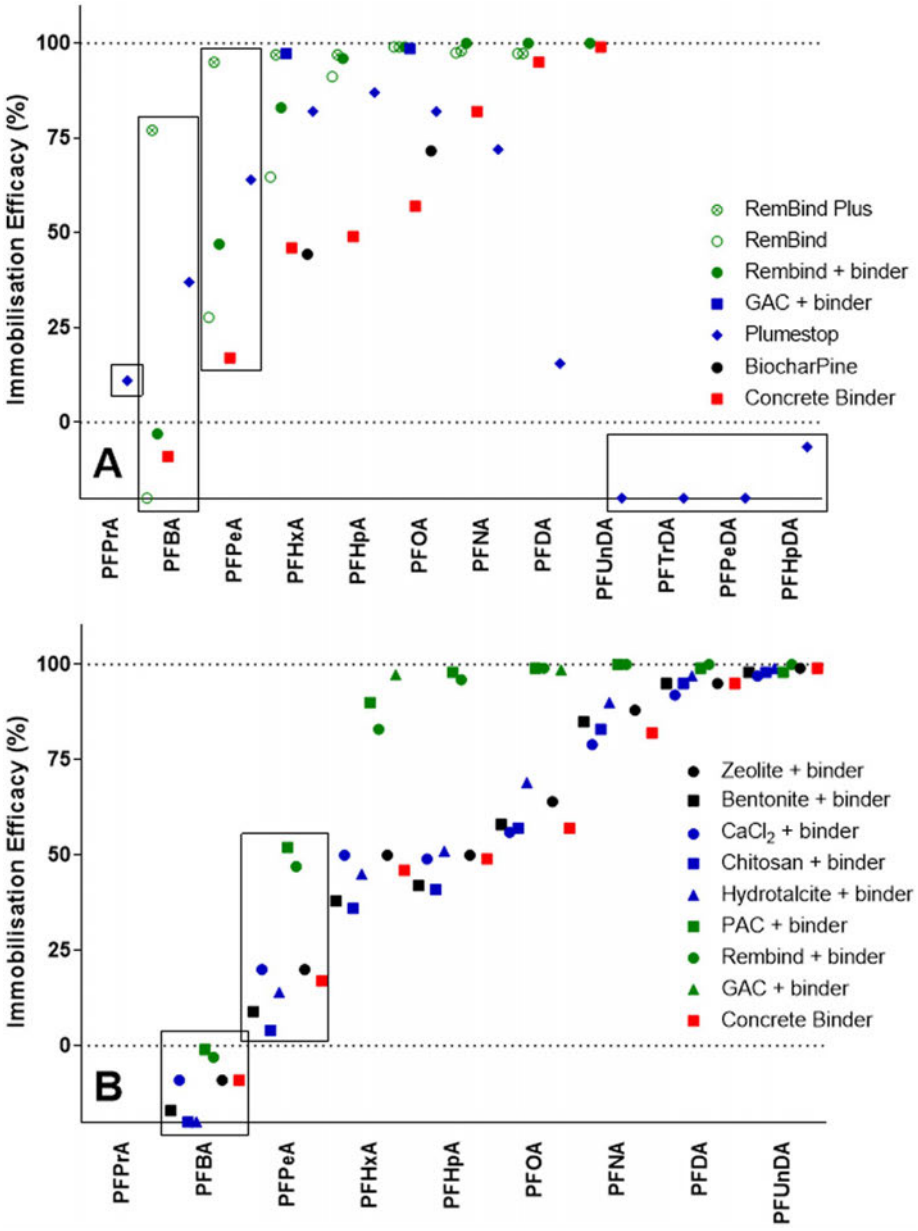


Fig. 2 Comparison of PFCA immobilisation efficacy when different amendment strategies were applied to contaminated soil. Data points may be cross-referenced with information in Table 1 to glean information on application rates, curing times and methods used for the assessment of PFAS leachability. PAC, Rembind® and RemBind Plus® [38], compost, montmorillonite [43], pine biochar [36], MatCARE^{TM} [39], PlumeStop® [34], GAC and CB [33], all other amendments with binder [42]. Points lower than -25 are shown at -25. Some results may be averages over several soil types, conditions and/or replicates, or the most realistic application rate. (**A**) Includes the activated carbon based amendments; (**B**) includes only studies involving a concrete binder

Remediation Effectiveness

A common strategy for determining immobilisation efficacy is the assessment of contaminant leaching, with a comparison between pre- and post-amendment values. Leaching assays are routinely undertaken to characterise the soil's mobile phase with data then utilised to estimate ground or surface water contamination potential. Leaching assays may also be utilised to classify waste for disposal and/or to demonstrate the effectiveness of soil amendment strategies. This may be achieved through the use of numerous leaching tests, including the Australian Standard Leaching Procedure (ASLP; AS4439-1997), Synthetic Precipitation Leaching Procedure (SPLP; USEPA method 1312), Toxicity Characteristic Leaching Procedure (TCLP; USEPA method 1311), TCLP variations (e.g. ASTM D3987-85), Multiple Extraction Procedure (MEP; USEPA method 1320) and Leaching Environmental Assessment Framework methods (LEAF; USEPA methods 1313-1316). The aforementioned leaching procedures vary in operational parameters including leaching fluid pH, buffering capacity, ionic strength, single versus multiple extractions, solid-to-solution ratio, contact time, agitation, maximum

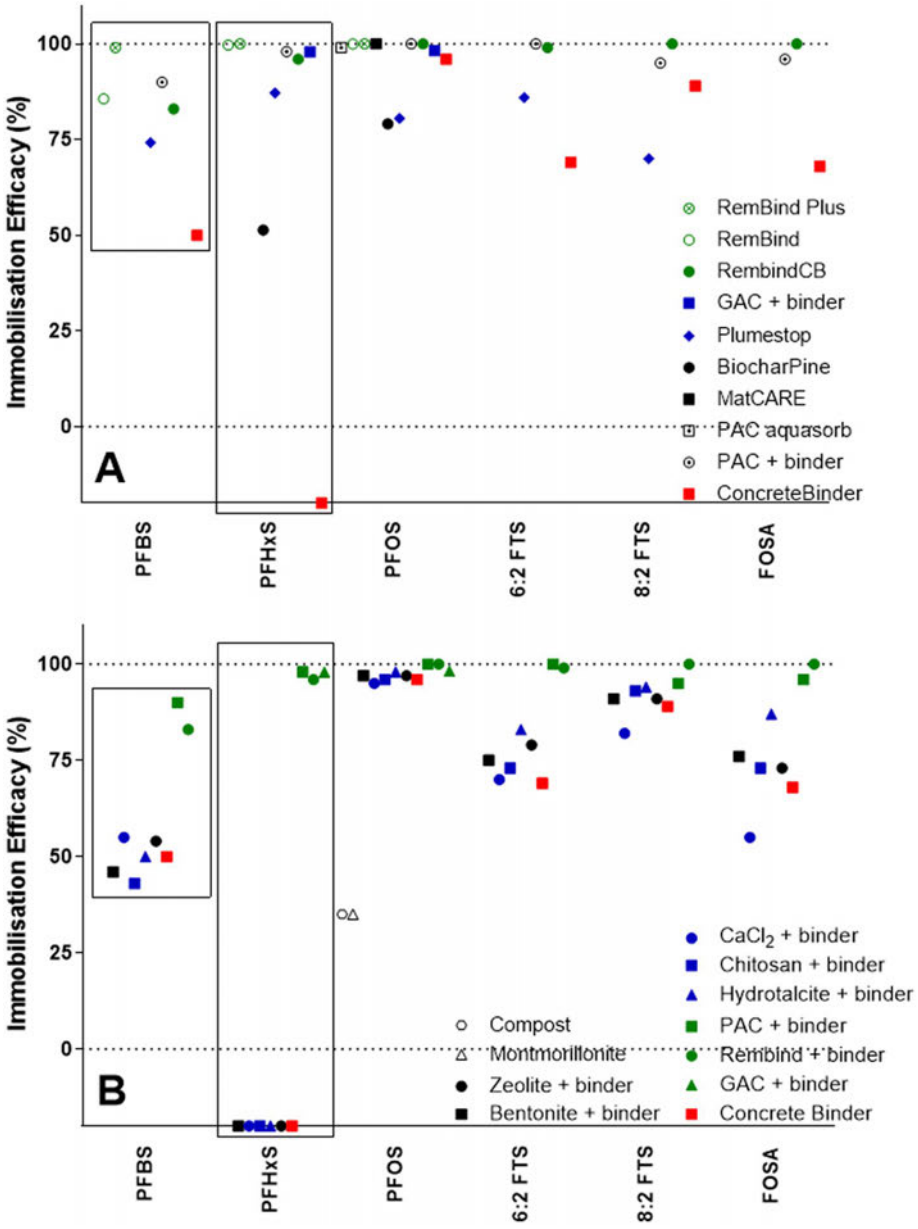


Fig. 3 Comparison of PFSA, FTS and FOSA immobilisation efficacy when different amendment strategies were applied to contaminated soil. (**A**) Includes the activated carbon based and composite amendments; (**B**) includes compost, montmorillonite and studies involving a concrete binder. Data point sources as described in Fig. 2 and Table 1

particle size, batch versus column tests; all of which will influence PFAS leachability outcomes. For example, differences in fluid pH (e.g. buffered TCLP at pH 4.93 versus unbuffered ASLP using deionised water) will influence leachability due to the impact of pH on sorption-desorption (as detailed in "Mechanisms of Immobilisation") while particle size differences (the maximum particle size for AS4439 is 2.4 mm versus 9.5 mm for TCLP) will also influence leaching outcomes due to disparities in reactive surface areas.

Notwithstanding the methodological differences between leaching assays, data from PFAS immobilisation studies (Table 1) are represented in Figs. 2 and 3 to provide an overview of immobilisation efficacy for different amendment strategies applied in both laboratory and field-based studies for PFAS varying in carbon chain length and functional group. Treatment efficacy was calculated, as in Sörengård et al. [34] by:

$$\Delta Re = \left(1 - \frac{c^t_{aq}}{c^u_{aq}}\right) \times 100 \quad (1)$$

where c^t_{aq} is the PFAS concentration in the leachate of the treated soil and c^u_{aq} of the untreated soil leachate.

Values greater than zero indicate that the amendment strategy decreased PFAS leachability compared to unamended soil with increasing values up to a maximum of 100 indicating increasing treatment efficacy up to complete immobilisation. Negative values may also be calculated whereby the addition of the soil amendment results in enhanced PFAS leachability compared to unamended soil. Negative values may also result from analytical variability particularly when PFAS concentrations are being reported near the level of quantification. Conceivably precursor transformation may influence PFAS immobilisation efficacy; however, data illustrating this is lacking due to analytical

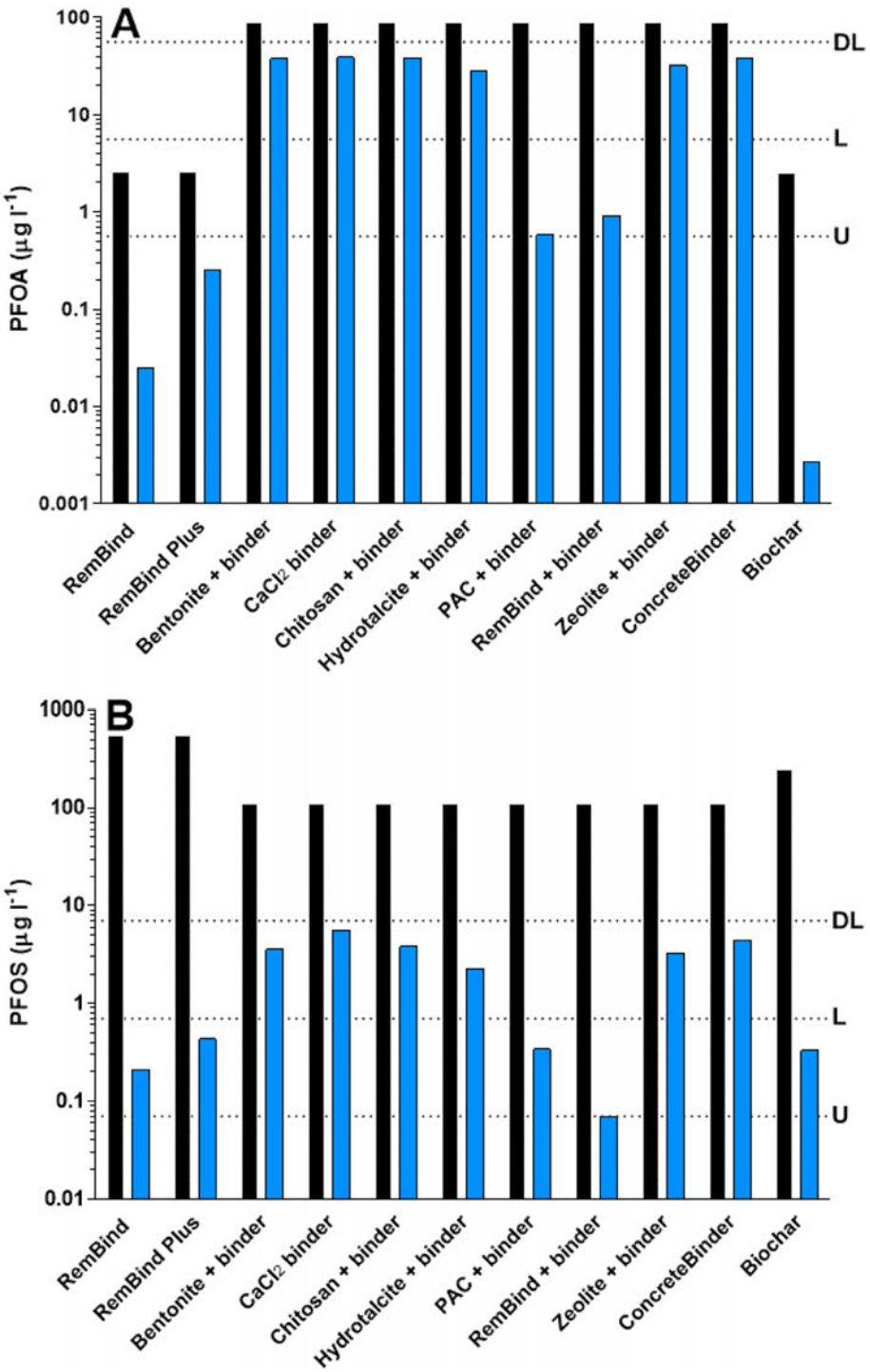


Fig. 4 Change in PFOA (**A**) and PFOS (**B**) leachability following treatment of soil with amendments (as detailed in Table 1). PFOA and PFOS leachability pre- (■) and post-amendment (■) is presented in the context of regulatory standards for unlined (**U**), lined (**L**) and double-lined (**DL**) landfills [63]. Amendments shown: RemBind [38], biochar [35], amendments with binder [42]

challenges associated with precursor identification and quantification. The plot of treatment efficacy, depicted in Figs. 2 and 3, provides a high-level approach for comparing data across amendment strategies. However, efficacy calculations do not reflect whether the extent of immobilisation was suitable against regulatory standards (i.e. landfill leaching criteria, water quality standards). As a result, Fig. 4a, b highlight PFOA and PFOS pre- and post-amendment leaching results in the context of regulatory standards.

As shown in Fig. 2, treatment efficacy trends were observed for PFCAs when different amendment strategies were utilised; PFAS immobilisation efficacy increased with increasing carbon chain length although some variability was observed for C_{10}-C_{14} compounds in the study of Sörengård et al. [34]. For $\leq C_6$ PFCAs, immobilisation efficacy for most treatments was <50% with the exception of three amendments incorporating activated carbon. Activated carbon amendments were highly effective at reducing leachability of $\geq C_8$ PFCAs in amended soil as exemplified by RemBind® and RemBind Plus® amendments [38]. At loadings of 25% and 15% w/w respectively, >97% reduction in leachability was observed for C_8-C_{10} PFCAs. For PlumeStop®, a decrease in immobilisation efficacy was observed for $>C_7$ PFCA possibly due to reduced hydrophobic interactions [34]. While only a limited number of studies have assessed the impact of biochar addition on PFCA leachability, Askeland et al. [36] observed increasing immobilisation efficacy with increasing carbon chain length. However, compared to activated carbon amendments, biochar appears to be less effective at reducing PFCA leachability, though further comparative studies with equivalent amendment loadings and leaching assessment methodologies would be beneficial. While the addition of bentonite, $CaCl_2$, chitosan, hydrotalcite and zeolite in conjunction with a concrete binder had little effect on treatment efficacy compared to the binder alone, the addition of activated carbon-based amendments with concrete binders enhanced immobilisation efficacy compared to binder alone, particularly for C_5-C_9 PFCAs. When immobilisation efficacy was compared between RemBind® amendments with and without the addition of concrete binders, C_5-C_7 PFCA treatment efficacy was enhanced by inclusion of the binding agent, however, this effect was not observed for longer chain PFCAs.

Immobilisation trends were less apparent for PFSAs compared to PFCAs (Fig. 3). For activated carbon-based amendments, higher immobilisation efficacy was observed for short-chain compounds (perfluorobutane sulfonic acid (PFBS) and PFHxS) compared to the equivalent carbon chain length carboxylic acids. Although some variability in PFSA immobilisation efficacy was observed for PlumeStop® [34], the remainder of the activated carbon-based amendments reduced PFSA leachability, irrespective of carbon chain length and degree of fluorination, by >80%. Limited data points are available for biochar amendments, however, similar trends were observed for PFSAs and PFCAs. Similarly, the addition of bentonite, $CaCl_2$, chitosan, hydrotalcite and zeolite in conjunction with a concrete binder had little effect on PFSA treatment efficacy compared to the binder alone [42].

Figure 4 shows PFOA and PFOS leachability pre- and post-amendment addition from selected studies, with reference to landfill regulatory guidelines [63]. In soil containing high PFOA leachability pre-treatment (~90 $\mu g\ L^{-1}$), irrespective of amendment type, leachability post-treatment was reduced to an acceptable level for soil disposal into a double-lined landfill, although for most treatments there was no advantage of adding an amendment (0.2% w/w) over the binder alone (10% w/w, Figure 4a). However, carbon-based amendments (PAC + binder, RemBind® + binder [42]) performed significantly better, reducing PFOA leachability to achieve the single-lined landfill criterion. For soil with low PFOA leachability pre-treatment (<3 $\mu g\ L^{-1}$), addition of RemBind® (25% w/w), RemBind Plus® (15% w/w) [38] and biochar (5% w/w) [35] reduced PFOA leachability to below the unlined landfill criterion. Although landfill acceptance criteria are lower for PFOS compared to PFOA, all treatments were able to reduce PFOS leachability to at least the double-lined landfill criterion (Fig. 4b). However, carbon-based amendments (RemBind® RemBind Plus® Biochar, PAC + binder, RemBind® + binder) achieved the single-lined landfill criterion at application rates ranging from 5-25% w/w.

Mechanisms of Immobilisation

A reduction in PFAS leachability occurs as a result of a number of sorption mechanisms. Sorption mechanisms are dependent on physico-chemical properties of PFAS and amendments and are influenced by the surrounding soil and environmental conditions. The following conditions will impact PFAS sorption:

1. C chain length and function group influence hydrophobic and electrostatic interactions respectively
2. Amendments may influence sorption through changes in soil pH (electrostatic interactions), by providing surfaces for hydrophobic interactions, and cation bridging.
3. PFAS adsorption studies performed on soils with varying characteristics (e.g. OC, clay, pH, anion exchange capacity (AEC) and protein) [64–70] have found that soil pH, organic carbon and clay content all play important roles in sorption through a combination of electrostatic and hydrophobic interactions [71].
4. Most PFAS have pKa<2 and thus are anions under most environmental circumstances. However, some PFAS (e.g. PFOSA, pKa 6.2-6.5), do not form anions under many circumstances [42, 72], which will impact sorption strategies based on direct electrostatic interactions.

PFAS have widely varying physico-chemical properties, and in particular, both the functional group and fluorinated C chain length affect sorption behaviour. PFAS may exist as uncharged, anionic, cationic, or zwitterionic molecules, although the most commonly observed compounds (PFOS and PFOA), both form anions. Charge differences affect sorption and desorption processes, and impacts the efficacy of soil amendments. The sulfonate functional group of PFSAs is considered to be a hard base, having higher sorption onto oxide surfaces than the soft base of the carboxylate group in PFCAs [73]. However, different amendments vary in their PFAS immobilisation efficacy due to the complex interplay of properties. Surface charge is a significant parameter, for example with anionic PFAS, sorption increases with increasingly positive surface charge [74].

Activated carbon and biochar have a number of different functional groups on the amendment surface, depending on the temperature of production, which will influence electrostatic interactions. More functional groups are present on the surface when production occurs at a lower temperature, therefore electrostatic interactions are likely to be higher; however, hydrophobic interactions may be the predominant PFAS sorption mechanism, as carbonaceous material produced at higher temperature have higher PFAS sorption capacities. pH influences will impact electrostatic interactions as an increase in pH will result in competition for sorption sites, between OH- groups and anionic PFAS [73].

PFAS octanol-water partitioning coefficients are influenced by C-chain length (e.g. PFHxA K_{OW}=3.12 versus PFOA K_{OW}=4.59 [75]), while log K_{OC} has been shown to increase by 0.6 and 0.83 with each additional fluorinated carbon for PFCAs and PFSAs respectively [67]. As such sorption efficacy of varying carbon chain length compounds to soil and soil amendments is influenced by K_{OW} through hydrophobic interactions [42, 66]. It has been reported that PFAS hemi-micelles and bilayers may form through self-aggregation on amendment surfaces [76] which is influenced by sorbent pore size, organic matter fraction, surface area and degree of carbonisation [36, 42].

In addition to electrostatic and hydrophobic interactions, PFAS may also form divalent cation bridges, with ions such as Ca^{2+} [77] and Mg^{2+}. Smaller PFAS are more likely to participate in divalent cation bridging, as observed by Campos Pereira et al. [67], potentially due to their shorter C-F tail, which makes them less hydrophobic, and subsequently less likely to sorb via hydrophobic interactions. Carbon nanotubes (CNT) with a variety of metal cations (Co, Mn, Mg and Al) on their outer and inner surface were found to enhance PFOA sorption by a factor of 6 compared to CNT containing inner surface Fe as a consequence of enhanced electrostatic interactions [60]. In addition, ligand exchange may occur between the carboxyl group of PFCAs and hydroxyl groups on metal oxides [76], forming inner sphere complexes via covalent metal-ligand bonds.

Compared to anionic PFAS, fewer sorption studies have been undertaken on cation, zwitterionic and neutral PFAS [42]. A study on cationic and zwitterionic PFAS sorption in soils [78], found that sorption of these compounds was non-linear, in contrast to anionic PFAS, however, electrostatic and hydrophobic interactions were the predominant mechanisms controlling PFAS sorption. Cationic PFAS sorption was correlated with soil organic matter content and was reversible. In contrast, sorption of zwitterionic

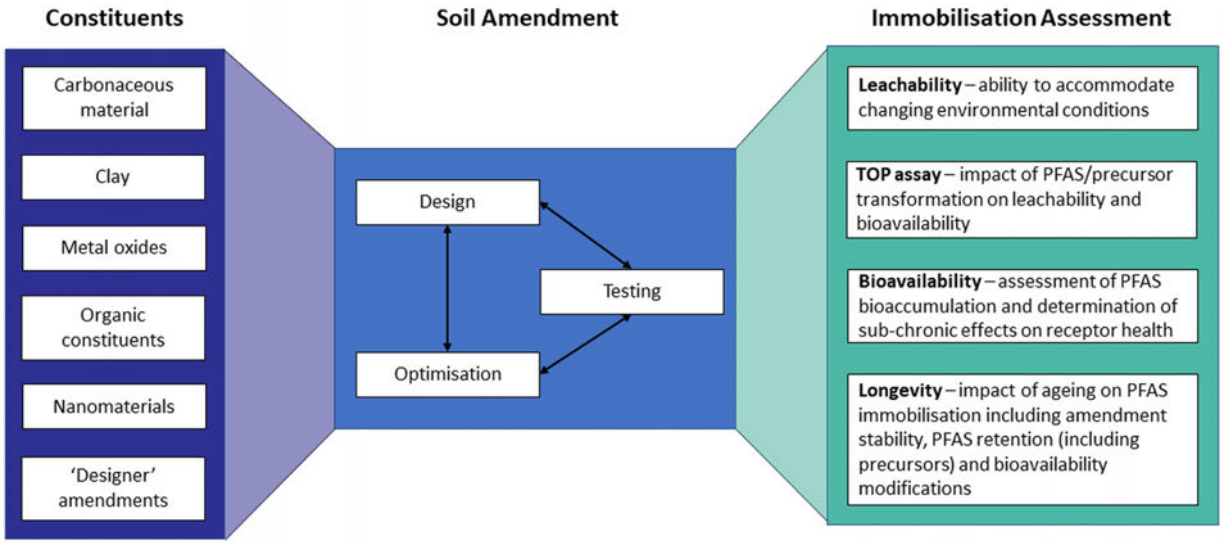


Fig. 5 Assessment framework for the design, optimisation and validation of PFAS immobilisation efficacy and longevity

PFAS was hysteretic rather than reversible and was hypothesised to be due to entrapment in porous structures present in inorganic soil components [78]. Differences in behaviour between cationic and zwitterionic PFAS highlight the necessity of further studies to assess the influence of soil amendments on PFAS fate and transport and immobilisation efficacy.

When binding agents are utilised, encapsulation also contributes to the decrease in PFAS leachability. Although the addition of cement binders may raise the pH to around 10 [42], thereby decreasing the impact of electrostatic interactions, the decrease in surface area and reduction in hydraulic conductivity of stabilised/solidified material results in reduced PFAS leachability.

Conclusions and Future Research Needs

As detailed in "Remediation Effectiveness", a common approach for assessing the efficacy of PFAS immobilisation is the use of leaching methodologies (e.g. SPLP, TCLP, ASLP). These approaches are simplistic, however, differences in operational parameters may restrict true comparison of immobilisation efficacy between treatments and studies. In addition, these approaches for the assessment of PFAS immobilisation utilise operationally defined procedures which may generate methodological artefacts, such as perceived enhanced contaminant mobility via colloidal generation [79–81]. Water-dispersible naturally occurring colloids are generated as a result of vigorous shaking during the batch extraction process or by leaching under elevated pH. Colloids exhibit high specific surface area and charge, which are effective sorbents for PFAS. Although an understanding of colloidal facilitated mobility of PFAS is limited, this transport mechanism has been shown to be significant for other contaminants of concern including metal(loid)s, mono-aromatic hydrocarbons, polycyclic aromatic hydrocarbons, polychlorinated biphenyls and organochlorine pesticides [82–87]. The use of the Leaching Environmental Assessment Framework (LEAF) [88] may overcome some the aforementioned limitations as the framework incorporates a number of standardized testing methods (including assays to assess pH dependency, liquid:solid dependency, percolation and mass transfer) and generic or application-specific release models. In addition, the LEAF overcomes single-point leaching tests that assess a specific environmental scenario and can accommodate defined particle sizes and monoliths (i.e. minimized colloidal generation) which are relevant for solidified materials.

Post immobilisation assessment should provide further consideration to the influence of aging and environmental factors on long-term immobilisation efficacy. Limited studies have assessed immobilisation stability over extended timeframes, however, PFAS immobilisation longevity was demonstrated in RemBind® amended soil following a 3-year aging period [38]. Although small increases in PFAS leachability (ASLP) were observed in aged samples when 2 month and 3-year leachability data was compared, PFAS leachability after 3-years was reduced by >99% compared to unamended soil. Additional studies like this are needed to elucidate the long-term effect of soil amendments on PFAS immobilisation. However, a limiting factor for ageing studies is the timeframe required to assess longevity. Conceivably, wetting and drying (at elevated temperature) cycles could be introduced into protocols as a means to accelerate ageing processes. This may provide indicative information regarding the impact of ageing on immobilisation stability although interpretation of data may be confounded by the difficulty in replicating natural ageing processes in the laboratory [89].

Transformation of PFAS and/or precursor compounds may potentially occur post-treatment via biotic and abiotic oxidation processes. Although little research has been undertaken to investigate the rate and extent of post-immobilisation transformation, the total oxidisable potential (TOP) assay [90] may provide an approach for quantifying transformation. However, as the name suggests, the assay quantifies the impact of oxidation on PFCA formation, although it fails to elucidate timeframes for such processes. Nevertheless, this information may provide a worst-case scenario for PFAS immobilisation stability. In the aforementioned 3-year RemBind ageing study [38], it was proposed that the minor increase in PFAS leachability in aged immobilised soil may have resulted from the generation of labile PFCAs through precursor compound transformation, however, it is conceivable that minor increases in PFAS leachability may have also resulted from immobilising agent breakdown. For some soil amendments with organic modifications (e.g. amine-modified clays), constituents may be utilised by the indigenous microflora as a carbon and energy source, thereby potentially impacting amendment integrity and PFAS sorption. The stability of these and other soil amendments has not been assessed in the context of PFAS sorption and retention; further assessment of this is required to ensure long-term stability of PFAS immobilised soil.

While leaching tests are utilised to understand the leaching profile of immobilised soil and/or determine the regulatory acceptability of stabilised material for disposal, data generated from these methods do not provide information regarding the influence of soil amendments on PFAS biological exposure and impact. If PFAS leachability can be reduced to below the criterion for unlined landfills, conceivably immobilised soil could remain on site; in such a case, other assessment methodologies (i.e. bioavailability assessment) would be required to ensure stabilised material was environmentally benign. Conceivably, leaching approaches may provide a conservative estimate of labile/exchangeable PFAS available to plants, however, other

release mechanisms may be pertinent for ecological receptors facilitated by oxidative processes (of precursor compounds or immobilising agent) and/or pH changes (e.g. in gut environments). However, limited studies have been undertaken whereby changes in PFAS bioavailability (e.g. decrease in PFAS bioaccumulation) as a result of amendment application have been quantified. Bräunig et al. [38] reported that PFAS bioaccumulation in *E. fetida* decreased by 74-98% following immobilisation of a soil with 25% w/w RemBind®, although earthworm weight loss was reported, presumably due to decreased nutrient availability. These potential ecological impacts require further investigation in addition to the assessment of potential sub-chronic health effects including oxidative stress, DNA damage and reproductive issues.

Due to the variability in physicochemical properties of legacy and replacement PFAS (e.g. ADONA, GenX), a single agent may not be adequate/suitable to immobilise all compounds of concern in impacted soil. As such, soil amendments may need to be tailored to site-specific conditions. To drive future PFAS soil amendment research and development, a robust assessment framework is essential to elucidate not only immobilisation efficacy but longevity of immobilisation processes. The schematic framework detailed in Fig. 5 provides key assessment components required to test and validate the efficacy, longevity and biological impact of amendments for PFAS immobilisation in soil. This information is critical to provide a lines-of-evidence approach for the application of sustainable, cost-effective, immobilisation strategies to minimise the impact of PFAS on environmental health.

Acknowledgements The authors would like to acknowledge the Australian Government and the University of South Australia for supporting J.A.S. with a Research Training Program Scholarship.

Declarations

Conflict of Interest The authors declare that they have no conflict of interest.

References

1. Dauchy X, Boiteux V, Bach C, Rosin C, Munoz JF. Per- and polyfluoroalkyl substances in firefighting foam concentrates and water samples collected near sites impacted by the use of these foams. Chemosphere. 2017;183:53–61. https://doi.org/10.1016/j.chemosphere.2017.05.056.
2. Kotthoff M, Müller J, Jürling H, Schlummer M, Fiedler D. Perfluoroalkyl and polyfluoroalkyl substances in consumer products. Environ Sci Pollut Res. 2015;22(19):14546–59. https://doi.org/10.1007/s11356-015-4202-7.
3. KEMI. Occurrence and Use of Highly Fluorinated Substances and Alternatives. KEMI (Swedish Chemicals Agency); 2015.
4. United Nations Environment Programme. Stockholm Convention; 2021. http://chm.pops.int/.
5. Wang J, Shi G, Yao J, Sheng N, Cui R, Su Z, et al. Perfluoropolyether carboxylic acids (novel alternatives to PFOA) impair zebrafish posterior swim bladder development via thyroid hormone disruption. Environ Int. 2020;134:105317. https://doi.org/10.1016/j.envint.2019.105317.
6. DeWitt JC, editor. Toxicological Effects of Perfluoroalkyl and Polyfluoroalkyl Substances. Springer; 2015.
7. Xu C, Jiang ZY, Liu Q, Liu H, Gu A. Estrogen receptor beta mediates hepatotoxicity induced by perfluorooctane sulfonate in mouse. Environ Sci Pollut Res. 2017;24(15):13414–23. https://doi.org/10.1007/s11356-017-8943-3.
8. Dong GH, Zhang YH, Zheng L, Liu W, Jin YH, He QC. Chronic effects of perfluorooctanesulfonate exposure on immunotoxicity in adult male C57BL/6 mice. Arch Toxicol. 2009;83(9):805–15. https://doi.org/10.1007/s00204-009-0424-0.
9. Lee I, Viberg H. A single neonatal exposure to perfluorohexane sulfonate (PFHxS) affects the levels of important neuroproteins in the developing mouse brain. NeuroToxicology. 2013;37:190–6. https://doi.org/10.1016/j.neuro.2013.05.007.
10. Shi X, Du Y, Lam PKS, Wu RSS, Zhou B. Developmental toxicity and alteration of gene expression in zebrafish embryos exposed to PFOS. Toxicol Appl Pharmacol. 2008;230(1):23–32. https://doi.org/10.1016/j.taap.2008.01.043.
11. Li K, Gao P, Xiang P, Zhang X, Cui X, Ma LQ. Molecular mechanisms of PFOA-induced toxicity in animals and humans: Implications for health risks. Environ Int. 2017;99:43–54. https://doi.org/10.1016/j.envint.2016.11.014.
12. Miller A, Elliott JE, Elliott KH, Lee S, Cyr F. Temporal trends of perfluoroalkyl substances (PFAS) in eggs of coastal and offshore birds: Increasing PFAS levels associated with offshore bird species breeding on the Pacific coast of Canada and wintering near Asia. Environ Toxicol Chem. 34(8):1799-808. https://doi.org/10.1002/etc.2992.
13. Molina ED, Balander R, Fitzgerald SD, Giesy JP, Kannan K, Mitchell R, et al. Effects of air cell injection of perfluorooctane sulfonate before incubation on development of the white leghorn chicken (Gallus domesticus) embryo. Environ Toxicol Chem. 2006;25(1):227–32.
14. Groffen T, Eens M, Bervoets L. Do concentrations of perfluoroalkylated acids (PFAAs) in isopods reflect concentrations in soil and songbirds? A study using a distance gradient from a fluorochemical plant. Sci Total Environ. 2019;657:111–23. https://doi.org/10.1016/j.scitotenv.2018.12.072.
15. Ase Høisæter, Pfaff A, Breedveld GD. Leaching and transport of PFAS from aqueous film-forming foam (AFFF) in the unsaturated soil at a firefighting training facility under cold climatic conditions. J Contam Hydrol. 2019;222:112–122. https://doi.org/10.1016/j.jconhyd.2019.02.010.
16. Hepburn E, Madden C, Szabo D, Coggan TL, Clarke B, Currell M. Contamination of groundwater with per- and polyfluoroalkyl substances (PFAS) from legacy landfills in an urban re-development precinct. Environ Pollut. 2019;248:101–13. https://doi.org/10.1016/j.envpol.2019.02.018.
17. Filipovic M, Woldegiorgis A, Norstrm K, Bibi M, Lindberg M, sters AH. Historical usage of aqueous film forming foam: A case study of the widespread distribution of perfluoroalkyl acids from a military airport to groundwater, lakes, soils and fish. Chemosphere. 2015;129:39-45. https://doi.org/10.1016/j.chemosphere.2014.09.005.
18. Semerd J, Hatasov N, Grasserov A, ern T, Filipov A, Han A, et al. Screening for 32 per- and polyfluoroalkyl substances (PFAS) including GenX in sludges from 43 WWTPs located in the Czech Republic - Evaluation of potential accumulation in vegetables after application of biosolids. Chemosphere. 2020;261:128018. https://doi.org/10.1016/j.chemosphere.2020.128018.
19. Gallen C, Eaglesham G, Drage D, Nguyen TH, Mueller J. A mass estimate of perfluoroalkyl substance (PFAS) release

from Australian wastewater treatment plants. Chemosphere. 2018;208:975–83. https://doi.org/10.1016/j.chemosphere.2018.06.024.
20. Szabo D, Coggan TL, Robson TC, Currell M, Clarke BO. Investigating recycled water use as a diffuse source of per- and polyfluoroalkyl substances (PFASs) to groundwater in Melbourne, Australia. Sci Total Environ. 2018;644:1409–17. https://doi.org/10.1016/j.scitotenv.2018.07.048.
21. Brusseau ML, Anderson RH, Guo B. PFAS concentrations in soils: Background levels versus contaminated sites. Sci Total Environ. 2020;740:140017. https://doi.org/10.1016/j.scitotenv.2020.140017.
22. Washington JW, Yoo H, Ellington JJ, Jenkins TM, Libelo EL. Concentrations, Distribution, and Persistence of Perfluoroalkylates in Sludge-Applied Soils near Decatur, Alabama, USA. Environ Sci Technol. 2010;44(22):8390–6. https://doi.org/10.1021/es1003846.
23. Coggan TL, Moodie D, Kolobaric A, Szabo D, Shimeta J, Crosbie ND, et al. An investigation into per- and polyfluoroalkyl substances (PFAS) in nineteen Australian wastewater treatment plants (WWTPs). Heliyon. 2019;5(8):e02316. https://doi.org/10.1016/j.heliyon.2019.e02316.
24. Dombrowski PM, Kakarla P, Caldicott W, Chin Y, Sadeghi V, Bogdan D, et al. Technology review and evaluation of different chemical oxidation conditions on treatability of PFAS. Remediat J. 28(2):135-50. https://doi.org/10.1002/rem.21555.
25. Stoiber T, Evans S, Naidenko OV. Disposal of products and materials containing per- and polyfluoroalkyl substances (PFAS): A cyclical problem. Chemosphere. 2020;260:127659. https://doi.org/10.1016/j.chemosphere.2020.127659.
26. Garca AN, Viciano N, Font R. Products obtained in the fuel-rich combustion of PTFE at high temperature. J Anal Appl Pyrolysis. 2007;80(1):85-91. https://doi.org/10.1016/j.jaap.2007.01.004.
27. Senevirathna S, Mahinroosta R. Remediation of Soil and Groundwater Contaminated with Per-and Poly-Fluoroalkyl Substances (PFAS). In: Soil and Groundwater Remediation Technologies: A Practical Guide. CRC Press 2020:109-24.
28. Ross I, McDonough J, Miles J, Storch P, Thelakkat Kochunarayanan P, Kalve E, et al. A review of emerging technologies for remediation of PFASs. Remediat J. 2018;28(2):101–26. https://doi.org/10.1002/rem.21553.
29. Lampert DJ. Emerging Research Needs for Assessment and Remediation of Sediments Contaminated with Per-and Poly-fluoroalkyl Substances. Current Pollution Reports. 2018;4(4):277–9. https://doi.org/10.1007/s40726-018-0098-4.
30. Ahmed MB, Johir MAH, McLaughlan R, Nguyen LN, Xu B, Nghiem LD. Per- and polyfluoroalkyl substances in soil and sediments: Occurrence, fate, remediation and future outlook. Science of the Total Environment. 2020;748. https://doi.org/10.1016/j.scitotenv.2020.141251.
31. Bolan N, Sarkar B, Yan Y, Li Q, Wijesekara H, Kannan K, et al. Remediation of poly- and perfluoroalkyl substances (PFAS) contaminated soils To mobilize or to immobilize or to degrade? J Hazard Mater. 2021;401:123892. https://doi.org/10.1016/j.jhazmat.2020.123892.
32. Mahinroosta R, Senevirathna L. A review of the emerging treatment technologies for PFAS contaminated soils. J Environ Manag. 2020;255:109896. https://doi.org/10.1016/j.jenvman.2019.109896.
33. Sörengard M, Gago-Ferrero P, Kleja DB, Ahrens L. Laboratory-scale and pilot-scale stabilization and solidification (S/S) remediation of soil contaminated with per- and polyfluoroalkyl substances (PFASs). J Hazard Mater. 2021;402:123453. https://doi.org/10.1016/j.jhazmat.2020.123453.
34. Sörengard M, Kleja DB, Ahrens L. Stabilization of per- and polyfluoroalkyl substances (PFASs) with colloidal activated carbon (PlumeStop) as a function of soil clay and organic matter content. J Environ Manag. 2019;249:109345. https://doi.org/10.1016/j.jenvman.2019.109345.
35. Sormo E, Silvani L, Bjerkli N, Hageman N, Zimmerman AR, Hale SE, et al. Stabilization of PFAS-contaminated soil with activated biochar. Science of The Total Environment. 2021;763:144034. https://doi.org/10.1016/j.scitotenv.2020.144034.
36. Askeland M, Clarke BO, Cheema SA, Mendez A, Gasco G, Paz-Ferreiro J. Biochar sorption of PFOS, PFOA, PFHxS and PFHxA in two soils with contrasting texture. Chemosphere. 2020;249.
37. Silvani L, Cornelissen G, Botnen Smebye A, Zhang Y, Okkenhaug G, Zimmerman AR, et al. Can biochar and designer biochar be used to remediate per- and polyfluorinated alkyl substances (PFAS) and lead and antimony contaminated soils? Sci Total Environ. 2019;694:133693. https://doi.org/10.1016/j.scitotenv.2019.133693.
38. Brunig J, Baduel C, Barnes CM, Mueller JF. Sorbent assisted immobilisation of perfluoroalkyl acids in soils effect on leaching and bioavailability. J Hazard Mater. 2021:125171. https://doi.org/10.1016/j.jhazmat.2021.125171.
39. Das P, Arias EVA, Kambala V, Mallavarapu M, Naidu R. Remediation of perfluorooctane sulfonate in contaminated soils by modified clay adsorbenta risk-based approach. Water Air Soil Pollut. 2013;224(12):1714. https://doi.org/10.1007/s11270-013-1714-y.
40. Kabiri S, Centner M, McLaughlin MJ. Durability of sorption of per- and polyfluorinated alkyl substances in soils immobilised using common adsorbents: 1. Effects of perturbations in pH. Sci Total Environ. 2021;766:144857. https://doi.org/10.1016/j.scitotenv.2020.144857.
41. Kabiri S, McLaughlin MJ. Durability of sorption of per- and polyfluorinated alkyl substances in soils immobilized using common adsorbents: 2. Effects of repeated leaching, temperature extremes, ionic strength and competing ions. Sci Total Environ. 2021;766:144718. https://doi.org/10.1016/j.scitotenv.2020.144718.
42. Sörengard M, Kleja DB, Ahrens L. Stabilization and solidification remediation of soil contaminated with poly- and perfluoroalkyl substances (PFASs). J Hazard Mater. 2019;367:639–46. https://doi.org/10.1016/j.jhazmat.2019.01.005.
43. Hale SE, Arp HPH, Slinde GA, Wade EJ, Bjørseth K, Breedveld GD, et al. Sorbent amendment as a remediation strategy to reduce PFAS mobility and leaching in a contaminated sandy soil from a Norwegian firefighting training facility. Chemosphere. 2017;171:9–18. https://doi.org/10.1016/j.chemosphere.2016.12.057.
44. Kupryianchyk D, Hale SE, Breedveld GD, Cornelissen G. Treatment of sites contaminated with perfluorinated compounds using biochar amendment. Chemosphere. 2016;142:35–40. https://doi.org/10.1016/j.chemosphere.2015.04.085.
45. Brennan A, Moreno Jimnez E, Alburquerque JA, Knapp CW, Switzer C. Effects of biochar and activated carbon amendment on maize growth and the uptake and measured availability of polycyclic aromatic hydrocarbons (PAHs) and potentially toxic elements (PTEs). Environ Pollut. 2014;193:79–87. https://doi.org/10.1016/j.envpol.2014.06.016.
46. Vasilyeva GK, Strijakova ER, Nikolaeva SN, Lebedev AT, Shea PJ. Dynamics of PCB removal and detoxification in historically contaminated soils amended with activated carbon. Environ Pollut. 2010;158(3):770–7. https://doi.org/10.1016/j.envpol.2009.10.010.
47. Julien F, Baudu M, Mazet M. Relationship between chemical and physical surface properties of activated carbon. Water Res. 1998;32(11):3414–24. https://doi.org/10.1016/S0043-1354(98)00109-2.
48. Yu Q, Zhang R, Deng S, Huang J, Yu G. Sorption of perfluorooctane sulfonate and perfluorooctanoate on activated carbons and resin: Kinetic and isotherm study. Water Res. 2009;43(4):1150–1158. https://doi.org/10.1016/j.watres.2008.12.001.
49. Zhang D, Luo Q, Gao B, Chiang SYD, Woodward D, Huang Q. Sorption of perfluorooctanoic acid, perfluorooctane sulfonate and perfluoroheptanoic acid on granular activated carbon.

Chemosphere. 2016;144:2336–42. https://doi.org/10.1016/j.chemosphere.2015.10.124.
50. Sörengård M, stblom E, Khler S, Ahrens L. Adsorption behavior of per- and polyfluoralkyl substances (PFASs) to 44 inorganic and organic sorbents and use of dyes as proxies for PFAS sorption. J Environ Chem Eng. 2020;8(3):103744. https://doi.org/10.1016/j.jece.2020.103744.
51. Ochoa-Herrera V, Sierra-Alvarez R. Removal of perfluorinated surfactants by sorption onto granular activated carbon, zeolite and sludge. Chemosphere. 2008;72(10):1588–93. https://doi.org/10.1016/j.chemosphere.2008.04.029.
52. Tomczyk A, Sokołowska Z, Boguta P. Biochar physicochemical properties: Pyrolysis temperature and feedstock kind effects. Reviews in Environmental Science and Bio/Technology. 2020:1–25. https://doi.org/10.1007/s11157-020-09523-3.
53. Hagemann N, Spokas K, Schmidt HP, Kgi R, Bhler M, Bucheli T. Activated Carbon, Biochar and Charcoal: Linkages and Synergies across Pyrogenic Carbons ABCs. Water. 2018;10(2):182. https://doi.org/10.3390/w10020182.
54. Sarkar B, Rusmin R, Ugochukwu UC, Mukhopadhyay R, Manjaiah KM. Chapter 5 - Modified clay minerals for environmental applications. In: Mercurio M, Sarkar B, Langella A, editors. Modified Clay and Zeolite Nanocomposite Materials. 2019:113–127. https://doi.org/10.1016/B978-0-12-814617-0.00003-7.
55. Zhang R, Yan W, Jing C. Mechanistic study of PFOS adsorption on kaolinite and montmorillonite. Colloids Surf A Physicochem Eng Asp. 2014;462:252–8. https://doi.org/10.1016/j.colsurfa.2014.09.019.
56. Xiao F, Zhang X, Penn L, Gulliver JS, Simcik MF. Effects of monovalent cations on the competitive adsorption of perfluoroalkyl acids by Kaolinite: Experimental studies and modeling. Environ Sci Technol. 2011;45(23):10028–35. https://doi.org/10.1021/es202524y.
57. Aly YH, McInnis DP, Lombardo SM, Arnold WA, Pennell KD, Hatton J, et al. Enhanced adsorption of perfluoro alkyl substances for in situ remediation. Environ Sci Water Res Technol. 2019;5:1867–75. https://doi.org/10.1039/C9EW00426B.
58. Anderson EL, Mousavi MPS, Aly YH, Chen XV, Simcik MF, Bhlmann P. Remediation of perfluorooctylsulfonate contamination by in Situ Sequestration: Direct monitoring of PFOS binding to polyquaternium polymers. ACS Omega. 2019;4(1):1068–76. https://doi.org/10.1021/acsomega.8b03275.
59. Liu Y, Su G, Wang F, Jia J, Li S, Zhao L, et al. Elucidation of the molecular determinants for optimal perfluorooctanesulfonate adsorption using a combinatorial nanoparticle library approach. Environ Sci Technol. 2017;51(12):7120–7. https://doi.org/10.1021/acs.est.7b01635.
60. Li C, Schffer A, Squaris JM, Lszl K, Tth A, Tombcz E, et al. Surface-associated metal catalyst enhances the sorption of perfluorooctanoic acid to multi-walled carbon nanotubes. J Colloid Interface Sci. 2012;377(1):342–346. https://doi.org/10.1016/j.jcis.2012.03.038.
61. Liu L, Li D, Li C, Ji R, Tian X. Metal nanoparticles by doping carbon nanotubes improved the sorption of perfluorooctanoic acid. J Hazard Mater. 2018;351:206–14. https://doi.org/10.1016/j.jhazmat.2018.03.001.
62. Liu L, Liu Y, Li C, Ji R, Tian X. Improved sorption of perfluorooctanoic acid on carbon nanotubes hybridized by metal oxide nanoparticles. Environ Sci Pollut Res. 2018;25(16):15507–17. https://doi.org/10.1007/s11356-018-1728-5.
63. Heads of EPAs Australia and New Zealand (HEPA). PFAS National Environmental Management Plan Version 2.0; 2020.
64. Chen H, Reinhard M, Yin T, Nguyen TV, Tran NH, Gin KYH. Multi-compartment distribution of perfluoroalkyl and polyfluoroalkyl substances (PFASs) in an urban catchment system. Water Res. 2019;154:227–37. https://doi.org/10.1016/j.watres.2019.02.009.
65. Higgins CP, Luthy RG. Sorption of Perfluorinated Surfactants on Sediments. Environ Sci Technol. 2006;40(23):7251–6. https://doi.org/10.1021/es061000n.
66. Milinovic J, Lacorte S, Vidal M, Rigol A. Sorption behaviour of perfluoroalkyl substances in soils. Sci Total Environ. 2015;511:63–71. https://doi.org/10.1016/j.scitotenv.2014.12.017.
67. Campos Pereira H, Ullberg M, Kleja DB, Gustafsson JP, Ahrens L. Sorption of perfluoroalkyl substances (PFASs) to an organic soil horizon Effect of cation composition and pH. Chemosphere. 2018;207:183–91. https://doi.org/10.1016/j.chemosphere.2018.05.012.
68. Oliver DP, Li Y, Orr R, Nelson P, Barnes M, McLaughlin MJ, et al. The role of surface charge and pH changes in tropical soils on sorption behaviour of per-and polyfluoroalkyl substances (PFASs). Sci Total Environ. 2019;673:197–206. https://doi.org/10.1016/j.scitotenv.2019.04.055.
69. Qian J, Shen M, Wang P, Wang C, Hou J, Ao Y, et al. Adsorption of perfluorooctane sulfonate on soils: Effects of soil characteristics and phosphate competition. Chemosphere. 2017;168:1383–8. https://doi.org/10.1016/j.chemosphere.2016.11.114.
70. Li F, Fang X, Zhou Z, Liao X, Zou J, Yuan B, et al. Adsorption of perfluorinated acids onto soils: Kinetics, isotherms, and influences of soil properties. Sci Total Environ. 2019;649:504–14. https://doi.org/10.1016/j.scitotenv.2018.08.209.
71. Li Y, Oliver DP, Kookana RS. A critical analysis of published data to discern the role of soil and sediment properties in determining sorption of per and polyfluoroalkyl substances (PFASs). Sci Total Environ. 2018;628:110–20. https://doi.org/10.1016/j.scitotenv.2018.01.167.
72. Rayne S, Forest K. Perfluoroalkyl sulfonic and carboxylic acids: A critical review of physicochemical properties, levels and patterns in waters and wastewaters, and treatment methods. J Environ Sci Health A. 2009;44(12):1145–99. https://doi.org/10.1080/10934520903139811.
73. Du Z, Deng S, Bei Y, Huang Q, Wang B, Huang J, et al. Adsorption behavior and mechanism of perfluorinated compounds on various adsorbentsa review. Journal of Hazardous Materials. 2014;274:443–54. doi: https://doi.org/10.1016/j.jhazmat.2014.04.038.
74. Campos-Pereira H, Kleja DB, Sjstedt C, Ahrens L, Klysubun W, Gustafsson JP. The Adsorption of Per- and Polyfluoroalkyl Substances (PFASs) onto Ferrihydrite Is Governed by Surface Charge. Environ Sci Technol. 2020;54(24):15722–30. https://doi.org/10.1021/acs.est.0c01646.
75. Arp HPH, Niederer C, Goss KU. Predicting the Partitioning Behavior of Various Highly Fluorinated Compounds. Environ Sci Technol. 2006;40(23):7298–304. https://doi.org/10.1021/es060744y.
76. Liu L, Liu Y, Gao B, Ji R, Li C, Wang S. Removal of perfluorooctanoic acid (PFOA) and perfluorooctane sulfonate (PFOS) from water by carbonaceous nanomaterials: A review. Crit Rev Environ Sci Technol. 2020;50(22):2379–414. https://doi.org/10.1080/10643389.2019.1700751.
77. Ebrahimi F, Lewis AJ, Sales CM, Suri R, McKenzie ER. Linking PFAS partitioning behavior in sewage solids to the solid characteristics, solution chemistry, and treatment processes. Chemosphere. 2021;271:129530. https://doi.org/10.1016/j.chemosphere.2020.129530.
78. Xiao F, Jin B, Golovko SA, Golovko MY, Xing B. Sorption and Desorption Mechanisms of Cationic and Zwitterionic Per- and Polyfluoroalkyl Substances in Natural Soils: Thermodynamics and Hysteresis. Environ Sci Technol. 2019;53(20):11818–27. https://doi.org/10.1021/acs.est.9b05379.
79. MacKay AA, Gschwend PM. Enhanced Concentrations of PAHs in Groundwater at a Coal Tar Site. Environ Sci Technol. 2001;35(7):1320–8. https://doi.org/10.1021/es0014786.

80. Lead JR, Wilkinson KJ. Aquatic colloids and nanoparticles: current knowledge and future trends. Environ Chem. 2006;3(3):159–71. https://doi.org/10.1071/EN06025.
81. Zhou J, Fileman T, Evans S, Donkin P, Readman J, Mantoura R, et al. The partition of fluoranthene and pyrene between suspended particles and dissolved phase in the Humber Estuary: a study of the controlling factors. Sci Total Environ. 1999;243:305–21. https://doi.org/10.1016/S0048-9697(99)00404-0.
82. Sen TK, Khilar KC. Review on subsurface colloids and colloid-associated contaminant transport in saturated porous media. Adv Colloid Interf Sci. 2006;119(2–3):71–96. https://doi.org/10.1016/j.cis.2005.09.001.
83. Benhabib K, Simonnot MO, Faure P, Sardin M. Evidence of colloidal transport of PAHs during column experiments run with contaminated soil samples. Environ Sci Pollut Res. 2017;24(10):9220–8. https://doi.org/10.1007/s11356-017-8586-4.
84. Eganhouse RP, DiFilippo E, Pontolillo J, Orem W, Hackley P, Edwards BD. DDT and related compounds in pore water of shallow sediments on the Palos Verdes Shelf, California, USA. Mar Chem. 2018;203:78–90. https://doi.org/10.1016/j.marchem.2018.05.003.
85. Valsala R, Govindarajan SK. Co-colloidal BTEX and Microbial Transport in a Saturated Porous System: Numerical Modeling and Sensitivity Analysis. Transp Porous Media. 2019;127(2):269–94. https://doi.org/10.1007/s11242-018-1191-2.
86. Dai G, Liu X, Liang G, Han X, Shi L, Cheng D, et al. Distribution of organochlorine pesticides (OCPs) and poly chlorinated biphenyls (PCBs) in surface water and sediments from Baiyangdian Lake in North China. J Environ Sci. 2011;23(10):1640–1649. https://doi.org/10.1016/S1001-0742(10)60633-X.
87. Lin Q, Xu X, Bao Q, Oh K, Chen D, Zhang L, et al. Influence of water-dispersible colloids from organic manure on the mechanism of metal transport in historically contaminated soils: coupling colloid fractionation with high-energy synchrotron analysis. J Soils Sediments. 2016;16(2):349–59. https://doi.org/10.1007/s11368-015-1233-0.
88. U S EPA. Leaching Environmental Assessment Framework (LEAF) How-To Guide, SW-846 Update VII Rev. 1. U.S. Environmental Protection Agency; 2019.
89. Alexander M. Aging, Bioavailability, and Overestimation of Risk from Environmental Pollutants. Environ Sci Technol. 2000;34(20):4259–65. https://doi.org/10.1021/es001069+.
90. Ross I, Houtz E, Kalve E, McDonough J, Hurst J, Miles J. PFASs and the TOP Assay. Industrial Fire Journal. 2018;Q1:26–7.

Publisher's Note Springer Nature remains neutral with regard to jurisdictional claims in published maps and institutional affiliations.

Part I

Modelling

Overview

Part I of the thesis comprises of two closely-linked chapters on Monte Carlo molecular modelling. Chapter 3 presents an overview of the modelling methodology, detailed results and discussion of a series of simulations with PFOS and PFBS interacting with a graphite surface. These simulations included differing surface charges and solution chemistry, and results were interpreted against both experimental results and theoretical expectation.

Chapter 4 describes in detail the functionality, implementation and underlying theory of the original software, R-MCMolecSim, developed for these simulations. This includes additional theoretical work devised for numerical calculation of long-range interactions. The visualisation capabilities of R-MCMolecSim are illustrated using a set of additional simulations undertaken with PFOA and PFDA.

Chapter 3

Modelling of PFAS-surface interactions: Effect of surface charge and solution ions

It was shown that immobilisation of PFAS in soils varies in a complex fashion with amendment composition, experimental conditions and PFAS molecular structure. At the molecular level, immobilisation is governed by the sorption of PFAS molecules to the constituent materials of immobilisation agents and soils. Following the finding that activated carbon based amendments were the best performing in terms PFAS immobilisation efficacy, it was of interest to study the interactions between PFAS molecules and carbon surfaces in more detail.

A Monte Carlo molecular simulation approach was utilised to simulate and subsequently analyse a series of systems consisting of either 16 PFBS molecules or 16 PFOS molecules and a carbon (graphite) surface to determine the influence of molecule size, surface charge, and solution chemistry (H^+, OH^-, and Ca^{2+} ions) on sorption to a carbon surface. PFOS was selected being one of the most prevalent and regulated PFAS, with PFBS chosen to examine the effect of C chain length while retaining the same functional group. This required the development of bespoke software and development of parts of the underlying theory. This allowed not only simulation with the required properties to be run, but the relative contributions of the van der Waals and electrostatic interactions to the overall potential to be quantified.

Results were interpreted with reference to theoretical expectations, experimental results from literature, and results of other published simulation studies. The main finding was the importance of surface charge in PFSA sorption. Simulation results were also affected to a lesser extent by changes in molecule size, H^+, OH^- and Ca^{2+} concentrations. The role of divalent cation bridging via Ca^{2+} and electrolytic screening were also compared and discussed.

This chapter was published in Chemosphere, as "Modelling of PFAS-Surface Interactions: Effect of Surface Charge and Solution Ions".[1] Supplementary information, published along side this chapter, is located in Appendix A, and the relevant code is provided in Appendix E.

[1]Reprinted courtesy of Elsevier, Chemosphere (See Appendix F for further details).

Chemosphere 319 (2023) 137910

Contents lists available at ScienceDirect

Chemosphere

journal homepage: www.elsevier.com/locate/chemosphere

Modelling of PFAS-surface interactions: Effect of surface charge and solution ions

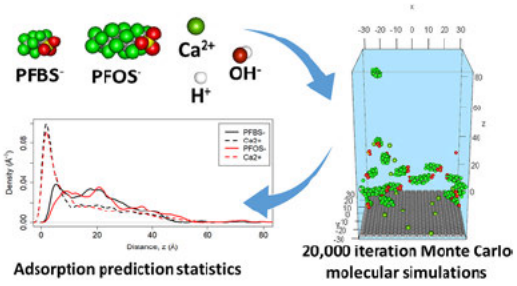
Julie A. Sleep [a,*], Stanley J. Miklavcic [b], Albert L. Juhasz [a]

[a] Future Industries Institute, University of South Australia, Mawson Lakes, SA, 5095, Australia
[b] Phenomics and Bioinformatics Research Centre, University of South Australia, Mawson Lakes, SA, 5095, Australia

HIGHLIGHTS

- Monte carlo molecular simulation of PFOS and PFBS interacting with graphite in an aqueous medium performed.
- Interactions with surface varied with surface charge, H+, OH- and Ca2+ concentrations.
- Surface charge played an important role, divalent cation bridging observed with negative surfaces.

GRAPHICAL ABSTRACT



ARTICLE INFO

Handling Editor: Junfeng Niu

Keywords:
PFAS
Molecular simulation
Surface interactions
Intermolecular forces

ABSTRACT

Per-: and poly-fluoroalkyl substances (PFAS) are a class of substances of increasing concern as environmental contaminants. The interactions between PFAS and surfaces play an important role in PFAS transport and remediation. Previous studies have found PFAS adsorption to be dependent upon properties including pH, organic matter and particle size, along with PFAS functional group and carbon chain length. It is hypothesised that a theoretical examination of PFAS-surface interactions, via Monte Carlo molecular simulation, would show differences resulting from changes in surface charge, H^+, OH^-, Ca^{2+} concentrations and PFAS carbon chain length. Monte Carlo molecular simulations of perfluorooctane and perfluorobutane sulfonic acids interacting with a graphite surface in an aqueous medium were performed. Variations in surface charge, H^+, OH^- and Ca^{2+} concentrations were made. The distance-dependent density of molecules from the surface was analysed as a proxy for PFAS adsorption to the surface. Simulation results showed differences in surface behaviour that depended on surface charge, H^+, OH^- and Ca^{2+} concentrations, along with carbon chain length, with surface charge playing the most prominent role in controlling PFAS adsorption. For negatively charged surfaces, adsorption due to divalent cation bridging was observed in Ca^{2+} solutions. Modelling, such as in this study, of the thermodynamic equilibrium behaviour of low concentrations of molecules, in scenarios where both adsorption and mobility of PFAS occur, can aid in the design and testing of sorptive surfaces for amendment-based PFAS remediation.

Abbreviations: Per- and poly-fluoroalkyl substances, (PFAS); perfluorooctanoic acid, (PFOA); perfluorooctane sulfonic acid, (PFOS); perfluorohexanoic acid, (PFHxA); perfluorohexane sulfonic acid, (PFHxS); perfluorobutane sulfonic acid, (PFBS); perfluorinated sulfonic acids, (PFSAs); perfluorinated carboxylic acids, (PFCAs).

* Corresponding author.
E-mail addresses: julie.sleep@mymail.unisa.edu.au (J.A. Sleep), stan.miklavcic@unisa.edu.au (S.J. Miklavcic), albert.juhasz@unisa.edu.au (A.L. Juhasz).

https://doi.org/10.1016/j.chemosphere.2023.137910
Received 17 August 2022; Received in revised form 1 December 2022; Accepted 17 January 2023
Available online 24 January 2023
0045-6535/© 2023 The Authors. Published by Elsevier Ltd. This is an open access article under the CC BY-NC-ND license (http://creativecommons.org/licenses/by-nc-nd/4.0/).

1. Introduction

Per- and poly-fluoroalkyl substances (PFAS) are emerging as a class of substances of increasing concern as environmental contaminants, which are found in a range of fire-fighting, household and other products (Kotthoff et al., 2015). They consist of either a completely or partially fluorinated carbon backbone and a functional group that is often a carboxylic or sulfonic acid. The adsorption of PFAS onto surfaces, for example soil or sediment particles, is a contributing factor to their fate and transport in the environment (Zareitalabad et al., 2013). Suspended particles are common PFAS carriers in aqueous environments (Chen et al., 2019), while adsorption is also an important mechanism for the development of remediation strategies to minimise PFAS exposure (Du et al., 2014). At environmental pH, the most common PFAS such as perfluorinated sulfonic acids (PFSAs) are usually anionic (Barzen-Hanson et al., 2017) and thus adsorption onto particles is thought to occur through one of two predominant mechanisms (Li et al., 2018). Adsorption may occur through direct attractive electrostatic interaction with positively charged soil surfaces. On the other hand, adsorption onto negatively charged soil surfaces may also occur in the presence of divalent cations through divalent cation bridges (Li et al., 2018). Hydrophobic effects, responsible for aggregate formation, may also influence adsorption, while van der Waals interactions and H-bonding were thought to be insignificant (Li et al., 2018; Du et al., 2014).

PFAS functional groups and their carbon backbone lengths are both factors influencing adsorption. For instance, PFSAs are more readily adsorbed than perfluorinated carboxylic acids (PFCAs) (Du et al., 2014). For example, perfluorooctane sulfonic acid (PFOS) and perfluorohexane sulfonic acid (PFHxS) have been found to adsorb to a greater extent than perfluorooctanoic acid (PFOA) and perfluorohexanoic acid (PFHxA) on hematite, kaolinite and montmorillonite surfaces (Zhao et al., 2014). Greater adsorption has also been observed with increasing carbon chain length, which may result from enhanced hydrophobic effects, which contribute to the adsorption process (Du et al., 2014). In (Li et al., 2019), it was found that the longer chain PFAS had a greater propensity to adsorb to soil, and those with a sulfonate functional group adsorbed to a greater extent than did those with a carboxyl functional group. It has also been observed that PFAS with carbon chain lengths of 10 or more were more likely to be present on suspended particles, while those with chains shorter than seven carbon units were more likely to be dissolved in the aqueous phase (Chen et al., 2019).

Coupled with the molecular properties of PFAS, the sorbent surface also plays an important role in PFAS adsorption. Studies found that negatively charged hematite had a greater adsorption capacity for PFOS, PFOA, PFHxS and PFHxA, compared to (negatively charged) kaolinite and (positively charged) montmorillonite (Zhao et al., 2014). When organic constituents were present, PFAS adsorption increased with organic carbon concentration (Anderson et al., 2019; Jeon et al., 2011), giving evidence for hydrophobic effects, while increased adsorption with increasing salt concentrations, provides evidence for electrostatic interactions influencing the degree of adsorption (Jeon et al., 2011).

With regard to solution pH, varying pH affects absorption behaviour by altering the state of charge of both the molecules and the surface. It is generally observed that increasing pH results in decreased PFAS adsorption, though increasing pH can also create more basic sites for divalent cation bridging, and thus contribute to an increase in adsorption of anionic PFAS (Du et al., 2014). On the other hand, cationic PFAS may adsorb more readily to negatively charged surfaces under high pH conditions. However, many additional factors come into play in complex environmental settings, though less adsorption to particles is often observed in environmental sampling at higher pH. For instance, adsorption kinetics are strongly influenced by the number and size of pores and the diameter of the adsorbent particles (Du et al., 2014).

Molecular modelling can help to understand and even quantify PFAS adsorption behaviour. Its benefits include insights into adsorption mechanisms, the role played by molecular structure and charge, along with the roles of surface and medium properties. Simulation outcomes can even be of use in the prediction of the environmental fate of PFAS, and the design of amendments for remediation. A small number of works involving theoretical modelling of PFAS molecules interacting with surfaces have been carried out to date.

A molecular dynamics study (He et al., 2013) of PFOS in an aqueous electrolyte solution containing K^+ ions in the presence of a TiO_2 surface showed a difference in adsorption behaviour at different crystal planes. It also showed that sulfonate head groups formed bridges with the surface via K^+ ions. A subsequent study (He et al., 2015) extended this work to examine the effect of different PFOS concentrations as well as the effect of Ca^{2+} on the structural assembly at the TiO_2 surface. Another molecular dynamics study (Zhang et al., 2015) involved PFOS interacting with a SiO_2 surface, including a layer of either hexane, butyl benzene or butyl benzoic acid. The study found that both inorganic and organic substances played a role in surface adsorption of PFOS.

In this paper, we report on a complementary theoretical investigation of PFAS adsorption behaviour onto graphite surfaces from an aqueous solution. In contrast to earlier work (He et al., 2013, 2015; Zhang et al., 2015), we focus on adsorption behaviour at equilibrium. Using the Monte Carlo molecular simulation method to describe the equilibrium statistical mechanics properties of this system, we study the effect on adsorption of PFAS chain length, surface charge as well as solution concentration of H^+, OH^- and Ca^{2+}.

2. Materials and methods

2.1. Monte Carlo simulations

The Monte Carlo simulation method was employed to calculate the equilibrium statistical properties of the system. This choice of method was motivated by the advantages of collecting equilibrium statistics of a dynamic system involving both adsorption and desorption processes. An ensemble of molecular configurations of the system was generated (and statistics collected) by randomly translating and rotating each of a finite number N of PFAS molecules and simple ionic species. With each random translation and rotation of a solute molecule, and random translation of a mobile ion, the change in total system energy, Δw, is determined. As described in (Hansen and McDonald, 1986), if the system energy change, following a translation or rotation, is negative (indicating a more favourable configuration), the new configuration is accepted. If the energy change is positive (a less favourable configuration), the new configuration is also accepted but with probability

$$p_a = e^{-\beta \Delta w} \tag{1}$$

where

$$\beta = \frac{1}{k_B T} \quad ,$$

k_B is the Boltzmann constant and T is temperature in Kelvin.

Statistics on the molecule positions and orientations are collected for each accepted new configuration. To avoid (or reduce the likelihood of) any dependence on the initial starting position, a significant number (2500 per molecule) of translation and rotations were performed during a so-called equilibration stage, with no statistics collected during this phase. The results shown here were based on data collected during the subsequent production stage.

The initial simulation box size was 60 × 60 × 60 Å, containing 16 PFBS or PFOS molecules, up to 32 additional ions (H^+, OH^- and/or Ca^{2+}) and implicit water throughout box. A layer of 1397 carbon atoms, arranged in the structure and atomic separation of graphite make up one wall of the box at $z = 0$. The water in the box extends infinitely in the z direction, so molecules are unrestricted in how far they can move away from the surface. Periodic boundary conditions were implemented in relation to molecular moves in the lateral directions. That is, any

molecules or atoms thereof that move outside of the sides of the box, are translated to their periodic reflection in the original box.

The surface charges considered were $\sigma_{surf} = 0$, 16/3600 e/Å^2, +16/3600 e/Å^2 and +32/3600 e/Å^2. The 2D structures of PFBS and PFOS are shown in Fig. 1(a) and (b), respectively. The 3D molecular structural coordinates (Gindulyte et al., 2019), partial charges (Gindulyte et al., 2019; Ionescu et al., 2015), and OPLS-AA based Lennard-Jones parameters (Hardacre et al., 2010; Van Der Spoel et al., 2005; Lin and Heinz, 2016) are listed in Supplementary Tables S1–S2. Lennard-Jones parameter estimates were obtained for the graphite surface (Song and Cappelletti, 1994; Klapetek, 2012) and mobile ions (Lin and Heinz, 2016; Van Der Spoel et al., 2005) ions. The translation step size was 0.5 Å, while the angular rotation change was randomly selected between 5 and 5° for rotation about each of the axes, x, y and z. All scenarios considered were electro-neutral.

2.2. Intermolecular potential calculations

In our simulations we considered only pairwise intermolecular potential calculations between atomic species. Although the PFAS molecules are finite in size and comprise multiple interaction sites, the concentration of the molecules themselves is dilute. Consequently, we anticipate that intermolecular interactions will be dominated by these two-body terms, particularly the long-ranged, Coulomb interactions, and hence we do not calculate three body and higher order interactions. Interactions between molecular species in solution as well as between solution molecules and the surface were treated at the atomic level. That is, on the one hand the interaction between a pair of PFAS molecules was taken to be the sum of pairwise interactions between atoms on opposing molecules. On the other hand, the interaction between a PFAS molecule and the surface was similarly taken as the sum of pair interactions between atomic sites on the molecule with all atomic sites defining the surface. All atomic site-atomic site potentials were modelled as the sum of a Coulomb potential, a van der Waals potential, and a long-range interaction:

$$w(r_{ij}) = w_C(r_{ij}) + w_{vdw}(r_{ij}) + w_{ext} \tag{2}$$

The effects of water were incorporated via the use of implicit water with dielectric screening.

2.3. Short-range electrostatic interactions

The dielectric-screened Coulomb potential was given by the expression (Israelachvili, 2011)

$$w_C(|\mathbf{r}_i \quad \mathbf{r}_j|) = \frac{q_i q_j}{4\pi\epsilon_0\epsilon_r|\mathbf{r}_i \quad \mathbf{r}_j|} = \frac{q_i q_j}{4\pi\epsilon_0\epsilon_r r_{ij}} \tag{3}$$

where $r_{ij} = |\mathbf{r}_i \quad \mathbf{r}_j|$ is the distance between the atoms at positions $\mathbf{r}_i$ and $\mathbf{r}_j$, q_i and q_j are the charges on atoms i and j, $\epsilon_0 = 8.8542 \times 10^{12}$ C^{2}N^{1}m^{2} is the vacuum permittivity, and ϵ_r is the relative permittivity of the aqueous medium.

2.4. van der Waals interaction

The van der Waals interaction was modelled by the standard 6–12 Lennard-Jones potential (Israelachvili, 2011), involving an atom-atom repulsion and an atom-atom dispersion attraction. This is expressed in the form

$$w_{vdw}(r_{ij}) = 4\epsilon_{ij}\left[\left(\frac{\sigma_{ij}}{r_{ij}}\right)^{12} \quad \left(\frac{\sigma_{ij}}{r_{ij}}\right)^{6}\right] \tag{4}$$

where ϵ_{ij} refers to the maximum energy of attraction (or 'well depth') in J and σ_{ij} is the separation at which the potential energy for atoms i and j is zero.

Intramolecular interactions, i.e., interactions between atoms within any given molecule were not included since the molecules (and surface) were assumed to be in a state of fixed internal conformation. This assumption is appropriate for PFOS, PFBS as well as other small counterions. Since intermolecular and molecule-surface interactions are treated as sums of interatomic Coulomb, dispersion and hard-sphere interactions, we do not include angular dependent interactions (such as charge-dipole, dipole-dipole and dipole-quadropole) (Hirschfelder et al., 1954) or dipole-surface interactions (Miklavcic, 1997). We assume the effects of the latter to be captured in the simulation process as different molecular orientations are sampled.

2.5. Long-range electrostatic interactions

The system under study assumes an infinite extent in the lateral direction parallel to the surface. Consequently, in addition to the direct and explicit interaction between any given atomic site and all other atoms within the simulation box, each charge site experiences an interaction with the total charge distribution outside the box (both surface and solution charges). It is impractical to evaluate explicitly this external interaction contribution, w_{ext}, which is to be added to the right hand side of Eq (2). Instead, we assume that the charge distribution outside the simulation box takes the form of the simulated equilibrium distribution generated by the mobile charges inside the box. This net mobile charge distribution, denoted $\rho_{eq}(z)$, which will be a function only of distance z from the surface, is combined with the smoothed out surface charge density, σ_{surf}, confined to the plane of the surface at $z = 0$. The external interaction potential experienced by a charge site, q_i, at a height, z_i, is given by the triple integral

$$w_{ext}(z_i) = 8\int_0^{\infty}\left[\frac{\rho_{eq}(z) + \sigma_{surf}\delta(z)}{4\pi\epsilon_0\epsilon_r} \times \int_0^{\pi/4}\left(\int_{b/\cos\theta}^{\infty}\frac{r\mathrm{d}r}{\sqrt{r^2 + (z \quad z_i)^2}}\right)\mathrm{d}\theta\right]\mathrm{d}z, \tag{5}$$

which effectively expresses the sum of all interactions from surface and

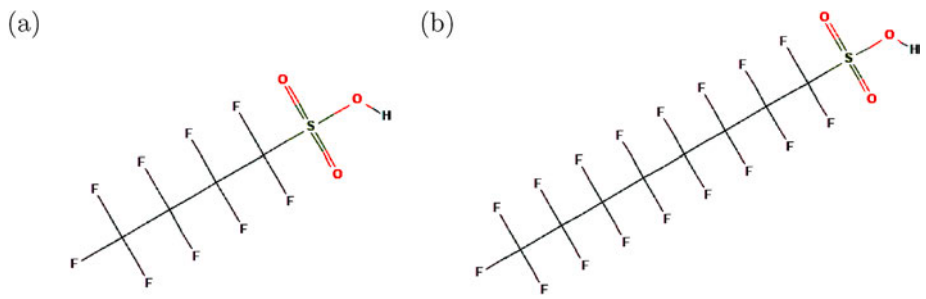


Fig. 1. (a) Structure of PFBS, CAS number 375-73-5 (Gindulyte et al., 2019). (b) Structure of PFOS, CAS number 1763-23-1 (Gindulyte et al., 2019). 3D structure coordinates given in Supplementary Tables S1 and S2.

distributed charges outside the box, from all eight half-quadrant sectors about the central charge. This integral is in line with the proposed external field contribution of (Jönsson et al., 1980). To simplify the calculations we replace the above integral for the external volume beyond the $2b \times 2b$ box, with an integral for an equivalent cylindrical external volume of minimum radius $a = 2b/\sqrt{\pi}$ measured from the central ion:

$$w_{ext}(z_i) = \int_0^{\infty} \left[\frac{\rho_{eq}(z) + \sigma_{surf}\delta(z)}{4\pi\epsilon_0\epsilon_r} \int_0^{2\pi} \left(\int_a^{\infty} \frac{r\mathrm{d}r}{\sqrt{r^2 + (z \quad z_i)^2}} \right) \mathrm{d}\theta \right] \mathrm{d}z. \qquad (6)$$

Since the charge distribution does not depend on angle, the θ integral can be performed explicitly. Moreover, utilizing the properties of the δ-function, a further integration of the surface term can be performed. The final expression implemented in this paper is

$$w_{ext}(z_i) = \frac{1}{2\varepsilon_0\epsilon_r} \left[\sigma_{surf} \int_a^{\infty} \frac{r\mathrm{d}r}{\sqrt{r^2 + z_i^2}} + \int_0^{\infty} \left(\rho_{eq}(z) \int_a^{\infty} \frac{r\mathrm{d}r}{\sqrt{r^2 + (z \quad z_i)^2}} \right) \mathrm{d}z \right]. \qquad (7)$$

The remaining integrals have been evaluated numerically using the trapezoidal rule over a radial range from $r_0 = round(a)$ to $r_{\max} = 10,000$ Å, in radial steps of $\Delta r = 10$ Å, and steps of $\Delta z = 1$ Å in the z-direction. The results of these calculations, based on an equilibrium charge distribution resulting from an initial, external potential-free, production simulation of 20,000 iterations per molecule, are shown in panels (e) and (f) of Supplementary Figs. S4–S11. It is clear from these that the above choice of $r_{\max}$ is sufficient to capture the effective range of the external field. Subsequent production simulations of 20,000 iterations per molecule incorporating these potentials were performed to include the effect of the external field. The results of these production runs are shown in Section 3.

2.6. Implementation and computation

All code was written in the R statistical programming language (R Core Team, 2018), and the simulation was performed using R v4.0.0, under Red Hat Enterprise Linux Server V 7.7 (64-bit). Production runs of 20,000 iterations per molecule were performed, with running time between 18 and 48 h, dependent on the size and number of molecules and ions present in the simulation. The Lennard-Jones and Coulomb interactions were non-truncated, which was computationally possible due to the range of the potential relative to the box size. Similarly, for each potential calculation periodic conditions were assumed centred on the molecule in question (x and y directions). Contributions to the total energy of the system included all intermolecular van der Waals and Coulomb interactions between all atoms (surface and mobile) according to the minimum image convention. Probability density functions were calculated using the R function 'density' with a bandwidth of 1 Å. Information on the system treated in each simulation run is listed in Table 1.

3. Results and discussion

In our investigation we considered a number of different scenarios to reflect the different situations studied experimentally. Bearing in mind that PFAS encounter a broad spectrum of surfaces in real-world situations, we considered the effect of surface charge on the extent of PFAS adsorption. The charge state of the PFAS molecules relative to the state of surface charge will naturally be a key factor in governing the degree of adsorption. It will either act in opposition to or in conjunction with van der Waals effects. In Section 3.1 we discuss the adsorption behaviour for a neutral surface, both with neutral and negatively charged PFAS. Next, in Sections 3.2 and 3.3 we study the respective systems of PFAS near a positively charged surface and a negatively charged surface. In each case, counterion species are included to balance the charges on either PFAS or the charged surface. As *in situ* PFAS solution systems invariably contain added electrolytes, we are also interested in the influence of additional mobile ions on adsorption behaviour. To this end, we include in our simulation study cases involving added monovalent ions, and divalent cations within the confines of our simulation model. We examine the role of these ions, looking for evidence of activity beyond simple electrolyte screening, such as cation bridging of PFAS molecules to surface molecules.

In this work, we present results in terms of the thermodynamic equilibrium, inhomogeneous PFAS molecular density, as a function of distance from the surface. We also show a few snapshots of configurations taken during the equilibration stage of the simulation, to emphasize points of our discussion. Additional snapshots are included in the Supplementary Information.

Table 1
Details of the system set up for the 12 different simulation scenarios featuring either uncharged PFOS and PFBS molecules, or $PFOS^-$ and $PFBS^-$ anions. The number of PFAS molecules, n_{PFAS}, the number of hydrogen counterions, n_H^+, hydroxide ions n_{OH}^-, and calcium divalent cations n_{Ca}^{2+}, are listed along with the surface charge, σ_{surf}.

Figures	PFAS	n_{PFAS}	n_H^+	n_{OH}	n_{Ca}^{2+}	σ_{surf} (e/Å^2)
Fig. 2(a)	PFOS	16	0	0	0	0
	PFBS	16	0	0	0	0
Fig. 2(b)	PFOS	16	16	0	0	0
	PFBS	16	16	0	0	0
Figs. 3(a) and 4(a)	PFOS	16	0	0	0	$+\frac{16}{3600}$
	PFBS	16	0	0	0	$+\frac{16}{3600}$
Figs. 3(b) and 4(b)	PFOS	16	0	16	0	$+\frac{32}{3600}$
	PFBS	16	0	16	0	$+\frac{32}{3600}$
Figs. 3(c) and 4(c)	PFOS	16	8	8	0	$+\frac{16}{3600}$
	PFBS	16	8	8	0	$+\frac{16}{3600}$
Figs. 3(d) and 4(d)	PFOS	16	16	16	0	$+\frac{16}{3600}$
	PFBS	16	16	16	0	$+\frac{16}{3600}$
Figs. 5(a) and 6(a)	PFOS	16	32	0	0	$\frac{16}{3600}$
	PFBS	16	32	0	0	$\frac{16}{3600}$
Figs. 5(b) and 6(b)	PFOS	16	0	0	16	$\frac{16}{3600}$
	PFBS	16	0	0	16	$\frac{16}{3600}$
Figs. 6(c) and 7(a)-(d)	PFOS	32	0	0	0	$\frac{16}{1800}, 0$
	PFBS	16	0	0	16	$\frac{16}{1800}, 0$

3.1. Neutral surface and molecules

Although usually in a dissociated state under normal pH conditions, it proves to be instructive to first consider the case of neutral molecules (and neutral surface) in order to establish a point of reference or benchmark from which to understand the case of charged molecules. Fig. 2(a) shows the ensemble average (i.e. equilibrium) molecular distribution (Å ^{3}) as a function of distance from the surface to the centre of the molecules. This distribution is equivalently defined as the thermodynamic probability of finding the centre of a given PFAS molecule at a distance z from the surface plane.

When the surface is uncharged, the molecules interact with the surface only through van der Waals potentials. Naturally, there remain

the electrostatic attractions between partially charged groups on different molecules. In the absence of any net intermolecular electrostatic repulsion, the electrostatic interactions between partial charges are likely to result in a thermodynamic equilibrium that is governed by attractive dipole-dipole interactions. The major repulsive contributor is then the very short-ranged Lennard-Jones repulsion. Consequently, one can appreciate the accumulation at the surface (in both cases of molecule) as well as a second layer of PFBS at around 40–60 Å: the inner-most adsorbed layer is more tightly bound, with the shorter chained PFBS positioned closer to the surface. The intermolecular repulsions limit the build-up of this first layer of molecules and instead induces the build-up of a second layer, at around 50 Å. This excluded volume phenomenon is commonly seen in hard sphere systems or systems with a strong (short-ranged) repulsive interaction (Israelachvili, 2011). In the case of the longer-chained PFOS, its rigid, lengthy 8 carbon chain prevents the build-up of a tightly bound inner-most layer under these conditions. This arises as much from energetic as from entropic considerations.

When the PFAS molecules are in a dissociated state (a net valence of 1), net electrostatic forces become the dominant intermolecular repulsions. Being of much longer range than the Lennard Jones repulsions, these Coulomb repulsions further limit the clustering of molecules at the surface. This is demonstrated in Fig. 2(b) which shows less pronounced and broader peaks in the density distribution of PFBS adjacent to the surface with little or no distinct layer present. As the surface itself remains neutral in this system, it is clear that the effect is largely due to intermolecular interactions. The neutralizing counterions contribute to the screening of the Coulomb repulsions between the larger PFBS (or PFOS) anions, as can be seen by the responsive H^+ concentration profile. Comparing the PFBS and PFOS density profiles, it would appear that the Coulomb repulsions between the molecules act as an equaliser, putting the shorter chain PFBS on equal footing with the longer chained PFOS . In other words, the electrostatic repulsion dominates over any energetic or configurational influence of the chains.

3.2. Positively charged surfaces

Although a somewhat artificial scenario, the case of a positively charged surface with a solution of neutralizing PFAS anions provides an interesting comparison. In contrast to the preceding case the attractive molecule-surface Coulomb interaction more than compensates for the intermolecular repulsion. The effect (which is the most marked of all cases studied, in that it has the highest density of ions close to the surface) is the result of the system's tendency to sample preferentially the energetically favourable positions close to the surface, instead of the entropically favourable bulk solution. The curves in Fig. 3 attest to the decisive influence of the molecule-surface attraction. This is based partly on the fact that both PFOS and PFBS show very similar behaviour (again, despite their size differences), and partly on the fact that the curves exhibit fewer and less pronounced fluctuations. We remark that in the case in Fig. 3(a) there is no mobile ion screening of either the intermolecular or molecule-surface interactions. Electrostatic screening by a low concentration of simple monovalent ions, shown in Fig. 3(b) would have little net effect as it would reduce the molecule-surface electrostatic attraction at the same time as reducing the electrostatic repulsion between the PFAS molecules. The importance of surface charge for sorption on positively charge surfaces is in agreement with the experimental study of (Campos-Pereira et al., 2020), on Ferrihydrite, where it was found that the surface charge was the governing factor in PFAS sorption rates.

Since it is invariably the case that a physical system will also contain a free electrolyte, it is interesting to see how simple mobile ions might affect the adsorption potential of PFAS ions. In Fig. 3(c) and (d) we illustrate the possible response to an added electrolyte under two concentration conditions. One low and one higher concentrations were chosen, shown in Fig. 3 (b) and (c), and can be compared with the zero concentration of Fig. 3(a). In Fig. 3(c) mobile ions are seen to effect a reduction in the densities of PFOS and PFBS equally, allowing the negatively charge OH ions to build up a diffuse layer adjacent to the surface. The positively charged ions in turn create a diffuse layer outside of the compact PFAS layer. It is interesting that the size of the PFAS molecule has an influence on the extent of surface-screening by the simple counterions. In the case of the larger PFOS molecule, volume exclusion is likely the reason for the smaller peak of the OH distribution.

Doubling the concentration of mobile ions appears to have several interesting coordinated effects. Not only do the mobile ions screen the surface, they also effectively screen the PFAS ions. In the case of the larger PFOS molecule, the surface screening reduces the energetic attraction with the surface, swinging the balance in favour of greater entropic freedom (and reduced intermolecular repulsion) away from the surface. In conjunction with this (and the ensuing reduced excluded volume restriction), the simple ions distribute in much the same way as they do in the presence of PFBS . The slight increase in the peak in the density of adsorbed PFBS molecules, is likely due to a reduced electrostatic repulsion between the molecules, allowing more to be closer to the surface. Support for this hypothesis can be found in the increased activity of the mobile cations within the same region occupied by the PFBS layer, and in the absence of a substantial cation density within the PFOS layer.

The effects of surface charge, volume exclusion and increase in electrolyte concentrations discussed above, are also clearly observed in the corresponding snapshots of the molecular simulations for PFOS in Fig. 4. Those for PFBS can be found in Supplementary Figs. S14–17.

3.3. Negatively charged surfaces

Fig. 5(a) and (b) present results of simulations of systems comprising negatively charged surfaces and solutions of net negatively charged PFAS molecules, plus either H^+ or Ca^{2+} counterions. These conditions are arguably more likely to occur in real world experimental scenarios than positive surface charges. Under common pH conditions found in nature, most surfaces in contact with aqueous solutions will be negatively charged, consequently the behaviour of PFAS molecules in the presence of a negatively charged surface is of significant practical

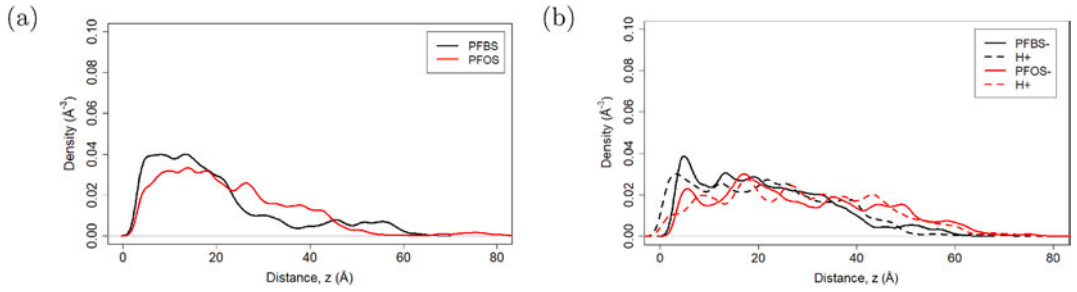


Fig. 2. Inhomogeneous density distributions of PFAS molecules, PFOS (——), PFBS (——) as a function of distance (in z direction in Å) of centre of molecule from an uncharged surface. PFAS molecules and surface are assumed net neutral. (a) Solution contains no additional ions. (b) Solution contains 16 H^+ counterions (– –, – –).

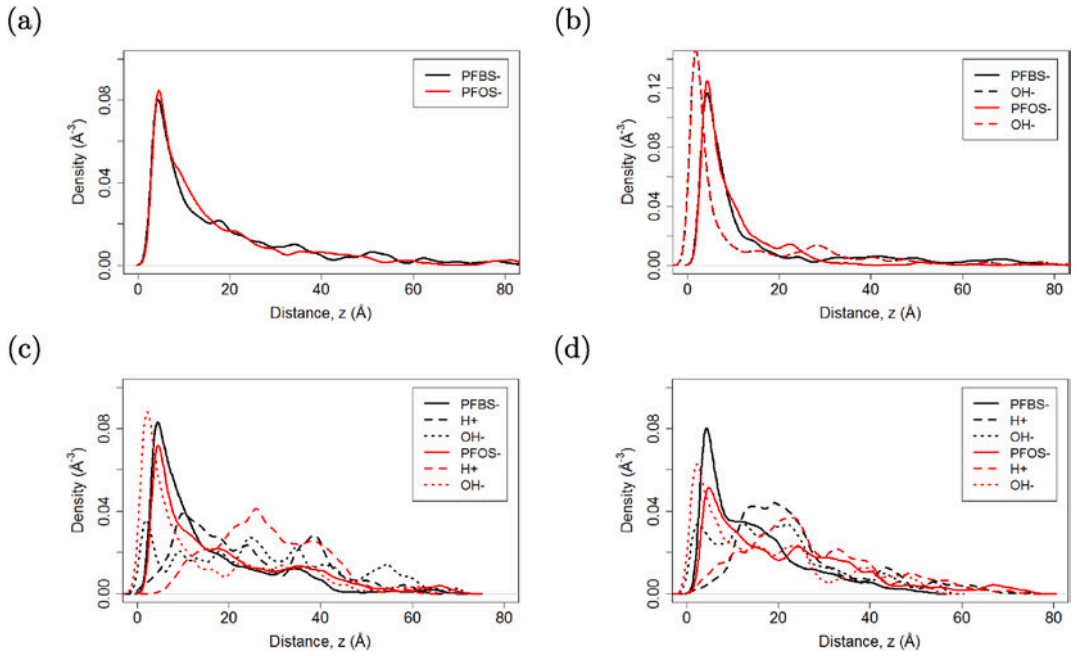


Fig. 3. Inhomogeneous density distributions of PFAS anions, $PFOS^-$ (——), $PFBS^-$ (——), as a function of distance (in the z direction) of molecule centres from a positively charged surface. In (a)–(d) the same number of PFAS molecules are modelled, along with (a) no additional ions, (b) 16 OH^- anions (– –, – –) and twice the surface charge of (a), (c) 8 H^+ counterions (– –, – –) and 8 OH^- anions (····, ····) and the same surface charge as (a), (d) 16 H^+ counterions (– –, – –) and 16 OH^- anions (····, ····) and the same surface charge as (a).

interest.

As in our earlier study involving mobile counterions, in the case of monovalent cations, the predominant effect is the screening of electrostatic interactions. In the case shown in Fig. 5(a), many of the cations move to the surface as thermodynamically preferred counterions to the negative surface charge. The distributions of both PFOS and PFBS molecules tend to be similar, remaining clustered just beyond the peak of the diffuse layer of counterions. Fig. 6(a) shows the increased H^+ near the surface, and spread in the z direction.

When divalent cations were introduced (Fig. 5(b)), there is a noticeable shift of the PFAS molecule back toward the surface, which is readily explained as a result of divalent cation bridging between the surface, and both the PFBS and PFOS (Supplementary Fig. S19(a) and Fig. 6(b)). Divalent cations have been shown experimentally to increase the adsorption of some PFAS for negatively charged surfaces (Ebrahimi et al., 2021; Campos Pereira et al., 2018). In qualitative agreement, we find an increase in the adsorption of both PFOS and PFBS with the addition of Ca^{2+}, relative to the case of an equally charged negative surface with added H^+ ions.

3.4. Surfaces with mixed charge

A simulation was also conducted with a surface containing both negative and neutral charged surface regions, as shown in Fig. 6 (c) and Supplementary Fig. S20 (a). The resulting densities varied in the x direction in correspondence with the changed surface charge, and this is shown for PFBS and PFOS in Fig. 7. These figures show the increased attraction of the H^+ to the negatively charged portion of the surface. The distribution of PFBS and PFOS is akin to the case of a fully negative surface with H^+ surface as seen in Fig. 5(a). Additionally, as discussed in experimental work such as (Cai et al., 2022), there is also an increased density of counter ions present in the solution co-located with the PFOS and PFBS anions, attracted by their negatively charged functional groups. However, as was seen in the other cases with a negatively charged surface presented in these simulations, the electrostatic attraction between the surface and the counter ions is the dominant factor under the conditions presented here.

3.5. Relative contributions of van der Waals and Coulomb potentials

Contributions of van der Waals and Coulomb potentials to the total potential of each simulation was also calculated, expressed as the magnitude of the van der Waals contribution over the total potential $|w_{vdw}|/(|w_C| + |w_{vdw}|)$. In the case of uncharged PFOS and PFBS, the calculated van der Waals contributions were on average 89% of the total interaction. With the removal of the H^+ charge from the functional group on the molecules, and with the addition of surface charge this dropped to 13%. In all the other simulation scenarios, the addition of solution ions reduces this further and the average contribution from the van der Waals potentials ranged from 0.5% to 5%. The magnitude of the van der Waals potentials were on average higher for the PFOS molecules, due to their increased size.

4. Conclusions and outlook

Results of Monte Carlo simulations have revealed differences in adsorption behaviour with surface charge, ion type, and four and eight carbon chain length perfluorinated sulfonic acid (PFSA) molecules. Compared with PFSA molecules in the presence of a neutral surface, higher adsorption occurred for positively charged surfaces, even with a screening electrolyte. Higher adsorption was also found with negatively charged surfaces in the presence of divalent Ca^{2+} cations due to cation bridge formation with the graphite surface.

The novel contribution of this work lies in the application of Monte Carlo molecular simulations to scenarios that differ from previously performed (molecular dynamics) simulations. By looking at low concentrations of molecules and in scenarios where both adsorption and mobility of per- and polyfluoroalkyl substances (PFAS) occur, the work may be of relevance to the design and testing of sorptive surfaces for amendment-based remediation. The carbon surface is of interest due the prevalence of many carbon-based products, such as powdered (Sörengård et al., 2019a), granulated (Sörengård et al., 2021) and liquid activated carbon (Sörengård et al., 2019b), along with carbon nanotubes (Li et al., 2012), used as substances for PFAS remediation.

It was hypothesised that a theoretical examination of PFAS-surface

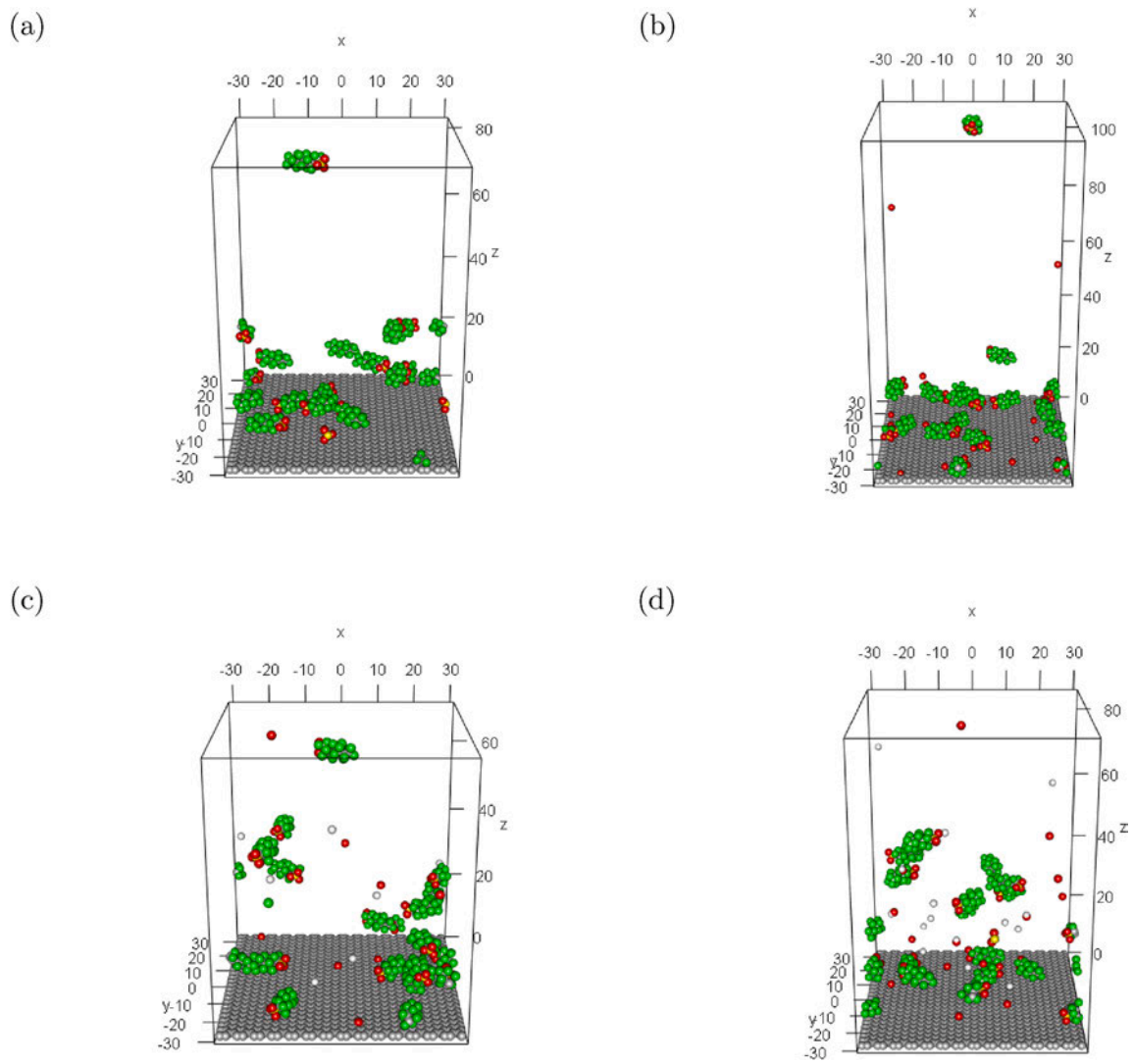


Fig. 4. PFOS anion simulation positions at 20,000 iterations per molecule for positively charged surfaces with (a) no added ions (b) 16 OH^- (red) and twice the surface charge of (a), (c) 8 H^+ (white), 8 OH^- and (d) 16 H^+, 16 OH^-.

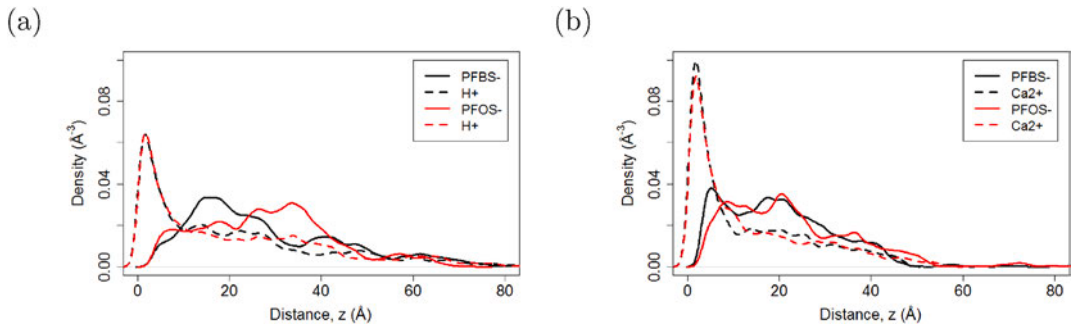


Fig. 5. Inhomogeneous density distributions of PFAS anions, $PFOS^-$ (——), $PFBS^-$ (——), as a function of distance (in the *z* direction) of centre of molecule from a negatively charged surface. In both (a) and (b) the same number are present, along with (a) 32 H^+ cation counterions (– –, – –) and (b) 16 Ca^{2+} divalent counterions (– –, – –).

interactions, via Monte Carlo molecular simulation, would reveal differences in adsorption behaviour resulting from changes in surface charge, divalent cation concentrations and PFAS carbon chain length. This was indeed found. As our focus has been on determining thermodynamic equilibrium behaviour, while previous work emphasised transient behaviour and the approach to equilibrium, it is interesting to contrast the respective works. In molecular dynamics simulations of perfluorooctane sulfonic acid (PFOS) at the Titanium oxide interface, high concentrations of molecules were simulated with the initial condition of densely packed molecules with an initial placement of just 8 Å from the surface (He et al., 2013, 2015). The subsequent adsorption results showed higher rates of adsorption compared to the current study.

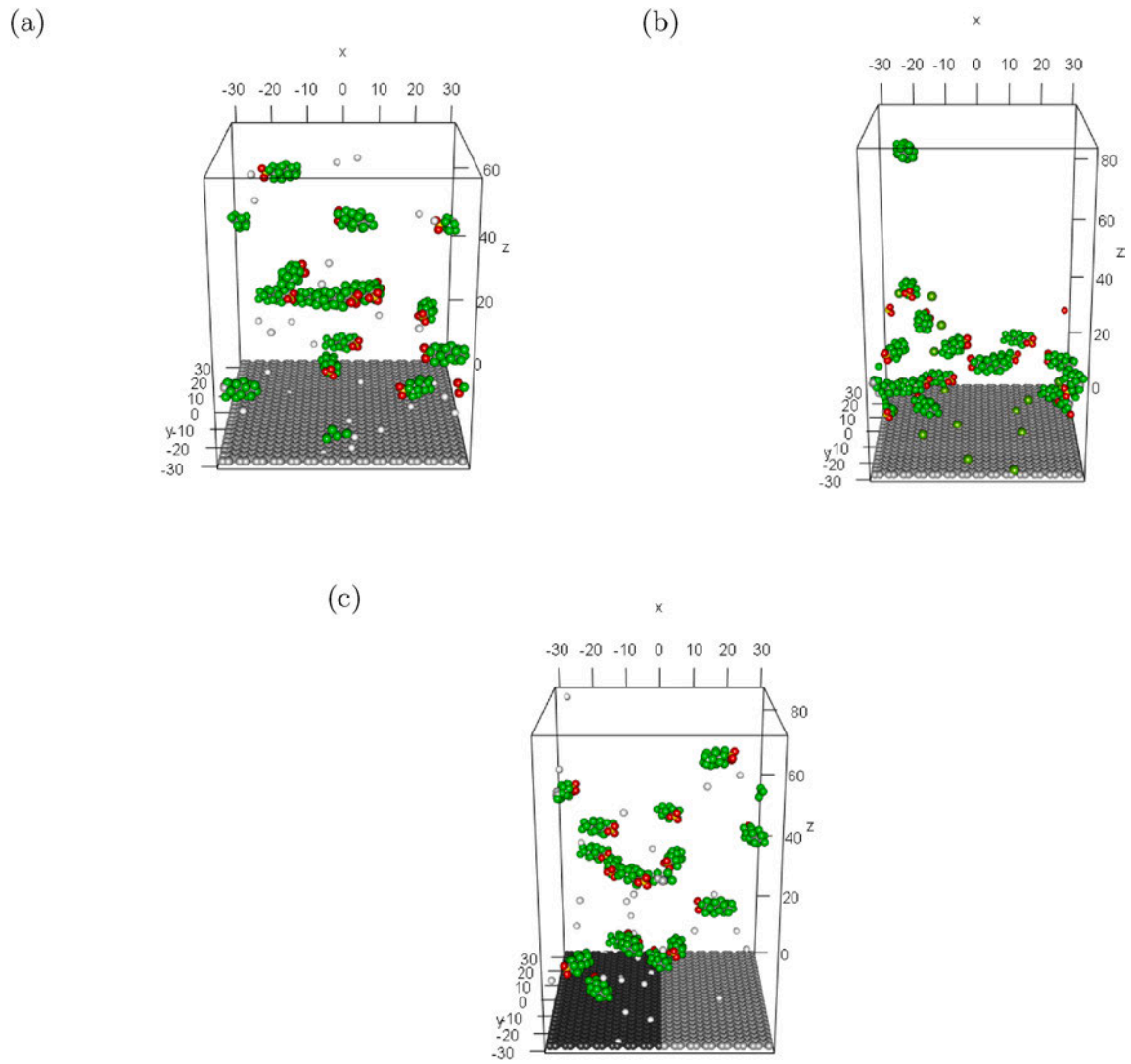


Fig. 6. PFOS anion simulation positions at 20,000 iterations per molecule for negatively charged surfaces with (a) 32 H^+ (white) (b) 16 Ca^{2+} (green) and (c) 32 H^+, half negative (left hand side, $x < 0$, dark grey), half neutral surface (right hand side, $x > 0$, light grey).

Our results, however, are more closely aligned with those of (Zhang et al., 2015), where low concentrations of molecules were studied. In that work, as in ours, multiple peaks were found in some cases, indicating both adsorption of some molecules, and mobility of others.

Due to the differing properties of experimental systems, including pH, soil composition, surface charges, organic materials and ion concentrations, comparison of theoretical and experimental results requires much care. Cai et al. (2022) present an interesting study on the effect of Ca^{2+}, Mg^{2+} and Na^+ findings screening effects of ions both at the surface and of PFAS functional groups. The present work shows both interactions, but without the reduced sorption for the PFBS shown in the experimental work, which may be due to the absence of organic material and explicit hydrophobic interactions in the simulation study. Indeed (Campos Pereira et al., 2018), shows a preference between short and long chain PFAS between different components of the soil organic matter. Even the presence of bubbles in solid-water mixtures greatly influences PFAS sorption (Meng et al., 2014), a factor which again is not captured in simulations to date. Future work matching experimental conditions to the simulation conditions would likely prove to be very useful in the quantification of sorption mechanisms, along with the relative importance of both types of screenings discussed by (Cai et al., 2022).

This work constitutes a basis for a more detailed modelling study featuring differences in sorptive behaviour of PFAS with varying functional groups, carbon chain length, charge, along with the effects of different surface composition and structure. While often the difference between the use of implicit and explicit water molecules may not have any effect on adsorption modelling results (e.g. (Liu et al., 2022)), this varies for different scenarios, and is also an area for future research for the specific case of PFAS adsorption simulations.

Author contributions

Julie A Sleep: Conceptualization, Methodology, Software, Formal Analysis, Visualisation, Writing - Original Draft. Stanley J Miklavcic: Supervision, Methodology, Writing - Review and Editing. Albert L Juhasz: Supervision, Methodology, Writing - Review and Editing.

Declaration of competing interest

The authors declare that they have no known competing financial interests or personal relationships that could have appeared to influence the work reported in this paper.

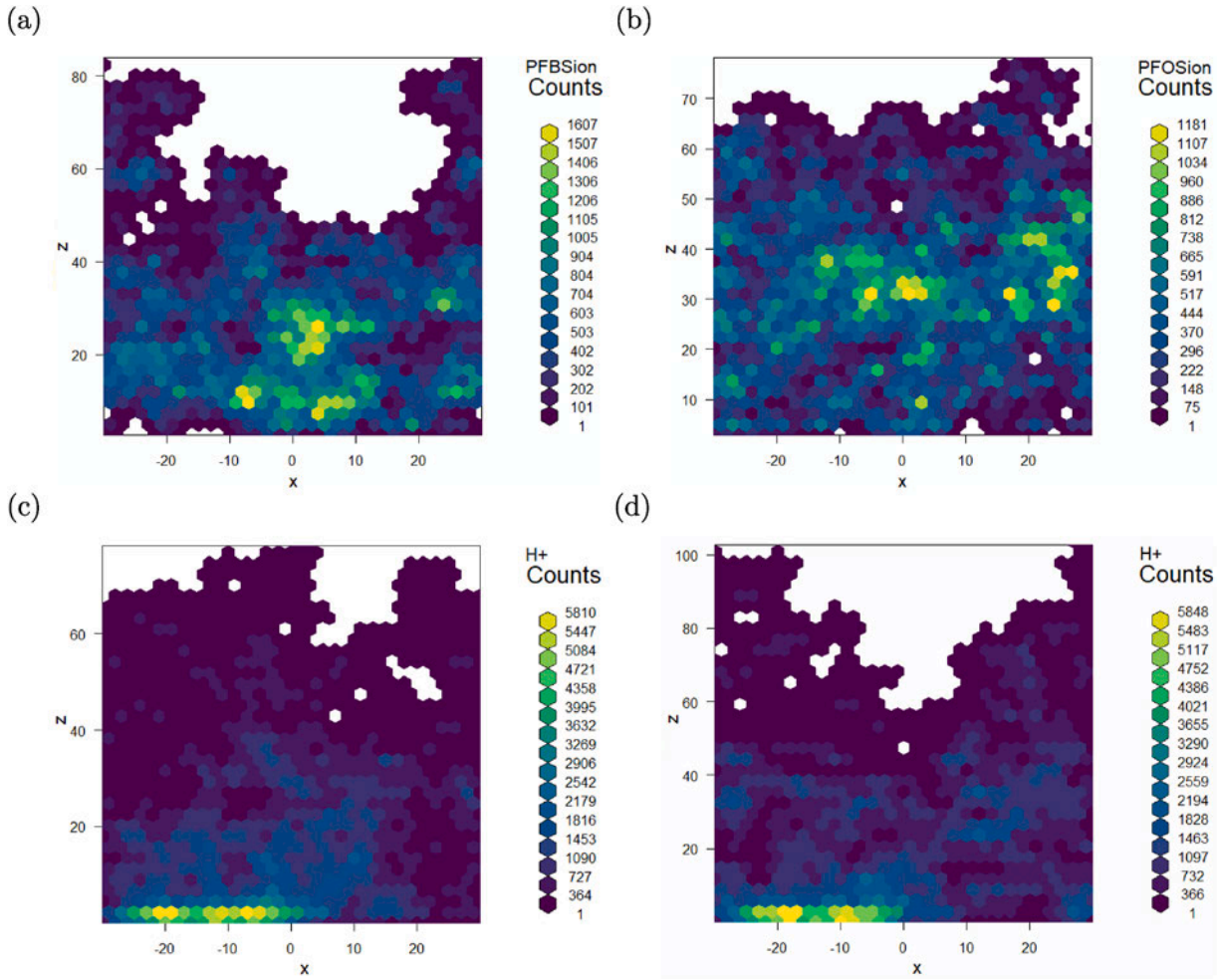


Fig. 7. Heat maps showing ion count during simulation as a function of height (z) and lateral position (x): (a) PFBS anion, (b) PFOS anion, (c) H^+ corresponding to case in (a), and (d) H^+ corresponding to case in (b) for 32 H^+, half negative (left hand side of plots $x < 0$), half neutral surface (right hand side of plots $x > 0$). Scale ranges from low density (dark blue) to high density (yellow); regions not sampled by an ion type appear in white.

Data availability

Data will be made available on request.

Acknowledgments

The authors would like to acknowledge the Australian Government and the University of South Australia for supporting J.A.S. with a Research Training Program Scholarship, and the University of South Australia for access to High Performance Computing facility Tango 2.0.

Appendix A. Supplementary data

Supplementary data to this article can be found online at https://doi.org/10.1016/j.chemosphere.2023.137910.

References

Anderson, R.H., Adamson, D.T., Stroo, H.F., 2019. Partitioning of poly- and perfluoroalkyl substances from soil to groundwater within aqueous film-forming foam source zones. J. Contam. Hydrol. 220, 59–65. https://doi.org/10.1016/j.jconhyd.2018.11.011.

Barzen-Hanson, K.A., Davis, S.E., Kleber, M., Field, J.A., 2017. Sorption of fluorotelomer sulfonates, fluorotelomer sulfonamido betaines, and a fluorotelomer sulfonamido amine in national foam aqueous film-forming foam to soil. Environ. Sci. Technol. 51 (21), 12394–12404. https://doi.org/10.1021/acs.est.7b03452.

Cai, W., Navarro, D.A., Du, J., Ying, G., Yang, B., McLaughlin, M.J., Kookana, R.S., 2022. Increasing ionic strength and valency of cations enhance sorption through hydrophobic interactions of pfas with soil surfaces. Sci. Total Environ. 817, 152975 https://doi.org/10.1016/j.scitotenv.2022.152975.

Campos Pereira, H., Ullberg, M., Kleja, D.B., Gustafsson, J.P., Ahrens, L., 2018. Sorption of perfluoroalkyl substances (PFASs) to an organic soil horizon – effect of cation composition and pH. Chemosphere 207, 183–191. https://doi.org/10.1016/j.chemosphere.2018.05.012.

Campos-Pereira, H., Kleja, D.B., Sjöstedt, C., Ahrens, L., Klysubun, W., Gustafsson, J.P., 2020. The adsorption of per- and polyfluoroalkyl substances (PFASs) onto ferrihydrite is governed by surface charge. Environ. Sci. Technol. 54 (24), 15722–15730. https://doi.org/10.1021/acs.est.0c01646.

Chen, H., Reinhard, M., Yin, T., Nguyen, T.V., Tran, N.H., Gin, K.Y.-H., 2019. Multi-compartment distribution of perfluoroalkyl and polyfluoroalkyl substances (PFASs) in an urban catchment system. Water Res. 154, 227–237. https://doi.org/10.1016/j.watres.2019.02.009.

Du, Z., Deng, S., Bei, Y., Huang, Q., Wang, B., Huang, J., Yu, G., 2014. Adsorption behavior and mechanism of perfluorinated compounds on various adsorbents—a review. J. Hazard Mater. 274, 443–454. https://doi.org/10.1016/j.jhazmat.2014.04.038.

Ebrahimi, F., Lewis, A.J., Sales, C.M., Suri, R., McKenzie, E.R., 2021. Linking PFAS partitioning behavior in sewage solids to the solid characteristics, solution chemistry, and treatment processes. Chemosphere 271, 129530. https://doi.org/10.1016/j.chemosphere.2020.129530.

Gindulyte, A., Shoemaker, B.A., Yu, B., He, J., Zhang, J., Chen, J., Zaslavsky, L., Thiessen, P.A., Li, Q., He, S., Kim, S., Cheng, T., Bolton, E.E., 2019. PubChem 2019 update: improved access to chemical data. Nucleic Acids Res. 47 (D1), D1102–D1109. https://doi.org/10.1093/nar/gky1033.

Hansen, J.-P., McDonald, I.R., 1986. Theory of Simple Liquids, second ed. Academic Press.

Hardacre, C., Holbrey, J.D., Mullan, C.L., Nieuwenhuyzen, M., Youngs, T.G., Bowron, D. T., Teat, S.J., 2010. Solid and liquid charge-transfer complex formation between 1-methylnaphthalene and 1-alkyl-cyanopyridinium bis {(trifluoromethyl) sulfonyl} imide ionic liquids. Phys. Chem. Chem. Phys. 12 (8), 1842–1853. https://doi.org/10.1039/B921160H.

He, G., Pan, G., Zhang, M., 2013. Assembling structures and dynamics properties of perfluorooctane sulfonate (PFOS) at water–titanium oxide interfaces. J. Colloid Interface Sci. 405, 189–194. https://doi.org/10.1016/j.jcis.2013.05.003.

He, G., Zhang, M., Zhou, Q., Pan, G., 2015. Molecular dynamics simulations of structural transformation of perfluorooctane sulfonate (PFOS) at water/rutile interfaces. Chemosphere 134, 272–278. https://doi.org/10.1016/j.chemosphere.2015.04.056.

Hirschfelder, J.O., Curtiss, C.F., Bird, R.B., 1954. Molecular Theory of Gases and Liquids. John Wiley & Sons Inc. (N.Y.).

Ionescu, C.-M., Sehnal, D., Falginella, F.L., Pant, P., Pravda, L., Bouchal, T., Vařeková, R. S., Geidl, S., Koča, J., 2015. AtomicChargeCalculator: interactive web-based calculation of atomic charges in large biomolecular complexes and drug-like molecules. J. Cheminf. 7 (1), 50. https://doi.org/10.1186/s13321-015-0099-x.

Israelachvili, J.N., 2011. Intermolecular and Surface Forces, third ed. Academic Press.

Jeon, J., Kannan, K., Lim, B.J., An, K.G., Kim, S.D., 2011. Effects of salinity and organic matter on the partitioning of perfluoroalkyl acid (PFAs) to clay particles. J. Environ. Monit. 13 (6), 1803–1810. https://doi.org/10.1039/C0EM00791A.

Jönsson, B., Wennerström, H., Halle, B., 1980. Ion distributions in lamellar liquid crystals. A comparison between results from Monte Carlo simulations and solutions of the Poisson-Boltzmann equation. J. Phys. Chem. 84 (17), 2179–2185. https://doi.org/10.1021/j100454a014.

Klapetek, P., 2012. Quantitative Data Processing in Scanning Probe Microscopy: SPM Applications for Nanometrology. Elsevier. https://doi.org/10.1016/C2011-0-09615-1.

Kotthoff, M., Müller, J., Jürling, H., Schlummer, M., Fiedler, D., 2015. Perfluoroalkyl and polyfluoroalkyl substances in consumer products. Environ. Sci. Pollut. Control Ser. 22 (19), 14546–14559. https://doi.org/10.1007/s11356-015-4202-7.

Li, C., Schäffer, A., Séquaris, J.-M., László, K., Tóth, A., Tombácz, E., Vereecken, H., Ji, R., Klumpp, E., 2012. Surface-associated metal catalyst enhances the sorption of perfluorooctanoic acid to multi-walled carbon nanotubes. J. Colloid Interface Sci. 377 (1), 342–346. https://doi.org/10.1016/j.jcis.2012.03.038.

Li, Y., Oliver, D.P., Kookana, R.S., 2018. A critical analysis of published data to discern the role of soil and sediment properties in determining sorption of per and polyfluoroalkyl substances (PFASs). Sci. Total Environ. 628, 110–120. https://doi.org/10.1016/j.scitotenv.2018.01.167.

Li, F., Fang, X., Zhou, Z., Liao, X., Zou, J., Yuan, B., Sun, W., 2019. Adsorption of perfluorinated acids onto soils: kinetics, isotherms, and influences of soil properties. Sci. Total Environ. 649, 504–514. https://doi.org/10.1016/j.scitotenv.2018.08.209.

Lin, T.-J., Heinz, H., 2016. Accurate force field parameters and pH resolved surface models for hydroxyapatite to understand structure, mechanics, hydration, and biological interfaces. J. Phys. Chem. C 120 (9), 4975–4992. https://doi.org/10.1021/acs.jpcc.5b12504.

Liu, M., Jin, Y., Pan, J., 2022. Relevance of implicit and explicit solvent in density-functional theory study of adsorption at electrochemical nacl/al interface. Mater. Today Commun. 31, 103425 https://doi.org/10.1016/j.mtcomm.2022.103425.

Meng, P., Deng, S., Lu, X., Du, Z., Wang, B., Huang, J., Wang, Y., Yu, G., Xing, B., 2014. Role of air bubbles overlooked in the adsorption of perfluorooctanesulfonate on hydrophobic carbonaceous adsorbents. Environ. Sci. Technol. 48 (23), 13785–13792. https://doi.org/10.1021/es504108u.

Miklavcic, S.J., 1997. Effective dipole potentials after angle averaging. Phys. Rev. E. 56 (1), 1142–1147. https://doi.org/10.1103/PhysRevE.56.1142.

R Core Team, R., 2018. A Language and Environment for Statistical Computing. R Foundation for Statistical Computing, Vienna, Austria. https://www.R-project.org/.

Song, J., Cappelletti, R., 1994. Lennard-Jones-potential calculation of C 60 stage-one graphite. Phys. Rev. B 50 (19), 14678. https://doi.org/10.1103/PhysRevB.50.14678.

Sörengård, M., Kleja, D.B., Ahrens, L., 2019a. Stabilization and solidification remediation of soil contaminated with poly- and perfluoroalkyl substances (PFASs). J. Hazard Mater. 367, 639–646. https://doi.org/10.1016/j.jhazmat.2019.01.005.

Sörengård, M., Kleja, D.B., Ahrens, L., 2019b. Stabilization of per- and polyfluoroalkyl substances (PFASs) with colloidal activated carbon (PlumeStop®) as a function of soil clay and organic matter content. J. Environ. Manag. 249, 109345 https://doi.org/10.1016/j.jenvman.2019.109345.

Sörengård, M., Gago-Ferrero, P., Kleja, D.B., Ahrens, L., 2021. Laboratory-scale and pilot-scale stabilization and solidification (S/S) remediation of soil contaminated with per- and polyfluoroalkyl substances (PFASs). J. Hazard Mater. 402, 123453 https://doi.org/10.1016/j.jhazmat.2020.123453.

Van Der Spoel, D., Lindahl, E., Hess, B., Groenhof, G., Mark, A.E., Berendsen, H.J., 2005. Gromacs: fast, flexible, and free. J. Comput. Chem. 26 (16), 1701–1718. https://doi.org/10.1002/jcc.20291.

Zareitalabad, P., Siemens, J., Hamer, M., Amelung, W., 2013. Perfluorooctanoic acid (PFOA) and perfluorooctanesulfonic acid (PFOS) in surface waters, sediments, soils and wastewater – a review on concentrations and distribution coefficients. Chemosphere 91 (6), 725–732. https://doi.org/10.1016/j.chemosphere.2013.02.024.

Zhang, R., Yan, W., Jing, C., 2015. Experimental and molecular dynamic simulation study of perfluorooctane sulfonate adsorption on soil and sediment components. J. Environ. Sci. 29, 131–138. https://doi.org/10.1016/j.jes.2014.11.001.

Zhao, L., Bian, J., Zhang, Y., Zhu, L., Liu, Z., 2014. Comparison of the sorption behaviors and mechanisms of perfluorosulfonates and perfluorocarboxylic acids on three kinds of clay minerals. Chemosphere 114, 51–58. https://doi.org/10.1016/j.chemosphere.2014.03.098.

Chapter 4

R-MCMolecSim: Original R-based software and extended numerical methods for Monte Carlo molecular simulations incorporating long-range interactions

4.1 Introduction

This chapter details the development and methodology of the R-MCMolecSim software developed and used in Chapter 3 to model interactions between PFAS and surfaces [38]. The aim was to investigate the theoretical interactions at a molecular level in order to identify possible mechanisms of sorption, along with theoretical explanations for the differences in the extent of sorption and how these change with molecular, surface and solution properties. Monte Carlo molecular modelling was undertaken to study the interaction between one of a number of types of PFAS and a carbon (graphite) surface, as a function surface charge, solution ion species, and molecule size. PFOA was chosen as an example molecule to illustrate software outputs, being a commonly observed and regulated PFAS, with PFDA chosen to examine the effect of a larger molecule size on computational time.

Previous work on the modelling of molecular-level PFAS-surface interactions [39, 40, 41] had utilised molecular dynamics simulations. He et al. [39] examined the difference between varying crystal planes on sorption. The same authors [40] looked at the effects of Ca^{2+} and PFOS concentration, while Zhang et al. [41] studied the effects of layers of butyl benzoic acid, butyl benzene and hexane on PFAS sorption. The Monte Carlo simulation method was chosen as the most appropriate modelling method to calculate

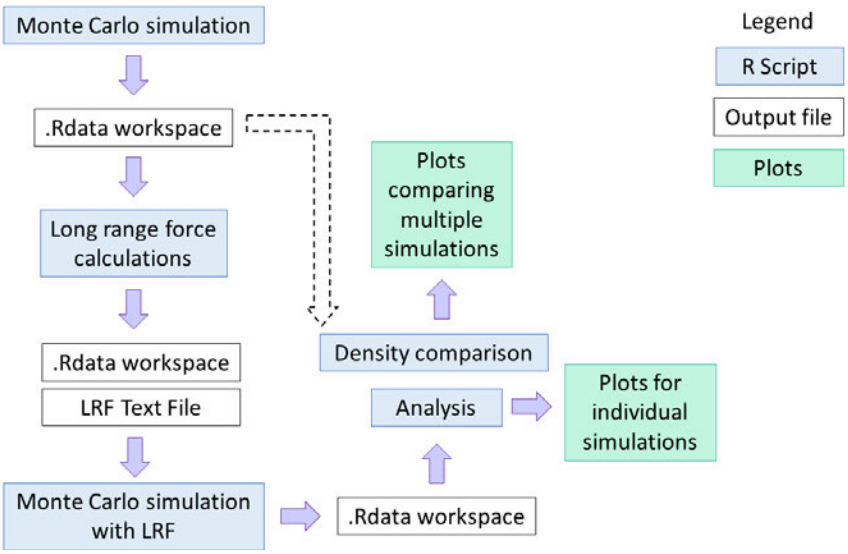


Figure 4.1: Structure of the R-MCMolecSim simulation code

equilibrium properties of different systems. This method has the advantage of calculating equilibrium statistical mechanics of systems that potentially involve both adsorption and desorption processes.

Existing Monte Carlo molecular modelling software packages [42, 43, 44], are either focussed on the modelling of quantum systems, or are written in the languages Fortran or C++. Here, it was desired to undertake the modelling using the R statistical programming language [45], to take advantage of inbuilt mathematical and statistical functions and high-quality visualisation capabilities, for both the plotting of statistical output data and the visualisation of molecular configurations within the 3-D simulation space. The software developed was designed to be flexible and extensible, in order to include different simulation components and to accommodate changes in these, as required to answer questions of scientific interest.

Configurations of the system contributing to the ensemble were generated by randomly translating and rotating molecules in the system, determining whether to accept the changes and, if accepted, calculating and recording the system state variables, including the change in total system energy. The total computation time varied between 18 and 48 hours for 20,000 iterations per molecule, depending on the number and size of molecules and ions present in the system.

An overview of the structure of the code is presented in Figure 4.1. If long range forces are not desired, the dashed path in the figure may be followed.

4.2 Setup and initialisation

4.2.1 Simulation box set up and periodic boundary conditions

A snapshot of an example physical system is shown in Figure 4.2. The box size ($2b \times 2b \times nb$) can be adjusted via a parameter `b`. For convenience we restrict the base to be a square, in the x and y dimensions with arbitrary extension in the z-direction. The fixed surface atom placements and their number need to be re-calculated upon a change of box size. The default size adopted in Chapter 3 was b = 30 Å, resulting in a simulation box of square base size 60 Å× 60 Å, and initially of height 60 Å. The default simulation box contains 16 primary[1] molecules, up to 32 additional ions (H^+, OH^- and/or Ca^{2+}) and implicit water throughout the box. Implicit water entails that water is modelled as a medium that affects interactions between molecules. Interactions are dependent on the parameter ε_r, the relative permittivity of the medium, in our case, water. In contrast, explicit water would entail inclusion of each water molecule explicitly in the simulation, which is discussed in future work. The fixed layer of surface atoms, making up the base of the box at $z = 0$, is, by default, a layer of carbon atoms arranged as a layer of graphite. The medium in the box is assumed to extend infinitely in the z direction. Molecules are thus theoretically unrestricted in how far they are permitted to move away from the surface. Periodic boundary conditions were implemented in the lateral (x and y) directions. That is, molecules or parts thereof that move beyond the lateral boundaries of the box, are translated to their periodic reflection inside the box.

4.2.2 Input parameters and other simulation features

Various input parameters of the simulated system are listed with their descriptions in Table 4.1. The simulation code also involves a number of physical constants such as Boltzmann's constant (stored in variable `kB`), the electron charge (`e`), Avogadro's number (`N_A`) and the vacuum permittivity (`eps_0`). Primary molecules of interest are introduced, defined and described via an input file as shown in Table 4.2. How this file is utilised is discussed in more detail in Section 4.2.3. The simulation code can currently accommodate up to three ion types in the solution which, by default, are H^+, OH^- and Ca^{2+}. These three ion types can easily be substituted for other types simply by changing the charge and the Lennard-Jones (LJ) parameter values provided in this input file. There are additional options listed at the top of the simulation script, including the option to test for the effect of starting the simulation under different initial molecule positions, or the effect of changing the LJ parameters of molecules, that are not included in Table 4.1. However, these options are described in detail in Chapter 3 and Appendix

[1] In our case these were per and poly-fluoroalkyl substances (PFAS), including the example in this chapter, PFOA, and the PFOS and PFBS of Chapter 3 (See Glossary).

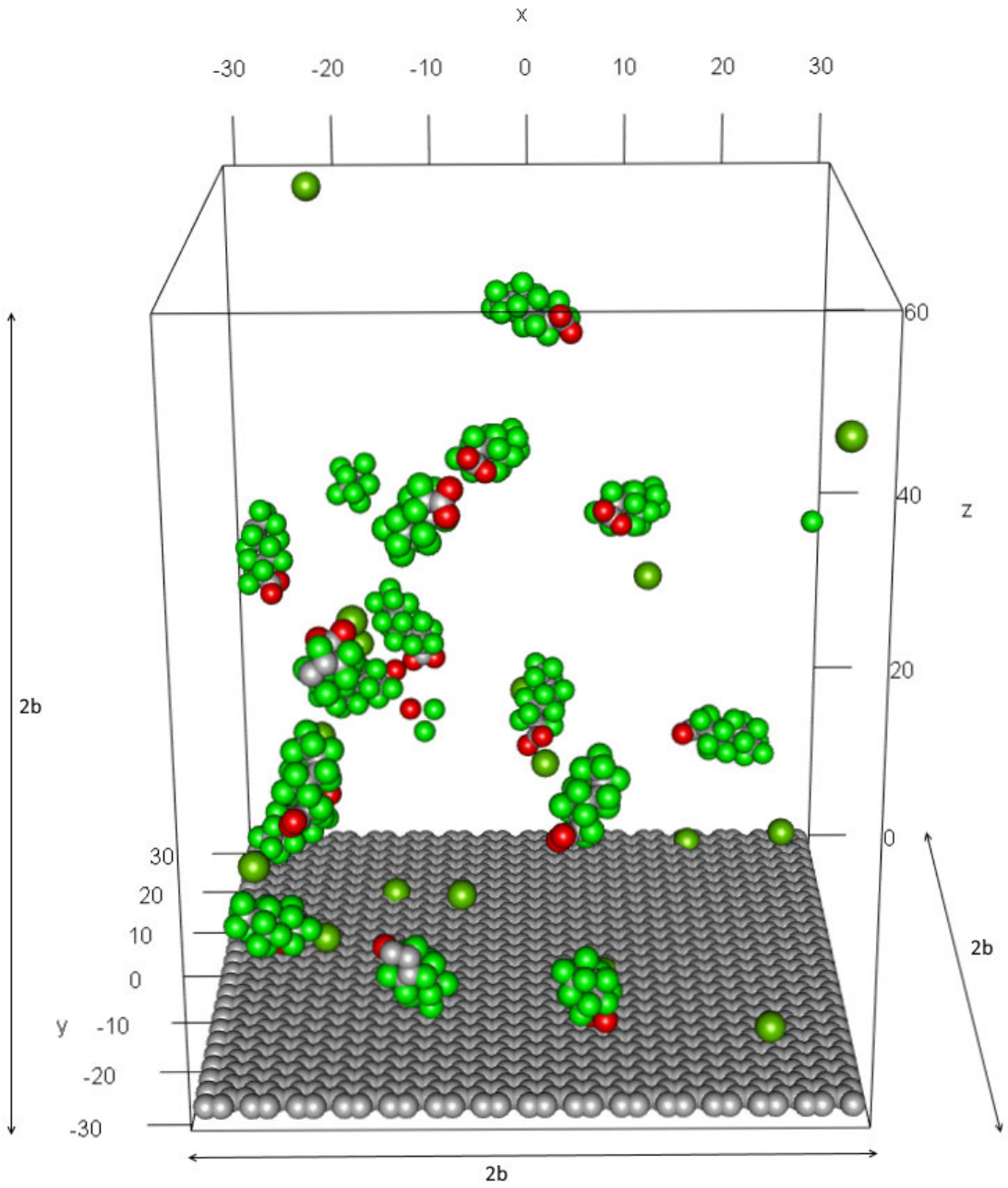


Figure 4.2: Simulation box of dimensions $2b \times 2b \times 2b$ showing fixed surface atoms (grey), mobile PFOA anions (clusters of spheres), and mobile Ca^{2+} ions (single green spheres). Molecule colours are standard CPK colours.

Table 4.1: Variable input parameters

Variable	Type	Description
`numsteps`	integer	Number of Monte Carlo (MC) simulation steps
`N`	integer	Number of primary (e.g. PFAS) molecules
`Nci`	integer	Number of ions of first type (e.g. H^+)
`Ndiv`	integer	Number of ions of third type (e.g. Ca^{2+})
`Noh`	integer	Number of ions of second type (e.g. OH^-)
`b`	numeric	Half box dimension
`boxh`	numeric	Half box height for initial placements
`stepSize`	numeric	MC step size in Å
`charge_C`	numeric	charge on each atom in the surface in eV
`eps_water`	numeric	relative permittivity of solution liquid at the desired temperature (e.g. water at 20°C)
`wDepth_C`	numeric	LJ well depth for surface molecules in kJ mol^{-1}
`sigma_C`	numeric	LJ sigma for surface molecules in Å
`liquidName`	string	Name of primary molecule, e.g. "PFOA"
`unix`	Boolean	Suppresses plotting and directory changes when set to true
`debug`	Boolean	Prints extra statements during runtime for debugging purposes
`mixedSurfaceCharge`	Boolean	Enables mixed surface charge when set to true, homogeneous surface charge when set to false

Table 4.2: Example structure of primary molecule input file format, for PFOA

Num	Elem	x	y	z	Name	Sigma	WellDepth	Charge
1	F	-1.0539	1.9481	-0.2014	F1	2.95	0.2218	-0.37216
2	F	0.5434	1.2581	-1.5025	F2	2.95	0.2218	-0.37593
3	F	1.2215	1.6487	1.0783	F3	2.95	0.2218	-0.38007
⋮	⋮	⋮	⋮	⋮	⋮	⋮	⋮	⋮

A.

In the default system, the 3D coordinates of molecules were obtained from [1]. Partial charges on atoms of the molecules were calculated as in [1, 46], and the OPLS-AA Lennard-Jones parameters were obtained from [47, 48, 49]. Examples of these can be found in Appendix A, Supplementary Tables S1 and S2. Lennard-Jones parameters for the default graphite surface were obtained from [50, 51], while similar data for mobile ions were obtained from [47, 49]. A default step size limit for ion or molecule translations in any of the three directions was set at 0.5 Å, while angular rotation changes were randomly determined between -5° and 5° about each of the x, y and z axes. Surface charges are set at values such as $\sigma_{surf} = 0$ and $\sigma_{surf} = -16/3600$ e/Å^2. As an additional option the simulation code allows the surface to posses a non-uniform surface charge. The default setting for this option is for the surface to be divided into two halves along $x = 0$, with each half having a different surface charge.

Molecules are placed in their respective initial positions according to a series of x, y and z coordinates which may be randomised, if desired. The code only automatically checks to ensure that molecules are above the surface. Consequently, if randomisation of initial molecule positions is performed, these positions must be inspected manually to ensure molecules are not overlapping. It was shown in Chapter 3 that a change in initial molecule positions has little effect on equilibrium density results, provided the simulation was run for a sufficiently long time, and provided that molecules were not placed too far from the surface. As explained below, the first few thousand steps, e.g. 2,500 MC steps per molecule, were treated as belonging to an equilibration run. The outputs from these steps were excluded from the subsequent data generation from which statistical analyses were performed. This cut-off point (that is, the separation between equilibration runs and production runs) can be changed in the data analysis scripts if an examination of the potential energy plot shows that equilibrium is reached sooner or later than the default value, depending on the system being studied.

4.2.3 Simulation initialisation

At the beginning of the simulation the parameters are initialised. The surface is plotted and stored in both an R data frame and written to the `(mixed)surface_fromR.csv` file for inspection and validation of its molecular structure. Different surfaces can be substituted, via a file of the same format as the .csv file and stored in the data frame `surface`. Next, the molecule properties are read in from the file `structuresliquidname.txt`, where `liquidname` is the name of the main molecule type under consideration, e.g. PFOA, as shown in Table 4.2. There are N primary molecules, which are stored in a list `pfasList`, as shown graphically in Figure 4.3. Each object in the list consists of multiple vectors, containing values of the parameters `sigma`, `wDepth`, `charge`, and co-ordinates `x`, `y` and `z` for each atom within the molecule. Additionally, each object contains vectors `origx`, `origy` and `origz` which store a copy of the coordinates of the atoms that make up the molecule, defined with their centre at the origin (0,0,0). These arrays are used to aid in the calculation and tracking of rotations of the molecules. The units of these stored parameter values are as shown in Table 4.1, with the exception of the well depth which is converted at this initialisation stage into the SI units of J mol^{-1} as required for the calculations. Three additional vectors are also created and used once at the beginning of the simulation only. These are called `xplacepfas`, `yplacepfas` and `zplacepfas` and store the initial coordinates of the molecule centres.

Each solution ion is similarly placed in the lists `ciList` (H^+ counterions), `ohList` (OH^- ions) and `divList` (Ca^{2+} divalent cations). These are easily modified to accommodate other mobile ions of one's choosing. Initial positions are visualised using the `plot3d` and `spheres3d` R functions, with standard CPK colours for atoms. All of the

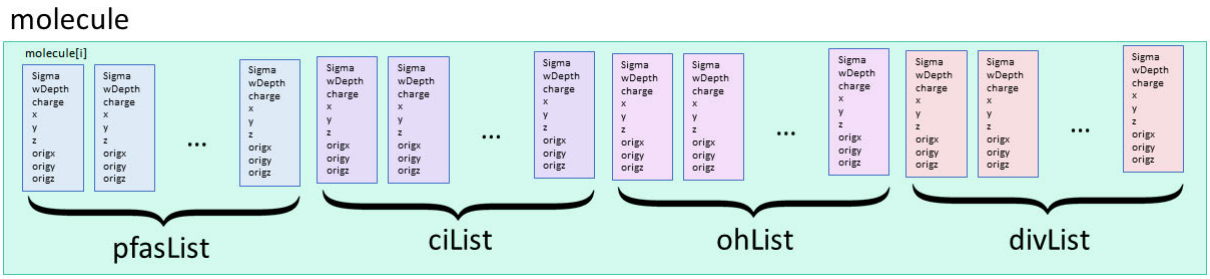


Figure 4.3: Structure of the combined R list object containing all the PFAS and ions, with each list item containing values for the 9 listed parameters

non-surface molecules are stored together in the list `molecule` depicted in Figure 4.3. This is the list which is iterated and updated at each MC step of the simulation.

4.3 Calculations

With the freely mobile molecules and ions, as well as the fixed surface atoms defined by their respective positions, state of charge, and chemical character, the total interaction energy within the simulation box is given by the pairwise sum of all interatomic potentials plus contributions for interactions with external fields. The potentials considered were the 6-12 Lennard-Jones dispersion interaction and the Coulomb potential for electrostatic interactions. Lennard-Jones and Coulomb interactions were not truncated, which was computationally possible due to the size of the simulation box. For each interaction potential calculation, the simulation box was centred on the molecule under current consideration, assuming periodic conditions. The calculation of the total system energy thus incorporated the intermolecular van der Waals and Coulomb interactions between every atom according to the minimum image convention.

The initial total potential energy is calculated as the sum of the interaction potentials between all pairs of atoms. The code iterates at three nested levels. Firstly, it loops across each molecule, `j`, in the simulation, stored in the list `molecule`. Then, it loops across each atom, `s`, of the jth molecule under consideration. For each atom `s`, the potential energies of interaction between all surface atoms, `sa`, and all atoms of the mobile molecules and mobile ions, `k`, are calculated. For each of these pairwise atom-atom calculations, the first step is to calculate the separation between the atoms. Here the minimum image convention relating to the periodic boundary condition is applied. That is, if an atom is further than `b` Å away in either the x or y (not z) direction from a given atom, then the closest periodic reflected position of that first atom is used. This distance is stored in the variable `D` in Å, and `D_m` in m. SI units are used for all calculations within the code, with conversions from input values performed as required. The measurements in Å are retained for use in the visualisations. Once a separation is

obtained, the potential energy is calculated (according to the procedure described in the following sections) and stored in the variable `totalPotential`.

4.3.1 Atom-atom potentials

The total interaction energy between a given pair of molecules was taken to be the sum of pairwise atom-atom interactions. The interaction energy between a molecule and the surface was likewise taken to be the sum of pairwise atom-atom interactions between all atoms in the molecule and the atoms making up the surface. Each atom-atom potential comprised of a Coulomb potential and a van der Waals potential.

$$w(r_{ij}) = w_C(r_{ij}) + w_{vdw}(r_{ij}) \tag{4.1}$$

The effects of the medium, e.g. water, are taken into account via the use of an implicit liquid and dielectric screening.

4.3.2 Electrostatic interaction

The dielectrically screened, electrostatic interaction between atom i and atom j was calculated using the Coulomb potential [52]

$$w_C(|\mathbf{r}_i - \mathbf{r}_j|) = \frac{q_i q_j}{4\pi\varepsilon_0\varepsilon_r|\mathbf{r}_i - \mathbf{r}_j|} = \frac{q_i q_j}{4\pi\varepsilon_0\varepsilon_r r_{ij}} \tag{4.2}$$

where $r_{ij} = |\mathbf{r}_i - \mathbf{r}_j|$ is the distance between the atom positions at $\mathbf{r}_i$ and $\mathbf{r}_j$, q_i and q_j are the atomic charges on i and j atoms respectively, ε_r is the relative permittivity (dielectric constant) of the medium and ε_0 is the vacuum permittivity.

4.3.3 Lennard-Jones potential

Van der Waals interactions were modelled as a standard 6-12 Lennard-Jones potential [52], incorporating an atom-atom repulsion and a dispersion attraction. The following expression was implemented

$$w_{vdw}(r_{ij}) = 4\varepsilon_{ij}\left[\left(\frac{\sigma_{ij}}{r_{ij}}\right)^{12} - \left(\frac{\sigma_{ij}}{r_{ij}}\right)^{6}\right] \tag{4.3}$$

where ε_{ij} refers to the well depth (maximum energy of attraction) in Joules (J) and σ_{ij} the separation at which the potential between atoms i and j is zero.

Intramolecular interactions between atoms within a molecule as well as between surface atoms were excluded as the molecules and surface were assumed to be internally

rigid. This assumption is appropriate for PFSA and PFCA molecules. As the intermolecular interactions are treated as sums of atomic Coulomb, dispersion and repulsive interactions, angular dependent interactions (e.g. charge-dipole, dipole-dipole, etc.) [53] and dipole-surface [54] interactions are not included. The effects of some of these multipole interactions are potentially captured in the simulation process due to the different molecular orientations that are included in the simulation.

4.3.4 Long-range electrostatic interactions

In addition to the direct interactions between any given atom and all other atoms in the simulation box, a charged atom experiences an interaction with the charge distribution outside the box. This distribution comprises the surface charge external to the box, as well as the molecules and ions in the external medium. It is not practical to explicitly calculate this external contribution, w_{ext}, which must be added to the right hand side of Eq 4.1 to give the total interaction energy between a given atom and the rest of the system. However, it is reasonable to expect that the equilibrium charge distribution normal to the surface outside the simulation box will be equal to the simulated equilibrium distribution generated by the mobile charges inside the box. As we assume translation invariance in the lateral direction, this net distribution of mobile charges, $\rho_{eq}(z)$, will only be a function of distance z from the surface. The density of charge is complemented by the average surface charge density, σ_{surf}, which is located only at the surface, $z = 0$. Hence, the external interaction energy experienced by a charge, q_i, at a height, z_i, due to all external charges ($|x|$, $|y| \geq b$) is given by

$$w_{ext}(z_i) = 8 \int_0^{\infty} \left[\frac{\rho_{eq}(z) + \sigma_{surf}\delta(z)}{4\pi\varepsilon_0\varepsilon_r} \int_0^{\pi/4} \left(\int_{b/\cos\theta}^{\infty} \frac{r\mathrm{d}r}{\sqrt{r^2 + (z - z_i)^2}} \right) \mathrm{d}\theta \right] \mathrm{d}z, \qquad (4.4)$$

which expresses the sum of the interactions from both the surface and distributed charges outside the box, from all eight half-quadrant sectors about the central charge, depicted in Figure 4.4. This integral is consistent with the proposed external field contribution discussed by [55].

To simplify the calculations, we have replaced the above integral for the external volume beyond the $2b \times 2b$ box, with an integral for an equivalent cylindrical external volume. This equivalent volume is depicted conceptually in Figure 4.5. The external cylindrical volume would start outside the cylinder of radius of a, given by

$$a = \frac{2b}{\sqrt{\pi}} \qquad (4.5)$$

The resulting integral can then be re-written, as measured from a central ion, as

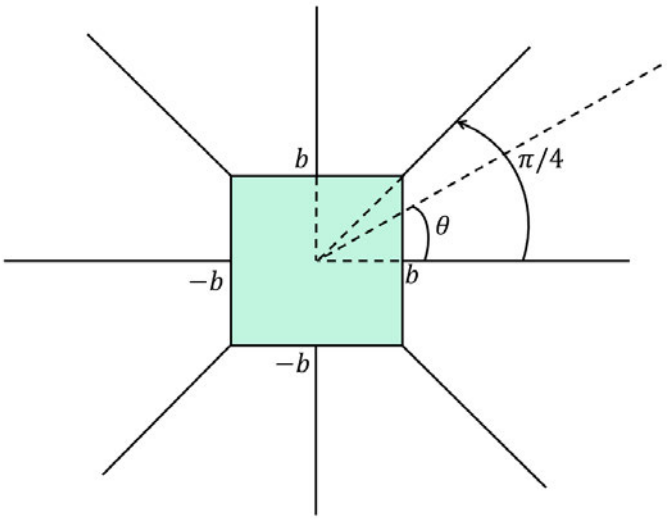


Figure 4.4: The structure of the eight half-quadrants around the simulation box (top view). The integration for the external field contribution, Eq 4.4, is performed over all space external to the shaded region.

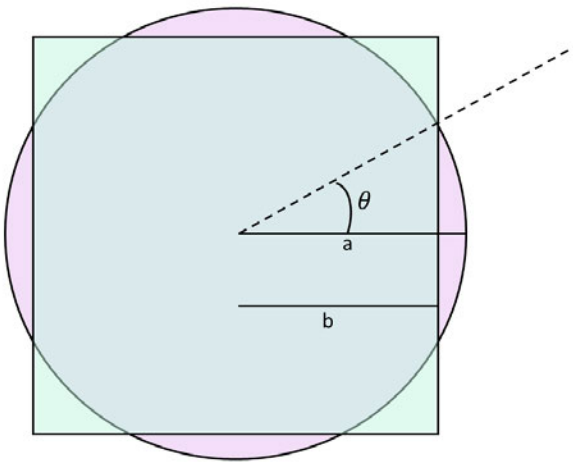


Figure 4.5: Conceptual diagram of the replacement of the square based prism of half-width b by a circular cylinder of radius a of equal volume (top view)

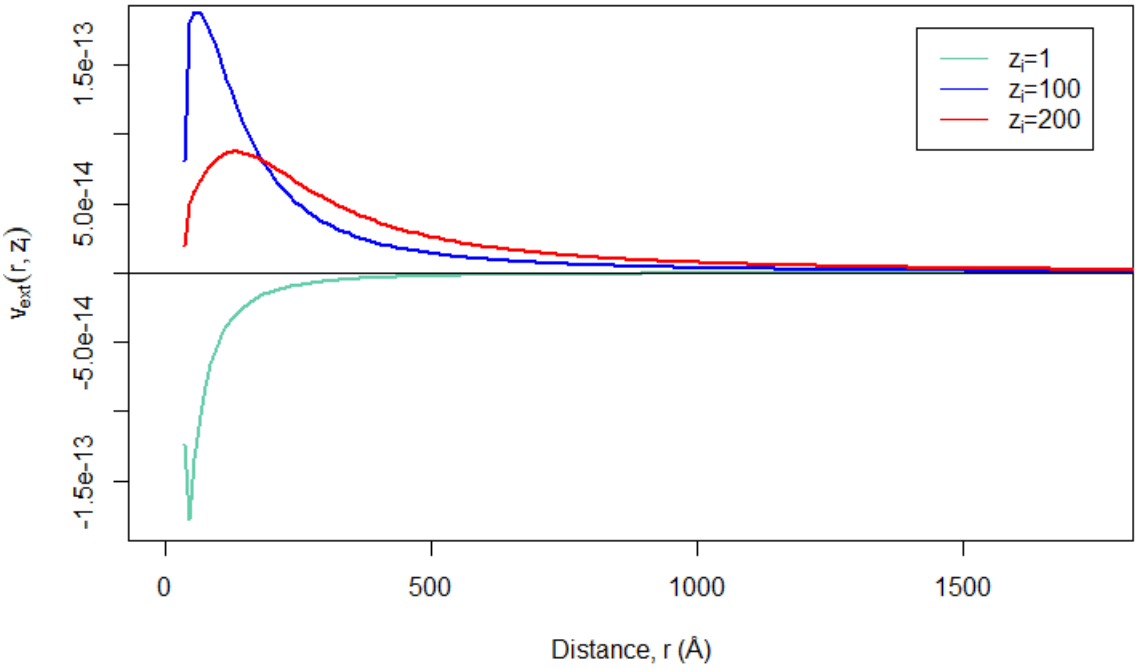


Figure 4.6: Plot of external potential contribution, v_{ext}, as a function of radial distance r. Shown are external potential for three values of z for a PFDA + Ca^{2+} system.

$$w_{ext}(z_i) = \int_0^\infty \left[\frac{\rho_{eq}(z) + \sigma_{surf}\delta(z)}{4\pi\varepsilon_0\varepsilon_r} \int_0^{2\pi} \left(\int_a^\infty \frac{r\mathrm{d}r}{\sqrt{r^2 + (z - z_i)^2}} \right) \mathrm{d}\theta \right] \mathrm{d}z. \tag{4.6}$$

Furthermore, given that the charge distribution would no longer depend on angle, the θ integral can be explicitly performed. Utilizing the properties of the δ-function, further integration of the surface term can also be performed. The final expression implemented is thus

$$w_{ext}(z_i) = \frac{1}{2\varepsilon_0\varepsilon_r} \left[\sigma_{surf} \int_a^\infty \frac{r\mathrm{d}r}{\sqrt{r^2 + z_i^2}} + \int_0^\infty \left(\rho_{eq}(z) \int_a^\infty \frac{r\mathrm{d}r}{\sqrt{r^2 + (z - z_i)^2}} \right) \mathrm{d}z \right]. \tag{4.7}$$

The integrals that remain in Eq 4.7 are evaluated numerically using the trapezoidal rule from $r_0 = round(a)$ to $r_{max} = 10,000$ Å, in steps of Δr =10 Å, and from z =1 Å to z_{max} in increments of $\Delta z = 1$ Å. It is adequate to set z_{max} (for both of the variables `maxzi` and `maxzj`) to any value that is larger than the highest distance from the surface z that any molecule reaches during the initial simulation. By inspecting Figure 4.6 it is possible to confirm if the choice of r_{max} was sufficient to capture the effective range of the external field for each simulation setup. Should it not be sufficient, this value can be altered and stored in `rmax`; the choice of Δr is stored in `deltar`.

4.4 Monte Carlo simulation

Once the system is set up with all molecules in place and the initial total potential energy calculated, the procedure is ready to perform the Monte Carlo simulation proper. Each step is randomly decided, sampled from a $U(0,1)$ distribution via the R function `runif(1)`, to determine whether to take a translation step or a rotation of a given molecule. A value of less than or equal to 0.5 results in a translation, while a random value greater than 0.5, results in a rotation.

4.4.1 Rotations and translations

If a rotation is selected, three random angles α, β, γ (stored in `degX`, `degY` and `degZ`, respectively) are produced within the range specified, for example between -5 and 5 degrees. The molecule is then rotated by these three amounts about the x, y and z axes, respectively. It is in this calculation, that the `origx`, `origx` and `origz` coordinates introduced earlier are used. In these vectors is stored information on the orientation of the molecule centred at the origin, (0,0,0). This information is used in the three following rotation equations. For rotation about the x axis the new atomic coordinates are calculated using

$$\begin{cases} x_1 &= x_0 \\ y_1 &= y_0 \cos\left(\frac{\alpha\pi}{180}\right) - z_0 \sin\left(\frac{\alpha\pi}{180}\right) \\ z_1 &= y_0 \sin\left(\frac{\alpha\pi}{180}\right) + z_0 \cos\left(\frac{\alpha\pi}{180}\right) \end{cases} . \tag{4.8}$$

Similarly, for rotation about the y axis the new atomic coordinates are,

$$\begin{cases} x_2 &= z_1 \sin\left(\frac{\beta\pi}{180}\right) + x_1 \cos\left(\frac{\beta\pi}{180}\right) \\ y_2 &= y_1 \\ z_2 &= z_1 \cos\left(\frac{\beta\pi}{180}\right) - x_1 \sin\left(\frac{\beta\pi}{180}\right) \end{cases} . \tag{4.9}$$

Finally, for rotation about the z axis the rotated atomic coordinates are,

$$\begin{cases} x_3 &= x_2 \cos\left(\frac{\gamma\pi}{180}\right) - y_2 \sin\left(\frac{\gamma\pi}{180}\right) \\ y_3 &= x_2 \sin\left(\frac{\gamma\pi}{180}\right) + y_2 \cos\left(\frac{\gamma\pi}{180}\right) \\ z_3 &= z_2 \end{cases} . \tag{4.10}$$

The differences between these origin-centred final coordinates (x_3, y_3, z_3) and the initial origin-centred values (x_0, y_0, z_0) are then added to the actual atom coordinates for the molecule, to get its new rotated atomic coordinates for the new step.

Translations, or moves, are determined by the step size, `m`, as defined in Table 4.1, with a default value of 0.5 Å. Three random numbers are generated in the range $(-m, m)$

via a uniform distribution in each of the x, y and z directions, and the position of the molecule is updated accordingly. The algorithm checks to see if the translation or rotation leaves the molecule inside the box, in the x and y directions, and if not, applies a periodic translation. In the case of the surface at $z = 0$, there are different cases for a translation or a rotation. If a rotation results in the molecule being placed through the surface, the rotation is rejected and the original position is restored. If a translation puts part or all of the molecule below the surface, the random x and y translations are kept but the z translation is rejected and the original z coordinates are retained.

4.4.2 Long-range force implementation

In order to calculate long range forces for multiple simulation runs at once, the variable `fileList` can be used to store the strings of the .RData file locations from the initial MC simulation run. Densities are calculated for each molecule and ion type in the simulation, across z intervals from -0.5 Å to `maxzj` Å of size 1 Å e.g. (-0.5,0.5), (0.5,1.5),... These densities are calculated using the R function `hist`. The charge for each species is used to calculate the net charge distribution in the z direction. This is stored in `netCharge1` and calculated as the sum across all primary molecule and solution ion types. These values are then written to the `Netcharges/TotalNetCharge.txt` files. The potential calculations utilising Eq 4.7 and the net charges are stored in `wlr_i` for each `z_i`. `wlr_final` is equal to `wlr_i`$\times$ `e` where `e` is the electron charge. Potentials are written to the `NetCharges/LongRangePotential.txt` files.

The long range force calculations are incorporated by running the `Simulation_withLRF` R script. This works as per the initial MC simulation described above, with the additional input of long range potentials, w_{ext}, from the text file, into `lrList`. The external potential values are obtained by selecting the potential for the interval of z co-ordinates of the nearest Å, via the `ceiling` function. This potential value is then multiplied by the charge on the atom, and this long range electrostatic contribution is included every time a potential calculation is performed.

4.4.3 Change in potential calculation

The new total interaction energy is then compared to the energy associated with the previous step. Following the method detailed in [56], if the potential energy difference[2], following a rotation or translation, is negative, which is indicative of a more favourable configuration, the new system configuration is accepted and the current potential energy value and molecule positions are updated. If the difference is positive, corresponding to a less favourable configuration, the configuration may potentially still be accepted, with

[2]This difference is calculated as after−before.

Table 4.3: Simulation output variables

Variable	Description
`u_tot_list`	Total potential after each MC iteration
`SurfaceAtomPotentials`	Total potential between molecules and surface at each MC iteration
`centreToSurface`	Distance in Å from the centre of each molecule to the surface at each MC iteration
`maxToSurface`	Distance in Å from the highest point of each molecule to the surface at each iteration
`xRotStore`	x rotation of each molecule at each iteration
`yRotStore`	y rotation of each molecule at each iteration
`zRotStore`	z rotation of each molecule at each iteration

probability equal to

$$p_a = e^{-\beta \Delta w} \tag{4.11}$$

where

$$\beta = \frac{1}{k_B T} \ ,$$

k_B is Boltzmann's constant and T is the temperature in Kelvin. Statistics regarding molecular orientations and locations for each accepted new configuration are collected and stored. If a rotation or translation is rejected, the system details at step $i + 1$ are set to those at step i. This continues until the final number of required MC steps has been reached. All objects in the R workspace are written to a .RData file, for use in subsequent calculations and visualisations.

4.5 Analysis

The primary simulation analyses and outputs are outlined in the sections below, with Table 4.3 containing the most important of the output variables. Example plots of these and their interpretations appear thereafter. Visualisations produced by the scripts fall into two main categories, those corresponding to a single simulation scenario, and those that combine and compare multiple simulation results.

4.5.1 Single simulation run statistics

The code to produce the potential energy plot for a single simulation run is part of the `Analysis` script. An example output is shown in Figure 4.7. These plots are useful for determining when equilibrium has been reached, and hence the point separating the equilibration section from the production section. This value is stored in the variable `cropPoint`, that determines the portion of data utilised for statistical analysis of the

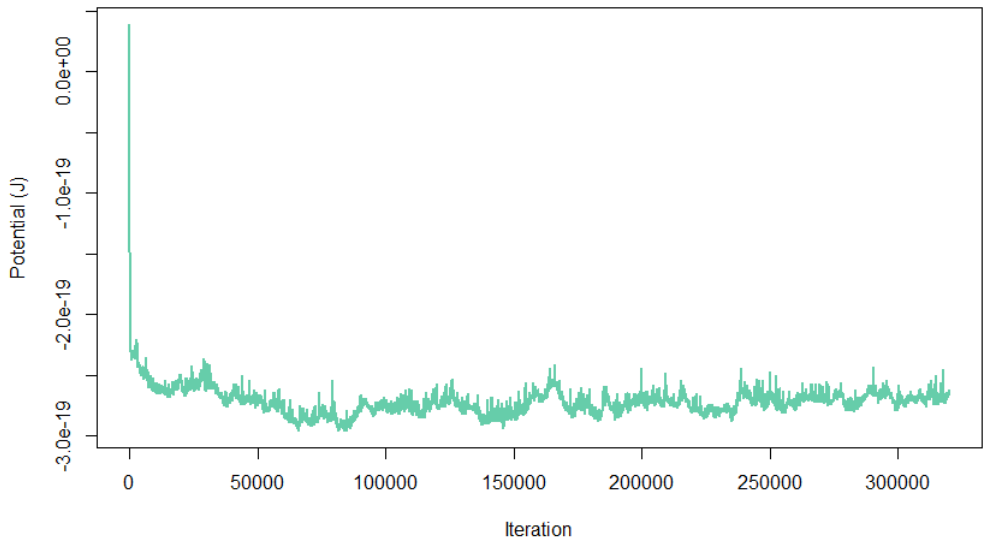


Figure 4.7: Example potential energy plot as a function of iteration number for a PFOA ion only system with a positive surface charge.

simulation. A script has also been written to produce a plot of overlain potentials for comparing multiple simulation runs. An example can be seen in Supplementary Figure A.3.

The plot of the final simulation positions, Figure 4.8, shows the system as a whole at the last step of the simulation. However, co-ordinates are saved for every iteration of the simulation so that the system's configuration at any point of the simulation may be inspected. Note that the system configuration at iteration 0, is not the same as the initial configuration found with plotting a snapshot of the equilibrated system at the start point of the production run, e.g. at iteration 2,500. The rotations of the molecules at each iteration are stored, and can be retrieved via the code in Appendix E. If molecular rotations are of interest, it may also be useful to plot molecule rotations as a function of distance from the surface.

4.5.2 Density calculations and plots

For surface interaction studies, we are primarily interested in the ensemble average number per unit volume of each type of molecule and ion as function of the distance from the surface face. This is calculated in the `DensityComparison` script. An example of such a plot is shown in Figure 4.9, where the red and black curves designate two different simulation scenarios, while the different line types differentiate the molecular and ionic species. This plot showing results of two separate simulation studies, was extended to show results of three case studies in Supplementary Figure A.1. While it is easy to extend this further to include a greater number of different species of molecules and ions, it may be advisable to produce separate plots so that these can be seen more

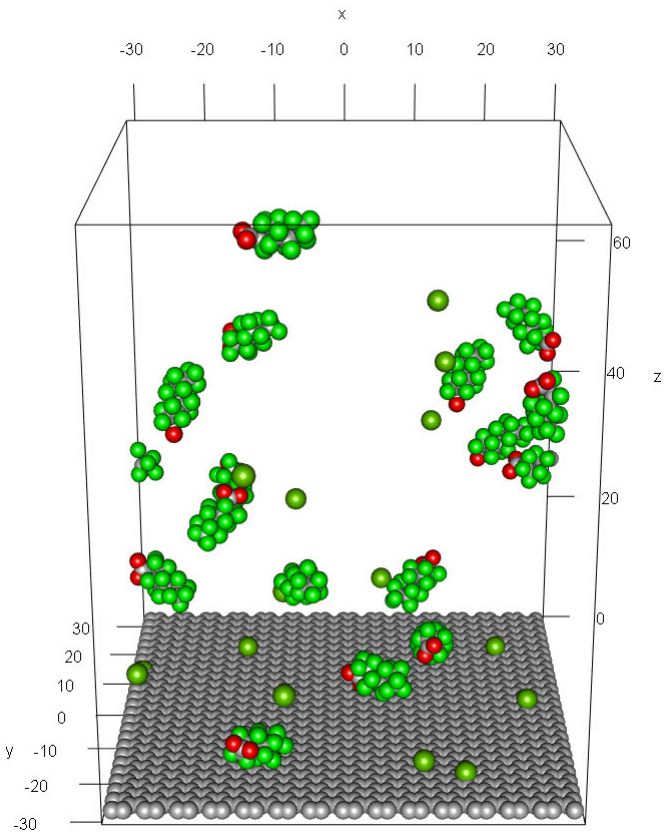


Figure 4.8: Snapshot of the simulation system in its final configuration for the case of PFOA with Ca^{2+} ions and a negative surface charge.

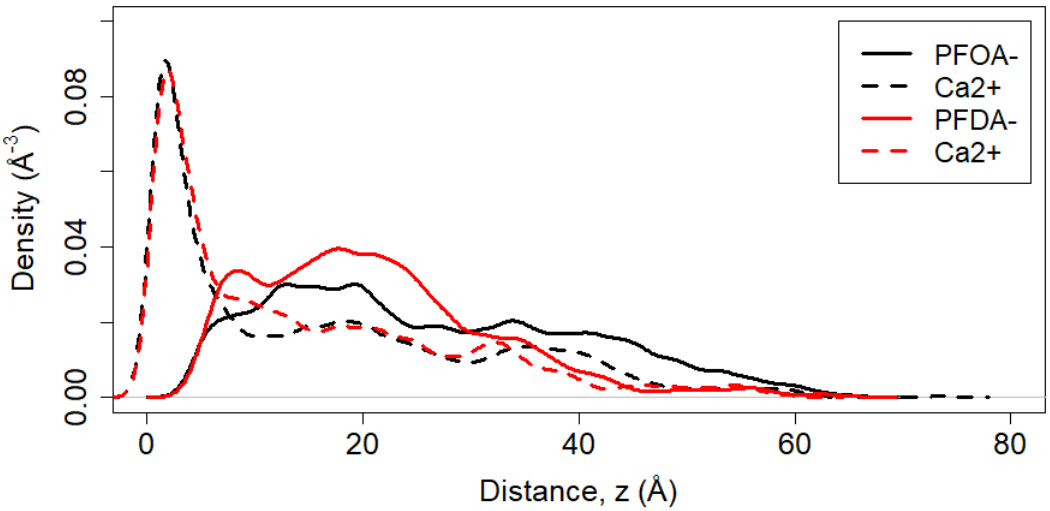


Figure 4.9: Plots of number density profiles as a function of distance from the surface. The results compared the distributions obtained from independent simulation of PFOA and PFDA both involving Ca^{2+} ions and a negative surface charge.

clearly. In the case of nonuniform surface charges, the molecule and ion densities may also be plotted as a 2D heat map, across the x and z dimensions, with the colour indicating the density magnitudes as shown in Figure 4.10.

4.5.3 Long-range force plots

In addition to plots showing the decay with distance of the external interaction potential, shown in Figure 4.6 and discussed above with regard to the choice of r_{max}, two other plots were produced by the external potential code. The first was a plot of the net charge density profile, shown in Figure 4.11. It was observed that this goes to zero as z increased, indicating that the chosen z_{max} value was sufficiently large. The second output is shown in Figure 4.12. This shows the external potential subjected to a negative and positive unit charge respectively, as a function of the distance z from the surface. A point of interest is the position where the lines cross the axis at zero potential, this is the point where the external potential due to the surface charge is equal to the contribution due to the mobile charges in the box medium.

4.6 Conclusions and future work

The R-MCMolecSim software described in this chapter applied the Monte Carlo simulation method to calculate equilibrium properties of systems involving a solution of charged molecules and ions interacting with a charged surface. The software can model a range of different rigid molecules, solution ions in an implicit water medium, and molecular surfaces. It analyses many aspects of the system, including the statistics of molecule and ion distribution from the surface, molecule rotations and the calculation of the relative contributions of van der Waals and electrostatic interactions to the total energy. The program represents a useful addition to the body of available research software in that it allows access to equilibrium Monte Carlo molecular simulations by researchers not conversant with the Fortan language, or unable to purchase expensive commercial software packages. All simulation aspects including analysis and visualisation features require only a free R [45] installation.

While the R-MCMolecSim software can currently model a range of scenarios, for example molecule-surface interactions, including adsorption and desorption, the model and code can be extended in many ways. One of those is the replacement of the implicit water medium with an explicit one. That is, explicit water molecules could also be included in the simulation box at a specified density and iterated over in the same manner as the molecules and ions in the current simulations. Another extension is to model systems involving two parallel surfaces confining the liquid phase between them. Alternatively, a bulk solution phase could be modelled using a box containing

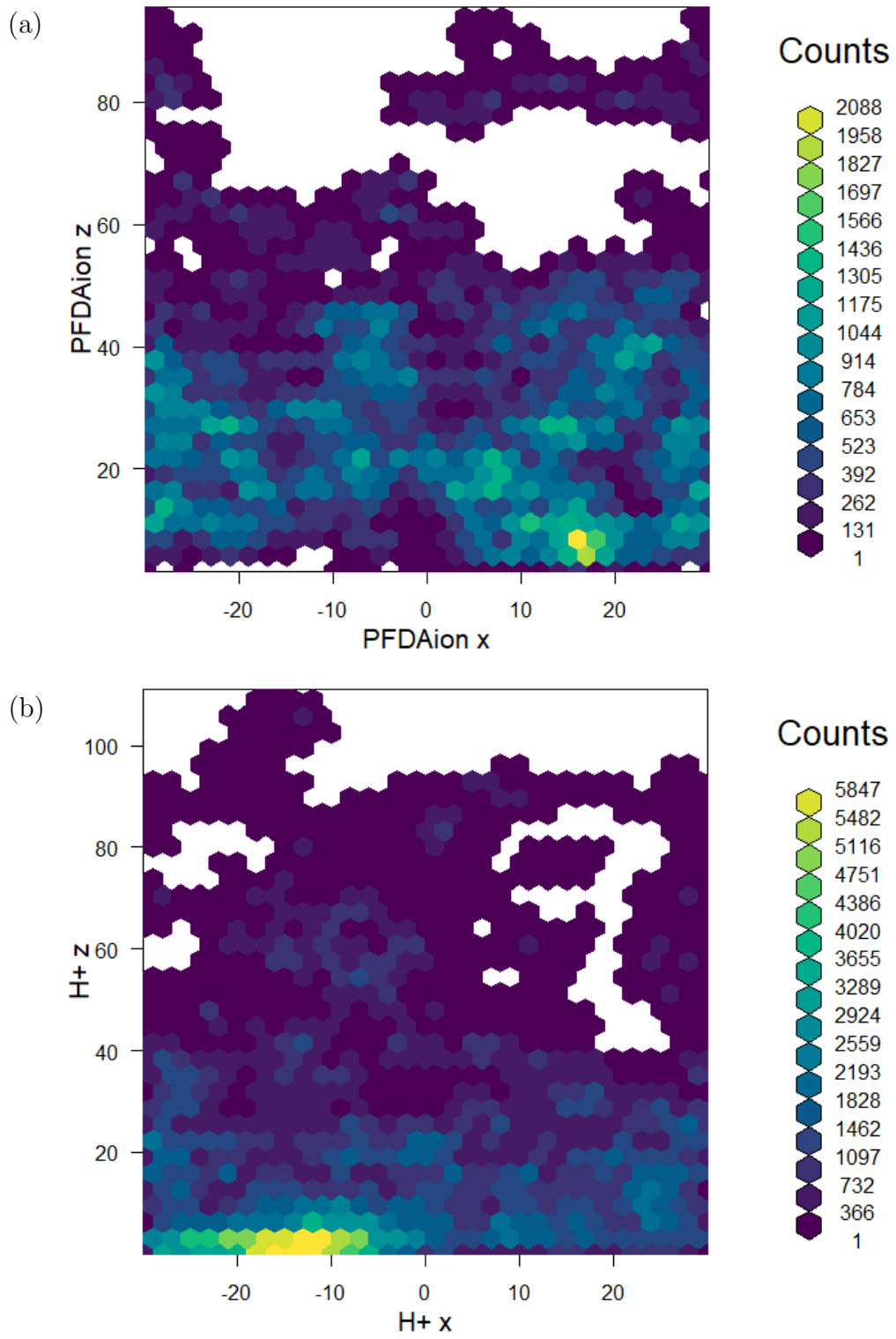


Figure 4.10: 2D density plots for (a) PFDA and (b) H^+ on surface of mixed charge

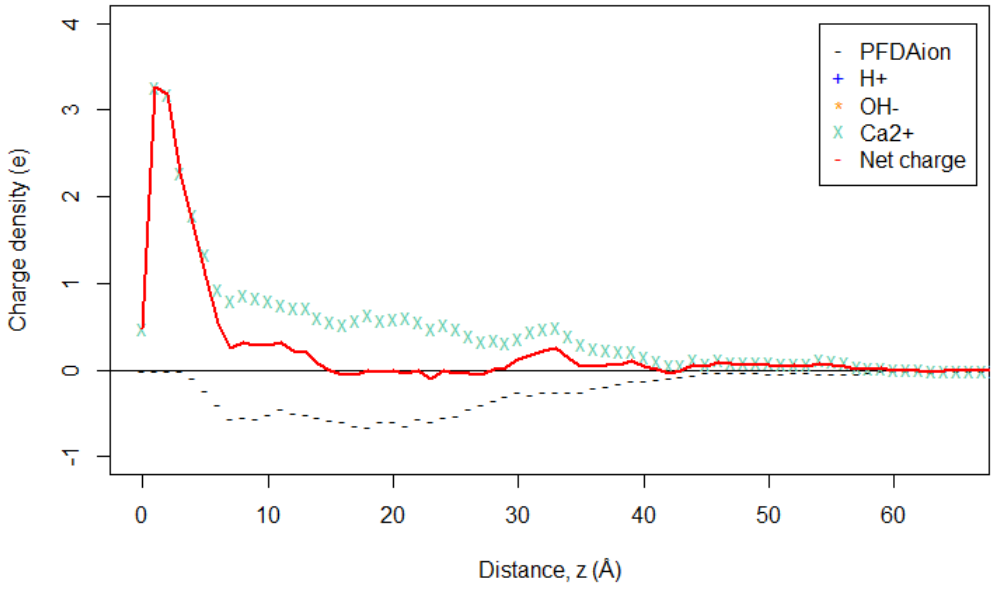


Figure 4.11: Plots of ensemble-averaged charge density distributions as a function of distance z from the surface for a system comprising PFDA anions, Ca^{2+} ions and a negative surface charge. Shown are individual charge distributions and the net charge distribution.

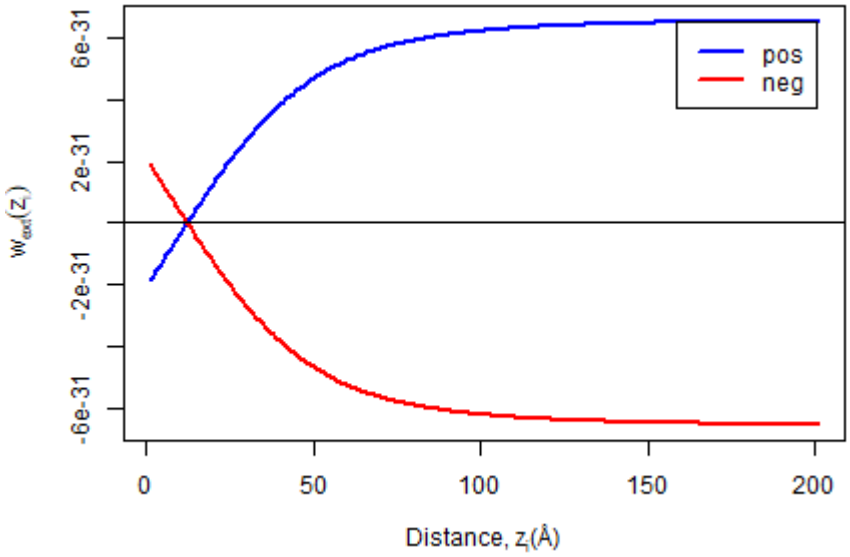


Figure 4.12: Plots of external potential as a function of z experienced by a positive and negative unit charge respectively for the case of a system of PFDA anions, with Ca^{2+} counterions and a negative surface charge.

just the solution, with periodic boundary conditions across all six faces. Finally, the interface between the user and the program could be improved to make it easier to change various parameters as well as to initialise the simulation, including a more automated construction of the molecular surfaces.

Part II

Environmental investigations

Overview

Part II of the thesis comprises three environmental investigations into PFAS. The first examines PFAS concentrations in biosolid samples from waste water treatment plants, the second investigates PFAS prevalence in soils from locations where aqueous film-forming foams have been used, and the third focuses on the immobilisation of PFAS within such soils.

Throughout the three studies, experimental measurements are analysed and compared to what is theoretically expected based on sorption theory. This included the effects of PFAS size, surface charges, pH and correlation with measured element concentrations.

Chapter 5

Perfluoroalkyl, fluorotelomer sulfonate, and perfluorooctane sulfonamide contamination in biosolids: Composition, co-contamination and re-use implications

This chapter details a thorough investigation of PFAS contamination in archived biosolid samples from twelve waste water treatment plants located across Australia, including historical biosolid stockpiles dating back many decades from one of these locations. It appeared in the journal Environmental Pollution with the title "Perfluoroalkyl, fluorotelomer sulfonate, and perfluorooctane sulfonamide contamination in biosolids: Composition, co-contamination and re-use implications".[1] Supplementary information associated with this work appears in Appendix B. The sample analysis was carried out externally by ALS Ltd.

As seen in Chapter 2, most particularly in Figure 2.1, biosolids represent a significant vector for soil contamination with PFAS, and a wide range of molecules may be present. Twenty-eight different PFAS, covering those examined in the review on immobilisation plus several others, were measured in this study. The analysis was extended beyond the usual reporting of PFAS concentrations, to include quantification of correlations between the different PFAS measured and between PFAS and other factors such as metal concentrations and pH. These findings were discussed in the context of the theoretical interactions between PFAS anions and different surfaces, linking with the

[1]Reprinted courtesy of Elsevier, Environmental Pollution (See Appendix F for further details).

theoretical work of Chapter 3 on sorption. For real-world relevance, concentrations were compared to international regulatory values, and post-oxidation PFAS concentrations were measured for a representative subset of locations to investigate long-term precursor transformation.

The analytical suite of 28 PFAS compounds used in this chapter was what was externally available at the time, and was large in comparison to the 3 PFAS listed or under consideration for listing in the Stockholm convention. Knowledge and interest in additional PFAS is expanding constantly, and methods become overtaken by more modern techniques over time. Some underestimation of PFAS can also occur due to under-extraction from complex matrices. The following article was published in 2020, and since that time knowledge and publications on PFAS have been growing rapidly. Additionally, guidelines for biosolids have been established for allowable PFAS concentrations in the Australian context.

It is noted that these samples were originally collected for purposes other than PFAS analysis and their collection methods and storage are detailed in the methods section and references contained therein. It is advised that this chapter does not make reference to additional source pathways of contamination in relation to biosolid stockpiles which may have been treated with PFAS containing substances such as some historically used herbicides, or to contamination which may have occurred during collection, storage and processing. The redacted text in Section 5.3.1[2] can be read as containing the revised population ranges of over 500,000, less than 10,000 and over 500,000 people respectively.

[2]This section is labelled as 3.1 within the published work.

Environmental Pollution 266 (2020) 115120

Contents lists available at ScienceDirect

Environmental Pollution

journal homepage: www.elsevier.com/locate/envpol

Perfluoroalkyl, fluorotelomer sulfonate, and perfluorooctane sulfonamide contamination in biosolids: Composition, co-contamination and re-use implications☆

Julie A. Sleep *, Albert L. Juhasz

Future Industries Institute, University of South Australia, Mawson Lakes, SA, 5095, Australia

ARTICLE INFO

Article history:
Received 3 April 2020
Received in revised form
17 June 2020
Accepted 25 June 2020
Available online 8 July 2020

Keywords:
Perfluoroalkyl substances
Biosolids
Co-contamination
TOP assay

ABSTRACT

In this study, biosolids from 12 waste water treatment plants across Australia were analysed to quantify the concentration of 28 per- and polyfluoroalkyl substances (PFAS). PFAS concentration varied significantly between locations (5.4 150 μg kg^{-1}) while perfluorooctane sulfonic acid (PFOS) was the predominant analyte in 9 of 12 biosolid samples (4.7 86 μg kg^{-1}) contributing 17 93% to the total PFAS concentration. However, in WWTP2 and WWTP10, PFAS composition differed significantly, with fluorotelomer sulfonic acids (FTSAs) and perfluorooctane sulfonamide-based substances (FOSAMs), precursor compounds of restricted PFAS, contributing significantly to Σ_{28} PFAS concentration. Five additional biosolid samples from historical stockpiles of varying ages located at WWTP3 were analysed to assess changes in Σ_{28} PFAS concentration with biosolid age (10 50 years). While temporal trends in Σ_{28} PFAS or individual PFAS concentration were not observed, a strong negative correlation was observed between pH and Σ_{28} PFAS concentration over a pH range of 4.1 6.6. Three samples (WWTP2, 3 and 10) were selected for further analysis using the total oxidisable precursor (TOP) assay to provide insights into the potential impact of oxidative transformation on individual PFAS concentration. Treatment with persulfate resulted in the decrease of 6:2 and 8:2 FTS (WWTP2), MeFOSE (WWTP2 and 3), EtFOSE (WWTP2), MeFOSAA (WWTP2, 3, 10) and EtFOSAA (WWTP2, 3, 10) with an increase in C_4 C_9 PFCAs (1 232 μg kg^{-1}), while changes in PFSA concentrations were negligible (< 7 μg kg^{-1}). Application of PFAS biosolids international guidance to samples analysed highlighted that 24 88% of biosolids exceeded regulatory standards, although this number increased when precursor compound oxidation was taken into consideration.

© 2020 Elsevier Ltd. All rights reserved.

1. Introduction

Per- and poly-fluoroalkyl substances (PFAS) are anthropogenic substances, manufactured for use in products ranging from aqueous film forming foams (AFFF) and stain repellents to fast food packaging and dental floss (Barzen-Hanson et al., 2017; Kotthoff et al., 2015; Guo et al., 2009). A listing of individual PFAS names and abbreviations is located in Supplementary Table S1. PFAS consist of fully or partially fluorinated carbon backbones, along with varying functional groups, both of which contribute to toxicity and affect environmental behaviour (Rayne and Forest, 2009). The high strength of their carbon-fluorine bonds make these substances persistent (Yamashita et al., 2008), and their accumulation in soil, water, plants and animals at all trophic levels (Munoz et al., 2017), poses a hazard to communities in contact with impacted land and water resources.

Waste water treatment plants (WWTPs) play a significant role in the transfer of PFAS from contamination point sources to other locations. Landfill leachates, AFFF and waste from metal plating industries have been found to be significant sources of perfluorinated sulfonic acids (PFSAs) found in WWTP sludges, while textile and carpet protection agents are contributing sources of perfluorinated carboxylic acids (PFCAs) (Alder and van der Voet, 2015). Pathways for these PFAS to exit the WWTP include effluent discharge, biosolid applications to land and the supply of recycled water.

An examination of the concentrations of PFCAs, PFSAs and

☆ This paper has been recommended for acceptance by Jörg Rinklebe.

* Corresponding author.
E-mail addresses: sleja001@mymail.unisa.edu.au, julie.sleep@mymail.unisa.edu.au (J.A. Sleep).

https://doi.org/10.1016/j.envpol.2020.115120
0269-7491/© 2020 Elsevier Ltd. All rights reserved.

perfluorooctane sulfonamide (PFOSA) in sludge from 1165 WWTPs in Bavaria, Germany over the period 2008–2013, revealed PFAS concentrations decreased over the period for many WWTPs. However, 16% of the WWTPs showed increases in PFAS concentration over this time frame (Ulrich et al., 2016). In a study of 20 Swiss WWTPs, no significant differences in temporal PFAS concentrations over the time period 1993–2008 were found (Sun et al., 2011). In contrast, over the time period of 2008–2011, perfluorooctane sulfonic acid (PFOS) concentrations in digested sludge from 45 Swiss WWTPs decreased (Alder and van der Voet, 2015). In the United States, tests for 12 PFAS in limed biosolids collected from 2005 to 2013 every 2–3 months showed that concentrations remained generally unchanged over time, except for occasional concentration spikes and some temporal variability (Armstrong et al., 2016).

High PFAS concentrations in WWTPs are of concern due to their eventual transfer into the environment, both via effluent discharge, water reuse and biosolid applications. Studies have found elevated concentrations in sediments near discharge areas (Higgins et al., 2005). Biosolids, derived from WWTP sludge, are used widely in agriculture, forestry and landscaping. The use of PFAS-contaminated biosolids for these purposes is of some concern, leading to the retention of PFAS in soil, uptake of PFAS by agricultural crops (Blaine et al., 2014; Wen et al., 2018), and the leaching of PFAS into groundwater (Lee and Mabury, 2014) and drainage waters (Gottschall et al., 2010).

Biosolids are often applied in agriculture on repeated, rather than a single occasion, while soils may also become contaminated due to industrial use and waste disposal. In a comparative study of soil-biosolid mixtures in both industrially impacted soils, and municipal soils subjected to repeated application of biosolids, PFSA concentrations were found to be higher in the latter soils, and PFCA concentrations in the former (Blaine et al., 2014). In the study of (Blaine et al., 2014), the average concentration of the three most prevalent contaminants in industrially impacted soil were found to be PFDA (93 μg kg^{-1}), PFOA (79 μg kg^{-1}) and PFOS (50 μg kg^{-1}). Municipal soils had significantly higher PFOS contamination with the three highest contaminants being PFOS (319 μg kg^{-1}), PFDS (61 μg kg^{-1}) and PFOA (15 μg kg^{-1}). In Australia, biosolids are commonly applied to agricultural lands, with an estimated annual transfer of 8 kg of PFOS and 2 kg of PFOA (Gallen et al., 2018).

The goal of this study was to examine the variation in PFAS concentration and composition in biosolids from a selection of geographically distant WWTPs, as well as in historical stockpiles of varying ages. PFAS concentration was related to biosolids physicochemical properties, including pH and trace element concentrations. In addition, an investigation was undertaken into which of the less common PFAS, such as fluorotelomer sulfonic acids (FTSAs) and perfluorooctane sulfonamide-based substance (FOSAMs), were present in biosolid samples, and how these compounds make a contribution to total PFAS concentration, both directly and as potential transformation product precursors. This data was collated and set in the context of environmental guidelines for the use of biosolids for agricultural application.

2. Materials and methods

2.1. Biosolid samples and characterisation

Seventeen samples from 12 WWTPs (WWTP1-WWTP12) located across six Australian states and territories were selected from archived biosolids, originally collected in 2009 for studies analysing metal speciation in biosolids (Donner et al., 2011; Donner et al., 2012; Donner et al., 2015). Collection points and treatment methods varied across the different WWTPs, with a summary given in Supplementary Table S2. Samples were collected from stages ranging from sludge belt-presses, fresh biosolid stockpiles, and aged stockpiles dating back to the 1970s and earlier, while 2 samples (WWTP6 and 12) were limed. All samples were air dried and stored in sealed glass jars at room temperature. Reverse aqua regia digests had been previously performed on archived biosolids; data detailing Al, Fe, Mo, Cu, Zn, C, N, P K, Mg, Se, Mn, Na, Ni, Cr, Cd and Pb concentration were made available, along with electrical conductivity (EC) and pH measurements. Detailed methods for the EC, pH, C and S measurements are described in (Donner et al., 2015), and for the metals in (Donner et al., 2012).

2.2. PFAS extraction and analysis

Biosolids (2 g) in polypropylene vials were extracted with CH_3OH:H_2O (10 mL, 1:1) adjusted to pH 9–10 using NH_4OH (20 μL). Mixtures were tumbled on an end-over end shaker (60 rpm for 1 h) after which samples were centrifuged at 4335 g, room temperature for 20 min. Supernatants were collected and transferred to new polypropylene vials with CH_2O_2 added to adjust the pH to 3–4. Liquid samples were applied to Envirocarb solid phase extraction cartridges for sample clean-up. Methanol eluates were stored at 4 °C prior to PFAS quantification using LC-MS/MS.

Analysis targeted priority PFAS (28 compounds listed in Table S1) using LC-MS/MS (1290 Infinity II HPLC system coupled online with a 6495 B Triple-Quadrupole MS platform, Agilent Technologies), incorporating 13C surrogate compounds and USEPA method 537/ASTM D7979-17. Prepared samples were injected onto a ZORBAX Eclipse Plus C18, 3.0 × 50 mm, 1.8 μm (Agilent Technologies) with PFAS separated using 5 mM ammonium acetate in water and 5 mM ammonium acetate in 95% methanol mobile phases. Eluted PFAS were ionised using an Agilent Jet Steam ESI source in negative ion mode in multiple reaction monitoring (MRM) mode for priority PFAS compounds. PFAS results were corrected for mass labelled extracted internal standards which were added prior to sample preparation to assess matrix effects and verify sample processing. PFAS analytes without a commercially available mass labelled analogue were corrected using a closely eluting mass labelled PFAS compound.

2.3. Total oxidisable precursor assay

The total oxidisable precursor (TOP) assay was utilised to provide insights into the potential impact of oxidative transformation on individual PFAS concentration. Three samples were selected for TOP assessment (WWTP2, 3 and 10) which was undertaken as described by (Houtz and Sedlak, 2012). Briefly, following biosolid extraction using basic methanol (as detailed above), extracts were incubated with potassium persulfate (60 mM) and sodium hydroxide (0.125 M) at 85 °C for 6 h. After neutralisation, PFAS were quantified using LC-MS/MS as detailed above.

2.4. QA/QC

During the quantification of PFAS in biosolids, the recovery of 13C-PFAS internal standards, applied the extraction process, ranged from 36 to 167% with mean and median values of 95.5% and 97.0% respectively. Low recoveries (< 60%) were observed for some long chain PFAS (PFUnDA, PFDoDA and PFTeDA) and perfluorooctane sulphonamide substances (MeFOSA, EtFOSA, MeFOSE, EtFOSE) in 2 biosolid samples. 13C-PFAS spiked recoveries in sample extracts ranged from 67.7 to 124% with mean and median values of 92.2% and 91.9% respectively.

2.5. Statistical analysis

Fig. 1 was prepared using the software Circos (Krzywinski et al., 2009); correlation analysis was performed using the R package 'Corrplot' (Wei and Simko, 2017), while linear regression calculations were performed using the R 'lm' function (R Core Team, 2018).

3. Results and discussion

3.1. Total PFAS concentrations

Total PFAS concentration (Σ_{28}PFAS), varied considerably between WWTP biosolids, with concentrations ranging from 5.35 to 145 μg kg^{-1}, as shown in Fig. 1. These concentrations are similar to values reported for biosolids in an earlier Australian study (Σ_9PFAS; 5–150 μg kg^{-1}) (Gallen et al., 2016) and from biosolid assessments in Finland (Σ_4PFAS; 18–113 μg kg^{-1}) (Perkola and Sainio, 2013). In contrast, PFAS concentrations in 94 U.S. WWTP biosolid samples were significantly higher (Σ_{12}PFAS), ranging from 354 to 940 μg kg^{-1} (Venkatesan and Halden, 2013).

The highest Σ_{28}PFAS concentrations were measured in biosolids from WWTP1 (145 μg kg^{-1}), WWTP2 (130 μg kg^{-1}) and WWTP3 (122 μg kg^{-1}). Despite the detection of elevated Σ_{28}PFAS concentrations in these biosolids, the WWTPs in these areas serve vastly different population sizes. WWTP1 catchment area serves in excess of [redacted] people and includes an air-force base and industrial areas. WWTP2 is located in a town of approximately [redacted] people, including an air-force base, yet presented similar overall PFAS concentrations to WWTP1. The WWTP3 catchment area includes approximately [redacted] people, including an air-force base. Trade waste potentially enters these sites from locations with PFAS usage, from both the aforementioned bases and from industry. The types of PFAS contributing to the composition of the PFAS contamination, however, was significantly different in WWTP2 compared to

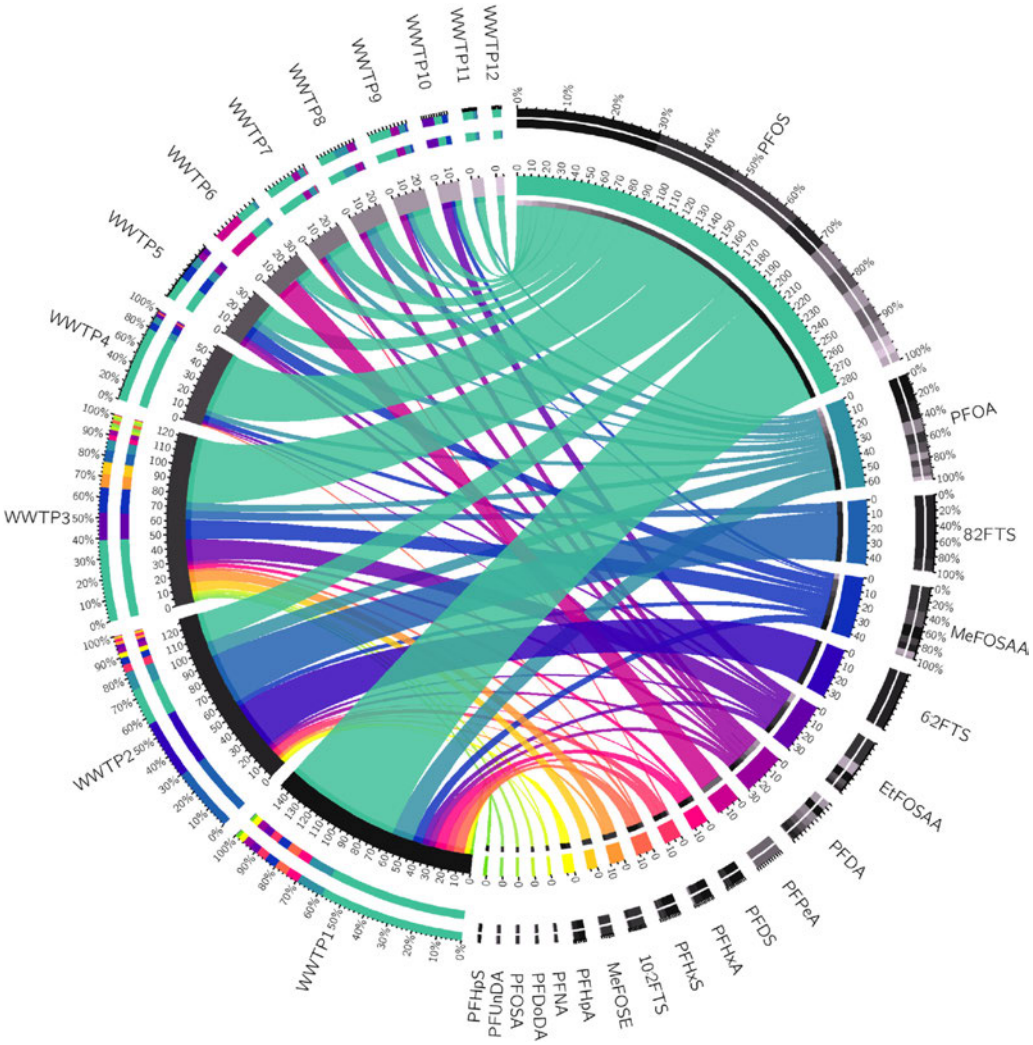


Fig. 1. Concentrations (μg kg^{-1}) and composition of PFAS in biosolids from 12 Australian waste water treatment plants. On the right hand side of the circle, moving clockwise, individual PFAS are shown ordered by decreasing total (average) concentration across all plants. This is followed by WWTPs, ordered by decreasing total PFAS concentration. The size of the link connecting an individual PFAS with a WWTP represents the concentration present, sized according the inner numbered scale (μg kg^{-1}). Values less than 0.5 μg kg^{-1} are not shown.

WWTP1 and 3. WWTP1, 2 and 3 were the only locations from the 12 to have a nearby air-force base, indicating this is associated with high PFAS levels in biosolids from Australian WWTPs. In contrast biosolids from WWTP 4–9, distant from air-force bases, had moderate Σ_{28}PFAS concentrations (23.0–57.0 μg kg^{-1}). Low Σ_{28}PFAS concentrations (5.35–14.7 μg kg^{-1}) were detected in biosolids from WWTP10, 11 and 12, which may be reflective of the small population sizes they serve and/or low PFAS inputs from industrial sources.

3.2. PFAS composition

Fig. 1 shows PFAS composition in biosolids from each WWTP (left hand side), and the total concentration of each individual PFAS ordered clock-wise in decreasing concentration (right hand side). PFAS including PFBS, PFBA, PFTeDA, MeFOSA, EtFOSE and 4:2 FTS were below the level of reporting (0.02–0.1 μg L^{-1}, see Supplementary Table S1) in all samples and as such were not included in Fig. 1. A full table of concentrations is also given in Supplementary Table S3.

For most biosolids, PFOS was the predominant constituent, representing, on average, 53% of the Σ_{28}PFAS concentration, and varying from 17% (WWTP2) to 93% (WWTP12). PFOS concentrations ranged from 4.7 μg kg^{-1} (WWTP10) to 85.7 μg kg^{-1} (WWTP1). Along with PFOS, PFOA was the only other PFAS detected above the limit of reporting (LOR) in every biosolid sample. PFOA concentration ranged from 0.35 μg kg^{-1} (WWTP12 and 10), to 16 μg kg^{-1} (WWTP1) with percentage composition averaging 10.6% and ranging from 2.39% (WWTP10) to 34.3% (WWTP8).

In biosolids from WWTP2, 8:2 FTS and 6:2 FTS were the predominant PFAS contributing 30% (38.4 μg kg^{-1}) and 27% (34.7 μg kg^{-1}), respectively to the Σ_{28}PFAS concentration. This was unique among sites studied and may be reflective of fluorotelomer-based AFFF originating from the nearby air-force base. In WWTP10 biosolids, EtFOSAA was the predominant PFAS, contributing 45.4% of the Σ_{28}PFAS measured (6.65 μg kg^{-1}).

PFPeA was only detected above the LOR in biosolids from WWTP6, and was the major contributor to Σ_{28}PFAS concentration at this location (17.4 μg kg^{-1}; 57.8% of Σ_{28}PFAS). It is unclear why this location exhibited a unique PFAS profile. A previous study observed PFPeA in 86% of Australian WWTP influents sampled, and in all liquid effluent processing stages (primary, secondary, final and recycled water) (Coggan et al., 2019). However, it was reported that although PFPeA was not detectable in any primary sludge, PFPeA was found in 20% of secondary sludge, and 33% of lagoon sludge (Coggan et al., 2019). In a review across multiple countries, changes in PFPeA concentrations from influent to sludge stages varied significantly between WWTP (Arvaniti and Stasinakis, 2015). Hence, differences in processing methods, may have resulted in PFPeA being retained in WWTP6 biosolids. Alternatively high influent concentrations may have been initially present relative to other WWTPs. High PFPeA concentrations found in some river locations have been suggested to arise from metal-electroplating processes, however, this was associated with high concentrations of 6:2 F TS, a precursor of PFPeA (Zhang et al., 2016). As 6:2 FTS was below the LOR in WWTP6 biosolids, as was PFHxA (a major degradation product of 6:2 FTS (Zhang et al., 2016; Wang and Shih, 2011)) it is unlikely that the occurrence of PFPeA arose from 6:2 FTS transformation in this case.

WWTP1, 2 and 3 samples were the most diverse in PFAS composition, containing 10, 13 and 14 different PFAS respectively. WWTP3 biosolids was the only sample location containing long chain compounds, PFUnDA and PFDoDA, while WWTP2 and WWTP3 were the only two found to contain detectable concentrations of FTSAs and PFNA.

3.3. Historical biosolid stockpiles

Five additional biosolid samples were analysed from WWTP3, taken from stockpiles ranging in age from approximately 10 to 40 years old at the time of collection (WWTP3H1–H5). Σ_{28}PFAS concentration in historical biosolid samples varied from 163 to 596 μg kg^{-1}, with the biosolids stockpile from the 1990s–2000s (WWTP3H1), containing the highest PFAS concentration. As seen in Fig. 2, no clear temporal trend in Σ_{28} or individual PFAS concentration was observed, however, all WWTP3 samples had similar relative proportions of each PFAS, irrespective of age.

PFOS predominated the PFAS composition in all WWTP3 samples, ranging from 37 to 61% (60.0–360 μg kg^{-1}), while potential precursor compounds (EtFOSAA and MeFOSAA) were present at

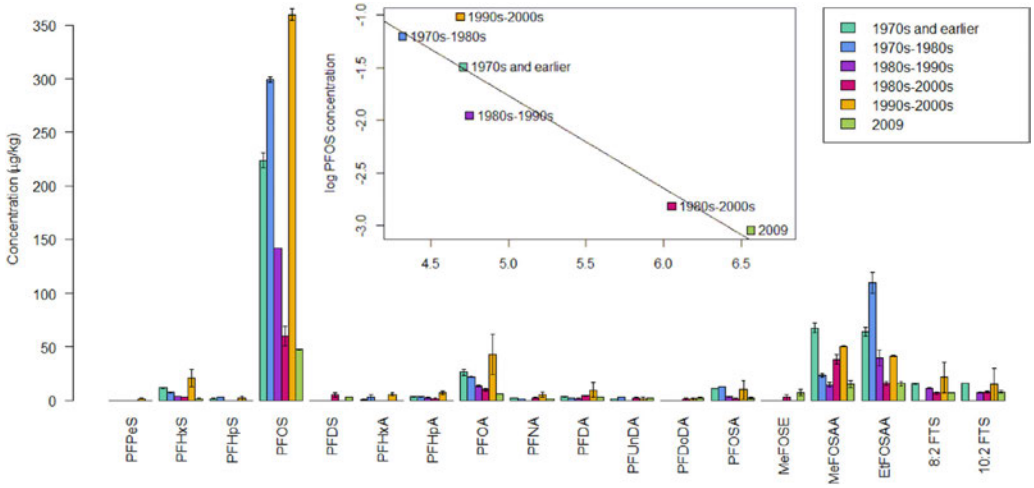


Fig. 2. Individual PFAS concentration (μg kg^{-1}) in WWTP biosolid samples from aged WWTP3 biosolid stockpiles. Data are ordered from oldest to youngest, error bars indicate the range of measurements. Inset: pH vs log(PFOS) for WWTP3 biosolid stockpiles (The equation of the fitted line is given by $\log(C_{PFOS})$ 8.88 pH + 2.64. R^2 value of 0.85 and p-value of 0.005).

concentrations ranging from 16.0 to 110 μg kg^{-1} and 14.7–67.7 μg kg^{-1}, respectively. In contrast to biosolids collected from other localities, WWTP3 was the only location to contain detectable concentrations of PFOSA, PFDoDA, PFUnDA, PFPeS and MeFOSE.

3.4. Relationships between PFAS and biosolid characteristics

Fig. 3 shows a correlation analysis of selected PFAS concentrations and biosolid properties, inclusive of all 17 biosolid samples (12 locations plus historical samples). Full correlation analyses are presented in Supplementary Tables S4–S6. The majority of PFAS concentrations were positively correlated with each other and with metal concentrations. In the latter case, the strongest correlations were observed with cadmium, chromium, lead and nickel concentrations. PFOS concentrations were found to be correlated strongly with all PFAS except 6:2 FTS (weakly negative) 8:2 FTS and PFDoDA (weakly positive). 6:2 and 8:2 FTS concentrations correlated with high sulphur concentrations, while high concentrations of carbon, nitrogen, phosphorus, potassium, magnesium and selenium were associated with low PFAS concentrations, as were pH and EC measurements. A strong (negative) correlation was also observed in the historical data between pH and Σ_{28}PFAS, particularly between pH and PFOS, as shown in the inset of Fig. 2.

This analysis, however, does not allow the distinction between relationships arising from biosolid influences on PFAS sorption, and those that are the result of processing large amounts of industrial waste containing high concentrations of both heavy metals and PFAS. Sorption and leaching play important roles in determining the concentration of PFAS present in biosolids. It is, however, difficult to link sorption propensity to biosolid characteristics without having knowledge of concentrations of PFAS at previous processing stages.

At environmental pH, PFAS, such as PFCAs and PFSAs, usually form anions and interact with surfaces in biosolids and soil mainly through direct electrostatic interactions with positively charged surfaces, or with negatively charged surfaces via divalent cation bridges (Li et al., 2018). Potential divalent cation forming elements measured in this study include Cr, Cu, Fe, Pb, Mn, Mg, Ni and Zn which, with the exception of Mn were positively correlated with the majority of PFAS concentrations. Aside from direct sorption and cation bridging, hydrophobic interactions, involving micelle and bilayer formation, can also be important (Du et al., 2014; Li et al., 2018), potentially affecting final PFAS destinations in the WWTP processing stages.

Functional head group and carbon chain length both play a role in establishing sorption rates, with PFSAs more readily adsorbed than PFCAs (Du et al., 2014). The longer the C chain length, the more

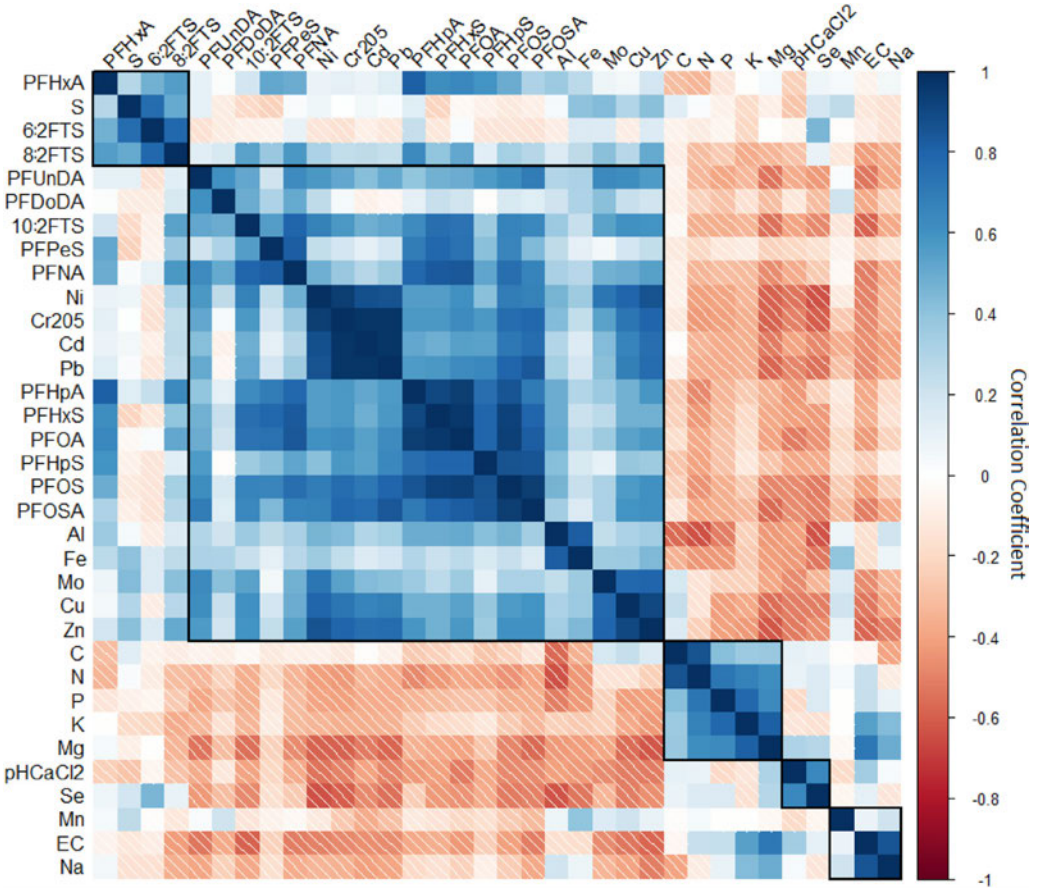


Fig. 3. Correlation between PFAS and biosolid physico-chemical properties, ordered by hierarchical clustering. Clusters for n 5 are denoted by black squares. The value of the correlation coefficient is indicated by the colour intensity, with diagonal stripes indicating negative correlations. For a full listing of correlation coefficients see Supplementary Tables S4–S6. (For interpretation of the references to colour in this figure legend, the reader is referred to the Web version of this article.)

hydrophobic the molecules, resulting in higher sorption propensity (Du et al., 2014). This is reflected in our results, with molecules of carbon chain lengths of 4 or 5 C backbone atoms being mostly less than the LOR. It has been observed that PFAS sorption decreases with increasing pH (Zhao et al., 2014), due to protonation of adsorbent surfaces leading to fewer sorption sites. This is consistent with our findings of negative correlation between pH and the majority of PFAS; this being clear across the pH range 4.1–6.6 for aged biosolids. At higher pH values, however, increasing pH can create more basic sites for divalent cation bridging, thus contributing to an increase in sorption. Salinity and organic matter have been found to increase PFAS sorption (Jeon et al., 2011), however, both Na and C concentrations were found to be negatively correlated with most PFAS concentrations in the biosolid samples.

3.5. Precursors and transformation

Three samples (WWTP2, 3 and 10) were selected for further analysis using the total oxidisable precursor (TOP) assay to provide insights into the potential impact of oxidative transformation on individual PFAS concentration. These samples were selected because they contained elevated concentration (WWTP2 and 3) or significant proportions (WWTP10) of potential precursor compounds including 6:2 F TS, 8:2 F TS, MeFOSE, EtFOSE, MeFOSAA and EtFOSAA. As detailed by (Houtz and Sedlak, 2012; Kim and Kannan, 2007; Ellis et al., 2004), oxidation of known and unknown precursor compounds in environmental samples may result in an increase in PFCA concentration leading to changes in contaminated matrix risk profiles. Although oxidation of precursor compounds such as fluorotelomers is complex, reactions with hydroxyl radicals produced during the TOP assay result in the formation of a series of PFCAs including C_{n+1}, C_n, C_{n-1} etc. down to the C_4 acid (Houtz and Sedlak, 2012). As suggested by (Houtz and Sedlak, 2012), the greatest yield of PFCAs following fluorotelomer oxidation is C_{n-1} followed by C_n then C_{n-2}. In addition, although fluorotelomers alcohols and fluorotelomer methacrylates are not routinely measured PFAS analytes, transformation of these compounds has been shown to result in the production of regulatory driven PFCAs (i.e. PFOA) (Liu and Avendaño, 2013).

Following application of the TOP assay, changes in Σ_{28}PFAS concentration were observed compared to pre-oxidation values. This was most evident for WWTP2 where a 23% increase in Σ_{28}PFAS concentration was observed. Increases in PFAS concentration in the range of 21% (Ye, 2014) to 150% (Houtz et al., 2016) as a result of precursor oxidation have been reported for waste water treatment plant effluents and river water, although the contribution from known (e.g. 6:2 F TS, 8:2 F TS, MeFOSE, EtFOSE, MeFOSAA and EtFOSAA) and unknown precursors is difficult to quantify. Although limited TOP data is available regarding PFCA formation from precursor compounds in biosolids, conceivably the high organic carbon in biosolids may limit precursor oxidation by consumption of oxidant load. This may result in partial PFAS oxidation when matrix interference is significant. This may explain the similarity in Σ_{28}PFAS concentration in pre- and post-TOP assay results for WWTP3 and 10. However, following TOP assessment, the biggest impact on WWTP2, 3 and 10 was the change in PFAS composition and concentration in each sample. Fig. 4 shows changes in individual PFAS in WWTP2, 3 and 10 following oxidation; treatment with persulfate resulted in the decrease of 6:2, 8:2 and 10:2 FTS (WWTP2 and 3), MeFOSE (WWTP2 and 3), EtFOSE (WWTP2), MeFOSAA (WWTP2, 3, 10) and EtFOSAA (WWTP2, 3, 10) with an increase in C_4–C_9 PFCAs, while changes in PFSA concentrations were negligible (< 7 μg kg^{-1}).

In all 3 samples, the most significant change in PFCA concentration was for PFOA. In WWTP2, the increase in PFOA concentration (from 12 to 60 μg kg^{-1}) may have resulted from the oxidation of 8:2 FTS (Houtz and Sedlak, 2012) in addition to transformation of MeFOSE, MeFOSAA and EtFOSAA. EtFOSE degradation in activated sludge via intermediaries including EtFOSAA, EtFOSA, PFOSA, perfluoroctane sulfinate (PFOSI) has been shown to result in increases in PFOS (Rhoads et al., 2008), or PFOS and PFOA (Lange, 2000) concentration. Similarly, transformation of EtFOSE in water by hydroxyl radicals has been shown to result in PFOA as a final product (Nguyen et al., 2013). Although 8:2 FTS was not present in WWTP10, and at low concentrations in WWTP3, significant increases in PFOA concentration post oxidation were also observed in these samples, presumably due to MeFOSE, EtFOSE, MeFOSAA and EtFOSAA oxidation. Increases in shorter chain length PFCAs (e.g. PFBA, PFPeA, PFHxA) in WWTP2 may also have resulted from the oxidation of 6:2 F TS, although contributions from 8:2 FTS oxidation cannot be excluded. PFBA, PFPeA and PFHxA occurrence as a result of 6:2 FTS oxidation have previously been observed in dilute activated sludge (Wang et al., 2011), while the oxidation of unknown precursors may have also resulted in the formation of short chain PFCAs in WWTP2, 3 and 10. Although a small loss in PFOS was observed in WWTP2, it is unlikely the result of its transformation due to chemical stability, rather experimental error associated with differences in mass balance pre- and post-TOPA.

The TOP assay offers a method to understand the potential magnitude of the precursor pool in environmental matrices, however, it does not provide information regarding the rate of (a)biotic transformation, or of the specific final degradation products resulting from environmental transformation. As such, TOP assay results may represent a worst-case scenario. Nevertheless, in some regulatory jurisdictions, the use of the TOP assay is prescribed (Ross et al., 2018). Current environmental guidelines for biosolids, as discussed in the proceeding section, only consider measurements of PFOS and PFOA, omitting information gleaned from the TOP assay on potential transformation of precursor compounds.

3.6. Biosolid contamination guidelines

Table 1 shows Σ_{28}PFAS, PFOS and PFOA concentrations for all samples, including those from historical stockpiles, compared to biosolids guideline values from Australia (HEPA, 2019), Germany (Wiechmann et al., 2013) and the U.S.A (Maine D.E.P., 2018). What is evident from Table 1, is that PFAS guideline values vary considerably with regard to regulatory jurisdiction, even by several orders of magnitude. Variation in PFAS guideline values is influenced by choice of parameters used in risk calculations including soil:biosolid mixing ratios and plant uptake rates, which vary significantly across species and accumulation endpoints for individual PFAS. However, application of these guidelines to biosolids studied in this paper highlight that 24%–88% of biosolids exceed regulatory standards for agricultural reuse. When assessed according to the Maine DEP guidance (the most stringent case), only two locations (WWTP10 and 12) had biosolids which were acceptable for reuse. When TOP assay data was used in these cases, WWTP10 biosolids would exceed acceptability criteria for reuse, with concentrations of both PFOS (7.7 μg kg^{-1}) and PFOA (33 μg kg^{-1}) greater than guideline values. As precursor compounds are not regulated or are not quantified in standard PFAS analyses (e.g. FTOH, unknown precursors), the use of TOP assay data may add rigour regarding the suitability of biosolids reuse.

4. Conclusions

In recent years, a considerable amount of information has

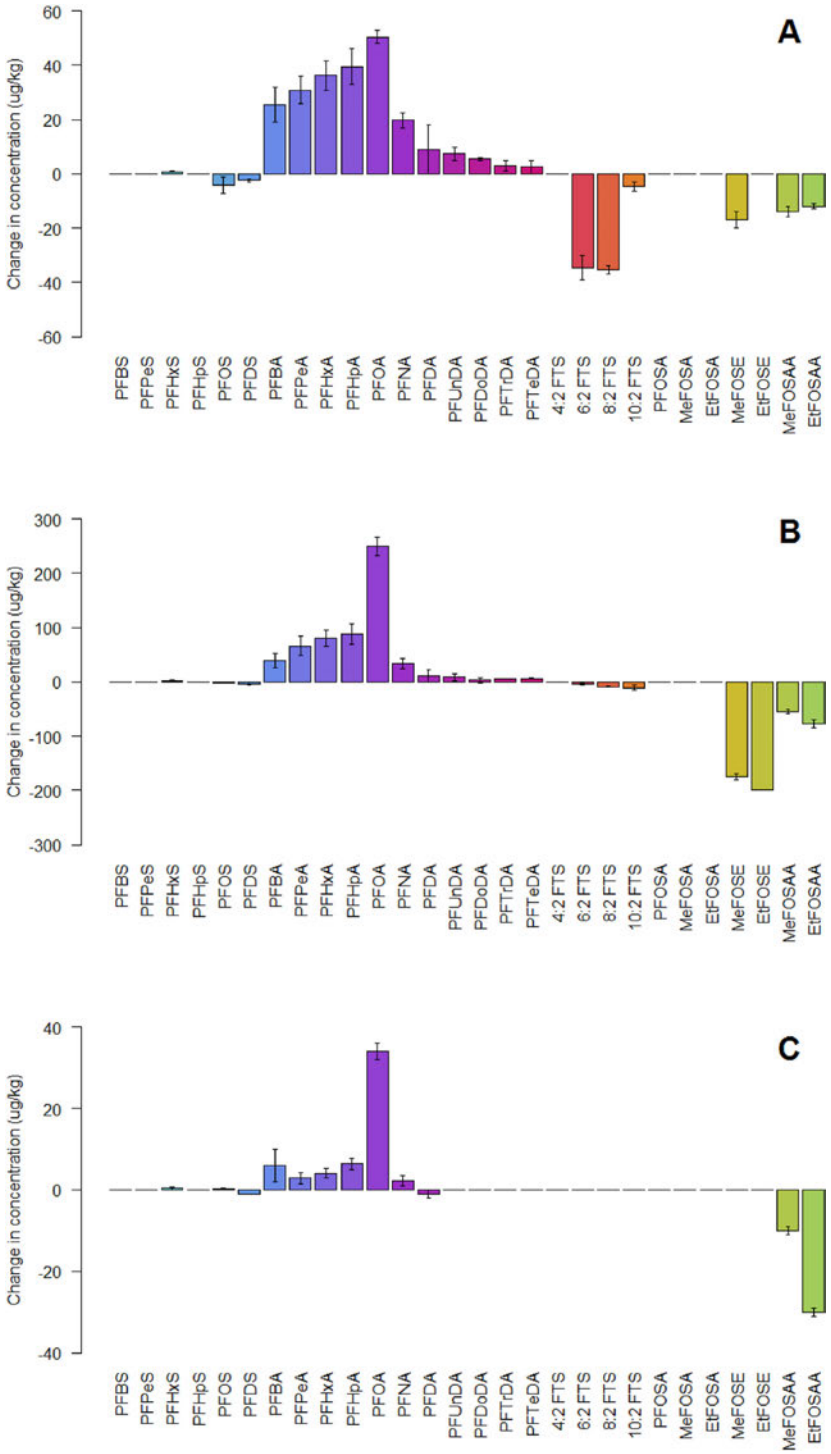


Fig. 4. Mean change in post-oxidation PFAS concentration (μg kg ^{1}) for WWTP2 (A), 3 (B) and 10 (C). Error bars indicate the range in PFAS concentration change from duplicate analysis.

Table 1
Σ_{28} PFAS, PFOS, PFOA, Cd, Cu, Zn concentrations in 17 biosolid samples from 12 waste water treatment plants across Australia. Biosolids exceeding guideline values for PFOS and PFOA are indicated, and a biosolid grade classification of A, B or C calculated from metal concentrations are listed.!

Biosolid Sample	Σ_{28}PFAS (μg kg ^{1})	PFOS (μg kg ^{1})	Restricted under[a]	PFOA kg ^{1})	Restr.under	PFAS Overall	Cd (mg kg ^{1})	Grade[b]	Cu (mg kg ^{1})	Grade	Zn (mg kg ^{1})	Grade	Metals Overall
WWTP3H1	596	360	A,M,G	43.0	M	A,M,G	11.8	C	946	C	1561	C	C
WWTP3H4	490	299	A,M,G	22.0	M	A,M,G	27.1	♠[d]	1080	C	1700	C	♠
WWTP3H5	449	224	A,M,G	26.3	M	A,M,G	21.3	♠	1170	C	1510	C	♠
WWTP3H3	239	141	A,M,G	13.4	M	A,M,G	32.7	♠	1190	C	2130	C	♠
WWTP3H2	163	60.0	A,M	10.0	M	A,M	6.08	B	1430	C	1950	C	C
WWTP1	145	85.7	A,M	16.0	M	A,M	1.33	B	477	B	467	B	B
WWTP2	130	22.3	A,M	11.4	M	A,M	4.13	B	512	B	1340	B	B
WWTP3	122	47.7	A,M	6.00	M	A,M	2.60	B	604	B	825	B	B
WWTP4	57.0	45.4	A,M	4.00	M	A,M	0.794	A	337	B	397	B	B
WWTP5	35.3	13.7	A,M	5.65	M	A,M	1.28	B	334	B	540	B	B
WWTP6	30.0	11.0	A,M	1.65	♣	A,M	1.18	B	186	B	567	B	B
WWTP7	25.5	16.5	A,M	4.00	M	A,M	2.99	B	323	B	587	B	B
WWTP8	23.4	10.4	A,M	8.00	M	A,M	1.39	B	765	C	647	B	C
WWTP9	23.0	13.0	A,M	4.00	M	A,M	1.08	B	286	B	567	B	B
WWTP10	14.7	4.65	♣[c]	0.350	♣	♣	0.201	A	96.0	A	102	A	A
WWTP11	7.00	5.50	M	1.50	♣	M	2.96	B	1060	C	1330	B	C
WWTP12	5.35	5.00	♣	0.350	♣	♣	5.87	B	416	B	332	B	B

[a] A Australian NEMP, M Maine DEP, G German Umweltbundesamt. NEMP guideline for PFOS 9 μg kg ^{1}, PFOA 100 μg kg ^{1} (HEPA, 2019). Maine DEP guideline for PFOS 5.2 μg kg ^{1}, PFOA 2.5 μg kg ^{1} (Maine D.E.P., 2018), German UBA guideline for PFOS and PFOA 100 μg kg ^{1} (Wiechmann et al., 2013).
[b] Classification cut-offs for grade (A,B,C) biosolids are Cd (1,11,20) mg kg ^{1}, Cu (100,750,2500) mg kg ^{1}, Zn (200,1400,2500) mg kg ^{1} (EPA S.A., 2015). Final grade may be of lesser quality due to concentrations of hexavalent Cr, Chlordane and Dieldrin (not measured).
[c] ♣ Passes relevant guideline concentrations.
[d] ♠ Contamination level higher than Class C biosolid limit.

emerged regarding the concentration of PFAS in environmental matrices including surface water, groundwater, waste water, soil, sediment, sludge and biosolids. Data derived from this study contributes to the growing international PFAS-biosolid database and adds valuable information to limited knowledge regarding PFAS concentration and composition in the Australian context. This is significant given that biosolids are utilised in Australian agriculture and guidance regarding PFAS acceptability criteria is in its infancy. PFAS were detected in all biosolid samples collected from WWTP across six Australian States and Territories. While Σ_{28}PFAS concentrations ranged from 5.35 to 145 μg kg^{-1}, no relationship was observed between concentration and WWTP catchment area indicating that trade waste may significantly impact PFAS-biosolid outcomes. When assessed against Australian PFAS regulatory guidelines, 9 of 12 samples exceed the PFOS concentration criterion (9 μg kg^{-1}) although all samples were below the PFOA guidance value (100 μg kg^{-1}). However, considering more stringent PFAS-biosolid guidance from Maine DEP, PFOA values were exceeded (10 of 12 samples), with potentially higher exceedances obtained following the assessment of precursor compounds. This highlights potential issues associated with precursor compounds of restricted PFAS and warrants investigation of agricultural land where frequent application of biosolids has been undertaken.

Main finding

Biosolids from 12 Australian waste water treatment plants were analysed for 28 PFAS. 24–88% of biosolids exceeded international regulatory standards.

CRediT authorship contribution statement

Julie A. Sleep: Formal analysis, Visualization, Writing - original draft. **Albert L. Juhasz:** Conceptualization, Writing - review & editing.

Declaration of competing interest

The authors declare that they have no known competing financial interests or personal relationships that could have appeared to influence the work reported in this paper.

Acknowledgments

Funding: The authors would like to acknowledge the Australian Government and the University of South Australia for supporting J.A.S. with a Research Training Program Scholarship. The authors would also like to acknowledge [redacted] Professor Stanley Miklavcic for feedback on the manuscript.

Appendix A. Supplementary data

Supplementary data to this article can be found online at https://doi.org/10.1016/j.envpol.2020.115120.

References

Alder, A.C., van der Voet, J., 2015. Occurrence and point source characterization of perfluoroalkyl acids in sewage sludge. Chemosphere 129, 62–73. https://doi.org/10.1016/j.chemosphere.2014.07.045.
Armstrong, D.L., Lozano, N., Rice, C.P., Ramirez, M., Torrents, A., 2016. Temporal trends of perfluoroalkyl substances in limed biosolids from a large municipal water resource recovery facility. J. Environ. Manag. 165, 88–95. https://doi.org/10.1016/j.jenvman.2015.09.023.
Arvaniti, O.S., Stasinakis, A.S., 2015. Review on the occurrence, fate and removal of perfluorinated compounds during wastewater treatment. Sci. Total Environ. 524–525, 81–92. https://doi.org/10.1016/j.scitotenv.2015.04.023.
Barzen-Hanson, K.A., Roberts, S.C., Choyke, S., Oetjen, K., McAlees, A., Riddell, N., McCrindle, R., Ferguson, P.L., Higgins, C.P., Field, J.A., 2017. Discovery of 40 classes of per- and polyfluoroalkyl substances in historical aqueous film-forming foams (AFFFs) and AFFF-impacted groundwater. Environ. Sci. Technol. 51 (4), 2047. https://doi.org/10.1021/acs.est.6b05843. –2057.
Blaine, A.C., Rich, C.D., Sedlacko, E.M., Hundal, L.S., Kumar, K., Lau, C., Mills, M.A., Harris, K.M., Higgins, C.P., 2014. Perfluoroalkyl acid distribution in various plant compartments of edible crops grown in biosolids-amended soils. Environ. Sci. Technol. 48 (14), 7858–7865. https://doi.org/10.1021/es500016s.
Coggan, T.L., Moodie, D., Kolobaric, A., Szabo, D., Shimeta, J., Crosbie, N.D., Lee, E., Fernandes, M., Clarke, B.O., 2019. An investigation into per- and polyfluoroalkyl

substances (PFAS) in nineteen Australian wastewater treatment plants (WWTPs). Heliyon 5 (8), e02316. https://doi.org/10.1016/j.heliyon.2019.e02316.
Donner, E., Howard, D.L., de Jonge, M.D., Paterson, D., Cheah, M.H., Naidu, R., Lombi, E., 2011. X-ray absorption and micro x-ray fluorescence spectroscopy investigation of copper and zinc speciation in biosolids. Environ. Sci. Technol. 45 (17), 7249–7257. https://doi.org/10.1021/es201710z.
Donner, E., Ryan, C., Howard, D., Zarcinas, B., Scheckel, K., McGrath, S., de Jonge, M., Paterson, D., Naidu, R., Lombi, E., 2012. A multi-technique investigation of copper and zinc distribution, speciation and potential bioavailability in biosolids. Environ. Pollut. 166, 57–64. https://doi.org/10.1016/j.envpol.2012.02.012.
Donner, E., Scheckel, K., Sekine, R., Popelka-Filcoff, R., Bennett, J., Brunetti, G., Naidu, R., McGrath, S., Lombi, E., 2015. Non-labile silver species in biosolids remain stable throughout 50 years of weathering and ageing. Environ. Pollut. 205, 78–86. https://doi.org/10.1016/j.envpol.2015.05.017.
Du, Z., Deng, S., Bei, Y., Huang, Q., Wang, B., Huang, J., Yu, G., 2014. Adsorption behavior and mechanism of perfluorinated compounds on various adsorbents: a review. J. Hazard Mater. 274, 443–454. https://doi.org/10.1016/j.jhazmat.2014.04.038.
Ellis, D.A., Martin, J.W., De Silva, A.O., Mabury, S.A., Hurley, M.D., Sulbaek Andersen, M.P., Wallington, T.J., 2004. Degradation of fluorotelomer alcohols: a likely atmospheric source of perfluorinated carboxylic acids. Environ. Sci. Technol. 38 (12), 3316–3321. https://doi.org/10.1021/es049860w.
EPA S.A., 2015. South Australian Biosolids Guidelines for the Safe Handling and Reuse of Biosolids. Environmental Protection Authority South Australia.
Gallen, C., Drage, D., Kaserzon, S., Baduel, C., Gallen, M., Banks, A., Broomhall, S., Mueller, J., 2016. Occurrence and distribution of brominated flame retardants and perfluoroalkyl substances in Australian landfill leachate and biosolids. J. Hazard Mater. 312, 55–64. https://doi.org/10.1016/j.jhazmat.2016.03.031.
Gallen, C., Eaglesham, G., Drage, D., Nguyen, T.H., Mueller, J., 2018. A mass estimate of perfluoroalkyl substance (PFAS) release from Australian wastewater treatment plants. Chemosphere 208, 975–983. https://doi.org/10.1016/j.chemosphere.2018.06.024.
Gottschall, N., Topp, E., Edwards, M., Russell, P., Payne, M., Kleywegt, S., Curnoe, W., Lapen, D., 2010. Polybrominated diphenyl ethers, perfluorinated alkylated substances, and metals in tile drainage and groundwater following applications of municipal biosolids to agricultural fields. Sci. Total Environ. 408 (4), 873–883. https://doi.org/10.1016/j.scitotenv.2009.10.063.
Guo, Z., Liu, X., Krebs, K.A., Roache, N.F., 2009. Perfluorocarboxylic Acid Content in 116 Articles of Commerce.
HEPA, 2019. PFAS National Environmental Management Plan. National Chemicals Working Group of the Heads of EPAs Australia and New Zealand.
Higgins, C.P., Field, J.A., Criddle, C.S., Luthy, R.G., 2005. Quantitative determination of perfluorochemicals in sediments and domestic sludge. Environ. Sci. Technol. 39 (11), 3946–3956. https://doi.org/10.1021/es048245p.
Houtz, E.F., Sedlak, D.L., 2012. Oxidative conversion as a means of detecting precursors to perfluoroalkyl acids in urban runoff. Environ. Sci. Technol. 46 (17), 9342–9349. https://doi.org/10.1021/es302274g.
Houtz, E.F., Sutton, R., Park, J.-S., Sedlak, M., 2016. Poly- and perfluoroalkyl substances in wastewater: significance of unknown precursors, manufacturing shifts, and likely afff impacts. Water Res. 95, 142–149. https://doi.org/10.1016/j.watres.2016.02.055.
Jeon, J., Kannan, K., Lim, B.J., An, K.G., Kim, S.D., 2011. Effects of salinity and organic matter on the partitioning of perfluoroalkyl acid (PFAs) to clay particles. J. Environ. Monit. 13 (6), 1803–1810. https://doi.org/10.1039/C0EM00791A.
Kim, S.-K., Kannan, K., 2007. Perfluorinated acids in air, rain, snow, surface runoff, and lakes: relative importance of pathways to contamination of urban lakes. Environ. Sci. Technol. 41 (24), 8328–8334. https://doi.org/10.1021/es072107t.
Kotthoff, M., Müller, J., Jürling, H., Schlummer, M., Fiedler, D., 2015. Perfluoroalkyl and polyfluoroalkyl substances in consumer products. Environ. Sci. Pollut. Control Ser. 22 (19), 14546–14559. https://doi.org/10.1007/s11356-015-4202-7.
Krzywinski, M.I., Schein, J.E., Birol, I., Connors, J., Gascoyne, R., Horsman, D., Jones, S.J., Marra, M.A., 2009. Circos: an information aesthetic for comparative genomics. Genome Res. 19 (9), 1639–1645. https://doi.org/10.1101/gr.092759.109.
Lange, C.C., 2000. The Aerobic Biodegradation of N-EtFOSE Alcohol by the Microbial Activity Present in Municipal Wastewater Treatment Sludge. Pace Analytical Services.
Lee, H., Mabury, S.A., 2014. Global Distribution of Polyfluoroalkyl and Perfluoroalkyl Substances and Their Transformation Products in Environmental Solids. John Wiley and Sons, Ltd, pp. 797–826. https://doi.org/10.1002/9781118339558.ch27. Ch. 27.
Li, Y., Oliver, D.P., Kookana, R.S., 2018. A critical analysis of published data to discern the role of soil and sediment properties in determining sorption of per and polyfluoroalkyl substances (PFASs). Sci. Total Environ. 628, 110–120. https://doi.org/10.1016/j.scitotenv.2018.01.167.
Liu, J., Avendaño, S.M., 2013. Microbial degradation of polyfluoroalkyl chemicals in the environment: a review. Environ. Int. 61, 98–114. https://doi.org/10.1016/j.envint.2013.08.022.
Maine D.E.P., 2018. Beneficial use of solid wastes. In: Maine Solid Waste Management Rules. Maine Department of Environmental Protection, pp. 1–28. Ch. 418.
Munoz, G., Budzinski, H., Babut, M., Drouineau, H., Lauzent, M., Menach, K.L., Lobry, J., Selleslagh, J., Simonnet-Laprade, C., Labadie, P., 2017. Evidence for the trophic transfer of perfluoroalkylated substances in a temperate macrotidal estuary. Environ. Sci. Technol. 51 (15), 8450–8459. https://doi.org/10.1021/acs.est.7b02399.
Nguyen, T.V., Reinhard, M., Gin, K.Y.-H., 2013. Rate laws and kinetic modeling of n-ethyl perfluorooctane sulfonamidoethanol (N-EtFOSE) transformation by hydroxyl radical in aqueous solution. Water Res. 47 (7), 2241–2250. https://doi.org/10.1016/j.watres.2013.01.047.
Perkola, N., Sainio, P., 2013. Survey of perfluorinated alkyl acids in Finnish effluents, storm water, landfill leachate and sludge. Environ. Sci. Pollut. Control Ser. 20 (11), 7979–7987. https://doi.org/10.1007/s11356-013-1518-z.
R Core Team, R., 2018. A Language and Environment for Statistical Computing. R Foundation for Statistical Computing, Vienna, Austria. https://www.R-project.org/.
Rayne, S., Forest, K., 2009. Perfluoroalkyl sulfonic and carboxylic acids: a critical review of physicochemical properties, levels and patterns in waters and wastewaters, and treatment methods. Journal of Environmental Science and Health Part A 44 (12), 1145–1199. https://doi.org/10.1080/10934520903139811.
Rhoads, K.R., Janssen, E.M.-L., Luthy, R.G., Criddle, C.S., 2008. Aerobic biotransformation and fate of n-ethyl perfluorooctane sulfonamidoethanol (N-EtFOSE) in activated sludge. Environ. Sci. Technol. 42 (8), 2873–2878.
Ross, I., Houtz, E., Kalve, E., McDonough, J., Hurst, J., Miles, J., 2018. PFASs and the TOP assay. Industrial Fire Journal Q1 26–27.
Sun, H., Gerecke, A.C., Giger, W., Alder, A.C., 2011. Long-chain perfluorinated chemicals in digested sewage sludges in Switzerland. Environ. Pollut. 159 (2), 654–662. https://doi.org/10.1016/j.envpol.2010.09.020.
Ulrich, H., Freier, K.P., Gierig, M., 2016. Getting on with persistent pollutants: decreasing trends of perfluoroalkyl acids (PFAAs) in sewage sludge. Chemosphere 161, 527–535. https://doi.org/10.1016/j.chemosphere.2016.07.048.
Venkatesan, A.K., Halden, R.U., 2013. National inventory of perfluoroalkyl substances in archived US biosolids from the 2001 EPA national sewage sludge survey. J. Hazard Mater. 252, 413–418. https://doi.org/10.1016/j.jhazmat.2013.03.016.
Wang, F., Shih, K., 2011. Adsorption of perfluorooctanesulfonate (PFOS) and perfluorooctanoate (PFOA) on alumina: influence of solution pH and cations. Water Res. 45 (9), 2925–2930.
Wang, N., Liu, J., Buck, R.C., Korzeniowski, S.H., Wolstenholme, B.W., Folsom, P.W., Sulecki, L.M., 2011. 6:2 fluorotelomer sulfonate aerobic biotransformation in activated sludge of waste water treatment plants. Chemosphere 82 (6), 853–858. https://doi.org/10.1016/j.chemosphere.2010.11.003.
Wei, T., Simko, V., 2017. R Package "Corrplot": Visualization of a Correlation Matrix, Version 0.84. https://github.com/taiyun/corrplot.
Wen, B., Pan, Y., Shi, X., Zhang, H., Hu, X., Huang, H., Lv, J., Zhang, S., 2018. Behavior of N-ethyl perfluorooctane sulfonamido acetic acid (N-EtFOSAA) in biosolids amended soil-plant microcosms of seven plant species: accumulation and degradation. Sci. Total Environ. 642, 366–373. https://doi.org/10.1016/j.scitotenv.2018.06.073.
Wiechmann, B., Dienemann, C., Kabbe, C., Brandt, S., Vogel, I., Roskosch, A., 2013. Sewage Sludge Management in Germany. Umweltbundesamt.
Yamashita, N., Taniyasu, S., Petrick, G., Wei, S., Gamo, T., Lam, P.K., Kannan, K., 2008. Perfluorinated acids as novel chemical tracers of global circulation of ocean waters. Chemosphere 70 (7), 1247–1255. https://doi.org/10.1016/j.chemosphere.2007.07.079.
Ye, F., 2014. Distribution and Behavior of Perfluoroalkyl Acid Precursors in the Aquatic Environment and Their Importance in Total Perfluoroalkyl Substances, Ph.D. Thesis. Yokohama National Unviersity.
Zhang, X., Lohmann, R., Dassuncao, C., Hu, X.C., Weber, A.K., Vecitis, C.D., Sunderland, E.M., 2016. Source attribution of poly- and perfluoroalkyl substances (PFASs) in surface waters from Rhode Island and the New York metropolitan area. Environ. Sci. Technol. Lett. 3 (9), 316â€"321. https://doi.org/10.1021/acs.estlett.6b00255.
Zhao, L., Bian, J., Zhang, Y., Zhu, L., Liu, Z., 2014. Comparison of the sorption behaviors and mechanisms of perfluorosulfonates and perfluorocarboxylic acids on three kinds of clay minerals. Chemosphere 114, 51–58. https://doi.org/10.1016/j.chemosphere.2014.03.098.

Chapter 6

Composition and transformation of PFAS contamination profiles in AFFF impacted soils and leachates

6.1 Introduction

Aqueous film forming foams (AFFFs) were developed during the 1960s and have been used extensively to extinguish hydrocarbon fuel fires, with particularly high use by the defence/military sector [57]. AFFF usage has resulted in extensive contamination, including groundwater, lakes, soils and fauna [58, 59], with concentrations of per- and poly-fluoroalkyl substances (PFAS) in AFFF contaminated soils being found to persist at high concentrations decades after their use [59]. There is need for ongoing research on identification, monitoring and remediation of AFFF contaminated sites. Such research has begun to appear in the literature, such as methods for identifying AFFF-based contamination in certain environments based on chemical signatures [60].

AFFF compositions vary in PFAS included in their formulations, and many AFFF formulations are proprietary. The two overarching classes of AFFF identified in the literature are electrochemical fluorination-based and fluorotelomer-based AFFF [60]. In a study of seven US military-certified AFFF formulations (Ansul, Angus, Chemguard, 3M, National Foam, Buckeye and FSP), ten distinct fluorochemical classes were identified via ultraperformance liquid chromatography (UPLC) and quadrupole time of flight mass spectrometry (QTOF-MS) [61]. The individual PFAS types identified in these AFFF included anionic, cationic, and zwitterionic molecules with perfluorinated carbon chains of lengths between 4 to 12 [61]. In another study, Luo et al. [62] characterised PFAS in AFFF via liquid chromatography, ion mobility spectrometry and mass spectrometry (LC-IMS-MS). The AFFF formulations studied were Chemguard (3% and 6%), FireAde MIL (3% and 6%), Firestopper, Fomtec, Phos-Check, Solberg Arctic and Tridol (Angus

Fire, 3% and 6%). This non-targeted analysis identified 124 PFAS-like features, varying with each AFFF and included 20 new PFAS-like homologous series that have not been previously described in similar analyses [62]. Hierarchical clustering on AFFF composition similarity showed Chemguard, FireAde and Fomtec were similar, Phos-Check, Firestopper and Solberg formed another (more varied) cluster and Tridol a third.

PFAS concentrations in soils vary widely from background concentrations to those of soils where extensive contamination has occurred. Composition of this contamination varies according PFAS source. In addition to AFFF-impacted areas, such as firefighting training areas, air force bases and airports, contamination may also occur due to other sources, including manufacturing plants [21], landfill, and application of contaminated biosolids [22]. PFAS concentrations are determined by many factors including initial PFAS contamination, ongoing inputs, rainfall, leaching and sorption rates. Sorption and leaching rates are complex and impacted by soil pH and composition (including clay, organic matter and carbon content), in conjunction with the types of PFAS present. Filipovic et al. [59] measured soil concentrations at an AFFF contaminated site with values ranging from 2.18-8,520 $\mu g\ kg^{-1}$ for perfluorooctane sulfonic acid (PFOS) and <0.12-287 $\mu g\ kg^{-1}$ for perfluorooctanoic acid (PFOA). Surface water concentrations at this site were up to 45.1 ng L^{-1} for PFOS and 8.8 ng L^{-1} for PFOA, while ground water concentrations were significantly higher, up to 42,200 ng L^{-1} for PFOS and 4,4700 ng L^{-1} for PFOA [59]. Houtz et al. [63] found soil PFAS concentrations of up to 6,200 and 800 $\mu g\ kg^{-1}$ for 6:2 and 8:2 fluorotelomer sulfonate (FTS), 3,400 $\mu g\ kg^{-1}$ of perfluorooctane sulfonamide (FOSA), up to 1,300, 2,000, 320, 5,200 and 20 $\mu g\ kg^{-1}$ for the C_5-C_9 perfluoroalkyl carboxylic acids (PFCAs), 610, 13,000, 430 and 20,000 for $C_{4,6,7,8}$ perfluoroalkyl sulfonic acids (PFSAs) along with 1,700 $\mu g\ kg^{-1}$ perfluorohexane sulfonamide (FHxSA) and 1,600 $\mu g\ kg^{-1}$ perfluorohexane sulfonamide amine (PFHxSaAM). In addition to the standard anionic PFAS commonly measured, one study [64] found when measuring soil cores from AFFF impacted areas that cations and zwitterions contributed up to 97% of total PFAS, indicating a much wider range of investigated PFAS may be needed to determine contamination scale.

There also exist differences in PFAS contamination profiles of AFFF products versus those of AFFF-impacted environments as discussed by Yan et al. [65]. Precursor compounds may be present in impacted soil, and there is potential for transformation of polyfluoroalkyl substances to perfluoroalkyl substances, in particular PFCAs. Transformation rates and pathways have been found to vary, with biotransformation thought to play a role in AFFF-derived PFAS contamination [65]. The differences in occurrence and transformation of all types of PFAS precursors has not been thoroughly investigated to date according to Yan et al. [65]. In groundwater, [58] detected mostly fluorotelomer sulfonates (FTSs), but when testing the AFFF source material identified predominantly fluoralythioamido sulfonates and only small concentrations of FTSs. Houtz et al. [63]

measured perfluorohexane sulfonamide amine (PFHxSAm) in soil samples but not in corresponding AFFF samples, also indicating transformation. Studies investigating the oxidation of AFFFs (3M, National Foam, Ansul Chemguard and Buckeye) found that the majority of precursor molecules were converted to PFCAs and PFSAs, and while only 3M had PFAAs present before oxidation, all AFFFs did after oxidation [63].

The following chapter aims to compare PFAS concentrations in twelve soils from Australian sites suspected to have been impacted by historical AFFF usage, and a thirteenth soil with added AFFF, specifically Angus Fire. It was hypothesised that soil contamination across sites would vary in both scale and diversity of PFAS present. Methods utilised to obtain PFAS and element concentrations in soils are detailed, then concentrations across all soils were examined and contrasted. The chapter analysed the transformation of precursors in samples with freshly added AFFF over multiple time points. Correlations between PFAS and elemental concentrations in both types of soils are discussed and complex relationships between samples quantified via a principal component analysis.

6.2 Materials and methods

6.2.1 Soil sampling and preparation

Soil samples were collected from Australian sites suspected to have been impacted by AFFF usage. Field collected soils P1 and P3 were from fuel storage areas, P4-P6, P10 and P11 from airports, P7-P9 and P12 from defence sites. Soil from the A horizon (top 20 cm) was collected in 20 L polypropylene buckets. Soils were subsequently air dried at room temperature, homogenised, and then sieved to retain the <250 μm size fraction. This particle size was chosen due to use in subsequent human health exposure assessments. In addition to field collected soils, 100 ml of Angus fire AFFF was mixed with 200 ml of MilliQ water then added to 1.0 kg of uncontaminated soil (Ferrosol), denoted by P20, to achieve a soil with Σ_{28}PFAS concentration of approximately 1,200 μg kg^{-1} and 60% water holding capacity. During addition of Angus fire AFFF to soil, material was homogenised by hand mixing for 20 minutes duration to ensure PFAS soil distribution homogeneity. P20 samples were incubated at room temperature (at 22°C) in the dark at 60% water holding capacity with sub-samples removed for PFAS quantification after 10 ($P20_{10}$), 33 ($P20_{33}$), 180 ($P20_{180}$) and 400 days ($P20_{400}$).

6.2.2 Chemical analysis

Inorganic constituents, total organic carbon (TOC) and pH were measured using standard wet chemistry methodologies [66], EPA methods 3015a (2007) and 6020A (1998).

The 28 PFAS selected for investigation included multiple common PFAS families, their full names, abbreviation the level of reporting (LOR) are given in Supplementary Table C.1. Measurement of soil PFAS concentrations was performed at Envirolab Services Pty Ltd and ALS Global Ltd. These facilities are accredited by the National Association of Testing Authorities (NATA) for testing of PFAS in biological and environmental matrices. PFAS concentrations were determined using liquid chromatography with tandem mass spectrometry (LC-MS/MS) following USEPA method 537 and ASTM D7979-17. ^{13}C PFAS surrogate standards were applied during the extraction process and their recovery rates quantified during PFAS analysis. For soils, mean recovery of $^{13}C_8$ PFOS was 100.6% (n=70; range 85-119%; median 100%), and $^{13}C_2$ PFOA mean recovery was 103.5% (n = 70; range 84-116%; median 106%). For leachates, mean recovery of $^{13}C_8$ PFOS was 97.7% (n = 48; range 91-123%; median 97%) and $^{13}C_2$ PFOA mean recovery was 101.8% (n = 48; 96-106%; median 102%). To measure the accuracy of PFAS quantification independent of the sample matrices, laboratory control spikes were included. Mean recoveries for these in soils were 89.9% for $^{13}C_4$ PFOS (n = 40, range 71.1-115%; median 92.7%) and 120.6% for $^{13}C_4$ PFOA (n = 40; range 113-130%; median 121%). Mean recovery in leachates was 115.7% for $^{13}C_4$ PFOS (n = 11; 107-120%; median 116%) and 123.0% for $^{13}C_4$ PFOA (n = 11; range 119-128%; median 124%).

The total oxidisable precursor (TOP) assay was also applied to soil and leachate samples. This assay provided insights into possible impacts of oxidative transformation on PFAS concentrations, and was conducted by the aforementioned testing facilities using a method similar to Houtz and Sedlak [67]. For soils during the TOP assay, mean recovery of $^{13}C_2$ PFOA was 105.8% (n = 63; range 77-134%; median 104%) and mean oxidation efficiency of $^{13}C_8$ FOSA was 98.6% (n = 63; range 90-117%; median 98%). For leachates during the TOP assay, mean recovery of $^{13}C_2$ PFOA was 92.7% (n = 42; range 75-103%; median 95%) and mean oxidation efficiency of $^{13}C_8$ FOSA was 98.0% (n = 42; range 91-100%; median 98%). Supplementary Table C.2 details the minimum, maximum and mean values for the surrogate recovery and oxidation efficiency values.

6.2.3 Leaching procedure

PFAS leachability was assessed using the Australian Standard Leaching Procedure (ASLP) (Standards Australia, 1997) [68] as recommended in [2]. Batch leaching tests utilised soil and deionised water (pH 7) at a solid to solution ratio of 1:20. Soil-water mixtures were tumbled end-over-end at 30±2 rpm for 18±2 hours at room temperature. Leachates were centrifuged at 2950 g for 30 minutes as per [69]. PFAS concentrations were quantified in leachates using LC-MS/MS as outlined in the previous section. For comparison with guideline values outcomes of leachability assessments were not adjusted for dilution in line with recommendations [2]. For comparison with with soil concentrations, leachate

concentrations were adjusted in line with the 1:20 solid:solution ratio.

6.2.4 Statistical analysis

All analysis and plotting was performed using the R [45] language, with the exception of Figures 6.5 and 6.11 (GraphPad Prism version 10.1.0). The principal component analysis was undertaken in R using the `prcomp` function, with scaling set to true. Correlation plots were produced with the `corrplot` function from the package of the same name, with scaling as described in the individual figure captions.

6.3 Results

6.3.1 PFAS concentrations in field collected soil samples

Σ_{28}PFAS concentrations for each soil are presented in Figure 6.1(a), PFSAs in panel (b), PFCAs in panel (c) and the remaining PFAS in panel (d). Figure 6.2 (a) shows the average concentrations of different PFAS across samples, as a percentage of the Σ_{28}PFAS. Values are provided in Supplementary Table C.3. The concentration of Σ_{28}PFAS in field collected AFFF impacted soil (P1-P13) ranged from 17.5-33,500 μg kg^{-1}. PFSA were the predominant PFAS class in 10 of 12 soils, comprising 60.8-97.1% of the Σ_{28}PFAS concentration. For soils P1 and P3, PFCA were the most prevalent class of PFAS comprising 60.4 and 100% of the Σ_{28}PFAS concentration respectively. PFOS was present in 11 of 12 soils (all except P3) at concentrations ranging from 16.5 (P1) to 28,500 μg kg^{-1} (P10), constituting 29.7-91.8% (median = 84.1%) of the Σ_{28} PFAS concentration. Of the other sulfonic acids, PFHxS was also present in 11 of 12 soils (again, not in P3), although the concentration was lower (5.5-2,850 μg kg^{-1}) compared to PFOS but higher than PFBS (1.0-160 μg kg^{-1}; number of soils: n = 10), PFPeS (1-290 μg kg^{-1}; n = 10), PFHpS (1-530 μg kg^{-1}; n = 10) and PFDS (20.5-60.0 μg kg^{-1}; n = 7). PFHxA (1.5-355 μg kg^{-1}) and PFOA (1.0- 275 μg kg^{-1}) were the most prevalent of the PFCAs, being present in 11 of 12 soils. The composition of Soil P3 was distinct from other field collected soils, containing only low concentrations of long chain PFCAs (8.0 μg kg^{-1} of PFNA and 9.5 μg kg^{-1} of PFUnDA).

Fluorotelomer sulfonates were detected in 6 of 12 field collected soils with 6:2 FTS (n = 4), 8:2 FTS (n = 6) and 10:2 FTS (n = 2) concentrations ranging from 14.5-705 μg kg^{-1}, 2.0-215 μg kg^{-1} and 5.0-10 μg kg^{-1}. Of the sulfonamides, only FOSA was above the LOR, and present in 6 of 12 soils (20-60 μg kg^{-1}). Of the 28 compounds analysed, six (MeFOSA, MeFOSE, MeFOSAA, EtFOSA, EtFOSE, EtFOSAA, PFTeDA) were below the level of reporting in all soil samples (1-50 μg kg^{-1}; see Supplementary Table C.1).

When compared to regulatory guidelines [70], all soils were below the PFOA human

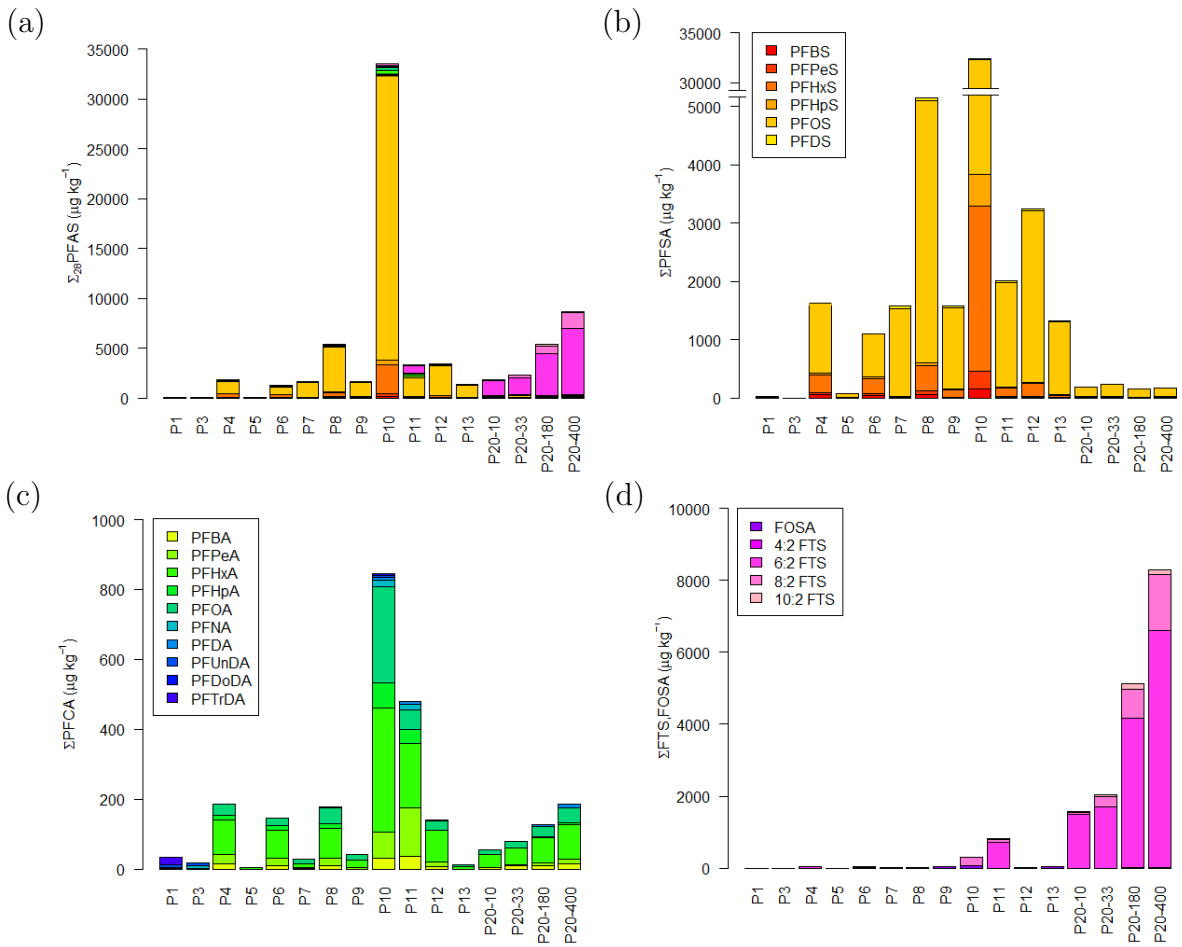


Figure 6.1: PFAS soil concentrations (µg kg^{-1}) for (a) Σ_{28}PFAS, (b) PFSAs, (c) PFCAs, and (d) FTSs and FOSA.

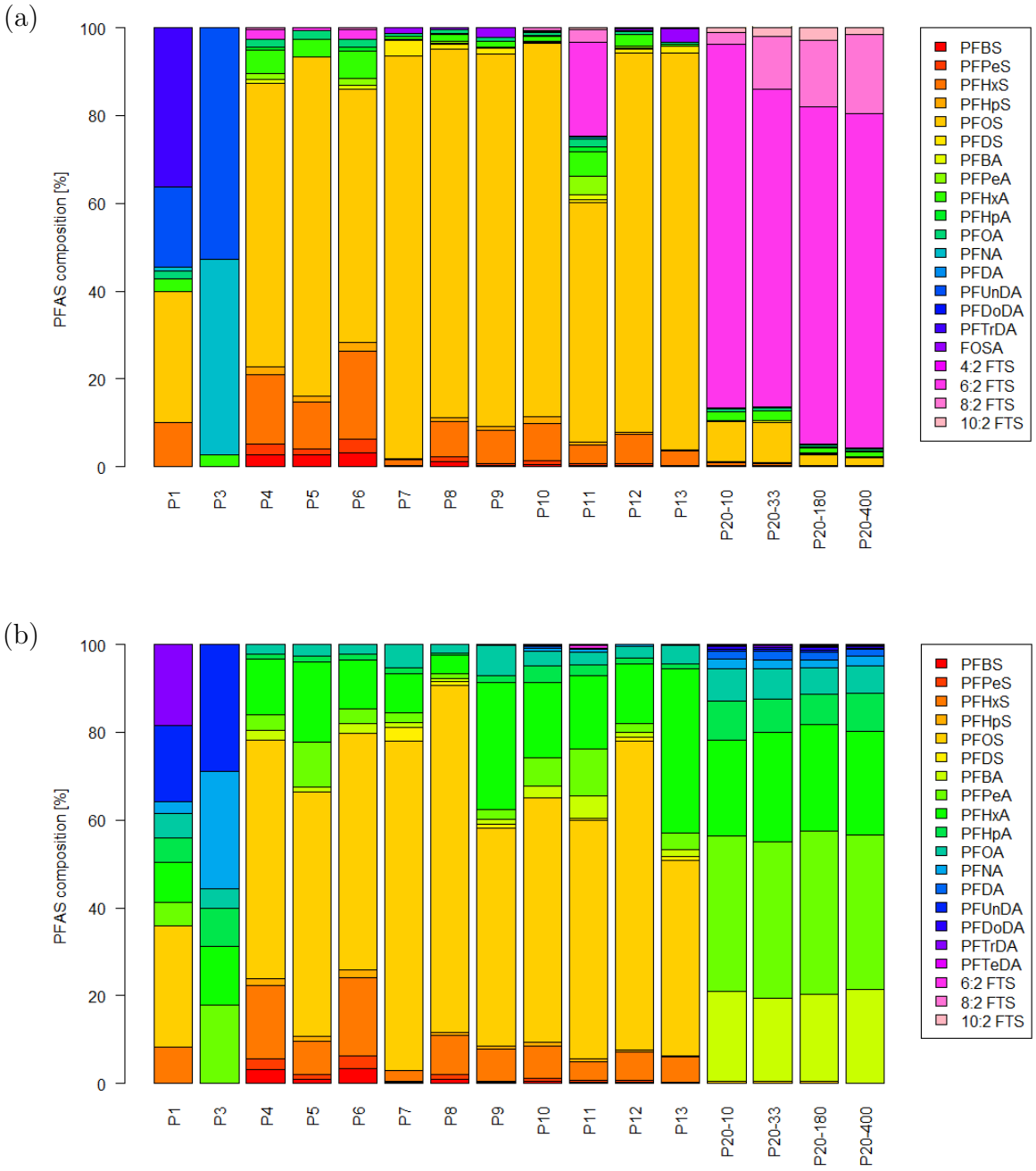


Figure 6.2: Composition of PFAS in soils (a) pre- (original samples) and (b) post-TOP assay

health investigation level of 50 mg kg^{-1} for industrial/commercial settings, while for the equivalent value for PFOS + PFHxS of 20 mg kg^{-1}, all soils were below with the exception of P10 (30.9 mg kg^{-1}). When PFOS concentrations were compared to the interim ecological soil guideline value of 10 μg kg^{-1}, exceedances were observed in all soils where PFOS was detected.

When compared to other studies, observed PFOS concentrations were within the range of that found by [59] with the exception of the non-detect in P3, and the high PFOS concentration of P10 (28,500 μg kg^{-1}), which was >3-fold the maximum reported in that study (8,520 μg kg^{-1}). However, PFOS concentrations of 20,000 μg kg^{-1} have been observed in other studies [63], which is of the same order of magnitude as reported here. PFOA concentrations, ranging from <LOR to 275 μg kg^{-1}, were similar to that of [59] (<0.12-287 μg kg^{-1}), but lower than the maximum observed by [63] (430 μg kg^{-1}).

In terms of comparisons of composition, many studies have either looked only at PFOS and PFOA, or have looked at a wider range of PFAS in untargeted analyses covering not only anionic, but cationic and zwitterionic PFAS. Houtz et al. [63] measured a similar range of PFAS, and the distribution between PFSAs and PFCAs was comparable, with PFSAs comprising a higher proportion of PFAS than PFCAs. The proportions of FTS were low in all soils except for P11, where 6:2 FTS and 8:2 FTS constituted 21% and 3% respectively of total Σ_{28}PFAS. This suggest that at sites P1-P10 and P13 electrochemical fluorination (ECF)-based AFFF were predominantly used. At P11 potentially both ECF and fluorotelomer based AFFF were used, given the presence of both FTS and PFSAs.

6.3.2 PFAS concentrations and temporal changes in Angus Fire impacted soil

In the soil with added Angus Fire AFFF, aged under laboratory conditions for 10 ($P20_{10}$), 33 ($P20_{33}$), 180 ($P20_{180}$) and 400 days ($P20_{400}$), significantly different PFAS compositions were observed compared to field collected soils. PFAS concentrations for P20 samples are provided in Supplementary Table C.4, plotted against sample ageing time in Figure 6.3 and additionally shown contrasted with field collected soils in Figures 6.1 and 6.2. Ageing P20 over 400 days resulted in increasing concentration of Σ_{28}PFAS ranging from 1,810 at 10 days to 8,660 μg kg^{-1} at 400 days. The main component in P20 was FTS ranging from 87% ($P20_{10}$) to 96% ($P20_{400}$). The total concentration of the 4 measured FTSs increased more than 5-fold over the ageing period from 1,570 to 8,300 μg kg^{-1}, as shown in Figure 6.1(d). 6:2 FTS was the predominant PFAS at all 4 time points, increasing from 1,500 to 6,600 μg kg^{-1} and comprising between 73-83% of Σ_{28}PFAS while 8:2 FTS increased from 48.5-1,550 μg kg^{-1} and comprised 3-18% of Σ_{28}PFAS. This is comparable to Houtz et al. [63], where 6:2 FTS was found at much higher concentrations

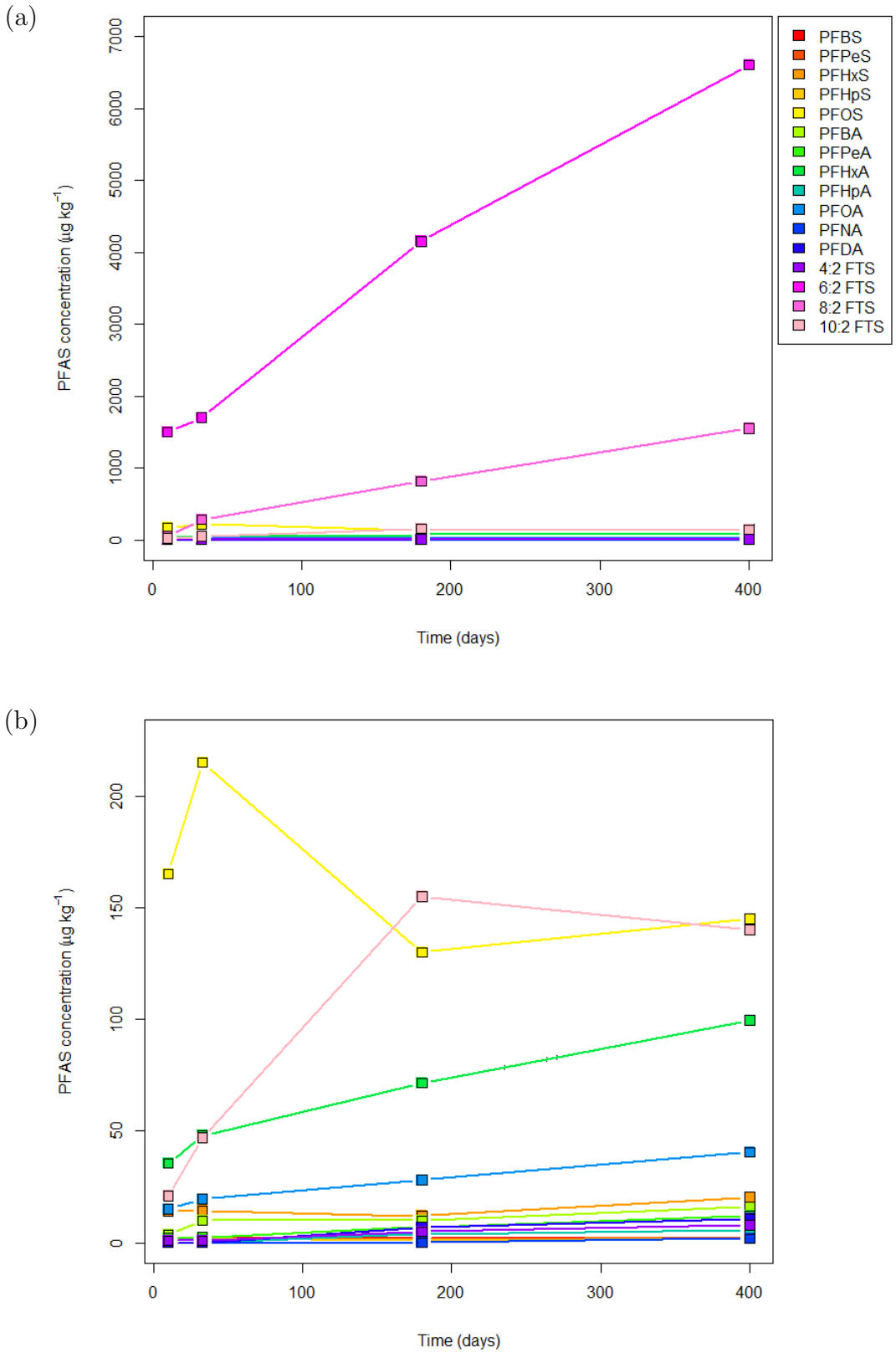


Figure 6.3: Change in individual PFAS concentration (µg kg^{-1}) in P20 over time for (a) all PFAS, (b) excluding 6:2 and 8:2 FTS

(up to 6,200 μg kg^{-1}) than 8:2 FTS (up to 800 μg kg^{-1}). PFOS remained relatively stable across sampling time points (130-215 μg kg^{-1}) with no clear temporal trend in concentration, although as a proportion of Σ_{28}PFAS declined from 9% to 2%.A slight increase in PFOA was observed, ranging from 15 μg kg^{-1} at 10 days to 40.5 at 400 days, but accounting for 1% or less of the overall PFAS concentrations. The entire range of C_{4-10} PFCAs all experienced an increase in concentration over time, the highest being PFHxA, with an increase from 35.5 to 99.5 μg kg^{-1}.

The increase in 6:2 FTS and PFCAs was assumed to be due to the transformation of precursor molecules by microbial or other processes. In an experimental analysis [61] of Angus Fire composition, 6:2 fluorotelomer thioether amido sulfonate (FtTAoS), 6:2 and 8:2 fluorotelomer thioether with trimethyl and quaternary amine functional structures were identified by QTOF-MS. These compounds have been observed to be transformed to FTS by microbial transformation [71]. Transformation of AFFF precursors in WWTP sludge into 6:2 FTS has also been observed under particular circumstances [72]. Additionally, studies report 6:2 FTS as being aerobically transformed itself into other PFAS including PFCAs [73]. Aerobic transformation of FtTAoS was observed by [71], of which FTS molecules including 6:2 FTS are possible transformation products. These precursor PFAS however were not measured in this study, so quantitative assessment or speculation regarding what has occurred in these samples was beyond the analytical capabilities of the study.

6:2 FTS half life in soil measured by [73] from AFFF impacted areas ranged from 43.3 to >224 days, however, here we did not observe any decline in 6:2 FTS at the 400 day mark. Examination of Figure 6.3(a) suggests that 6:2 FTS may continue increasing beyond 400 days as concentrations had yet to plateau. Non-targeted analysis could be utilised to investigate the hypothesis of microbial transformation and help to better understand the transformation pathways and rates of transformation. Indeed, precursors and fluorinated intermediates are not commonly measured, and so may be accumulating at rates not known [71], which is an important concept discussed further in future work.

6.3.3 Correlations

Correlations between PFAS and soil element concentrations are depicted in Figure 6.4 noting this includes the P1-P13 samples and a single P20 soil sample ($P20_{10}$). PFAS and elements are ordered by hierarchical clustering, with the clusters of level $h = 5$ designated on the figure by black squares. Each cluster shows variables which are correlated with each other across soil measurements. The upper-left cluster contains silica, PFDS and FOSA, noting that silica is quite distinct in that it has negative correlations to almost all other substances. This is inline with experimental work [32] where sorption of PFOA and PFOS onto silica was not reported. Due to its negative surface charge, it was

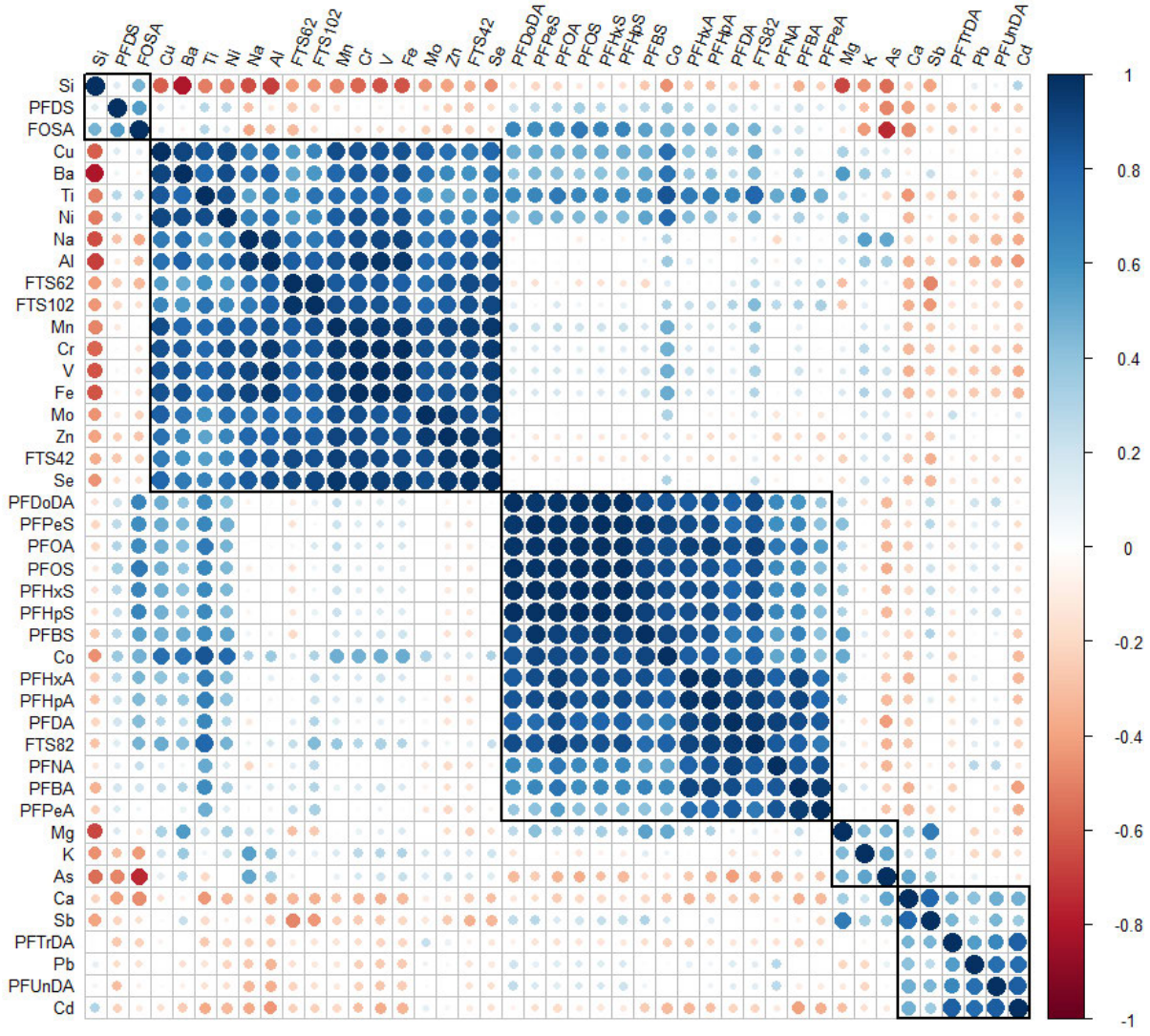


Figure 6.4: Correlation plot of PFAS and elements present across soils with hierarchical clustering. The colour and size of each circle corresponds to the Pearson correlation co-efficient (shown in the right-hand side legend) and indicates if there is a positive or negative association between each pair of variables, and the strength of this.

reasoned that this was due to electrostatic interactions being the driving force in the process of PFAS sorption. The second cluster contains 4:2, 6:2 and 10:2 FTS, along with a large number of metal ions such as copper, titanium, nickel, aluminium, chromium, iron and zinc. The third contains C_{4-10} and C_{12} PFCAs, and C_{4-8} PFSAs, along with 8:2 FTS and cobalt. A fourth cluster contains magnesium, potassium and arsenic, while the remaining C_{11} and C_{13} PFCAs are strongly correlated across samples with lead, cadmium, antimony and calcium. From this analysis is can be hypothesised that ion concentrations of both positive and negative charge, may be involved in increased PFAS sorption, a phenomena also observed in the theoretical work of Chapter 3 [38].

6.3.4 PFAS concentration in soil post-TOP assay

Section 6.3.2 highlighted that precursor transformation was an important factor driving changes in soil PFAS concentration over time, particularly for Angus Fire amended soil. The total oxidisable precursor (TOP) assay is a method that provides insights into potential impacts of oxidative transformation on individual PFAS concentrations. This is achieved by the application of persulfate ($S_2O_8^{2-}$) and heat [67]. The scale of some PFAS precursor molecules present in contaminated soils can be resolved using the TOP assay. This oxidation process leads to a decrease of known oxidisable compounds, such FTS and FOSA, and an increase in PFCAs [67, 74, 75]. Figure 6.5 shows pre- and post-TOP assay concentrations for Σ_{28}PFAS, PFSAs, PFCAs and PFOA. PFOA was highlighted in this plot as it was the only PFCA that had a soil guideline value in Australia [2]. Results for individual PFAS are given in Supplementary Tables C.5 and C.6, for field collected samples (P1-P13) and P20 Angus Fire impacted soils (P20) respectively.

Figure 6.5(a) shows that pre- vs post-TOP assay Σ_{28}PFAS concentration for most soils were similar, falling close to the 1:1 line with the exception of P20 soils. For Angus Fire amended soil, a significant increase in Σ_{28}PFAS concentration resulted from the application of the TOP assay, indicating the presence of a significant precursor burden outside of the measured 28 PFAS. Figure 6.5(b) shows that PFSA concentrations remain relatively unchanged following TOP assay application, while Figure 6.5(c) highlights that PFCA concentrations increase significantly. PFCAs are generally the resultant molecule after the transformation of other functional groups by the application of the TOP assay[67, 74, 75].

More specifically, for field collected soils, P1-13, from Supplementary Table C.5 we see absolute changes in Σ_{28}PFAS concentration that range from -0.5 μg kg^{-1} (P1) to 9,730 μg kg^{-1} (P10). Looking at relative increases in Σ_{28}PFAS this ranged from a small loss of -0.898% (P6) to an increase of 86.5% (P13). This indicates some variability that may be either due to precursor molecules or experimental variability but this is dwarfed

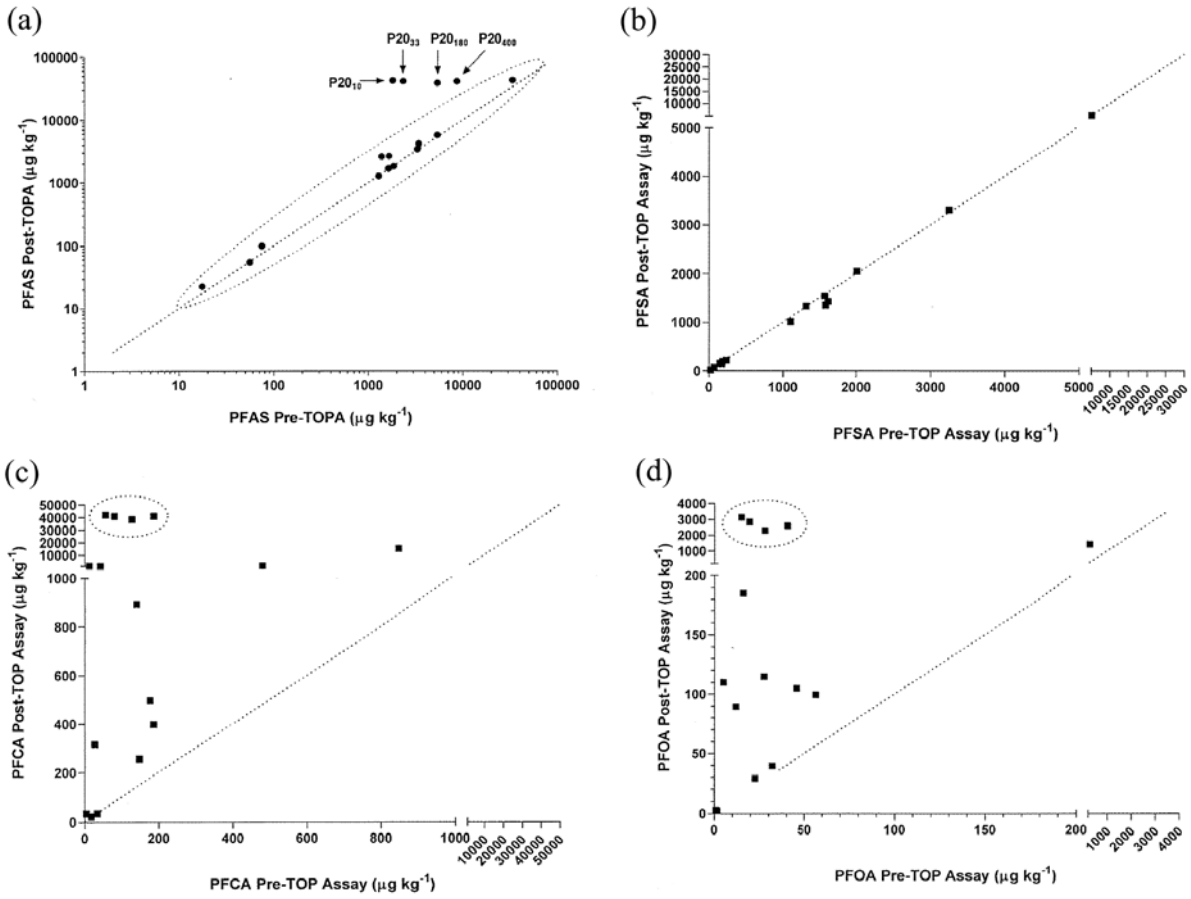


Figure 6.5: PFAS concentration (µg kg^{-1}) in soils pre vs post- TOP assay (a) Σ_{28}PFAS (b) PFSAs (c) PFCAs (d) PFOA. A 1:1 relationship is detailed by a dotted line, while P20 soils are labelled in (a) and circled in (c) and (d).

by the increases we see in the P20 soils (Supplementary Table C.6), which ranged from 40,600 µg kg^{-1} at 10 days to 32,500 µg kg^{-1} at 400 days, representing a percentage increase in Σ_{28}PFAS of 2240% at 10 days to 375% at 400 days.

PFCA increases for the field collected soils ranged from 1.73-36.5 fold for PFBA, 1.18-36.6 fold for PFPeA, 0.73-137 fold for PFHxA and 0.23-10 fold for PFOA as observed in Supplementary Table C.5. With the exception of soil P3 which had negligible PFAS, the PFCA with highest absolute increase in each soil with the application of the TOP assay was PFHxA (3.5-7,045 µg kg^{-1}). The second highest increase in concentration varied among soils between PFPeA for soils P1, 4, 6, 7, 10 and 11, and PFOA for soils P8, 9, 12 and 13. For the P20 soils (Supplementary Table C.6), PFCA increases were highest for PFPeA at up to a 7,500 fold increase at 10 days. PFBA increases were up to 2,480 fold and PFHxA 26.1 fold. These large increases are due in part to the high concentrations of FTS (particularly 6:2 FTS) and other precursor molecules in the P20 soil and the relatively low to moderate initial concentrations of these shorter chain PFCAs.

FOSA decreased, as expected, by 100% in soils where it was initially present. FTS

concentrations decreased by 100% across most samples, with a small number of samples having some remaining FTS concentrations corresponding to oxidation efficacy of 91-99% across soils. Observed changes in PFSA concentrations pre- and post-TOP assay are also given in Tables C.5 and C.6. Observed PFOS losses ranged from 0 (P12) to -18% (P4), and while it is possible that this may be due solely to measurement variations, decreases in PFSAs were also observed in contaminated soils from the shorter PFBS up to the longer PFDS by Zhao et al. [76], warranting further investigation.

From the TOP assay it was observed that precursor populations were decreasing with soil ageing, and from pre- assay measurements that FTS populations were increasing. In the previous section it was observed that many components of Angus Fire are outside of the PFAS tested. However, many of these are transformed over time into PFAS such as 6:2 FTS, and FTS are transformed into PFCAs with application of the TOP assay, as seen in the data. It is hypothesised that the historically impacted soils had low precursor burdens, due to leaching and previous transformation. Zhao et al. [76] applied the TOP assay to suspected contaminated soils at an oil refinery and found increases in PFCA with application of the TOP assay of between 0 and 47.5 μg kg^{-1}. Changes from 4 to 112 fold, in Σ28 PFCA concentrations were observed in house dust [77].

While the P20 soils differed in composition at different stages of the ageing process, their composition is more homogenous after the application of the TOP assay. The FTS have been transformed into the C_4, C_5 and C_6, and lesser extent C_7 and C_8 PFCAs, which was also observed for soil sample P11. The P20 samples additionally underwent transformation in composition across their 400 day ageing period, with unknown precursor molecules transformed into 4:2, 6:2 and 8:2 FTS molecules.

6.3.5 Relationships between samples

A principal component analysis (PCA) was performed on the individual PFAS sample measurements in order to examine patterns in data, in particular relationships between both samples and individual measured PFAS concentrations. These data were not averaged, but were scaled to have unit variance. Variables plotted against the first two dimensions are shown in Figure 6.6. In Dimension 1, the contribution to the variation was predominantly from PFCA and PFSA families. Dimension 2 variation was predominantly from the FTS family in one direction, and some of the longer chain compounds like PFTrDA and PFUnDA in the other. When comparing this to correlations studied in Figure 6.4 it can be seen that PFAS clusters observed in that analysis are also observed in this figure. Obtaining similar results across different methods increases confidence in conclusions drawn, in particular that PFAS concentrations are related to each other across samples.

Individual samples are shown plotted in Figure 6.7, where it can be seen that soil

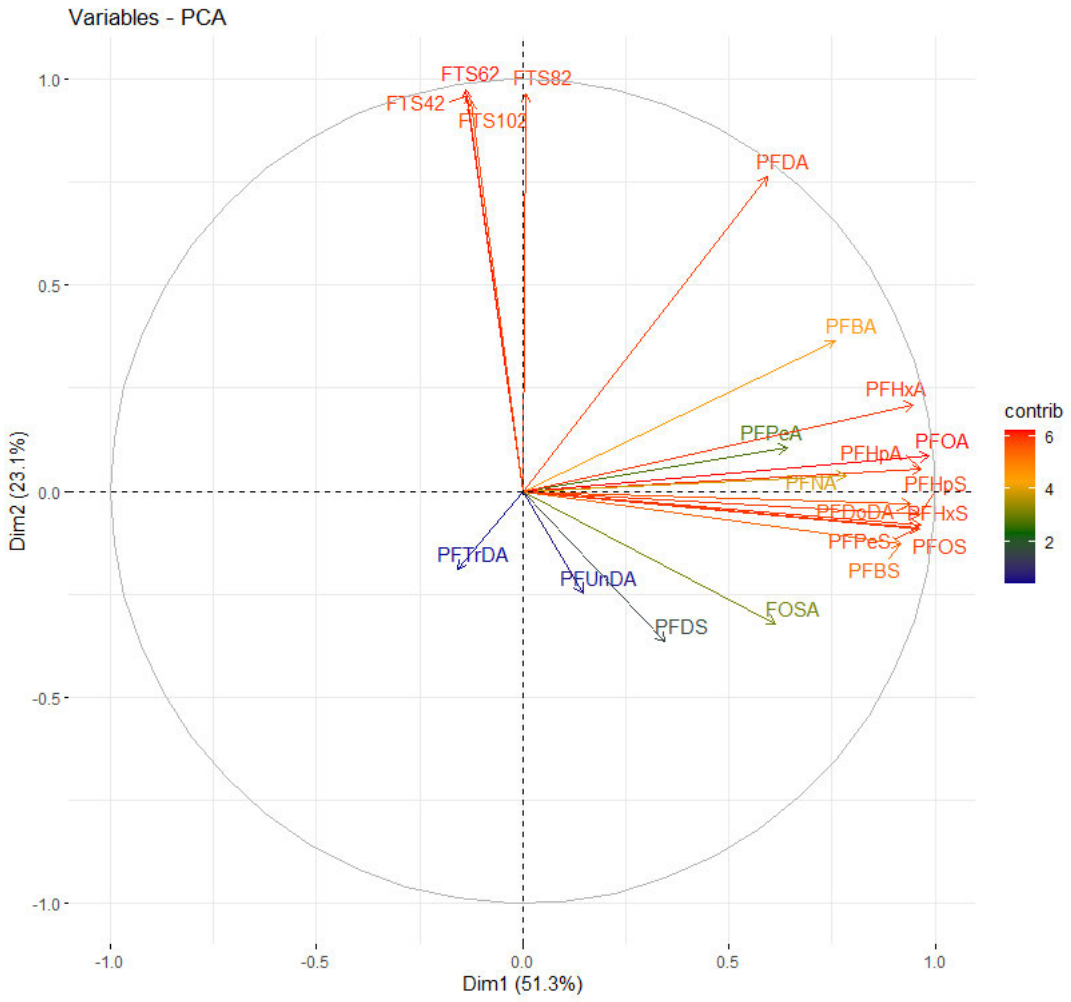


Figure 6.6: PFAS plotted against the first two principal components. Variables are coloured by the magnitude of their contribution to the components.

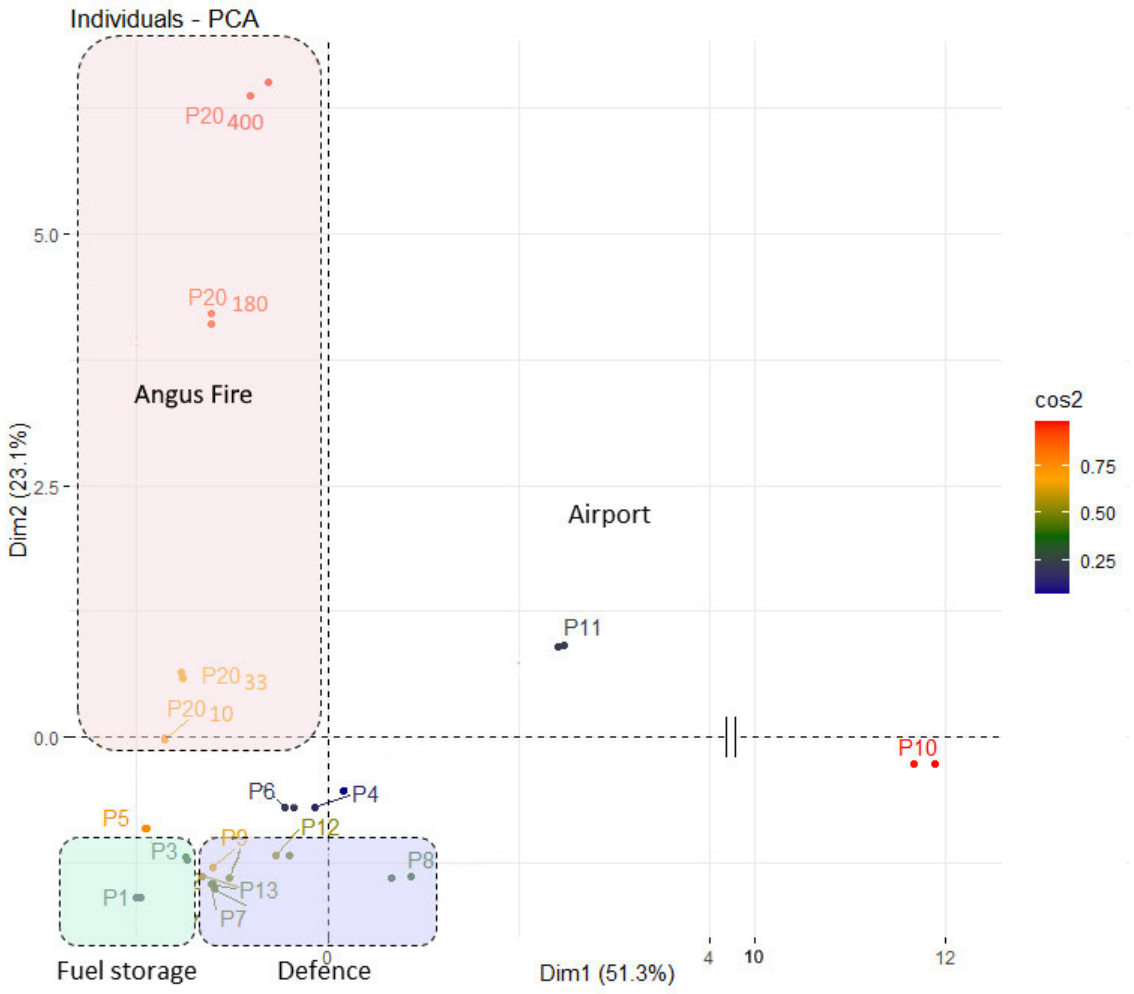


Figure 6.7: Individual samples plotted against the first two principal components. Points are coloured by their representation quality.

P10 is located on the far right due to high PFCA and PFSA concentrations, but close to the dimension 2 axis due to low FTS concentrations. P20 samples are located high on the dimension 2 axis due to their high FTS concentrations. P20 samples move further away from the x-axis with ageing due to increasing FTS concentrations that comprise the majority of dimension 2. Within the first two dimensions, it can be seen that soils are clustered based on site usage, with P20 soils in the upper left quadrant, fuel storage area soils in the far bottom left (P1, P3) and defence soils (P7-P9 and P12) being negative on dimension 2, but around the axis on Dimension 1. Airport soils P4-P6, P10 and P11 were the most dispersed, being around the axis on dimension 2 but with large variation in dimension 1. It is hypothesised that this may be due to similar AFFF being used at defence sites due to nation-wide defence contracts in fire fighting acquisitions. Similarly, the variability at airports may be due to different airport operators contracting different fire fighting systems. Values of the coordinates for

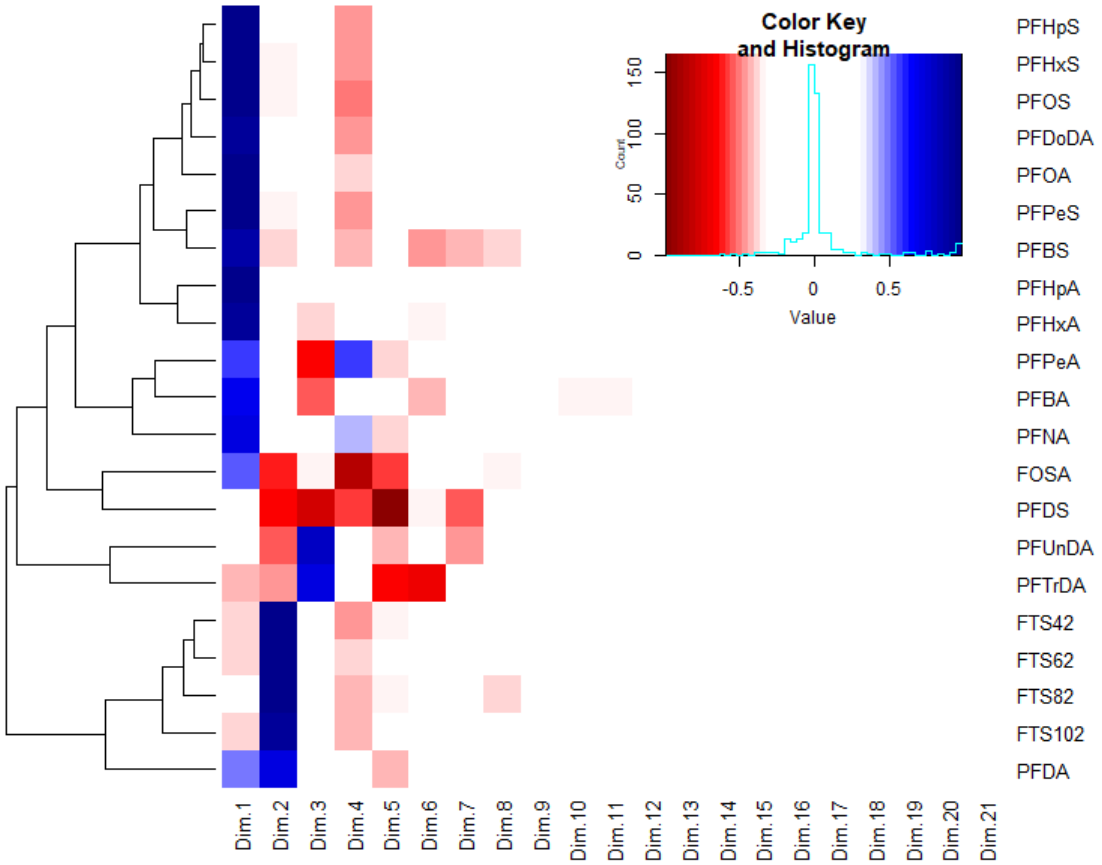


Figure 6.8: Values of the coordinates for the contributions of each PFAS to each of the dimensions.

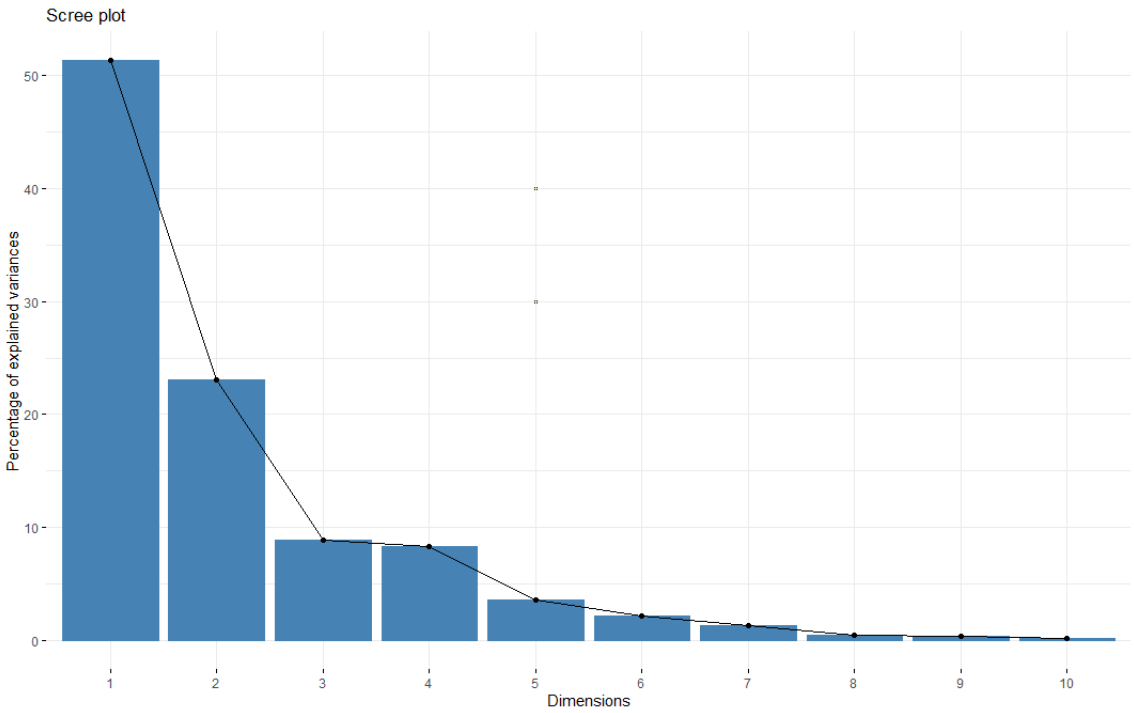


Figure 6.9: Scree plot showing percentage of variance in the data that is explained by each principal component

all dimensions, can be seen in Figure 6.8. Dimension 1 comprises positive contributions from the majority of PFSAs and PFCAs with the exception of the C_{11} and C_{13} PFCAs, while dimension 2 comprises positive contributions from FTSs and PFDA. It can be seen that dimension 3 involves most strongly positive PFUnDA and PFTrDA and negative PFDS , while Dimension 4 involves positive PFPeA and negative FOSA. The scree plot shown in Figure 6.9 depicts the percentage of variation in the data that is explained by each principal component. The first and second principal components account for 51.2% and 23.1% of overall variation in data, respectively.

The use of PCA in investigating source attribution of PFAS contamination is a currently emerging area. It has been applied to Italian spatial PFAS data by Giglioli et al. [78] with some similarity to PFAS in each dimension, though FTS were not measured which prevents direct comparison. With an extended data set and information on AFFF for some sites, PCA could be a promising technique for source identification for contamination of unknown origins.

6.3.6 PFAS concentrations in leachate

Leaching of PFAS from soil plays a critical role in risk assessments associated with contaminated soil remediation, disposal and/or reuse [79]. In the Australian context, there are guideline values based on leaching tests for disposal of contaminated soil in landfill sites [2]. Leaching procedures were performed on all soils and resulting PFAS composi-

tion and concentrations are presented in Figure 6.10(a) and Supplementary Tables C.7 and C.8. In addition, the TOP assay was also applied to corresponding leachate samples in order to gain an understanding of precursor burden.

Field collected soil leachate

The concentration of Σ_{28}PFAS in P1-P13 leachates ranged from 1.43-1440 μg L^{-1} (Supplementary Table C.7). PFSAs were the predominant PFAS family in 11 of 12 leachates, comprising 55.9-99.0% of the Σ_{28}PFAS concentration. For the P3 leachate, PFCAs were the prevalent class of PFAS comprising 81.5% of the Σ_{28}PFAS concentration. PFOS was present in all leachates, with concentrations ranging from 0.11 (P1) to 1,100 μg L^{-1} (P10), constituting 18.5-94.8% (median = 78.4%) of the Σ_{28}PFAS concentration. PFHxS was present in 11 of 12 leachates (not P3), although concentrations were lower (0.28-155 μg L^{-1}) compared to PFOS.

When compared to regulatory guidelines [70] (Supplementary Table C.9), all soils failed the unlined landfill disposal guideline due to PFOS+PFHxS leachate concentrations exceeding 0.07 μg L^{-1}, and PFOA exceeded 0.56 μg L^{-1} for 8 of 12 leachates. Soil P3 was suitable for disposal in clay/single lined composite lined landfills based on low leachate concentrations of both PFOA and PFOS+PFHxS, and soils P1, P3 and P5 met the conditions for disposal in double composite lined landfill. Soils P4 and P6-P13 were unsuitable for disposal without prior treatment due to PFOS+PFHxS concentrations exceeding 7 μg L^{-1}.

Angus Fire impacted soil leachate

Σ_{28}PFAS concentrations in P20 leachates increased with ageing time, from 80.1 μg L^{-1} at 10 days to 455 μg L^{-1} at 400 days (Supplementary Table C.8). FTS were the predominant PFAS class across all P20 leachates, comprising 90.1-96.5% of the Σ_{28}PFAS concentration. Of the FTS family, 6:2 FTS had the highest concentration, ranging from 70.5-415 μg L^{-1} and comprising 78-91% of Σ_{28}PFAS. PFOS, PFHxS and PFOA were present in all P20 leachates, with concentrations ranging from 2.2 ($P20_{180}$) to 4.85 μg L^{-1} ($P20_{33}$), 0.605-4.25 μg L^{-1}, and 1.35-2.90 μg L^{-1} respectively.

Angus fire impacted leachate concentrations were also compared to regulatory guidelines [70] as per Supplementary Table C.9. All P20 leachates failed the unlined landfill disposal guideline due to both PFOS+PFHxS concentrations exceeding 0.07 μg L^{-1} and PFOA concentrations exceeding 0.56 μg L^{-1}. They were also unsuitable for clay/single lined composite lined landfills based on the leachate concentrations of PFOS+PFHxS (2.86-5.61μg L^{-1}) exceeding the 0.7 μg L^{-1} guideline value. However, all P20 samples were suitable for disposal in double composite lined landfills.

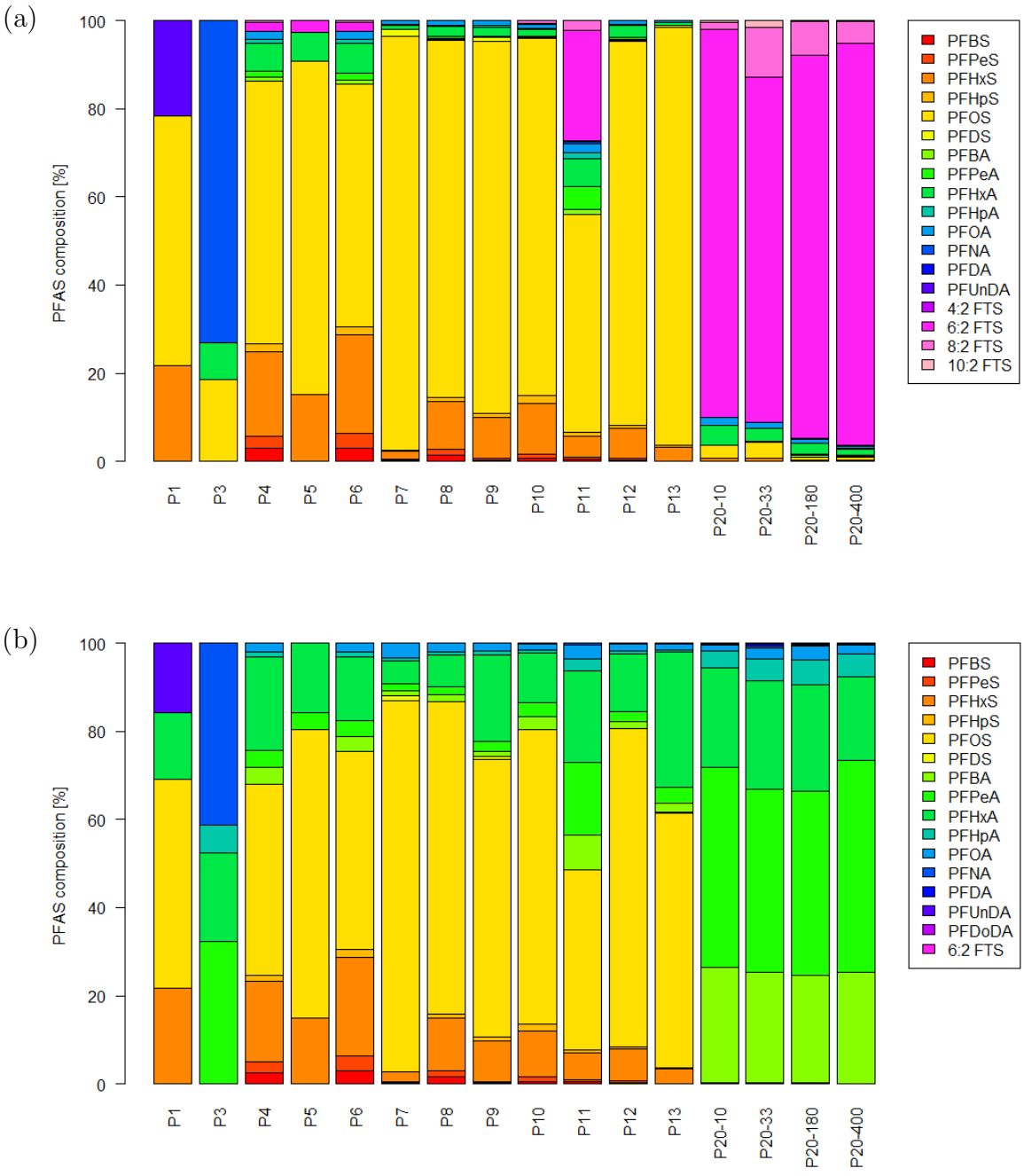


Figure 6.10: Composition of PFAS in (a) pre and (b) post TOP assay leachate.

6.3.7 Soil-leachate comparison

Table 6.1 gives leachable PFAS fractions for samples, as calculated by the dilution factor adjusted soil leachate concentrations divided by the soil concentrations. It can be seen that differences between soil and soil leachate PFAS concentrations were observed, but mostly dependent on carbon chain length and independent of soil. There were differences in leachability between the P1-P13 samples and the P20 samples, which could be associated with a number of potential factors including soil properties.

As calculated from Table 6.1, the ratio of leachable fraction to soil fraction[1] (excluding cases of zero leachability) observed for PFBS ranged from 0.80 to 1.4:1, 0.55 to 1.2:1 for PFHpS, 0.27 to 0.95:1 for PFOS, and 0.17 to 0.52:1 for PFDS. The ratios for C_4-C_7 PFCAs ranged from 0.93 to 2.2:1, PFOA from 0.88 to 2.1:1, PFNA from 8.4 to 1.1:1 and PFDA from 0.30 to 0.85:1. There is a slight contrast to the leachability study of Chapter 7 which aligned more closely to the ratios observed in [80].[2] The maximum leachabilities[3] observed by Kabiri et al. [81] were also lower than both this study and those of Rayner et al. [80].

Variation between soil and leachate concentrations was experimentally observed in the literature [80, 81]. PFAS carbon chain length is known to influence sorption properties (see Supplementary Figure C.1) and this is widely reported in the literature. Chen et al. [27] determined experimentally that PFAS of C_{10} or longer carbon chain had increased likelihood of being adsorbed on suspended particles, while PFAS shorter than C_7 were, in contrast, more likely to be dissolved in the aqueous phase. This is due to PFAS with longer fluorinated carbon chains being more hydrophobic [82], and thus likely to have stronger affinity for surfaces, due to both greater contact area between the molecules and surface and stronger interactions. Shorter chain PFAS have regularly been shown to have higher solubility in water than their longer counterparts [83]. While this may account for some of the differences in soil and leachate concentrations, it is also seen in Table 6.1 and Supplementary Figure C.2 that some PFAS are found at increased concentrations in leachate relative to their soil concentrations. These leachability measurements of over 100% may be related to both the sorption behaviour and the experimental methodology of the ASLP and are also observed and discussed in the separate leaching experiments of Chapter 7. Kabiri et al. [81] also observed leaching of over 100% in their work and attributed this to the higher concentrations and subsequent lower precision in soil than in leachate measurements. However, Rayner et al. [80], examined the ASLP and four other leaching methods and observed significant differences

[1] In Table 6.1 this is presented as a dilution factor, where, for example, a dilution factor of 80 corresponds to a leachable fraction to soil fraction of 0.80:1.

[2] Rayner et al. [80] obtained C_4-C_8 PFCA measured mean ratios of leachable fractions to soil fractions ranging from the order 2:1 to 4:1, for PFNA 1:1 and PFDA closer to 0:1. For C_4-C_8 PFSAs mean ratios were approximately 5:1 for PFBS, 2:1 for PFHpS, to 1:1 for PFOS, and close to 0:1 for C_9-C_{11} PFSAs.

[3] 1.9:1 for PFBA and 1.6:1 for PFOA.

Table 6.1: Dilution factor adjusted leachate concentrations as a percentage of soil concentrations (%, 3.s.f.). * denotes detection in leachate but not soil, 0 detection in soil but not leachate, and blank - detection in neither sample.

	P1	P3	P4	P5	P6	P7	P8	P9
PFBS			106	0	96.2	80.0	100	82.9
PFPeS			108	0	102	145	98.3	94.3
PFHxS	102		117	108	110	116	108	105
PFHpS			90.9	0	92.3	115	88.1	83.6
PFOS	89.1	*	88.3	74.1	93.2	83.3	77.8	85.7
PFDS						33.3	16.5	51.6
PFBA			111		121	0	106	
PFPeA			102		96.5	0	93.0	137
PFHxA	0	200	114	123	104	118	106	124
PFHpA			105		103	*	99.3	*
PFOA	0		100	0	93.3	99.2	98.9	103
PFNA	0	109	0		0		0	
PFUnDA	56.0	0						
PFTrDA	0							
FOSA						0	0	0
6:2 FTS			96.3	300	94.5		*	
8:2 FTS			78.6		96.0			

	P10	P11	P12	P13	$P20_{10}$	$P20_{33}$	$P20_{180}$	$P20_{400}$
PFBS	104	105	93.7	0.0	0	100	125	137
PFPeS	93.1	108	102	0.0	0	50.0	0	108
PFHxS	109	95.7	97.8	77.8	86.4	104	116	122
PFHpS	94.3	96.0	95.7	100	0	55.0	0	0
PFOS	77.2	75.6	94.9	81.6	27.3	45.1	33.8	34.5
PFDS	40.0	0.0	27.2	27.8				
PFBA	113	94.3	118		0	0	157	150
PFPeA	98.0	103	110		0	220	209	192
PFHxA	110	95.1	96.1	94.3	203	158	200	131
PFHpA	106	93.5	*		*	*	180	126
PFOA	98.2	99.1	90.9	88.0	180	169	207	133
PFNA	91.2	83.5	0					0
PFDA	85.0	30.0				*	37.1	0
PFUnDA	0							
PFDoDA	0							
FOSA	0		0	0				
4:2 FTS					0	250	132	135
6:2 FTS	104	97.9			94.0	124	123	126
8:2 FTS	82.8	63.0	0	0	53.6	107	54.3	29.7
10:2 FTS	0	0			33.8	87.2	9.68	5.14

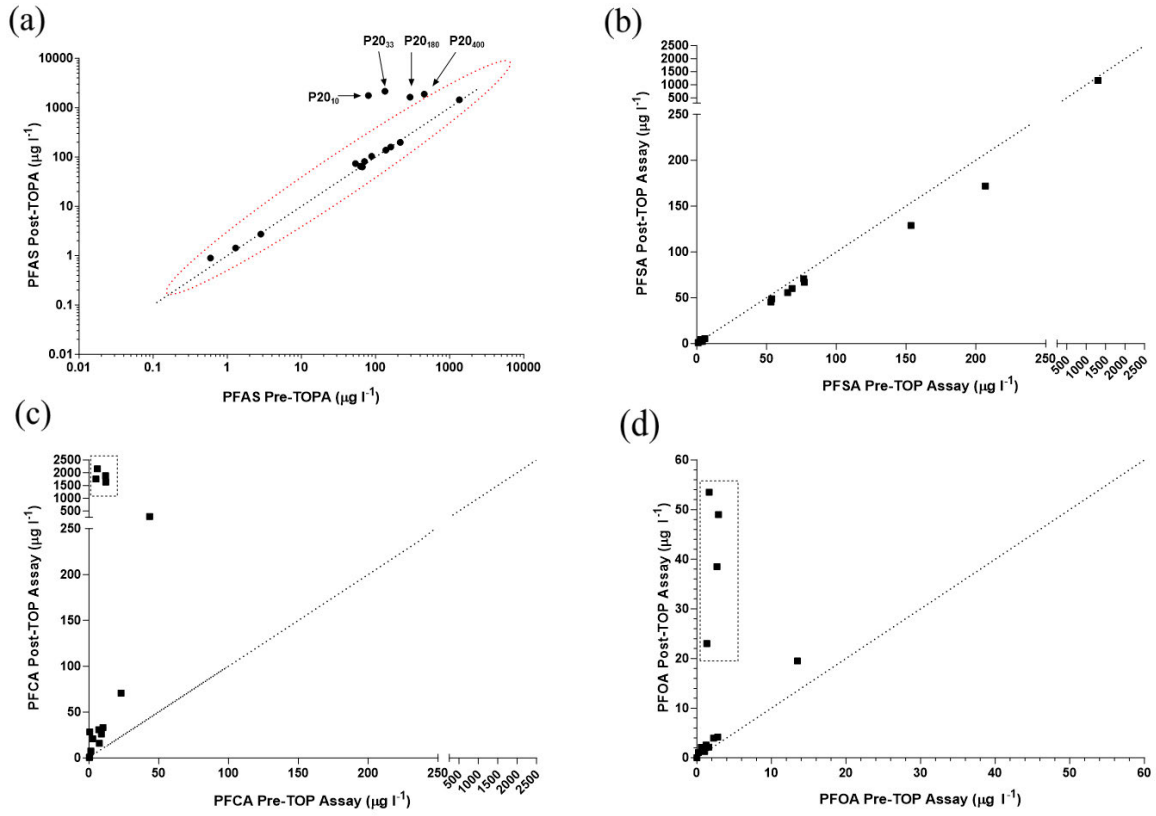


Figure 6.11: PFAS concentration (µg L^{-1}) in leachate pre vs post- TOP assay (a) Σ_{28}PFAS (b) PFSAs (c) PFCAs (d) PFOA. A 1:1 relationship is detailed by a dotted line, while P20 soils are labelled in (a) and within a box in (c) and (d).

between soil concentrations and leachate fractions. Their experimental work found liquid:soil ratio and duration of tumbling during the leaching process were correlated with the amount of leached PFAS observed.

6.3.8 PFAS concentration in leachate post-TOP assay

As performed with soils, it was also of interest to investigate the potential impacts of oxidative transformation on PFAS in soil leachates, along with resolving the scale of PFAS precursors. Figure 6.10 shows the composition of PFAS in leachates before and after the TOP assay application. The general observation from this figure was that FTS and unknown precursors are transformed into PFCAs, in particular PFBA, PFPeA and PFHxA. Pre- and post-TOP assay concentrations for Σ_{28}PFAS, PFSAs, PFCAs and PFOA are shown in Figure 6.11. Supplementary Tables C.10 and C.11 give the post TOP assay individual PFAS concentrations in leachates for field collected and Angus Fire impacted soils respectively, and Supplementary Tables C.12 and C.13 the percentage change.

Figure 6.11(a) shows that pre- vs post-TOP assay Σ_{28}PFAS concentration for most leachates were similar, falling close to the 1:1 line except for P20 leachates. For An-

gus Fire amended soil, an increase in Σ_{28}PFAS concentration resulted from the TOP assay application, indicating the presence of a leachable precursor burden outside of the measured 28 PFAS. Figure 6.11(b) indicated that PFSA concentrations remained relatively unchanged following TOP assay application, while Figure 6.11(c) highlights increased PFCA concentrations following TOP assay application, in line with literature [67, 74, 75].

Small changes in Σ_{28}PFAS were observed for field collected soil leachates as a result of oxidation of precursors and experimental variability. Relative changes in Σ_{28}PFAS ranged from -8.3% for P8 to +36.7% for P13 (Supplementary Table C.12). Increases in PFBA in field collected soil leachates ranged from 0.78 μg L^{-1} (P7) to 39.2 μg L^{-1} (P10), with relative increases ranging from 272% (P6) to 2180% (P10). PFPeA increases ranged from 0.105 μg L^{-1} (P5) to 40.4 μg L^{-1} (P10) and relative increases ranged from 144% (P6) to 1,110% (P10). Observed PFHxA increases were between 0.13 μg L^{-1} (P3) and 22.2 μg L^{-1} (P13) with percentage increases between 124% (P6) and 6,720% (P13).

In contrast, large differences in pre- and post-TOP assay Σ_{28}PFAS in leachates were observed for P20 soils (Supplementary Table C.13). These ranged from 1,340 μg L^{-1} at 180 days to 2,020 μg L^{-1} at 33 days. As observed in the soils, the range of percentage increases of Σ_{28}PFAS in leachates decreased over time from 2,100% at 10 days to 314% at 400 days. These changes included oxidation of the large FTS component of P20 in addition to suspected precursors, and an increase in PFCAs. Increases in PFCAs for the P20 samples were also significantly higher. For PFBA, increases ranged from 399-540 μg L^{-1}, PFPeA 684-904 μg L^{-1} and PFHxA 354-526 μg L^{-1}. These represented significant relative increases of up to 325,000% (PFPeA, $P20_{33}$).

Changes in ΣPFAS with application of the TOP assay vary in the literature. Increases in landfill leachate with application of the TOP assay have found to be small [84], hypothesised as due to precursors having been already leached or transformed. Median ΣPFAS was found to increase with application of the TOP assay in contaminated soils in another study by 4-72% [85]. ΣPFAS in sediment and suspended particulate matter was up to 53.1 μg kg^{-1} for pre-TOPA analyses but around 337 μg kg^{-1} after the TOPA application [86]. While not directly comparable, Al Amin et al. [87] measured increases in ΣPFAS of up to 534-fold with application of a modified version of the TOP assay to diluted AFFF samples and up to 7-fold for contaminated soils. 6:2 FTS, 6:2 Fluorotelomer sulfonamidoalkyl betaine (6:2 FTAB) and Perfluorohexane sulfonamide (FHxSA) were found to be prevalent precursors at a fire-fighting training area by Martin et al. [88], with 6:2 FTS and 6:2 FTAB being transformed under the TOP assay to C_3-C_7 PFCAs, and FHxSA to C_5-C_6 PFCAs. Further investigation, and studies such as [88] with a wider range of PFAS, are required for further interpretation and comparison of the high increases due to TOP assay application across P20 samples.

6.4 Conclusions and future work

PFAS present in soils contaminated with AFFF are diverse in both their concentration and composition, differing according to whether they were historically impacting and subject to years of leaching and potential transformation, or whether they were freshly impacted soils, aged and stored under laboratory conditions. The study of correlations between PFAS concentration and other elements in soil, showed a strong negative correlation of all but two PFAS with silica, in agreement with experimental results reported in the literature. There were also many strong positive correlations between most PFAS, and between PFAS and metal ions particularly, as also observed in Chapter 5's correlation analysis of PFAS and elements in biosolids.

Leachability of soil PFAS varied with carbon chain length, as observed in other work, and the TOP assay was applied to both soil and leachate samples, to determine the scale of PFAS precursors present. Precursor populations were found to be 33-fold higher in more recently impacted soil, aged under laboratory conditions rather than field collected soil (and 175-fold higher for leachates). This suggests that precursor populations are reduced under field conditions via mechanisms such as leaching and transformation. Comparison of soil and leachate concentrations, additionally added to the body of knowledge in the literature, and differences in leachability were observed across both soils and PFAS. Further work could be carried out using this and other available data in answer to questions raised around differences between observed leachate-soil ratios, especially those over 1.

The difference between observed leachate:soil ratios under the ASLP both between studies in this thesis and with external work is also an area requiring further investigations, with the role of different experimental conditions, including pH and tumbling duration, transformation during the leaching procedure, and differing soil properties of interest. It has also been noted that the applicability of leaching results such as the ASLP may not accurately reflect PFAS concentrations and leaching as observed under field conditions. Alternative methods for assessment have been recently forthcoming, for example the work of Rayner et al. on suction lysimeters [89], which was shown to more closely align with leaching result observed under field conditions.

Other future work could involve ageing of soils with different AFFF formulations, and comparison of long-term leaching and transformation with weathering, along with assessment of different leaching methods. Of potential interest in the future would be to collate further soils with different contamination sources, e.g. soils with repeated biosolid applications, soils in close proximity to manufacturing sites or landfill sites to compare factors influencing PFAS leachability. Work could also be undertaken to extend the range of PFAS measured to further identify precursor molecules and fluorinated intermediates as discussed in [71]. This could include the measurement and analysis of cationic and

zwitterionic PFAS that [64] found made up the majority of PFAS measured in the study of AFFF impacted soil cores.

As PFAS leachability in soils exceeded landfill acceptability criteria, the next chapter investigated the use of soil amendments for PFAS immobilisation and modelling approaches for predicting leachability endpoints.

Chapter 7

Measurement and prediction of PFAS immobilisation in AFFF-contaminated soils with RemBind® formulations

7.1 Introduction

Soil amendments are an effective in-situ method of PFAS remediation, and in Chapter 2 [90], it was observed that soil amendments based on activated carbon, including RemBind®, were the most effective at the immobilisation of a range of common PFAS such as perfluoroalkyl sulfonic acids (PFSAs) and perfluoroalkyl carboxylic acids (PFCAs). RemBind® (RB) is a powdered soil amendment developed by the CSIRO and Ziltek Pty Ltd (US Patent 8,940,958 B2). Designed for the purpose of immobilising contaminants within soils, it is composed of activated carbon, aluminium hydroxide and kaolin. It is thought that the aluminium hydroxide component of RB interacts with anionic PFAS via electrostatic interactions with their functional groups. The activated carbon and organic matter components of RB are thought to interact with the fluorinated carbon tail of anionic PFAS molecules, through hydrophobic and van der Waals interactions. The kaolin and organic matter components of RB provide a mechanism to bind cationic PFAS through electrostatic interactions. The activated carbon component may also bond with cation-forming PFAS. This may occur through hydrophobic interactions, although the hydrophobic or hydrophilic nature of the various structures present on an activated carbon surface is reported to be complex [91]. Long chain PFAS ($\geq C_8$) strongly bind to activated carbon. However, the interaction of shorter chain compounds ($\leq C_4$) with activated carbon may be weaker due to less contact area with a surface (and hence weaker Van der Waals interactions). Their shorter fluorinated carbon backbones

are also less hydrophobic, influencing potential hydrophobic surface interactions.

In the current study, two newer RemBind® products, RemBind®100 (RB100) and RemBind®300 (RB300) were assessed to determine the efficacy of PFAS immobilisation. RB100 and RB300 comprise of amorphous aluminium hydroxide in the form of pseudoboehmite, kaolin clay and activated carbon, although the precise composition of RB100 and RB300 cannot be detailed due to their proprietary nature. These products exhibit high capacity for PFAS sorption of approximately 2,000 μg g^{-1} [92]. The product formulations differ in their proportions of two different activated carbon types. The aim of this difference is to increase their respective abilities to be effective in different soil chemistries. Surface area and particle size differ between RB100 and RB300, and were quantified in [92], where it was also found that RB300 had higher pore volumes and surface areas across all measures examined. These products differ from the original RB and RemBind Plus® (RB+), which were superseded in 2018 by RB100 and RemBind® 100X (RB100X). RemBind Plus® (RB+), was a form of RB which contained a higher quality and proportions of both aluminium oxyhydroxides and activated carbon [93]. These products have been used in a number of published immobilisation studies, e.g. [93, 94, 95, 96].

Immobilisation studies using RB products, up until 2021 were evaluated and discussed in the review paper (Chapter 2) covering immobilisation of PFAS using a variety of soil amendments [90]. This work included laboratory and field-based immobilisation studies detailing the impact of soil amendment on PFAS leachabiliy. The works involving RB were those of Braunig et al. [93], Kabiri et al. [69, 97] and Sörengård et al. [95]. Bräunig et al. [93] applied RB and RB+ at 5-30% w/w to AFFF contaminated soil; the ageing period was 2 months. The initial concentrations were Σ_{12}PFAS=2,400-14,000 μg kg^{-1} for $C_{4,6,8}$ PFSAs and C_{4-10} PFCAs. They found that leaching and bioaccumulation (in earthworms and wheatgrass) decreased by up to 99.9% for PFOS, but varied with other PFAS and application rates. Effectiveness over three years was studied, and it was concluded that RB and RB+ were effective in the long term reduction of PFAAs in leachates, and reported reduced PFAS bioaccumulation factors (BAFs) and grass accumulation factors (GAFs) across the majority of cases studied. Sörengård et al. [95] applied concrete binder and RB together in a stabilisation and solidification study at 10% w/w binder and 0.2% w/w amendment. Aged for 4 months, soil was loamy sand and spiked with PFAS, with initial concentrations of Σ_{14}PFAS=6240-7310 μg kg^{-1} for C_{3-10} PFCAs, $C_{4,6,8}$ PFSA, 6:2, 8:2 FTS and PFOSA. It was found that the stabilisation and solidification approach with additives based on activated carbon, including RB, reduced leaching without significantly affecting physical matrix stability.

Kabiri et al. [69, 97] applied RB100 at 5% to AFFF contaminated loamy sand and sandy soils. Initial concentrations were Σ_{21}PFAS=700-37,200 μg kg^{-1} for $C_{4-8,10}$ PFSAs, C_{4-13} PFCAs, PFOSA, and 4:2, 6:2, 8:2 and 10:2 FTS. In [69] it was found that

reduction in PFAS leaching with RB100 application was stable under pH range of 4-9. In [97] it was found that extremes of temperature, and competing ions (orthophosphate and humic acid) caused no increase in PFAS leaching in RB100 immobilised soil.

Beyond these, more recent studies include those of Zhang et al. [98, 99], Biek et al. [33] and Juhasz et al. [92]. Zhang et al. [98] applied multiple amendments to 10 soils spiked with $C_{4,6,8}$PFSAs, C_{6-11}PFCAs, and GenX at 300 or 600 μg/kg (dry soil). They found that at day 52 and day 115, both RB100 and RB100X reduced leachable PFAS by 99%. The same authors [99] also measured PFAS uptake in Timothy grass planted in biosolid amended soil, finding that stabilization with RB (2% w/w) reduced PFAS bioavailability in biosolids to 3.35% of the total PFAS concentration compared to unamended samples. Biek et al. [33] applied RemBind at application rates ranging from 0.5-5% to PFAS contaminated soil and measured both uptake into a grass species and leachability, finding both a significant reduction in leachability (88.7-99.8%) and a 5-12 fold reduction in uptake by the grass. Juhasz et al. [92] applied RB100 and RB300 to reduce PFAS leachability by over 98% and relative bioavailability by over 70%, a study that this work expands upon with the inclusion of additional soils and fitting of models to immobilisation data.

It can be seen from the published literature that the immobilisation potential of the RemBind® family of products is significant, and applicable over a range of conditions. The aim of the present study was to undertake detailed analysis of data arising from bench scale immobilisation studies utilising RB100 and RB300 applied to five different AFFF contaminated soils, at application rates of 1, 2.5, 5 and 10% w/w, to determine immobilisation efficacy based on PFAS leachability. Additionally, models were fitted to this data in order to predict the application rates required to achieve immobilisation satisfying landfill disposal guidelines.

7.2 Materials and Methods

7.2.1 Soil sampling, preparation and immobilisation

Soils were collected from a number of locations across Australia suspected to have been impacted by historical AFFF usage. These samples are denoted by Z2-Z4 and Z7-Z9.[1]. Soil was collected from within the top 20 cm of the soil surface, in 20 L polypropylene buckets. Soils were air dried at room temperature, homogenised and then sieved to retain the <2 mm size fraction. This size fraction was different than the <250 μm fraction of Chapter 6, with the larger size fraction utilised for soil characterisation and associated

[1]A number of the soil samples on this chapter were sub-sampled from those collected in the same locations in Chapter 6, namely: Z2 and P10, Z3 and P11, Z4 and P12, and Z7 and P13. Samples from locations Z2-Z4 were also utilised in [92] and locations Z4 and Z7 in [100].

ecological experiments and the smaller particle size fraction part of wider experimental data utilised for in vivo and in vitro experiments relating to human health exposure assessment.

Soils were characterised to determine total organic carbon (TOC), pH and inorganic constituents using standard methodologies [66], EPA method 6020A (1998) and 3015a (2007). The 28 individual PFAS selected for investigation are listed in Supplementary Table D.1, along with their full names, abbreviation and the level of reporting (LOR). Measurement of soil PFAS concentrations was performed at ALS Global Ltd and Envirolab Services Pty Ltd, facilities accredited by the National Association of Testing Authorities (NATA) for testing of PFAS in environmental and biological matrices. Soil PFAS concentrations were determined using liquid chromatography with tandem mass spectrometry (LC-MS-MS) according to USEPA method 537 and ASTM D7979-17. Recovery values were as reported in Juhasz et al. [92], with $^{13}C_4$PFOS having mean recovery of 95.5% (n = 335; range 60.0–127%) and $^{13}C_8$PFOA 97.0% (n = 335; range 64.6–120%). Sample matrix independent mean spike recoveries over 28 individual PFAS compounds ranged from 93.5% for PFHxS, up to 108.8% for 4:2 FTS, with further details found in Juhasz et al. [92].

Bench-scale immobilisation studies were undertaken to determine the efficacy of RB100 and RB300 soil amendments on PFAS leachability. RB100 and RB300 were added to 400g of air-dried, <2 mm particle size fraction soil. Soils were treated with the adsorbents to achieve application rates of 1%, 2.5% , 5% and 10% w/w, and were mixed thoroughly. Deionized water was added to achieve a crumbly consistency with a water holding capacity of approximately 30%. Soil moisture contents were gravimetrically maintained over the 5-day ageing period, and these steps were all performed at room temperature.

7.2.2 PFAS leachability, analysis and QA/QC

PFAS leachability in both amended and unamended soils was assessed using the Australian Standard Leaching Procedure with deionised (DI) water (ASLP-DI) (ASLP; AS4439, 1997 [68]) according to the PFAS National Environmental Management Plan, version 2.0 [2]. Batch leaching tests utilised amended or unamended soil and deionized water at a solid to solution ratio of 1:20. Samples were tumbled end-over-end at 30 ± 2 rpm for 18 ± 2 hours. Leachates were then centrifuged at 2950 g for 30 minutes [69, 97], and filtration performed using 0.6-0.8 µm filters. When comparing to guideline values, the output values of the leachability assessments were not adjusted via the dilution ratio, as per the recommendations of [2]. However, when comparing the leachate concentrations to the soil concentrations they were adjust to ensure a meaningful comparison by the 1:20 soil:solution ratio. Concentrations of the 28 PFAS in leachate were determined

using LC-MS-MS as per USEPA method 537 / ASTM D7979-17. The 28 PFAS and respective limit of reporting (LOR) values are contained in Supplementary Table D.1, with the mean spike recovery values as per Juhasz et al. [92].

7.2.3 Statistical analysis and model fitting

Substitutions for values less than the LOR were not made for the purposes of model fitting; for further discussion around this point see [101]. The interval of potential values $[0, LOR]$ was used in efficacy calculations in the supplementary information, and 0 in the main text. Statistical analyses and plotting were carried out using R [45]. Exponential models were fitted using the nls() function (for determining non-linear least-squares estimates for non-linear models), for a model of the form

$$y = ae^{rx}$$

where y describes the PFAS concentration in leachate samples, x being the percentage of amendment added, and a and r are constants obtained from the model fitting process for each soil and RB formulation. The percentage of amendment required to be added, x_g was then calculated from the fitted model, via

$$x_g = \frac{\ln\left(\frac{y_g}{a}\right)}{r}$$

where y_g corresponds to the desired guideline concentration value.

7.3 Results and Discussion

7.3.1 PFAS concentration in soil pre-amendment

Soil PFAS concentrations before amendment are presented in Table 7.1, where it is seen that the Σ_{28}PFAS concentration in contaminated soils ranged from 445 (Z7) to 2,320,000 (Z9) μg kg^{-1}. PFSAs were the dominant class of PFAS comprising 62% (Z3) - 99% (Z8) of the Σ_{28}PFAS concentration. Of the PFSAs, PFOS was the most prevalent individual compound, ranging from 393 (Z7) to 2,000,000 (Z9) μg kg^{-1}. PFCAs accounted for 0.65% (Z8) - 15% (Z3) of the Σ_{28}PFAS concentrations. Within the PFCA family, PFHxA had the highest concentration in most soils, ranging from 1.65 μg kg^{-1} in Z7 to 41700 μg kg^{-1} in Z9. PFOA was less than this in all soils except Z7, with concentrations ranging from 1.90 (Z7) to 27,900 (Z9) μg kg^{-1}. 8:2 FTS was the most prevalent of the fluorotelomer sulfonates, being detected in all but 2 samples at concentrations of 3.10 (Z4) to 48,400 (Z9) μg kg^{-1}. FOSA was the most prevalent of the FOSAM family at 4.40 (Z3) - 6,730 (Z9) μg kg^{-1}. Six PFAS, namely MeFOSA, MeFOSE, EtFOSA,

Table 7.1: Mean soil PFAS concentrations in AFFF-impacted soil prior to immobilisation (μg kg^{-1}, 3 s.f.). MeFOSA, MeFOSE, EtFOSA, EtFOSE, 4:2 FTS and PFTeDA were <LOR for all soils. Replicate measure varied for concentrations greater than the LOR by an average of ±12%.

PFAS	Z2	Z3	Z4	Z7	Z8	Z9
PFBS	122	7.55	7.70	<LOR	83.5	3,070
PFPeS	202	10.4	13.2	0.50	117	4,300
PFHxS	2,390	106	202	16.3	4,470	74,200
PFHpS	348	20.3	19.3	1.80	3,810	65,200
PFOS	21,500	1,240	2,430	393	203,000	2,000,000
PFDS	31.2	12.3	27.7	8.65	448	6,660
PFBA	9.00	13.5	3.50	<LOR	<LOR	3,820
PFPeA	51.7	101	12.9	<LOR	93.5	7,480
PFHxA	302	140	74.7	1.65	731	41,700
PFHpA	66.3	31.0	6.80	<LOR	60.8	5,220
PFOA	210	40.7	20.9	1.90	499	27,900
PFNA	20.7	13.6	1.50	<LOR	<LOR	387
PFDA	9.10	5.00	1.45	<LOR	<LOR	2,670
PFUnDA	1.45	2.70	0.70	<LOR	<LOR	665
PFDoDA	2.35	0.70	1.00	0.60	<LOR	<LOR
PFTrDA	0.55	0.65	0.10	<LOR	<LOR	<LOR
FOSA	52.50	4.40	15.2	20.7	486	6,730
MeFOSAA	0.65	<LOR	0.30	<LOR	<LOR	<LOR
EtFOSAA	0.35	<LOR	1.80	<LOR	<LOR	<LOR
6:2 FTS	5.05	441	<LOR	<LOR	<LOR	18,800
8:2 FTS	135	71.0	3.10	<LOR	<LOR	48,400
10:2 FTS	0.30	7.30	<LOR	<LOR	<LOR	<LOR
Σ_6PFSA	24,500	1,400	2,700	420	212,000	2,150,000
PFSA %	96.5	61.6	94.9	94.4	99.1	92.8
Σ_{10}PFCA	686	348	124	4.15	1,380	93,200
PFCA %	2.70	15.3	4.35	0.932	0.647	4.02
PFOS+PFHxS	23,900	1,350	2,630	409	207,000	2,070,000
Σ_{28}PFAS	25,400	2,270	2,840	445	214,000	2,320,000

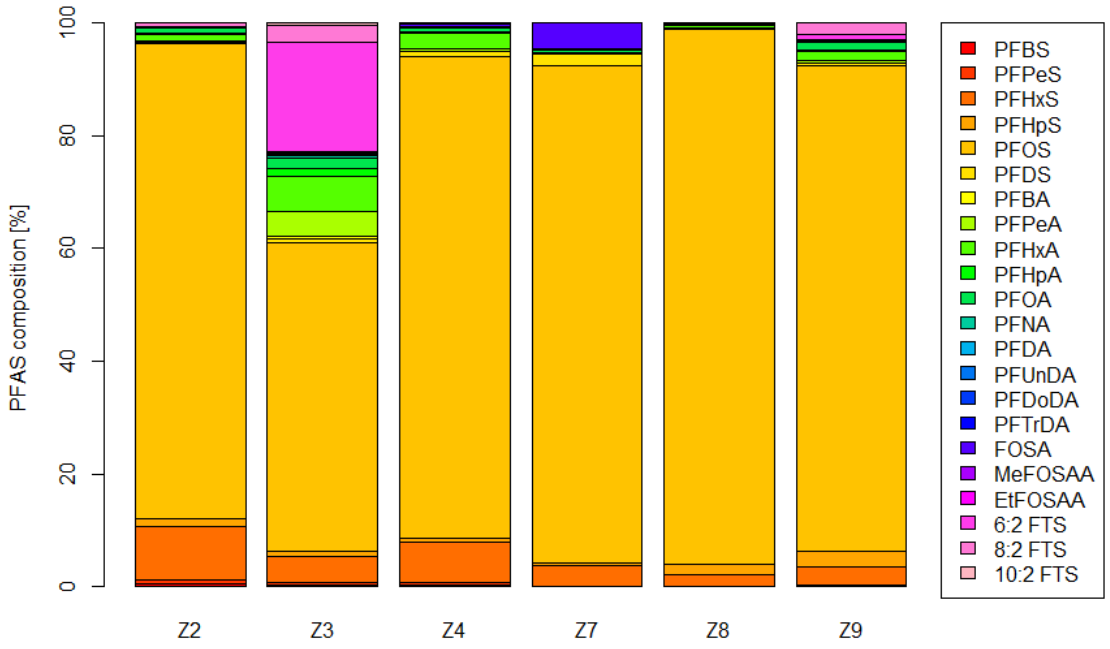


Figure 7.1: PFAS composition across soils Z2-Z4 and Z7-Z9 in the <2 mm soil particle size fraction.

EtFOSE, 4:2 FTS and PFTeDA were not detected in any of the soils. Figure 7.1 shows the composition of each sample as proportions, where it can be clearly seen that PFOS formed the largest proportion for all 6 soils, ranging from 54.7% (Z3) to 94.9% (Z8). PFHxS was the second highest for soils Z2 (9.39%), Z4 (7.10%), Z8 (9.09%) and Z9 (3.19%). Soil Z7 contained a high proportion of FOSA (4.64%), while Z3 contained a large proportion of both 6:2 FTS (19.4%) and PFHxA (6.14%). Supplementary Figure D.1 depicts a heat map of PFAS concentrations in the <2 mm soil fraction, with values normalised across each PFAS.

When compared to soil guideline values (Table 7.2, [2]), it can be seen that PFOS + PFHxS guideline values have the most impact on these soils, due to lower guideline values and higher PFOS concentrations. All soils were above at least one guideline value for garden soil. Soil Z7 met the requirements for ecological and public open space, residential and commercial land. Soil Z3 passed the requirements for residential with minimal opportunity to access soil and commercial land, while Z4 met the criteria for use as commercial land only. Soils Z2, Z8 and Z9 were highly contaminated and exceeded all guideline values except the PFOA guideline value for industrial land. The Σ_{28}PFAS concentrations in soils Z2, Z3 and Z4 were found to fall within the range of AFFF contaminated soils discussed in the introduction (700-37,200 μg kg^{-1}). Soil Z7 fell slightly below this range and soils Z8 and Z9 were well above this range. From a broader perspective than the contaminated soils examined earlier, the investigations and review of Brusseau et al. [102] found total PFAS contamination in soils of up to 460,000

Table 7.2: Local guideline values for garden soil, ecological and public land, residential soil and industrial land [2] and soils failing these at initial concentration measurements.

Guideline type	PFAS	Guideline conc. ($\mu g\ kg^{-1}$)	Soils failing	Soils passing both values
Residential soil incl. garden	PFOA PFOS+PFHxS	100 10	Z2, Z8, Z9 Z2, Z3, Z4, Z7, Z8, Z9	-
Public open space	PFOA PFOS+PFHxS	10,000 1,000	Z9 Z2, Z3, Z4, Z8, Z9	Z7
Residential with minimal opportunity for soil access	PFOA PFOS+PFHxS	20,000 2,000	Z9 Z2, Z4, Z8, Z9	Z3, Z7
Commercial / industrial	PFOA PFOS+PFHxS	50,000 20,000	- Z2, Z8, Z9	Z3, Z4, Z7

$\mu g\ kg^{-1}$ for an Australian Study, and 373,000 $\mu g\ kg^{-1}$ for a US study. While Z8 falls under these maximum reported concentrations, Z9 at 2,320,000 $\mu g\ kg^{-1}$ is significantly higher. Conceivably, high Σ_{28}PFAS in Z9 may result from repeat applications of AFFF or direct spills of AFFF concentrate.

7.3.2 PFAS leaching in soil pre-amendment

In addition to soil analyses, PFAS concentrations in leachates (DI water) of the <2 mm soil fraction were determined as presented in Table 7.3. The concentration of Σ_{28}PFAS in contaminated soil leachate ranged from 25.0 (Z7) to 14700 (Z9) $\mu g\ L^{-1}$. PFSAs were the dominant class of PFAS comprising 55 (Z3) - 99 (Z8) % of the Σ_{28}PFAS concentration. Within the PFSAs, PFOS was the most prevalent at 21.9 (Z7) - 10600 (Z8) $\mu g\ L^{-1}$. PFCAs comprised between 0.54 (Z8) and 29.5 (Z9) % of Σ_{28}PFAS concentrations. PFHxA was the most prevalent of this family with concentrations ranging from 0.115 (Z7) to 2160 (Z9) $\mu g\ L^{-1}$. PFOA concentrations in the leachate ranged from 1.14 (Z4) up to 944 (Z9) $\mu g\ L^{-1}$. 6:2 FTS had the highest concentrations from the FTS family with concentrations ranging from 0.585 (Z2) to 499 (Z8) $\mu g\ L^{-1}$. 10:2 FTS and PFTrDA, which were detected in the soils, were not present in these leachates at detectable levels (<0.05 and <0.02 $\mu g\ L^{-1}$ respectively). It was also observed that Z8 had the highest concentration of PFOS in leachate, in contrast to Z9 having the highest PFOS concentration in soil, which is discussed further in Section 7.3.3. The leachate from Z4 had the highest (and only) EtFOSAA (0.025 $\mu g\ L^{-1}$) and MeFOSAA (0.020 $\mu g\ L^{-1}$) concentrations, noting that Z4 had also the highest concentrations of EtFOSAA (1.8 $\mu g\ kg^{-1}$) of

Table 7.3: Mean leachate PFAS concentrations prior to immobilisation (μg L^{-1}, 3 s.f.). MeFOSA, MeFOSE, EtFOSA, EtFOSE, 4:2 FTS, 10:2 FTS, PFTrDA and PFTeDA were <LOR for all leachates. Replicate measure varied for concentrations greater than the LOR by an average of ±15%.

PFAS	Z2	Z3	Z4	Z7	Z8	Z9
PFBS	7.27	0.570	0.535	<LOR	5.45	228
PFPeS	177	0.635	0.755	0.0300	7.75	494
PFHxS	173	7.47	11.6	1.10	250	3380
PFHpS	291	1.45	1.28	0.110	232	387
PFOS	1050	59.0	122	21.9	10600	5290
PFDS	1.67	0.235	1.30	0.545	1.25	2.30
PFBA	1.60	1.75	0.250	<LOR	<LOR	272
PFPeA	3.69	9.45	1.14	<LOR	5.70	585
PFHxA	18.9	8.19	5.24	0.115	27.7	2160
PFHpA	3.63	2.15	0.520	0.025	2.05	361
PFOA	10.9	2.22	1.14	0.080	25.4	944
PFNA	0.880	0.880	0.110	<LOR	<LOR	21.1
PFDA	0.485	0.240	0.095	<LOR	<LOR	<LOR
PFUnDA	0.050	0.055	0.015	<LOR	<LOR	<LOR
PFDoDA	0.015	<LOR	0.010	0.030	<LOR	<LOR
FOSA	0.750	0.030	0.790	1.00	27.6	17.6
MeFOSAA	<LOR	<LOR	0.020	<LOR	<LOR	<LOR
EtFOSAA	<LOR	<LOR	0.025	<LOR	<LOR	<LOR
6:2 FTS	0.585	28.3	<LOR	<LOR	<LOR	499
8:2 FTS	7.38	3.03	0.175	<LOR	<LOR	34.6
Σ_6PFSA	1280	69.3	137	23.7	11100	9780
PFSA %	96.4	55.2	93.5	94.9	99.1	66.5
Σ_{10}PFCA	40.2	24.9	8.55	0.250	60.8	4340
PFCA %	3.03	19.9	5.81	1.00	0.543	29.5
PFOS+PFHxS	1230	66.4	134	23.0	10800	8670
Σ_{28}PFAS	1330	126	147	25.0	11200	14700

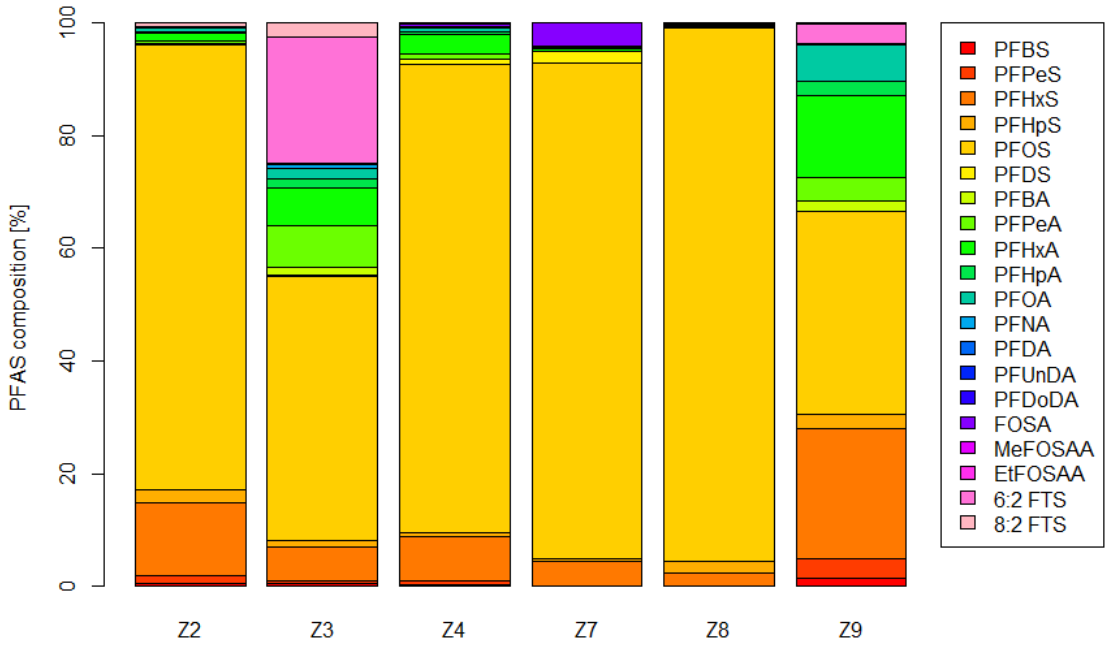


Figure 7.2: PFAS composition across soils Z2-Z4, and Z7-Z9 following leaching using ASLP (AS4439) (1997).

all the soils. Z9 had the highest concentration of PFOA in both soil (27,900 μg kg^{-1}) and leachate (944 μg L^{-1}) measurements.

The percentage composition of PFAS in leachates are plotted in Figure 7.2. As in soils, leachates contained PFOS as the predominant PFAS, ranging from 7.0% (Z3) to 94.8% (Z8). Leachates from Z3, Z4 and Z9 contained a significant proportion C_5-C_6 carboxylic acids, with up to 7.5% PFPeA (Z4) and 14.7% PFHxA (Z9). The Z3 leachate contained 22.5% 6:2 FTS, while Z9 and Z2 contained 23.0% and 13.0% PFHxS respectively. Z7 contained the highest proportion of FOSA (4.01%), although FOSA was detected in small amounts in all of the leachate samples. Supplementary Figure D.2 shows a heat map of leachate PFAS values normalised per PFAS.

The landfill acceptance criteria [2] (guideline values) for PFOA and PFOS+PFHxS concentrations in soil leachates, for unlined, clay or single composite lined, and double composite lined landfills are given in Table 7.4. It is seen that no soils are eligible for disposal in unlined, clay/single composite lined landfills or double composite lined landfills based on leachable fractions.

7.3.3 Soil-leachate comparison prior to amendment

When adjusted by the soil:solution dilution ratio of 1:20, the relationship between soil PFAS and leachate PFAS was close to 1:1 in some cases, but was more complex in others. Table 7.5 shows the leachable proportion of each PFAS in soil, this was calculated as the dilution adjusted leachate concentration divided by the soil concentration, multiplied by

Table 7.4: Suitability of unamended soils for landfill disposal based on landfill acceptance criteria [2] including leachable concentration (Guideline 1) and soil concentration (Guideline 2).

Landfill type	PFAS	Guideline 1 conc. ($\mu g\ L^{-1}$)	Guideline 2 conc. ($mg\ kg^{-1}$)	Soils failing G1	Soils failing G2	Soils passing all
Unlined	PFOA	0.56	50	Z2, Z3, Z4, Z8, Z9	-	-
	PFOS+ PFHxS	0.07	20	Z2, Z3, Z4, Z7, Z8, Z9	Z8, Z9	
Clay/single composite lined	PFOA	5.6	50	Z2, Z8, Z9	-	-
	PFOS+ PFHxS	0.7	50	Z2, Z3, Z4, Z7, Z8, Z9	Z8, Z9	
Double composite lined	PFOA	56	50	Z9	-	-
	PFOS+ PFHxS	7	50	Z2, Z3, Z4, Z7, Z8, Z9	Z8, Z9	

100 to obtain the value as a percentage. The differences between the soil and leachate concentrations appear to be determined predominately by carbon chain length. C_4-C_5 PFAS are consistently highly leachable, with leachability ranging from 115% (PFPeS Z4) - 356% (PFBA Z2). C_6-C_7 leachability ranged from 11.9% (PFHpS Z9) - 167% (PFHpS Z2). Indeed Z9 samples have notably and consistently lower leachability across almost all PFAS, presumably driven by soil physicochemical properties, such as organic carbon and clay content. Excluding Z9 values for PFOS (5%) and PFOA (68%), PFOS leachability ranged from 95-111%, and PFOA 82-109%. Long chain PFAS were often present in lower concentrations in the leachate than in the soil, with PFDS leachability ranging from 0.7% in Z9 to 126% in Z7, and PFUnDA from 41% in Z3 to 69% in Z2. The values in Table 7.5 raised questions as to why some PFAS are found at increased concentrations in leachate relative to their measured soil concentrations. Variation in leachability, including values of over 100%, is related to both the sorption behaviour, analytical variability and the experimental methodology of the ASLP. It is noted that analytical variability for low PFAS concentrations may result in large differences in percentage leached. Additionally there may be the potential for transformation of precursor molecules during the ASLP to shorter chain PFAS [81], and this requires further experimental investigation.

The general dependence of sorption on carbon chain length is known and reported in the literature. For example, Chen et al. [27] found in their experimental work that PFAS with carbon chain lengths of 10 or more were more likely to be adsorbed on suspended particles, while those shorter than C_7 were more likely to be dissolved in the aqueous phase. PFAS with longer fluorinated carbon chain are more hydrophobic, and are thus more likely to have a stronger affinity for surfaces, both because of greater contact area and stronger interactions. In contrast, shorter chain PFAS have been shown to have

Table 7.5: Dilution adjusted leachate concentrations as a percentage of soil concentrations (%, max 3 s.f.). Cells marked with * denote the PFAS was detected in leachate but not in soil, 0 denotes detected in soil but not in leachate, and blank indicates detection in neither sample.

PFAS	Z2	Z3	Z4	Z7	Z8	Z9
PFBS	119	151	139		131	148
PFPeS	174	122	115	120	133	230
PFHxS	145	141	114	135	112	91.1
PFHpS	167	143	133	122	122	11.9
PFOS	97.8	94.9	100	111	104	5.29
PFDS	107	38.2	94.0	126	5.59	0.69
PFBA	356	259	143			143
PFPeA	143	187	177		122	156
PFHxA	125	117	140	139	75.8	104
PFHpA	110	139	153	*	67.5	138
PFOA	104	109	109	84.2	102	67.8
PFNA	85.0	129	147			10.9
PFDA	107	96.0	131			0
PFUnDA	69.0	40.7	42.9			0
PFDoDA	12.8	0	20.0	100		
PFTrDA	0	0	0			
FOSA	28.6	13.64	104	96.9	114	5.22
MeFOSAA	0		133			
EtFOSAA	0		27.8			
6:2 FTS	232	128				53.0
8:2 FTS	110	85.3	113			1.43
10:2 FTS	0	0				

higher solubility in water than their longer counterparts [83].

Via an examination of the literature, it was found that PFAS leachability results are consistent with other studies. Rayner et al. [80], for example, examined five leaching methods, including the ASLP, and found significant differences between soil concentrations and leachate fractions. They found that C_4-C_8 PFCAs had mean ratios of leachable fractions to soil fractions of the order of 2-4. For PFNA this ratio was close to 1 and for PFDA closer to 0. For the C_4-C_7 PFSAs the mean ratio ranged from almost 5 for PFBS, 2 for PFHpS, to 1 for PFOS and close to 0 for C_9-C_{11} PFSAs. These literature results are consistent with our soil leachability results, presented above. Rayne et al. [80] additionally found that of the five studied leaching methodologies, both the Australian Standard Leaching Procdure) ASLP (utilised in this work), and the leaching assessment framework (LEAF) resulted in the highest PFAS concentrations. Across the methods, both the liquid:soil ratio and duration of tumbling were correlated with the leached PFAS concentrations. The trend of higher concentrations of short-chain PFAS in leachate was observed by Rayner et al. [80] across all methods studied.

7.3.4 Leachates after amendment: amendment efficacy

As discussed in the introduction, products from the RemBind® family have been shown to be among the most effective at reducing leachability of many PFAS, including PFOS, PFOA and PFHxS [90]. Previous immobilisation studies assessed products RB [93, 95, 33], RB+ [93], RB100 [69, 97, 98, 92], RB100X [98] and RB300 [92]. The assessments performed in this section add to this body of work, by extending the work of Juhasz et al. [92] on RB100 and RB300, with inclusion of additional soil samples and modelling of immobilisation efficacy.

Following the analysis of PFAS in soil and leachate in the six samples, bench scale immobilisation was performed on 5 of these soils. Soil Z8 was excluded from the study as the leachable PFOS concentration was deemed too high for practical inclusion in immobilisation experiments. Specifically, the ratio of amendment to soil that would be required to reduce the leachable PFOS concentration below guideline values would not be economically feasible. Soil amendments were added to PFAS-contaminated soil, as described in Section 7.2, for the purpose of investigating the efficacy of immobilisation as measured by changes in leachable PFAS concentrations. Two different products, RB100 and RB300 were added at applications of 1, 2.5, 5 and 10% w/w.

Figure 7.3 shows the measured efficacy for each of the four applications, with applications shown as different shapes, while soils are depicted in different colours. Similar to the immobilisation efficacy by carbon chain length plot of the in Chapter 2 using data from the literature, a similar trend was observed in efficacy data. While absolute values varied across soils, immobilisation efficacies were seen in some soils to exhibit a

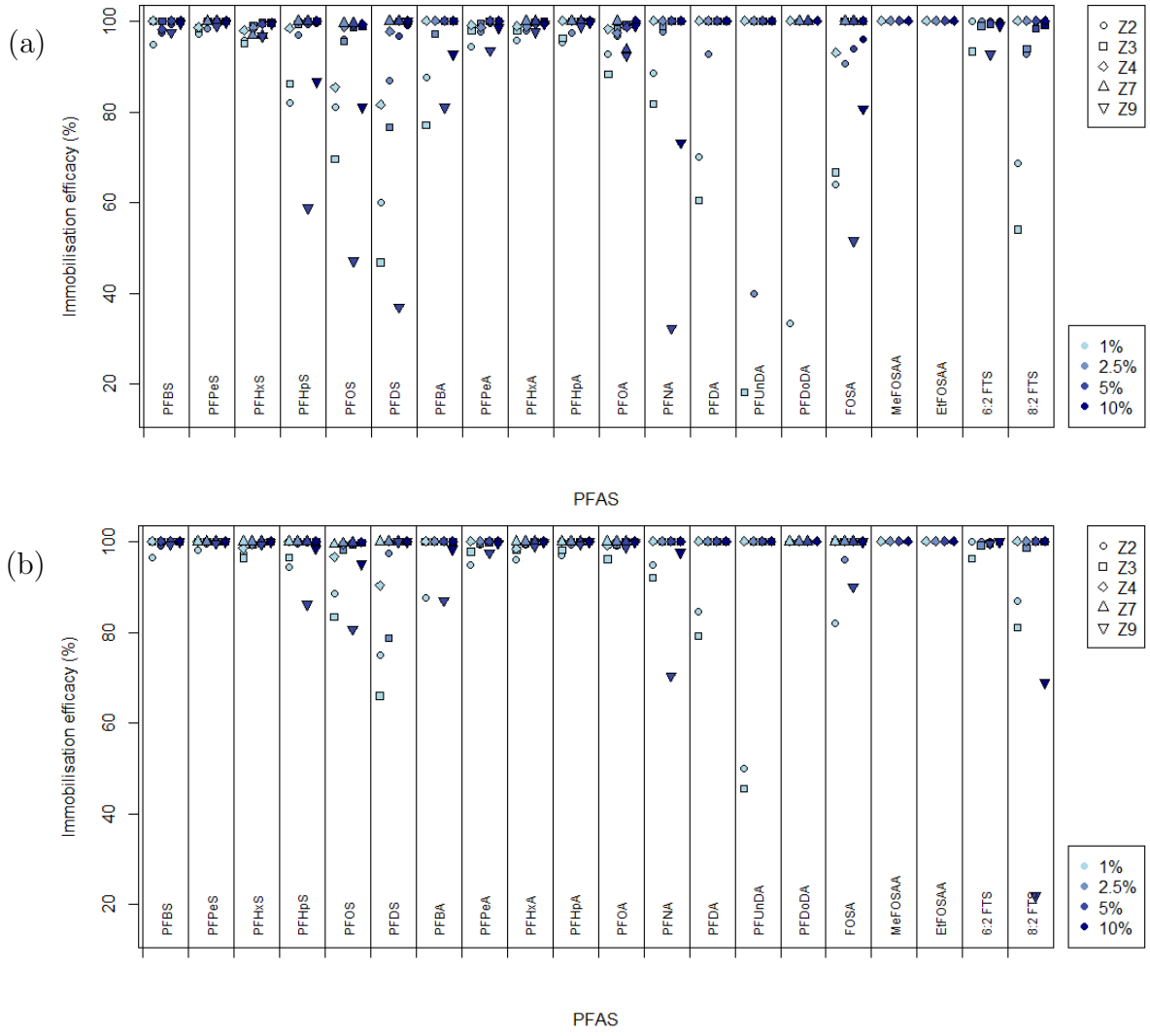


Figure 7.3: PFAS immobilisation efficacy at application rates of 1%, 2.5%, 5% and 10% w/w as a function of soil and PFAS for (a) RB100 and (b) RB300. Applications shown in different shades, while soils are depicted as different shapes.

Table 7.6: Σ_{28}PFAS immobilisation efficacy (%) of RB100, RB300 and relative efficacy of RB100 vs RB300 as a function of application rate (w/w %) and soil. 10% application rate was not applied to Z7 soil due to low initial PFAS concentrations.

RB100 efficacy				
App. rate	1	2.5	5	10
Z2	83.6	96.4	98.9	99.4
Z3	81.4	97.3	99.1	99.3
Z4	87.4	98.7	99.2	99.4
Z7		99.4	99.4	
Z9			76.8	91.9
RB300 efficacy				
App. rate	1	2.5	5	10
Z2	90.1	99.1	99.7	99.9
Z3	90.1	98.7	99.5	99.9
Z4	96.9	99.5	99.8	100
Z7		99.7	99.8	
Z9			91.6	98.0
Relative efficacy: RB100/RB300×100				
App. rate	1	2.5	5	10
Z2	92.8	97.2	99.3	99.5
Z3	90.4	98.5	99.6	99.4
Z4	90.2	99.3	99.3	99.4
Z7		99.8	99.7	
Z9			83.9	93.8

parabolic relationship with carbon chain length, with lower efficacies occurring towards the lowest and highest C chain lengths, across both PFCAs and PFSAs, and both RB formulations. Full listings of immobilisation efficacy values are given in Supplementary Tables D.2 to D.9, including uncertainty associated with values below the LOR. Supplementary Figures D.3 and D.4 show amounts of immobilised individual PFAS for each soil and RB formulation.

The Σ_{28}PFAS immobilisation efficacy results are presented in Table 7.6. For RB100 these ranged from 76.8% for the 5% application rate in soil Z9, to 99.4% for the 10% rate in soils Z2 and Z4. RB300 efficacy varied from 90.1% for the 1% application rate in soils Z2 and Z3, up to ∼100% (3 s.f.) for the 10% application rate where only 0.06 μg L^{-1} of measurable PFAS was in the leachate sample. It was observed, for both individual and Σ_{28}PFAS concentrations, that RB300 was more effective at immobilising PFAS in these samples, with smaller amounts of the product required to achieve the same immobilisation effect. This is highlighted by relative efficacy values for RB100 compared to RB300 (Table 7.6), which ranged from 83.9 for the Z9 sample at the 5% application rate, up to 99.8 for Z7 at the 2.5% application rate. The greater variation in relative efficacy at low application rates suggests that the improvements made to

RB300 compared to RB100 advocates preferential use of RB300 at lower application rates, primarily if not exclusively.

As identified by examination of Supplementary Tables D.2-D.9, reduced leaching of PFOA with RB100 ranged from 88.3% for Z3 at an application rate of 1%, to below detection for Z7 at 1%, and Z3 and Z4 at an application rate of 5%. With RB300, PFOA immobilisation efficacy ranged from 95.9% for Z2 at 1%, to ∼100% for Z7 at 1%, Z4 at 2.5%, Z3 at 5% and Z2 at 10%. PFOS immobilisation with RB100 ranged from 47.2% for Z9 at the lowest application rate of 5%, to 99.5% for Z7 at both 2.5 and 5% application rates. With RB300, PFOS immobilisation was also superior, ranging from 80.6% for Z9 (5% w/w) to ∼100% for Z4 at the 10% application rate. PFHxS immobilisation efficacy with RB100 varied from 95.0% at 1% application rate in Z3, to 99.7% at the 10% application rate for Z2, Z3 and Z4. RB300 was noticeably more effective for PFHxS immobilisation, with efficacy ranging from 96.4% for Z3 at 1% to ∼100% at 1, 2.5 and 5% for Z7 and 10% application rates for soils Z2 and Z3.

These efficacies are comparable to those of [97] where reduction in leachable PFAS from a soil remediated with 5% w/w RB100 was found to range between 91.8% and ∼100% in comparable data using the ASLP, with similar outcomes for other leaching methods.

7.3.5 Modelling PFAS immobilisation

Following examination of PFAS immobilisation data, an exponential model dependent on application rate was fitted in line with the aim of predicting the amendment application rate required to reduce PFAS leachability to below landfill disposal guidelines. As immobilisation does not change the soil content, in this section only landfill acceptance was examined based on leachate concentration. Only the subset of PFAS that were present in the initial leachate sample, and with values greater than the LOR for at least two amendment application rates were used in the model fitting.[2] The overlaid exponential curves of the form

$$y = ae^{rx}$$

for each soil, where x is the percentage of amendment added and y the leachate concentration in μg L^{-1}, are shown in Supplementary Figures D.5 and D.6, while individual fitted curves are shown for each PFAS and amendment type in Supplementary Figures D.7 to D.17. A selection of model fits for PFOA and the fits for the sum of PFOS and PFHxS are shown in Figures 7.4 and 7.5, respectively.

Values for the two fitted parameters, a and r are shown in Table 7.7. The parameter a corresponds to the fitted initial value, where the curve crosses the axis at $x = 0$, in

[2]This is due to the minimum requirement of 3 data points to fit an exponential model.

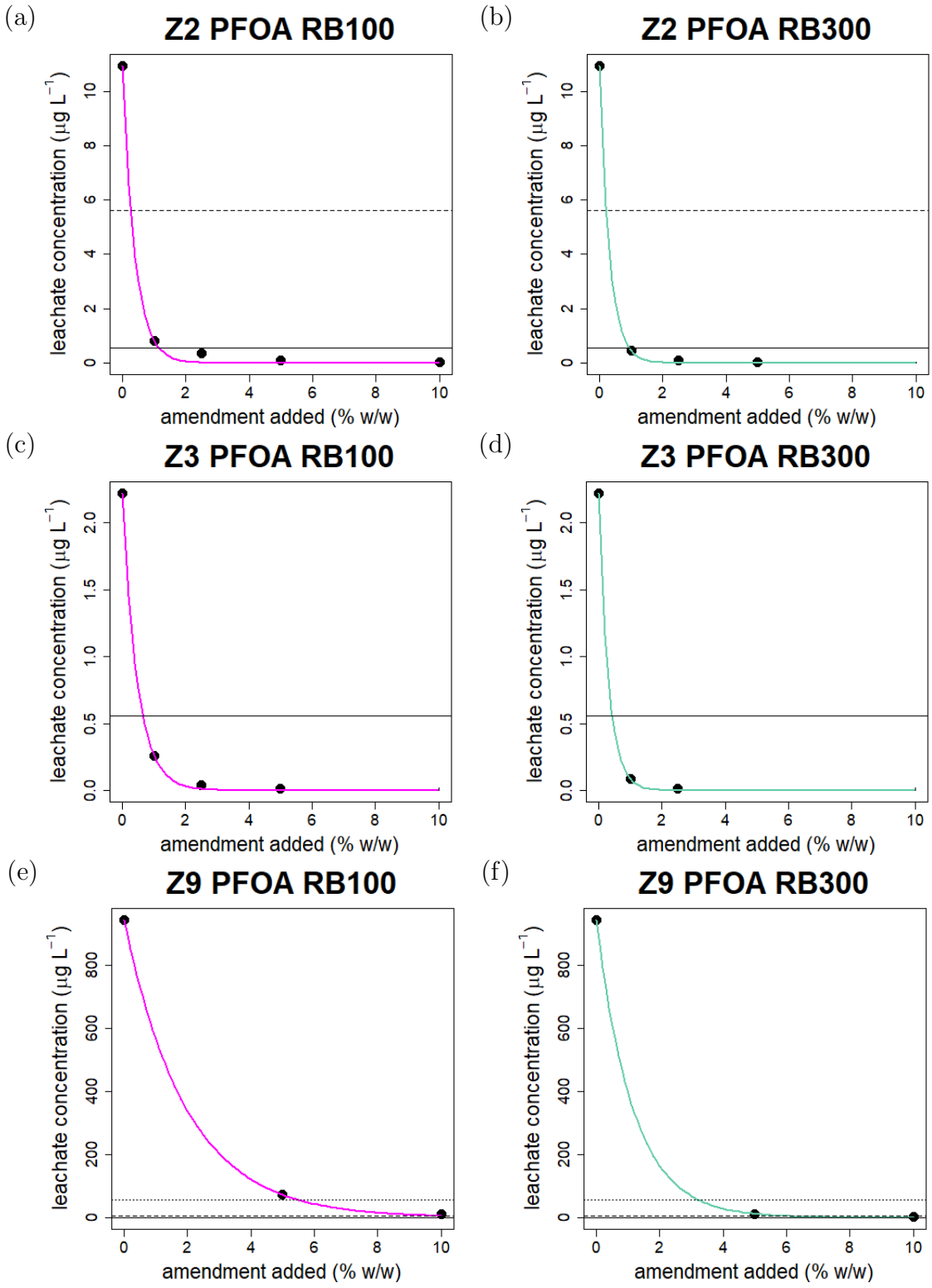


Figure 7.4: PFOA experimental leachate concentrations (points) and fitted models (coloured lines) for soils Z2, Z3 and Z9 and amendments RB100 and RB300. Horizontal lines show leachate guideline values of 0.56 (unlined; solid), 5.6 (single composite lined; dashed) and 56 µg L^{-1} (double composite lined; dotted).

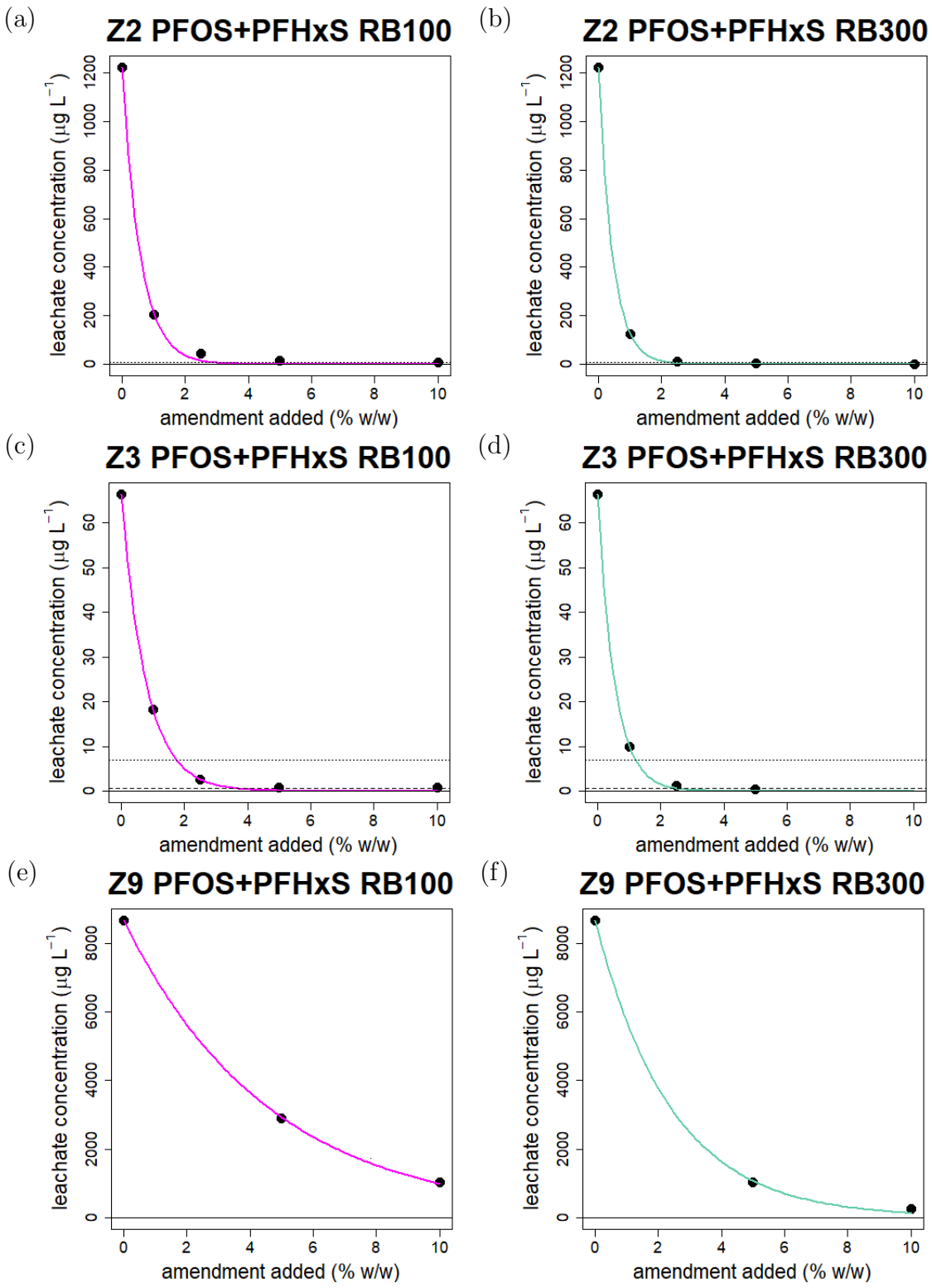


Figure 7.5: PFOS + PFHxS experimental leachate concentration (points) and fitted model (coloured lines) for soils Z2, Z3 and Z9 following amendment with (a) RB100 and (b) RB300. Horizontal lines show leachate guideline values of 0.07 (unlined; solid), 0.7 (single composite lined; dashed) and 7 µg L^{-1} (double composite lined; dotted).

Table 7.7: Fitted exponential model parameters a and r (3 s.f.) for PFAS immobilisation using RB100 and RB300.

Soil	PFAS	RB100		RB300	
		a	r	a	r
Z2	PFBS	7.27	-2.95	7.27	-3.33
	PFPeS	17.6	-3.54	17.6	-3.95
	PFHxS	173	-3.17	173	-3.69
	PFHpS	29.0	-1.70	29.0	-2.88
	PFOS	1050	-1.64	1049	-2.15
	PFDS	1.66	-0.873	1.67	-1.39
	PFPeA	3.69	-2.85	3.69	-2.96
	PFHxA	18.8	-3.15	18.8	-3.22
	PFHpA	3.63	-3.05	3.63	-3.45
	PFOA	10.9	-2.59	10.9	-3.20
	PFDA	0.484	-1.18		
	FOSA	0.748	-0.990		
	8:2 FTS	7.37	-1.13	7.38	-2.03
	PFOS+PFHxS	1221	-1.76	1222	-2.27
Z3	PFHxS	7.47	-3.00	7.47	-3.32
	PFOS	59.0	-1.20	58.9	-1.79
	PFDS	0.23	-0.602	0.231	-0.876
	PFPeA	9.44	-3.93	9.44	-3.78
	PFHxA	8.18	-3.87	8.18	-3.97
	PFOA	2.22	-2.13	2.22	-3.26
	6:2 FTS	28.2	-2.70	28.2	-3.29
	8:2 FTS	3.05	-0.868		
	PFOS+PFHxS	66.4	-1.29	66.41	-1.88
Z4	PFHxS	11.5	-3.87	11.55	-4.25
	PFOS	122	-1.92	122	-3.39
	PFOA	1.14	-1.44	5.24	-4.12
	PFOS+PFHxS	134	-2.00	134	-3.44
Z7	PFHxS	1.10	-1.35		
	PFOS	21.9	-2.13	21.9	-5.05
	PFOS+PFHxS	23.0	-2.04		
Z9	PFBS	227	-0.74		
	PFPeS	494	-0.896		
	PFHxS	3380	-0.678	3380	-0.994
	PFHpS	388	-0.187	387	-0.397
	PFOS	5340	-0.146	5290	-0.324
	PFBA	272	-0.319		
	PFPeA	584	-0.544	584	-0.738
	PFHxA	2160	-0.744	2160	-0.898
	PFHpA	360	-0.887		
	PFOA	943	-0.513	943	-0.874
	PFNA	21.6	-0.110		
	FOSA	17.6	-0.154		
	6:2 FTS	498	-0.523		
	8:2 FTS	37.4	0.008	35.9	-0.093
	PFOS+PFHxS	8670	-0.217	8670	-0.416

our case this value was always positive. r is related to the growth or decay rate, and corresponds to the rate of PFAS immobilised in soil. r was negative in every case except the outlier 8:2 FTS immobilisation in soil Z9, where concentrations did not decline at either amendment application rate (Supplementary Figure D.16).

The amount of RB100 and RB300 required to achieve leachable concentrations under landfill disposal guidelines, x_g, was calculated via the fitted model using the equation

$$x_g = \frac{\ln\left(\frac{y_g}{a}\right)}{r}$$

where y_g is the desired guideline concentration. These results are summarised in Table 7.8.

To achieve leachate acceptability for double composite lined and unlined landfills, it was calculated that RB100 should be added to Z2 at 2.9% w/w and 5.6% w/w respectively. Lower amounts of RB300 were required to achieve these landfill criteria (2.3% and 4.3% respectively); the difference being more significant with decreasing leachate acceptability values. Similar results were observed for the remaining soils, where lower amounts of RB300 were required compared to RB100 for PFAS leachate values to fall below landfill criteria. For Z7 and RB300, application rates were unable to be calculated due to leachability being <LOR at all tested application rates for both PFOA and PFHxS (see Supplementary Table D.3). Although Z9 failed landfill criteria based on the total concentration of PFOS+PFHxS (>20,000 µg kg^{-1}), modelling was still undertaken to investigate amount of RB100 and RB300 required to reduce leachable fractions to below landfill criteria. As shown in Table 7.8, impractical amounts of RB100 (32.9% w/w) and RB300 (17.1% w/w) would be required to meet double composite lined landfill leachate criteria. However, again modelling showed greater immobilisation efficacy for RB300 and demonstrated the application of the exponential model to predict PFAS leachability.

It can be seen in Table 7.8 that for all soils, the driving factor in application rate calculations was PFOS+PFHxS concentration. The amount of RB100 and RB300 required to immobilise PFOA to below guideline concentrations was significantly lower when assessed in isolation. For all soils, the amount of RB300 required to reduce the PFAS leachable fraction to below the corresponding landfill guideline, was lower than for RB100. However, as as there may be a cost difference between products, this should also be taken into consideration when determining optimal product and application rate for a site. It is also an important observation that immobilisation rates depended not only on the intial PFAS concentration but also varied with soils. This soil effect was noted in the increased immobilisation effectiveness of PFOS+PFHxS in Z4 relative to the less contaminated Z3. More cannot be concluded from the current data, but further controlled experiments investigating the dependence of immobilisation rates on soil

Table 7.8: Table of percentage required to get below leachable concentration guideline values for disposal in double composite lined (Double CL), clay/single composite lined (Clay SL) and unlined landfills. Cells marked with * were not fitted using the exponential model, as the minimum required data points were unavailable due to concentrations <LOR.

			RemBind application (% w/w) to reduce PFAS leachability to below landfill guideline values									
Landfill	PFAS	Guideline	Z2		Z3		Z4		Z7		Z9	
type		(μg L^{-1})	RB100	RB300	RB100	RB300	RB100	RB300	RB100	RB300	RB100	RB300
Double	PFOA	56	-	-	-	-	-	-	-	-	14.5	8.5
CL	PFOS+ PFHxS	7	**2.94**	**2.28**	**1.75**	**1.20**	**1.47**	**0.858**	**0.584**	* (<1)	**32.9**	**17.1**
Clay	PFOA	5.6	0.259	0.209	-	-	-	-	-	-	10	5.87
SL	PFOS+ PFHxS	0.7	**4.25**	**3.29**	**3.53**	**2.42**	**2.63**	**1.53**	**1.72**	* (<1)	**43.5**	**22.6**
Unlined	PFOA	0.56	1.15	0.93	0.646	0.423	* (<1)	* (<1)	-	-	5.51	3.23
	PFOS+ PFHxS	0.07	**5.56**	**4.30**	**5.32**	**3.64**	**3.78**	**2.20**	**2.85**	* (<5)	**54.1**	**28.2**

properties across a range of soils with equivalent PFAS concentrations and compositions could assist with quantifying these effects. Finally, although the exponential model generally fits the data well, it is not exact and thus when making a recommendation of the required % to be added, a margin of error should also be investigated and calculated. This would require an more detailed quantification of analysis of inter-sample variability and experimental errors.

7.4 Conclusions and future work

Analysis of data from bench-scale immobilisation studies was presented for PFAS contaminated soils immobilised with RB100 and RB300. Data covered five soils, four amendment application rates (1, 2.5, 5 and 10%), and 28 measured PFAS. Data regarding the reduction of leachable PFAS was shown to fit an exponential model. Based on this model, a method was developed for determining the amount of amendment required for soils to meet landfill disposal criteria. This work could be applied to other soils to estimate a starting point or range of application rates for soils of similar PFAS concentration and soil type, and extended to a more generally applicable model using the stragegies suggested below.

It was observed that immobilisation efficacy varied across the PFAS range studied, as well as with soil, functional group and carbon chain length. The lowest efficacies were measured for the long chain PFDS, PFDA, PFUnDA, PFDoDA, FOSA and 8:2 FTS, particularly at the lowest application rate. Efficacy of immobilisation for PFCAs generally decreased with chain length, for chains longer than 8 carbons in several soils, and for PFSAs from carbon chain length of 6 or more. RB100 and RB300 were both found to be effective immobilisation agents. Although RB100 required an overall higher application rate to achieve the same results as RB300, it should be noted that cost differences between the products were not taken into consideration. These factors would affect the calculation of an economically optimal intervention strategy.

Future work should involve a more detailed method dealing in with uncertainty in measurements in relation to application rate determination. Methods for estimating concentrations under the LOR for use in fitting approximate models would also be required in future iterations of the work to cope with cases were less than three measured data points above the LOR were available. Investigation and quantification of soil properties and influence on amendment efficacy could also be investigated in the future by undertaking experimental work that systematically examines differences in soil type in relation to amendment efficacy. Post immobilisation assessment could provide further insight into the influence of ageing and environmental factors on long-term immobilisation efficacy. Limited studies have been conducted to assess immobilisation stability

over longer time-frames, and so wetting and drying at elevated temperature cycles could be introduced into protocols to accelerate ageing processes. Multi-scale modelling could potentially provide and additional contribution in this area.

In the modelling of data presented here, it was found that r parameter values, corresponding to immobilisation rates, varied across all soil samples and PFAS. The results allude to a complex, yet hidden, relationship between soil properties and PFAS immobilisation. In theory, a characteristic application rate should reflect the ease (or difficulty) with which a particular PFAS can be immobilised in a given soil. This suggests that possible future efforts could be directed toward more detailed and extensive experimental studies to characterise soil composition and examine relationships with both initial PFAS leachability and immobilisation rates. Exponential modelling thereafter could potentially reveal a more consistent relationship between PFAS leaching, immobilisation and soil type, leading to the goal of a predictive model of amendment application efficacy.

Chapter 8

Conclusions and future work

8.1 Conclusions

Immobilisation of PFAS in soils is an area of emerging importance, as governments and private organisations grapple with the challenge of addressing historical PFAS contamination. The review undertaken at the beginning of this work provided an in-depth, quantitative comparison and assessment of PFAS immobilisation studies in soil. It found that across the range of soil and experimental conditions in published studies, activated carbon based amendments resulted in the highest immobilisation efficacies for PFAS. This analysis further highlighted differences in efficacy relating to PFAS carbon chain length and functional group. These findings underpinned and motivated both the subsequent theoretical simulations, with their focus on carbon surfaces and the inclusion of molecules of different carbon chain length, and the composite activated carbon-based immobilisation study contained in the final chapter. A schematic framework was also devised to outline the key assessment components required to test and validate the efficacy, longevity and biological impact of the application of PFAS immobilisation amendments in soils. This provided an evidence-based approach for the application of cost effective and sustainable immobilisation strategies, with the added objectives of minimising the impact of soil PFAS on environmental and human health.

While experimental works on topics relating to PFAS sorption, leaching and immobilisation are common, molecular level modelling of PFAS has rarely been presented in the published literature. The novel contribution of this work was on the application of Monte Carlo molecular simulation method to scenarios that differ from the three previously performed molecular dynamics simulations involving PFAS molecules [39, 40, 41]. The Monte Carlo simulation technique allowed focus to be placed on determining thermodynamic equilibrium behaviour, rather than either transient behaviour or the approach to equilibrium of molecular dynamic studies. By examining scenarios where both adsorption and mobility of PFAS may occur, the work is also of potential relevance to the

design and testing of sorptive surfaces for amendment-based remediation. In the work it was hypothesised that a theoretical study of PFAS-surface interactions, via Monte Carlo molecular simulation, would reveal differences in simulated behaviour resulting from changes in surface charge, divalent cation concentrations and PFAS carbon chain length, and this was indeed observed to be the case. The Monte Carlo simulations revealed differences in adsorption behaviour of PFSAs to graphite with surface charge, ion type, and carbon chain length. Higher adsorption was shown to occur for positively charged surfaces, compared to neutral surfaces, even in the presence of a screening electrolyte. Higher adsorption was also observed with negatively charged surfaces when divalent Ca^{2+} cations were included, due to cation bridge formation with the surface. The simulations in this work showed the role of van der Waals and electrostatic interactions, but did not show the reduced sorption for the PFBS observed in experimental work, possibly due to the absence in the model of both organic material and explicit hydrophobic interactions. Indeed, it was shown by [103] that there are differences in the interactions of short and long chain PFAS between different components of soil organic matter.

The developed simulation software in itself represents a significant contribution, providing access to a Monte Carlo molecular simulation model by an audience possibly not conversant with the Fortan language used in the majority of historical physics-based software, nor able to purchase expensive commercial simulation packages. The entire simulation, analysis and production of visualisations as seen throughout this work requires only a free R [45] software installation. The software developed here has the capability to simulate a range of rigid molecules and solution ions interacting with a single surface across an implicit aqueous medium. The software's functionality further extends to detailed analyses of all aspects of the simulation, including thermodynamic averaged molecular distance from the surface, statistics on the rotation of molecules, and calculations of relative contributions of van der Waals and electrostatic interactions.

An increasing amount of important information has emerged in recent times relating to the concentration of PFAS in environmental matrices such as surface water, groundwater, wastewater, soil, sediment, sludge and biosolids. The results of the analyses conducted in this thesis contributed to the growing international PFAS-biosolid concentration knowledge-base, and added valuable information on PFAS concentrations and composition in the Australian context. This is critical given that the re-use of biosolids occurs frequently and that guidelines for PFAS acceptability criteria in biosolids is only in its early stages of development in Australia. In this work, PFAS were detected in all waste water treatment plant (WWTP) biosolid samples analysed, ranging in concentration from 5.35 to 145 mg kg^{-1}. When assessed against regulatory guidelines, the majority of the samples exceeded the PFAS guideline concentration values. This is concerning given the critical role WWTPs play in effecting PFAS transfer into the environment,

not only through biosolid reuse but also recycled water reuse and effluence discharge to the environment. The study highlighted the diversity of PFAS contamination profiles across different sites, and consequently highlighted the inadequacy of measuring only regulated PFAS: PFOA, PFOS and PFHxS. Such limited investigation does not provide an adequate picture of the entire scope of PFAS contamination in WWTP biosolids. The correlations between PFAS and other substances present also raises questions on the influence of pH and substances, such as metal ions, on PFAS sorption and leaching behaviour in biosolids. There was no relationship observed between PFAS concentration and the size of WWTP catchment areas, indicating that other factors such as contamination source proximity, to, say air force bases or trade waste, likely play a more significant role in the observed levels of biosolid PFAS contamination. The work showed particularly the important correlation between pH and the extent of PFAS contamination in historical stockpiles. The correlation was higher than any temporal effects.

As in the study of biosolid samples, the AFFF contaminated soils studied were shown to vary both in total PFAS concentrations and diversity of PFAS molecules present. The TOP assay was applied to these samples, showing potential transformation of PFCA precursor molecules. The analysis of data from bench scale immobilisation studies were presented for PFAS contaminated soils immobilised with RB100 and RB300. The presented data covered five soils with amendment application rates of 1, 2.5, 5 and 10%, and 28 measured PFAS. The modelling of the reduction of leachable PFAS was shown to fit well with the exponential model, and a method for calculating the percentage of amendment required based on this model was presented. The soil analyses highlighted the variation in PFAS soil contamination present at a selection of Australian AFFF impacted sites, including many soils with leachble PFAS concentrations rendering them unsuitable for disposal to Australian landfill sites. With RemBind® being among the most effective immobilisation agents identified in the analyses of Chapter 2, the immobilisation study then examined the effectiveness of RemBind® in reducing leachable PFAS to permitted concentrations. This was shown to be an effective method at the bench-scale for all but the most highly contaminated soils. This work contributed to the body of immobilisation data studied at the beginning of this work.

Overall, the published works, data, analyses and software presented in this thesis represent a contribution to the knowledge base and available tools for understanding PFAS behaviour. These contributions span the areas of PFAS prevalence and sorption in complex soils, biosolids and immobilisation amendments, and more fundamental work relating to sorption to graphite surfaces. Together, this represents a marrying of experimental observations and theoretical computational modelling, based on established principles of theoretical physical chemistry.

8.1.1 Limitations

While the thesis represents a contribution as described above, there are many limitations of the work arising from project time-scales, funding, data availability or inherent in techniques utilised. A summary of some of the main limitations follows in chapter order. The comparison of PFAS immobilisation studies of Chapter 2, and in particular comparison of efficacy of immobilisation across different studies is limited by lack of consistent experimental conditions and soils. This limits conclusions about relative efficacy of different amendments on unknown soils or under varied conditions.

The most significant limitation of Chapter 3 is lack of experimental data to validate the modelling outcomes. This drawback is the main focus of the Section 8.2 on future work, and associated challenges are discussed in detail therein. Other limitations of both Chapter 3 and Chapter 4 include use of implicit water, and the simplified simulation set-up compared to real-world conditions, including a lack of organic matter and heterogeneous surfaces.

For Chapter 5, examining biosolids, main limitations were around the age and storage of samples, and varied sample types and collection methods. While at the time of analysis, all samples were dried, archived samples, they had been stored for significant periods. Potential transformation or degradation during collection, drying and storage was not able to be measured, and collection methods and sources of samples differ. Information on sample source types is included in Supplementary Table B.2, but means waste water treatment plants are not directly comparable, and limits the study to being a more exploratory investigation into potential variability in scope and scale of PFAS contamination in historical Australian biosolids.

In terms of the remaining experimental chapters, scope of PFAS measured, lack of any non-target analysis, or total organic fluorine measurement also limits conclusions that can be drawn from Chapters 6 and 7. Specifically for the immobilisation study, short time-span, short monitoring duration and lack of long-term validation limit the applicability of results, though others have conducted longer studies on RemBind® and similar AC-based amendments with promising results over 3-4 years [93, 34]. Lack of real world conditions present in bench-scale experiments, along with lack of accounting for heterogeneity associated with large-scale application techniques are also limitations of the work.

8.2 Future Work

Future work arising from this thesis spans a wide range of potential areas, from further software development, new simulations in conjunction with linked experimental sorption studies, to computational modelling and optimisation of amendment formulations and

application regimes. These ideas for potential research directions are elucidated in the sections below, and have been arranged into short-, medium- and long-term goals.

8.2.1 Short-term

The first natural extension of the work is the broader utilisation of the Monte Carlo simulation software to investigate additional factors such as functional group, carbon chain length, surface charge and surface structure. Ideally, these studies would be performed in conjunction with closely matching experimental work. Matching of experimental conditions, in a range of both simple and more complex scenarios, to the simulation conditions would prove useful in better identifying and quantifying sorption mechanisms. This work could either directly involve new experimental results, or seek to match the more fundamental, detailed PFAS sorption studies not previously modelled on a molecular level. An example of existing work that could be utilised includes the comprehensive experimental work on sorption of 12 PFAS to ferrihydrite surfaces with changing surface charge of Campos-Pereira et al. [104]. Another potential experimental study for future associated modelling is the recent investigation of the effect of N group and pore size in sorption to activated carbon of Zhang et al. [105]. Modelling that includes the components of composite amendments, such as aluminium hydroxide, kaolin clay and activated carbon, both individually and combined is also an interesting avenue of investigation. Modelling of other PFAS families including the currently used alternative molecules such as ADONA and GenX could also be of interest.

8.2.2 Medium-term

Once a sound foundation of fundamental molecular-level modelling studies has been established and experimentally validated, the results could also be used in a series of subsequent multi-scale models. Such modelling could include important processes such as competition for sorption sites between PFAS, sorption in complex systems with varying soil types and varying environmental conditions. The presence of bubbles in solid-water mixtures was shown to significantly influence PFAS sorption [106]. This has not been captured in simulations to date, and is another avenue for future work.

The simulation software, while useful as it stands for a range of scenarios, such as the surface interactions of Chapter 3, could be extended in multiple ways. These include the replacement of the implicit medium with an explicit one. That is, explicit water molecules could be included in the simulation box at a specified density and iterated over as per the same method as the molecules and solution ions in the current simulation. While the difference between implicit and explicit water molecules often does not affect adsorption modelling results [107], the influence varies for different scenarios. It would be of interest to undertake this comparison for the specific case of PFAS adsorption.

Another possible extension could involve enhancing the flexibility of the simulation set up. For example, it would be relevant to consider a simulation box containing two impenetrable, charged surfaces, one at the top and one at the bottom, or a box containing just a 3D solution, with periodic boundary conditions across all six faces. Lastly, on a more technical level the interface of the system could be improved to make it easier for users to change parameters and set up the simulation. In particular, this could include a more automated construction method of the molecular structure of the surfaces.

8.2.3 Long-term

The concentrations of both restricted PFAS and precursor compounds of restricted PFAS in biosolids warrants future investigation to determine concentrations in land where frequent applications of biosolids have been undertaken. The soil and biosolid components of the work could also be extended to include contrast studies of measured concentrations of historical samples compared with more recent ones in matching locations, to investigate the impact both of the cessation of AFFF product usage, and of the longevity of accumulated PFAS in the environment. Further insight into the relationship between PFAS and other elements could also be investigated by adding Cd, Zn etc. to the aforementioned experimental and modelling scenarios, and examining their impact on sorption. While there are many other important experiments and studies that could be performed, it is envisaged that the narrowing of the gulf between the experimental and theoretical work on PFAS sorption presents itself as both a valuable and natural progression of the analyses presented here.

In relation to immobilisation, computational modelling aiming to optimise surface properties could be utilised to aid in the selection of materials for composite immobilisation agents. Due to the different physicochemical properties of legacy and replacement PFAS, a single immobilisation agent may not adequately immobilise all compounds of concern in PFAS contaminated soils, and soil amendments may need to be tailored to site-specific conditions. Future PFAS soil amendment research and development, utilising a robust assessment framework would be useful to elucidate not only immobilisation efficacy but longevity of immobilisation. Post immobilisation assessments could provide further consideration into the influence of ageing and environmental factors on long-term immobilisation efficacy. Limited studies have been conducted to assess immobilisation stability over longer time frames. However, a limiting factor for ageing studies is the time frame required to assess longevity. Conceivably, wetting and drying under elevated temperature cycles could be introduced into protocols to accelerate the ageing processes, and multiscale modelling could aid with this objective.

Bibliography

[1] A. Gindulyte, B. A. Shoemaker, B. Yu, J. He, J. Zhang, J. Chen, L. Zaslavsky, P. A. Thiessen, Q. Li, S. He, S. Kim, T. Cheng, and E. E. Bolton, "PubChem 2019 update: Improved access to chemical data," *Nucleic Acids Research*, vol. 47, no. D1, pp. D1102–D1109, 2019.

[2] Heads of EPAs Australia and New Zealand (HEPA), *PFAS National Environmental Management Plan Version 2.0*. 2020.

[3] United Nations Environment Programme, *Stockholm Convention on Persistent Organic Pollutions (POPs)*. Secretariat of the Stockholm Convention (SSC), 2018.

[4] United Nations Environment Programme, "Chemicals proposed for listing under the convention." http://chm.pops.int/TheConvention/ThePOPs/ChemicalsProposedforListing/tabid/2510/Default.aspx, 2019.

[5] M. Ateia, A. Maroli, N. Tharayil, and T. Karanfil, "The overlooked short-and ultrashort-chain poly-and perfluorinated substances: A review," *Chemosphere*, vol. 220, pp. 866–882, 2019.

[6] S. Rayne and K. Forest, "Perfluoroalkyl sulfonic and carboxylic acids: A critical review of physicochemical properties, levels and patterns in waters and wastewaters, and treatment methods," *Journal of Environmental Science and Health Part A*, vol. 44, no. 12, pp. 1145–1199, 2009.

[7] R. C. Buck, S. H. Korzeniowski, E. Laganis, and F. Adamsky, "Identification and classification of commercially relevant per-and poly-fluoroalkyl substances (PFAS)," *Integrated environmental assessment and management*, vol. 17, no. 5, pp. 1045–1055, 2021.

[8] J. C. DeWitt, ed., *Toxicological Effects of Perfluoroalkyl and Polyfluoroalkyl Substances*. Springer, 2015.

[9] I. T. Cousins, R. Vestergren, Z. Wang, M. Scheringer, and M. S. McLachlan, "The precautionary principle and chemicals management: The example of perfluoroalkyl acids in groundwater," *Environment International*, vol. 94, pp. 331–340, 2016.

[10] K. Li, P. Gao, P. Xiang, X. Zhang, X. Cui, and L. Q. Ma, "Molecular mechanisms of PFOA-induced toxicity in animals and humans: Implications for health risks," *Environment International*, vol. 99, pp. 43–54, 2017.

[11] X. Shao, F. Ji, Y. Wang, L. Zhu, Z. Zhang, X. Du, A. C. K. Chung, Y. Hong, Q. Zhao, and Z. Cai, "Integrative chemical proteomics-metabolomics approach reveals acaca/acacb as direct molecular targets of PFOA," *Analytical Chemistry*, vol. 90, no. 18, pp. 11092–11098, 2018.

[12] S. A. Beach, J. L. Newsted, K. Coady, and J. P. Giesy, "Ecotoxicological evaluation of perfluorooctanesulfonate (PFOS)," in *Reviews of Environmental Contamination and Toxicology*, pp. 133–174, Springer, 2006.

[13] C. McCarthy, W. Kappleman, and W. DiGuiseppi, "Ecological considerations of per-and polyfluoroalkyl substances (PFAS)," *Current Pollution Reports*, vol. 3, no. 4, pp. 289–301, 2017.

[14] P. E. Goodrum, J. K. Anderson, A. L. Luz, and G. K. Ansell, "Application of a framework for grouping and mixtures toxicity assessment of PFAS: A closer examination of dose-additivity approaches," *Toxicological Sciences*, vol. 179, no. 2, pp. 262–278, 2020.

[15] US EPA. https://www.epa.gov/sites/production/files/2018-11/documents/factsheet_pfbs-genx-toxicity_values_11.14.2018.pdf, 2018.

[16] Z. Wang, J. C. DeWitt, C. P. Higgins, and I. T. Cousins, "A never-ending story of per- and polyfluoroalkyl substances (PFASs)?," *Environmental Science & Technology*, vol. 51, no. 5, pp. 2508–2518, 2017.

[17] S. Zhang, K. Chen, W. Li, Y. Chai, J. Zhu, B. Chu, N. Li, J. Yan, S. Zhang, and Y. Yang, "Varied thyroid disrupting effects of perfluorooctanoic acid (PFOA) and its novel alternatives hexafluoropropylene-oxide-dimer-acid (GenX) and ammonium 4,8-dioxa-3h-perfluorononanoate (ADONA) in vitro," *Environment International*, vol. 156, p. 106745, 2021.

[18] W. F. Hartz, M. K. Björnsdotter, L. W. Yeung, A. Hodson, E. R. Thomas, J. D. Humby, C. Day, I. E. Jogsten, A. Kärrman, and R. Kallenborn, "Levels and distribution profiles of per-and polyfluoroalkyl substances (PFAS) in a high Arctic Svalbard ice core," *Science of the Total Environment*, vol. 871, p. 161830, 2023.

[19] G. Casas, J. Iriarte, L. A. D'Agostino, J. L. Roscales, A. Martinez-Varela, M. Vila-Costa, J. W. Martin, B. Jiménez, and J. Dachs, "Inputs, amplification and

sinks of perfluoroalkyl substances at coastal Antarctica," *Environmental Pollution*, vol. 338, p. 122608, 2023.

[20] U. K. Vedagiri, R. H. Anderson, H. M. Loso, and C. M. Schwach, "Ambient levels of PFOS and PFOA in multiple environmental media," *Remediation Journal*, vol. 28, no. 2, pp. 9–51, 2018.

[21] T. Groffen, M. Eens, and L. Bervoets, "Do concentrations of perfluoroalkylated acids (PFAAs) in isopods reflect concentrations in soil and songbirds? A study using a distance gradient from a fluorochemical plant," *Science of the Total Environment*, vol. 657, pp. 111–123, 2019.

[22] J. W. Washington, H. Yoo, J. J. Ellington, T. M. Jenkins, and E. L. Libelo, "Concentrations, distribution, and persistence of perfluoroalkylates in sludge-applied soils near Decatur, Alabama, USA," *Environmental Science & Technology*, vol. 44, no. 22, pp. 8390–8396, 2010.

[23] A. Garg, N. P. Shetti, S. Basu, M. N. Nadagouda, and T. M. Aminabhavi, "Treatment technologies for removal of per- and polyfluoroalkyl substances (PFAS) in biosolids," *Chemical Engineering Journal*, vol. 453, p. 139964, 2023.

[24] D. Szabo, T. L. Coggan, T. C. Robson, M. Currell, and B. O. Clarke, "Investigating recycled water use as a diffuse source of per- and polyfluoroalkyl substances (PFASs) to groundwater in Melbourne, Australia," *Science of The Total Environment*, vol. 644, pp. 1409 – 1417, 2018.

[25] E. S. Coffin, D. M. Reeves, and D. P. Cassidy, "PFAS in municipal solid waste landfills: Sources, leachate composition, chemical transformations, and future challenges," *Current Opinion in Environmental Science & Health*, vol. 31, p. 100418, 2023.

[26] C. dan Gan, M. yi Peng, H. bo Liu, and J. yan Yang, "Concentration and distribution of metals, total fluorine, per- and poly-fluoroalkyl substances (PFAS) in vertical soil profiles in industrialized areas," *Chemosphere*, vol. 302, p. 134855, 2022.

[27] H. Chen, M. Reinhard, T. Yin, T. V. Nguyen, N. H. Tran, and K. Y.-H. Gin, "Multi-compartment distribution of perfluoroalkyl and polyfluoroalkyl substances (PFASs) in an urban catchment system," *Water Research*, vol. 154, pp. 227–237, 2019.

[28] G. Munoz, H. Budzinski, M. Babut, H. Drouineau, M. Lauzent, K. L. Menach, J. Lobry, J. Selleslagh, C. Simonnet-Laprade, and P. Labadie, "Evidence for the

trophic transfer of perfluoroalkylated substances in a temperate macrotidal estuary," *Environmental Science & Technology*, vol. 51, no. 15, pp. 8450–8459, 2017.

[29] G. Munoz, L. Mercier, S. V. Duy, J. Liu, S. Sauvé, and M. Houde, "Bioaccumulation and trophic magnification of emerging and legacy per- and polyfluoroalkyl substances (PFAS) in a St. Lawrence River food web," *Environmental Pollution*, vol. 309, p. 119739, 2022.

[30] Z. Du, S. Deng, Y. Bei, Q. Huang, B. Wang, J. Huang, and G. Yu, "Adsorption behavior and mechanism of perfluorinated compounds on various adsorbents—a review," *Journal of Hazardous Materials*, vol. 274, pp. 443–454, 2014.

[31] Y. Li, D. P. Oliver, and R. S. Kookana, "A critical analysis of published data to discern the role of soil and sediment properties in determining sorption of per and polyfluoroalkyl substances (PFASs)," *Science of the Total Environment*, vol. 628, pp. 110–120, 2018.

[32] M. S. Hellsing, S. Josefsson, A. V. Hughes, and L. Ahrens, "Sorption of perfluoroalkyl substances to two types of minerals," *Chemosphere*, vol. 159, pp. 385–391, 2016.

[33] S. K. Biek, L. S. Khudur, L. Rigby, N. Singh, M. Askeland, and A. S. Ball, "Assessing the impact of immobilisation on the bioavailability of PFAS to plants in contaminated Australian soils," *Environmental Science and Pollution Research*, pp. 1–13, 2024.

[34] D. A. Navarro, S. Kabiri, J. Ho, K. C. Bowles, G. Davis, M. J. McLaughlin, and R. S. Kookana, "Stabilisation of PFAS in soils: Long-term effectiveness of carbon-based soil amendments," *Environmental Pollution*, vol. 323, p. 121249, 2023.

[35] M. Wang, K. J. Rivenbark, H. Nikkhah, B. Beykal, and T. D. Phillips, "In vitro and in vivo remediation of per- and polyfluoroalkyl substances by processed and amended clays and activated carbon in soil," *Applied Soil Ecology*, vol. 196, p. 105285, 2024.

[36] S. E. Hearon, A. A. Orr, H. Moyer, M. Wang, P. Tamamis, and T. D. Phillips, "Montmorillonite clay-based sorbents decrease the bioavailability of per- and polyfluoroalkyl substances (PFAS) from soil and their translocation to plants," *Environmental Research*, vol. 205, p. 112433, 2022.

[37] A. Esmaeilian, N. Quinete, P. R. Gardinali, and K. O'Shea, "The effects of soil properties and sorbent amendments on immobilization of perfluorooctane sulfonate

(PFOS) in contrasting soils: Experimental and numerical study," *Journal of Environmental Chemical Engineering*, vol. 11, no. 2, p. 109509, 2023.

[38] J. A. Sleep, S. J. Miklavcic, and A. L. Juhasz, "Modelling of PFAS-surface interactions: Effect of surface charge and solution ions," *Chemosphere*, vol. 319, p. 137910, 2023.

[39] G. He, G. Pan, and M. Zhang, "Assembling structures and dynamics properties of perfluorooctane sulfonate (PFOS) at water–titanium oxide interfaces," *Journal of Colloid and Interface Science*, vol. 405, pp. 189–194, 2013.

[40] G. He, M. Zhang, Q. Zhou, and G. Pan, "Molecular dynamics simulations of structural transformation of perfluorooctane sulfonate (PFOS) at water/rutile interfaces," *Chemosphere*, vol. 134, pp. 272–278, 2015.

[41] R. Zhang, W. Yan, and C. Jing, "Experimental and molecular dynamic simulation study of perfluorooctane sulfonate adsorption on soil and sediment components," *Journal of Environmental Sciences*, vol. 29, pp. 131–138, 2015.

[42] M. G. Martin, "MCCCS Towhee: a tool for Monte Carlo molecular simulation," *Molecular Simulation*, vol. 39, no. 14-15, pp. 1212–1222, 2013.

[43] B. Stenqvist, A. Thuresson, A. Kurut, R. Vácha, and M. Lund, "Faunus – a flexible framework for Monte Carlo simulation," *Molecular Simulation*, vol. 39, no. 14-15, pp. 1233–1239, 2013.

[44] W. L. Jorgensen and J. Tirado–Rives, "Molecular modeling of organic and biomolecular systems using BOSS and MCPRO," *Journal of Computational Chemistry*, vol. 26, no. 16, pp. 1689–1700, 2005.

[45] R Core Team, *R: A Language and Environment for Statistical Computing*. R Foundation for Statistical Computing, Vienna, Austria, 2018.

[46] C.-M. Ionescu, D. Sehnal, F. L. Falginella, P. Pant, L. Pravda, T. Bouchal, R. S. Vařeková, S. Geidl, and J. Koča, "AtomicChargeCalculator: Interactive web-based calculation of atomic charges in large biomolecular complexes and drug-like molecules," *Journal of Cheminformatics*, vol. 7, no. 1, p. 50, 2015.

[47] D. Van Der Spoel, E. Lindahl, B. Hess, G. Groenhof, A. E. Mark, and H. J. Berendsen, "Gromacs: fast, flexible, and free," *Journal of Computational Chemistry*, vol. 26, no. 16, pp. 1701–1718, 2005.

[48] C. Hardacre, J. D. Holbrey, C. L. Mullan, M. Nieuwenhuyzen, T. G. Youngs, D. T. Bowron, and S. J. Teat, "Solid and liquid charge-transfer complex formation

between 1-methylnaphthalene and 1-alkyl-cyanopyridinium bis {(trifluoromethyl) sulfonyl} imide ionic liquids," *Physical Chemistry Chemical Physics*, vol. 12, no. 8, pp. 1842–1853, 2010.

[49] T.-J. Lin and H. Heinz, "Accurate force field parameters and pH resolved surface models for hydroxyapatite to understand structure, mechanics, hydration, and biological interfaces," *The Journal of Physical Chemistry C*, vol. 120, no. 9, pp. 4975–4992, 2016.

[50] P. Klapetek, *Quantitative Data Processing in Scanning Probe Microscopy: SPM Applications for Nanometrology*. Elsevier, 2012.

[51] J. Song and R. Cappelletti, "Lennard-Jones-potential calculation of C 60 stage-one graphite," *Physical Review B*, vol. 50, no. 19, p. 14678, 1994.

[52] J. N. Israelachvili, *Intermolecular and Surface Forces*. Academic Press, third ed., 2011.

[53] J. O. Hirschfelder, C. F. Curtiss, and R. B. Bird, *Molecular theory of gases and liquids*. John Wiley & Sons Inc. (N.Y.), 1954.

[54] S. J. Miklavcic, "Effective dipole potentials after angle averaging," *Physical Review E*, vol. 56, no. 1, pp. 1142–1147, 1997.

[55] B. Jönsson, H. Wennerström, and B. Halle, "Ion distributions in lamellar liquid crystals. A comparison between results from Monte Carlo simulations and solutions of the Poisson-Boltzmann equation," *The Journal of Physical Chemistry*, vol. 84, no. 17, pp. 2179–2185, 1980.

[56] J.-P. Hansen and I. R. McDonald, *Theory of simple liquids*. Academic Press, 2nd ed., 1986.

[57] C. A. Moody and J. A. Field, "Perfluorinated surfactants and the environmental implications of their use in fire-fighting foams," *Environmental Science and Technology*, vol. 34, no. 18, pp. 3864–3870, 2000.

[58] M. M. Schultz, D. F. Barofsky, and J. A. Field, "Quantitative determination of fluorotelomer sulfonates in groundwater by LC MS/MS," *Environmental Science and Technology*, vol. 38, no. 6, pp. 1828–1835, 2004.

[59] M. Filipovic, A. Woldegiorgis, K. Norström, M. Bibi, M. Lindberg, and A.-H. Österås, "Historical usage of aqueous film forming foam: A case study of the widespread distribution of perfluoroalkyl acids from a military airport to groundwater, lakes, soils and fish," *Chemosphere*, vol. 129, pp. 39–45, 2015.

[60] B. J. Ruyle, H. M. Pickard, D. R. LeBlanc, A. K. Tokranov, C. P. Thackray, X. C. Hu, C. D. Vecitis, and E. M. Sunderland, "Isolating the AFFF signature in coastal watersheds using oxidizable PFAS precursors and unexplained organofluorine," *Environmental Science & Technology*, vol. 55, no. 6, pp. 3686–3695, 2021.

[61] B. J. Place and J. A. Field, "Identification of novel fluorochemicals in aqueous film-forming foams used by the US military," *Environmental Science & Technology*, vol. 46, no. 13, pp. 7120–7127, 2012.

[62] Y.-S. Luo, N. A. Aly, J. McCord, M. J. Strynar, W. A. Chiu, J. N. Dodds, E. S. Baker, and I. Rusyn, "Rapid characterization of emerging per- and polyfluoroalkyl substances in aqueous film-forming foams using ion mobility spectrometry–mass spectrometry," *Environmental Science & Technology*, vol. 54, no. 23, pp. 15024–15034, 2020.

[63] E. F. Houtz, C. P. Higgins, J. A. Field, and D. L. Sedlak, "Persistence of perfluoroalkyl acid precursors in AFFF-impacted groundwater and soil," *Environmental Science and Technology*, vol. 47, no. 15, pp. 8187–8195, 2013.

[64] A. Nickerson, A. C. Maizel, P. R. Kulkarni, D. T. Adamson, J. J. Kornuc, and C. P. Higgins, "Enhanced extraction of AFFF-associated PFASs from source zone soils," *Environmental Science & Technology*, vol. 54, no. 8, pp. 4952–4962, 2020.

[65] P.-F. Yan, S. Dong, K. D. Pennell, and N. L. Cápiro, "A review of the occurrence and microbial transformation of per- and polyfluoroalkyl substances (PFAS) in aqueous film-forming foam (AFFF)-impacted environments," *Science of The Total Environment*, vol. 927, p. 171883, 2024.

[66] D. W. Nelson and L. E. Sommers, *Total Carbon, Organic Carbon, and Organic Matter*, ch. 34, pp. 961–1010. John Wiley & Sons, Ltd, 1996.

[67] E. F. Houtz and D. L. Sedlak, "Oxidative conversion as a means of detecting precursors to perfluoroalkyl acids in urban runoff," *Environmental Science & Technology*, vol. 46, no. 17, pp. 9342–9349, 2012.

[68] Standards Australia, "As 4439.3: Wastes, sediments and contaminated soils, part 3: Preparation of leachates-bottle leaching procedure," 1997.

[69] S. Kabiri, M. Centner, and M. J. McLaughlin, "Durability of sorption of per- and polyfluorinated alkyl substances in soils immobilised using common adsorbents: 1. Effects of perturbations in pH," *Science of The Total Environment*, vol. 766, p. 144857, 2021.

[70] National Chemicals Working Group of the Heads of EPAs Australia and New Zealand, "PFAS national environmental management plan version 2.0," 2020.

[71] K. C. Harding-Marjanovic, E. F. Houtz, S. Yi, J. A. Field, D. L. Sedlak, and L. Alvarez-Cohen, "Aerobic biotransformation of fluorotelomer thioether amido sulfonate (Lodyne) in AFFF-amended microcosms," *Environmental Science and Technology*, vol. 49, no. 13, pp. 7666–7674, 2015.

[72] L. A. D'Agostino and S. A. Mabury, "Aerobic biodegradation of 2 fluorotelomer sulfonamide–based aqueous film–forming foam components produces perfluoroalkyl carboxylates," *Environmental Toxicology and Chemistry*, vol. 36, no. 8, pp. 2012–2021, 2017.

[73] P.-F. Yan, S. Dong, K. E. Manz, M. J. Woodcock, C. Liu, M. P. Mezzari, L. M. Abriola, K. D. Pennell, and N. L. Cápiro, "Aerobic biotransformation of 6:2 fluorotelomer sulfonate in soils from two aqueous film-forming foam (AFFF)-impacted sites," *Water Research*, vol. 249, p. 120941, 2024.

[74] S.-K. Kim and K. Kannan, "Perfluorinated acids in air, rain, snow, surface runoff, and lakes: Relative importance of pathways to contamination of urban lakes," *Environmental Science & Technology*, vol. 41, no. 24, pp. 8328–8334, 2007.

[75] D. A. Ellis, J. W. Martin, A. O. De Silva, S. A. Mabury, M. D. Hurley, M. P. Sulbaek Andersen, and T. J. Wallington, "Degradation of fluorotelomer alcohols: A likely atmospheric source of perfluorinated carboxylic acids," *Environmental Science & Technology*, vol. 38, no. 12, pp. 3316–3321, 2004.

[76] M. Zhao, Y. Yao, X. Dong, M. Baqar, B. Fang, H. Chen, and H. Sun, "Nontarget identification of novel per- and polyfluoroalkyl substances (PFAS) in soils from an oil refinery in southwestern China: A combined approach with TOP assay," *Environmental Science and Technology*, vol. 57, no. 48, pp. 20194–20205, 2023.

[77] A. L. Juhasz, A. Keith, R. Jones, and F. Kastury, "Impact of precursors and bioaccessibility on childhood PFAS exposure from house dust," *Science of The Total Environment*, vol. 889, p. 164306, 2023.

[78] S. Giglioli, L. Colombo, and A. Azzellino, "Cluster and multivariate analysis to study the diffuse contamination of emerging per-and polyfluoroalkyl substances (PFAS) in the Veneto Region plain (North-eastern Italy)," *Chemosphere*, vol. 319, p. 137916, 2023.

[79] D. A. Navarro, S. S. Kabiri, K. Bowles, E. R. Knight, J. Braeunig, P. Srivastava, N. J. Boxall, G. Douglas, J. Mueller, M. J. McLaughlin, *et al.*, "Review on meth-

ods for assessing and predicting leaching of PFAS from solid matrices," *Current Pollution Reports*, vol. 10, no. 4, pp. 628–647, 2024.

[80] J. L. Rayner, D. Slee, S. Falvey, R. Kookana, E. Bekele, G. Stevenson, A. Lee, and G. B. Davis, "Laboratory batch representation of PFAS leaching from aged field soils: Intercomparison across new and standard approaches," *Science of The Total Environment*, vol. 838, p. 156562, 2022.

[81] S. Kabiri, W. Tucker, D. A. Navarro, J. Bräunig, K. Thompson, E. R. Knight, T. M. H. Nguyen, C. Grimison, C. M. Barnes, C. P. Higgins, J. F. Mueller, R. S. Kookana, and M. J. McLaughlin, "Comparing the leaching behavior of per- and polyfluoroalkyl substances from contaminated soils using static and column leaching tests," *Environmental Science & Technology*, vol. 56, no. 1, pp. 368–378, 2022.

[82] M. Park, S. Wu, I. J. Lopez, J. Y. Chang, T. Karanfil, and S. A. Snyder, "Adsorption of perfluoroalkyl substances (PFAS) in groundwater by granular activated carbons: Roles of hydrophobicity of PFAS and carbon characteristics," *Water Research*, vol. 170, p. 115364, 2020.

[83] G. Ding and W. J. G. M. Peijnenburg, "Physicochemical properties and aquatic toxicity of poly- and perfluorinated compounds," *Critical Reviews in Environmental Science & Technology*, vol. 43, no. 6, pp. 598–678, 2013.

[84] S. L. Capozzi, A. L. Leang, L. A. Rodenburg, B. Chandramouli, D. A. Delistraty, and C. H. Carter, "PFAS in municipal landfill leachate: Occurrence, transformation, and sources," *Chemosphere*, vol. 334, p. 138924, 2023.

[85] J. Wellmitz, N. Bandow, and J. Koschorreck, "Long-term trend data for PFAS in soils from German ecosystems, including TOP assay," *Science of The Total Environment*, vol. 893, p. 164586, 2023.

[86] B. Göckener, A. Fliedner, K. Weinfurtner, H. Rüdel, A. Badry, and J. Koschorreck, "Tracking down unknown PFAS pollution – The direct TOP assay in spatial monitoring of surface waters in Germany," *Science of The Total Environment*, vol. 898, p. 165425, 2023.

[87] M. Al Amin, Y. Luo, F. Shi, L. Yu, Y. Liu, A. Nolan, O. S. Awoyemi, M. Megharaj, R. Naidu, and C. Fang, "A modified TOP assay to detect per- and polyfluoroalkyl substances in aqueous film-forming foams (AFFF) and soil," *Frontiers in Chemistry*, vol. Volume 11 - 2023, 2023.

[88] D. Martin, G. Munoz, S. Mejia-Avendaño, S. V. Duy, Y. Yao, K. Volchek, C. E. Brown, J. Liu, and S. Sauvé, "Zwitterionic, cationic, and anionic perfluoroalkyl

and polyfluoroalkyl substances integrated into total oxidizable precursor assay of contaminated groundwater," *Talanta*, vol. 195, pp. 533–542, 2019.

[89] J. L. Rayner, A. Lee, S. Corish, S. Leake, E. Bekele, and G. B. Davis, "Advancing the use of suction lysimeters to inform soil leaching and remediation of PFAS source zones," *Groundwater Monitoring & Remediation*, vol. 44, no. 3, pp. 49–60, 2024.

[90] J. A. Sleep and A. L. Juhasz, "A review of immobilisation-based remediation of per- and poly-fluoroalkyl substances (PFAS) in soils," *Current Pollution Reports*, vol. 7, pp. 524–539, 2021.

[91] E. A. Müller and K. E. Gubbins, "Molecular simulation study of hydrophilic and hydrophobic behavior of activated carbon surfaces," *Carbon*, vol. 36, no. 10, pp. 1433–1438, 1998.

[92] A. L. Juhasz, F. Kastury, C. Herde, and W. Tang, "Application of soil amendments for reducing PFAS leachability and bioavailability," *Environmental Pollution*, vol. 307, p. 119498, 2022.

[93] J. Bräunig, C. Baduel, C. M. Barnes, and J. F. Mueller, "Sorbent assisted immobilisation of perfluoroalkyl acids in soils – effect on leaching and bioavailability," *Journal of Hazardous Materials*, p. 125171, 2021.

[94] S. Lath, D. A. Navarro, D. Losic, A. Kumar, and M. J. McLaughlin, "Sorptive remediation of perfluorooctanoic acid (PFOA) using mixed mineral and graphene/carbon-based materials," *Environmental Chemistry*, vol. 15, no. 8, pp. 472–480, 2018.

[95] M. Sörengård, D. B. Kleja, and L. Ahrens, "Stabilization and solidification remediation of soil contaminated with poly- and perfluoroalkyl substances (PFASs)," *Journal of Hazardous Materials*, vol. 367, pp. 639 – 646, 2019.

[96] M. Sörengård, D. B. Kleja, and L. Ahrens, "Stabilization of per- and polyfluoroalkyl substances (PFASs) with colloidal activated carbon (PlumeStop®) as a function of soil clay and organic matter content," *Journal of Environmental Management*, vol. 249, p. 109345, 2019.

[97] S. Kabiri and M. J. McLaughlin, "Durability of sorption of per- and polyfluorinated alkyl substances in soils immobilized using common adsorbents: 2. Effects of repeated leaching, temperature extremes, ionic strength and competing ions," *Science of The Total Environment*, vol. 766, p. 144718, 2021.

[98] W. Zhang and Y. Liang, "Performance of different sorbents toward stabilizing per- and polyfluoroalkyl substances (PFAS) in soil," *Environmental Advances*, vol. 8, p. 100217, 2022.

[99] W. Zhang and Y. Liang, "Changing bioavailability of per- and polyfluoroalkyl substances (PFAS) to plant in biosolids amended soil through stabilization or mobilization," *Environmental Pollution*, vol. 308, p. 119724, 2022.

[100] T. Cáceres, R. Jones, F. Kastury, and A. L. Juhasz, "Soil amendments reduce PFAS bioaccumulation in eisenia fetida following exposure to AFFF-impacted soil," *Environmental Pollution*, vol. 358, p. 124489, 2024.

[101] D. R. Helsel, "Fabricating data: How substituting values for nondetects can ruin results, and what can be done about it," *Chemosphere*, vol. 65, no. 11, pp. 2434–2439, 2006.

[102] M. L. Brusseau, R. H. Anderson, and B. Guo, "PFAS concentrations in soils: Background levels versus contaminated sites," *Science of the Total Environment*, vol. 740, p. 140017, 2020.

[103] H. Campos Pereira, M. Ullberg, D. B. Kleja, J. P. Gustafsson, and L. Ahrens, "Sorption of perfluoroalkyl substances (PFASs) to an organic soil horizon – Effect of cation composition and pH," *Chemosphere*, vol. 207, pp. 183 – 191, 2018.

[104] H. Campos-Pereira, D. B. Kleja, C. Sjöstedt, L. Ahrens, W. Klysubun, and J. P. Gustafsson, "The adsorption of per- and polyfluoroalkyl substances (PFASs) onto ferrihydrite is governed by surface charge," *Environmental Science & Technology*, vol. 54, no. 24, pp. 15722–15730, 2020.

[105] Y. Zhang, Y. Xu, B. Shi, and X. Huang, "The influence of nitrogen-containing functional groups and pore structure on the adsorption of per- and polyfluoroalkyl substances in ultrapure and real water," *Journal of Environmental Chemical Engineering*, vol. 12, no. 2, p. 112082, 2024.

[106] P. Meng, S. Deng, X. Lu, Z. Du, B. Wang, J. Huang, Y. Wang, G. Yu, and B. Xing, "Role of air bubbles overlooked in the adsorption of perfluorooctanesulfonate on hydrophobic carbonaceous adsorbents," *Environmental Science & Technology*, vol. 48, no. 23, pp. 13785–13792, 2014.

[107] M. Liu, Y. Jin, and J. Pan, "Relevance of implicit and explicit solvent in density-functional theory study of adsorption at electrochemical NaCl/Al interface," *Materials Today Communications*, vol. 31, p. 103425, 2022.

Appendix A

Supplementary information: Modelling of PFAS-surface interactions: Effect of surface charge and solution ions

Supplementary information for Modelling of PFAS-Surface Interactions: Effect of Surface Charge and Solution Ions

Julie A. Sleep, Stanley J. Miklavcic, Albert L. Juhasz

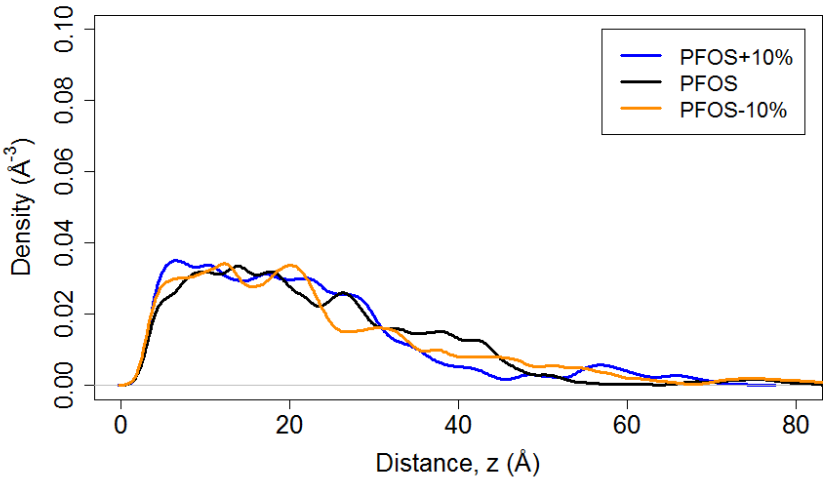
December 2, 2022

Supplementary Table S1: 3D structure [1], Lennard jones parameters (OPLS-AA [2, 3]), partial charges [4], for PFBS anion. Some values are rounded for ease of display.

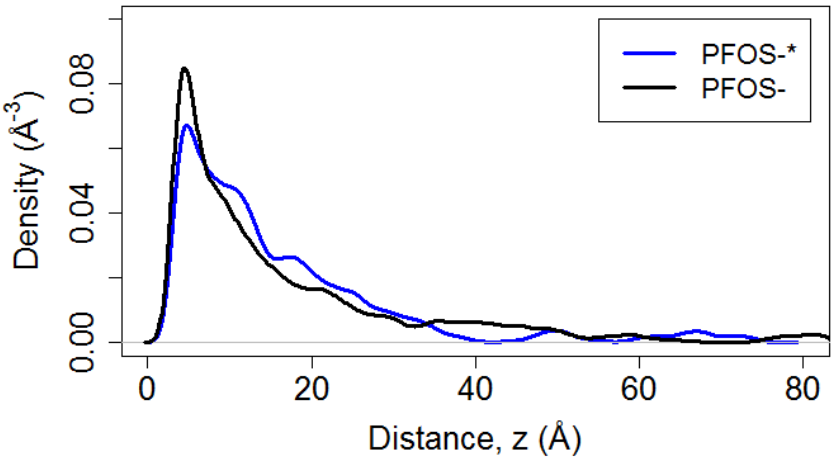
Num	Elem	Coordinates (Å)			σ	ε	q
		x	y	z	(Å)	(kJ mol^{-1})	(e)
1	S	1.968	-0.744	-0.402	3.55	1.046	2.35
2	F	-0.653	1.970	0.831	2.95	0.222	-0.38
3	F	0.403	1.892	-1.067	2.95	0.222	-0.40
4	F	1.973	1.392	1.057	2.95	0.222	-0.39
5	F	0.643	-0.183	1.732	2.95	0.222	-0.39
6	F	-2.100	1.017	-1.281	2.95	0.222	-0.38
7	F	-0.629	-0.548	-1.601	2.95	0.222	-0.40
8	F	-2.508	0.042	1.312	2.95	0.222	-0.40
9	F	-2.857	-1.409	-0.280	2.95	0.222	-0.40
10	F	-1.040	-1.519	0.909	2.95	0.222	-0.40
11	O	3.223	-0.992	0.610	2.96	0.879	-0.54
12	O	2.468	-0.084	-1.590	2.96	0.879	-0.73
13	O	1.187	-1.962	-0.472	2.96	0.879	-0.72
14	C	-0.084	1.1082	-0.060	3.50	0.276	0.58
15	C	1.107	0.445	0.613	3.50	0.276	0.22
16	C	-1.191	0.242	-0.639	3.50	0.276	0.49
17	C	-1.912	-0.665	0.328	3.50	0.276	0.89

Supplementary Table S2: 3D structure [1], Lennard jones parameters (OPLS-AA [2, 3]), partial charges [4], for PFOS anion. Some values are rounded for ease of display.

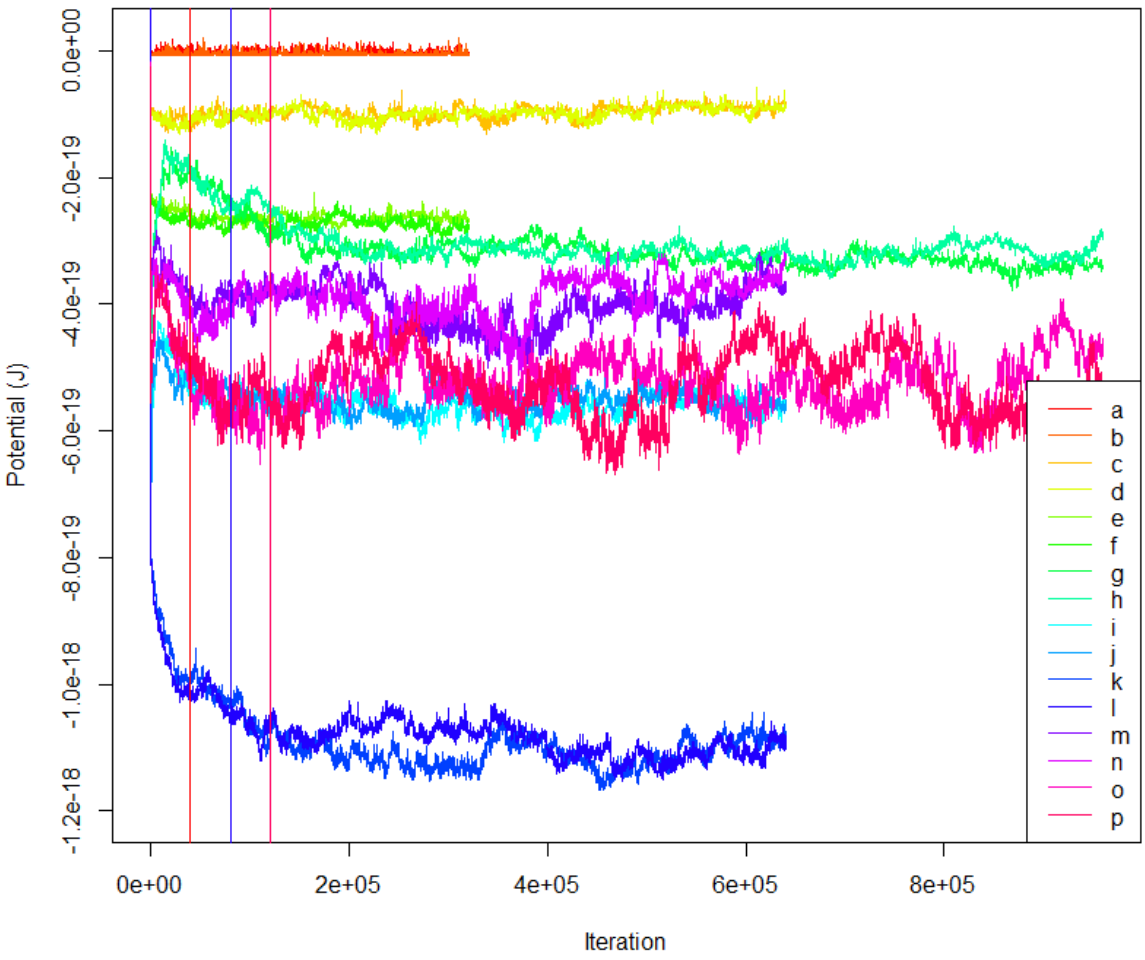
Num	Elem	Coordinates (Å)			σ	ε	q
		x	y	z	(Å)	(kJ mol^{-1})	(e)
1	S	4.065	-0.753	-0.171	3.55	1.046	2.40
2	F	-0.764	-1.695	-0.728	2.95	0.222	-0.37
3	F	0.797	-1.571	0.775	2.95	0.222	-0.38
4	F	0.071	0.651	-1.862	2.95	0.222	-0.37
5	F	1.593	-0.891	-1.740	2.95	0.222	-0.39
6	F	-0.093	0.740	1.719	2.95	0.222	-0.37
7	F	-1.526	-0.889	1.744	2.95	0.222	-0.37
8	F	2.493	1.609	-1.377	2.95	0.222	-0.38
9	F	1.153	1.895	0.310	2.95	0.222	-0.37
10	F	-2.558	1.558	1.377	2.95	0.222	-0.37
11	F	-1.322	1.912	-0.369	2.95	0.222	-0.37
12	F	2.312	-0.178	1.624	2.95	0.222	-0.37
13	F	3.639	1.456	1.107	2.95	0.222	-0.37
14	F	-2.493	-0.164	-1.691	2.95	0.222	-0.37
15	F	-3.837	1.377	-0.959	2.95	0.222	-0.37
16	F	-4.593	-0.229	1.140	2.95	0.222	-0.38
17	F	-3.191	-1.756	0.483	2.95	0.222	-0.38
18	F	-4.840	-1.164	-0.816	2.95	0.222	-0.38
19	O	5.112	-0.839	1.076	2.96	0.879	-0.49
20	O	4.740	-0.126	-1.288	2.96	0.879	-0.69
21	O	3.397	-2.032	-0.298	2.96	0.879	-0.68
22	C	-0.008	-0.816	-0.025	3.50	0.276	0.61
23	C	0.863	-0.019	-0.988	3.50	0.276	0.57
24	C	-0.900	-0.008	0.911	3.50	0.276	0.61
25	C	1.865	0.944	-0.363	3.50	0.276	0.61
26	C	-1.951	0.926	0.329	3.50	0.276	0.63
27	C	2.944	0.420	0.571	3.50	0.276	0.26
28	C	-3.040	0.344	-0.559	3.50	0.276	0.57
29	C	-3.929	-0.702	0.067	3.50	0.276	0.96



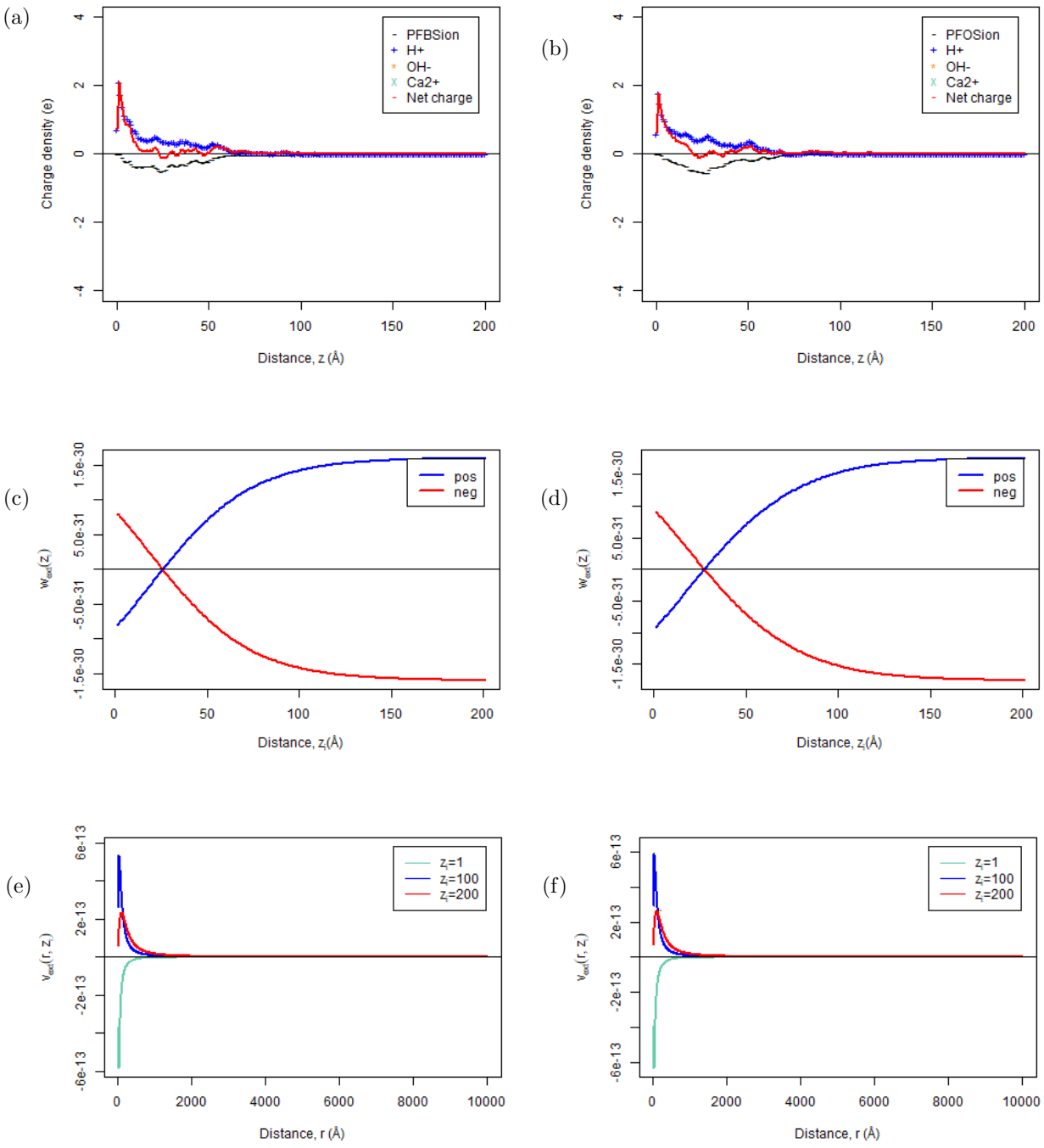
Supplementary Figure S1: PFOS simulation run with ±10% of OPLSAA parameter values given in Tables S1 and S2, showing the effects of changes in the Lennard-Jones interaction potential parameters.



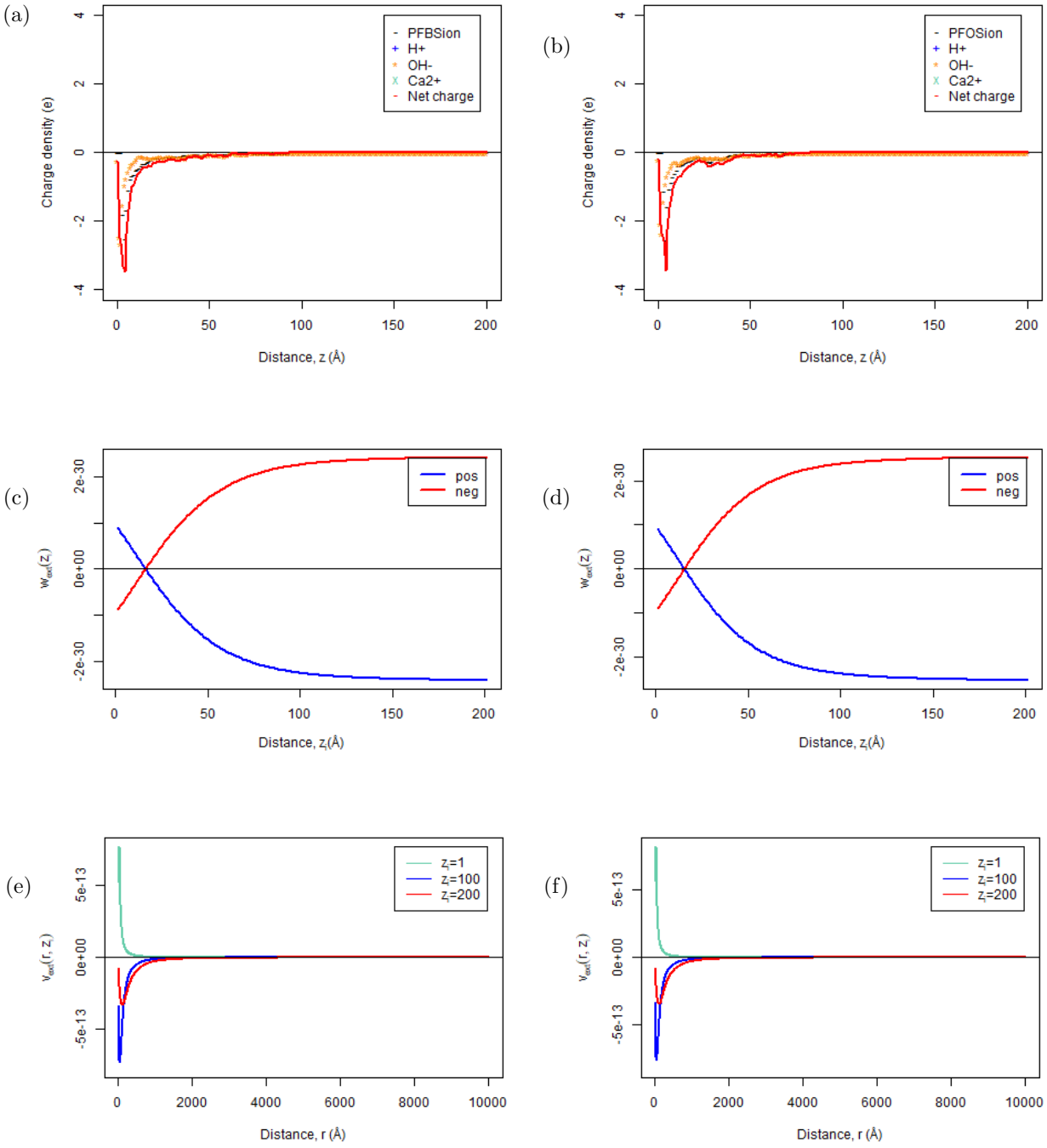
Supplementary Figure S2: PFOS simulation runs with different random starting configurations.



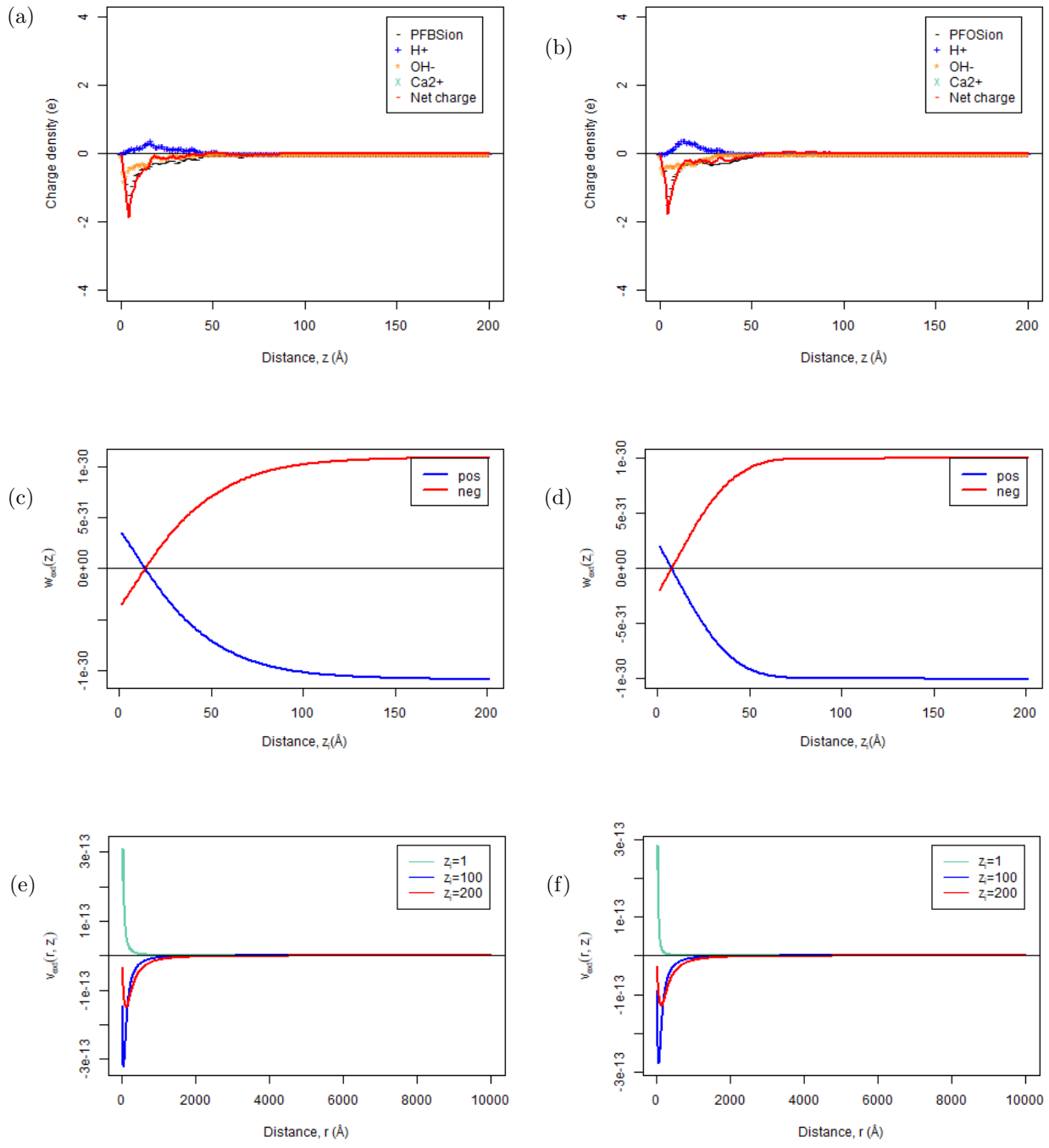
Supplementary Figure S3: Potential energy at each step of simulation: (a) PFBS 0Ca 0H 0OH 0surf (b) PFOS 0Ca 0H 0OH 0surf (c) PFBSion 0Ca 16H 0OH 0surf (d) PFOSion 0Ca 16H 0OH 0surf (e) PFBSion 0Ca 0H 0OH +1surf (f) PFOSion 0Ca 0H 0OH +1surf (g) PFBSion 0Ca 32H 0OH -1surf (h) PFOSion 0Ca 32H 0OH -1surf (i) PFBSion 16Ca 0H 0OH -1surf (j) PFOSion 16Ca 0H 0OH -1surf (k) PFBSion 0Ca 0H 16OH +2surf (l) PFOSion 0Ca 0H 16OH +2surf (m) PFBSion 0Ca 8H 8OH +1surf (n) PFOSion 0Ca 8H 8OH +1surf (o) PFBSion 0Ca 16H 16OH +1surf (p) PFOSion 0Ca 16H 16OH +1surf. Lines designate the cut-off point for the initial statistics collection.



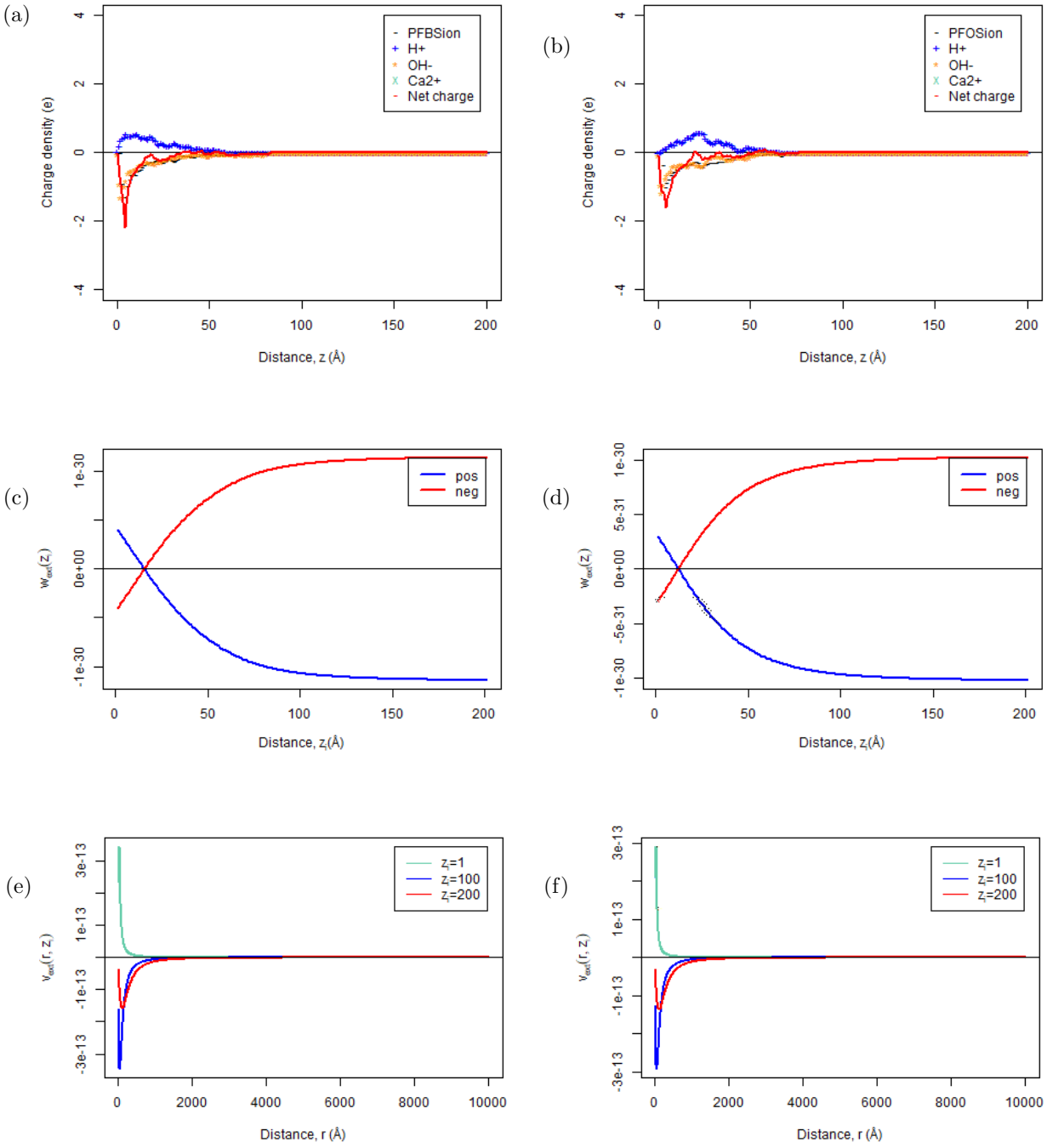
Supplementary Figure S4: (a) 16 PFBS ion 32H+ -1S net charge as a function of z, (b) 16 PFOS ion 32H+ -1S net charge as a function of z, (c) and (d) external potential $w_{ext}(z_i)$ as a function of distance from surface, z_i, for positively and negatively charged atoms (e) and (f) $v_{ext}(r, z_i)$ (external potential divided by charge) evaluated at each radial distance, r, shown for three values of z_i.



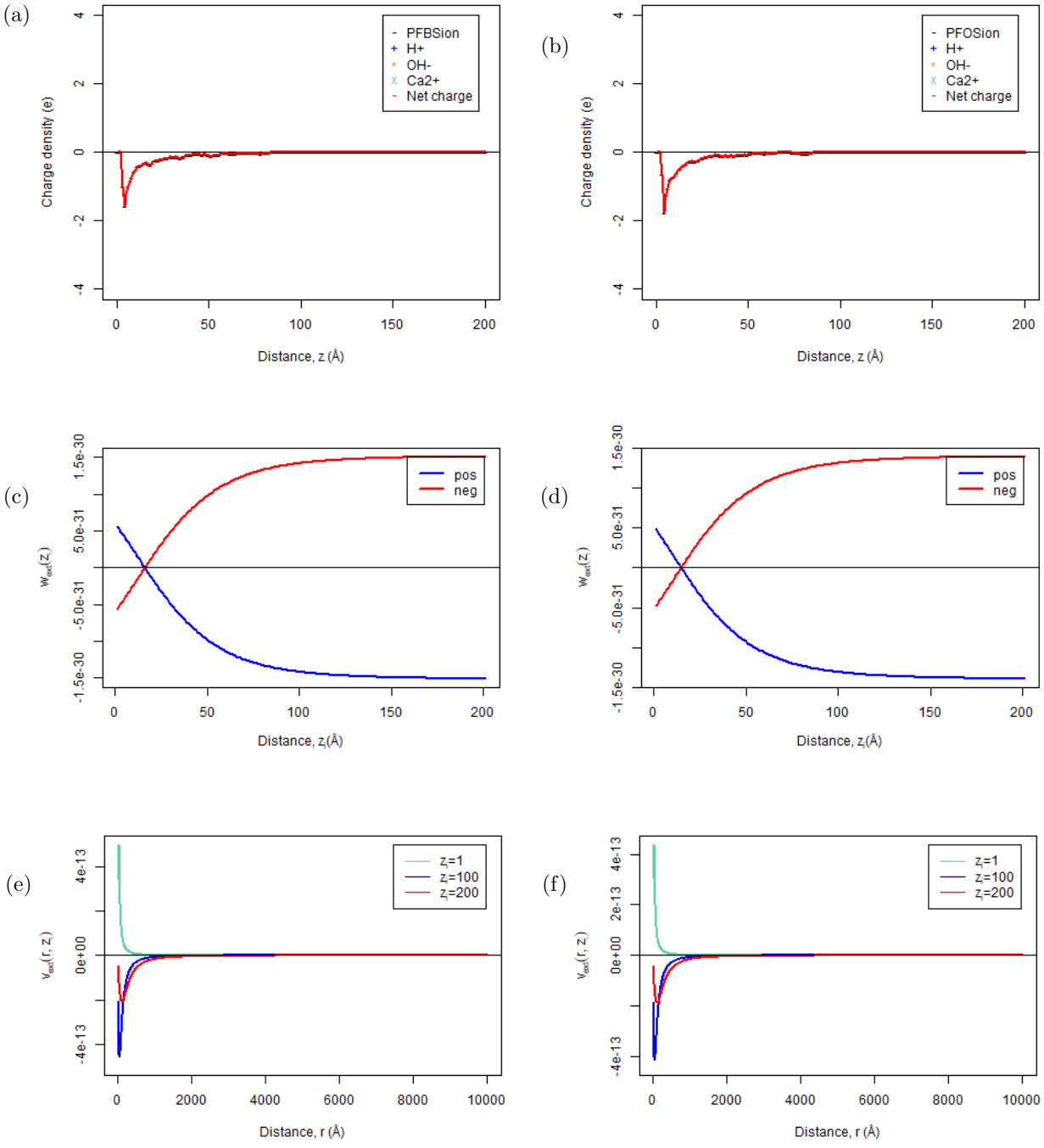
Supplementary Figure S5: 16PFBSion 0H 16OH +1S, 16PFOSion 0H 16OH +2S. See caption S4 for panel information.



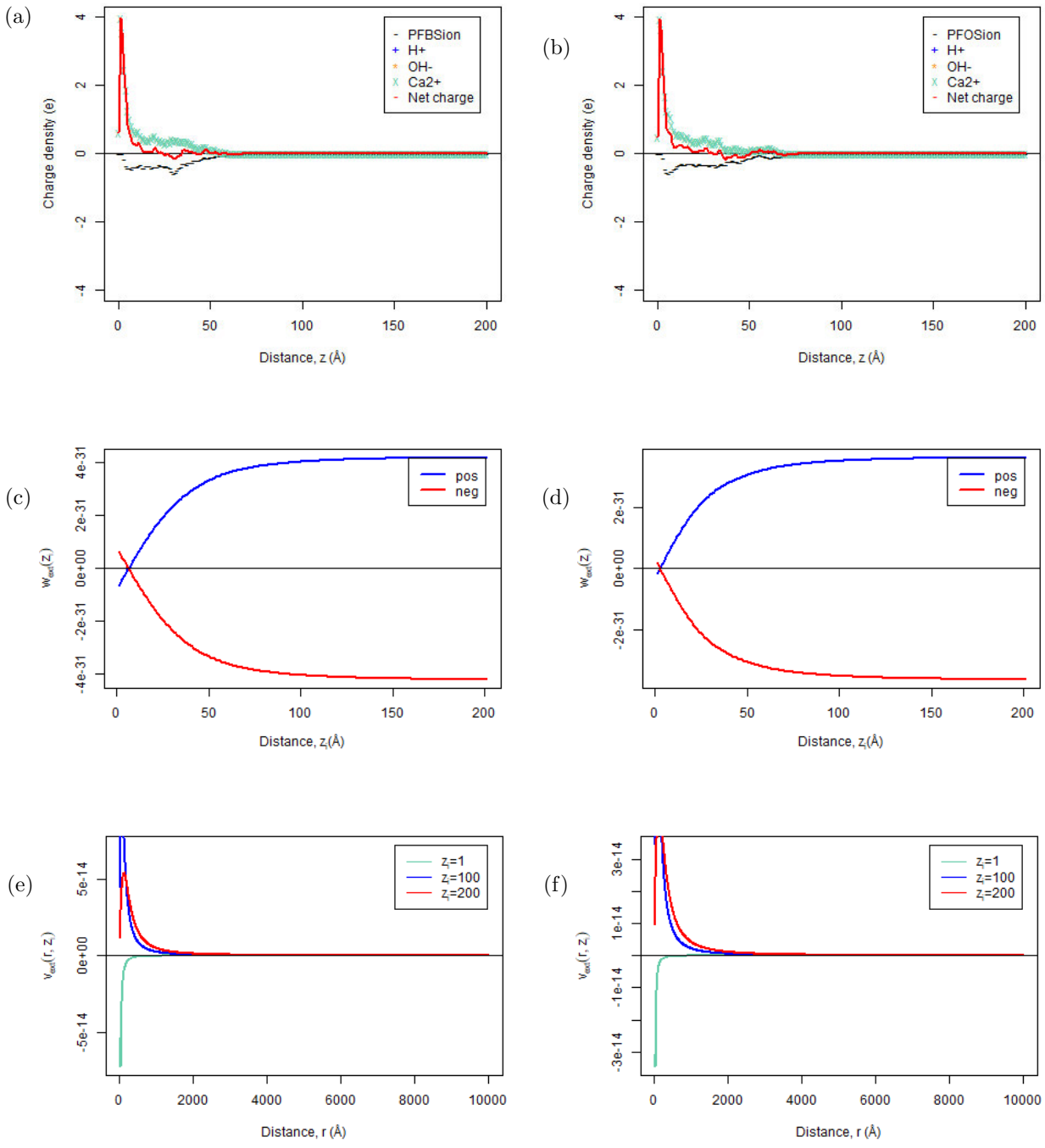
Supplementary Figure S6: 16PFBSion 8H 8OH +1S, 16PFOSion 8H 8OH +1S. See caption S4 for panel information.



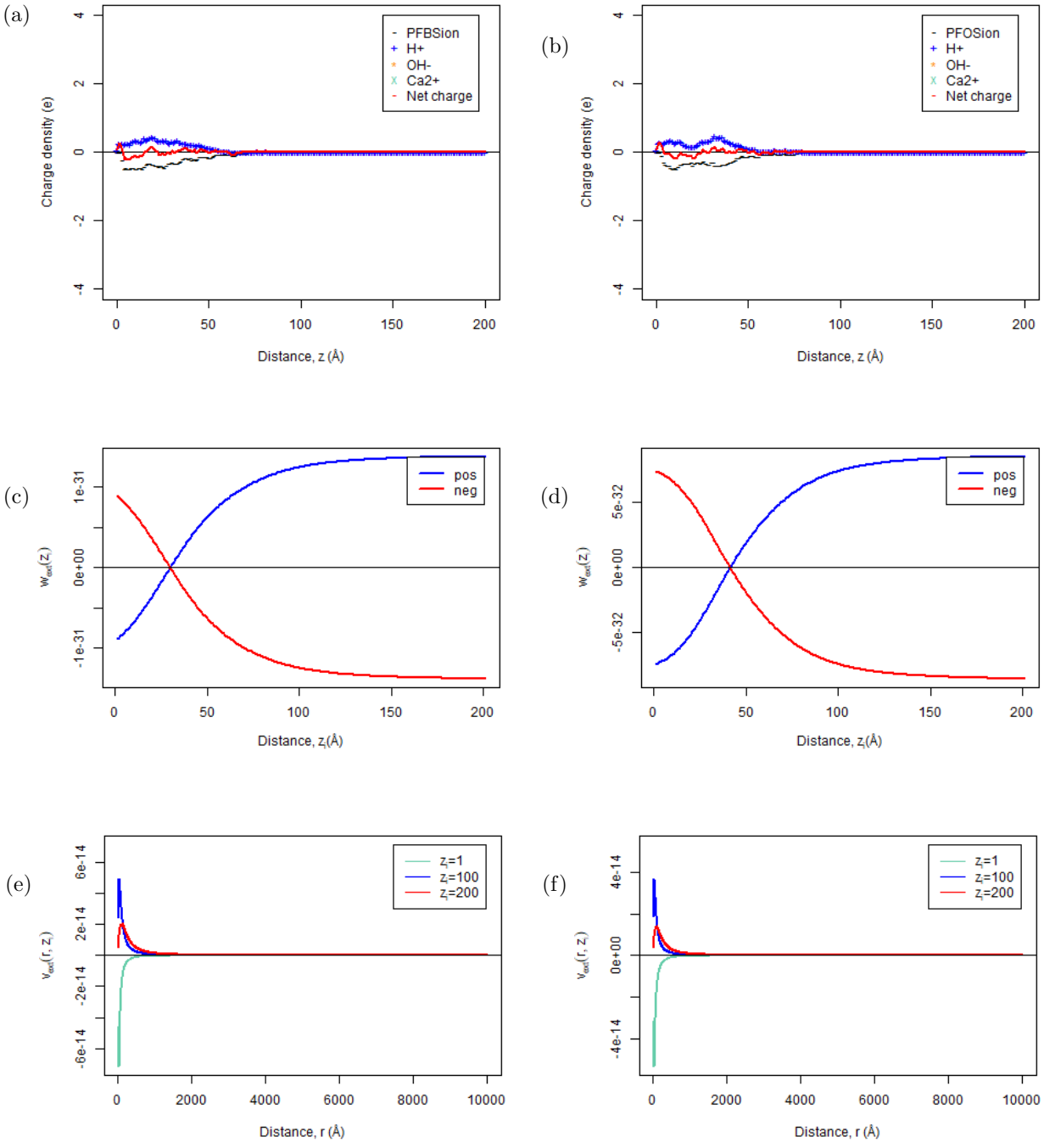
Supplementary Figure S7: 16PFBSion 16H 16OH +1S, 16PFOSion 16H 16OH +1S. See caption S4 for panel information.



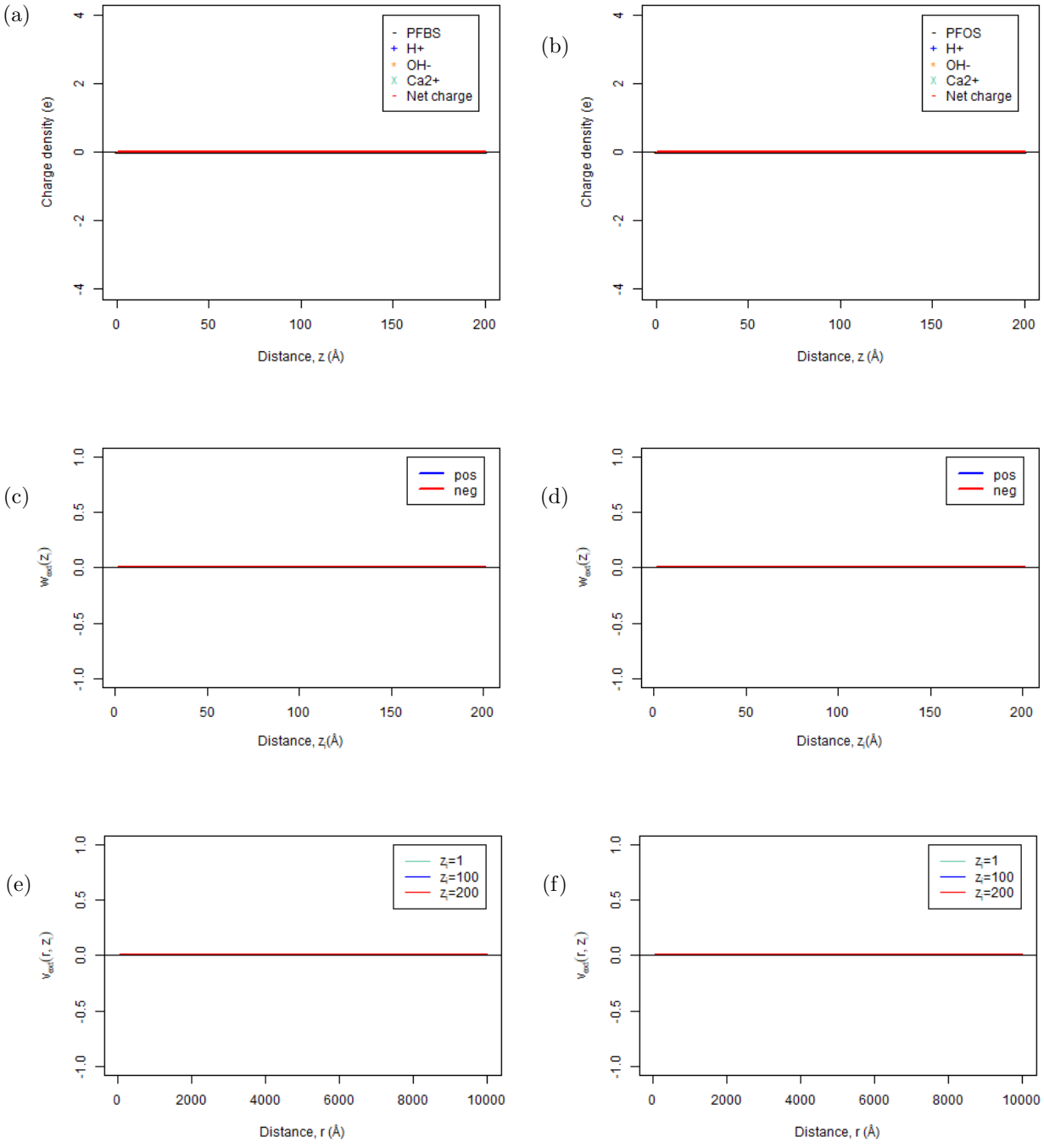
Supplementary Figure S8: 16PFBSion +1S, 16PFOSion +1S. See caption S4 for panel information.



Supplementary Figure S9: 16PFOSion 16Ca2+ -2S, 16PFOSion 16Ca2+ -2S. See caption S4 for panel information.

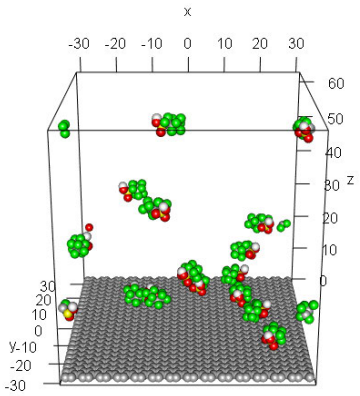


Supplementary Figure S10: PFBSion 16H 0S, PFOSion 16H 0S. See caption S4 for panel information.

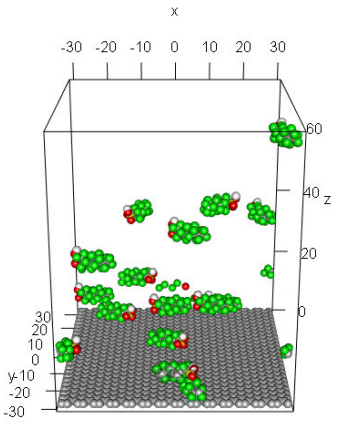


Supplementary Figure S11: PFBS 0H 0S, PFOS 0H 0S. See caption S4 for panel information.

(a)

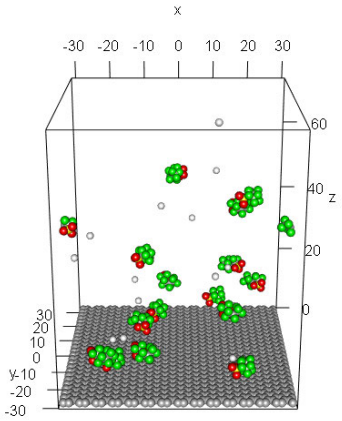


(b)

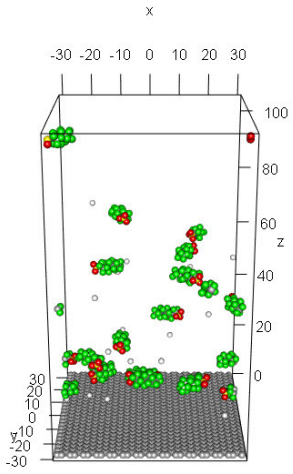


Supplementary Figure S12: (a) PFBS and (b) PFOS simulation positions at 20,000 iterations (neutral surface).

(a)

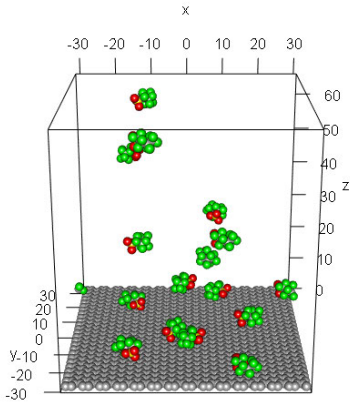


(b)

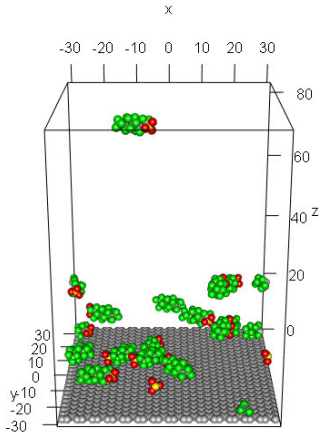


Supplementary Figure S13: (a) PFBS anion and (b) PFOS anion simulation positions at 20,000 iterations (16 H^+ (white), neutral surface).

(a)

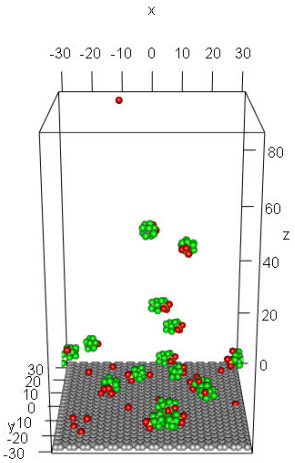


(b)

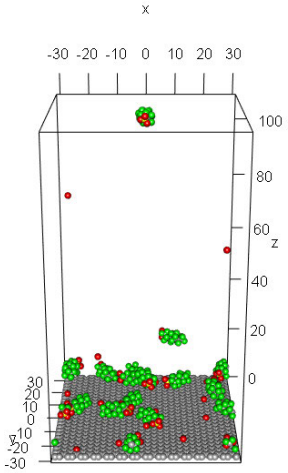


Supplementary Figure S14: (a) PFBS anion and (b) PFOS anion simulation positions at 20,000 iterations (positive surface).

(a)

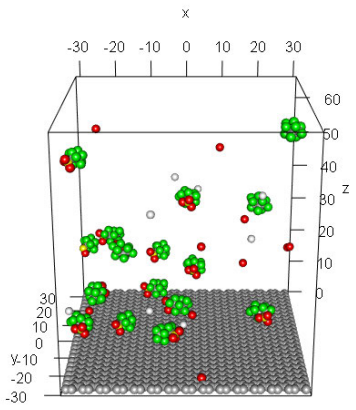


(b)

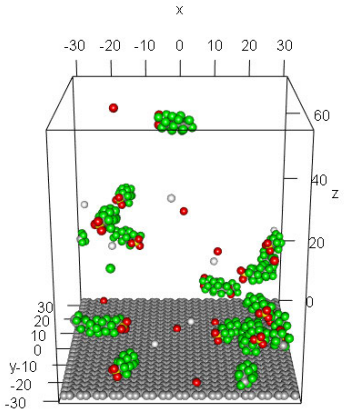


Supplementary Figure S15: (a) PFBS anion and (b) PFOS anion simulation positions at 20,000 iterations (16 OH^- (red), positive surface).

(a)

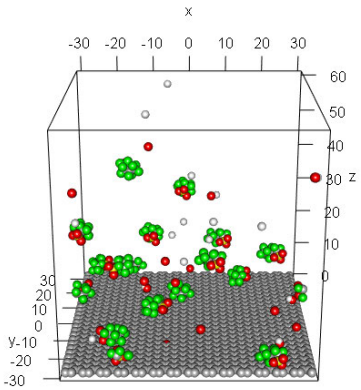


(b)

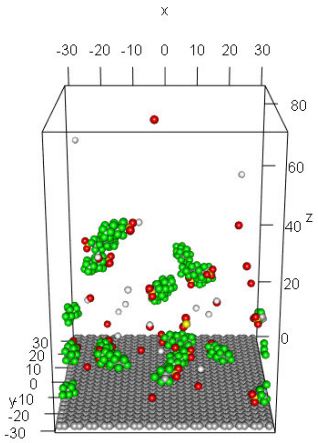


Supplementary Figure S16: (a) PFBS anion and (b) PFOS anion simulation positions at 20,000 iterations (8 H^+ (white), 8 OH^- (red), positive surface).

(a)

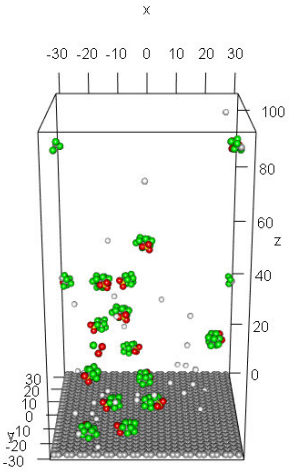


(b)

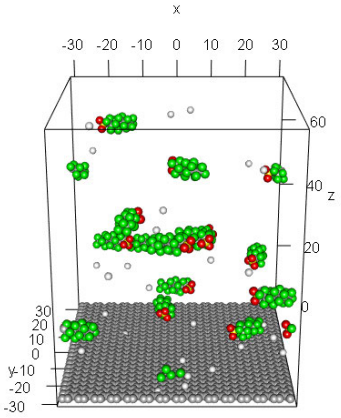


Supplementary Figure S17: (a) PFBS anion and (b) PFOS anion simulation positions at 20,000 iterations (16 H^+, 16 OH^-, positive surface).

(a)

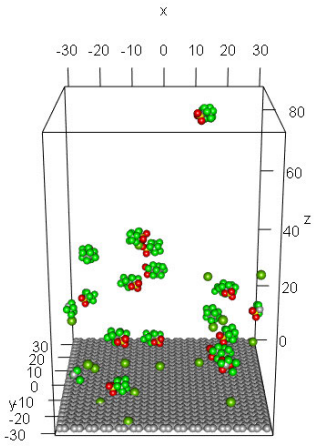


(b)

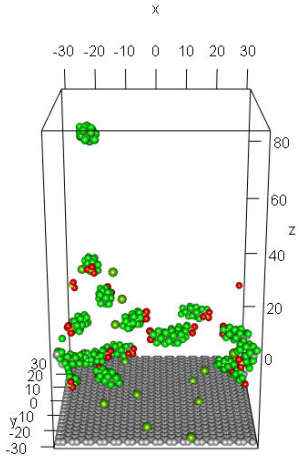


Supplementary Figure S18: (a) PFBS anion and (b) PFOS anion simulation positions at 20,000 iterations (32 H^+, negative surface).

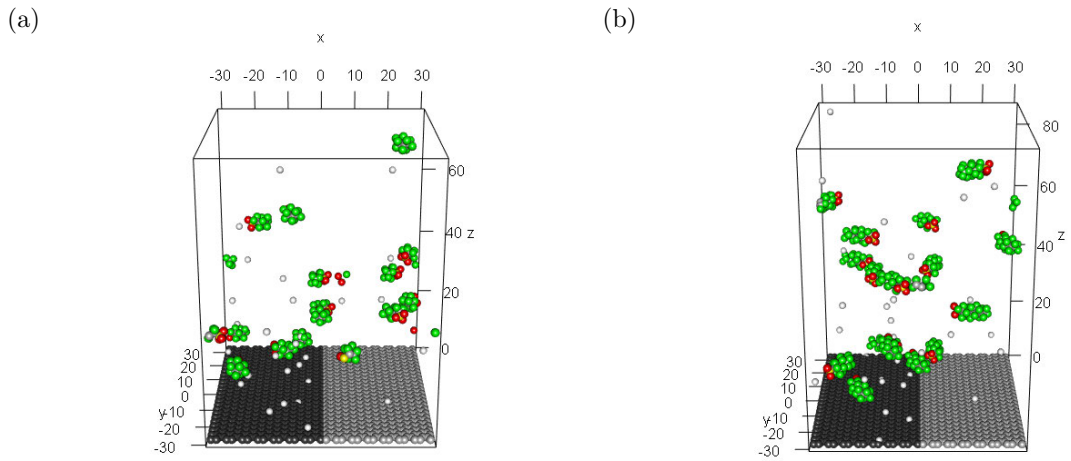
(a)



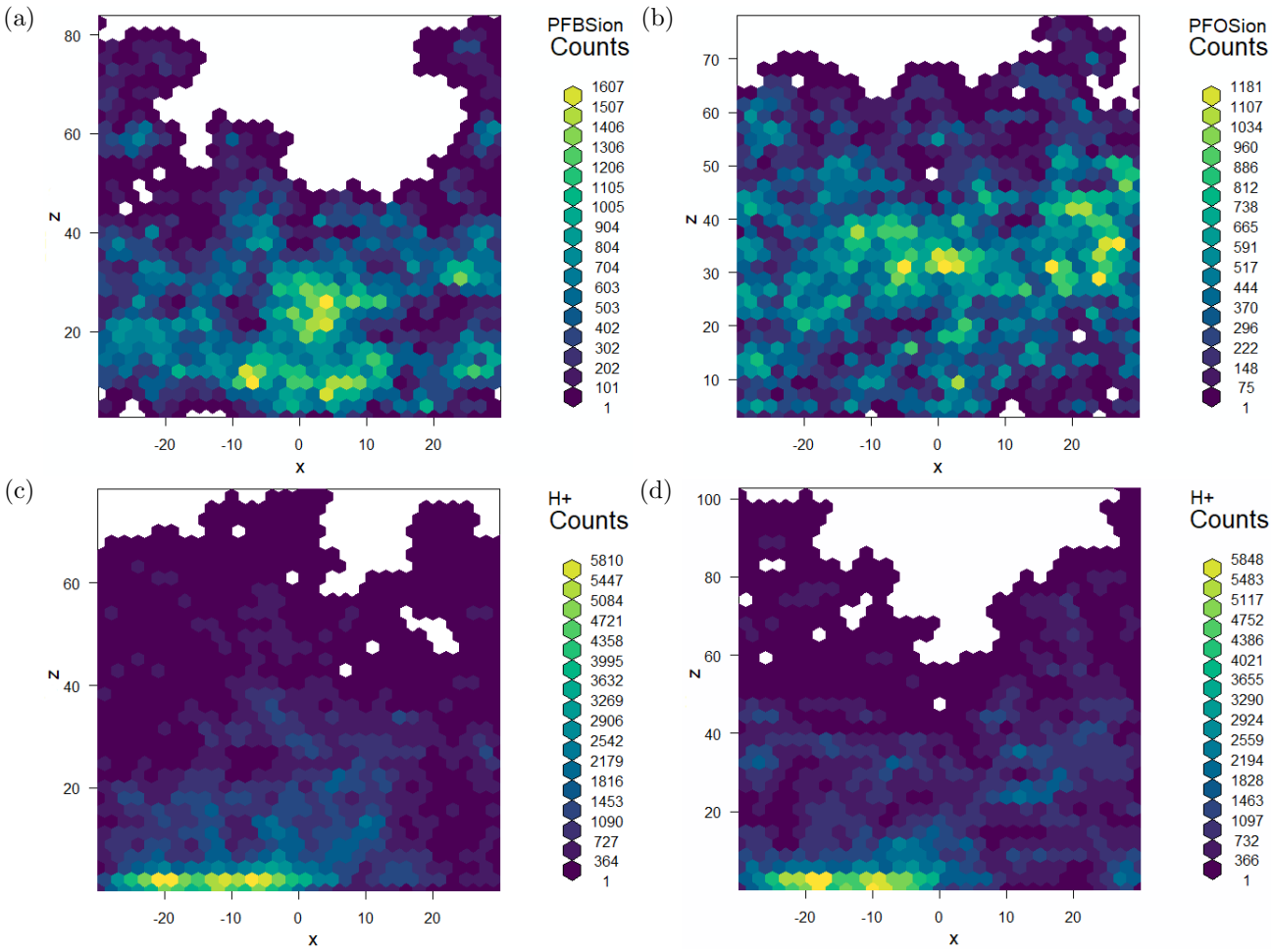
(b)



Supplementary Figure S19: (a) PFBS anion and (b) PFOS anion simulation positions at 20,000 iterations (16 Ca^{2+} (green), negative surface).



Supplementary Figure S20: (a) PFBS anion and (b) PFOS anion simulation positions at 20,000 iterations (32 H^+, half negative (left hand side, $x < 0$, dark grey), half neutral surface (right hand side, $x > 0$, light grey)).



Supplementary Figure S21: Heat maps showing ion count during simulation as a function of height (z) and lateral position (x): (a) PFBS anion, (b) PFOS anion, (c) H^+ corresponding to case in (a), and (d) H^+ corresponding to case in (b) for 32 H^+, half negative (left hand side of plots $x < 0$), half neutral surface (right hand side of plots $x > 0$). Scale ranges from low density (dark blue) to high density (yellow); regions not sampled by an ion type appear in white.

References

[1] A. Gindulyte, B. A. Shoemaker, B. Yu, J. He, J. Zhang, J. Chen, L. Zaslavsky, P. A. Thiessen, Q. Li, S. He, S. Kim, T. Cheng, E. E. Bolton, PubChem 2019 update: Improved access to chemical data, Nucleic Acids Research 47 (D1) (2019) D1102–D1109. doi:https://doi.org/10.1093/nar/gky1033.

[2] D. Van Der Spoel, E. Lindahl, B. Hess, G. Groenhof, A. E. Mark, H. J. Berendsen, Gromacs: fast, flexible, and free, Journal of Computational Chemistry 26 (16) (2005) 1701–1718. doi:https://doi.org/10.1002/jcc.20291.

[3] C. Hardacre, J. D. Holbrey, C. L. Mullan, M. Nieuwenhuyzen, T. G. Youngs, D. T. Bowron, S. J. Teat, Solid and liquid charge-transfer complex formation between 1-methylnaphthalene and 1-alkyl-cyanopyridinium bis {(trifluoromethyl) sulfonyl} imide ionic liquids, Physical Chemistry Chemical Physics 12 (8) (2010) 1842–1853. doi:https://doi.org/10.1039/B921160H.

[4] C.-M. Ionescu, D. Sehnal, F. L. Falginella, P. Pant, L. Pravda, T. Bouchal, R. S. Vařeková, S. Geidl, J. Koča, AtomicChargeCalculator: Interactive web-based calculation of atomic charges in large biomolecular complexes and drug-like molecules, Journal of Cheminformatics 7 (1) (2015) 50. doi:https://doi.org/10.1186/s13321-015-0099-x.

Appendix B

Supplementary information: Perfluoroalkyl, fluorotelomer sulfonate, and perfluorooctane sulfonamide contamination in biosolids: Composition, co-contamination and re-use implications

Supplementary Information:

Perfluoroalkyl, fluorotelomer sulfonate, and perfluorooctane sulfonamide contamination in biosolids: Composition, co-contamination and re-use implications

Julie A. Sleep, Albert L. Juhasz

S1.1 Chemicals and reagents

During the quantification of PFAS concentration, labelled-PFAS, including $^{13}C_3$ PFPeA, $^{13}C_2$ PFHxA, $^{13}C_4$ PFHpA, $^{13}C_4$ PFOA, $^{13}C_5$ PFNA, $^{13}C_2$ PFDA, $^{13}C_2$ PFUnDA, $^{13}C_2$ PFDoDA, $^{13}C_2$ PFTeDA, $^{13}C_2$ 4:2FTS, $^{13}C_2$ 6:2FTS, $^{13}C_2$ 8:2FTS, $^{13}C_8$ FOSA, d_3 N MeFOSA, d_5 N EtFOSA, d_7 N MeFOSE, d_9 N EtFOSE, d_3 N MeFOSA and d_5 N EtFOSAA (Wellington Laboratories, Canada; see Table S2 for abbreviations) were utilised. Analytical grade reagents (ammonium acetate, sodium hydroxide, potassium persulfate, ammonium hydroxide, formic acid) and solvents (methanol) utilize for the extraction, oxidation and analysis of PFAS were purchased from Sigma-Aldrich, Agilent Technologies and Thermo Fisher Scientific (Australia).

Table S1: PFAS analysed in this study, abbreviations used and limits of reporting (LOR). Compounds fell into the broad groups of perfluoroalkyl sulfonic acids (PFSAs), perfluoroalkyl carboxylic acids (PFCAs), perfluorooctane sulfonamide-based substances (FOSAMs) and fluorotelomer sulfonic acids (FTSAs).

Chemical name	Abbreviation	CAS No.	Family	Fluorinated Carbon Tail Length	LOR[†] ($\mu g\ L^{-1}$)	LOR TOPA ($\mu g\ kg^{-1}$)
Perfluorobutane sulfonic acid	PFBS	375-73-5	PFSAs	C_4	0.02	0.1
Perfluoropentane sulfonic acid	PFPeS	2706-91-4		C_5	0.02	0.1
Perfluorohexane sulfonic acid	PFHxS	355-46-4		C_6	0.02	0.1
Perfluoroheptane sulfonic acid	PFHpS	375-92-8		C_7	0.02	0.1
Perfluorooctane sulfonic acid	PFOS	1763-23-1		C_8	0.01	0.1
Perfluorodecane sulfonic acid	PFDS	335-77-3		C_{10}	0.02	0.2
Perfluorobutanoic acid	PFBA	375-22-4	PFCAs	C_4	0.1	0.2
Perfluoropentanoic acid	PFPeA	2706-90-3		C_5	0.02	0.2
Perfluorohexanoic acid	PFHxA	307-24-4		C_6	0.02	0.1
Perfluoroheptanoic acid	PFHpA	375-85-9		C_7	0.02	0.1
Perfluorooctanoic acid	PFOA	335-67-1		C_8	0.01	0.1
Perfluorononanoic acid	PFNA	375-95-1		C_9	0.02	0.1
Perfluorodecanoic acid	PFDA	335-76-2		C_{10}	0.02	0.5
Perfluoroundecanoic acid	PFUnDA	2058-94-8		C_{11}	0.02	0.5
Perfluorododecanoic acid	PFDoDA	307-55-1		C_{12}	0.02	0.5
Perfluorotridecanoic acid	PFTrDA	72629-94-8		C_{13}	0.02	0.5
Perfluorotetradecanoic acid	PFTeDA	376-06-7		C_{14}	0.05	5
Perfluorooctane sulfonamide	PFOSA	754-91-6	FOSAMs	C_8	0.02	1
N-Methyl perfluorooctane sulfonamide	MeFOSA	31506-32-8		C_8	0.05	1
N-Ethyl perfluorooctane sulfonamide	EtFOSA	4151-50-2		C_8	0.05	1
N-Methyl perfluorooctane sulfonamidoethanol	MeFOSE	24448-09-7		C_8	0.05	1
N-Ethyl perfluorooctane sulfonamidoethanol	EtFOSE	1691-99-2		C_8	0.05	5
N-Methyl perfluorooctane sulfonamidoacetic acid	MeFOSAA	2355-31-9		C_8	0.02	0.2
N-Ethyl perfluorooctane sulfonamidoacetic acid	EtFOSAA	2991-50-6		C_8	0.02	0.2
4:2 Fluorotelomer sulfonic acid	4:2FTS	757124-72-4	FTSAs	C_4	0.05	0.1
6:2 Fluorotelomer sulfonic acid	6:2FTS	27619-97-2		C_6	0.05	0.1
8:2 Fluorotelomer sulfonic acid	8:2FTS	39108-34-4		C_8	0.05	0.1
10:2 Fluorotelomer sulfonic acid	10:2FTS	120226-60-0		C_{10}	0.05	0.1

[†] This LOR can be converted to ($\mu g\ kg^{-1}$) for these samples by a multiplying by 66.7.

Table S2: WWTP details including sampling point of biosolid sample, plant processing method, approximate population served and proximity to an air force (RAAF) base.

Biosolid sample	Sampling point	Approximate population range served	Proximity to RAAF base as range (km)
WWTP1	Biosolid stockpile	>500,000	0-50
WWTP2	Bottom of drained lagoon	<10,000	0-50
WWTP3	Biosolid stockpile	>500,000	0-50
WWTP4	Biosolid stockpile	100,000-500,000	-
WWTP5	Unknown	50,000-100,000	-
WWTP6	Lime amended biosolids	10,000-50,000	-
WWTP7	Sludge	100,000-500,000	-
WWTP8	Sludge	10,000-50,000	-
WWTP9	Sludge	100,000-500,000	-
WWTP10	Biosolid stockpile	10,000-50,000	-
WWTP11	Sludge belt press	10,000-50,000	-
WWTP12	Lime amended biosolids	100,000-500,000	-

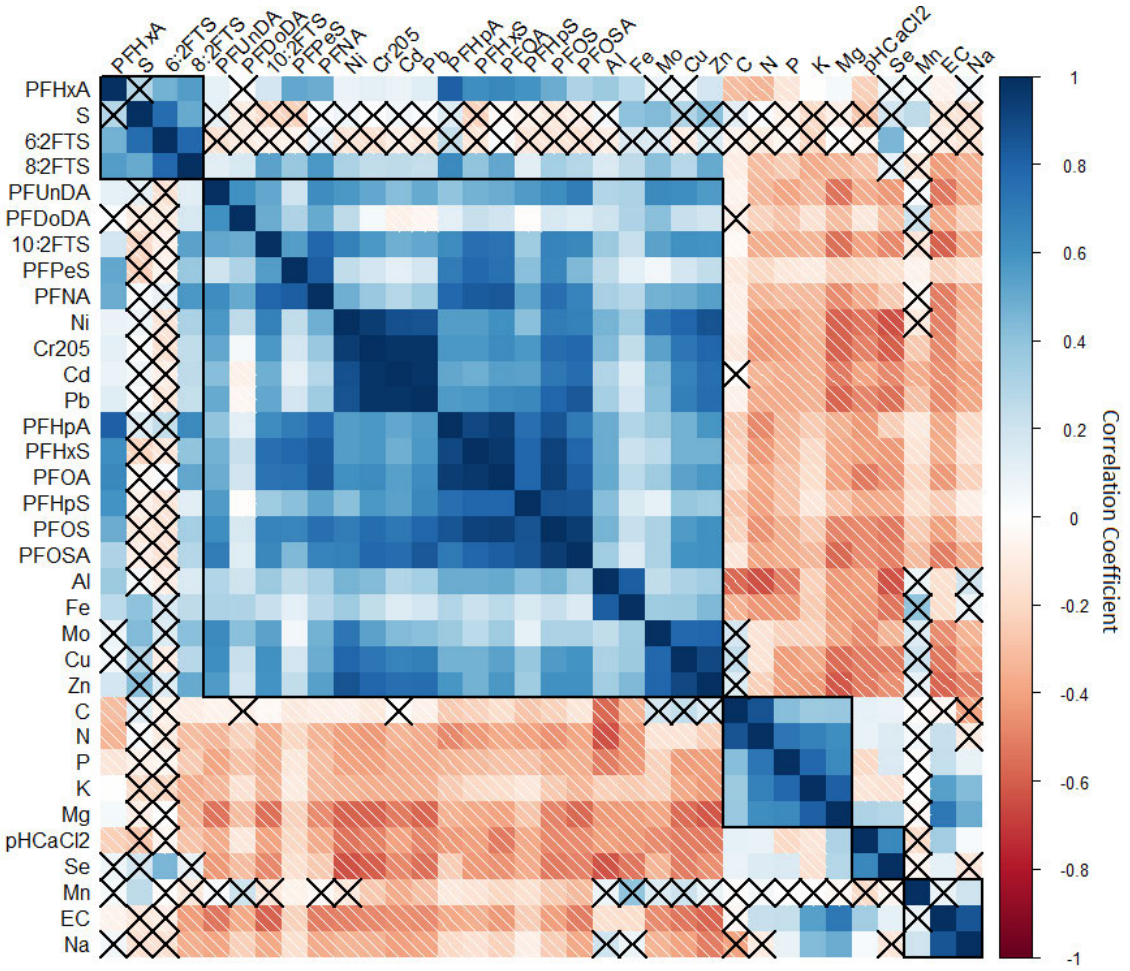


Figure S1: Correlation between PFAS and biosolid physico-chemical properties, ordered by hierarchical clustering. Clusters for $n = 5$ are denoted by black squares. The value of the correlation coefficient is indicated by the colour intensity, with diagonal stripes indicating negative correlations. The X indicates correlations that were not significant at p=0.05.

Table S3: Individual and total PFAS (mean) concentrations in μg kg^{-1}. Concentrations less than the LOR are denoted by 0.

	PFPeS	PFHxS	PFHpS	PFOS	PFDS	PFPeA	PFHxA	PFHpA	PFOA	PFNA	PFDA	PFUnDA	PFDoDA	PFOSA	MeFOSE	MeFOSAA	EtFOSAA	62FTS	82FTS	102FTS	TotalPFAS
WWTP1	0	7.65	1.65	85.7	8	0	6	3.65	16	0	5	0	0	0	0	6.65	5	0	0	0	145.3
WWTP2	0	0.65	0	22.3	1.3	0	5.3	3.3	11.35	1.3	3.3	0	0	0	0	4.35	2	34.65	38.35	1.65	129.8
WWTP3	0	1.65	0	47.65	3	0	0	0	6	1.3	3	2	2.35	2	7.35	15.35	15.65	0	6.7	8	122
WWTP4	0	1	0	45.35	0	0	0	0	4	0	1.35	0	0	0	0	3.65	1.65	0	0	0	57
WWTP5	0	0	0	13.65	0	0	0	0	5.65	0	4	0	0	0	0	9	3	0	0	0	35.3
WWTP6	0	0	0	11	0	17.35	0	0	1.65	0	0	0	0	0	0	0	0	0	0	0	30
WWTP7	0	0	0	16.5	0	0	1	0	4	0	4	0	0	0	0	0	0	0	0	0	25.5
WWTP8	0	0	0	10.35	0	0	0	0	8	0	5	0	0	0	0	0	0	0	0	0	23.35
WWTP9	0	0	0	13	0	0	0	0	4	0	5	0	0	0	0	1	0	0	0	0	23
WWTP10	0	0	0	4.65	0	0	0	0	0.35	0	0	0	0	0	0	3	6.65	0	0	0	14.65
WWTP11	0	0	0	5.5	0	0	0	0	1.5	0	0	0	0	0	0	0	0	0	0	0	7
WWTP12	0	0	0	5	0	0	0	0	0.35	0	0	0	0	0	0	0	0	0	0	0	5.35

Table S4: Correlation coefficients (2 s.f.) between PFAS concentrations and physico-chemical Properties

	PFPeS	PFHxS	PFHpS	PFOS	PFDS	PFPeA	PFHxA	PFHpA	PFOA	PFNA	PFDA	PFUnDA	PFDoDA	PFOSA	MeFOSE	MeFOSAA	EtFOSAA	X62FTS	X82FTS	X102FTS	TotalPFAS
EC	-0.22	-0.36	-0.24	-0.40	0.03	0.09	-0.06	-0.38	-0.43	-0.50	-0.21	-0.52	-0.37	-0.50	-0.29	-0.57	-0.47	-0.09	-0.42	-0.59	-0.47
pHh2o	-0.21	-0.41	-0.37	-0.49	0.00	0.63	-0.24	-0.44	-0.53	-0.37	-0.52	-0.36	-0.11	-0.48	-0.03	-0.45	-0.48	-0.08	-0.31	-0.39	-0.51
pHCaCl2	-0.20	-0.41	-0.37	-0.48	-0.04	0.64	-0.24	-0.43	-0.52	-0.36	-0.52	-0.36	-0.12	-0.47	-0.04	-0.45	-0.47	-0.05	-0.29	-0.39	-0.50
C	-0.12	-0.23	-0.27	-0.22	-0.20	0.01	-0.31	-0.25	-0.17	-0.09	0.12	-0.06	-0.09	-0.13	-0.06	-0.09	-0.18	-0.07	-0.09	-0.04	-0.21
N	-0.21	-0.43	-0.39	-0.45	-0.23	0.05	-0.33	-0.47	-0.38	-0.34	0.11	-0.33	-0.22	-0.39	-0.15	-0.40	-0.41	-0.11	-0.31	-0.35	-0.46
Al	0.25	0.49	0.42	0.46	0.38	-0.17	0.36	0.49	0.50	0.33	0.36	0.29	0.20	0.35	0.11	0.44	0.34	-0.09	0.16	0.36	0.47
Cd	0.11	0.49	0.54	0.71	-0.20	-0.16	0.08	0.51	0.55	0.28	0.01	0.42	-0.08	0.76	-0.13	0.54	0.84	-0.08	0.26	0.48	0.72
Cr267	0.19	0.58	0.58	0.77	-0.07	-0.18	0.12	0.58	0.63	0.38	0.12	0.52	0.04	0.79	-0.03	0.64	0.85	-0.16	0.25	0.58	0.78
Cr205	0.19	0.58	0.58	0.77	-0.07	-0.18	0.12	0.58	0.63	0.38	0.12	0.52	0.04	0.79	-0.03	0.63	0.85	-0.16	0.25	0.58	0.78
Cu	0.18	0.48	0.38	0.56	0.14	-0.30	0.06	0.48	0.53	0.50	0.22	0.62	0.22	0.59	0.13	0.66	0.59	-0.09	0.28	0.60	0.60
Fe1	0.12	0.21	0.17	0.22	0.33	-0.25	0.27	0.30	0.26	0.27	0.24	0.31	0.31	0.15	0.27	0.27	0.17	0.15	0.26	0.22	0.25
Fe2	0.13	0.25	0.20	0.26	0.33	-0.24	0.25	0.30	0.29	0.28	0.23	0.33	0.31	0.19	0.27	0.29	0.20	0.08	0.21	0.24	0.28
K	-0.10	-0.19	-0.13	-0.25	0.09	-0.13	0.00	-0.25	-0.18	-0.32	0.35	-0.33	-0.16	-0.32	-0.12	-0.36	-0.34	-0.20	-0.37	-0.34	-0.30
Mg	-0.22	-0.37	-0.28	-0.49	0.16	-0.07	0.05	-0.34	-0.40	-0.47	0.08	-0.53	-0.31	-0.56	-0.23	-0.57	-0.56	-0.01	-0.33	-0.55	-0.53
Mn	-0.07	-0.14	-0.16	-0.25	0.43	-0.19	0.05	-0.11	-0.20	-0.04	-0.07	0.03	0.21	-0.31	0.23	-0.15	-0.30	-0.02	-0.12	-0.14	-0.25
Mo	0.05	0.26	0.10	0.32	0.36	-0.27	0.07	0.37	0.35	0.48	0.29	0.63	0.41	0.32	0.37	0.55	0.35	0.15	0.41	0.54	0.39
Na	-0.17	-0.15	-0.08	-0.25	0.26	-0.16	0.06	-0.20	-0.23	-0.37	-0.06	-0.38	-0.23	-0.37	-0.17	-0.33	-0.35	-0.15	-0.35	-0.38	-0.30
Ni	0.25	0.55	0.41	0.70	0.06	-0.23	0.09	0.56	0.60	0.48	0.22	0.58	0.26	0.67	0.16	0.67	0.71	-0.14	0.32	0.67	0.71
P	-0.12	-0.32	-0.28	-0.36	-0.17	-0.20	-0.13	-0.33	-0.29	-0.30	0.22	-0.38	-0.28	-0.35	-0.25	-0.36	-0.36	-0.06	-0.25	-0.35	-0.38
Pb	0.18	0.57	0.64	0.80	-0.21	-0.15	0.13	0.56	0.63	0.36	0.07	0.50	-0.05	0.85	-0.12	0.60	0.91	-0.12	0.24	0.51	0.80
S	-0.23	-0.22	-0.07	-0.11	0.15	-0.29	0.29	0.13	-0.04	0.03	0.01	0.11	-0.10	-0.09	-0.03	-0.11	0.02	0.76	0.50	-0.20	-0.06
Se	-0.16	-0.43	-0.36	-0.51	-0.05	0.30	0.07	-0.25	-0.44	-0.25	-0.37	-0.42	-0.30	-0.49	-0.25	-0.49	-0.48	0.45	0.09	-0.47	-0.50
Zn	0.24	0.48	0.36	0.61	0.04	-0.17	0.19	0.58	0.57	0.54	0.23	0.56	0.19	0.61	0.08	0.62	0.62	0.15	0.50	0.60	0.65

Table S5: Correlation coefficients (2 s.f.) between PFAS concentrations

	PFPeS	PFHxS	PFHpS	PFOS	PFDS	PFPeA	PFHxA	PFHpA	PFOA	PFNA	PFDA	PFUnDA	PFDoDA	PFOSA	MeFOSE	MeFOSAA	EtFOSAA	X62FTS	X82FTS	X102FTS	TotalPFAS
PFPeS	1	0.79	0.41	0.65	-0.12	-0.06	0.52	0.69	0.75	0.82	0.68	0.21	0.30	0.45	-0.08	0.47	0.20	-0.06	0.37	0.55	0.61
PFHxS	0.79	1	0.79	0.92	0.11	-0.16	0.61	0.91	0.97	0.84	0.64	0.47	0.22	0.80	-0.08	0.80	0.61	-0.13	0.40	0.75	0.91
PFHpS	0.41	0.79	1	0.87	0.14	-0.13	0.59	0.75	0.79	0.52	0.37	0.56	-0.01	0.85	-0.17	0.58	0.83	-0.13	0.12	0.35	0.87
PFOS	0.65	0.92	0.87	1	-0.06	-0.16	0.49	0.85	0.93	0.76	0.48	0.61	0.16	0.94	-0.09	0.77	0.85	-0.13	0.34	0.66	0.99
PFDS	-0.12	0.11	0.14	-0.06	1	-0.12	0.41	0.22	0.07	0.07	0.24	0.23	0.33	-0.17	0.37	0.08	-0.13	0.03	0.00	0.04	-0.02
PFPeA	-0.06	-0.16	-0.13	-0.16	-0.12	1	-0.15	-0.18	-0.20	-0.15	-0.31	-0.15	-0.10	-0.14	-0.08	-0.18	-0.15	-0.06	-0.14	-0.15	-0.16
PFHxA	0.52	0.61	0.59	0.49	0.41	-0.15	1	0.81	0.65	0.50	0.55	0.10	0.01	0.30	-0.19	0.22	0.21	0.47	0.56	0.18	0.50
PFHpA	0.69	0.91	0.75	0.85	0.22	-0.18	0.81	1	0.94	0.79	0.62	0.40	0.11	0.70	-0.17	0.68	0.58	0.23	0.63	0.63	0.86
PFOA	0.75	0.97	0.79	0.93	0.07	-0.20	0.65	0.94	1	0.84	0.70	0.50	0.19	0.83	-0.10	0.80	0.67	0.02	0.51	0.74	0.94
PFNA	0.82	0.84	0.52	0.76	0.07	-0.15	0.50	0.79	0.84	1	0.67	0.63	0.51	0.66	0.18	0.79	0.45	0.09	0.58	0.79	0.78
PFDA	0.68	0.64	0.37	0.48	0.24	-0.31	0.55	0.62	0.70	0.67	1	0.25	0.30	0.32	0.04	0.48	0.12	0.02	0.35	0.49	0.48
PFUnDA	0.21	0.47	0.56	0.61	0.23	-0.15	0.10	0.40	0.50	0.63	0.25	1	0.61	0.70	0.53	0.66	0.71	-0.15	0.13	0.52	0.66
PFDoDA	0.30	0.22	-0.01	0.16	0.33	-0.10	0.01	0.11	0.19	0.51	0.30	0.61	1	0.13	0.92	0.32	0.05	-0.10	0.17	0.49	0.19
PFOSA	0.45	0.80	0.85	0.94	-0.17	-0.14	0.30	0.70	0.83	0.66	0.32	0.70	0.13	1	-0.04	0.80	0.94	-0.14	0.28	0.65	0.96
MeFOSE	-0.08	-0.08	-0.17	-0.09	0.37	-0.08	-0.19	-0.17	-0.10	0.18	0.04	0.53	0.92	-0.04	1	0.13	-0.02	-0.08	0.03	0.29	-0.04
MeFOSAA	0.47	0.80	0.58	0.77	0.08	-0.18	0.22	0.68	0.80	0.79	0.48	0.66	0.32	0.80	0.13	1	0.65	-0.12	0.42	0.91	0.82
EtFOSAA	0.20	0.61	0.83	0.85	-0.13	-0.15	0.21	0.58	0.67	0.45	0.12	0.71	0.05	0.94	-0.02	0.65	1	-0.14	0.16	0.45	0.87
X62FTS	-0.06	-0.13	-0.13	-0.13	0.03	-0.06	0.47	0.23	0.02	0.09	0.02	-0.15	-0.10	-0.14	-0.08	-0.12	-0.14	1	0.79	-0.08	-0.07
X82FTS	0.37	0.40	0.12	0.34	0.00	-0.14	0.56	0.63	0.51	0.58	0.35	0.13	0.17	0.28	0.03	0.42	0.16	0.79	1	0.53	0.40
X102FTS	0.55	0.75	0.35	0.66	0.04	-0.15	0.18	0.63	0.74	0.79	0.49	0.52	0.49	0.65	0.29	0.91	0.45	-0.08	0.53	1	0.70
TotalPFAS	0.61	0.91	0.87	0.99	-0.02	-0.16	0.50	0.86	0.94	0.78	0.48	0.66	0.19	0.96	-0.04	0.82	0.87	-0.07	0.40	0.70	1

Table S6: Correlation coefficients (2 s.f.) between physico-chemical properties

	EC	pHh2o	pHCaCl2	C	N	Al	Cd	Cr267	Cr205	Cu	Fe1	Fe2	K	Mg	Mn	Mo	Na	Ni	P	Pb	S	Se	Zn
EC	1	0.36	0.35	-0.05	0.22	-0.16	-0.46	-0.48	-0.48	-0.53	-0.17	-0.17	0.55	0.72	0.08	-0.46	0.85	-0.50	0.23	-0.47	-0.13	0.10	-0.57
pHh2o	0.36	1	1.00	0.07	0.07	-0.39	-0.42	-0.51	-0.51	-0.52	-0.42	-0.42	-0.14	0.31	-0.16	-0.47	0.07	-0.55	-0.19	-0.50	-0.30	0.64	-0.54
pHCaCl2	0.35	1.00	1	0.10	0.09	-0.40	-0.40	-0.49	-0.49	-0.51	-0.43	-0.43	-0.14	0.31	-0.18	-0.47	0.04	-0.53	-0.19	-0.48	-0.28	0.64	-0.52
C	-0.05	0.07	0.10	1	0.87	-0.56	-0.02	-0.12	-0.12	0.23	-0.34	-0.35	0.36	0.38	-0.02	0.17	-0.40	-0.07	0.42	-0.08	0.13	0.08	0.15
N	0.22	0.07	0.09	0.87	1	-0.64	-0.34	-0.42	-0.42	-0.15	-0.44	-0.46	0.67	0.61	0.04	-0.14	-0.10	-0.41	0.72	-0.36	0.03	0.15	-0.23
Al	-0.16	-0.39	-0.40	-0.56	-0.64	1	0.30	0.43	0.43	0.32	0.83	0.85	-0.24	-0.43	0.08	0.25	0.20	0.47	-0.51	0.34	0.05	-0.62	0.35
Cd	-0.46	-0.42	-0.40	-0.02	-0.34	0.30	1	0.97	0.97	0.67	0.14	0.17	-0.36	-0.52	-0.36	0.44	-0.40	0.87	-0.36	0.98	0.05	-0.48	0.76
Cr267	-0.48	-0.51	-0.49	-0.12	-0.42	0.43	0.97	1	1.00	0.73	0.25	0.28	-0.35	-0.58	-0.26	0.53	-0.34	0.94	-0.40	0.97	0.00	-0.60	0.80
Cr205	-0.48	-0.51	-0.49	-0.12	-0.42	0.43	0.97	1.00	1	0.73	0.25	0.28	-0.35	-0.58	-0.26	0.53	-0.34	0.94	-0.40	0.97	0.01	-0.59	0.80
Cu	-0.53	-0.52	-0.51	0.23	-0.15	0.32	0.67	0.73	0.73	1	0.36	0.39	-0.38	-0.55	0.21	0.78	-0.39	0.80	-0.41	0.68	0.29	-0.51	0.91
Fe1	-0.17	-0.42	-0.43	-0.34	-0.44	0.83	0.14	0.25	0.25	0.36	1	1.00	-0.25	-0.41	0.40	0.35	0.07	0.36	-0.43	0.18	0.40	-0.52	0.44
Fe2	-0.17	-0.42	-0.43	-0.35	-0.46	0.85	0.17	0.28	0.28	0.39	1.00	1	-0.27	-0.44	0.41	0.35	0.09	0.39	-0.46	0.21	0.35	-0.57	0.45
K	0.55	-0.14	-0.14	0.36	0.67	-0.24	-0.36	-0.35	-0.35	-0.38	-0.25	-0.27	1	0.81	-0.01	-0.23	0.44	-0.34	0.79	-0.34	-0.19	-0.16	-0.43
Mg	0.72	0.31	0.31	0.38	0.61	-0.43	-0.52	-0.58	-0.58	-0.55	-0.41	-0.44	0.81	1	-0.03	-0.39	0.49	-0.59	0.64	-0.57	-0.08	0.29	-0.62
Mn	0.08	-0.16	-0.18	-0.02	0.04	0.08	-0.36	-0.26	-0.26	0.21	0.40	0.41	-0.01	-0.03	1	0.14	0.20	-0.12	0.00	-0.29	0.26	-0.05	0.09
Mo	-0.46	-0.47	-0.47	0.17	-0.14	0.25	0.44	0.53	0.53	0.78	0.35	0.35	-0.23	-0.39	0.14	1	-0.34	0.73	-0.22	0.41	0.44	-0.33	0.79
Na	0.85	0.07	0.04	-0.40	-0.10	0.20	-0.40	-0.34	-0.34	-0.39	0.07	0.09	0.44	0.49	0.20	-0.34	1	-0.34	0.09	-0.38	-0.16	-0.13	-0.51
Ni	-0.50	-0.55	-0.53	-0.07	-0.41	0.47	0.87	0.94	0.94	0.80	0.36	0.39	-0.34	-0.59	-0.12	0.73	-0.34	1	-0.40	0.86	0.06	-0.64	0.87
P	0.23	-0.19	-0.19	0.42	0.72	-0.51	-0.36	-0.40	-0.40	-0.41	-0.43	-0.46	0.79	0.64	0.00	-0.22	0.09	-0.40	1	-0.36	-0.08	0.16	-0.41
Pb	-0.47	-0.50	-0.48	-0.08	-0.36	0.34	0.98	0.97	0.97	0.68	0.18	0.21	-0.34	-0.57	-0.29	0.41	-0.38	0.86	-0.36	1	0.02	-0.54	0.76
S	-0.13	-0.30	-0.28	0.13	0.03	0.05	0.05	0.00	0.01	0.29	0.40	0.35	-0.19	-0.08	0.26	0.44	-0.16	0.06	-0.08	0.02	1	0.18	0.41
Se	0.10	0.64	0.64	0.08	0.15	-0.62	-0.48	-0.60	-0.59	-0.51	-0.52	-0.57	-0.16	0.29	-0.05	-0.33	-0.13	-0.64	0.16	-0.54	0.18	1	-0.45
Zn	-0.57	-0.54	-0.52	0.15	-0.23	0.35	0.76	0.80	0.80	0.91	0.44	0.45	-0.43	-0.62	0.09	0.79	-0.51	0.87	-0.41	0.76	0.41	-0.45	1

Appendix C

Supplementary information for Chapter 6

Table C.1: PFAS compounds fell into the broad groups of perfluoroalkyl sulfonic acids (PFSAs), perfluoroalkyl carboxylic acids (PFCAs), perfluorooctane sulfonamide-based substances (FOSAMs) and fluorotelomer sulfonic acids (FTSAs).

Chemical name	Abbreviation	CAS No.	Family	Fluorinated Carbon Tail Length	LOR Soil ($\mu g\ kg^{-1}$)	LOR Leachate ($\mu g\ L^{-1}$)
Perfluorobutane sulfonic acid	PFBS	375-73-5	PFSAs	C_4	1.0	0.01
Perfluoropentane sulfonic acid	PFPeS	2706-91-4		C_5	1.0	0.01
Perfluorohexane sulfonic acid	PFHxS	355-46-4		C_6	1.0	0.01
Perfluoroheptane sulfonic acid	PFHpS	375-92-8		C_7	1.0	0.01
Perfluorooctane sulfonic acid	PFOS	1763-23-1		C_8	1.0	0.01
Perfluorodecane sulfonic acid	PFDS	335-77-3		C_{10}	2.0	0.02
Perfluorobutanoic acid	PFBA	375-22-4	PFCAs	C_4	2.0	0.2
Perfluoropentanoic acid	PFPeA	2706-90-3		C_5	2.0	0.02
Perfluorohexanoic acid	PFHxA	307-24-4		C_6	1.0	0.01
Perfluoroheptanoic acid	PFHpA	375-85-9		C_7	10	0.01
Perfluorooctanoic acid	PFOA	335-67-1		C_8	1.0	0.01
Perfluorononanoic acid	PFNA	375-95-1		C_9	5.0	0.01
Perfluorodecanoic acid	PFDA	335-76-2		C_{10}	5.0	0.02
Perfluoroundecanoic acid	PFUnDA	2058-94-8		C_{11}	5.0	0.02
Perfluorododecanoic acid	PFDoDA	307-55-1		C_{12}	5.0	0.05
Perfluorotridecanoic acid	PFTrDA	72629-94-8		C_{13}	5.0	0.10
Perfluorotetradecanoic acid	PFTeDA	376-06-7		C_{14}	50	0.50
Perfluorooctane sulfonamide	PFOSA	754-91-6	FOSAMs	C_8	10	0.10
N-Methyl perfluorooctane sulfonamide	MeFOSA	31506-32-8		C_8	10	0.05
N-Ethyl perfluorooctane sulfonamide	EtFOSA	4151-50-2		C_8	10	0.10
N-Methyl perfluorooctane sulfonamidoethanol	MeFOSE	24448-09-7		C_8	10	0.05
N-Ethyl perfluorooctane sulfonamidoethanol	EtFOSE	1691-99-2		C_8	2.0	0.02
N-Methyl perfluorooctane sulfonamidoacetic acid	MeFOSAA	2355-31-9		C_8	2.0	0.02
N-Ethyl perfluorooctane sulfonamidoacetic acid	EtFOSAA	2991-50-6		C_8	2.0	0.02
4:2 Fluorotelomer sulfonic acid	4:2FTS	757124-72-4	FTSAs	C_4	1.0	0.01
6:2 Fluorotelomer sulfonic acid	6:2FTS	27619-97-2		C_6	1.0	0.01
8:2 Fluorotelomer sulfonic acid	8:2FTS	39108-34-4		C_8	2.0	0.02
10:2 Fluorotelomer sulfonic acid	10:2FTS	120226-60-0		C_{10}	2.0	0.02

† This LOR can be converted to ($\mu g\ kg^{-1}$) for these samples by a multiplying by 66.7.

Table C.2: Surrogate recovery and oxidation efficiency values for pre- and post-TOP assay analyses of P1-P13 and P20 soils.

	PFAS quantification pre-TOP assay		PFAS quantification post-TOP assay	
	Surrogate $^{13}C_8$ PFOS	Surrogate $^{13}C_2$ PFOA	Surrogate $^{13}C_2$ PFOA	Oxidation Efficiency $^{13}C_8$ FOSA
P1-13	99	102	99	105
	106	102	96	107
	102	105	95	105
	100	106	97	98
	101	102	95	105
	103	107	98	105
	116	116	96	111
	109	114	96	102
	109	110	94	105
	105	111	95	117
	115	109	97	104
	105	106	94	104
	119	106	96	104
	110	107	95	102
	102	107	106	100
	102	111	112	97
	107	108	105	97
	108	108	113	94
	101	109	111	99
	105	108	114	100
	97	101	99	95
	102	99	98	91
	102	104	100	95
	108	104	109	90
	99	103	104	93
	101	101	106	92
P20	97	94	123	98
	94	91	122	98
	96	113	114	97
	100	112	124	99
	99	108	104	92
	96	106	93	99
	98	101	115	99
	96	89	118	97
	98	87	86	99
	89	92	89	93
Min	89	87	86	90
Max	119	116	124	117
Mean	103	104	103	100

Table C.3: PFAS concentrations in P1-P13 soils (μg kg^{-1}, max 3 significant figures, s.f.) and % of Σ_{28}PFAS (max 2 s.f.).

	P1	P3	P4	P5	P6	P7	P8	P9	P10	P11	P12	P13
PFBS	0	0	51	2	39.5	3	60	3.5	160	10	9.5	1
	0%	0%	3%	3%	3%	0%	1%	0%	0%	0%	0%	0%
PFPeS	0	0	45.5	1	41	2	59	7	290	12	13.5	2
	0%	0%	2%	1%	3%	0%	1%	0%	1%	0%	0%	0%
PFHxS	5.5	0	290	8	255	22.5	435	125	2850	140	225	45
	10%	0%	16%	11%	20%	1%	8%	8%	9%	4%	7%	3%
PFHpS	0	0	33	1	26	2	42	16.5	530	25	18.5	4
	0%	0%	2%	1%	2%	0%	1%	1%	2%	1%	1%	0%
PFOS	16.5	0	1,200	58	740	1,500	4,500	1,400	28,500	1,800	2,950	1,250
	30%	0%	65%	77%	58%	92%	84%	85%	85%	55%	86%	91%
PFDS	0	0	0	0	0	57	60	22.5	34.5	21	36	20.5
	0%	0%	0%	0%	0%	3%	1%	1%	0%	1%	1%	1%
PFBA	0	0	15	0	10	2	10	0	32	35	6	0
	0%	0%	1%	0%	1%	0%	0%	0%	0%	1%	0%	0%
PFPeA	0	0	26.5	0	20	2.5	20	3.5	74.5	140	15	0
	0%	0%	1%	0%	2%	0%	0%	0%	0%	4%	0%	0%
PFHxA	1.5	0.5	98.5	3	81	11	86	22.5	355	185	89.5	7
	3%	3%	5%	4%	6%	1%	2%	1%	1%	6%	3%	1%
PFHpA	0	0	13	0	12.5	0	13.5	0	72	38.5	0	0
	0%	0%	1%	0%	1%	0%	0%	0%	0%	1%	0%	0%
PFOA	1	0	32	1.5	22.5	12	45.5	16	275	56.5	27.5	5
	2%	0%	2%	2%	2%	1%	1%	1%	1%	2%	1%	0%
PFNA	0.5	8	1	0	0.5	0	1.5	0	17	17	2	0
	1%	44%	0%	0%	0%	0%	0%	0%	0%	1%	0%	0%
PFDA	0	0	0	0	0	0	0	0	10	7	0	0
	0%	0%	0%	0%	0%	0%	0%	0%	0%	0%	0%	0%
PFUnDA	10	9.5	0	0	0	0	0	0	5	0	0	0
	18%	53%	0%	0%	0%	0%	0%	0%	0%	0%	0%	0%
PFDoDA	0	0	0	0	0	0	0	0	6	0	0	0
	0%	0%	0%	0%	0%	0%	0%	0%	0%	0%	0%	0%
PFTrDA	20	0	0	0	0	0	0	0	0	0	0	0
	36%	0%	0%	0%	0%	0%	0%	0%	0%	0%	0%	0%
FOSA	0	0	0	0	0	20	20	35	60	0	20	45
	0%	0%	0%	0%	0%	1%	0%	2%	0%	0%	1%	3%
4:2 FTS	0	0	0	0	0	0	0	0	0	0	0	0
	0%	0%	0%	0%	0%	0%	0%	0%	0%	0%	0%	0%
6:2 FTS	0	0	40.5	0.5	27.5	0	0	0	14.5	705	0	0
	0%	0%	2%	1%	2%	0%	0%	0%	0%	21%	0%	0%
8:2 FTS	0	0	7	0	5	0	0	0	215	100	3	1
	0%	0%	0%	0%	0%	0%	0%	0%	1%	3%	0%	0%
10:2 FTS	0	0	0	0	0	0	0	0	5	10	0	0
	0%	0%	0%	0%	0%	0%	0%	0%	0%	0%	0%	0%
Σ_{28}PFAS	55	18	1,850	75	1,281	1,630	5,353	1,652	33,500	3,300	3,420	1,380

Table C.4: PFAS concentrations in P20 soil (μg kg^{-1}, max 3 s.f.) and % of Σ_{28}PFAS (max 2 s.f.).

	$P20_{10}$	$P20_{33}$	$P20_{180}$	$P20_{400}$
PFBS	2	2	2	1.9
	0%	0%	0%	0%
PFPeS	2	2	1.5	2.5
	0%	0%	0%	0%
PFHxS	14	14.5	12	20.5
	1%	1%	0%	0%
PFHpS	1	2	1	1.9
	0%	0%	0%	0%
PFOS	165	215	130	145
	9%	9%	2%	2%
PFDS	0	0	0	0
	0%	0%	0%	0%
PFBA	3.5	10	10	16
	0%	0%	0%	0%
PFPeA	2	2.5	7	12
	0%	0%	0%	0%
PFHxA	35.5	48	71.5	99.5
	2%	2%	1%	1%
PFHpA	0	0	4	5.85
	0%	0%	0%	0%
PFOA	15	19.5	28	40.5
	1%	1%	1%	0%
PFNA	0	0	0	1.9
	0%	0%	0%	0%
PFDA	0	0	7	10.75
	0%	0%	0%	0%
PFUnDA	0	0	0	0
	0%	0%	0%	0%
PFDoDA	0	0	0	0
	0%	0%	0%	0%
PFTrDA	0	0	0	0
	0%	0%	0%	0%
FOSA	0	0	0	0
	0%	0%	0%	0%
4:2 FTS	1	1	5	7.85
	0%	0%	0%	0%
6:2 FTS	1,500	1,700	4,150	6,600
	83%	73%	77%	76%
8:2 FTS	48.5	280	810	1,550
	3%	12%	15%	18%
10:2 FTS	21	47	155	140
	1%	2%	3%	2%
Σ_{28}PFAS	1,810	2,340	5,390	8,660

Table C.5: Differences in PFAS concentrations in P1-P13 soils pre vs post- TOP assay (μg kg^{-1}, 3 s.f.), and percentage change (%, 3 s.f.), which is blank when the PFAS was not detected in the original sample.

PFAS	P1	P3	P4	P5	P6	P7	P8	P9	P10	P11	P12	P13
PFBS	0	0	5	-1	3.5	0.5	-3	1	65	2	1.5	1
			10%	-50%	9%	17%	-5%	29%	41%	20%	16%	100%
PFPeS	0	0	-1	0	-3.5	1.5	0.5	1.5	-10	2	3.5	1.5
			-2%	0%	-9%	75%	1%	21%	-3%	17%	26%	75%
PFHxS	-1	0	15	-0.5	-30	18.5	75	65	300	0	50	105
	-18%		5%	-6%	-12%	82%	17%	52%	11%	0%	22%	233%
PFHpS	0	0	-2.5	0	-3	0.5	-2	3.5	-95	-1.5	1	1
			-8%	0%	-12%	25%	-5%	21%	-18%	-6%	5%	25%
PFOS	-1.5	0	-210	-3	-55	-250	50	-100	-4,500	50	0	-100
	-9%		-18%	-5%	-7%	-17%	1%	-7%	-16%	3%	0%	-8%
PFDS	0	0	0	0	0	-5	-4.5	-1.5	-1	-6	-3.5	-0.5
						-9%	-8%	-7%	-3%	-29%	-10%	-2%
PFBA	0	0	26	1	16.5	18.5	25	31	1,168	145	41	42.5
			173%		165%	925%	250%		3,650%	414%	683%	
PFPeA	3	4	39	10	23.5	32	38.5	56.5	2,730	225	76.5	95
			147%		118%	1,280%	193%	1,610%	3,660%	161%	510%	
PFHxA	3.5	2.5	132	15	59	139	164	733	7,050	380	481	958
	233%	500%	134%	500%	73%	1,260%	191%	3,260%	1,990%	205%	537%	13,700%
PFHpA	3	2	9	1.5	4	21	14.5	39.5	1,530	43.5	53.5	29
			69%		32%		107%		2120%	113%		
PFOA	2	1	7.5	1	6.5	77.5	59.5	169	1,180	43	87.5	105
	200%		23%	67%	29%	646%	131%	1,060%	427%	76%	318%	2,100%
PFNA	1	-2	-1	0	-0.5	0.5	1	2	313	4.5	9	3
	200%	-25%	-100%		-100%		67%		1,840%	26%	450%	
PFDA	0	0	0	0	0	0	0	0	135	1	2.5	0
									1,350%	14%		
PFUnDA	-0.5	-3	0	0	0	0	0	0	89	0	0	0
	-5%	-32%							1,780%			
PFDoDA	0	0	0	0	0	0	0	0	51	0	0	0
									850%			
PFTrDA	-10	0	0	0	0	0	0	0	30	0	0	0
	-50%											
PFTeDA	0	0	0	0	0	0	0	0	0	0	0	0
FOSA	0	0	0	0	0	-20	-20	-35	-60	0	-20	-45
						-100%	-100%	-100%	-100%		-100%	-100%
4:2 FTS	0	0	0	0	0	0	0	0	0	0	0	0
6:2 FTS	0	0	-40	-0.5	-27.5	0	0	0	-14.5	-682	0	0
			-99%	-100%	-100%				-100%	-97%		
8:2 FTS	0	0	-7	0	-5	0	0	0	-207	-91	-3	-1
			-100%		-100%				-96%	-91%	-100%	-100%
10:2 FTS	0	0	0	0	0	0	0	0	-5	-10	0	0
									-100%	-100%		
Σ_{28} PFAS	-0.5	4.5	-28.5	23.5	-11.5	34.5	399	965	9,730	106	780	1,190
	-0.909%	25.0 %	-1.54 %	31.3%	-0.898%	2.11%	7.45%	58.4%	29.0%	3.20%	22.8%	86.5%

Table C.6: Differences in PFAS concentrations in P20 soil pre vs post- TOP assay (μg kg^{-1}, 3 s.f.), and percentage change (%, 3 s.f.), which is blank when the PFAS was not detected in the original sample.

PFAS	$P20_{10}$	$P20_{33}$	$P20_{180}$	$P20_{400}$
PFBS	0	0.5	0	-0.5
	0%	25%	0%	-26%
PFPeS	0	1	0.5	-0.25
	0%	50%	33%	-10%
PFHxS	-2	2.5	4.5	-10.9
	-14%	17%	38%	-53%
PFHpS	0	1	1	-1.9
	0%	50%	100%	-100%
PFOS	10	-25	0	-111
	6%	-12%	0%	-77%
PFDS	0	0	0	0
PFBA	8,700	7,740	7,690	8,734
	248,000%	77,400%	76,900%	54,600%
PFPeA	15,000	14,700	14,500	14,500
	750,000%	590,000%	207,000%	121,000%
PFHxA	9,260	10,200	9,380	9,550
	26,100%	21,300%	13,100%	9,600%
PFHpA	3,750	3,100	2,650	3,590
			66,200%	61,400%
PFOA	3,140	2,830	2,270	2,560
	20,900%	14,500%	8,110%	6,320%
PFNA	900	825	730	878
				46,200%
PFDA	795	825	673	609
			9,610%	5,670%
PFUnDA	170	178	170	170
PFDoDA	240	255	260	145
PFTrDA	95	113	114	44
PFTeDA	100	103	100	62
FOSA	0	0	0	0
4:2 FTS	-1	-1	-5	-7.85
	-100%	-100%	-100%	-100%
6:2 FTS	-1,500	-1,700	-4,130	-6,570
	-100%	-100%	-100%	-100%
8:2 FTS	-48.5	-280	-796	-1,530
	-100%	-100%	-98%	-99%
10:2 FTS	-21	-47	-153	-132
	-100%	-100%	-99%	-95%
Σ_{28}PFAS	40,600	38,900	33,400	32,500
	2,240%	1,660%	620%	375%

Table C.7: PFAS concentrations in P1-P13 leachates (μg L^{-1}, max 3 s.f.) and % of Σ_{28}PFAS (max 2 s.f.).

	P1	P3	P4	P5	P6	P7	P8	P9	P10	P11	P12	P13
PFBS	0	0	2.7	0	1.9	0.12	3	0.145	8.35	0.525	0.445	0
	0%	0%	3%	0%	3%	0%	1%	0%	1%	0%	0%	0%
PFPeS	0	0	2.45	0	2.1	0.145	2.9	0.33	13.5	0.645	0.69	0
	0%	0%	3%	0%	3%	0%	1%	0%	1%	0%	0%	0%
PFHxS	0.28	0	17	0.43	14	1.3	23.5	6.55	155	6.7	11	1.75
	22%	0%	19%	15%	22%	2%	11%	9%	11%	5%	7%	3%
PFHpS	0	0	1.5	0	1.2	0.115	1.85	0.69	25	1.2	0.885	0.2
	0%	0%	2%	0%	2%	0%	1%	1%	2%	1%	1%	0%
PFOS	0.735	0.11	53	2.15	34.5	62.5	175	60	1,100	68	140	51
	57%	18%	60%	76%	55%	94%	81%	84%	81%	49%	87%	95%
PFDS	0	0	0	0	0	0.95	0.495	0.58	0.69	0	0.49	0.285
	0%	0%	0%	0%	0%	1%	0%	1%	0%	0%	0%	1%
PFBA	0	0	0.83	0	0.605	0	0.53	0	1.8	1.65	0.355	0
	0%	0%	1%	0%	1%	0%	0%	0%	0%	1%	0%	0%
PFPeA	0	0	1.35	0	0.965	0	0.93	0.24	3.65	7.2	0.825	0
	0%	0%	2%	0%	2%	0%	0%	0%	0%	5%	1%	0%
PFHxA	0	0.05	5.6	0.185	4.2	0.65	4.55	1.4	19.5	8.8	4.3	0.33
	0%	8%	6%	7%	7%	1%	2%	2%	1%	6%	3%	1%
PFHpA	0	0	0.68	0	0.645	0.115	0.67	0.29	3.8	1.8	0.39	0
	0%	0%	1%	0%	1%	0%	0%	0%	0%	1%	0%	0%
PFOA	0	0	1.6	0	1.05	0.595	2.25	0.825	13.5	2.8	1.25	0.22
	0%	0%	2%	0%	2%	1%	1%	1%	1%	2%	1%	0%
PFNA	0	0.435	0	0	0	0	0	0	0.775	0.71	0	0
	0%	73%	0%	0%	0%	0%	0%	0%	0%	1%	0%	0%
PFDA	0	0	0	0	0	0	0	0	0.425	0.105	0	0
	0%	0%	0%	0%	0%	0%	0%	0%	0%	0%	0%	0%
PFUnDA	0.28	0	0	0	0	0	0	0	0	0	0	0
	22%	0%	0%	0%	0%	0%	0%	0%	0%	0%	0%	0%
6:2 FTS	0	0	1.95	0.075	1.3	0	0.1	0	0.755	34.5	0	0
	0%	0%	2%	3%	2%	0%	0%	0%	0%	25%	0%	0%
8:2 FTS	0	0	0.275	0	0.24	0	0	0	8.9	3.15	0	0
	0%	0%	0%	0%	0%	0%	0%	0%	1%	2%	0%	0%
10:2 FTS	0	0	0	0	0	0	0	0	0	0	0	0
	0%	0%	0%	0%	0%	0%	0%	0%	0%	0%	0%	0%
PFOS+ PFHxS	1.02	0.11	70 .0	2.58	48.5	63.8	199	66.6	1,260	74.7	151	52.8
Σ_{28}PFAS	1.30	0.595	88.9	2.84	62.7	66.5	216	71.1	1,356	138	161	53.8

Table C.8: PFAS concentrations in P20 leachates ($\mu g\ L^{-1}$, max 3 s.f.) and % of Σ_{28}PFAS (max 2 s.f.).

	$P20_{10}$	$P20_{33}$	$P20_{180}$	$P20_{400}$
PFBS	0	0.1	0.125	0.13
	0%	0%	0%	0%
PFPeS	0	0.05	0	0.135
	0%	0%	0%	0%
PFHxS	0.605	0.755	0.695	1.25
	1%	1%	0%	0%
PFHpS	0	0.055	0	0
	0%	0%	0%	0%
PFOS	2.25	4.85	2.2	2.5
	3%	4%	1%	1%
PFDS	0	0	0	0
	0%	0%	0%	0%
PFBA	0	0	0.785	1.2
	0%	0%	0%	0%
PFPeA	0	0.275	0.73	1.15
	0%	0%	0%	0%
PFHxA	3.6	3.8	7.15	6.5
	4%	3%	2%	1%
PFHpA	0.115	0.165	0.36	0.37
	0%	0%	0%	0%
PFOA	1.35	1.65	2.9	2.7
	2%	1%	1%	1%
PFDA	0	0.1	0.13	0
	0%	0%	0%	0%
4:2 FTS	0	0.125	0.33	0.53
	0%	0%	0%	0%
6:2 FTS	70.5	105	255	415
	88%	78%	87%	91%
8:2 FTS	1.3	15	22	23
	2%	11%	8%	5%
10:2 FTS	0.355	2.05	0.75	0.36
	0%	2%	0%	0%
PFOS+PFHxS	2.86	5.61	2.90	3.75
Σ_{28}PFAS	80.1	134	293	455

Table C.9: Suitability of soils for landfill disposal based on landfill acceptance criteria [2] including leachable concentration (Guideline 1) and soil concentration (Guideline 2).

Landfill type	PFAS	Guideline 1 conc. ($\mu g\ L^{-1}$)	Guideline 2 conc. ($mg\ kg^{-1}$)	Soils failing G1	Soils failing G2	Soils passing all
Unlined	PFOA	0.56	50	P4, P6-P12, P20	-	(P1, P3, P5, P13)
	PFOS+ PFHxS	0.07	20	P1-13, P20	-	-
Clay/single composite lined	PFOA	5.6	50	P10	-	(P1-9, P11-13, P20)
	PFOS+ PFHxS	0.7	50	P1, P4-P13, P20	-	**P3**
Double composite lined	PFOA	56	50	-	-	(P1-13, P20)
	PFOS+ PFHxS	7	50	P4, P6-13,	-	**P1, P3, P5, P20**

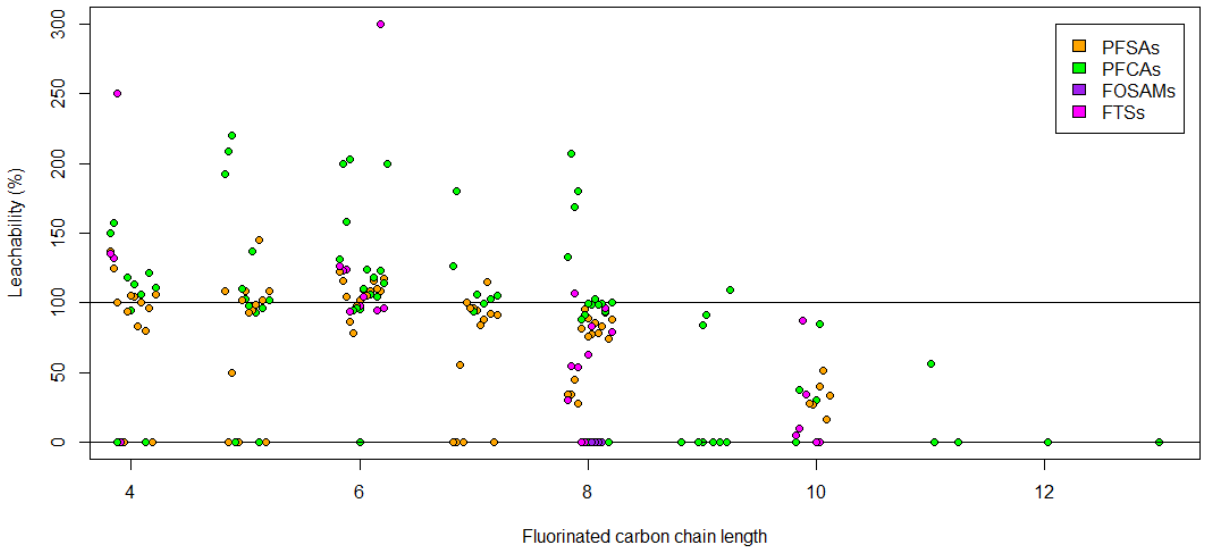


Figure C.1: PFAS leachability vs fluorinated carbon chain length. Points shown at zero had detectable PFAS concentrations in the soil but not in the leachate.

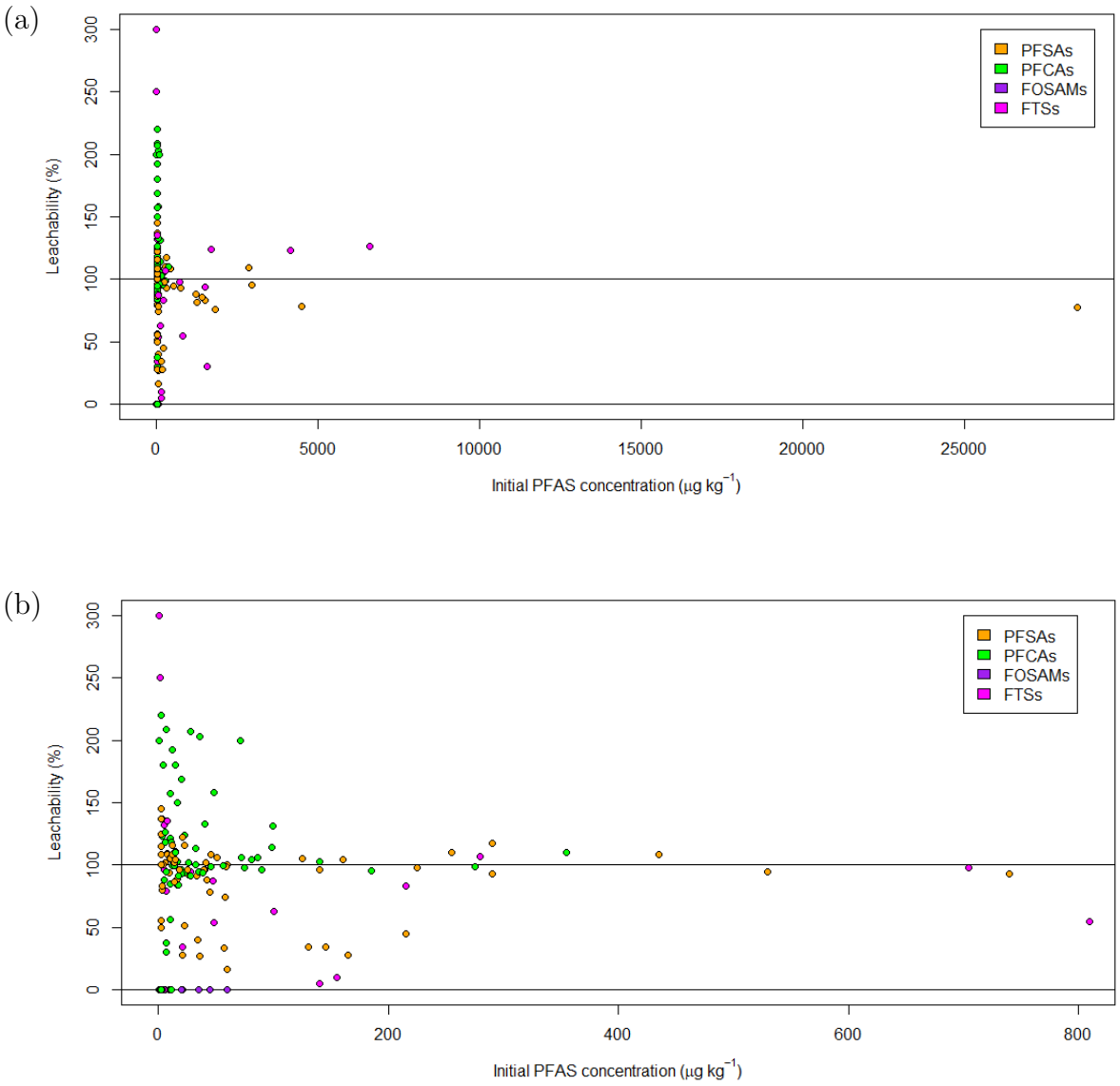


Figure C.2: PFAS leachability vs initial concentration (a) all soils (b) soils with lower initial concentrations. Points shown at zero had detectable PFAS concentrations in the soil but not in the leachate. Higher ($> 150\%$) leachability values are observed at lower concentrations, which may be reflective of variability in concentrations closer to the limits of quantification along with impacts of adjustments for dilution factors.

Table C.10: PFAS concentrations in P1-13 post-TOPA leachates (μg L^{-1}, max 3 s.f.) and % of Σ_{28}PFAS (max 2 s.f.).

	P1	P3	P4	P5	P6	P7	P8	P9	P10	P11	P12	P13
PFBS	0	0	2.7	0	1.9	0.16	3	0.15	8.4	0.535	0.475	0.01
	0%	0%	3%	0%	3%	0%	2%	0%	1%	0%	0%	0%
PFPeS	0	0	2.45	0	2.15	0.165	2.95	0.31	13.5	0.68	0.72	0
	0%	0%	2%	0%	3%	0%	1%	0%	1%	0%	0%	0%
PFHxS	0.31	0	19	0.41	14.5	1.35	23.5	7.4	150	8.5	11.5	2.5
	22%	0%	18%	15%	22%	2%	12%	9%	10%	6%	7%	3%
PFHpS	0	0	1.45	0	1.25	0.125	1.9	0.69	24	1.035	0.86	0.17
	0%	0%	1%	0%	2%	0%	1%	1%	2%	1%	1%	0%
PFOS	0.68	0	45	1.8	29	53	140	51	965	56	115	42.5
	48%	0%	43%	66%	45%	84%	71%	63%	67%	41%	72%	58%
PFDS	0	0	0	0	0	0.71	0.385	0.49	0.73	0	0.34	0.11
	0%	0%	0%	0%	0%	1%	0%	1%	0%	0%	0%	0%
PFBA	0	0	3.95	0	2.25	0.78	3.1	1.05	41	11	2.4	1.55
	0%	0%	4%	0%	3%	1%	2%	1%	3%	8%	2%	2%
PFPeA	0	0.29	4	0.105	2.35	0.905	3.25	1.75	44	22.5	3.6	2.65
	0%	32%	4%	4%	4%	1%	2%	2%	3%	16%	2%	4%
PFHxA	0.215	0.18	22	0.43	9.4	3.35	14.5	16	165	28.5	21	22.5
	15%	20%	21%	16%	15%	5%	7%	20%	11%	21%	13%	31%
PFHpA	0	0.055	1.04	0	0.705	0.415	1.25	0.62	10	3.9	1.1	0.42
	0%	6%	1%	0%	1%	1%	1%	1%	1%	3%	1%	1%
PFOA	0	0	2.15	0	1.25	2.1	3.95	1.45	19.5	4.15	2.55	1.05
	0%	0%	2%	0%	2%	3%	2%	2%	1%	3%	2%	1%
PFNA	0	0.37	0	0	0	0	0	0	1.1	0.64	0.105	0.06
	0%	41%	0%	0%	0%	0%	0%	0%	0%	0%	0%	0%
PFDA	0	0	0	0	0	0	0	0	0.665	0	0	0
	0%	0%	0%	0%	0%	0%	0%	0%	0%	0%	0%	0%
PFUnDA	0.225	0	0	0	0	0	0	0	0	0	0	0
	16%	0%	0%	0%	0%	0%	0%	0%	0%	0%	0%	0%
PFDoDA	0	0	0	0	0	0	0	0	0	0	0	0
	0%	0%	0%	0%	0%	0%	0%	0%	0%	0%	0%	0%
6:2 FTS	0	0	0	0	0	0	0	0	0	0	0	0
	0%	0%	0%	0%	0%	0%	0%	0%	0%	0%	0%	0%
Σ_{28}PFAS	1.43	0.895	104	2.75	64.8	63.1	198	80.9	1,440	137	160	73.5

Table C.11: PFAS concentrations in P20 post-TOPA leachates (μg L^{-1}, max 3 s.f.) and % of Σ_{28}PFAS (max 2 s.f.).

	$P20_{10}$	$P20_{33}$	$P20_{180}$	$P20_{400}$
PFBS	0.19	0.06	0	0
	0%	0%	0%	0%
PFPeS	0.285	0.18	0.135	0
	0%	0%	0%	0%
PFHxS	2.25	1.2	1.05	1.25
	0%	0%	0%	0%
PFHpS	0	0	0	0
	0%	0%	0%	0%
PFOS	1.8	3.95	1.6	1.05
	0%	0%	0%	0%
PFDS	0	0	0	0
	0%	0%	0%	0%
PFBA	460	540	400	475
	26%	25%	24%	25%
PFPeA	800	895	685	905
	45%	41%	42%	48%
PFHxA	400	530	395	360
	23%	25%	24%	19%
PFHpA	65.5	110	93	96.5
	4%	5%	6%	5%
PFOA	23	53.5	49	38.5
	1%	2%	3%	2%
PFNA	3.95	9.35	5.75	4.75
	0%	0%	0%	0%
PFDA	2.75	9.05	3.75	1.55
	0%	0%	0%	0%
PFUnDA	0.825	2.3	0.985	0
	0%	0%	0%	0%
PFDoDA	0.655	2.05	0.83	0
	0%	0%	0%	0%
6:2 FTS	0.3	0.135	0.29	1.35
	0%	0%	0%	0%
Σ_{28}PFAS	1,760	2,160	1,640	1,880

Table C.12: Changes in PFAS concentrations in leachate with application of the TOP assay. First row is raw difference in concentration (μg L^{-1}, max 3 s.f.), alternate rows are percentage change (%, max 3 s.f.). * denotes the PFAS was not present in the initial sample, blank that the PFAS was not present in either sample.

	P1	P3	P4	P5	P6	P7	P8	P9	P10	P11	P12	P13
PFBS	0	0	0	0	0	0.04	0	0.005	0.05	0.01	0.03	0.01
			0%		0%	33%	0%	3%	1%	2%	7%	*
PFPeS	0	0	0	0	0.05	0.02	0.05	-0.02	0	0.035	0.03	0
			0%		2%	14%	2%	-6%	0%	5%	4%	
PFHxS	0.03	0	2	-0.02	0.5	0.05	0	0.85	-5	1.8	0.5	0.75
	11%		12%	-5%	4%	4%	0%	13%	-3%	27%	5%	43%
PFHpS	0	0	-0.05	0	0.05	0.01	0.05	0	-1	-0.165	-0.025	-0.03
			-3%		4%	9%	3%	0%	-4%	-14%	-3 %	-15%
PFOS	-0.055	-0.11	-8	-0.35	-5.5	-9.5	-35	-9	-135	-12	-25	-8.5
	-7%	-100%	-15%	-16%	-16%	-15%	-20%	-15%	-12%	-18%	-18%	-17%
PFDS	0	0	0	0	0	-0.24	-0.11	-0.09	0.04	0	-0.15	-0.175
						-25%	-22%	-16%	6%		-31%	-61%
PFBA	0	0	3.12	0	1.65	0.78	2.57	1.05	39.2	9.35	2.05	1.55
			376%		272%	*	485%	*	2,180%	567%	576%	*
PFPeA	0	0.29	2.65	0.105	1.39	0.905	2.32	1.51	40.4	15.3	2.78	2.65
		*	196%	*	144%	*	249%	629%	1,110%	213%	336%	*
PFHxA	0.215	0.13	16.4	0.245	5.2	2.7	9.95	14.6	146	19.7	16.7	22.2
	*	260%	293%	132%	124%	415%	219%	1,040%	746%	224%	388%	6720%
PFHpA	0	0.055	0.36	0	0.06	0.3	0.58	0.33	6.2	2.1	0.71	0.42
		*	53%		9%	261%	87%	114%	163%	117	182	*
PFOA	0	0	0.55	0	0.2	1.51	1.7	0.625	6	1.35	1.3	0.83
			34%		19%	253%	76%	76%	44%	48%	104%	377%
PFNA	0	-0.065	0	0	0	0	0	0	0.325	-0.07	0.105	0.06
		-15%							42%	-10 %	*	*
PFDA	0	0	0	0	0	0	0	0	0.24	-0.105	0	0
									56%	-100%		
PFUnDA	-0.055	0	0	0	0	0	0	0	0	0	0	0
	-20%											
PFDoDA	0	0	0	0	0	0	0	0	0	0	0	0
4:2 FTS	0	0	0	0	0	0	0	0	0	0	0	0
6:2 FTS	0	0	-1.95	-0.075	-1.3	0	-0.1	0	-0.755	-34.5	0	0
			-100%	-100%	-100%		-100%		-100%	-100%		
8:2 FTS	0	0	-0.275	0	-0.24	0	0	0	-8.9	-3.15	0	0
			-100%		-100%				-100%	-100%		
10:2 FTS	0	0	0	0	0	0	0	0	0	0	0	0
Total	0.135	0.3	14.8	-0.095	2.05	-3.43	-18.0	9.86	87.25	-0.345	-0.98	19.7
	10.4%	50.4 %	16.6%	-3.3%	3.3%	-5.2%	-8.3%	13.9%	6.4%	-0.3%	-0.6%	36.7%

Table C.13: Changes in PFAS concentrations in leachate with application of the TOP assay for P20 samples.

	$P20_{10}$	$P20_{33}$	$P20_{180}$	$P20_{400}$
PFBS	0.19	-0.04	-0.125	-0.13
	*	-40%	-100%	-100%
PFPeS	0.285	0.13	0.135	-0.135
	*	260%	*	-100%
PFHxS	1.645	0.445	0.355	0
	272%	59%	51%	0%
PFHpS	0	-0.055	0	0
		-100%		
PFOS	-0.45	-0.9	-0.6	-1.45
	-20%	-19%	-27%	-58%
PFDS	0	0	0	0
PFBA	460	540	399	474
	*	*	50,900%	39,500%
PFPeA	800	895	684	904
	*	325,000%	93,700%	78,600%
PFHxA	396	526	388	354
	11,000%	13,800%	5,420%	5,440%
PFHpA	65.4	110	92.6	96.1
	56,900%	66,600%	25,700%	26,000%
PFOA	21.7	51.9	46.1	35.8
	1,600%	3,140%	1,590%	1,330%
PFNA	3.95	9.35	5.75	4.75
	*	*	*	*
PFDA	2.75	8.95	3.62	1.55
	*	8,950%	2,790%	*
PFUnDA	0.825	2.3	0.985	0
	*	*	*	
PFDoDA	0.655	2.05	0.83	0
	*	*	*	
4:2 FTS	0	-0.125	-0.33	-0.53
		-100%	-100%	-100%
6:2 FTS	-70.2	-105	-255	-414
	-100%	-100%	-100%	-100%
8:2 FTS	-1.3	-15	-22	-23
	-100%	-100%	-100%	-100%
10:2 FTS	-0.355	-2.05	-0.75	-0.36
	-100%	-100%	-100%	-100%
Total	1,680	2,020	1,340	1,430
	2,100%	1,510%	458%	314%

Appendix D

Supplementary information for Chapter 7

Table D.1: PFAS level of reporting (LOR) for liquid and solid matrices, grouped into perfluoroalkyl sulfonic acids (PFSAs), perfluoroalkyl carboxylic acids (PFCAs), perfluorooctane sulfonamide-based substances (FOSAMs) and fluorotelomer sulfonic acids (FTSAs).

Chemical name	Abbreviation	CAS No.	Family	Fluor. C Tail Length	LOR (µg L^{-1})	LOR (µg kg^{-1})
Perfluorobutane sulfonic acid	PFBS	375-73-5	PFSAs	C_4	0.02	0.1
Perfluoropentane sulfonic acid	PFPeS	2706-91-4		C_5	0.02	0.1
Perfluorohexane sulfonic acid	PFHxS	355-46-4		C_6	0.02	0.1
Perfluoroheptane sulfonic acid	PFHpS	375-92-8		C_7	0.02	0.1
Perfluorooctane sulfonic acid	PFOS	1763-23-1		C_8	0.01	0.1
Perfluorodecane sulfonic acid	PFDS	335-77-3		C_{10}	0.02	0.2
Perfluorobutanoic acid	PFBA	375-22-4	PFCAs	C_4	0.1	0.2
Perfluoropentanoic acid	PFPeA	2706-90-3		C_5	0.02	0.2
Perfluorohexanoic acid	PFHxA	307-24-4		C_6	0.02	0.1
Perfluoroheptanoic acid	PFHpA	375-85-9		C_7	0.02	0.1
Perfluorooctanoic acid	PFOA	335-67-1		C_8	0.01	0.1
Perfluorononanoic acid	PFNA	375-95-1		C_9	0.02	0.1
Perfluorodecanoic acid	PFDA	335-76-2		C_{10}	0.02	0.5
Perfluoroundecanoic acid	PFUnDA	2058-94-8		C_{11}	0.02	0.5
Perfluorododecanoic acid	PFDoDA	307-55-1		C_{12}	0.02	0.5
Perfluorotridecanoic acid	PFTrDA	72629-94-8		C_{13}	0.02	0.5
Perfluorotetradecanoic acid	PFTeDA	376-06-7		C_{14}	0.05	5
Perfluorooctane sulfonamide	PFOSA	754-91-6	FOSAMs	C_8	0.02	1
N-Methyl perfluorooctane sulfonamide	MeFOSA	31506-32-8		C_8	0.05	1
N-Ethyl perfluorooctane sulfonamide	EtFOSA	4151-50-2		C_8	0.05	1
N-Methyl perfluorooctane sulfonamidoethanol	MeFOSE	24448-09-7		C_8	0.05	1
N-Ethyl perfluorooctane sulfonamidoethanol	EtFOSE	1691-99-2		C_8	0.05	5
N-Methyl perfluorooctane sulfonamidoacetic acid	MeFOSAA	2355-31-9		C_8	0.02	0.2
N-Ethyl perfluorooctane sulfonamidoacetic acid	EtFOSAA	2991-50-6		C_8	0.02	0.2
4:2 Fluorotelomer sulfonic acid	4:2FTS	757124-72-4	FTSAs	C_4	0.05	0.1
6:2 Fluorotelomer sulfonic acid	6:2FTS	27619-97-2		C_6	0.05	0.1
8:2 Fluorotelomer sulfonic acid	8:2FTS	39108-34-4		C_8	0.05	0.1
10:2 Fluorotelomer sulfonic acid	10:2FTS	120226-60-0		C_{10}	0.05	0.1

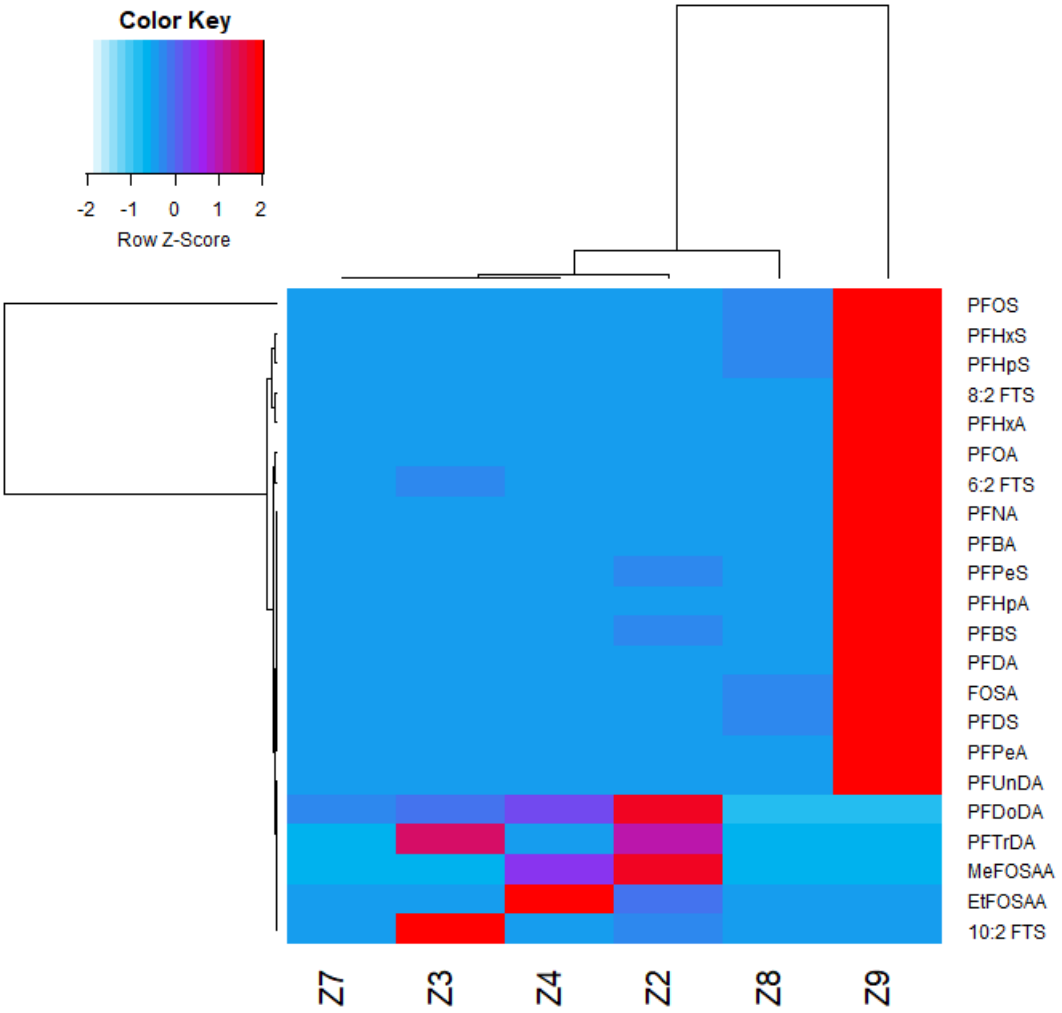


Figure D.1: Heat map of PFAS concentrations across soils Z2-Z4 and Z7-Z9 in the <2 mm soil fraction, normalised per PFAS. Colour scale indicates row-normalised concentration Z-score.

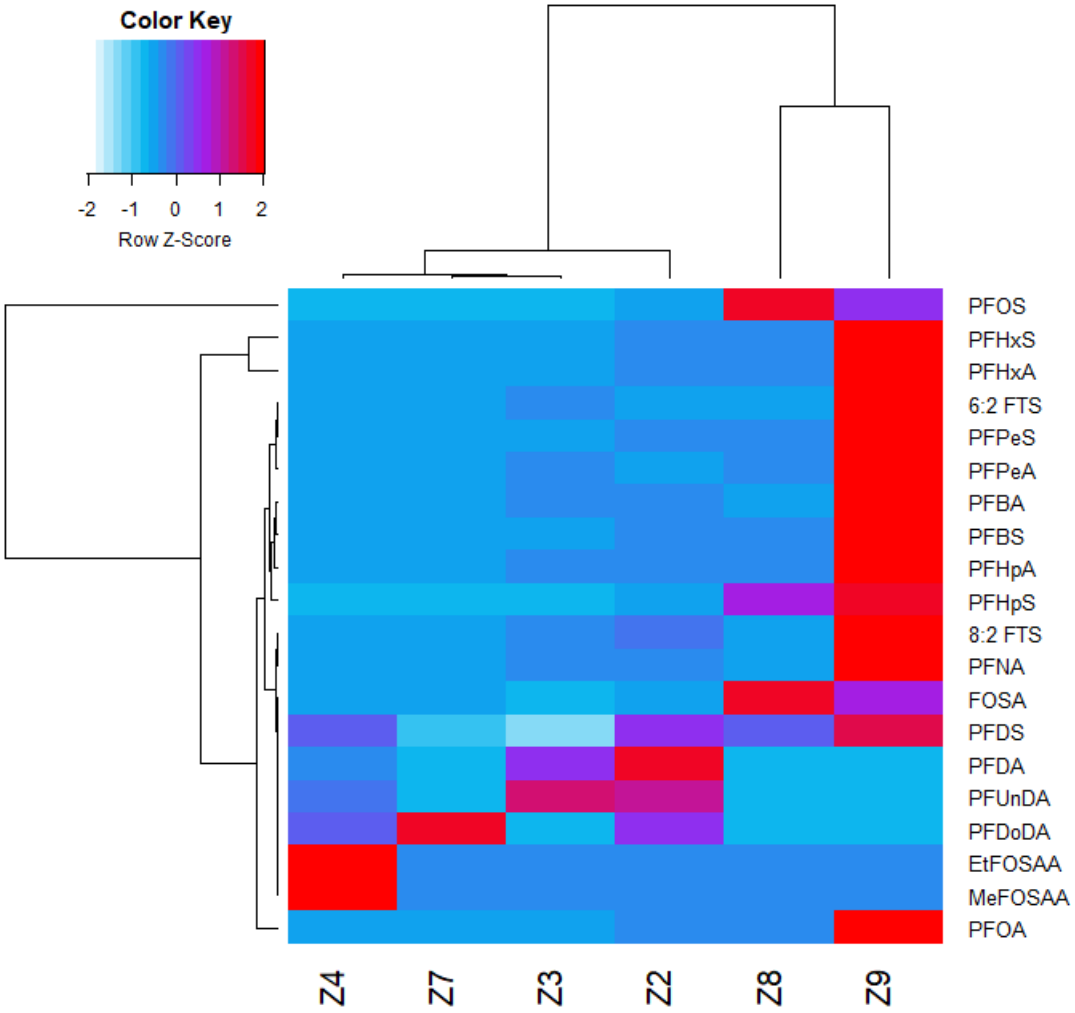


Figure D.2: Heat map of PFAS concentrations across soils Z2-Z4, and Z7-Z9 in leachable fraction, normalised per PFAS. Colour scale indicates row-normalised concentration Z-score.

Table D.2: RB100 PFAS immobilisation efficacy at an application of 1% w/w. Where leachate values were <LOR, an immobilisation range was calculated using leachate values of 0 and LOR.

PFAS	Z2	Z3	Z4
PFBS	94.8	96.5-100	96.3-100
PFPeS	97.1	96.9-98.4	97.4-98.7
PFHxS	95.8	95.0	97.9
PFHpS	82.1	86.2	98.4
PFOS	81.1	69.6	85.4
PFDS	60.1	46.8	81.5
PFBA	87.5	77.1	60.0-100
PFPeA	94.3	98.0	99.1
PFHxA	95.8	97.9	98.9
PFHpA	95.3	96.3	96.2-100
PFOA	92.6	88.3	98.2
PFNA	88.6	81.8	81.8-100
PFDA	70.1	60.4	78.9-100
PFUnDA	-40.0-(-16.7)	18.2	20.0-100
PFDoDA	20.0-33.3		0-100
FOSA	64.0	66.7	93.0
MeFOSAA			33.3-100
EtFOSAA			42.9-100
6:2 FTS	91.5-100	93.3	
8:2 FTS	68.6	54.0	71.4-100

Table D.3: RB300 PFAS immobilisation efficacy at an application of 1% w/w.

PFAS	Z2	Z3	Z4	Z7
PFBS	96.4	96.5-100	96.3-100	
PFPeS	98.1	96.9-100	97.4-100	33.3-100
PFHxS	97.5	96.4	98.6	98.2-100
PFHpS	94.4	96.5	98.4-100	81.8-100
PFOS	88.4	83.5	96.6	99.4
PFDS	75.1	66.0	90.4	96.3-100
PFBA	87.5	94.3-100	60.0-100	
PFPeA	94.9	97.7	98.2-100	
PFHxA	96.0	98.1	98.4	82.6-100
PFHpA	96.8	98.1	96.2-100	20.0-100
PFOA	95.9	96.2	99.1	87.5-100
PFNA	94.9	92.0	81.8-100	
PFDA	84.5	79.2	78.9-100	
PFUnDA	50.0	45.5	20.0-100	
PFDoDA	20.0-100		0.0-100	33.3-100
FOSA	82.0	33.3-100	97.5-100	98.0-100
MeFOSAA			33.3-100	
EtFOSAA			42.9-100	
6:2 FTS	91.5-100	96.3		
8:2 FTS	86.9	81.0	71.4-100	

Table D.4: RB100 PFAS immobilisation efficacy at an application of 2.5% w/w.

PFAS	Z2	Z3	Z4	Z7
PFBS	97.3	96.5-100	96.3-98.1	
PFPeS	98.4	96.9-100	97.4-100	33.3-100
PFHxS	98.0	98.9	98.7	96.8
PFHpS	96.9	98.6-99.3	98.4-100	81.8-100
PFOS	96.0	95.6	98.7	99.5
PFDS	86.8	76.6	96.9-97.7	96.3-100
PFBA	93.8-100	94.3-97.1	60-100	
PFPeA	97.7	99.5	97.8-98.7	
PFHxA	97.8	99.3	98.8	82.6-100
PFHpA	97.4	99.1-100	96.2-100	20-100
PFOA	96.8	98.2	97.4	87.5-100
PFNA	96.6-97.7	97.7-98.9	81.8-100	
PFDA	92.8	91.7-100	78.9-100	
PFUnDA	50.0-40.0	63.6-100	20-100	
PFDoDA	20.0-100		0-100	33.3-100
FOSA	90.7	33.3-100	97.5-100	98.0-100
MeFOSAA			33.3-100	
EtFOSAA			42.9-100	
6:2 FTS	91.5-100	98.9		
8:2 FTS	92.7	93.9	71.4-100	

Table D.5: RB300 PFAS immobilisation efficacy at an application of 2.5% w/w.

PFAS	Z2	Z3	Z4	Z7
PFBS	99.1	96.5-100	96.3-100	
PFPeS	99.5	96.9-100	97.4-100	33.3-100
PFHxS	99.4	99.3	99.4	98.2-100
PFHpS	99.5	98.6-100	98.4-100	81.8-100
PFOS	99.0	98.0	99.4	99.6
PFDS	97.3	78.7	98.5-100	96.3-100
PFBA	93.8-100	94.3-100	60.0-100	
PFPeA	99.2	99.6	98.2-100	
PFHxA	99.2	99.6	99.6	82.6-100
PFHpA	99.2	99.1-100	96.2-100	20-100
PFOA	99.1	99.3	99.1-100	87.5-100
PFNA	97.7-100	97.7-100	81.8-100	
PFDA	95.9-100	91.7-100	78.9-100	
PFUnDA	66.7-100	63.6-100	20.0-100	
PFDoDA	20.0-100		0-100	33.3-100
FOSA	94.7-96.0	33.3-100	97.5-100	98-100
MeFOSAA			33.3-100	
EtFOSAA			42.9-100	
6:2 FTS	91.5-100	99.2		
8:2 FTS	98.9	97.7-98.5	71.4-100	

Table D.6: RB100 PFAS immobilisation efficacy at an application of 5% w/w.

	Z2	Z3	Z4	Z7	Z9
PFBS	99.2	96.5-100	96.3-100		97.6
PFPeS	99.5	96.9-100	97.4-100	33.3-100	98.9
PFHxS	99.3	99.6	99.3	96.8	96.7
PFHpS	99.2	98.6-100	98.4-100	81.8-100	58.9
PFOS	98.9	98.6	99.1	99.5	47.2
PFDS	96.7	91.5-100	98.5-100	96.3-100	37.0
PFBA	93.8-100	94.3-100	60-100		81.0
PFPeA	99.5	99.8-100	98.2-100		93.5
PFHxA	99.2	99.7-99.8	99.2-99.4	82.6-100	97.6
PFHpA	99.3-99.6	99.1-100	96.2-100	20.0-100	98.8
PFOA	98.9	99.3	98.7	87.5-93.8	92.4
PFNA	97.7-100	97.7-100	81.8-100		32.2
PFDA	95.9-100	91.7-100	78.9-100		-2950-0
PFUnDA	66.7-100	63.6-100	20.0-100		
PFDoDA	20.0-100		0-100	33.3-100	
FOSA	94.0	33.3-100	97.5-100	98-100	51.6
MeFOSAA			33.3-100		
EtFOSAA			42.9-100		
6:2 FTS	91.5-100	99.4			92.7
8:2 FTS	98.6-98.9	98.3	71.4-100		-28.7

Table D.7: RB300 PFAS immobilisation efficacy at an application of 5% w/w.

	Z2	Z3	Z4	Z7	Z9
PFBS	99.7	96.5-100	96.3-100	0.0	99.3
PFPeS	99.8	96.9-100	97.4-100	33.3-100	99.5
PFHxS	99.7	99.6	99.7-99.8	98.2-100	99.3
PFHpS	99.8	98.6-100	98.4-100	81.8-100	86.2
PFOS	99.6	99.2	99.8	99.7	80.6
PFDS	98.8-100	91.5-100	98.5-100	96.3-100	56.5-100
PFBA	93.8-100	94.3-100	60.0-100		87.0
PFPeA	99.5-100	99.8-99.9	98.2-100		97.5
PFHxA	99.7	99.8-100	99.6-100	82.6-100	98.9
PFHpA	99.4-100	99.1-100	96.2-100	20-100	99.4
PFOA	99.6	99.5-100	99.1-100	87.5-100	98.7
PFNA	97.7-100	97.7-100	81.8-100		70.4
PFDA	95.9-100	91.7-100	78.9-100		
PFUnDA	66.7-100	63.6-100	20-100		
PFDoDA	20-100		0-100	33.3-100	
FOSA	97.3-100	33.3-100	97.5-100	98-100	90.0
MeFOSAA			33.3-100		
EtFOSAA			42.9-100		
6:2 FTS	91.5-100	99.6			99.6
8:2 FTS	99.3-100	98.3-100	71.4-100		21.9

Table D.8: RB100 PFAS immobilisation efficacy at an application of 10% w/w.

	Z2	Z3	Z4	Z9
PFBS	99.7-99.9	96.5-100	96.3-100	99.5
PFPeS	99.8	96.9-100	97.4-100	99.7
PFHxS	99.7	99.7	99.7	99.3
PFHpS	99.6	98.6-100	98.4-100	86.6
PFOS	99.3	98.8	99.3	81.0
PFDS	98.5-99.1	91.5-100	98.5-100	99.1-100
PFBA	93.8-100	94.3-100	60-100	92.7
PFPeA	99.5-100	99.8-100	98.2-100	98.6
PFHxA	99.7	99.8-100	99.4-99.6	99.4
PFHpA	99.4-100	99.1-100	96.2-100	99.7
PFOA	99.6	99.3-99.5	99.1-100	98.9
PFNA	97.7-100	97.7-100	81.8-100	73.2
PFDA	95.9-100	91.7-100	78.9-100	-2450-0
PFUnDA	66.7-100	63.6-100	20-100	
PFDoDA	20.0-100		0-100	
FOSA	94.7-96	33.3-100	97.5-100	80.6
MeFOSAA			33.3-100	
EtFOSAA			42.9-100	
6:2 FTS	91.5-100	99.5		99.1
8:2 FTS	98.6-99	98.2-99	71.4-100	-9.4

Table D.9: RB300 PFAS immobilisation efficacy at an application of 10% w/w.

	Z2	Z3	Z4	Z9
PFBS	99.7-100	96.5-100	96.3-100	100
PFPeS	99.9-100	96.9-100	97.4-100	100
PFHxS	99.9	99.7-100	99.8-100	99.9
PFHpS	99.9-100	98.6-100	98.4-100	98.4
PFOS	99.9	99.8	100	95.1
PFDS	98.8-100	91.5-100	98.5-100	56.5-100
PFBA	93.8-100	94.3-100	60.0-100	98.3-98.3
PFPeA	99.5-100	99.8-100	98.2-100	99.6
PFHxA	99.9	99.8-100	99.6-100	99.8
PFHpA	99.4-100	99.1-100	96.2-100	100
PFOA	99.9-100	99.5-100	99.1-100	99.8
PFNA	97.7-100	97.7-100	81.8-100	97.6-97.6
PFDA	95.9-100	91.7-100	78.9-100	
PFUnDA	66.7-100	63.6-100	20-100	
PFDoDA	20-100		0-100	
FOSA	97.3-100	33.3-100	97.5-100	94.3-100
MeFOSAA			33.3-100	
EtFOSAA			42.9-100	
6:2 FTS	91.5-100	99.8-100		99.8-100
8:2 FTS	99.3-100	98.3-100	71.4-100	68.9

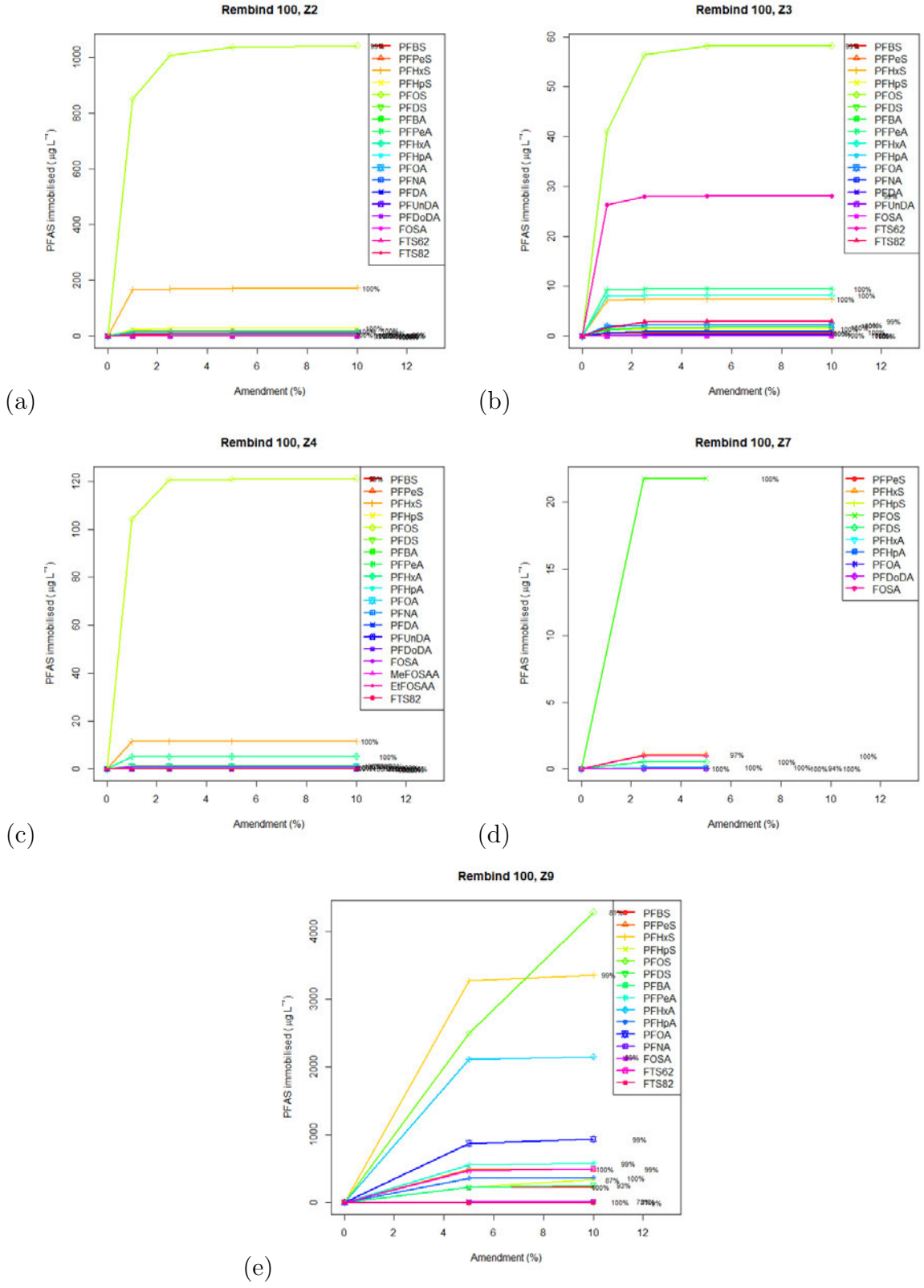


Figure D.3: Leachable PFAS reduction (µg L^{-1}) in (a) Z2 (b) Z3 (c) Z4 (d) Z7 and (e) Z9 soil amended with RB100. Points indicate experimental data, connecting lines for visualisation purposes only.

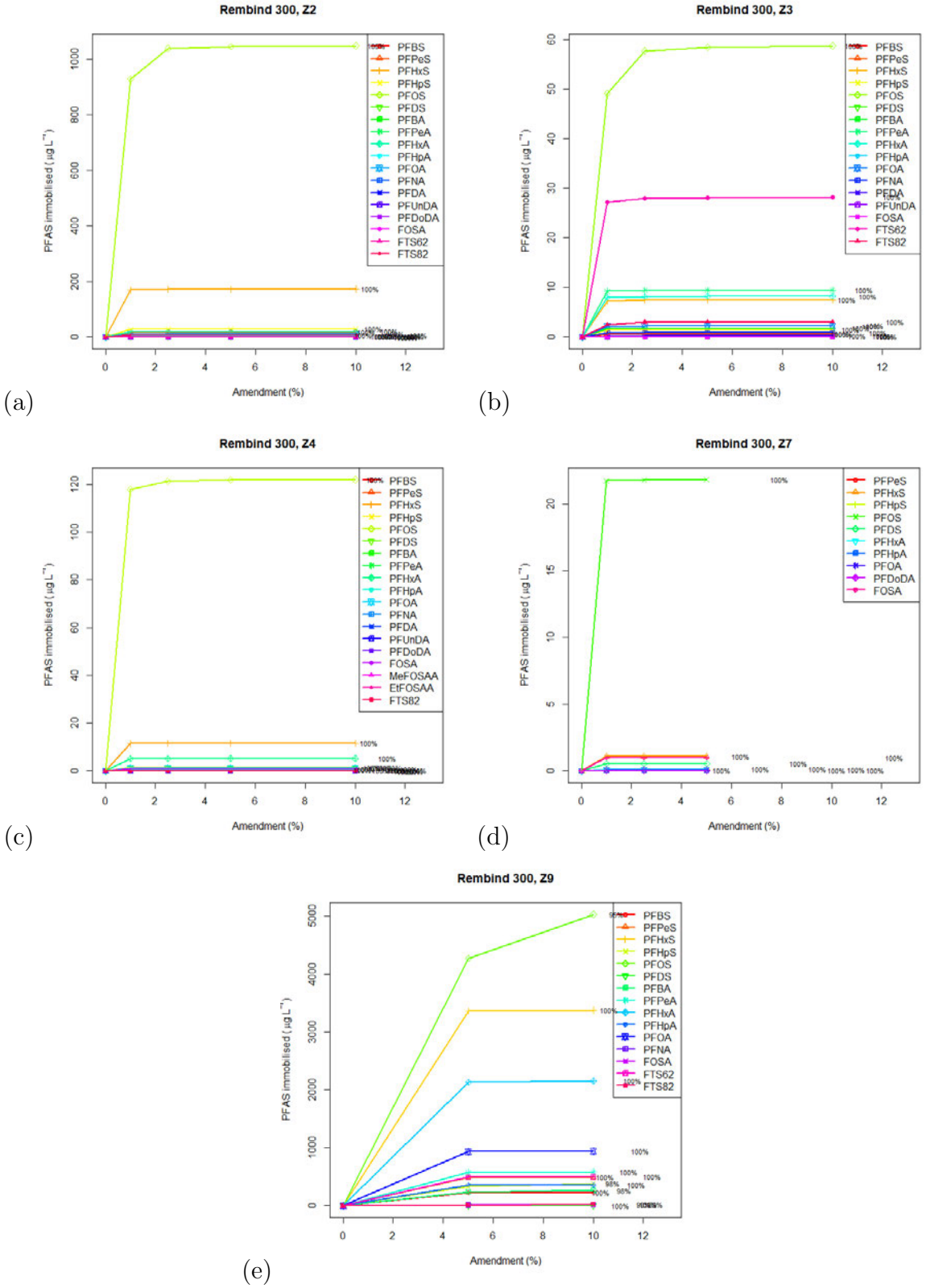


Figure D.4: Leachable PFAS reduction (µg L^{-1}) in (a) Z2 (b) Z3 (c) Z4 (d) Z7 and (e) Z9 soil amended with RB300. Points indicate experimental data, connecting lines for visualisation purposes only.

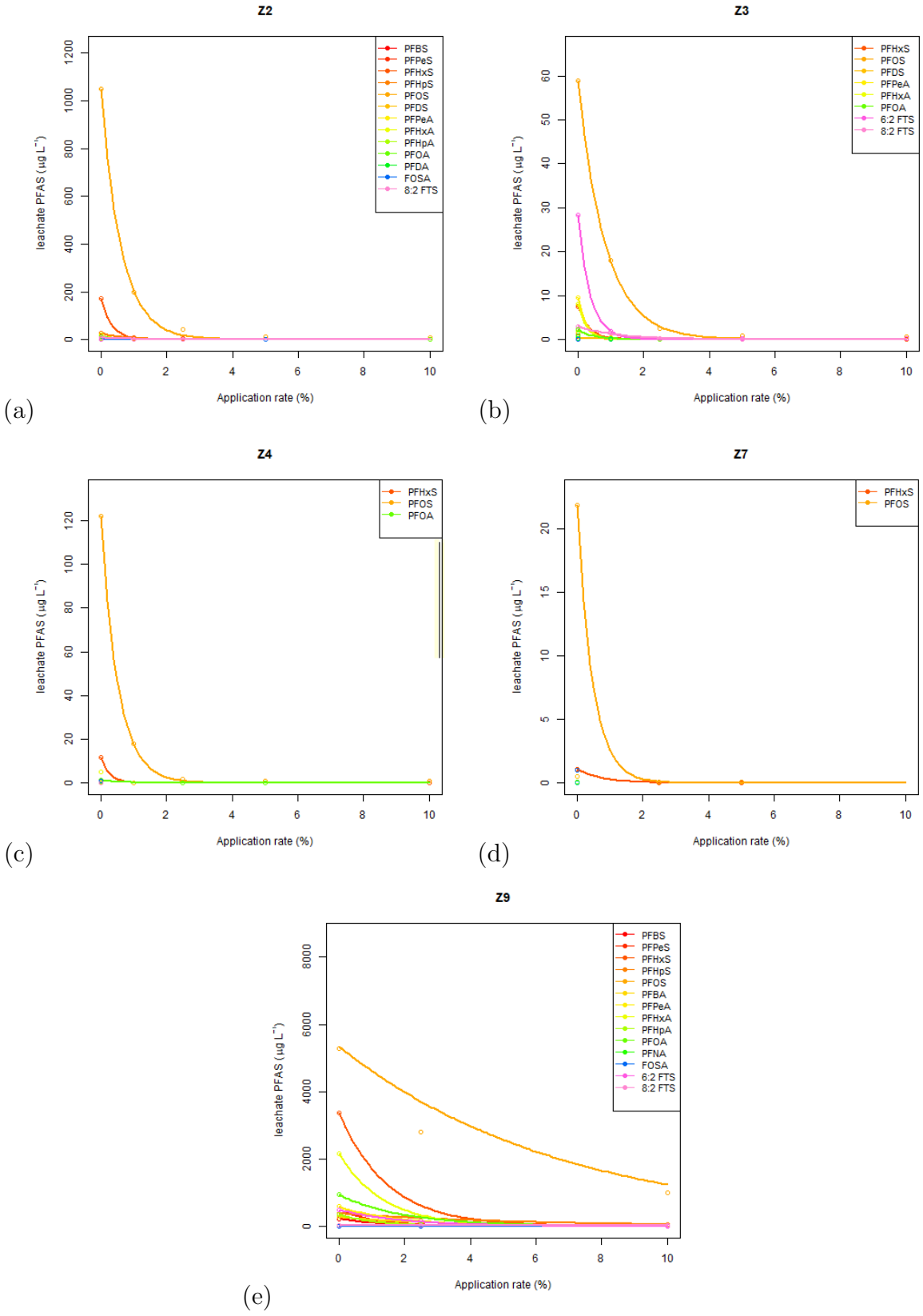


Figure D.5: PFAS concentration in leachable fraction following immobilisation with RB 100: (a) Z2, (b) Z3, (c) Z4, (d) Z7, (e) Z9. Points indicate experimental data and coloured lines the fitted model.

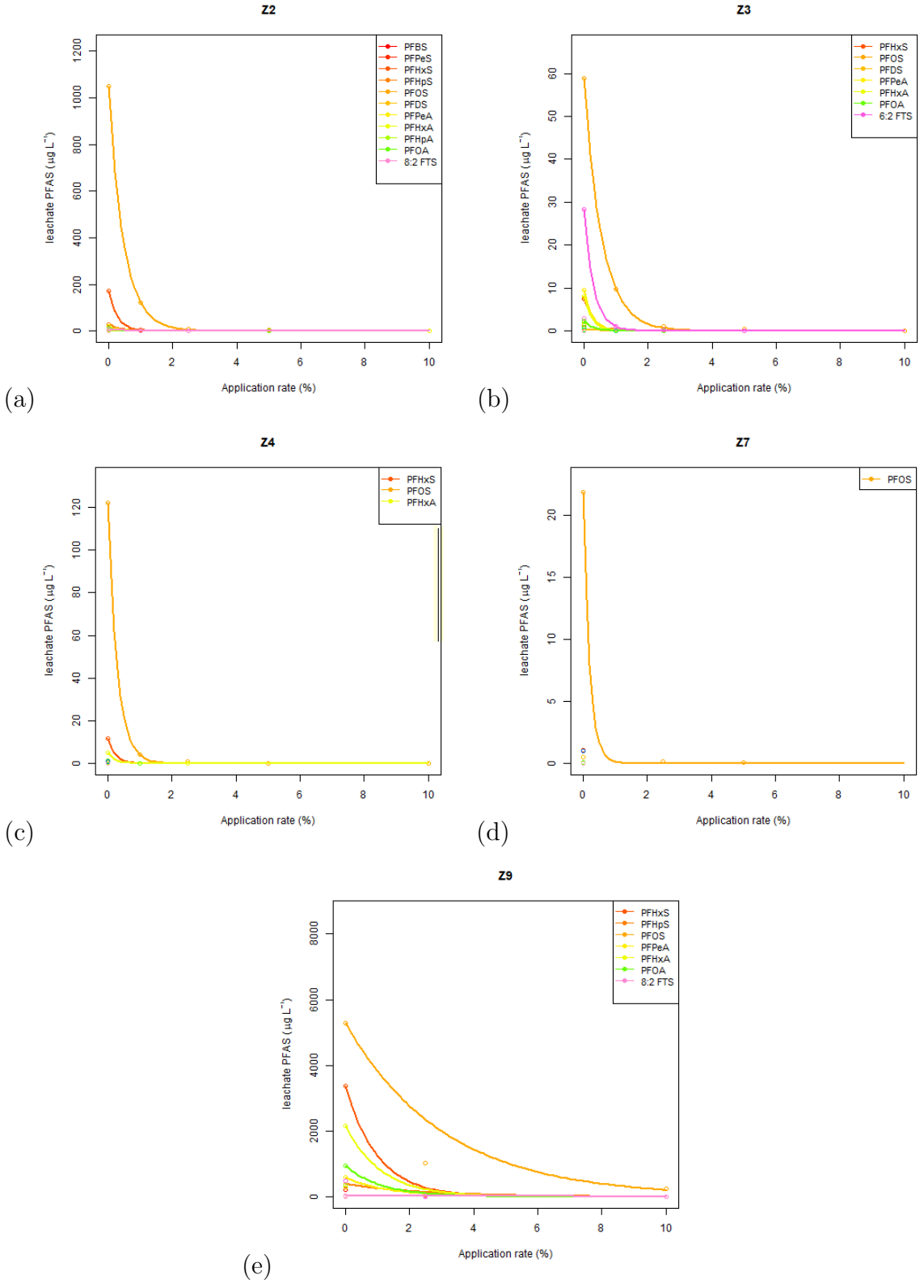


Figure D.6: PFAS concentration in leachable fraction following immobilisation with RemBind 300: (a) Z2, (b) Z3, (c) Z4, (d) Z7, (e) Z9. Points indicate experimental data and coloured lines the fitted model.

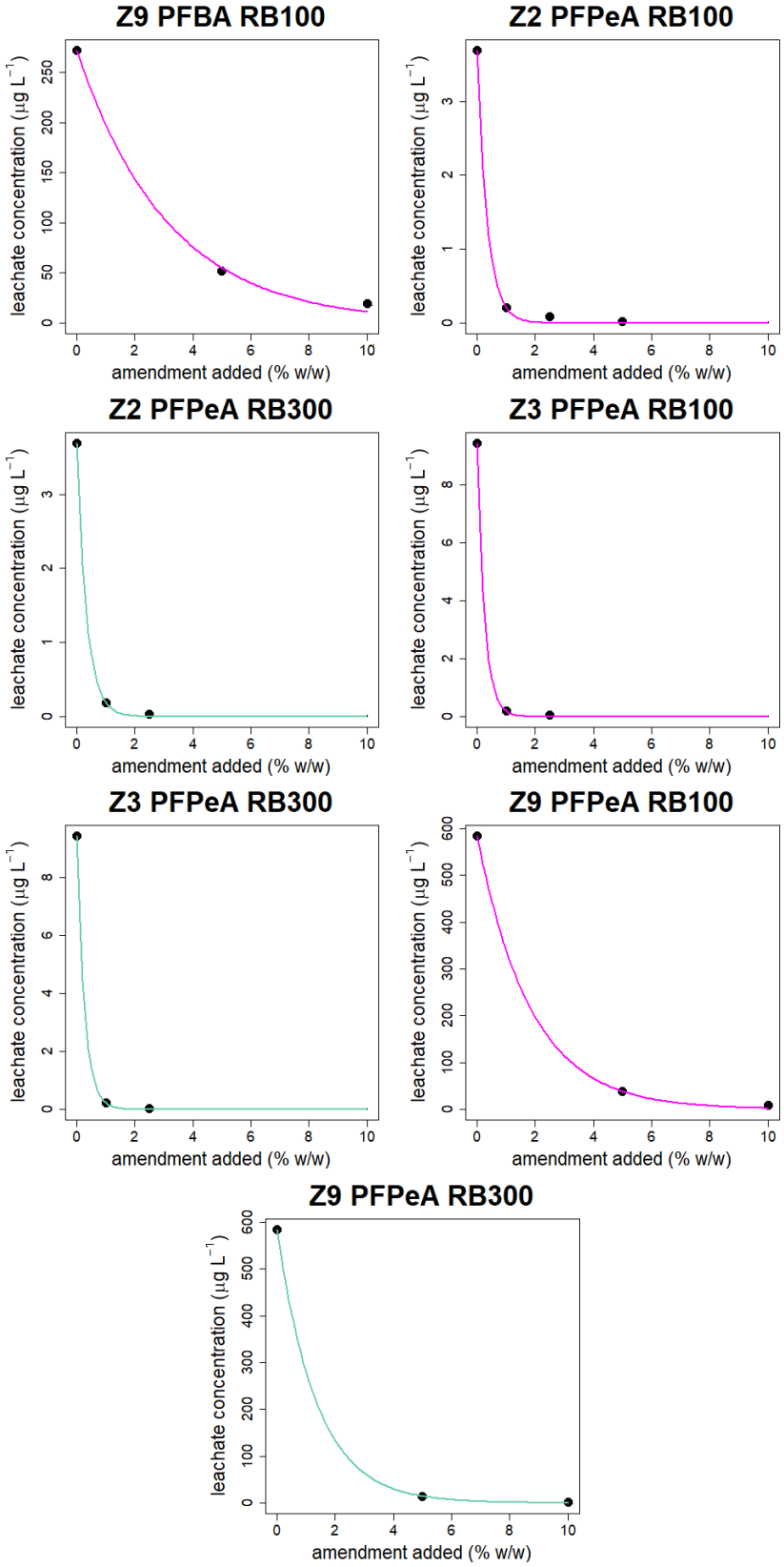


Figure D.7: Fitted exponentials by PFAS family: Short chain PFCAs. Points indicate experimental data.

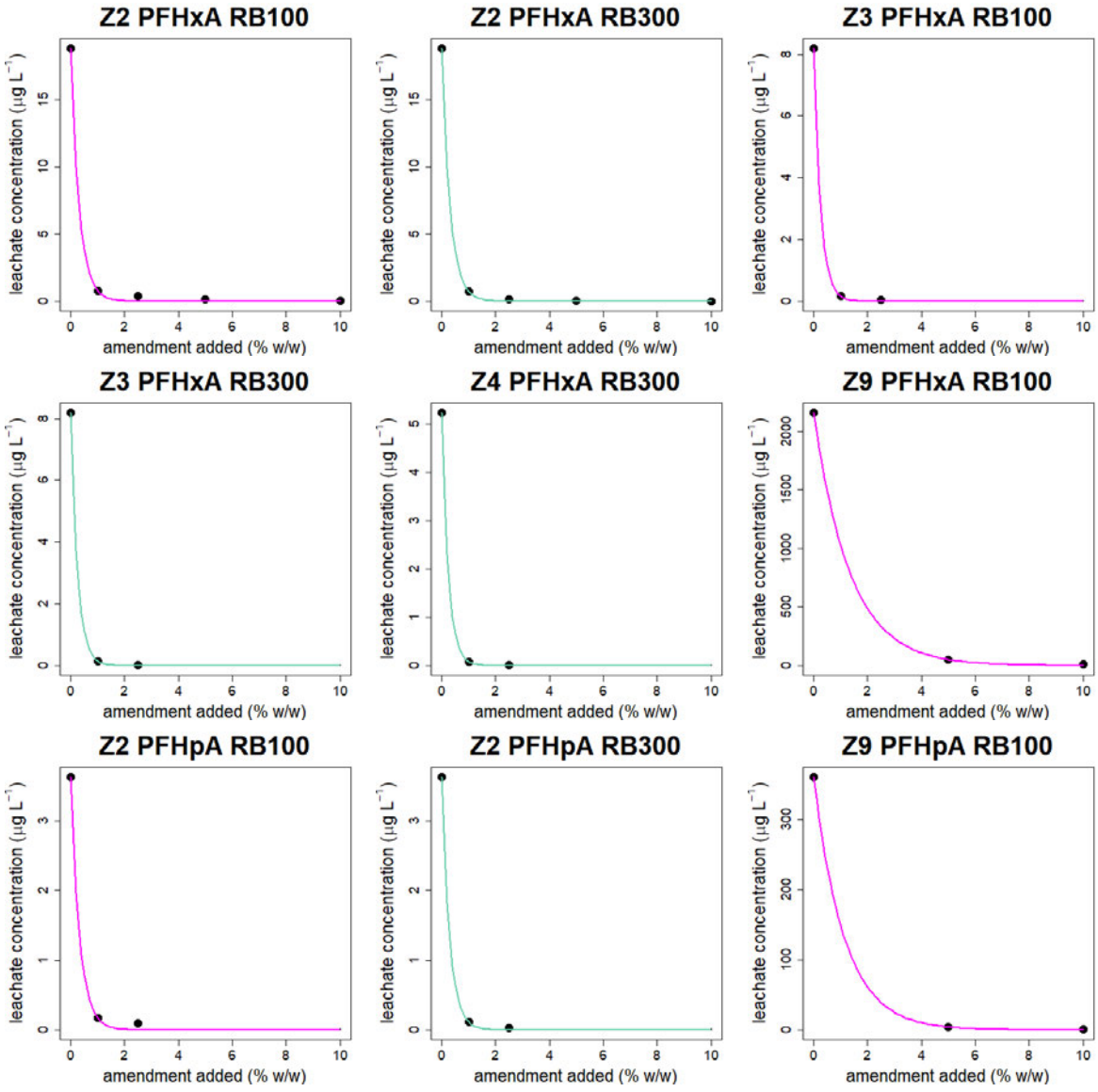


Figure D.8: Fitted exponentials by PFAS family: Medium chain PFCAs. Points indicate experimental data.

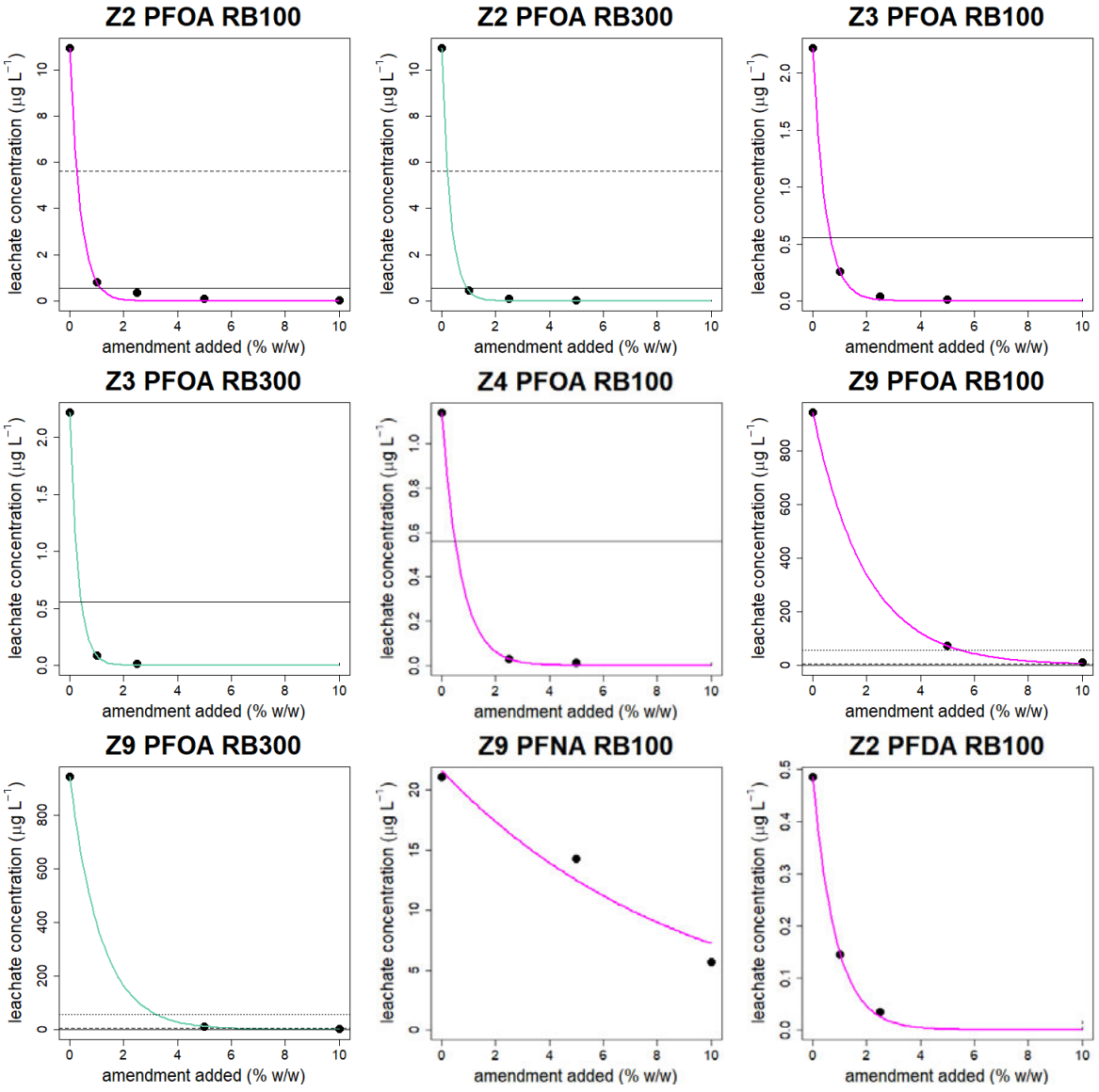


Figure D.9: Fitted exponentials by PFAS family: Long chain PFCAs. Points indicate experimental data.

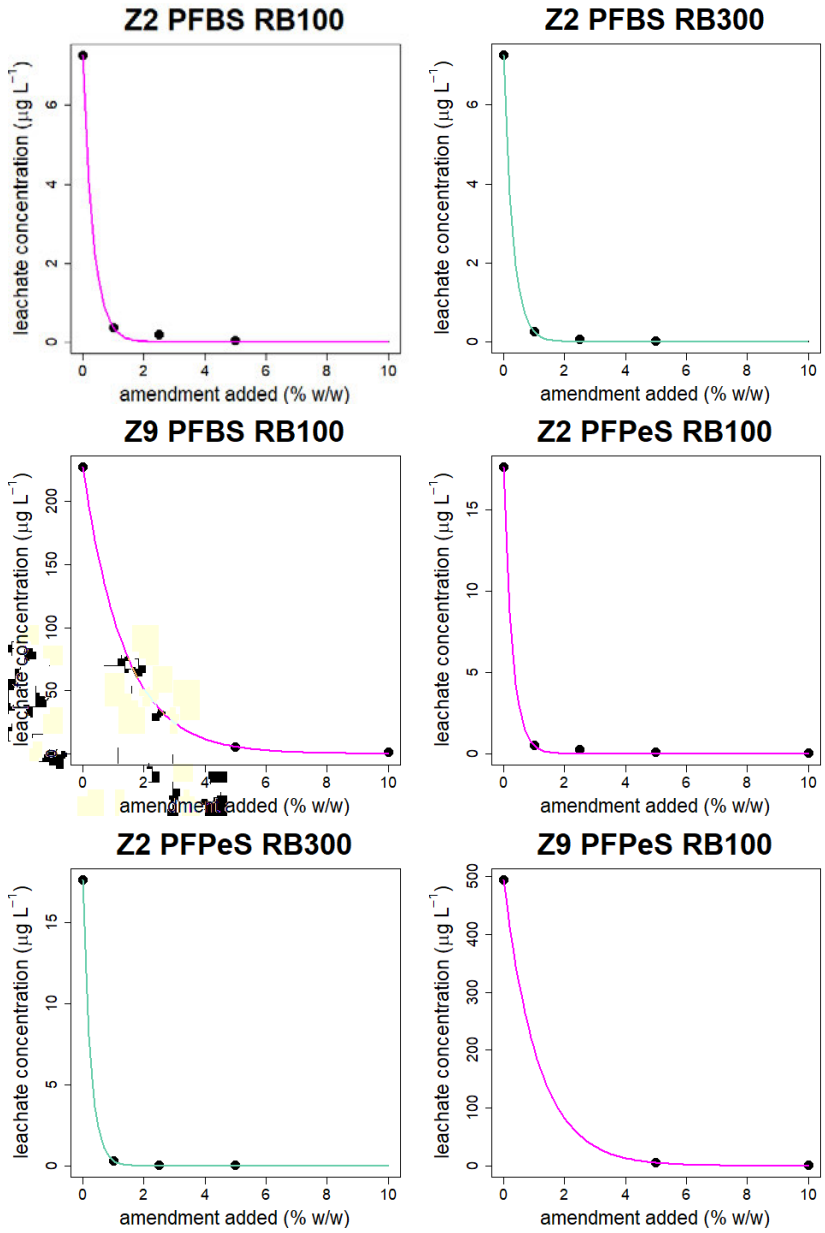


Figure D.10: Fitted exponentials by PFAS family: Short chain PFSAs. Points indicate experimental data.

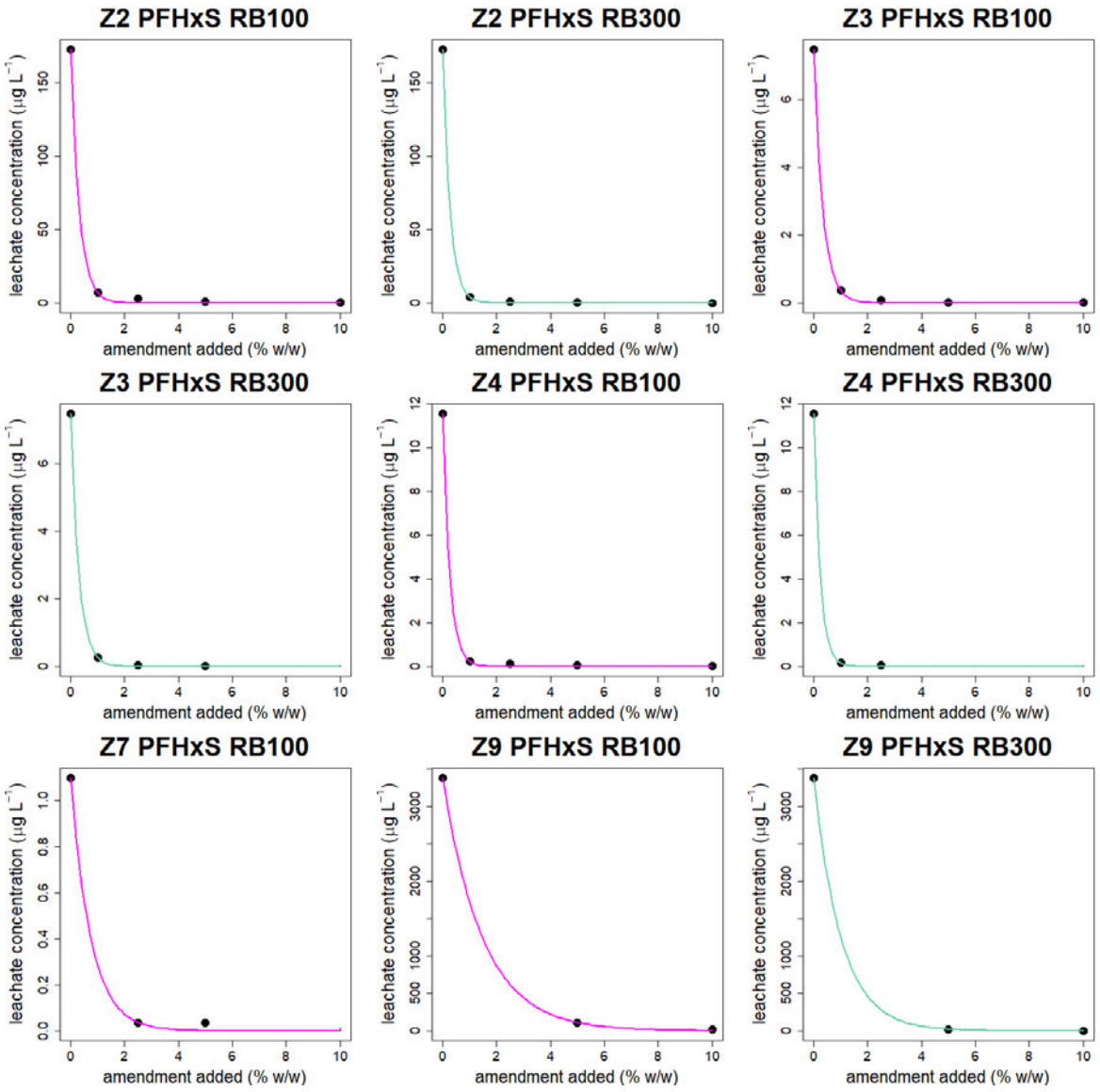


Figure D.11: Fitted exponentials by PFAS: PFHxS. Points indicate experimental data.

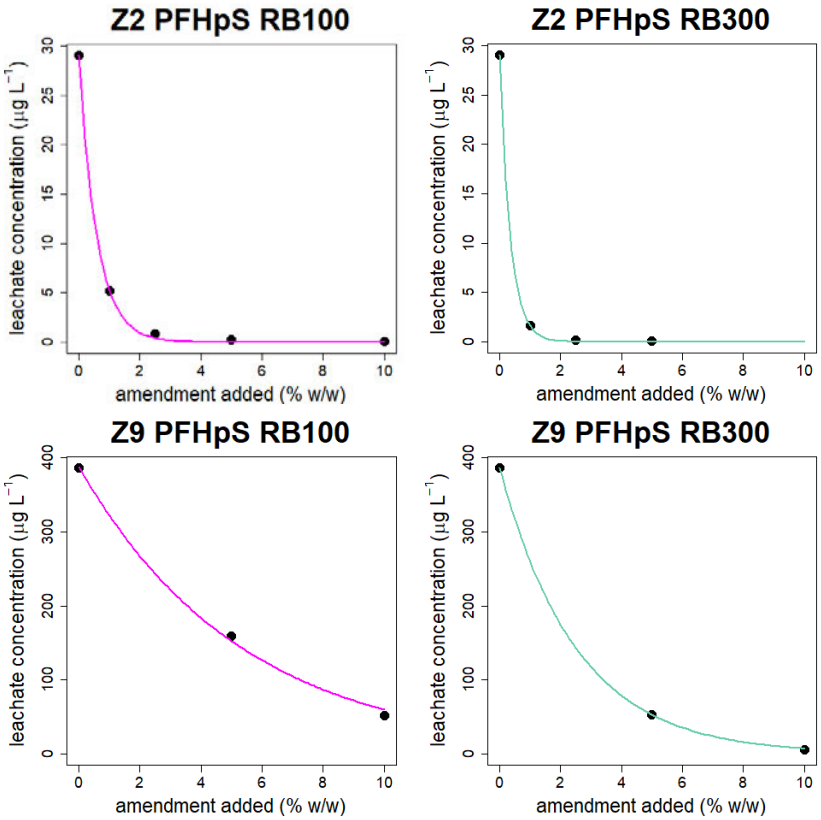


Figure D.12: Fitted exponentials by PFAS: PFHpS. Points indicate experimental data.

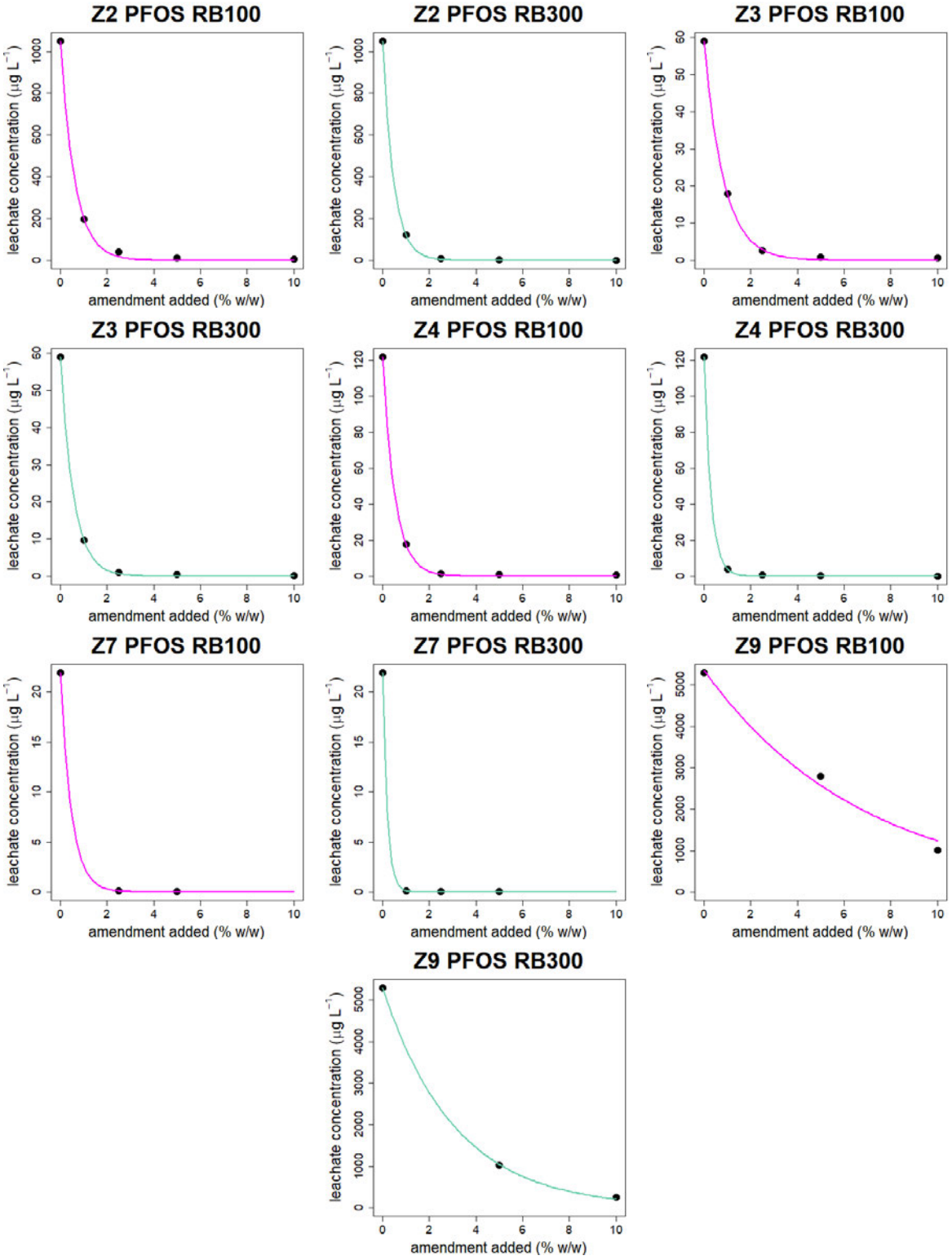


Figure D.13: Fitted exponentials by PFAS: PFOS. Points indicate experimental data.

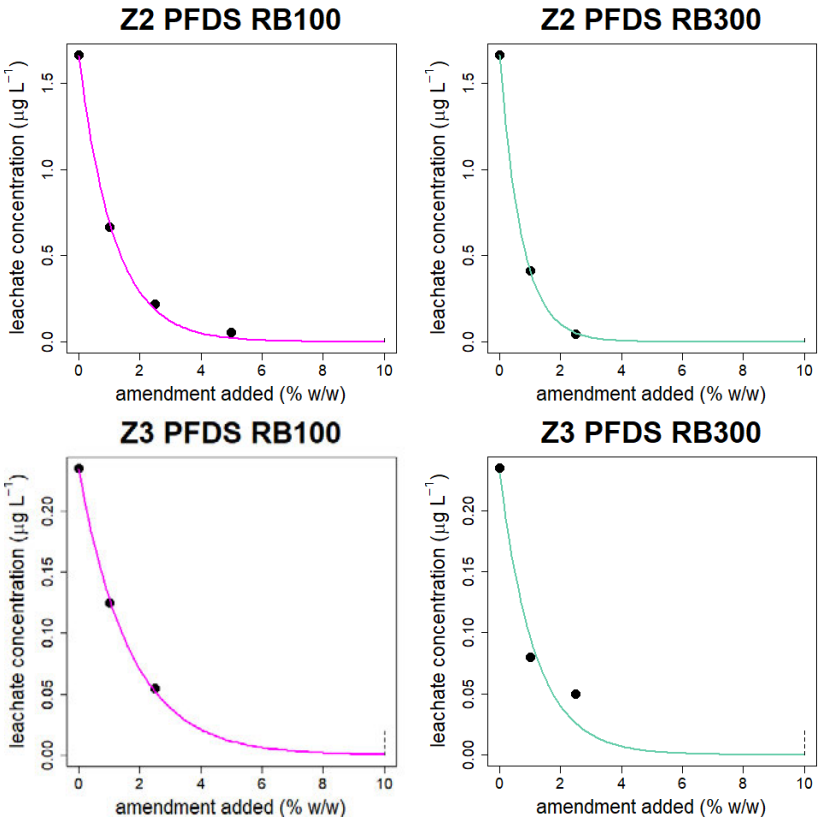


Figure D.14: Fitted exponentials by PFAS family: Long chain PFSAs. Points indicate experimental data.

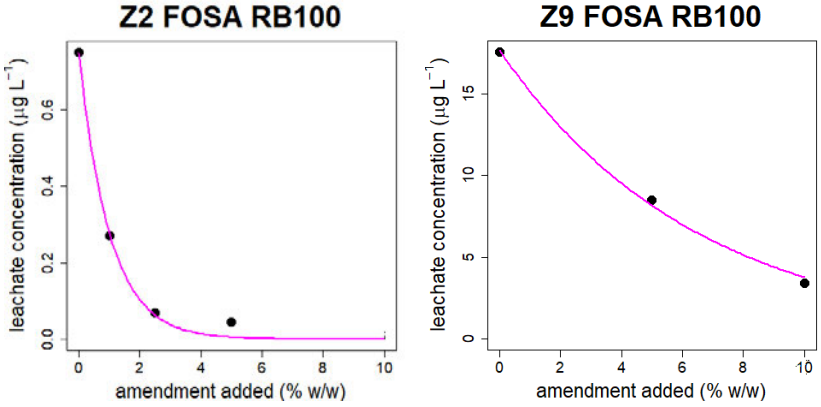


Figure D.15: Fitted exponentials by PFAS family: FOSAMs. Points indicate experimental data.

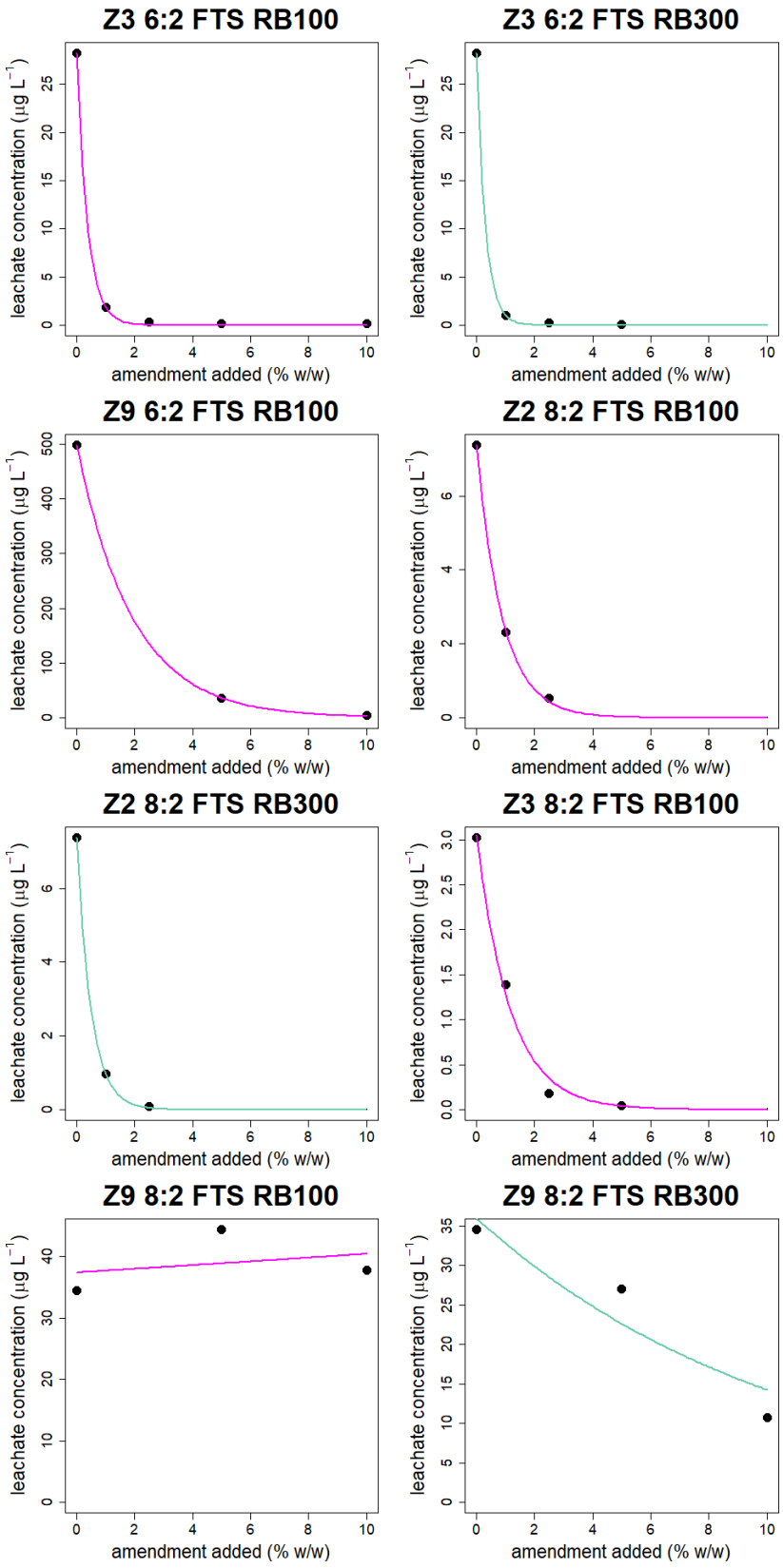


Figure D.16: Fitted exponentials by PFAS family: FTSAs. Points indicate experimental data.

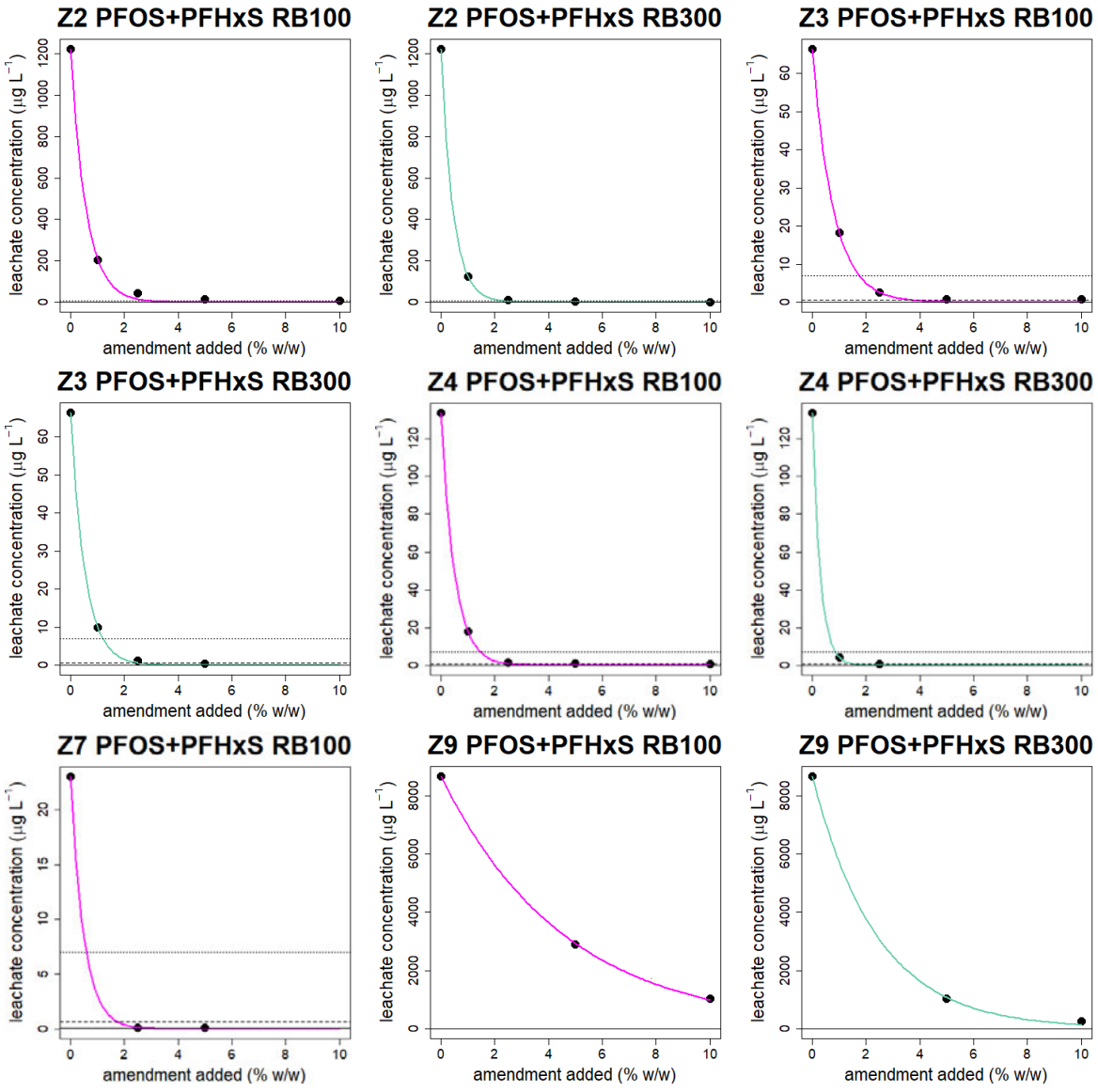


Figure D.17: Fitted exponentials: PFOS+PFHxS. Points indicate experimental data.

Table D.10: Residual sum of squares (RSS), total sum of squares (TSS) and R^2 values for RB100 fitted models.

Soil	PFAS	RSS	TSS	R^2
Z2	PFBS	3.93×10^{-2}	3.75×10^{1}	0.999
	PFPeS	8.42×10^{-2}	2.43×10^{2}	1.00
	PFHxS	1.27×10^{1}	2.31×10^{4}	0.999
	PFHpS	3.24×10^{-1}	6.20×10^{2}	0.999
	PFOS	8.02×10^{2}	8.00×10^{5}	0.999
	PFDS	3.05×10^{-3}	1.57	0.998
	PFPeA	7.14×10^{-3}	9.66	0.999
	PFHxA	1.96×10^{-1}	2.74×10^{2}	0.999
	PFHpA	8.69×10^{-3}	8.16	0.999
	PFOA	1.30×10^{-1}	9.03×10^{1}	0.999
	PFDA	1.08×10^{-4}	1.10×10^{-1}	0.999
	FOSA	1.69×10^{-3}	3.20×10^{-1}	0.995
	8:2 FTS	1.42×10^{-2}	2.52×10^{1}	0.999
	PFOS+PFHxS	1.15×10^{3}	1.09×10^{6}	0.999
Z3	PFHxS	7.28×10^{-3}	4.32×10^{1}	1.00
	PFOS	1.10	2.49×10^{3}	1.00
	PFDS	2.03×10^{-5}	1.65×10^{-2}	0.999
	PFPeA	1.98×10^{-3}	5.80×10^{1}	1.00
	PFHxA	2.97×10^{-3}	4.35×10^{1}	1.00
	PFOA	1.09×10^{-3}	3.39	1.00
	6:2 FTS	1.32×10^{-1}	6.12×10^{2}	1.00
	8:2 FTS	3.94×10^{-2}	5.71	0.993
	PFOS+PFHxS	1.11	3.17×10^{3}	1.00
Z4	PFHxS	3.18×10^{-2}	1.04×10^{2}	1.00
	PFOS	2.22	1.11×10^{4}	1.00
	PFOA	2.01×10^{-4}	8.33×10^{-1}	1.00
	PFOS+PFHxS	2.83	1.33×10^{4}	1.00
Z7	PFHxS	1.14×10^{-3}	7.56×10^{-1}	0.998
	PFOS	9.90×10^{-3}	3.17×10^{2}	1.00
	PFOS+PFHxS	1.80×10^{-2}	3.48×10^{2}	1.00
Z9	PFBS	9.28×10^{-1}	3.35×10^{4}	1.00
	PFPeS	2.68	1.60×10^{5}	1.00
	PFHxS	3.52×10^{2}	7.32×10^{6}	1.00
	PFHpS	1.12×10^{2}	5.84×10^{4}	0.998
	PFOS	1.06×10^{5}	9.26×10^{6}	0.989
	PFBA	8.85×10^{1}	3.77×10^{4}	0.998
	PFPeA	3.32×10^{1}	2.11×10^{5}	1.00
	PFHxA	1.31×10^{2}	3.02×10^{6}	1.00
	PFHpA	9.99×10^{-1}	8.54×10^{4}	1.00
	PFOA	2.03×10^{1}	5.45×10^{5}	1.00
	PFNA	6.00	1.20×10^{2}	0.950
	FOSA	2.64×10^{-1}	1.03×10^{2}	0.997
	6:2 FTS	4.20	1.53×10^{5}	1.00
	8:2 FTS	4.60×10^{1}	5.09×10^{1}	0.097
	PFOS+PFHxS	1.95×10^{3}	3.17×10^{7}	1.00

Table D.11: Residual sum of squares (RSS), total sum of squares (TSS) and R^2 values for RB300 fitted models.

Soil	PFAS	RSS	TSS	R^2
Z2	PFBS	4.40×10^{-3}	3.84×10^{1}	1.00
	PFPeS	7.48×10^{-3}	2.30×10^{2}	1.00
	PFHxS	1.20	2.36×10^{4}	1.00
	PFHpS	2.01×10^{-2}	6.08×10^{2}	1.00
	PFOS	4.08×10^{1}	8.34×10^{5}	1.00
	PFDS	4.02×10^{-5}	1.44	1.00
	PFPeA	7.71×10^{-4}	8.56	1.00
	PFHxA	2.33×10^{-2}	2.77×10^{2}	1.00
	PFHpA	8.61×10^{-4}	8.44	1.00
	PFOA	1.09×10^{-2}	8.66×10^{1}	1.00
	8:2 FTS	1.16×10^{-3}	3.17×10^{1}	1.00
	PFOS+PFHxS	6.42×10^{1}	1.14×10^{6}	1.00
Z3	PFHxS	3.22×10^{-3}	4.06×10^{1}	1.00
	PFOS	4.59×10^{-1}	2.58×10^{3}	1.00
	PFDS	8.61×10^{-4}	1.97×10^{-2}	0.956
	PFPeA	1.54×10^{-3}	5.79×10^{1}	1.00
	PFHxA	1.20×10^{-3}	4.36×10^{1}	1.00
	PFOA	2.06×10^{-4}	3.14	1.00
	6:2 FTS	6.05×10^{-2}	5.80×10^{2}	1.00
	PFOS+PFHxS	6.02×10^{-1}	2.99×10^{3}	1.00
Z4	PFHxS	4.19×10^{-3}	8.72×10^{1}	1.00
	PFOS	5.56×10^{-1}	1.17×10^{4}	1.00
	PFHxA	3.93×10^{-4}	1.79×10^{1}	1.00
	PFOS+PFHxS	5.78×10^{-1}	1.14×10^{4}	1.00
Z7	PFOS	1.02×10^{-2}	3.57×10^{2}	1.00
Z9	PFHxS	2.20×10^{1}	7.55×10^{6}	1.00
	PFHpS	1.26	8.59×10^{4}	1.00
	PFOS	3.26×10^{3}	1.47×10^{7}	1.00
	PFPeA	2.85	2.21×10^{5}	1.00
	PFHxA	1.47×10^{1}	3.07×10^{6}	1.00
	PFOA	3.06	5.85×10^{5}	1.00
	8:2 FTS	3.33×10^{1}	2.96×10^{2}	0.888
	PFOS+PFHxS	1.80×10^{4}	4.31×10^{7}	1.00

Appendix E

Monte Carlo simulation source code

E.1 Monte Carlo simulation

```
#============================================================
# PFAS on Solid Substrates ---
# Author: Julie Sleep
# Monte Carlo PFSAs on Graphite
# Version of 03/11/2022
# Incorporates plus minus 10% parameter testing (via input files called plus 10 and -10 only)
# Incorporates different starting position testing (via input PFOSionsds and normPlacement boolean)
# Incorporates option for a mixed Surface charge (via mixedSurfaceChargeBoolean)
#============================================================

#---------------------------------------
#Variable parameters required to be set:
#---------------------------------------
unix=TRUE #Set to true when runing on unix machine to suppress plotting
#unix=FALSE #Set to false to include plotting
#debug=TRUE # Set to true to print out acceptance values
debug=FALSE # Set to false to suppress print out
#mixedSurfaceCharge = TRUE #half according to charge_C, other half zero
mixedSurfaceCharge = FALSE #regular homogeneous surface charge
normPlacement = TRUE
#normPlacement = FALSE

numSteps = 20000 #Number of monte carlo steps
#numSteps = 10000 #Number of monte carlo steps
#numSteps = 200 #Number of monte carlo steps
stepSize = 0.5 #Angstrom, was 0.5

#liquidName = "PFOS"
#liquidName = "PFOSion"
#liquidName = "PFBS"
#liquidName = "PFBSion"
#liquidName = "PFOA"
#liquidName = "PFOAion"
liquidName = "PFDAion"
#liquidName = "PFOSminus10"
#liquidName = "PFOSplus10"
#liquidName = "PFOSionds"

N = 16 #number of PFAS molecules
Nci = 0 # number of positive counterions (H+)
Ndiv = 0 # number of divalent cations (Ca2+)
Noh = 0 # Number of negative counterions (OH-)

# Charge balance on carbon in eV, later multiplied by e to convert to C
#charge_C = 0 #Neutral
#charge_C = -16/1397 #Negative
charge_C = 16/1397 #Positive
#charge_C = 2*16/1397 #Double positive

if(mixedSurfaceCharge==TRUE){#convert charge to just cover the 711 molecules
  charge_C=charge_C*1397/711
}

if(unix==FALSE){
  library(scatterplot3d)
  library(rgl)
}

#Clear workspace and set directory
if(unix==FALSE){
  #rm(list=ls())
  getwd()
  setwd("PFAS/Soil/SoilMolecular")
  #setwd("..")
}

#Measure system time
sTime = proc.time()

#Monte Carlo and Molecule Parameters
set.seed(1) #for random number generation
```

```
Ntot = N + Nci + Noh + Ndiv #Total number of ions
if(liquidName=="PFOS" || liquidName == "PFOSion"){
  pfosColours = c("yellow", rep("green",17), rep("red",3),rep("grey",8),"white")
}
if(liquidName=="PFBS" || liquidName == "PFBSion"){
  pfosColours = c("yellow", rep("green",9), rep("red",3),rep("grey",4),"white")
}
if(liquidName=="PFOSplus10" || liquidName == "PFOSminus10"){
  pfosColours = c("yellow", rep("green",17), rep("red",3),rep("grey",8),"white")
}
if(liquidName=="PFOSionds"){
  pfosColours = c("yellow", rep("green",17), rep("red",3),rep("grey",8),"white")
}

#Box dimensions
b = 30 #Dimensions of (half) box (Angstroms)
boxh = 30 # (half) height of box
colfunc <- colorRampPalette(c("aquamarine3", "cornflowerblue", "darkorchid3",
                              "deeppink3"))#,"darkgoldenrod2","darkolivegreen3"))
colourpfas = colfunc(N)

#Physical Constants
e = 1.60217662e-19 #- e charge
kB = 1.38064852e-23 # Boltzmann
eps_water = 80.1 # relative permittivity of Water at 20 degrees
eps_0 = 8.854187817620e-12 # vacuum permittivity
N_A = 6.022140857e23 #Avogadros number
T = 300 # Temp in Kelvin
#n1 = 1.00029 #Refractive indexes Air
#eps1 = 1.00059 #Air #Dielectric constants
#eps_air = 1.00054

#Surface constants
wDepth_C = 2.12267 #kJ mol-1 HOPG (/1000/NA in eqn)
sigma_C = 2.9 #Angstroms (to m in eqn)
#wDepth_HOPG = 0.4393 #kJ mol-1 HOPG
#sigma_HOPG = 3.851 #Angstrom HOPG

#Variables for storing values
u_tot = 0
lj_tot = 0
coul_tot = 0
totalPotential = 0 #Total for all molecules

#Temporary store variables used inside loop
atom_sTot = 0

#vectors and matrices for storing results
u_tot_list = c() #list of total potential at each step
potentMatrix = matrix(numeric(Ntot^2), nrow=Ntot, ncol=Ntot) #Potentials between each molecule
surfaceAtomPotentials = numeric(Ntot) #Potentials between molecules and surface
centreToSurface = matrix(numeric(Ntot*(numSteps+1)),
                         nrow=numSteps+1, ncol=Ntot) #Storing z value for accepted moves
maxToSurface = matrix(numeric(Ntot*(numSteps+1)),
                      nrow=numSteps+1, ncol=Ntot) #Storing z value for accepted moves
xRotStore  = matrix(numeric(Ntot*(numSteps+1)), nrow=numSteps+1, ncol=Ntot) # x rotation for accepted moves
yRotStore  = matrix(numeric(Ntot*(numSteps+1)), nrow=numSteps+1, ncol=Ntot) # y for accepted moves
zRotStore  = matrix(numeric(Ntot*(numSteps+1)), nrow=numSteps+1, ncol=Ntot) # z value for accepted moves

#============================================================================
# System structure creation, placing and plotting
#============================================================================
#Some points in a box to plot
Sub = seq(-b,b, by=1.42)
NNN = 10
xx = runif(NNN,-b,b)
yy = runif(NNN,-b,b)
zz = runif(NNN,0,boxh)
ions = data.frame(xx,yy,zz)
if(unix==FALSE){
  ionplot = scatterplot3d(ions,
                          color="white", pch = "*",
                          xlab = expression(paste("x (",ring(A),")")),
```

```
                          ylab = expression(paste("y (",ring(A),")")),
                          zlab = expression(paste("z (",ring(A),")")),
                          xlim=c(-b,b), ylim=c(-b,b), zlim=c(0,boxh*2)
  )
}
#============================================================
#Plot and store a bottom surface
surfaceX = vector()
surfaceY = vector()
surfaceZ = vector()

#Starting positions
gZ = 0
gY = b
gX = -b
rowCount = 1
surfCount = 0

while (gY>=-b && gY<=b){

  #For all odd numbered rows (including the first)
  if(rowCount%%2 == 1){
    #For each atom in an odd row
    for (j in 1:29){
      surfCount = surfCount +1 # Count number of atoms in surface
      if(j == 1){#first molecule
        gX = -b
      }
      else if((j %% 2) == 0){#even molecules
        gX = gX + 1.42
      }
      else{# odd molecules
        gX = gX + 2.84
      }
      if(unix==FALSE){ ionplot$points3d(x=gX, y=gY, z=gZ, pch=21, col="black", bg="grey") }

      #Add atom to data frame
      surfaceX = c(surfaceX, gX)
      surfaceY = c(surfaceY, gY)
      surfaceZ = c(surfaceZ, gZ)
    }#end for each atom
  }#end for odd row
  else if (rowCount%%2 == 0){#For all even numbered rows (second and onward --- different offset)

    #For each atom in an even row
    for (j in 1:28){
      surfCount = surfCount + 1 # Count number of atoms in surface
      if(j == 1){#first molecule
        gX = -b+1.42+0.71
      }
      else if((j %% 2) == 0){#even molecules
        gX = gX + 1.42
      }
      else{# odd molecules
        gX = gX + 2.84
      }
      if(unix==FALSE){ ionplot$points3d(x=gX, y=gY, z=gZ, pch=21, col="black", bg="grey")}
      #Add atom to data frame
      surfaceX = c(surfaceX, gX)
      surfaceY = c(surfaceY, gY)
      surfaceZ = c(surfaceZ, gZ)

    }#end for within row
  }#end for even rows

  #shift y to next row, and increment counter
  gY = gY - 1.23
  rowCount = rowCount + 1
}#end while rows within bounds

print(paste(surfCount,"atoms in surface, check =", length(surfaceX)))
surfaceAtoms = rep("C", surfCount)
surfaceEpsilon = rep(wDepth_C, surfCount)
```

```
surfaceSigma = rep(sigma_C, surfCount)
if(mixedSurfaceCharge == TRUE){#HETEROGENEOUS CHARGE
surfaceCharge = c(rep(c(rep(charge_C,15),rep(0,14),
                        rep(charge_C,14),rep(0,14))
                      ,24),
                  rep(charge_C,15),rep(0,14))
}else{#HOMOGENEOUS CHARGE
  surfaceCharge = rep(charge_C, surfCount)
}
surface = data.frame(atoms = surfaceAtoms, x = surfaceX, y = surfaceY, z = surfaceZ,
                     wDepth = surfaceEpsilon, sigma = surfaceSigma, charge = surfaceCharge)

#Write surface to file
if(mixedSurfaceCharge == TRUE){
  write.csv(surface, file = "Mixed_Surface_fromR.csv")
}else{
  write.csv(surface, file = "Surface_fromR.csv")
}

#-------------------------------------------------------------
# Read in pfas molecules # PFOS - pubchem
#-------------------------------------------------------------
pfasFileName = paste0("Structures/",liquidName,".txt")
pfas = read.table(pfasFileName, header=TRUE)
pfas$sigma  = pfas$Sigma #in angstrom
pfas$wDepth = pfas$WellDepth*4185.8 #was in kcal/mol need to be in J/mol x 4185.8
pfas$charge = pfas$Charge #in e
pfas$origx = pfas$x # A copy of co-ordinates centred at 0,0,0
pfas$origy = pfas$y
pfas$origz = pfas$z

#Make list of N pfas
pfasList = rep(list(pfas), N)

#calculate placement lists
if(normPlacement == TRUE){
  xplacepfas = rep(c(-15, 5, -5, 15), 4)
  yplacepfas = rep(c(15, 15, 5, 5, -5, -5, -15, -15), 2)
  zplacepfas = c(rep(10, 8), rep(20, 8))
} else {
  xplacepfas = rep(c(-12, 4, -6, 17), 4)
  yplacepfas = rep(c(12, 17, 4, 6, -4, -6, -12, -17), 2)
  zplacepfas = c(rep(12, 8), rep(18, 8))
}

print(paste("Placing", Ntot, " ", liquidName, "molecules in the box"))
#Offset molecules in box
for(i in 1:N){
  pfasList[[i]]$x = pfasList[[i]]$x + xplacepfas[i]
  pfasList[[i]]$y = pfasList[[i]]$y + yplacepfas[i]
  pfasList[[i]]$z = pfasList[[i]]$z + zplacepfas[i]
}

if(unix==FALSE){
  #plot structures in box
  for(i in 1:N){
    ionplot$points3d(pfasList[[i]]$x, pfasList[[i]]$y, pfasList[[i]]$z, pch=21,
                     col="black", bg=colourpfas[i], cex=1.75)
  }
  #convert to 2d
  pfasCor <- ionplot$xyz.convert(pfas$x,pfas$y,pfas$z)
}

#-------------------------------------------------------------
# Place H+ counterions in box
#-------------------------------------------------------------
if(Nci>0){
  #Properties of a single counter ion type (i.e. H+)
  counterIon = data.frame(atomType="H",x=0,y=0,z=0, sigma=1.6, wDepth=0.03, charge=1)
  counterIon$origx = counterIon$x
  counterIon$origy = counterIon$y
  counterIon$origz = counterIon$z
```

```
  #Make list of Nci counter ions (e.g. 16 H+)
  ciList = rep(list(counterIon),Nci)

  #calculate placement lists (For ONLY H+)
  xplaceci = rep(c(-5, 15, -15, 5), 8)
  yplaceci = rep(c(15, 15, 5, 5, -5, -5, -15, -15), 4)
  zplaceci = c(rep(10, 8), rep(30, 8), rep(20,8), rep(40,8))

  #calculate placement lists (For case with both 8 H+ and 8 OH-)
  if(Noh>0){
    xplaceci = rep(c(-5, 15, -15, 5), 8)
    yplaceci = rep(c(15, 15, 5, 5, -5, -5, -15, -15), 4)
    zplaceci = c(rep(c(10,10,20,20),2),rep(c(15,15,25,25),2))
  }


  print(paste("Placing", Nci, "counterions in the box"))
  #Offset molecules in box
  for(i in 1:Nci){
    ciList[[i]]$x = ciList[[i]]$x + xplaceci[i]
    ciList[[i]]$y = ciList[[i]]$y + yplaceci[i]
    ciList[[i]]$z = ciList[[i]]$z + zplaceci[i]
  }

  if(unix==FALSE){
    #plot structures in box
    for(i in 1:Nci){
      ionplot$points3d(ciList[[i]]$x, ciList[[i]]$y, ciList[[i]]$z, pch=21,
                       col="black", bg="yellow", cex=1.75)
    }
  }
}else{
  ciList = NULL
}

#------------------------------------------------------------
# Place OH- counterions in box
#------------------------------------------------------------
if(Noh>0){
  #Properties of a single counter ion type
  #Lin 16b, wdepth published in kcal/mol, converted to kj/mol
  ohIon = data.frame(atomType="OH",x=0,y=0,z=0, sigma=3.7, wDepth=0.33472, charge=-1)
  ohIon$origx = ohIon$x
  ohIon$origy = ohIon$y
  ohIon$origz = ohIon$z

  #Make list of Noh counter ions (e.g. 16 OH-)
  ohList = rep(list(ohIon),Noh)

  #calculate placement lists for case of OH only
  xplaceoh = rep(c(-5, 15, -15, 5), 8)
  yplaceoh = rep(c(15, 15, 5, 5, -5, -5, -15, -15), 4)
  zplaceoh = c(rep(10, 8), rep(30, 8), rep(20,8), rep(40,8))

  #calculate placement lists (For case with both 8 H+ and 8 OH-)
  if(Nci>0){
    xplaceoh = rep(c(-5, 15, -15, 5), 8)
    yplaceoh = rep(c(15, 15, 5, 5, -5, -5, -15, -15), 4)
    zplaceoh = c(rep(c(20,20,10,10),2),rep(c(25,25,15,15),2))
  }

  print(paste("Placing", Noh, "OH ions in the box"))
  #Offset molecules in box
  for(i in 1:Noh){
    ohList[[i]]$x = ohList[[i]]$x + xplaceoh[i]
    ohList[[i]]$y = ohList[[i]]$y + yplaceoh[i]
    ohList[[i]]$z = ohList[[i]]$z + zplaceoh[i]
  }

  if(unix==FALSE){
    #plot structures in box
    for(i in 1:Noh){
      ionplot$points3d(ohList[[i]]$x, ohList[[i]]$y, ohList[[i]]$z, pch=21,
```

```
                      col="black", bg="red", cex=1.75)
    }
  }
}else{
  ohList = NULL
}

#-------------------------------------------------------------
# Place divalent cations in box
#-------------------------------------------------------------
if(Ndiv>0){
  #Properties of a single cation type (i.e. Ca2+) from Gromacs OPLS-AA
  divIon = data.frame(atomType="Ca",x=0,y=0,z=0, sigma=2.41203, wDepth=1.88136, charge=2)
  divIon$origx = divIon$x
  divIon$origy = divIon$y
  divIon$origz = divIon$z

  #Make list of Nci counter ions (e.g. 16 H+)
  divList = rep(list(divIon),Ndiv)

  #calculate placement lists
  xplacediv = rep(c(-5, 15, -15, 5), 8)
  yplacediv = rep(c(15, 15, 5, 5, -5, -5, -15, -15), 4)
  zplacediv = c(rep(10, 8), rep(30, 8), rep(20,8), rep(40,8))

  print(paste("Placing", Ndiv, "divalent cations in the box"))
  #Offset molecules in box
  for(i in 1:Ndiv){
    divList[[i]]$x = divList[[i]]$x + xplacediv[i]
    divList[[i]]$y = divList[[i]]$y + yplacediv[i]
    divList[[i]]$z = divList[[i]]$z + zplacediv[i]
  }

  if(unix==FALSE){
    #plot structures in box
    for(i in 1:Ndiv){
      ionplot$points3d(divList[[i]]$x, divList[[i]]$y, divList[[i]]$z, pch=21,
                       col="black", bg="magenta", cex=2.75)
    }
  }
}else{
  divList = NULL
}


#@@@
```

```
            xlab="x", ylab="y", zlab="z")
    for(i in 2:Noh){
      spheres3d(ohList[[i]]$x, ohList[[i]]$y, ohList[[i]]$z, col="red",
                radius=1.2)
    }
  }

  if(Ndiv>0){
    #Divalent cations
    spheres3d(divList[[1]]$x, divList[[1]]$y, divList[[1]]$z, col="chartreuse3",
              type="s", radius=1.5, xlim=c(-30,30), ylim=c(-30,30), zlim=c(0,60),
              xlab="x", ylab="y", zlab="z")
    for(i in 2:Ndiv){
      spheres3d(divList[[i]]$x, divList[[i]]$y, divList[[i]]$z, col="chartreuse3",
                radius=1.5)
    }
  }
  #Surface
  if(mixedSurfaceCharge == TRUE){
    surfaceColour = c(rep(c(rep("gray27",15),rep("grey",14),
                                          rep("gray27",14),rep("grey",14))
                                        ,24),
                                    rep("gray27",15),rep("grey",14))
  }else{
    surfaceColour = "grey"
  }
  spheres3d(surface$x, surface$y, surface$z, col=surfaceColour, radius=1.2)


  #rgl.snapshot("initialpos4.png",fmt="png")
  #play3d( spin3d( axis = c(0, 0, 1), rpm = 10), duration = 10 )
}
#-------------------------------------------------------------------------------
#Add in check for z below surface
for(i in 1:N){
  print(paste("checking below surface",i))
  print(min(pfasList[[i]]$z))
}
if(Nci>0){
  for(i in 1:Nci){
    print(paste("checking below surface",i))
    print(min(ciList[[i]]$z))
  }
}
if(Noh>0){
  for(i in 1:Noh){
    print(paste("checking below surface",i))
    print(min(ohList[[i]]$z))
  }
}
if(Ndiv>0){
  for(i in 1:Ndiv){
    print(paste("checking below surface",i))
    print(min(divList[[i]]$z))
  }
}

#===============================================================================
#Store pfas and counterions
molecule = c(pfasList,ciList,ohList,divList)

#===============================================================================
#Initialise variables
for(i in 1:N){
  centreToSurface[1,i] = zplacepfas[i]  #6*i # pfas centre 6 Ang to surface, 12
  maxToSurface[1,i] = max(molecule[[i]]$z) # pfas max Ang to surface
  xRotStore[1,i] = 0 # pfas rotation starts at 0
  yRotStore[1,i] = 0 # pfas rotation starts at 0
  zRotStore[1,i] = 0 # pfas rotation starts at 0
}
if(Nci>0){
  for(i in 1:Nci){
    centreToSurface[1,N+i] = zplaceci[i]
```

```
    maxToSurface[1,N+i] = max(molecule[[N+i]]$z) # pfas max Ang to surface
    xRotStore[1,N+i] = 0 # ci rotation starts at 0
    yRotStore[1,N+i] = 0 # ci rotation starts at 0
    zRotStore[1,N+i] = 0 # ci rotation starts at 0
  }
}
if(Noh>0){
  for(i in 1:Noh){
    centreToSurface[1,N+Nci+i] = zplaceoh[i]
    maxToSurface[1,N+Nci+i] = max(molecule[[N+Nci+i]]$z) # pfas max Ang to surface
    xRotStore[1,N+Nci+i] = 0 # ci rotation starts at 0
    yRotStore[1,N+Nci+i] = 0 # ci rotation starts at 0
    zRotStore[1,N+Nci+i] = 0 # ci rotation starts at 0
  }
}
if(Ndiv>0){
  for(i in 1:Ndiv){
    centreToSurface[1,N+Nci+Noh+i] = zplacediv[i]
    maxToSurface[1,N+Nci+i] = max(molecule[[N+Nci+Noh+i]]$z) # pfas max Ang to surface
    xRotStore[1,N+Nci+Noh+i] = 0 # ci rotation starts at 0
    yRotStore[1,N+Nci+Noh+i] = 0 # ci rotation starts at 0
    zRotStore[1,N+Nci+Noh+i] = 0 # ci rotation starts at 0
  }
}

#=============================================================================
# Part 1
# Calculate inital total potential
# Storing the sub totals for later use
#=============================================================================

print("================================================")
print("Calculating initial Total Potential")

# ====================================================================
for(j in 1:Ntot){#For each molecule in the box
  print(paste("Initial potential Molecule j =",j))
  molj = molecule[[j]] #extract current molecule
  moljTot = 0 #total for j=1,2, etc.

  #====================================================================
  # For each atom in molecule j under consideration
  for (s in 1:nrow(molj)){ #s is the atom in the mol

    atom_sTot = 0 #Total for each atom s within a molecule, S=C1,F2, etc. with surface

    #---------------------------------------------------------
    # Surface-atom calculations for mol j
    #---------------------------------------------------------

    #-------------------------------------------------------------------------------
    # Pairwise pfas atom-surface atom calculations
    #-------------------------------------------------------------------------------
    for (sa in 1:surfCount){#sa is the atom in the surface

      aasTot = 0

      #calculate separation between pfas and surface atom being investigated
      rawx = abs(surface$x[sa] - molj$x[s])
      rawy = abs(surface$y[sa] - molj$y[s])

      #adjust for period boundary conditions (further away than b=30Angstrom pairs see neighbours)
      # quotient * b (gives 30 or 0) minus remainder
      # i.e. raw 59, gives 1*30-29=1, raw 15 gives 0-15=-15 (is squared so sign irrelevant)
      deltax = (rawx%/%b)*b - rawx%%b
      deltay = (rawy%/%b)*b - rawy%%b

      D = sqrt( deltax^2 + deltay^2 +
                  (surface$z[sa] - molj$z[s])^2)
      D_m = D*1e-10 #convert to m

      #---------------------------------
      #6-12 Lennard Jones potential
```

```
  # eps_ij: well depth, sigma_ij:dependent on molecules
  # For the sigma_ij = (sigmaii * sigmajj)^1/2
  # Convert everything to SI units
  wDepth = sqrt(molj$wDepth[s]/1000*surface$wDepth[sa]/1000)/N_A #in J
  sigma = sqrt(molj$sigma[s]*1e-10*surface$sigma[sa]*1e-10)#in m
  u_lj = 4*wDepth*((sigma/D_m)^12 - (sigma/D_m)^6)

  #-----------------------------------
  #Coulomb potential
  q1 = molj$charge[s]*e
  q2 = surface$charge[sa]*e #electron charge e to get from eV to J
  u_c = q1*q2/(4*pi*eps_0*eps_water*D_m)#D_m is separation in m

  #==============================
  #Atom-Atom totals
  aasTot = u_lj + u_c #total for one pair

  #print(paste("aas Tot", s, sa, "=", aasTot))

  atom_sTot = atom_sTot + aasTot #total for one atom s of molecule j with all of surface

}#end for sa : each molecule in the surface

#print(paste("s ", s," atom_sTot ", atom_sTot))

#update totals
#surfaceAtomPotentials[j] = surfaceAtomPotentials[j] + atom_sTot
#add atom s total to total for molecule j with surface

#-------------------------------------------------------------------------------
# Inter molecular calculations (not surface)
#-------------------------------------------------------------------------------

#-------------------------------------------------------------------------------
#For other molecules in the box
#But not molecule j itself
notJ = 1:Ntot
notJ = notJ[-j]

for(k in notJ){

  molk = molecule[[k]]
  molkTot = 0

  #-----------------------------------------------------------------------------
  # Pairwise atom-atom calculations
  #-----------------------------------------------------------------------------
  for (t in 1:nrow(molk)){#t is the atom in the otherMol

    pairTot = 0

    #calculate actual separation between molecule atoms being investigated
    rawx = abs(molk$x[t] - molj$x[s])
    rawy = abs(molk$y[t] - molj$y[s])

    #adjust for period boundary conditions (further away than b=30Angstrom pairs see neighbours)
    deltax = (rawx%/%b)*b - rawx%%b
    deltay = (rawy%/%b)*b - rawy%%b

    D = sqrt(deltax^2 + deltay^2 + (molk$z[t] - molj$z[s])^2)
    D_m = D*1e-10 #convert to m

    #-----------------------------------
    #6-12 Lennard Jones potential
    # eps_ij: well depth, sigma_ij:dependent on molecules
    # For the sigma_ij = (sigmaii * sigmajj)^1/2
    # Convert everything to SI units
    wDepth = sqrt(molj$wDepth[s]/1000*molk$wDepth[t]/1000)/N_A #in J
    sigma = sqrt(molj$sigma[s]*1e-10*molk$sigma[t]*1e-10)#in m
    u_lj = 4*wDepth*((sigma/D_m)^12 - (sigma/D_m)^6)

    #-----------------------------------
    #Coulomb potential
```

```
        q1 = molj$charge[s]*e
        q2 = molk$charge[t]*e #electron charge e to get from eV to C
        u_c = q1*q2/(4*pi*eps_0*eps_water*D_m)#D_m is separation in m

        #================================
        #Atom-Atom totals
        pairTot = u_lj + u_c #total for one pair

        molkTot = molkTot + pairTot #total for one atom of j with all of molecule k

      }#end for t each molecule in the other molecule(k)

      atom_sTot = atom_sTot + molkTot #add mol k total to total for the s atom

      #Add the molk totals to the potential matrix for k=1,2,...
      potentMatrix[j,k] = potentMatrix[j,k] + molkTot

    }#end for each other molecule k

    #add total for one atom with all other atoms in all molecules
    #store in total for that molecule
    moljTot = moljTot + atom_sTot

  } #end for s each atom in the current molecule

  #Overall total potential
  totalPotential = totalPotential + moljTot

  print(paste("Total for Molecule :", j, "=",moljTot))

}#end j for each molecule in the box

print(paste("Final total:", totalPotential))


#=============================================================================
# Part 2
# Monte Carlo Simulation
#=============================================================================

print("================================================")
print("Performing Simulation")
print(paste("Step size:",stepSize))
print(paste("Number of Steps:", numSteps))

for(i in 1:numSteps){
  if(debug==TRUE) { print(paste("Monte Carlo Step:",i)) }

  for(j in 1:Ntot){#For each molecule in the box

    if(debug==TRUE) { print(paste("Molecule: j =", j)) }

    u_tot = 0
    newSurfacePotential = 0 # stores updated potential for each molecule j with surface
    newMatrixRow = numeric(Ntot)#Stores updated potential of j with every k.

    oldPotential = rowSums(potentMatrix)[j] + surfaceAtomPotentials[j]
    newPotential = 0;
    diffPotential = 0;

    #extract current molecule
    molj = molecule[[j]] #copy to update with move

    #---------------------------------------------------------------
    # Make a move or a rotation
    #---------------------------------------------------------------
    # For each molecule in the box
    # Decide on a move or a rotation
    moveOrRot = runif(1)
    if(moveOrRot<=0.5){#make a move

      # For a move
      m = stepSize #moveLength;
```

```
  # Produce 3 random numbers for x,y,z
  mvx = runif(1, min=-m, max=m)
  mvy = runif(1, min=-m, max=m)
  mvz = runif(1, min=-m, max=m)

  # Move the molecule in that direction
  newx = molj$x + mvx
  newy = molj$y + mvy
  newz = molj$z + mvz


}#end make a move
else{#make a rotation
  #=====================================================
  # Rotating of molecule about 3 axis
  #=====================================================

  # For a rotation
  # Produce 3 random numbers for x,y,z axis rotation
  maxDegrees = 5#maximum rotation to turn about on each axis
  degX = runif(1, -5, 5)#turn between 0 and 5 degrees
  degY = runif(1, -5, 5)#turn between 0 and 5 degrees
  degZ = runif(1, -5, 5)#turn between 0 and 5 degrees

  #Rotate coordinates of molj$origx,... about each axis for degX degrees
  #molecules are rotated around (0,0,0), then translated to actual position

  #x 1
  angle1= degX*pi/180
  rotx1 = molj$origx
  roty1 = molj$origy*cos(angle1) - molj$origz*sin(angle1)
  rotz1 = molj$origy*sin(angle1) + molj$origz*cos(angle1)

  #y 2
  angle2= degY*pi/180
  rotx2 = rotz1*sin(angle2) + rotx1*cos(angle2)
  roty2 = roty1
  rotz2 = rotz1*cos(angle2) - rotx1*sin(angle2)

  #z 3
  angle3= degZ*pi/180
  rotx3 = rotx2*cos(angle3) - roty2*sin(angle3)
  roty3 = rotx2*sin(angle3) + roty2*cos(angle3)
  rotz3 = rotz2

  #Calculate difference between original and rotated
  diffx = rotx3 - molj$origx
  diffy = roty3 - molj$origy
  diffz = rotz3 - molj$origz

  #store in newx by adding diffx,...
  newx = molj$x + diffx
  newy = molj$y + diffy
  newz = molj$z + diffz

}#end make a rotation

#=================================================================
#Check if outside box / apply periodic Boundary Conditions
#check if inside the box in x and y directions only
if(max(newx)>b){
  #print("Outside box on RHS")
  for(m in 1:length(newx)){
    if(newx[m]>b){
      oldx = newx[m]
      newx[m] = newx[m]-2*b
      #print(paste("Old",oldx,"New",newx[m]))
    }
  }
}
if(min(newx)< -b){
  #print("Outside box on LHS")
```

```
  for(m in 1:length(newx)){
    if(newx[m]< -b){
      oldx = newx[m]
      newx[m] = newx[m]+2*b
      #print(paste("Old",oldx,"New",newx[m]))
    }
  }
}
if(max(newy)>b){
  #print("Outside box on back")
  for(m in 1:length(newy)){
    if(newy[m]>b){
      oldy = newy[m]
      newy[m] = newy[m]-2*b
    }
  }

}
if(min(newy)< -b){
  #print("Outside box on front")
  for(m in 1:length(newy)){
    if(newy[m]< -b){
      oldy = newy[m]
      newy[m] = newy[m]+2*b
    }
  }
}
if(min(newz)< 0){#If goes through bottom surface
  #print("Through bottom surface")
  #For a move, reject, keep z same
  if(moveOrRot<=0.5){
    newz = molj$z
    mvz = 0
  }
  else{#For a rotation, undo the whole rotation
    newx=molj$x
    newy=molj$y
    newz=molj$z

    rotx3 = molj$origx
    roty3 = molj$origy
    rotz3 = molj$origz
    degX = 0
    degY = 0
    degZ = 0
  }
}

#-----------------------------------------
#For both moves and rotations
#Store new coordinates

#update current ion
molj$x=newx
molj$y=newy
molj$z=newz

#For a rotation only
#Update also the origx,... to store starting rotation for next time
if(moveOrRot>0.5){
  molj$origx = rotx3
  molj$origy = roty3
  molj$origz = rotz3
  #rotating does not change the distance to surface
  centreToSurface[i+1,j] = centreToSurface[i,j]

  #rotating does change the max distance to surface
  maxToSurface[i+1,j] = max(molj$z)

  #rotating changes the angles
  xRotStore[i+1,j] = xRotStore[i,j] + degX
  yRotStore[i+1,j] = yRotStore[i,j] + degY
  zRotStore[i+1,j] = zRotStore[i,j] + degZ
```

```
  #subtract 360 if bigger than this angle
  if(xRotStore[i+1,j]>=360)
    xRotStore[i+1,j] = xRotStore[i+1,j] - 360
  if(yRotStore[i+1,j]>=360)
    yRotStore[i+1,j] = yRotStore[i+1,j] - 360
  if(zRotStore[i+1,j]>=360)
    zRotStore[i+1,j] = zRotStore[i+1,j] - 360

  #add 360 for negative angles
  if(xRotStore[i+1,j]<0)
    xRotStore[i+1,j] = xRotStore[i+1,j] + 360
  if(yRotStore[i+1,j]<0)
    yRotStore[i+1,j] = yRotStore[i+1,j] + 360
  if(zRotStore[i+1,j]<0)
    zRotStore[i+1,j] = zRotStore[i+1,j] + 360
}
else{#For a move only
  #Moving changes the distance to the surface
  centreToSurface[i+1,j] = centreToSurface[i,j] + mvz

  #moving does change the max distance to surface
  maxToSurface[i+1,j] = max(molj$z)

  #Moving does not change the rotation
  xRotStore[i+1,j] = xRotStore[i,j]
  yRotStore[i+1,j] = yRotStore[i,j]
  zRotStore[i+1,j] = zRotStore[i,j]
}

# ======================================================================
# CALCULATE CHANGE IN POTENTIAL FOR CURRENT MOLECULE
# Do each interaction pair potential
# Including its relationship with the bottom surface.
# ======================================================================

# For each atom in the molecule under consideration
for (s in 1:nrow(molj)){#s is the atom in the mol j

  tempSurfTot = 0

  #-------------------------------------------------------------------------------
  # Pairwise pfas atom-surface atom calculations
  #-------------------------------------------------------------------------------
  for (sa in 1:surfCount){#sa is the atom in the surface

    aasTot = 0

    #calculate separation between pfas and surface atom being investigated
    rawx = abs(surface$x[sa] - molj$x[s])
    rawy = abs(surface$y[sa] - molj$y[s])

    #adjust for period boundary conditions (further away than b=30Angstrom pairs see neighbours)
    deltax = (rawx%/%b)*b - rawx%%b
    deltay = (rawy%/%b)*b - rawy%%b

    D = sqrt(deltax^2 + deltay^2 + (surface$z[sa] - molj$z[s])^2)
    D_m = D*1e-10 #convert to m

    #-----------------------------------
    #6-12 Lennard Jones potential
    # eps_ij: well depth, sigma_ij:dependent on molecules
    # For the sigma_ij = (sigmaii * sigmajj)^1/2
    # Convert everything to SI units
    wDepth = sqrt(molj$wDepth[s]/1000*surface$wDepth[sa]/1000)/N_A #in J
    sigma = sqrt(molj$sigma[s]*1e-10*surface$sigma[sa]*1e-10)#in m
    u_lj = 4*wDepth*((sigma/D_m)^12 - (sigma/D_m)^6)

    #-----------------------------------
    #Coulomb potential
    q1 = molj$charge[s]*e
    q2 = surface$charge[sa]*e #electron charge e to get from eV to J
    u_c = q1*q2/(4*pi*eps_0*eps_water*D_m)#D_m is separation in m
```

```
    #==============================
    #Atom-Atom totals
    aasTot = u_lj + u_c #total for one pair

    #print(paste("aas Tot", s, sa, "=", aasTot))

    tempSurfTot = tempSurfTot + aasTot #total for one atom s of molecule j with all of surface

  }#end for sa : each molecule in the surface

  #Update totals
  newSurfacePotential = newSurfacePotential + tempSurfTot
  newPotential = newPotential + tempSurfTot


  #-----------------------------------------------------
  # Calculate potential with other molecules atoms
  #-----------------------------------------------------

  #===========================================
  #For other molecules in the box
  #But not molecule j itself
  notJ = 1:Ntot
  notJ = notJ[-j]
  for(k in notJ){

    molk = molecule[[k]]

    #===========================================
    # For other atoms within the molecule
    for (t in 1:nrow(molk)){#t is the atom in the pfas

      #calculate actual separation between molecule atoms being investigated
      rawx = abs(molk$x[t] - molj$x[s])
      rawy = abs(molk$y[t] - molj$y[s])

      #adjust for period boundary conditions (further away than b=30Angstrom pairs see neighbours)
      deltax = (rawx%/%b)*b - rawx%%b
      deltay = (rawy%/%b)*b - rawy%%b

      D = sqrt(deltax^2 + deltay^2 + (molk$z[t] - molj$z[s])^2)
      D_m = D*1e-10 #convert to m

      #----------------------------------
      #6-12 Lennard Jones potential
      # eps_ij =  #well depth
      # sigma_ij = #dependent on molecules
      # For the sigma_ij = (sigmaii * sigmajj)^1/2
      # Convert everything to SI units
      wDepth = sqrt(molj$wDepth[s]/1000*molk$wDepth[t]/1000)/N_A #in J
      sigma  = sqrt(molj$sigma[s]*1e-10*molk$sigma[t]*1e-10)#in m
      u_lj = 4*wDepth*((sigma/D_m)^12 - (sigma/D_m)^6)

      #----------------------------------
      #Coulomb potential
      q1 = molj$charge[s]*e
      q2 = molk$charge[t]*e #electron charge e to get from eV to J
      u_c = q1*q2/(4*pi*eps_0*eps_water*D_m)#D_m is separation in m

      #==============================
      #update totals
      newPotential = newPotential +  u_lj + u_c #Just keep adding

      #update also rows of the potential matrix
      newMatrixRow[k] = newMatrixRow[k] + u_lj + u_c

    }#end for t (each pfas atom)

  }# end k for each other molecule not j

} #end for s (each anion atom)
```

```
    #====================================
    # Decide whether to Accept or reject
    diffPotential = newPotential - oldPotential
    if(debug==TRUE) {
      print(paste("Old potential", oldPotential))
      print(paste("New potential", newPotential))
      print(paste("Difference", diffPotential))
    }

    #if potential lower, accept:
    if(newPotential<=oldPotential){
      if(debug==TRUE) { print("Move accepted outright") }

      #store new molecule position
      molecule[[j]]=molj

      #Update potentials
      totalPotential = totalPotential + diffPotential #total potential
      surfaceAtomPotentials[j] = newSurfacePotential #update surface atom potentials for mol j
      potentMatrix[j,] = newMatrixRow #totals for j with other mols
      potentMatrix[,j] = newMatrixRow

    }
    else{
      #if potential higher, accept with probability...
      acceptProb = exp(1)^(-(1/(kB*T))*diffPotential)
      randomProb = runif(1) #random num b/w 0 and 1
      tau = 1 #tau #increase if not converging. Unity preserves symmetry

      if(debug==TRUE) {
        print(paste("kB",kB,"T",T))
        print(paste("acceptance probability",acceptProb))
        print(paste("random probability",randomProb))
      }

      #if accepted
      if(randomProb<(1/tau)*acceptProb){

        if(debug==TRUE) { print("move acceptd with higher potential") }

        #store new molecule position
        molecule[[j]]=molj

        #Update totals
        totalPotential = totalPotential + diffPotential #total potential
        surfaceAtomPotentials[j] = newSurfacePotential #update surface atom potentials for mol j
        potentMatrix[j,] = newMatrixRow
        potentMatrix[,j] = newMatrixRow

      }#end inner if
      else{#Move is Rejected
        #For rejected moves, set centreToSurfaceDistance  back to previous value
        centreToSurface[i+1,j] = centreToSurface[i,j]
        maxToSurface[i+1,j] = maxToSurface[i,j]
        #For rejected moves, set RotStore  back to previous value
        xRotStore[i+1,j] = xRotStore[i,j]
        yRotStore[i+1,j] = yRotStore[i,j]
        zRotStore[i+1,j] = zRotStore[i,j]

        if(debug==TRUE) { print("move rejected") }

      }#end move rejected
    }#end not accept outright (else)

    #Update running list of total potentials (for plotting later)
    u_tot_list = c(u_tot_list, totalPotential)

    if(debug==TRUE) { print("----------------------------------------") }

  }#end j for each molecule in the box

}#end i (number of monte carlo steps)
```

```
print(paste("Final total:",totalPotential))

#Record and print computation time
fTime = proc.time()
elaps = fTime[3]-sTime[3]
print(paste0("Time taken: ",elaps," seconds"))

#=========================================================================
#SAVE WORKSPACE
#=========================================================================
outPutFile = paste0("MixedSurfaceCharge",N,liquidName,"_",Ndiv,"Ca_",Nci,"H_",Noh,"OH_",
                    sign(charge_C),"surf_",numSteps,"_",stepSize,"Ang.RData")
save.image(outPutFile)
```

E.2 Long-range force calculation

```
#-------------------------------------------------------------------
# Calculation of net charges and long range forces
# Author: Julie Sleep
# Writes to file and workspace
# Requires Monte_v51a_16PFAS or similar to be run first
# Need to run plotting script afterwards for figures
# Then run simulation with LRF script
#-------------------------------------------------------------------

getwd()
unix = TRUE
#unix = FALSE

if(unix==FALSE){
  setwd("PFAS/Soil/SoilMolecular")
  setwd("../../PFAS/Soil/SoilMolecular")
  #setwd("Results")
}

maxzi = 200.5
maxzj = 200.5
rmax = 10000 #maximum distance away from centre
deltar = 10 #interval for trapezoidal rule


fileList = list()

#Scenario 1: non-anion
fileList[1] = "Paper3Results/16PFBS_0Ca_0H_0OH_0surf_20000_0.5Ang.RData"
fileList[2] = "Paper3Results/16PFOS_0Ca_0H_0OH_0surf_20000_0.5Ang.RData"

#Scenario 2: anion with 16H+
fileList[3] = "Paper3Results/16PFBSion_0Ca_16H_0OH_0surf_20000_0.5Ang.RData"
fileList[4] = "Paper3Results/16PFOSion_0Ca_16H_0OH_0surf_20000_0.5Ang.RData"

#Scenario 3: anion with pos surface
fileList[5] = "Paper3Results/16PFBSion_0Ca_0H_0OH_1surf_20000_0.5Ang.RData"
fileList[6] = "Paper3Results/16PFOSion_0Ca_0H_0OH_1surf_20000_0.5Ang.RData"
#file = "PFOAResults/16PFOAion_0Ca_0H_0OH_1Surf_20000_0.5Ang.RData"

#Scenario 4: anion with 32 H+ and neg surface
fileList[7] = "Paper3Results/16PFBSion_0Ca_32H_0OH_-1surf_20000_0.5Ang.RData"
fileList[8] = "Paper3Results/16PFOSion_0Ca_32H_0OH_-1surf_20000_0.5Ang.RData"
#file = "16PFOAion_0Ca_32H_0OH_-1surf_20000_0.5Ang.RData"

#Scenario 5: anion with 16 Ca2+ and neg surface
fileList[9] = "Paper3Results/16PFBSion_16Ca_0H_0OH_-1surf_20000_0.5Ang.RData"
fileList[10] = "Paper3Results/16PFOSion_16Ca_0H_0OH_-1surf_20000_0.5Ang.RData"

#Scenario 6: anion with 16 OH- and double pos surface
fileList[11] = "Paper3Results/16PFBSion_0Ca_0H_16OH_1surf_20000_0.5Ang.RData"
fileList[12] = "Paper3Results/16PFOSion_0Ca_0H_16OH_1surf_20000_0.5Ang.RData"

#Scenario 7: anion with 8 H+, 8 OH- and pos surface
fileList[13] = "Paper3Results/16PFBSion_0Ca_8H_8OH_1surf_20000_0.5Ang.RData"
```

```
fileList[14] = "Paper3Results/16PFOSion_0Ca_8H_8OH_1surf_20000_0.5Ang.RData"
#file1 = "PFOAResults/16PFOAion_0Ca_8H_8OH_1surf_20000_0.5Ang.RData"

#Scenario 8: anion with 16 H+, 16 OH- and pos surface
fileList[15] = "Paper3Results/16PFBSion_0Ca_16H_16OH_1surf_20000_0.5Ang.RData"
fileList[16] = "Paper3Results/16PFOSion_0Ca_16H_16OH_1surf_20000_0.5Ang.RData"
#file1 = "PFOAResults/16PFOAion_0Ca_16H_16OH_1surf_20000_0.5Ang.RData"

#Scenario 4: anion with 32 H+ and neg surface
fileList[17] = "MixedSurfaceCharge16PFBSion_0Ca_32H_0OH_-1surf_20000_0.5Ang.RData"
fileList[18] = "MixedSurfaceCharge16PFOSion_0Ca_32H_0OH_-1surf_20000_0.5Ang.RData"
#file = "16PFOAion_0Ca_32H_0OH_-1surf_20000_0.5Ang.RData"


num_files = length(fileList)
#num_files = 2 #for debugging - the end file number

#start_file = 1
start_file = 17 #for debugging

#============================================================
for(fnum in start_file:num_files){

  print(paste("file ",fnum))

  file = fileList[[fnum]]
  load(file)

  #set cropping point
  cropPoint = 2500
  dataSize = numSteps+1-cropPoint
  croppedSurface1 = matrix(numeric(N*dataSize),
                           nrow=dataSize, ncol=N)

  #Store positions and calculate densities PFAS 1
  for(i in 1:N){
    for(j in 1:dataSize){
      #croppedSurface[j,i] = maxToSurface[cropPoint+j,i]
      croppedSurface1[j,i] = centreToSurface[cropPoint+j,i]
    }
  }

  #Counterions 1
  if(Nci>0){
    hydrogenData1 = matrix(numeric(Nci*dataSize),nrow=dataSize, ncol=Nci)
    for(i in (N+1):(N+Nci)){
      for(j in 1:dataSize){
        hydrogenData1[j,i-N] = centreToSurface[cropPoint+j,i]
      }
    }
  }

  #Divalent cations 1
  if(Ndiv>0){
    calciumData1 = matrix(numeric(Ndiv*dataSize),nrow=dataSize, ncol=Ndiv)
    for(i in (N+1):Ntot){
      for(j in 1:dataSize){
        calciumData1[j,i-N] = centreToSurface[cropPoint+j,i]
      }
    }
  }

  # Hydroxyl (as well as hydrogen)
  if(Noh>0 && Nci>0){
    ohData1 = matrix(numeric(Noh*dataSize),nrow=dataSize, ncol=Noh)
    for(i in (N+Nci+1):(N+Nci+Noh)){
      for(j in 1:dataSize){
        ohData1[j,i-(N+Nci)] = centreToSurface[cropPoint+j,i]
      }
    }
    # Just hydroxyl
  }else if(Noh>0){
    ohData1 = matrix(numeric(Noh*dataSize),nrow=dataSize, ncol=Noh)
```

```
  for(i in (N+Nci+1):(N+Nci+Noh)){
    for(j in 1:dataSize){
      ohData1[j,i-N] = centreToSurface[cropPoint+j,i]
    }
  }
}

#-------------------------------------------------------------
# Part I: Net Charge calculation
#-------------------------------------------------------------

#Histogram for PFAS
#pfasHist1 = hist(croppedSurface1, breaks=c(0:ceiling(max(croppedSurface1))))
pfasHist1 = hist(croppedSurface1, breaks=c(-0.5:maxzj))

#Histogram counterions
if(Nci>0){
  #hydroHist1 = hist(hydrogenData1, breaks=c(0:ceiling(max(hydrogenData1))))
  hydroHist1 = hist(hydrogenData1, breaks=c(-0.5:maxzj))
}

#Histogram oh
if(Noh>0){
  #hydroHist1 = hist(hydrogenData1, breaks=c(0:ceiling(max(hydrogenData1))))
  ohHist1 = hist(ohData1, breaks=c(-0.5:maxzj))
}

#Histogram divalen Ca2+
if(Ndiv>0){
  caHist1 = hist(calciumData1, breaks=c(-0.5:maxzj))
}

#Convert to charge distribution
obsPerPointP1 = nrow(croppedSurface1)
if(liquidName=="PFOSion" || liquidName=="PFBSion"){
  anionCharge=-1
  chargePfas1 = pfasHist1$counts*anionCharge/obsPerPointP1
} else  {
  chargePfas1 = pfasHist1$counts*0/obsPerPointP1
}
#
#  if(unix==FALSE){
# Plot Net Charges
#    plotFileName = paste0("../PaperFigures/NetCharge",liquidName,Nci,"H",Ndiv,"Ca",
#Noh,"OH",100*round(charge_C,2),"Surf.png")
#    png(plotFileName, height=400, width=450)
ymax = 4
ymin = -4
#    plot(x=pfasHist1$mids, chargePfas1, pch="-", ylim=c(ymin,ymax),
#         xlab="distance from surface (A)", ylab = "Net charge density (e)")
#    abline(h=0)
if(Nci>0){
  obsPerPointH1 = nrow(hydrogenData1)
  hydroCharge=1
  chargeHydrogen1 = hydroHist1$counts*hydroCharge/obsPerPointH1
  #      points(x=hydroHist1$mids, chargeHydrogen1, pch="+")
}

if(Noh>0){
  obsPerPointOH1 = nrow(ohData1)
  ohCharge=-1
  chargeOH1 = ohHist1$counts*ohCharge/obsPerPointOH1
  #      points(x=ohHist1$mids, chargeOH1, pch="*")
}

if(Ndiv>0){
  obsPerPointCa1 = nrow(calciumData1)
  caCharge=2
  chargeCa1 = caHist1$counts*caCharge/obsPerPointCa1
  #      points(x=caHist1$mids, chargeCa1, pch="x")
}

if(Nci==0 && Noh==0 && Ndiv==0){
```

```
  netCharge1 = chargePfas1
}

if(Nci>1 && Noh==0){
  netCharge1 = chargePfas1 + chargeHydrogen1
}

if(Nci==0 && Noh>1){
  netCharge1 = chargePfas1 + chargeOH1
}

if(Nci>1 && Noh>1){
  netCharge1 = chargePfas1 + chargeHydrogen1 + chargeOH1
}

if(Ndiv>0){
  netCharge1 = chargePfas1 + chargeCa1
}

#    points(x=pfasHist1$mids, y=netCharge1, type="l", lwd=2, col="red")
#    legend(x=maxzj*0.72, y=ymax, pch=c("-","+","*","x","-"),
#  legend=c(liquidName,"H+","OH-","Ca2+","Net charge"))
#    dev.off() #save image
#  }#end no plotting on unix

#mean(croppedSurface1)#means of individual data.
#mean(hydrogenData1)
#sum(netCharge1) #check for total overall charge

#Write net charges to file  *** NOTE these are in e and angstroms
if(mixedSurfaceCharge == FALSE){
  ncFile = paste0("NetCharges/TotalNetCharge",liquidName,Nci,"H",Ndiv,"Ca",
                  Noh,"OH",100*round(charge_C,2),"Surf.txt")
  write.table(netCharge1, ncFile, sep=" ")
}else if (mixedSurfaceCharge == TRUE){
  ncFile = paste0("NetCharges/TotalNetChargeMixedSurface",liquidName,Nci,"H",Ndiv,"Ca",
                  Noh,"OH",100*round(charge_C,2),"Surf.txt")
  write.table(netCharge1, ncFile, sep=" ")
}

#-----------------------------------------------------------------------
# Part II: Long range force calculation
#-----------------------------------------------------------------------

a = 2*b/sqrt(pi)

# Calculate the external potential for all z_i i=1,... 120
# (or maximum height from surface)
# For each z=1,..20 (or point where net charge is close to zero)
# z's in net charges refer to mid points of histogram bins.
# z=1 is for z between 0 and 1
# Note that indices to matrix start at 1, but represent z=0

# This section is performed for each simulation scenario
wlr_i = matrix(nrow=maxzi+0.5, 1)
wlr_final = matrix(nrow=maxzi+0.5, 1)
zi_store = rep(0, maxzi+0.5)
multistore = list()
for(zi in 0:(maxzi+0.5)){ #zi is the n - the height of the molecule in question at the centre of the box
  #print(paste("zi=",zi))
  r_store = rep(0, rmax)
  deltar_in_m = deltar*1e-10
  r_sequence = seq(round(a),rmax,deltar) #points to evaluate for trapezoidal rule

  for(r in r_sequence){

    #print(paste("r",r))

    temp_r_store = 0

    #calculation for surface
    d = sqrt(r^2 + zi^2)
    d_in_m = d*1e-10 #convert to m
```

```
    b_in_m = b*1e-10
    r_in_m = r*1e-10

    #surfaceChargeAng2 = sum(surfaceCharge)/((2*b)^2)
    surfaceChargeAng2 = sum(surface$charge)/((2*b)^2)
    #surfaceChargeM2 = sum(surfaceCharge)/((2*b_in_m)^2)

    #u_surf = e*surfaceChargeAng2/(4*pi*eps_0*eps_water*d)
    #u_surf = e*surfaceChargeM2/(4*pi*eps_0*eps_water*d_in_m)
    u_surf = e*surfaceChargeAng2/(4*pi*eps_0*eps_water*d_in_m)

    #print(paste("surf",u_surf))

    zj_store = rep(0, maxzj+0.5)

    for(zj in 0:(maxzj+0.5)){ #zj is the variable 'm'

      #calculation in solution
      d = sqrt(r^2 + (zi-zj)^2)
      d_in_m = d*1e-10 #convert to m

      #u_over_q1 = e*netCharge1[zj]/(4*pi*eps_0*eps_water*d)
      u_over_q1 = (e*netCharge1[zj]/((2*b)^2))/(4*pi*eps_0*eps_water*d_in_m)

      zj_store[zj] = u_over_q1

    }#End zj loop

    u_soln = sum(zj_store)
    #temp_r_store = (u_surf + sum(zj_store))*2*pi*r*deltar
    temp_r_store = (u_surf + u_soln)*2*pi*r*deltar_in_m

    #print(paste("temp_r",temp_r_store))

    #surface interaction + solution interaction
    #times 2*pi*2 for circumference of circle
    #times deltar for trapezoidal rule

    #Trapezoidal rule - first and last terms by 1/2
    if(r==round(a) || r==r_sequence[length(r_sequence)]){
      r_store[r] = 0.5 * temp_r_store
    } else {
      r_store[r] = temp_r_store
    }

  }#end r loop

  multistore[[zi+1]] = r_store

  zi_store[zi] = sum(r_store)

  wlr_i[zi] = zi_store[zi]

  #print(paste("total", wlr_i[zi]))

}#end zi loop


#PLOTS FOR DEBUGGING
if(unix==FALSE){
  plot(wlr_i)
  #plotFileName = paste0("../PaperFigures/Convergence",liquidName,Nci,"H",Ndiv,"Ca",
  #Noh,"OH",100*round(charge_C,2),"Surf.png")
  #png(plotFileName, height=300, width=450)
  #plot(part2_store, type="l", col="red")
  #points(-1*part3_store, type="l", col="blue")
  #legend("left", legend = c("part2","-part3"), col = c("red","blue"), lty=1)
  #dev.off()
}

wlr_final = wlr_i*e

# Plot WLR FINAL
```

```
  if(unix == FALSE){
    if(mixedSurfaceCharge == FALSE){
      plotFileName3 = paste0("../PaperFigures/LRF",liquidName,Nci,"H",Ndiv,"Ca",
                             Noh,"OH",100*round(charge_C,2),"Surf.png")
    }else if (mixedSurfaceCharge == TRUE){
      plotFileName3 = paste0("Chem2Results/Figures/MixedSurface_LRF",liquidName,Nci,"H",Ndiv,"Ca",
                             Noh,"OH",100*round(charge_C,2),"Surf.png")
    }
    png(plotFileName3, height=300, width=450)
    plot(wlr_final)
    abline(h=0)
    dev.off()  #save image
  }

  if(unix == FALSE){
    # Plot positive and negative lines
    if(mixedSurfaceCharge == FALSE){
      plotFileName2 = paste0("../PaperFigures/PosNegLRF",liquidName,Nci,"H",Ndiv,"Ca",
                             Noh,"OH",100*round(charge_C,2),"Surf.png")
    }
    else if(mixedSurfaceCharge == TRUE){
      plotFileName2 = paste0("Chem2Results/Figures/MixedSurface_PosNegLRF",liquidName,Nci,"H",Ndiv,"Ca",
                             Noh,"OH",100*round(charge_C,2),"Surf.png")
    }
    png(plotFileName2, height=300, width=450)
    posCurve = 1*e*wlr_final
    negCurve = -1*e*wlr_final
    axislim = max(max(posCurve),max(negCurve))
    plot(posCurve, col="blue", ylim = c(-1*axislim,1*axislim))
    points(negCurve, col="red")
    abline(h=0)
    dev.off()  #save image
  }

  #NEED TO CONVERT EVERYTHING TO M from AA
  #Final values are potentials, need to multiple by q_i during simulation
  #to get J. (not e anymore, writing wrl_final)
  if(mixedSurfaceCharge == FALSE){
    wlriFile = paste0("NetCharges/LongRangePotential",N,liquidName,Ndiv,"Ca",Nci,"H",
                      Noh,"OH",sign(charge_C),"Surf.txt")
  }else{
    wlriFile = paste0("NetCharges/MixedSurface_LongRangePotential",N,liquidName,Ndiv,"Ca",Nci,"H",
                      Noh,"OH",sign(charge_C),"Surf.txt")
  }
  write.table(wlr_final, wlriFile, sep=" ")

  #Save r workspace for later plotting
  if(mixedSurfaceCharge == FALSE){
    outPutFile = paste0("NetCharges/Workspace",N,liquidName,"_",Ndiv,"Ca_",Nci,"H_",Noh,"OH_",
                        sign(charge_C),"surf.RData")
  }else{
    outPutFile = paste0("NetCharges/MixedSurface_Workspace",N,liquidName,"_",Ndiv,"Ca_",Nci,"H_",Noh,"OH_",
                        sign(charge_C),"surf.RData")

  }
  save.image(outPutFile)
}
```

E.3 Monte Carlo simulation with long-range forces

```
#============================================================
# PFAS on Solid Substrates ---
# Author: Julie Sleep
# Monte Carlo PFSAs on Graphite
# Version of 21/03/2022
# Incorporates long range interactions
# as of 4W incorporates mixed surface option
#============================================================
#liquidList = c("PFOS","PFBS",rep(c("PFOSion","PFBSion"),7))
```

```
#ciNumberList = c(0,0,16,16,0,0,32,32,0,0,0,0,8,8,16,16)

#Variable parameters required to be set:

unix=TRUE #Set to true when runing on unix machine to suppress plotting
#unix=FALSE #Set to false to include plotting
#debug=TRUE # Set to true to print out acceptance values
debug=FALSE # Set to false to suppress print out
mixedSurfaceCharge = TRUE
#mixedSurfaceCharge = FALSE

#liquidName = "PFOS"
#liquidName = "PFOSion"
#liquidName = "PFBS"
#liquidName = "PFBSion"
#liquidName = "PFOA"
#liquidName = "PFOAion"
liquidName = "PFDAion"

N = 16 #number of PFAS molecules
Nci = 32 # number of positive counterions (H+)
Ndiv = 0 # number of divalent cations (Ca2+)
Noh = 0 # Number of negative counterions (OH-)

# Charge balance on carbon in eV, later multiplied by e to convert to C
#charge_C = 0 #Neutral
charge_C = -16/1397 #Negative
#charge_C = 16/1397 #Positive
#charge_C = 2*16/1397 #Double positive

if(mixedSurfaceCharge==TRUE){#convert charge to just cover the 711 molecules
  charge_C=charge_C*1397/711
}

numSteps = 20000 #Number of monte carlo steps
#numSteps = 10 #Number of monte carlo steps
stepSize = 0.5 #Angstrom, was 0.5

if(unix==FALSE){
  library(scatterplot3d)
  library(rgl)
}

#Clear workspace and set directory
if(unix==FALSE){
  #rm(list=ls())
  getwd()
  setwd("PFAS/Soil/SoilMolecular")
  #setwd("..")
}

#Measure system time
sTime = proc.time()

#Monte Carlo and Molecule Parameters
set.seed(1) #for random number generation
Ntot = N + Nci + Noh + Ndiv #Total number of ions
if(liquidName=="PFOS" || liquidName == "PFOSion"){
  pfosColours = c("yellow", rep("green",17), rep("red",3),rep("grey",8),"white")
}else if(liquidName=="PFBS" || liquidName == "PFBSion"){
  pfosColours = c("yellow", rep("green",9), rep("red",3),rep("grey",4),"white")
}else{
  pfosColours = c("yellow", rep("green",17), rep("red",3),rep("grey",8),"white")
}

#Box dimensions
b = 30 #Dimensions of (half) box (Angstroms)
boxh = 30 # (half) height of box
colfunc <- colorRampPalette(c("aquamarine3", "cornflowerblue", "darkorchid3",
                              "deeppink3"))#,"darkgoldenrod2","darkolivegreen3"))
colourpfas = colfunc(N)

#Physical Constants
```

```
e = 1.60217662e-19 #- e charge
kB = 1.38064852e-23 # Boltzmann
eps_water = 80.1 # relative permittivity of Water at 20 degrees
eps_0 = 8.854187817620e-12 # vacuum permittivity
N_A = 6.022140857e23 #Avogadros number
T = 300 # Temp in Kelvin
#n1 = 1.00029 #Refractive indexes Air
#eps1 = 1.00059 #Air #Dielectric constants
#eps_air = 1.00054

#Surface constants
wDepth_C = 2.12267 #kJ mol-1 HOPG (/1000/NA in eqn)
sigma_C = 2.9 #Angstroms (to m in eqn)
#wDepth_HOPG = 0.4393 #kJ mol-1 HOPG
#sigma_HOPG = 3.851 #Angstrom HOPG

#Variables for storing values
u_tot = 0
lj_tot = 0
coul_tot = 0
totalPotential = 0 #Total for all molecules

#Temporary store variables used inside loop
atom_sTot = 0

#vectors and matrices for storing results
u_tot_list = c() #list of total potential at each step
potentMatrix = matrix(numeric(Ntot^2), nrow=Ntot, ncol=Ntot) #Potentials between each molecule
surfaceAtomPotentials = numeric(Ntot) #Potentials between molecules and surface
centreToSurface = matrix(numeric(Ntot*(numSteps+1)), nrow=numSteps+1, ncol=Ntot) #Storing z value for accepted moves
maxToSurface = matrix(numeric(Ntot*(numSteps+1)), nrow=numSteps+1, ncol=Ntot) #Storing z value for accepted moves
xRotStore  = matrix(numeric(Ntot*(numSteps+1)), nrow=numSteps+1, ncol=Ntot) # x rotation for accepted moves
yRotStore  = matrix(numeric(Ntot*(numSteps+1)), nrow=numSteps+1, ncol=Ntot) # y for accepted moves
zRotStore  = matrix(numeric(Ntot*(numSteps+1)), nrow=numSteps+1, ncol=Ntot) # z value for accepted moves

#new for mixed surface
centreXcoords = matrix(numeric(Ntot*(numSteps+1)), nrow=numSteps+1, ncol=Ntot) #Storing x value for accepted moves
centreYcoords = matrix(numeric(Ntot*(numSteps+1)), nrow=numSteps+1, ncol=Ntot) #Storing y value for accepted moves


#=========================================================================
# System structure creation, placing and plotting
#=========================================================================
#Some points in a box to plot
Sub = seq(-b,b, by=1.42)
NNN = 10
xx = runif(NNN,-b,b)
yy = runif(NNN,-b,b)
zz = runif(NNN,0,boxh)
ions = data.frame(xx,yy,zz)
if(unix==FALSE){
  ionplot = scatterplot3d(ions,
                          color="white", pch = "*",
                          xlab = expression(paste("x (",ring(A),")")),
                          ylab = expression(paste("y (",ring(A),")")),
                          zlab = expression(paste("z (",ring(A),")")),
                          xlim=c(-b,b), ylim=c(-b,b), zlim=c(0,boxh*2)
  )
}
#=============================================================
#Plot and store a bottom surface
surfaceX = vector()
surfaceY = vector()
surfaceZ = vector()

#Starting positions
gZ = 0
gY = b
gX = -b
rowCount = 1
surfCount = 0

while (gY>=-b && gY<=b){
```

```
  #For all odd numbered rows (including the first)
  if(rowCount%%2 == 1){
    #For each atom in an odd row
    for (j in 1:29){
      surfCount = surfCount +1 # Count number of atoms in surface
      if(j == 1){#first molecule
        gX = -b
      }
      else if((j %% 2) == 0){#even molecules
        gX = gX + 1.42
      }
      else{# odd molecules
        gX = gX + 2.84
      }
      if(unix==FALSE){ ionplot$points3d(x=gX, y=gY, z=gZ, pch=21, col="black", bg="grey") }

      #Add atom to data frame
      surfaceX = c(surfaceX, gX)
      surfaceY = c(surfaceY, gY)
      surfaceZ = c(surfaceZ, gZ)
    }#end for each atom
  }#end for odd row
  else if (rowCount%%2 == 0){#For all even numbered rows (second and onward --- different offset)

    #For each atom in an even row
    for (j in 1:28){
      surfCount = surfCount + 1 # Count number of atoms in surface
      if(j == 1){#first molecule
        gX = -b+1.42+0.71
      }
      else if((j %% 2) == 0){#even molecules
        gX = gX + 1.42
      }
      else{# odd molecules
        gX = gX + 2.84
      }
      if(unix==FALSE){ ionplot$points3d(x=gX, y=gY, z=gZ, pch=21, col="black", bg="grey")}
      #Add atom to data frame
      surfaceX = c(surfaceX, gX)
      surfaceY = c(surfaceY, gY)
      surfaceZ = c(surfaceZ, gZ)

    }#end for within row
  }#end for even rows

  #shift y to next row, and increment counter
  gY = gY - 1.23
  rowCount = rowCount + 1
}#end while rows within bounds

print(paste(surfCount,"atoms in surface, check =", length(surfaceX)))
surfaceAtoms = rep("C", surfCount)
surfaceEpsilon = rep(wDepth_C, surfCount)
surfaceSigma = rep(sigma_C, surfCount)
if(mixedSurfaceCharge == TRUE){#HETEROGENEOUS CHARGE
  surfaceCharge = c(rep(c(rep(charge_C,15),rep(0,14),
                          rep(charge_C,14),rep(0,14))
                        ,24),
                    rep(charge_C,15),rep(0,14))
}else{#HOMOGENEOUS CHARGE
  surfaceCharge = rep(charge_C, surfCount)
}

surface = data.frame(atoms = surfaceAtoms, x = surfaceX, y = surfaceY, z = surfaceZ,
                     wDepth = surfaceEpsilon, sigma = surfaceSigma, charge = surfaceCharge)

#Write surface to file
if(mixedSurfaceCharge == FALSE){
  write.csv(surface, file = "LRF_Surface_fromR.csv")
}else{
  write.csv(surface, file = "LRF_Mixed_Surface_fromR.csv")
}
```

```
#-------------------------------------------------------------
# Read in pfas molecules # PFOS - pubchem
#-------------------------------------------------------------
pfasFileName = paste0("Structures/",liquidName,".txt")
pfas = read.table(pfasFileName, header=TRUE)
pfas$sigma  = pfas$Sigma #in angstrom
pfas$wDepth = pfas$WellDepth*4185.8 #was in kcal/mol need to be in J/mol x 4185.8
pfas$charge = pfas$Charge #in e
pfas$origx = pfas$x # A copy of co-ordinates centred at 0,0,0
pfas$origy = pfas$y
pfas$origz = pfas$z

#Make list of N pfas
pfasList = rep(list(pfas), N)

#calculate placement lists
xplacepfas = rep(c(-15, 5, -5, 15), 4)
yplacepfas = rep(c(15, 15, 5, 5, -5, -5, -15, -15), 2)
zplacepfas = c(rep(10, 8), rep(20, 8))

print(paste("Placing", Ntot, " ", liquidName, "molecules in the box"))
#Offset molecules in box
for(i in 1:N){
  pfasList[[i]]$x = pfasList[[i]]$x + xplacepfas[i]
  pfasList[[i]]$y = pfasList[[i]]$y + yplacepfas[i]
  pfasList[[i]]$z = pfasList[[i]]$z + zplacepfas[i]
}

if(unix==FALSE){
  #plot structures in box
  for(i in 1:N){
    ionplot$points3d(pfasList[[i]]$x, pfasList[[i]]$y, pfasList[[i]]$z, pch=21,
                     col="black", bg=colourpfas[i], cex=1.75)
  }
  #convert to 2d
  pfasCor <- ionplot$xyz.convert(pfas$x,pfas$y,pfas$z)
}

#-------------------------------------------------------------
# Place H+ counterions in box
#-------------------------------------------------------------
if(Nci>0){
  #Properties of a single counter ion type (i.e. H+)
  counterIon = data.frame(atomType="H",x=0,y=0,z=0, sigma=1.6, wDepth=0.03, charge=1)
  counterIon$origx = counterIon$x
  counterIon$origy = counterIon$y
  counterIon$origz = counterIon$z

  #Make list of Nci counter ions (e.g. 16 H+)
  ciList = rep(list(counterIon),Nci)

  #calculate placement lists (For ONLY H+)
  xplaceci = rep(c(-5, 15, -15, 5), 8)
  yplaceci = rep(c(15, 15, 5, 5, -5, -5, -15, -15), 4)
  zplaceci = c(rep(10, 8), rep(30, 8), rep(20,8), rep(40,8))

  #calculate placement lists (For case with both 8 H+ and 8 OH-)
  if(Noh>0){
    xplaceci = rep(c(-5, 15, -15, 5), 8)
    yplaceci = rep(c(15, 15, 5, 5, -5, -5, -15, -15), 4)
    zplaceci = c(rep(c(10,10,20,20),2),rep(c(15,15,25,25),2))
  }


  print(paste("Placing", Nci, "counterions in the box"))
  #Offset molecules in box
  for(i in 1:Nci){
    ciList[[i]]$x = ciList[[i]]$x + xplaceci[i]
    ciList[[i]]$y = ciList[[i]]$y + yplaceci[i]
    ciList[[i]]$z = ciList[[i]]$z + zplaceci[i]
  }
```

```
  if(unix==FALSE){
    #plot structures in box
    for(i in 1:Nci){
      ionplot$points3d(ciList[[i]]$x, ciList[[i]]$y, ciList[[i]]$z, pch=21,
                       col="black", bg="yellow", cex=1.75)
    }
  }
}else{
  ciList = NULL
}

#-------------------------------------------------------------
# Place OH- counterions in box
#-------------------------------------------------------------
if(Noh>0){
  #Properties of a single counter ion type
  #Lin 16b, wdepth published in kcal/mol, converted to kj/mol
  ohIon = data.frame(atomType="OH",x=0,y=0,z=0, sigma=3.7, wDepth=0.33472, charge=-1)
  ohIon$origx = ohIon$x
  ohIon$origy = ohIon$y
  ohIon$origz = ohIon$z

  #Make list of Noh counter ions (e.g. 16 OH-)
  ohList = rep(list(ohIon),Noh)

  #calculate placement lists for case of OH only
  xplaceoh = rep(c(-5, 15, -15, 5), 8)
  yplaceoh = rep(c(15, 15, 5, 5, -5, -5, -15, -15), 4)
  zplaceoh = c(rep(10, 8), rep(30, 8), rep(20,8), rep(40,8))

  #calculate placement lists (For case with both 8 H+ and 8 OH-)
  if(Nci>0){
    xplaceoh = rep(c(-5, 15, -15, 5), 8)
    yplaceoh = rep(c(15, 15, 5, 5, -5, -5, -15, -15), 4)
    zplaceoh = c(rep(c(20,20,10,10),2),rep(c(25,25,15,15),2))
  }

  print(paste("Placing", Noh, "OH ions in the box"))
  #Offset molecules in box
  for(i in 1:Noh){
    ohList[[i]]$x = ohList[[i]]$x + xplaceoh[i]
    ohList[[i]]$y = ohList[[i]]$y + yplaceoh[i]
    ohList[[i]]$z = ohList[[i]]$z + zplaceoh[i]
  }

  if(unix==FALSE){
    #plot structures in box
    for(i in 1:Noh){
      ionplot$points3d(ohList[[i]]$x, ohList[[i]]$y, ohList[[i]]$z, pch=21,
                       col="black", bg="red", cex=1.75)
    }
  }
}else{
  ohList = NULL
}

#-------------------------------------------------------------
# Place divalent cations in box
#-------------------------------------------------------------
if(Ndiv>0){
  #Properties of a single cation type (i.e. Ca2+) from Gromacs OPLS-AA
  divIon = data.frame(atomType="Ca",x=0,y=0,z=0, sigma=2.41203, wDepth=1.88136, charge=2)
  divIon$origx = divIon$x
  divIon$origy = divIon$y
  divIon$origz = divIon$z

  #Make list of Nci counter ions (e.g. 16 H+)
  divList = rep(list(divIon),Ndiv)

  #calculate placement lists
  xplacediv = rep(c(-5, 15, -15, 5), 8)
  yplacediv = rep(c(15, 15, 5, 5, -5, -5, -15, -15), 4)
  zplacediv = c(rep(10, 8), rep(30, 8), rep(20,8), rep(40,8))
```

```
  print(paste("Placing", Ndiv, "divalent cations in the box"))
  #Offset molecules in box
  for(i in 1:Ndiv){
    divList[[i]]$x = divList[[i]]$x + xplacediv[i]
    divList[[i]]$y = divList[[i]]$y + yplacediv[i]
    divList[[i]]$z = divList[[i]]$z + zplacediv[i]
  }

  if(unix==FALSE){
    #plot structures in box
    for(i in 1:Ndiv){
      ionplot$points3d(divList[[i]]$x, divList[[i]]$y, divList[[i]]$z, pch=21,
                       col="black", bg="magenta", cex=2.75)
    }
  }
}else{
  divList = NULL
}


#@@@
```

```
#-------------------------------------------------------------------------
#Add in check for z below surface
for(i in 1:N){
  print(paste("checking below surface",i))
  print(min(pfasList[[i]]$z))
}
if(Nci>0){
  for(i in 1:Nci){
    print(paste("checking below surface",i))
    print(min(ciList[[i]]$z))
  }
}
if(Noh>0){
  for(i in 1:Noh){
    print(paste("checking below surface",i))
    print(min(ohList[[i]]$z))
  }
}
if(Ndiv>0){
  for(i in 1:Ndiv){
    print(paste("checking below surface",i))
    print(min(divList[[i]]$z))
  }
}

#=========================================================================
#Store pfas and counterions
molecule = c(pfasList,ciList,ohList,divList)

#=========================================================================
#Initialise variables
for(i in 1:N){
  centreToSurface[1,i] = zplacepfas[i]  #6*i # pfas centre 6 Ang to surface, 12
  maxToSurface[1,i] = max(molecule[[i]]$z) # pfas max Ang to surface
  xRotStore[1,i] = 0 # pfas rotation starts at 0
  yRotStore[1,i] = 0 # pfas rotation starts at 0
  zRotStore[1,i] = 0 # pfas rotation starts at 0
  centreXcoords[1,i] = xplacepfas[i]
  centreYcoords[1,i] = yplacepfas[i]
}
if(Nci>0){
  for(i in 1:Nci){
    centreToSurface[1,N+i] = zplaceci[i]
    maxToSurface[1,N+i] = max(molecule[[N+i]]$z) # pfas max Ang to surface
    xRotStore[1,N+i] = 0 # ci rotation starts at 0
    yRotStore[1,N+i] = 0 # ci rotation starts at 0
    zRotStore[1,N+i] = 0 # ci rotation starts at 0
    centreXcoords[1,N+i] = xplaceci[i]
    centreYcoords[1,N+i] = yplaceci[i]
  }
}
if(Noh>0){
  for(i in 1:Noh){
    centreToSurface[1,N+Nci+i] = zplaceoh[i]
    maxToSurface[1,N+Nci+i] = max(molecule[[N+Nci+i]]$z) # pfas max Ang to surface
    xRotStore[1,N+Nci+i] = 0 # ci rotation starts at 0
    yRotStore[1,N+Nci+i] = 0 # ci rotation starts at 0
    zRotStore[1,N+Nci+i] = 0 # ci rotation starts at 0
    centreXcoords[1,N+Nci+i] = xplaceoh[i]
    centreYcoords[1,N+Nci+i] = yplaceoh[i]
  }
}
if(Ndiv>0){
  for(i in 1:Ndiv){
    centreToSurface[1,N+Nci+Noh+i] = zplacediv[i]
    maxToSurface[1,N+Nci+i] = max(molecule[[N+Nci+Noh+i]]$z) # pfas max Ang to surface
    xRotStore[1,N+Nci+Noh+i] = 0 # ci rotation starts at 0
    yRotStore[1,N+Nci+Noh+i] = 0 # ci rotation starts at 0
    zRotStore[1,N+Nci+Noh+i] = 0 # ci rotation starts at 0
    centreXcoords[1,N+Nci+Noh+i] = xplacediv[i]
    centreYcoords[1,N+Nci+Noh+i] = yplacediv[i]
  }
}
```

```
#================================================================
#Read in long range electrostatic potential file
print("================================================")
print("Reading in long range interaction file")
if(mixedSurfaceCharge==FALSE){
  wlriFileName = paste0("NetCharges/LongRangePotential",N,liquidName,Ndiv,"Ca",Nci,"H",
                        Noh,"OH",sign(charge_C),"Surf.txt")
}else{
  wlriFileName = paste0("NetCharges/MixedSurface_LongRangePotential",N,liquidName,Ndiv,"Ca",Nci,"H",
                        Noh,"OH",sign(charge_C),"Surf.txt")
}
wlri = read.table(wlriFileName, header=TRUE)
lrList = wlri$V1
#lrList$1 gives long range potential at z between zero and 1
#this needs to be calculated

#=============================================================================
# Part 1
# Calculate inital total potential
# Storing the sub totals for later use
#=============================================================================

print("================================================")
print("Calculating initial Total Potential")

# ================================================================
for(j in 1:Ntot){#For each molecule in the box
  if(debug==TRUE){
    print(paste("Initial potential Molecule j =",j))}
  molj = molecule[[j]] #extract current molecule
  moljTot = 0 #total for j=1,2, etc.

  #================================================================
  # For each atom in molecule j under consideration
  for (s in 1:nrow(molj)){ #s is the atom in the mol

    atom_sTot = 0 #Total for each atom s within a molecule, S=C1,F2, etc. with surface

    #------------------------------------------------------------
    # Surface-atom calculations for mol j
    #------------------------------------------------------------

    #-----------------------------------------------------------------------------
    # Pairwise pfas atom-surface atom calculations
    #-----------------------------------------------------------------------------
    for (sa in 1:surfCount){#sa is the atom in the surface

      aasTot = 0

      #calculate separation between pfas and surface atom being investigated
      rawx = abs(surface$x[sa] - molj$x[s])
      rawy = abs(surface$y[sa] - molj$y[s])

      #adjust for period boundary conditions (further away than b=30Angstrom pairs see neighbours)
      # quotient * b (gives 30 or 0) minus remainder
      # i.e. raw 59, gives 1*30-29=1, raw 15 gives 0-15=-15 (is squared so sign irrelevant)
      deltax = (rawx%/%b)*b - rawx%%b
      deltay = (rawy%/%b)*b - rawy%%b

      D = sqrt( deltax^2 + deltay^2 +
                  (surface$z[sa] - molj$z[s])^2)
      D_m = D*1e-10 #convert to m

      #-----------------------------------
      #6-12 Lennard Jones potential
      # eps_ij: well depth, sigma_ij:dependent on molecules
      # For the sigma_ij = (sigmaii * sigmajj)^1/2
      # Convert everything to SI units
      wDepth = sqrt(molj$wDepth[s]/1000*surface$wDepth[sa]/1000)/N_A #in J
      sigma = sqrt(molj$sigma[s]*1e-10*surface$sigma[sa]*1e-10)#in m
      u_lj = 4*wDepth*((sigma/D_m)^12 - (sigma/D_m)^6)
```

```
  #----------------------------------
  #Coulomb potential
  q1 = molj$charge[s]*e
  q2 = surface$charge[sa]*e #electron charge e to get from eV to J
  u_c = q1*q2/(4*pi*eps_0*eps_water*D_m)#D_m is separation in m

  #================================
  #Atom-Atom totals
  aasTot = u_lj + u_c #total for one pair

  #print(paste("aas Tot", s, sa, "=", aasTot))

  atom_sTot = atom_sTot + aasTot #total for one atom s of molecule j with all of surface

}#end for sa : each molecule in the surface

#print(paste("s ", s," atom_sTot ", atom_sTot))

#update totals
#surfaceAtomPotentials[j] = surfaceAtomPotentials[j] + atom_sTot
#add atom s total to total for molecule j with surface

#-------------------------------------------------------------------------------
# Inter molecular calculations (not surface)
#-------------------------------------------------------------------------------

#-------------------------------------------------------------------------------
#For other molecules in the box
#But not molecule j itself
notJ = 1:Ntot
notJ = notJ[-j]

for(k in notJ){

  molk = molecule[[k]]
  molkTot = 0

  #-----------------------------------------------------------------------------
  # Pairwise atom-atom calculations
  #-----------------------------------------------------------------------------
  for (t in 1:nrow(molk)){#t is the atom in the otherMol

    pairTot = 0

    #calculate actual separation between molecule atoms being investigated
    rawx = abs(molk$x[t] - molj$x[s])
    rawy = abs(molk$y[t] - molj$y[s])

    #adjust for period boundary conditions (further away than b=30Angstrom pairs see neighbours)
    deltax = (rawx%/%b)*b - rawx%%b
    deltay = (rawy%/%b)*b - rawy%%b

    D = sqrt(deltax^2 + deltay^2 + (molk$z[t] - molj$z[s])^2)
    D_m = D*1e-10 #convert to m

    #----------------------------------
    #6-12 Lennard Jones potential
    # eps_ij: well depth, sigma_ij:dependent on molecules
    # For the sigma_ij = (sigmaii * sigmajj)^1/2
    # Convert everything to SI units
    wDepth = sqrt(molj$wDepth[s]/1000*molk$wDepth[t]/1000)/N_A #in J
    sigma = sqrt(molj$sigma[s]*1e-10*molk$sigma[t]*1e-10)#in m
    u_lj = 4*wDepth*((sigma/D_m)^12 - (sigma/D_m)^6)

    #----------------------------------
    #Coulomb potential
    q1 = molj$charge[s]*e
    q2 = molk$charge[t]*e #electron charge e to get from eV to C
    u_c = q1*q2/(4*pi*eps_0*eps_water*D_m)#D_m is separation in m

    #================================
    #Atom-Atom totals
    pairTot = u_lj + u_c #total for one pair
```

```
        molkTot = molkTot + pairTot #total for one atom of j with all of molecule k

      }#end for t each molecule in the other molecule(k)

      atom_sTot = atom_sTot + molkTot #add mol k total to total for the s atom

      #-------------------------------------------------------------------------
      #Add the molk totals to the potential matrix for k=1,2,...
      potentMatrix[j,k] = potentMatrix[j,k] + molkTot

    }#end for each other molecule k

    #-------------------------------------------------------------------------
    #Add long range potential to atom_sTot
    #-------------------------------------------------------------------------
    lrPotS = lrList[ceiling(molj$z[s])] #get respective long range potential
    lrCoulomb = lrPotS*molj$charge[s] #multiple by valency (charge in units e*C)
    atom_sTot = atom_sTot + lrCoulomb

    #-------------------------------------------------------------------------
    #add total for one atom with all other atoms in all molecules
    #-------------------------------------------------------------------------
    #store in total for that molecule
    moljTot = moljTot + atom_sTot

  } #end for s each atom in the current molecule

  #Overall total potential
  totalPotential = totalPotential + moljTot

  if(debug==TRUE){
    print(paste("Total for Molecule :", j, "=",moljTot))
  }


}#end j for each molecule in the box

print(paste("Final total:", totalPotential))


#=============================================================================
# Part 2
# Monte Carlo Simulation
#=============================================================================

print("================================================")
print("Performing Simulation")
print(paste("Step size:",stepSize))
print(paste("Number of Steps:", numSteps))

for(i in 1:numSteps){
  if(debug==TRUE) { print(paste("Monte Carlo Step:",i)) }

  for(j in 1:Ntot){#For each molecule in the box

    if(debug==TRUE) { print(paste("Molecule: j =", j)) }

    u_tot = 0
    newSurfacePotential = 0 # stores updated potential for each molecule j with surface
    newMatrixRow = numeric(Ntot)#Stores updated potential of j with every k.

    oldPotential = rowSums(potentMatrix)[j] + surfaceAtomPotentials[j]
    newPotential = 0;
    diffPotential = 0;

    #extract current molecule
    molj = molecule[[j]] #copy to update with move

    #-----------------------------------------------------------------
    # Make a move or a rotation
    #-----------------------------------------------------------------
    # For each molecule in the box
```

```
# Decide on a move or a rotation
moveOrRot = runif(1)
if(moveOrRot<=0.5){#make a move

  # For a move
  m = stepSize #moveLength;

  # Produce 3 random numbers for x,y,z
  mvx = runif(1, min=-m, max=m)
  mvy = runif(1, min=-m, max=m)
  mvz = runif(1, min=-m, max=m)

  # Move the molecule in that direction
  newx = molj$x + mvx
  newy = molj$y + mvy
  newz = molj$z + mvz


}#end make a move
else{#make a rotation
  #=========================================================
  # Rotating of molecule about 3 axis
  #=========================================================

  # For a rotation
  # Produce 3 random numbers for x,y,z axis rotation
  maxDegrees = 5#maximum rotation to turn about on each axis
  degX = runif(1, -5, 5)#turn between 0 and 5 degrees
  degY = runif(1, -5, 5)#turn between 0 and 5 degrees
  degZ = runif(1, -5, 5)#turn between 0 and 5 degrees

  #Rotate coordinates of molj$origx,... about each axis for degX degrees
  #molecules are rotated around (0,0,0), then translated to actual position

  #x 1
  angle1= degX*pi/180
  rotx1 = molj$origx
  roty1 = molj$origy*cos(angle1) - molj$origz*sin(angle1)
  rotz1 = molj$origy*sin(angle1) + molj$origz*cos(angle1)

  #y 2
  angle2= degY*pi/180
  rotx2 = rotz1*sin(angle2) + rotx1*cos(angle2)
  roty2 = roty1
  rotz2 = rotz1*cos(angle2) - rotx1*sin(angle2)

  #z 3
  angle3= degZ*pi/180
  rotx3 = rotx2*cos(angle3) - roty2*sin(angle3)
  roty3 = rotx2*sin(angle3) + roty2*cos(angle3)
  rotz3 = rotz2

  #Calculate difference between original and rotated
  diffx = rotx3 - molj$origx
  diffy = roty3 - molj$origy
  diffz = rotz3 - molj$origz

  #store in newx by adding diffx,...
  newx = molj$x + diffx
  newy = molj$y + diffy
  newz = molj$z + diffz

}#end make a rotation

#=================================================================
#Check if outside box / apply periodic Boundary Conditions
#check if inside the box in x and y directions only
if(max(newx)>b){
  #print("Outside box on RHS")
  for(m in 1:length(newx)){
    if(newx[m]>b){
      oldx = newx[m]
      newx[m] = newx[m]-2*b
```

```
      #print(paste("Old",oldx,"New",newx[m]))
    }
  }
}
if(min(newx)< -b){
  #print("Outside box on LHS")
  for(m in 1:length(newx)){
    if(newx[m]< -b){
      oldx = newx[m]
      newx[m] = newx[m]+2*b
      #print(paste("Old",oldx,"New",newx[m]))
    }
  }
}
if(max(newy)>b){
  #print("Outside box on back")
  for(m in 1:length(newy)){
    if(newy[m]>b){
      oldy = newy[m]
      newy[m] = newy[m]-2*b
    }
  }

}
if(min(newy)< -b){
  #print("Outside box on front")
  for(m in 1:length(newy)){
    if(newy[m]< -b){
      oldy = newy[m]
      newy[m] = newy[m]+2*b
    }
  }
}
if(min(newz)< 0){#If goes through bottom surface
  #print("Through bottom surface")
  #For a move, reject, keep z same
  if(moveOrRot<=0.5){
    newz = molj$z
    mvz = 0
  }else{#For a rotation, undo the whole rotation
    newx=molj$x
    newy=molj$y
    newz=molj$z

    rotx3 = molj$origx
    roty3 = molj$origy
    rotz3 = molj$origz
    degX = 0
    degY = 0
    degZ = 0
  }
}

#-----------------------------------------
#For both moves and rotations
#Store new coordinates

#update current ion
molj$x=newx
molj$y=newy
molj$z=newz

#For a rotation only
#Update also the origx,... to store starting rotation for next time
if(moveOrRot>0.5){
  molj$origx = rotx3
  molj$origy = roty3
  molj$origz = rotz3

  #rotating does not change the distance to surface
  centreToSurface[i+1,j] = centreToSurface[i,j]

  #or change the centre of the molecule
```

```
  centreXcoords[i+1,j] = centreXcoords[i,j]
  centreYcoords[i+1,j] = centreYcoords[i,j]

  #rotating does change the max distance to surface
  maxToSurface[i+1,j] = max(molj$z)

  #rotating changes the angles
  xRotStore[i+1,j] = xRotStore[i,j] + degX
  yRotStore[i+1,j] = yRotStore[i,j] + degY
  zRotStore[i+1,j] = zRotStore[i,j] + degZ

  #subtract 360 if bigger than this angle
  if(xRotStore[i+1,j]>=360)
    xRotStore[i+1,j] = xRotStore[i+1,j] - 360
  if(yRotStore[i+1,j]>=360)
    yRotStore[i+1,j] = yRotStore[i+1,j] - 360
  if(zRotStore[i+1,j]>=360)
    zRotStore[i+1,j] = zRotStore[i+1,j] - 360

  #add 360 for negative angles
  if(xRotStore[i+1,j]<0)
    xRotStore[i+1,j] = xRotStore[i+1,j] + 360
  if(yRotStore[i+1,j]<0)
    yRotStore[i+1,j] = yRotStore[i+1,j] + 360
  if(zRotStore[i+1,j]<0)
    zRotStore[i+1,j] = zRotStore[i+1,j] + 360
}
else{#For a move only
  #Moving changes the distance to the surface
  centreToSurface[i+1,j] = centreToSurface[i,j] + mvz

  #moving does change the max distance to surface
  maxToSurface[i+1,j] = max(molj$z)

  #update these too --- NEW
  centreXcoords[i+1,j] = centreXcoords[i,j] + mvx
  centreYcoords[i+1,j] = centreYcoords[i,j] + mvy

  #Moving does not change the rotation
  xRotStore[i+1,j] = xRotStore[i,j]
  yRotStore[i+1,j] = yRotStore[i,j]
  zRotStore[i+1,j] = zRotStore[i,j]
}

# ======================================================================
# CALCULATE CHANGE IN POTENTIAL FOR CURRENT MOLECULE
# Do each interaction pair potential
# Including its relationship with the bottom surface.
# ======================================================================

# For each atom in the molecule under consideration
for (s in 1:nrow(molj)){#s is the atom in the mol j

  tempSurfTot = 0

  #--------------------------------------------------------------------------------
  # Pairwise pfas atom-surface atom calculations
  #--------------------------------------------------------------------------------
  for (sa in 1:surfCount){#sa is the atom in the surface

    aasTot = 0

    #calculate separation between pfas and surface atom being investigated
    rawx = abs(surface$x[sa] - molj$x[s])
    rawy = abs(surface$y[sa] - molj$y[s])

    #adjust for period boundary conditions (further away than b=30Angstrom pairs see neighbours)
    deltax = (rawx%/%b)*b - rawx%%b
    deltay = (rawy%/%b)*b - rawy%%b

    D = sqrt(deltax^2 + deltay^2 + (surface$z[sa] - molj$z[s])^2)
    D_m = D*1e-10 #convert to m
```

```
  #----------------------------------
  #6-12 Lennard Jones potential
  # eps_ij: well depth, sigma_ij:dependent on molecules
  # For the sigma_ij = (sigmaii * sigmajj)^1/2
  # Convert everything to SI units
  wDepth = sqrt(molj$wDepth[s]/1000*surface$wDepth[sa]/1000)/N_A #in J
  sigma = sqrt(molj$sigma[s]*1e-10*surface$sigma[sa]*1e-10)#in m
  u_lj = 4*wDepth*((sigma/D_m)^12 - (sigma/D_m)^6)

  #----------------------------------
  #Coulomb potential
  q1 = molj$charge[s]*e
  q2 = surface$charge[sa]*e #electron charge e to get from eV to J
  u_c = q1*q2/(4*pi*eps_0*eps_water*D_m)#D_m is separation in m

  #==============================
  #Atom-Atom totals
  aasTot = u_lj + u_c #total for one pair

  #print(paste("aas Tot", s, sa, "=", aasTot))

  tempSurfTot = tempSurfTot + aasTot #total for one atom s of molecule j with all of surface

}#end for sa : each molecule in the surface

#Update totals
newSurfacePotential = newSurfacePotential + tempSurfTot
newPotential = newPotential + tempSurfTot


#-------------------------------------------------
# Calculate potential with other molecules atoms
#-------------------------------------------------

#=========================================
#For other molecules in the box
#But not molecule j itself
notJ = 1:Ntot
notJ = notJ[-j]
for(k in notJ){

  molk = molecule[[k]]

  #=========================================
  # For other atoms within the molecule
  for (t in 1:nrow(molk)){#t is the atom in the pfas

    #calculate actual separation between molecule atoms being investigated
    rawx = abs(molk$x[t] - molj$x[s])
    rawy = abs(molk$y[t] - molj$y[s])

    #adjust for period boundary conditions (further away than b=30Angstrom pairs see neighbours)
    deltax = (rawx%/%b)*b - rawx%%b
    deltay = (rawy%/%b)*b - rawy%%b

    D = sqrt(deltax^2 + deltay^2 + (molk$z[t] - molj$z[s])^2)
    D_m = D*1e-10 #convert to m

    #----------------------------------
    #6-12 Lennard Jones potential
    # eps_ij =  #well depth
    # sigma_ij = #dependent on molecules
    # For the sigma_ij = (sigmaii * sigmajj)^1/2
    # Convert everything to SI units
    wDepth = sqrt(molj$wDepth[s]/1000*molk$wDepth[t]/1000)/N_A #in J
    sigma  = sqrt(molj$sigma[s]*1e-10*molk$sigma[t]*1e-10)#in m
    u_lj = 4*wDepth*((sigma/D_m)^12 - (sigma/D_m)^6)

    #----------------------------------
    #Coulomb potential
    q1 = molj$charge[s]*e
    q2 = molk$charge[t]*e #electron charge e to get from eV to J
    u_c = q1*q2/(4*pi*eps_0*eps_water*D_m)#D_m is separation in m
```

```
      #==============================
      #update totals
      newPotential = newPotential +  u_lj + u_c #Just keep adding

      #update also rows of the potential matrix
      newMatrixRow[k] = newMatrixRow[k] + u_lj + u_c

    }#end for t (each pfas atom)

  }# end k for each other molecule not j

  #-----------------------------------------------------------------------------
  #Add long range potential to newPotential
  #-----------------------------------------------------------------------------
  lrPotS = lrList[ceiling(molj$z[s])] #get respective long range potential
  lrCoulomb = lrPotS*molj$charge[s] #multiple by valency (charge in units e*C)
  newPotential = newPotential + lrCoulomb

} #end for s (each atom in molecule that was moved)

#====================================
# Decide whether to Accept or reject
diffPotential = newPotential - oldPotential
if(debug==TRUE) {
  print(paste("Old potential", oldPotential))
  print(paste("New potential", newPotential))
  print(paste("Difference", diffPotential))
}

#if potential lower, accept:
if(newPotential<=oldPotential){
  if(debug==TRUE) { print("Move accepted outright") }

  #store new molecule position
  molecule[[j]]=molj

  #Update potentials
  totalPotential = totalPotential + diffPotential #total potential
  surfaceAtomPotentials[j] = newSurfacePotential #update surface atom potentials for mol j
  potentMatrix[j,] = newMatrixRow #totals for j with other mols
  potentMatrix[,j] = newMatrixRow

}
else{
  #if potential higher, accept with probability...
  acceptProb = exp(1)^(-(1/(kB*T))*diffPotential)
  randomProb = runif(1) #random num b/w 0 and 1
  tau = 1 #tau #increase if not converging. Unity preserves symmetry

  if(debug==TRUE) {
    print(paste("kB",kB,"T",T))
    print(paste("acceptance probability",acceptProb))
    print(paste("random probability",randomProb))
  }

  #if accepted
  if(randomProb<(1/tau)*acceptProb){

    if(debug==TRUE) { print("move acceptd with higher potential") }

    #store new molecule position
    molecule[[j]]=molj

    #Update totals
    totalPotential = totalPotential + diffPotential #total potential
    surfaceAtomPotentials[j] = newSurfacePotential #update surface atom potentials for mol j
    potentMatrix[j,] = newMatrixRow
    potentMatrix[,j] = newMatrixRow

  }#end inner if
  else{#Move is Rejected
    #For rejected moves, set centreToSurfaceDistance  back to previous value
```

```
        centreToSurface[i+1,j] = centreToSurface[i,j]
        maxToSurface[i+1,j] = maxToSurface[i,j]
        centreXcoords[i+1,j] = centreXcoords[i,j]
        centreYcoords[i+1,j] = centreYcoords[i,j]

        #For rejected moves, set RotStore  back to previous value
        xRotStore[i+1,j] = xRotStore[i,j]
        yRotStore[i+1,j] = yRotStore[i,j]
        zRotStore[i+1,j] = zRotStore[i,j]

        if(debug==TRUE) { print("move rejected") }

      }#end move rejected
    }#end not accept outright (else)

    #Update running list of total potentials (for plotting later)
    u_tot_list = c(u_tot_list, totalPotential)

    if(debug==TRUE) { print("--------------------------------------") }

  }#end j for each molecule in the box

}#end i (number of monte carlo steps)

print(paste("Final total:",totalPotential))

#Record and print computation time
fTime = proc.time()
elaps = fTime[3]-sTime[3]
print(paste0("Time taken: ",elaps," seconds"))

#=============================================================================
#SAVE WORKSPACE
#=============================================================================
if(mixedSurfaceCharge == FALSE){
outPutFile = paste0("LRF_",N,liquidName,"_",Ndiv,"Ca_",Nci,"H_",Noh,"OH_",
                    sign(charge_C),"surf_",numSteps,"_",stepSize,"Ang.RData")
}else{
  outPutFile = paste0("LRF_MixedSurface_",N,liquidName,"_",Ndiv,"Ca_",Nci,"H_",Noh,"OH_",
                      sign(charge_C),"surf_",numSteps,"_",stepSize,"Ang.RData")

}
save.image(outPutFile)
```

E.4 Analysis of initial output

```
#=============================================================================
# Plotting and Post-Simulation Analysis
# Initial output (no LRF)
# Author: Julie Sleep
#=============================================================================
library(rgl)
library(magick)
library(scatterplot3d)
library(scales)

getwd()
#setwd("../")
setwd("PFAS/Soil/SoilMolecular")
#setwd("results")

#-------------------------------------------------------------
#Scenario 1: non-anion
#file = "Paper3Results/16PFBS_0Ca_0H_0OH_0surf_20000_0.5Ang.RData"
file = "Paper3Results/16PFOS_0Ca_0H_0OH_0surf_20000_0.5Ang.RData"

#Scenario 2: anion with 16H+
#file = "Paper3Results/16PFBSion_0Ca_16H_0OH_0surf_20000_0.5Ang.RData"
#file = "Paper3Results/16PFOSion_0Ca_16H_0OH_0Surf_20000_0.5Ang.RData"

#Scenario 3: anion with pos surface
```

```
#file = "Paper3Results/16PFBSion_0Ca_0H_0OH_1surf_20000_0.5Ang.RData"
#file = "Paper3Results/16PFOSion_0Ca_0H_0OH_1Surf_20000_0.5Ang.RData"
#file = "Paper3Results/16PFOAion_0Ca_0H_0OH_1Surf_20000_0.5Ang.RData"

#Scenario 4: anion with 32 H+ and neg surface
#file = "Paper3Results/16PFBSion_0Ca_32H_0OH_-1surf_20000_0.5Ang.RData"
#file = "Paper3Results/16PFOSion_0Ca_32H_0OH_-1surf_20000_0.5Ang.RData"

#Scenario 4b: anion with 32 H+ and neg mixed negative - neutral surface
#file = "Paper3Results/MixedSurfaceCharge16PFBSion_0Ca_32H_0OH_-1surf_20000_0.5Ang.RData"
#file = "Paper3Results/MixedSurfaceCharge16PFOSion_0Ca_32H_0OH_-1surf_20000_0.5Ang.RData"
#file = "Chem2Results/LRF_MixedSurface_16PFBSion_0Ca_32H_0OH_-1surf_20000_0.5Ang.RData"
#file = "Chem2Results/LRF_MixedSurface_16PFOSion_0Ca_32H_0OH_-1surf_20000_0.5Ang.RData"

#Scenario 5: anion with 16 Ca2+ and neg surface
#file = "Paper3Results/16PFBSion_16Ca_0H_0OH_-1surf_20000_0.5Ang.RData"
#file = "Paper3Results/16PFOSion_16Ca_0H_0OH_-1Surf_20000_0.5Ang.RData"

#Scenario 6: anion with 16 OH- and double pos surface
#file = "Paper3Results/16PFBSion_0Ca_0H_16OH_1surf_20000_0.5Ang.RData"
#file = "Paper3Results/16PFOSion_0Ca_0H_16OH_1surf_20000_0.5Ang.RData"

#Scenario 7: anion with 8 OH-, H+ and pos surface
#file = "Paper3Results/16PFBSion_0Ca_8H_8OH_1surf_20000_0.5Ang.RData"
#file = "Paper3Results/16PFOSion_0Ca_8H_8OH_1surf_20000_0.5Ang.RData"

#Scenario 8: anion with 16 OH-, H+ and pos surface
#file = "Paper3Results/16PFBSion_0Ca_16H_16OH_1surf_20000_0.5Ang.RData"
#file = "Paper3Results/16PFOSion_0Ca_16H_16OH_1surf_20000_0.5Ang.RData"

load(file)

#@@@@@@@@@@@@@@@@@@@@@@@@@@@@@@@@@@@@@@@@@@@@
#New final position visualisation
if(liquidName=="PFOS" || liquidName == "PFOSion"){
  pfosColours = c("yellow", rep("green",17), rep("red",3),rep("grey",8),"white")
}
if(liquidName=="PFBS" || liquidName == "PFBSion"){
  pfosColours = c("yellow", rep("green",9), rep("red",3),rep("grey",4),"white")
}
if(liquidName=="PFOA" || liquidName == "PFOAion"){
  pfosColours = c(rep("green",15), rep("red",2),rep("grey",8),"white")
}


open3d(windowRect=c(100,100,700,700))

plot3d(molecule[[1]]$x, molecule[[1]]$y, molecule[[1]]$z, col=pfosColours,
       type="s", radius=1.2, xlim=c(-30,30), ylim=c(-30,30), zlim=c(0,60),
       xlab="x", ylab="y", zlab="z")

for(i in 2:N){
  spheres3d(molecule[[i]]$x, molecule[[i]]$y, molecule[[i]]$z, col=pfosColours,
            radius=1.2)
}
#For Hydrogen counter ions
if(Nci>0){
  for(i in (N+1):(N+Nci)){
    spheres3d(molecule[[i]]$x, molecule[[i]]$y, molecule[[i]]$z, col="white",
              radius=1.0)
  }
}

#For OH- ions
if(Noh>0){
  for(i in (N+Nci+1):Ntot){
    spheres3d(molecule[[i]]$x, molecule[[i]]$y, molecule[[i]]$z, col="red",
              radius=1.2)
  }
}

#For divalent cat ions
if(Ndiv>0){
```

```
  for(i in (N+Nci+1):Ntot){
    spheres3d(molecule[[i]]$x, molecule[[i]]$y, molecule[[i]]$z,
              col="chartreuse3",
              radius=1.5)
  }
}

if(charge_C>0){chargeSign=1}
if(charge_C<0){chargeSign=-1}
if(charge_C==0){chargeSign=0}
#Surface
#Surface
if(mixedSurfaceCharge == TRUE){
  surfaceColour = c(rep(c(rep("gray27",15),rep("grey",14),
                          rep("gray27",14),rep("grey",14))
                        ,24),
                    rep("gray27",15),rep("grey",14))
}else{
  surfaceColour = "grey"
}
spheres3d(surface$x, surface$y, surface$z, col=surfaceColour, radius=1.2)

#spheres3d(surface$x, surface$y, surface$z, col="grey", radius=1.2)
#rgl.snapshot(paste0("../../PFOA/Figures/final",liquidName,Nci,"H",Ndiv,"Ca",
                    #Noh,"OH",chargeSign,"S.png"),fmt="png")

#UNCOMMENT TO SAVE --- Published style version
#rgl.snapshot(paste0("Chem2Results/Figures/LRFmixedSurfaceFinal",liquidName,Nci,"H",Ndiv,"Ca",
#Noh,"OH",chargeSign,"S.png"),fmt="png")

#rgl.postscript("finalpositions.pdf","pdf")
#play3d( spin3d( axis = c(0, 0, 1), rpm = 10), duration = 10 )

#=========================================================
#Plot the Potential over time
xx=1:(numSteps*Ntot)
plot(xx, u_tot_list, type="l", lwd=2, col="aquamarine3",
     xlab = "Iteration", ylab="Potential (J)")

#=========================================================
#Plot the max distance to the surface
colourPfas = rainbow(N)

xx=1:(numSteps+1)
plot(xx, maxToSurface[,1], type="l", col=colourPfas[1],
     xlim=c(1, numSteps+1),
     ylim=c(0, max(maxToSurface)),
     xlab="Monte Carlo Iteration Number",
     ylab="MOlecule max distance to surface")
for(i in 2:N){
  points(xx,maxToSurface[,i], type="l", col=colourPfas[i])
}
if(Nci>0){
  for(i in (N+1):N+Nci){
    points(xx,maxToSurface[,i], type="l", col="black", lty=2)
  }}
if(Ndiv>0){
  for(i in (N+Nci+1):Ntot){
    points(xx,maxToSurface[,i], type="l", col="black", lty=2)
  }}
abline(h=0.0)

#=============================================================
#Plot histogram as density line

#set cropping point
cropPoint = 2500
dataSize = numSteps+1-cropPoint
croppedSurface = matrix(numeric(Ntot*dataSize),
                        nrow=dataSize, ncol=Ntot)
for(i in 1:Ntot){
  newVector = numeric(dataSize)
  for(j in 1:dataSize){
```

```
    croppedSurface[j,i] = maxToSurface[cropPoint+j,i]
  }
}
colourPfas = rainbow(N)
heightMeans = numeric(Ntot)

dens.mim = list()
for(i in 1:Ntot){
  dens.mim[[i]] = density(maxToSurface[,i])
  heightMeans[i] = mean(maxToSurface[,i])
}

#Plot of PFAS
plot(dens.mim[[1]], xlim=c(2,90), ylim=c(0,0.3), col=colourPfas[1], lwd=2, main="")
for(i in 2:N){ lines(dens.mim[[i]], col=colourPfas[i], lwd=2) }

#Add counterions
for(i in (N+1):Ntot){ lines(dens.mim[[i]], col="black", lwd=2, lty=2)}

#Plot of just counterions
plot(dens.mim[[N+1]], col="black", lwd=2, lty=1, ylim=c(0,0.4), xlim=c(0,90), main="")
for(i in (N+1):Ntot){
  lines(dens.mim[[i]], col="black", lwd=2, lty=1)
}

#Plot of just divalent cations
plot(dens.mim[[N+Nci+1]], col="black", lwd=2, lty=1, ylim=c(0,0.4), xlim=c(0,110), main="")
for(i in (N+Nci+1):Ntot){
  lines(dens.mim[[i]], col="black", lwd=2, lty=1)
}

#Add a line for the mean
heightMeans
meanMean = mean(heightMeans)
meanMean
abline(v=meanMean, lwd=4)

#-------------------------------------
#Plot cropped density
for(i in 1:Ntot){
  dens.mim[[i]] = density(croppedSurface[,i])
  heightMeans[i] = mean(croppedSurface[,i])
}
plot(dens.mim[[1]], xlim=c(0,70), ylim=c(0,0.2), col=colourPfas[1], lwd=2)
for(i in 2:Ntot){
  lines(dens.mim[[i]], col=colourPfas[i], lwd=2)
}
for(i in (N+1):Ntot){
  lines(dens.mim[[i]], col=colourPfas[i-N], lty=2, lwd=2)
}
heightMeans
meanMean = mean(heightMeans)
meanMean
abline(v=meanMean, lwd=4)

#@@@
```

```
  xrot.mim[[i]] = density(xRotStore[,i], bandwidth = 10)
}
plot(xrot.mim[[1]], col=colourPfas[1], lwd=2, ylim=c(0,0.01), xlim=c(0,360), main = outPutFile)
for(i in 2:N){
  lines(xrot.mim[[i]], col=colourPfas[i], lwd=2)
}
nameList = c(rep("PFOS",N))
legend(x=12.5, y=5, legend=nameList, col=colourPfas,
       lty=c(rep(1,N),rep(2,N)), lwd=2)

#============================================================
#plot yrot Store
yrot.mim = list()
for(i in 1:N){
  yrot.mim[[i]] = density(yRotStore[,i], bandwidth = 10)
}
plot(yrot.mim[[1]], col=colourPfas[1], lwd=2, ylim=c(0,0.01), xlim=c(0,360), main = outPutFile)
for(i in 2:N){
  lines(yrot.mim[[i]], col=colourPfas[i], lwd=2)
}
nameList = c(rep("PFOS",N))
legend(x=12.5, y=5, legend=nameList, col=colourPfas,
       lty=c(rep(1,N),rep(2,N)), lwd=2)

#============================================================
#plot zrot Store
zrot.mim = list()
for(i in 1:Ntot){
  zrot.mim[[i]] = density(zRotStore[,i], bandwidth = 10)
}
plot(zrot.mim[[1]], col=colourPfas[1], lwd=2, ylim=c(0,0.01), xlim=c(0,360), main = outPutFile)
for(i in 2:Ntot){
  lines(zrot.mim[[i]], col=colourPfas[i], lwd=2)
}
nameList = c(rep("PFOS",N))
legend(x=12.5, y=5, legend=nameList, col=colourPfas,
       lty=c(rep(1,N),rep(2,N)), lwd=2)


#@@@@@@@@@@@@@@@@@@@@@@@@@@@@@@@@@@@@@@@@@@@@@@@@@@@@@@@@@
#Regular Visualisation
pfas = molecule[[i]]
finalplot$points3d(pfas$x, pfas$y, pfas$z, col="black", bg=pfosColours, cex=atomSize, pch=21)
colourPfas = rainbow(N)

#Some points in a box
Sub = seq(-b,b, by=1.42)
NN = 10
xx = runif(NN,-b,b)
yy = runif(NN,-b,b)
zz = runif(NN,0,boxh*3)

ions = data.frame(xx,yy,zz)
finalplot = scatterplot3d(ions, color="white",
                          pch = "*", xlab = expression(paste("x (",ring(A),")")),
                          ylab = expression(paste("y (",ring(A),")")),
                          zlab = expression(paste("z (",ring(A),")")),
                          xlim=c(-b,b), ylim=c(-b,b), zlim=c(0,50))

#Plot a bottom surface --- this is wrong structure
Sub =  seq(-b,b, by=0.4)
for(i in Sub){
  SubFrame = data.frame(Sub, i, 0)
  finalplot$points3d(SubFrame,col="lightgrey", pch=19, cex=0.5)
}

#option 2: molecular colours
pfosColours = c("yellow", rep("green",17), rep("red",3),rep("grey",8),"white")
atomSize = 1.7

# Plot of Cations
pfas = molecule[[1]]
finalplot$points3d(pfas$x, pfas$y, pfas$z, col="black", bg=pfosColours, cex=atomSize, pch=21)
```

```
for(i in 2:N){
  pfas = molecule[[i]]
  finalplot$points3d(pfas$x, pfas$y, pfas$z, col="black", bg=pfosColours, cex=atomSize, pch=21)
}
# Plot of Cations
pfas = molecule[[1]]
finalplot$points3d(pfas$x, pfas$y, pfas$z, pch=19, col=colourPfas[1], cex=1)
for(i in 2:N){
  pfas = molecule[[i]]
  finalplot$points3d(pfas$x, pfas$y, pfas$z, pch=19, col=colourPfas[i], cex=1)
}

#=====================================================
#Plot a top view surface

colfunc <- colorRampPalette(c("purple", "aquamarine3"))
coloursToUse = colfunc(10)

plot(1, 2, pch=19, col="white", xlim=c(-b,b), ylim=c(-b,b))
for(i in 1:Ntot){
  test = molecule[[i]]
  tX = test$x
  tY = test$y
  tZ = test$z
  ZasInt = round(tZ)+1
  Zcols = 1:length(tZ)
  print(i)
  for(j in 1:length(tZ)){
    Zcols[j] = coloursToUse[ZasInt[j]]
  }
  lightColours=alpha(Zcols, 0.15)
  points(tX, tY, pch=19, col=lightColours, xlim=c(-60,60), ylim=c(-60,60), cex=5)
}


#=========================================================
# VdW vs Coulomb interactions
#=========================================================
#=============================================================================
# Part 1
# Calculate final total potential
#=============================================================================

print("================================================")
print("Calculating final Total Potential")
finalPotential = 0
finalVdW = 0
finalCoulomb = 0

# ====================================================================
for(j in 1:Ntot){#For each molecule in the box
  print(paste("Final potential Molecule j =",j))
  molj = molecule[[j]] #extract current molecule
  moljTot = 0 #total for j=1,2, etc.

  #====================================================================
  # For each atom in molecule j under consideration
  for (s in 1:nrow(molj)){ #s is the atom in the mol

    atom_sTot = 0 #Total for each atom s within a molecule, S=C1,F2, etc. with surface

    #-----------------------------------------------------------
    # Surface-atom calculations for mol j
    #-----------------------------------------------------------

    #-----------------------------------------------------------------------------
    # Pairwise pfas atom-surface atom calculations
    #-----------------------------------------------------------------------------
    for (sa in 1:surfCount){#sa is the atom in the surface

      aasTot = 0

      #calculate separation between pfas and surface atom being investigated
```

```
  rawx = abs(surface$x[sa] - molj$x[s])
  rawy = abs(surface$y[sa] - molj$y[s])

  #adjust for period boundary conditions (further away than b=30Angstrom pairs see neighbours)
  # quotient * b (gives 30 or 0) minus remainder
  # i.e. raw 59, gives 1*30-29=1, raw 15 gives 0-15=-15 (is squared so sign irrelevant)
  deltax = (rawx%/%b)*b - rawx%%b
  deltay = (rawy%/%b)*b - rawy%%b

  D = sqrt( deltax^2 + deltay^2 +
              (surface$z[sa] - molj$z[s])^2)
  D_m = D*1e-10 #convert to m

  #-----------------------------------
  #6-12 Lennard Jones potential
  # eps_ij: well depth, sigma_ij:dependent on molecules
  # For the sigma_ij = (sigmaii * sigmajj)^1/2
  # Convert everything to SI units
  wDepth = sqrt(molj$wDepth[s]/1000*surface$wDepth[sa]/1000)/N_A #in J
  sigma = sqrt(molj$sigma[s]*1e-10*surface$sigma[sa]*1e-10)#in m
  u_lj = 4*wDepth*((sigma/D_m)^12 - (sigma/D_m)^6)



  #-----------------------------------
  #Coulomb potential
  q1 = molj$charge[s]*e
  q2 = surface$charge[sa]*e #electron charge e to get from eV to J
  u_c = q1*q2/(4*pi*eps_0*eps_water*D_m)#D_m is separation in m


  #================================
  #Atom-Atom totals
  aasTot = u_lj + u_c #total for one pair

  #update comparison totals
  finalVdW = finalVdW + u_lj
  finalCoulomb = finalCoulomb + u_c

  #print(paste("aas Tot", s, sa, "=", aasTot))

  atom_sTot = atom_sTot + aasTot #total for one atom s of molecule j with all of surface

}#end for sa : each molecule in the surface

#print(paste("s ", s," atom_sTot ", atom_sTot))

#-------------------------------------------------------------------------------
# Inter molecular calculations (not surface)
#-------------------------------------------------------------------------------

#-------------------------------------------------------------------------------
#For other molecules in the box
#But not molecule j itself
notJ = 1:Ntot
notJ = notJ[-j]

for(k in notJ){

  molk = molecule[[k]]
  molkTot = 0

  #-----------------------------------------------------------------------------
  # Pairwise atom-atom calculations
  #-----------------------------------------------------------------------------
  for (t in 1:nrow(molk)){#t is the atom in the otherMol

    pairTot = 0

    #calculate actual separation between molecule atoms being investigated
    rawx = abs(molk$x[t] - molj$x[s])
    rawy = abs(molk$y[t] - molj$y[s])
```

```
        #adjust for period boundary conditions (further away than b=30Angstrom pairs see neighbours)
        deltax = (rawx%/%b)*b - rawx%%b
        deltay = (rawy%/%b)*b - rawy%%b

        D = sqrt(deltax^2 + deltay^2 + (molk$z[t] - molj$z[s])^2)
        D_m = D*1e-10 #convert to m

        #-----------------------------------
        #6-12 Lennard Jones potential
        # eps_ij: well depth, sigma_ij:dependent on molecules
        # For the sigma_ij = (sigmaii * sigmajj)^1/2
        # Convert everything to SI units
        wDepth = sqrt(molj$wDepth[s]/1000*molk$wDepth[t]/1000)/N_A #in J
        sigma = sqrt(molj$sigma[s]*1e-10*molk$sigma[t]*1e-10)#in m
        u_lj = 4*wDepth*((sigma/D_m)^12 - (sigma/D_m)^6)

        #-----------------------------------
        #Coulomb potential
        q1 = molj$charge[s]*e
        q2 = molk$charge[t]*e #electron charge e to get from eV to C
        u_c = q1*q2/(4*pi*eps_0*eps_water*D_m)#D_m is separation in m

        #================================
        #Atom-Atom totals
        pairTot = u_lj + u_c #total for one pair

        molkTot = molkTot + pairTot #total for one atom of j with all of molecule k

        #update comparison totals
        finalVdW = finalVdW + u_lj
        finalCoulomb = finalCoulomb + u_c


      }#end for t each molecule in the other molecule(k)

      atom_sTot = atom_sTot + molkTot #add mol k total to total for the s atom

      #Add the molk totals to the potential matrix for k=1,2,...
      potentMatrix[j,k] = potentMatrix[j,k] + molkTot

    }#end for each other molecule k

    #add total for one atom with all other atoms in all molecules
    #store in total for that molecule
    moljTot = moljTot + atom_sTot

  } #end for s each atom in the current molecule

  #Overall final potential
  finalPotential = finalPotential + moljTot

  print(paste("Total for Molecule :", j, "=",moljTot))

}#end j for each molecule in the box

print(paste("Final total:", finalPotential))
print(paste("VDW total:", finalVdW))
print(paste("Coulomb total:", finalCoulomb))

forcePercent = (finalVdW / (finalCoulomb + finalVdW))*100

print (paste("VdW percent of total",forcePercent))
```

E.5 Analysis of output with long-range forces

```
#=========================================================================
# Plotting and Post-Simulation Analysis
# Analysis of output with long-range forces
# Author: Julie Sleep
#=========================================================================
library(rgl)
```

```
library(magick)
library(scatterplot3d)
library(scales)

getwd()
#setwd("../")
setwd("PFAS/Soil/SoilMolecular")
#setwd("results")

#-------------------------------------------------------------
#Scenario 1: non-anion -- No LRF
#file = "Paper3Results/16PFBS_0Ca_0H_0OH_0surf_20000_0.5Ang.RData"
#file = "Paper3Results/16PFOS_0Ca_0H_0OH_0surf_20000_0.5Ang.RData"

#Scenario 2: anion with 16H+
#file = "NewLRFResults/16PFBSion_0Ca_16H_0OH_0surf_20000_0.5Ang.RData"
#file = "NewLRFResults/16PFOSion_0Ca_16H_0OH_0Surf_20000_0.5Ang.RData"

#Scenario 3: anion with pos surface
#file = "NewLRFResults/16PFBSion_0Ca_0H_0OH_1surf_20000_0.5Ang.RData"
#file = "NewLRFResults/16PFOSion_0Ca_0H_0OH_1Surf_20000_0.5Ang.RData"

#Scenario 4: anion with 32 H+ and neg surface
#file = "NewLRFResults/16PFBSion_0Ca_32H_0OH_-1surf_20000_0.5Ang.RData"
#file = "NewLRFResults/16PFOSion_0Ca_32H_0OH_-1surf_20000_0.5Ang.RData"

#Scenario 5: anion with 16 Ca2+ and neg surface
file = "NewLRFResults/16PFBSion_16Ca_0H_0OH_-1surf_20000_0.5Ang.RData"
#file = "NewLRFResults/16PFOSion_16Ca_0H_0OH_-1Surf_20000_0.5Ang.RData"

#Scenario 6: anion with 16 OH- and double pos surface
#file = "NewLRFResults/16PFBSion_0Ca_0H_16OH_1surf_20000_0.5Ang.RData"
#file = "NewLRFResults/16PFOSion_0Ca_0H_16OH_1surf_20000_0.5Ang.RData"

#Scenario 7: anion with 8 OH-, H+ and pos surface
#file = "NewLRFResults/16PFBSion_0Ca_8H_8OH_1surf_20000_0.5Ang.RData"
#file = "NewLRFResults/16PFOSion_0Ca_8H_8OH_1surf_20000_0.5Ang.RData"

#Scenario 8: anion with 16 OH-, H+ and pos surface
#file = "NewLRFResults/16PFBSion_0Ca_16H_16OH_1surf_20000_0.5Ang.RData"
#file = "NewLRFResults/16PFOSion_0Ca_16H_16OH_1surf_20000_0.5Ang.RData"

load(file)

#@@@@@@@@@@@@@@@@@@@@@@@@@@@@@@@@@@@@@@@@@@@
#New final position visualisation
if(liquidName=="PFOS" || liquidName == "PFOSion"){
  pfosColours = c("yellow", rep("green",17), rep("red",3),rep("grey",8),"white")
}
if(liquidName=="PFBS" || liquidName == "PFBSion"){
  pfosColours = c("yellow", rep("green",9), rep("red",3),rep("grey",4),"white")
}
if(liquidName=="PFOA" || liquidName == "PFOAion"){
  pfosColours = c(rep("green",15), rep("red",2),rep("grey",8),"white")
}

open3d(windowRect=c(100,100,700,700))

plot3d(molecule[[1]]$x, molecule[[1]]$y, molecule[[1]]$z, col=pfosColours,
       type="s", radius=1.2, xlim=c(-30,30), ylim=c(-30,30), zlim=c(0,60),
       xlab="x", ylab="y", zlab="z")

for(i in 2:N){
  spheres3d(molecule[[i]]$x, molecule[[i]]$y, molecule[[i]]$z, col=pfosColours,
            radius=1.2)
}
#For Hydrogen counter ions
if(Nci>0){
  for(i in (N+1):(N+Nci)){
    spheres3d(molecule[[i]]$x, molecule[[i]]$y, molecule[[i]]$z, col="white",
              radius=1.0)
  }
}
```

```
#For OH- ions
if(Noh>0){
  for(i in (N+Nci+1):Ntot){
    spheres3d(molecule[[i]]$x, molecule[[i]]$y, molecule[[i]]$z, col="red",
              radius=1.2)
  }
}

#For divalent cat ions
if(Ndiv>0){
  for(i in (N+Nci+1):Ntot){
    spheres3d(molecule[[i]]$x, molecule[[i]]$y, molecule[[i]]$z,
              col="chartreuse3",
              radius=1.5)
  }
}

if(charge_C>0){chargeSign=1}
if(charge_C<0){chargeSign=-1}
if(charge_C==0){chargeSign=0}
#Surface
spheres3d(surface$x, surface$y, surface$z, col="grey", radius=1.2)
rgl.snapshot(paste0("../PaperFigures/final",liquidName,Nci,"H",Ndiv,"Ca",
                    Noh,"OH",chargeSign,"S.png"),fmt="png")

#=======================================================
#Plot the Potential over time
xx=1:(numSteps*Ntot)
plot(xx, u_tot_list, type="l", lwd=2, col="aquamarine3",
     xlab = "Iteration", ylab="Potential (J)")

#=======================================================
#Plot the max distance to the surface
colourPfas = rainbow(N)

xx=1:(numSteps+1)
plot(xx, maxToSurface[,1], type="l", col=colourPfas[1],
     xlim=c(1, numSteps+1),
     ylim=c(0, max(maxToSurface)),
     xlab="Monte Carlo Iteration Number",
     ylab="MOlecule max distance to surface")
for(i in 2:N){
  points(xx,maxToSurface[,i], type="l", col=colourPfas[i])
}
if(Nci>0){
  for(i in (N+1):N+Nci){
    points(xx,maxToSurface[,i], type="l", col="black", lty=2)
  }}
if(Ndiv>0){
  for(i in (N+Nci+1):Ntot){
    points(xx,maxToSurface[,i], type="l", col="black", lty=2)
  }}
abline(h=0.0)

#=============================================================
#Plot histogram as density line

#set cropping point
cropPoint = 2500
dataSize = numSteps+1-cropPoint
croppedSurface = matrix(numeric(Ntot*dataSize),
                        nrow=dataSize, ncol=Ntot)
for(i in 1:Ntot){
  newVector = numeric(dataSize)
  for(j in 1:dataSize){
    croppedSurface[j,i] = maxToSurface[cropPoint+j,i]
  }
}
colourPfas = rainbow(N)
heightMeans = numeric(Ntot)

dens.mim = list()
```

```
for(i in 1:Ntot){
  dens.mim[[i]] = density(maxToSurface[,i])
  heightMeans[i] = mean(maxToSurface[,i])
}

#Plot of PFAS
plot(dens.mim[[1]], xlim=c(2,90), ylim=c(0,0.3), col=colourPfas[1], lwd=2, main="")
for(i in 2:N){ lines(dens.mim[[i]], col=colourPfas[i], lwd=2) }

#Add counterions
for(i in (N+1):Ntot){ lines(dens.mim[[i]], col="black", lwd=2, lty=2)}

#Plot of just counterions
plot(dens.mim[[N+1]], col="black", lwd=2, lty=1, ylim=c(0,0.4), xlim=c(0,90), main="")
for(i in (N+1):Ntot){
  lines(dens.mim[[i]], col="black", lwd=2, lty=1)
}

#Plot of just divalent cations
plot(dens.mim[[N+Nci+1]], col="black", lwd=2, lty=1, ylim=c(0,0.4), xlim=c(0,110), main="")
for(i in (N+Nci+1):Ntot){
  lines(dens.mim[[i]], col="black", lwd=2, lty=1)
}

#Add a line for the mean
heightMeans
meanMean = mean(heightMeans)
meanMean
abline(v=meanMean, lwd=4)

#-----------------------------------
#Plot cropped density
for(i in 1:Ntot){
  dens.mim[[i]] = density(croppedSurface[,i])
  heightMeans[i] = mean(croppedSurface[,i])
}
plot(dens.mim[[1]], xlim=c(0,70), ylim=c(0,0.2), col=colourPfas[1], lwd=2)
for(i in 2:Ntot){
  lines(dens.mim[[i]], col=colourPfas[i], lwd=2)
}
for(i in (N+1):Ntot){
  lines(dens.mim[[i]], col=colourPfas[i-N], lty=2, lwd=2)
}
heightMeans
meanMean = mean(heightMeans)
meanMean
abline(v=meanMean, lwd=4)

#@@@
```

```
  lines(xrot.mim[[i]], col=colourPfas[i], lwd=2)
}
nameList = c(rep("PFOS",N))
legend(x=12.5, y=5, legend=nameList, col=colourPfas,
       lty=c(rep(1,N),rep(2,N)), lwd=2)

#=============================================================
#plot yrot Store
yrot.mim = list()
for(i in 1:N){
  yrot.mim[[i]] = density(yRotStore[,i], bandwidth = 10)
}
plot(yrot.mim[[1]], col=colourPfas[1], lwd=2, ylim=c(0,0.01), xlim=c(0,360), main = outPutFile)
for(i in 2:N){
  lines(yrot.mim[[i]], col=colourPfas[i], lwd=2)
}
nameList = c(rep("PFOS",N))
legend(x=12.5, y=5, legend=nameList, col=colourPfas,
       lty=c(rep(1,N),rep(2,N)), lwd=2)

#=============================================================
#plot zrot Store
zrot.mim = list()
for(i in 1:Ntot){
  zrot.mim[[i]] = density(zRotStore[,i], bandwidth = 10)
}
plot(zrot.mim[[1]], col=colourPfas[1], lwd=2, ylim=c(0,0.01), xlim=c(0,360), main = outPutFile)
for(i in 2:Ntot){
  lines(zrot.mim[[i]], col=colourPfas[i], lwd=2)
}
nameList = c(rep("PFOS",N))
legend(x=12.5, y=5, legend=nameList, col=colourPfas,
       lty=c(rep(1,N),rep(2,N)), lwd=2)

#@@@@@@@@@@@@@@@@@@@@@@@@@@@@@@@@@@@@@@@@@@@@@@@@@@@@@@@@@@@@
#Regular Visualisation
pfas = molecule[[i]]
finalplot$points3d(pfas$x, pfas$y, pfas$z, col="black", bg=pfosColours, cex=atomSize, pch=21)
colourPfas = rainbow(N)

#Some points in a box
Sub = seq(-b,b, by=1.42)
NN = 10
xx = runif(NN,-b,b)
yy = runif(NN,-b,b)
zz = runif(NN,0,boxh*3)

ions = data.frame(xx,yy,zz)
finalplot = scatterplot3d(ions, color="white",
                          pch = "*", xlab = expression(paste("x (",ring(A),")")),
                          ylab = expression(paste("y (",ring(A),")")),
                          zlab = expression(paste("z (",ring(A),")")),
                          xlim=c(-b,b), ylim=c(-b,b), zlim=c(0,50))

#Plot a bottom surface --- this is a plain surface not the modelled structure
Sub =  seq(-b,b, by=0.4)
for(i in Sub){
  SubFrame = data.frame(Sub, i, 0)
  finalplot$points3d(SubFrame,col="lightgrey", pch=19, cex=0.5)
}

#option 2: molecular colours
pfosColours = c("yellow", rep("green",17), rep("red",3),rep("grey",8),"white")
atomSize = 1.7

# Plot of Cations
pfas = molecule[[1]]
finalplot$points3d(pfas$x, pfas$y, pfas$z, col="black", bg=pfosColours, cex=atomSize, pch=21)
for(i in 2:N){
  pfas = molecule[[i]]
  finalplot$points3d(pfas$x, pfas$y, pfas$z, col="black", bg=pfosColours, cex=atomSize, pch=21)
}
# Plot of Cations
```

```
pfas = molecule[[1]]
finalplot$points3d(pfas$x, pfas$y, pfas$z, pch=19, col=colourPfas[1], cex=1)
for(i in 2:N){
  pfas = molecule[[i]]
  finalplot$points3d(pfas$x, pfas$y, pfas$z, pch=19, col=colourPfas[i], cex=1)
}

#=====================================================
#Plot a top view surface

colfunc <- colorRampPalette(c("purple", "aquamarine3"))
coloursToUse = colfunc(10)

plot(1, 2, pch=19, col="white", xlim=c(-b,b), ylim=c(-b,b))
for(i in 1:Ntot){
  test = molecule[[i]]
  tX = test$x
  tY = test$y
  tZ = test$z
  ZasInt = round(tZ)+1
  Zcols = 1:length(tZ)
  print(i)
  for(j in 1:length(tZ)){
    Zcols[j] = coloursToUse[ZasInt[j]]
  }
  lightColours=alpha(Zcols, 0.15)
  points(tX, tY, pch=19, col=lightColours, xlim=c(-60,60), ylim=c(-60,60), cex=5)
}
```

E.6 Long-range force visualisation

```
#-----------------------------------------------------------
# Long range force plots
# Author: Julie Sleep
#-----------------------------------------------------------
getwd()
setwd('PFAS/Soil/SoilMolecular')

fList = list()

#Scenario 1: non-anion
fList[1] = "NetCharges/Workspace16PFBS_0Ca_0H_0OH_0surf.RData"
fList[2] = "NetCharges/Workspace16PFOS_0Ca_0H_0OH_0surf.RData"

#Scenario 2: anion with 16H+
fList[3] = "NetCharges/Workspace16PFBSion_0Ca_16H_0OH_0surf.RData"
fList[4] = "NetCharges/Workspace16PFOSion_0Ca_16H_0OH_0surf.RData"

#Scenario 3: anion with pos surface
fList[5] = "NetCharges/Workspace16PFBSion_0Ca_0H_0OH_1surf.RData"
fList[6] = "NetCharges/Workspace16PFOSion_0Ca_0H_0OH_1surf.RData"

#Scenario 4: anion with 32 H+ and neg surface
fList[7] = "NetCharges/Workspace16PFBSion_0Ca_32H_0OH_-1surf.RData"
fList[8] = "NetCharges/Workspace16PFOSion_0Ca_32H_0OH_-1surf.RData"

#Scenario 5: anion with 16 Ca2+ and neg surface
fList[9] = "NetCharges/Workspace16PFBSion_16Ca_0H_0OH_-1surf.RData"
fList[10] = "NetCharges/Workspace16PFOSion_16Ca_0H_0OH_-1surf.RData"

#Scenario 6: anion with 16 OH- and double pos surface
fList[11] = "NetCharges/Workspace16PFBSion_0Ca_0H_16OH_1surf.RData"
fList[12] = "NetCharges/Workspace16PFOSion_0Ca_0H_16OH_1surf.RData"

#Scenario 7: anion with 8 H+, 8 OH- and pos surface
fList[13] = "NetCharges/Workspace16PFBSion_0Ca_8H_8OH_1surf.RData"
fList[14] = "NetCharges/Workspace16PFOSion_0Ca_8H_8OH_1surf.RData"

#Scenario 8: anion with 16 H+, 16 OH- and pos surface
fList[15] = "NetCharges/Workspace16PFBSion_0Ca_16H_16OH_1surf.RData"
fList[16] = "NetCharges/Workspace16PFOSion_0Ca_16H_16OH_1surf.RData"
```

```
num_f = length(fList)
#num_files = 7 #for debugging

start_f = 1
#start_file = 7 #for debugging

#============================================================
for(fno in start_f:num_f){

  print(paste("file ",fno))

  currentFile = fList[[fno]]
  load(currentFile)

  #plot vs Z
  fn3 = paste0("../LRFigures/WLRI",liquidName,Nci,"H",Ndiv,"Ca",
               Noh,"OH",sign(charge_C),"Surf.png")
  png(fn3, height=350, width=450)
  posCurve = 1*wlr_final
  negCurve = -1*wlr_final
  axislim = max(max(posCurve),max(negCurve))
  plot(posCurve, col="blue", ylim = c(-1*axislim,1*axislim),
       xlab = expression(paste("Distance, ",z[i],"(Å)")), type="l",
       ylab = expression("w"[ext](z[i])), lwd="2")
  points(negCurve, col="red", type="l", lwd="2")
  legend("topright", legend = c("pos","neg"), col = c("blue","red"), lty=1, lwd="2", inset=0.04)
  abline(h=0)
  dev.off()

  #plot vs R
  fn4 = paste0("../LRFigures/R",liquidName,Nci,"H",Ndiv,"Ca",
               Noh,"OH", sign(charge_C),"Surf.png")
  png(fn4, height=350, width=450)
  plot(r_sequence, r_store[r_sequence], type="l", lwd="2", col="aquamarine3",
       xlab = "Distance, r (Å)", ylab = expression("w"[ext](r))  )
  abline(h=0)
  dev.off()

  #plot vs Multiple R
  rplotrange1 = max(abs(min(multistore[[1]][r_sequence])),abs(max(multistore[[1]][r_sequence])))
  rplotrange2 = max(abs(min(multistore[[101]][r_sequence])),abs(max(multistore[[1]][r_sequence])))
  rplotrange3 = max(abs(min(multistore[[201]][r_sequence])),abs(max(multistore[[1]][r_sequence])))
  rplotrange=max(rplotrange1,rplotrange2,rplotrange3)
  print(rplotrange)
  fn4 = paste0("../LRFigures/MultiR",liquidName,Nci,"H",Ndiv,"Ca",
               Noh,"OH", sign(charge_C),"Surf.png")
  png(fn4, height=350, width=450)
  plot(r_sequence, multistore[[1]][r_sequence], type="l", lwd="2", col="aquamarine3",
       xlab = "Distance, r (Å)", ylab = expression("v"[ext](r,z[i])), ylim=c(-rplotrange,rplotrange))
  points(r_sequence, multistore[[101]][r_sequence], col="blue", lwd="2", type = "l")
  points(r_sequence, multistore[[201]][r_sequence], col="red", lwd="2", type = "l")
  abline(h=0)
  legend("topright", legend = c(expression(paste('z'[i],'=',1)), expression(paste('z'[i],'=',100)),
                                expression(paste('z'[i],'=',200))),
         col=c("aquamarine3","blue","red"), inset=0.04, lty=1)
  dev.off()


  # Plot Net Charges
  fn5 = paste0("../LRFigures/NetCharge",liquidName,Nci,"H",Ndiv,"Ca",
               Noh,"OH",sign(charge_C),"Surf.png")
  png(fn5, height=400, width=450)
  ymax = 4
  ymin = -4
  plot(x=pfasHist1$mids, chargePfas1, pch="-", ylim=c(ymin,ymax),
       xlab="Distance, z (Å)", ylab = "Charge density (e)", col="black")
  abline(h=0)

  if(Nci>0){
    points(x=hydroHist1$mids, chargeHydrogen1, pch="+", col="blue")
  }
  if(Noh>0){
    points(x=ohHist1$mids, chargeOH1, pch="*", col="darkorange")
```

```
  }
  if(Ndiv>0){
    points(x=caHist1$mids, chargeCa1, pch="x", col="aquamarine3")
  }

  points(x=pfasHist1$mids, y=netCharge1, type="l", lwd=2, col="red")
  legend(x=maxzj*0.72, y=ymax, pch=c("-","+","*","x","-"),
         legend=c(liquidName,"H+","OH-","Ca2+","Net charge"),
         col = c("black","blue","darkorange","aquamarine3","red"))


  dev.off()

}#End for each file
```

E.7 Density plotting of multiple simulations

```
#-------------------------------------------------------------
# Comparison on multiple results sets
# Author: Julie Sleep
#-------------------------------------------------------------

getwd()
setwd("PFAS/Soil/SoilMolecular")
#setwd("Results")

#Scenario 1: non-anion
#file1 = "NewLRFResults/16PFBS_0Ca_0H_0OH_0surf_20000_0.5Ang.RData"
#file2 = "NewLRFResults/16PFOS_0Ca_0H_0OH_0surf_20000_0.5Ang.RData"

#Scenario 2: anion with 16H+
file1 = "NewLRFResults/16PFBSion_0Ca_16H_0OH_0surf_20000_0.5Ang.RData"
file2 = "NewLRFResults/16PFOSion_0Ca_16H_0OH_0Surf_20000_0.5Ang.RData"

#Scenario 3: anion with pos surface
#file1 = "NewLRFResults/16PFBSion_0Ca_0H_0OH_1surf_20000_0.5Ang.RData"
#file2 = "NewLRFResults/16PFOSion_0Ca_0H_0OH_1Surf_20000_0.5Ang.RData"

#Scenario 4: anion with 32 H+ and neg surface
#file1 = "NewLRFResults/16PFBSion_0Ca_32H_0OH_-1surf_20000_0.5Ang.RData"
#file2 = "NewLRFResults/16PFOSion_0Ca_32H_0OH_-1surf_20000_0.5Ang.RData"

#Scenario 5: anion with 16 Ca2+ and neg surface
#file1 = "NewLRFResults/16PFBSion_16Ca_0H_0OH_-1surf_20000_0.5Ang.RData"
#file2 = "NewLRFResults/16PFOSion_16Ca_0H_0OH_-1Surf_20000_0.5Ang.RData"

#Scenario 6: anion with 16 OH- and double pos surface
#file1 = "NewLRFResults/16PFBSion_0Ca_0H_16OH_1surf_20000_0.5Ang.RData"
#file2 = "NewLRFResults/16PFOSion_0Ca_0H_16OH_1surf_20000_0.5Ang.RData"

#Scenario 7: anion with 8 H+, 8 OH- and pos surface
#file1 = "NewLRFResults/16PFBSion_0Ca_8H_8OH_1surf_20000_0.5Ang.RData"
#file2 = "NewLRFResults/16PFOSion_0Ca_8H_8OH_1surf_20000_0.5Ang.RData"

#Scenario 8: anion with 16 H+, 16 OH- and pos surface
#file1 = "NewLRFResults/16PFBSion_0Ca_16H_16OH_1surf_20000_0.5Ang.RData"
#file2 = "Paper3Results/16PFOSion_0Ca_16H_16OH_1surf_20000_0.5Ang.RData"

#=============================================================
#Plot histogram as density line

load(file1)

#save image pre
#png(paste0("../PaperFigures/density",Nci,"H",Ndiv,"Ca",
           #Noh,"OH",charge_C,"Surf",numSteps,".png"))

#ylimit = 0.04 #OK for most neutral surfaces (2,4,5)
#ylimit = 0.05 #OK for most neutral surfaces (1)
#ylimit = 0.09 #for charged surfaces (3)
if(Noh>0){
  ylimit=0.14
```

```
} else {
  ylimit = 0.1 #for strongly charged surfaces (6)
}

ylimit = 0.2 #for strongly charged surfaces (6)
ylimit = 0.1
#bwidth = 0.001 #was 1
bwidth = 1
#lwidth = 2 #was 3
lwidth = 3

#set cropping point
cropPoint = 2500
dataSize = numSteps+1-cropPoint
croppedSurface1 = matrix(numeric(N*dataSize),
                         nrow=dataSize, ncol=N)

#Store positions and calculate densities PFAS 1
for(i in 1:N){
  newVector = numeric(dataSize)
  for(j in 1:dataSize){
    #croppedSurface[j,i] = maxToSurface[cropPoint+j,i]
    croppedSurface1[j,i] = centreToSurface[cropPoint+j,i]
  }}

par(mgp=c(3,1,0))
par(mar=c(5,6,2,2)+0.1)

#Plot a single line for first type PFAS molecules
overall.dens1 = density(croppedSurface1, bw=bwidth)
plot(overall.dens1, lwd=lwidth, ylim=c(0,ylimit), xlim=c(0,80),
     #main=paste(Nci,"H",Ndiv,"Ca", Noh,"OH",charge_C,"Surf",numSteps),
     main="", xlab="Distance, z (Å)",
     ylab=expression(paste("Density (Å"^"-3",")")),
     cex.lab=1.6, cex.axis=1.6,
     lty=1)

#Counterions 1
if(Nci>0){
  hydrogenData1 = matrix(numeric(Nci*dataSize),nrow=dataSize,
                         ncol=Nci)
  for(i in (N+1):(N+Nci)){
    for(j in 1:dataSize){
      hydrogenData1[j,i-N] = centreToSurface[cropPoint+j,i]
    }
  }
  hydrogenDensity1 = density(hydrogenData1, bw=bwidth)
  lines(hydrogenDensity1,  lwd=lwidth, main="", col="black", lty=2)
}

#Divalent cations 1
if(Ndiv>0){
  calciumData1 = matrix(numeric(Ndiv*dataSize),nrow=dataSize, ncol=Ndiv)
  for(i in (N+1):Ntot){
    for(j in 1:dataSize){
      calciumData1[j,i-N] = centreToSurface[cropPoint+j,i]
    }
  }
  calciumDensity1 = density(calciumData1, bw=bwidth)
  lines(calciumDensity1,  lwd=lwidth, main="", col="black", lty=2)
}

# Hydroxyl and hydrogen
if(Noh>0 && Nci>0){
  ohData1 = matrix(numeric(Noh*dataSize),nrow=dataSize, ncol=Noh)
  for(i in (N+Nci+1):(N+Nci+Noh)){
    for(j in 1:dataSize){
      ohData1[j,i-(N+Nci)] = centreToSurface[cropPoint+j,i]
    }
  }
  ohDensity1 = density(ohData1, bw=bwidth)
  lines(ohDensity1,  lwd=lwidth, main="", col="black", lty=3)
  # Just hydroxyl
```

```
}else if(Noh>0){
  ohData1 = matrix(numeric(Noh*dataSize),nrow=dataSize, ncol=Noh)
  for(i in (N+Nci+1):(N+Nci+Noh)){
    for(j in 1:dataSize){
      ohData1[j,i-N] = centreToSurface[cropPoint+j,i]
    }
  }
  ohDensity1 = density(ohData1, bw=bwidth)
  lines(ohDensity1,  lwd=lwidth, main="", col="black", lty=3)
}

#-------------------------------------------------------------
#Add second PFAS to plot
load(file2)

cropPoint = 2500
dataSize = numSteps+1-cropPoint
croppedSurface2 = matrix(numeric(N*dataSize), nrow=dataSize, ncol=N)
for(i in 1:N){
  newVector = numeric(dataSize)
  for(j in 1:dataSize){
    #croppedSurface[j,i] = maxToSurface[cropPoint+j,i]
    croppedSurface2[j,i] = centreToSurface[cropPoint+j,i]
  }}

#Plot a 2nd single line for all second PFAS type molecules
overall.dens2 = density(croppedSurface2, bw=bwidth)
lines(overall.dens2, lwd=lwidth, main="", col="red", lty=1)

#Counterions 2
if(Nci>0){
  hydrogenData2 = matrix(numeric(Nci*dataSize),nrow=dataSize,
                         ncol=Nci)
  for(i in (N+1):(N+Nci)){
    for(j in 1:dataSize){
      hydrogenData2[j,i-N] = centreToSurface[cropPoint+j,i]
    }
  }
  hydrogenDensity2 = density(hydrogenData2, bw=bwidth)
  lines(hydrogenDensity2,  lwd=lwidth, main="", col="red", lty=2)
}

#Divalent cations 2
if(Ndiv>0){
  calciumData2 = matrix(numeric(Ndiv*dataSize),nrow=dataSize,
                        ncol=Ndiv)
  for(i in (N+1):Ntot){
    for(j in 1:dataSize){
      calciumData2[j,i-N] = centreToSurface[cropPoint+j,i]
    }
  }
  calciumDensity2 = density(calciumData2, bw=bwidth)
  lines(calciumDensity2,  lwd=lwidth, main="", col="red", lty=2)
}

# Hydroxyl2 and hydrogen
if(Noh>0 && Nci>0){
  ohData2 = matrix(numeric(Noh*dataSize),nrow=dataSize, ncol=Noh)
  for(i in (N+Nci+1):(N+Nci+Noh)){
    for(j in 1:dataSize){
      ohData2[j,i-(N+Nci)] = centreToSurface[cropPoint+j,i]
    }
  }
  ohDensity2 = density(ohData2, bw=bwidth)
  lines(ohDensity2,  lwd=lwidth, main="", col="red", lty=3)
  # Just hydroxyl
}else if(Noh>0){
  ohData2 = matrix(numeric(Noh*dataSize),nrow=dataSize, ncol=Noh)
  for(i in (N+1):Ntot){
    for(j in 1:dataSize){
      ohData2[j,i-N] = centreToSurface[cropPoint+j,i]
    }
  }
```

```
  ohDensity2 = density(ohData1, bw=bwidth)
  lines(ohDensity2,  lwd=lwidth, main="", col="red", lty=2)
}

#-------------------------------------------------------------
if(liquidName=="PFOS"){
  legend(x=65, y=ylimit, col=c("black","red"), lwd=lwidth,
         legend=c("PFBS","PFOS"), lty=c(1,1), cex=1.4)
} else if(Nci>0 && Noh>0){
  legend(x=64, y=ylimit, col=c("black","black","black","red","red","red"),
         lwd=lwidth,
         legend=c("PFBS-","H+","OH-","PFOS-","H+","OH-"), lty=c(1,2,3,1,2,3),
         cex=1.4)
} else if(Nci>0){
  legend(x=64, y=ylimit, col=c("black","black","red","red"), lwd=lwidth,
         legend=c("PFBS-","H+","PFOS-","H+"), lty=c(1,2,1,2), cex=1.4)
} else if(Ndiv>0){
  legend(x=64, y=ylimit, col=c("black","black","red","red"), lwd=lwidth,
         legend=c("PFBS-","Ca2+","PFOS-","Ca2+"), lty=c(1,2,1,2), cex=1.4)
} else if(Noh>0){
  legend(x=64, y=ylimit, col=c("black","black","red","red"), lwd=lwidth,
         legend=c("PFBS-","OH-","PFOS-","OH-"), lty=c(1,2,1,2), cex=1.4)
} else {
  legend(x=64, y=ylimit, col=c("black","red"), lwd=lwidth,
  legend=c("PFOA-","PFOS-"), lty=c(1,1), cex=1.4)
}

#H, OH, PFOS, PFOA
legend(x=64, y=ylimit, col=c("black","black","black","red","red","red"),
       lwd=lwidth,
       legend=c("PFOA-","H+","OH-","PFOS-","H+","OH-"), lty=c(1,2,3,1,2,3),
       cex=1.4)

#save image post
#png(paste0("../PaperFigures/density",Nci,"H",Ndiv,"Ca",
                      #Noh,"OH",charge_C,"Surf",numSteps,".png"))
#dev.off()

#END=================================================================
```

Appendix F

Documentation

F.1 Authorship statements

Signed statements detailing contribution to authorship are as follows:

University of South Australia

Statement of Authorship

Title of Paper	A Review of Immobilisation-Based Remediation of Per- and Poly-Fluoroalkyl Substances (PFAS) in Soils
Publication Status	☑ Published ☐ Accepted for Publication ☐ Submitted for Publication ☐ Unpublished and Unsubmitted work written in manuscript style
Publication Details Relevant reference details	Current Pollution Reports, 7, 524-539 (2021)

PRINCIPAL AUTHOR

Name of Principal Author (Candidate)	Julie A. Sleep	
Contribution to the Paper Brief description of your work in this publication	Conducted literature review, data collection, statistical analysis, lead author	
Overall Percentage (%)	70%	
Certification		
Signature *Signatures will be redacted by the Library at the time of publication*	Julie Sleep Digitally signed by Julie Sleep Date: 2022.06.01 12:23:33 +09'30'	Date 6/1/22

CO-AUTHOR CONTRIBUTIONS

By signing the Statement of Authorship, each author certifies that:

I. the candidate's stated contribution to the publication is accurate (as detailed above);

II. permission is granted for the candidate in include the publication in the thesis; and

III. the sum of all co-author contribution is equal to 100% less the candidate's stated contribution.

Name of Co-Author 1	Albert L. Juhasz	
% Contribution to the Paper	30%	
Signature *Signatures will be redacted by the Library at the time of publication*	Albert Juhasz Digitally signed by Albert Juhasz Date: 2024.12.05 14:45:18 +10'30'	Date
Name of Co-Author 2		

University of South Australia

Statement of Authorship

Title of Paper	Monte Carlo Simulation of Perfluoralkyl Acid-Surface Interactions: I. Effect of Surface Charge and Solution Ions
Publication Status	☑ Published ☐ Accepted for Publication ☐ Submitted for Publication ☐ Unpublished and Unsubmitted work written in manuscript style
Publication Details Relevant reference details	Chemosphere, 319, 137910, 2023

PRINCIPAL AUTHOR

Name of Principal Author (Candidate)	Julie A. Sleep	
Contribution to the Paper Brief description of your work in this publication	Conceptualisation, data collection, programming, statistical analysis, visualisation, lead author	
Overall Percentage (%)	89%	
Certification		
Signature *Signatures will be redacted by the Library at the time of publication*	Julie Sleep Digitally signed by Julie Sleep Date: 2022.06.01 12:30:05 +09'30'	Date 6/1/22

CO-AUTHOR CONTRIBUTIONS

By signing the Statement of Authorship, each author certifies that:

I. the candidate's stated contribution to the publication is accurate (as detailed above);

II. permission is granted for the candidate in include the publication in the thesis; and

III. the sum of all co-author contribution is equal to 100% less the candidate's stated contribution.

Name of Co-Author 1	Stanley J. Miklavcic	
% Contribution to the Paper	9%	
Signature *Signatures will be redacted by the Library at the time of publication*	[redacted]	Date 6/12/24
Name of Co-Author 2	Albert L. Juhasz	

University of South Australia

% Contribution to the Paper	2%	
Signature *Signatures will be redacted by the Library at the time of publication*	Albert Juhasz Digitally signed by Albert Juhasz Date: 2024.12.05 14:46:11 +10'30'	Date
Name of Co-Author 3		
% Contribution to the Paper		
Signature *Signatures will be redacted by the Library at the time of publication*		Date
Name of Co-Author 4		
% Contribution to the Paper		
Signature *Signatures will be redacted by the Library at the time of publication*		Date
Name of Co-Author 5		
% Contribution to the Paper		
Signature *Signatures will be redacted by the Library at the time of publication*		Date
Name of Co-Author 6		
% Contribution to the Paper		
Signature *Signatures will be redacted by the Library at the time of publication*		Date
Name of Co-Author 7		
% Contribution to the Paper		
Signature *Signatures will be redacted by the Library at the time of publication*		Date
Name of Co-Author 8		
% Contribution to the Paper		

The University of South Australia
www.unisa.edu.au
CRICOS Provider No. 00121B

University of South Australia

Statement of Authorship

Title of Paper	Perfluoroalkyl, fluorotelomer sulfonate, and perfluorooctane sulfonamide contamination in biosolids: Composition, co-contamination and re-use implications
Publication Status	☐ Published ☑ Accepted for Publication ☐ Submitted for Publication ☐ Unpublished and Unsubmitted work written in manuscript style
Publication Details Relevant reference details	Environmental Pollution, 266 (1), 115120 (2020)

PRINCIPAL AUTHOR

Name of Principal Author (Candidate)	Julie A. Sleep	
Contribution to the Paper Brief description of your work in this publication	Lead author, Statistical analysis and methodology, Visualisation, Writing - original draft and review/editing	
Overall Percentage (%)		
Certification		
Signature *Signatures will be redacted by the Library at the time of publication*	[redacted]	Date 9/1/25

CO-AUTHOR CONTRIBUTIONS

By signing the Statement of Authorship, each author certifies that:

I. the candidate's stated contribution to the publication is accurate (as detailed above);

II. permission is granted for the candidate in include the publication in the thesis; and

III. the sum of all co-author contribution is equal to 100% less the candidate's stated contribution.

Name of Co-Author 1	Albert L. Juhasz	
% Contribution to the Paper		
Signature *Signatures will be redacted by the Library at the time of publication*	[redacted]	Date 15/1/25
Name of Co-Author 2		

The University of South Australia
www.unisa.edu.au
CRICOS Provider No. 00121B

F.2 Publication reprinting permissions

Permissions from publishers to reprint articles.

F.2.1 Elsevier permissions

Publications 2 and 3 are reprinted courtesy of Elsevier.

The Elsevier policy https://www.elsevier.com/en-au/about/policies-and-standards/copyright/permissions states that "Authors can include their articles in full or in part in a thesis or dissertation for non-commercial purposes." and that "As an Elsevier journal author, you have the right to Include the article in a thesis or dissertation (provided that this is not to be published commercially) whether in full or in part, subject to proper acknowledgment; see the Copyright page for more information. No written permission from Elsevier is necessary. This right extends to the posting of your thesis to your university's repository provided that if you include the published journal article, it is embedded in your thesis and not separately downloadable."

F.2.2 Springer Nature permissions

The license for reprinting publication 1 from Springer Nature is contained on the following pages.

SPRINGER NATURE LICENSE
TERMS AND CONDITIONS
May 31, 2022

This Agreement between Ms. Julie Sleep ("You") and Springer Nature ("Springer Nature") consists of your license details and the terms and conditions provided by Springer Nature and Copyright Clearance Center.

License Number	5319680430047
License date	May 31, 2022
Licensed Content Publisher	Springer Nature
Licensed Content Publication	Current Pollution Reports
Licensed Content Title	A Review of Immobilisation-Based Remediation of Per- and Poly-Fluoroalkyl Substances (PFAS) in Soils
Licensed Content Author	Julie A. Sleep et al
Licensed Content Date	Sep 28, 2021
Type of Use	Thesis/Dissertation
Requestor type	academic/university or research institute
Format	print and electronic
Portion	full article/chapter
Will you be translating?	no
Circulation/distribution	50000 or greater
Author of this Springer Nature content	yes
Title	Modelling, Prevalence and Immobilisation of Per- and Poly-fluoroalkyl Substances
Institution name	University of South Australia
Expected presentation date	Dec 2022
Requestor Location	Ms. Julie Sleep [redacted] [redacted] Australia Attn: Ms. Julie Sleep
Total	0.00 AUD

Terms and Conditions

Springer Nature Customer Service Centre GmbH
Terms and Conditions

This agreement sets out the terms and conditions of the licence (the **Licence**) between you and **Springer Nature Customer Service Centre GmbH** (the **Licensor**). By clicking 'accept' and

completing the transaction for the material (**Licensed Material**), you also confirm your acceptance of these terms and conditions.

1. **Grant of License**

    1. The Licensor grants you a personal, non-exclusive, non-transferable, world-wide licence to reproduce the Licensed Material for the purpose specified in your order only. Licences are granted for the specific use requested in the order and for no other use, subject to the conditions below.

    2. The Licensor warrants that it has, to the best of its knowledge, the rights to license reuse of the Licensed Material. However, you should ensure that the material you are requesting is original to the Licensor and does not carry the copyright of another entity (as credited in the published version).

    3. If the credit line on any part of the material you have requested indicates that it was reprinted or adapted with permission from another source, then you should also seek permission from that source to reuse the material.

2. **Scope of Licence**

    1. You may only use the Licensed Content in the manner and to the extent permitted by these Ts&Cs and any applicable laws.

    2. A separate licence may be required for any additional use of the Licensed Material, e.g. where a licence has been purchased for print only use, separate permission must be obtained for electronic re-use. Similarly, a licence is only valid in the language selected and does not apply for editions in other languages unless additional translation rights have been granted separately in the licence. Any content owned by third parties are expressly excluded from the licence.

    3. Similarly, rights for additional components such as custom editions and derivatives require additional permission and may be subject to an additional fee. Please apply to Journalpermissions@springernature.com/bookpermissions@springernature.com for these rights.

    4. Where permission has been granted **free of charge** for material in print, permission may also be granted for any electronic version of that work, provided that the material is incidental to your work as a whole and that the electronic version is essentially equivalent to, or substitutes for, the print version.

    5. An alternative scope of licence may apply to signatories of the STM Permissions Guidelines, as amended from time to time.

- **Duration of Licence**

    1. A licence for is valid from the date of purchase ('Licence Date') at the end of the relevant period in the below table:

Scope of Licence	Duration of Licence
Post on a website	12 months
Presentations	12 months
Books and journals	Lifetime of the edition in the language purchased

- **Acknowledgement**

1. The Licensor's permission must be acknowledged next to the Licenced Material in print. In electronic form, this acknowledgement must be visible at the same time as the figures/tables/illustrations or abstract, and must be hyperlinked to the journal/book's homepage. Our required acknowledgement format is in the Appendix below.

- **Restrictions on use**

1. Use of the Licensed Material may be permitted for incidental promotional use and minor editing privileges e.g. minor adaptations of single figures, changes of format, colour and/or style where the adaptation is credited as set out in Appendix 1 below. Any other changes including but not limited to, cropping, adapting, omitting material that affect the meaning, intention or moral rights of the author are strictly prohibited.

2. You must not use any Licensed Material as part of any design or trademark.

3. Licensed Material may be used in Open Access Publications (OAP) before publication by Springer Nature, but any Licensed Material must be removed from OAP sites prior to final publication.

- **Ownership of Rights**

1. Licensed Material remains the property of either Licensor or the relevant third party and any rights not explicitly granted herein are expressly reserved.

- **Warranty**

IN NO EVENT SHALL LICENSOR BE LIABLE TO YOU OR ANY OTHER PARTY OR ANY OTHER PERSON OR FOR ANY SPECIAL, CONSEQUENTIAL, INCIDENTAL OR INDIRECT DAMAGES, HOWEVER CAUSED, ARISING OUT OF OR IN CONNECTION WITH THE DOWNLOADING, VIEWING OR USE OF THE MATERIALS REGARDLESS OF THE FORM OF ACTION, WHETHER FOR BREACH OF CONTRACT, BREACH OF WARRANTY, TORT, NEGLIGENCE, INFRINGEMENT OR OTHERWISE (INCLUDING, WITHOUT LIMITATION, DAMAGES BASED ON LOSS OF PROFITS, DATA, FILES, USE, BUSINESS OPPORTUNITY OR CLAIMS OF THIRD PARTIES), AND WHETHER OR NOT THE PARTY HAS BEEN ADVISED OF THE POSSIBILITY OF SUCH DAMAGES. THIS LIMITATION SHALL APPLY NOTWITHSTANDING ANY FAILURE OF ESSENTIAL PURPOSE OF ANY LIMITED REMEDY PROVIDED HEREIN.

- **Limitations**

1. ***BOOKS ONLY:***Where '**reuse in a dissertation/thesis**' has been selected the following terms apply: Print rights of the final author's accepted manuscript (for clarity, NOT the published version) for up to 100 copies, electronic rights for use only on a personal website or institutional repository as defined by the Sherpa guideline (www.sherpa.ac.uk/romeo/).

2. For content reuse requests that qualify for permission under the STM Permissions Guidelines, which may be updated from time to time, the STM Permissions Guidelines supersede the terms and conditions contained in this licence.

- **Termination and Cancellation**

1. Licences will expire after the period shown in Clause 3 (above).

2. Licensee reserves the right to terminate the Licence in the event that payment is not received in full or if there has been a breach of this agreement by you.

Appendix 1 — Acknowledgements:

For Journal Content:
Reprinted by permission from [**the Licensor**]: [**Journal Publisher** (e.g. Nature/Springer/Palgrave)] [**JOURNAL NAME**] [**REFERENCE CITATION** (Article name, Author(s) Name), [**COPYRIGHT**] (year of publication)
For **Advance Online Publication papers:**
Reprinted by permission from [**the Licensor**]: [**Journal Publisher** (e.g. Nature/Springer/Palgrave)] [**JOURNAL NAME**] [**REFERENCE CITATION** (Article name, Author(s) Name), [**COPYRIGHT**] (year of publication), advance online publication, day month year (doi: 10.1038/sj.[JOURNAL ACRONYM].)
For Adaptations/Translations:
Adapted/Translated by permission from [**the Licensor**]: [**Journal Publisher** (e.g. Nature/Springer/Palgrave)] [**JOURNAL NAME**] [**REFERENCE CITATION** (Article name, Author(s) Name), [**COPYRIGHT**] (year of publication)
Note: For any republication from the British Journal of Cancer, the following credit line style applies:
Reprinted/adapted/translated by permission from [**the Licensor**]: on behalf of Cancer Research UK: : [**Journal Publisher** (e.g. Nature/Springer/Palgrave)] [**JOURNAL NAME**] [**REFERENCE CITATION** (Article name, Author(s) Name), [**COPYRIGHT]** (year of publication)
For **Advance Online Publication** papers:
Reprinted by permission from The [**the Licensor**]: on behalf of Cancer Research UK: [**Journal Publisher** (e.g. Nature/Springer/Palgrave)] [**JOURNAL NAME**] [**REFERENCE CITATION** (Article name, Author(s) Name), [**COPYRIGHT**] (year of publication), advance online publication, day month year (doi: 10.1038/sj.[JOURNAL ACRONYM])
For Book content:
Reprinted/adapted by permission from [**the Licensor**]: [**Book Publisher** (e.g. Palgrave Macmillan, Springer etc) [**Book Title**] by [**Book author**(s)] [**COPYRIGHT**] (year of publication)

Other Conditions:

Version 1.3

Questions? customercare@copyright.com or +1-855-239-3415 (toll free in the US) or +1-978-646-2777.
